A MULTI-PARAMETER RADAR APPROACH TO STAND STRUCTURE AND FOREST BIOMASS ESTIMATION

PETER NILO TIANGCO

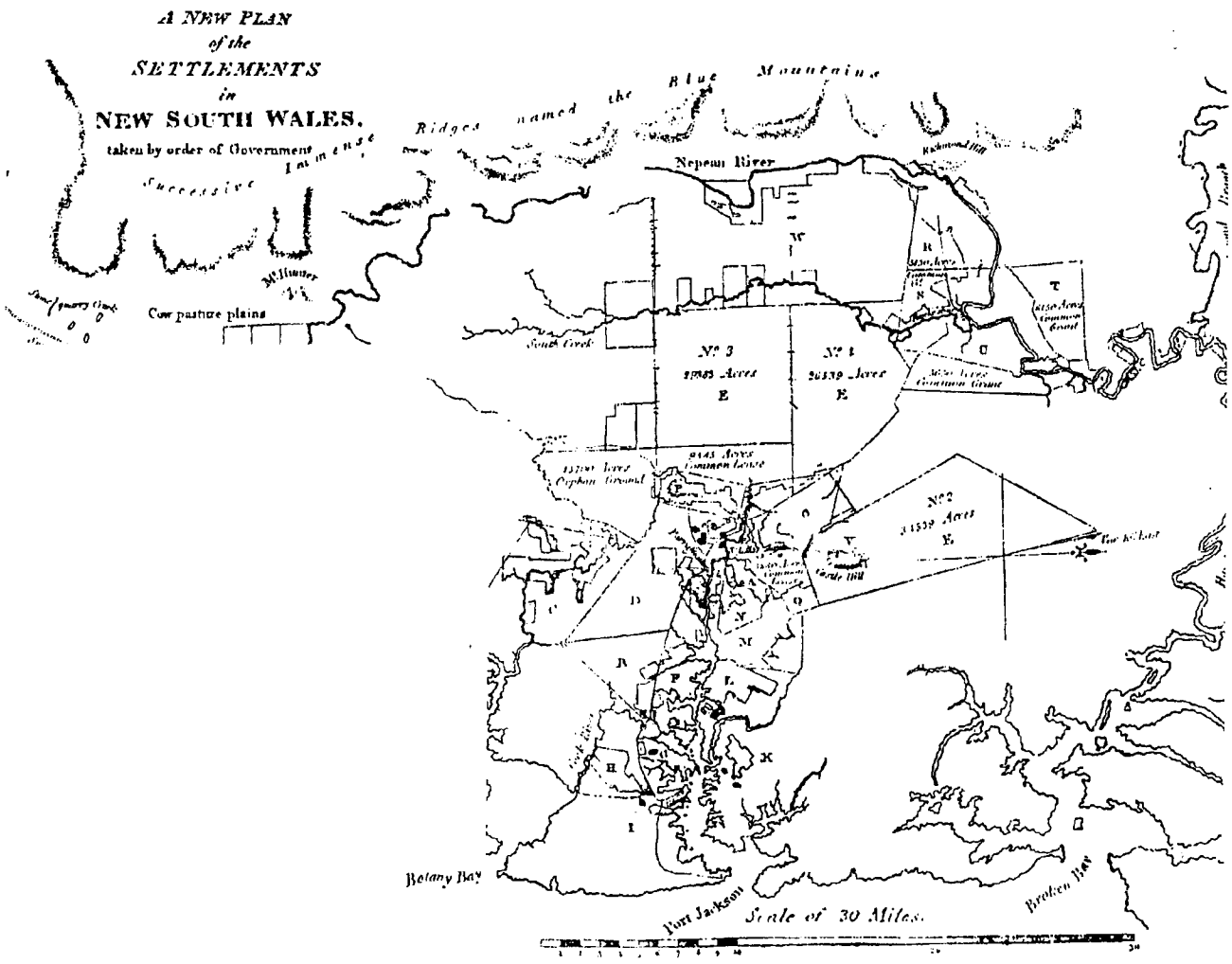

UNISURV S-57, 2000

Reports from

SCHOOL OF GEOMATIC ENGINEERING

THE UNIVERSITY OF NEW SOUTH WALES SYDNEY NSW 2052 AUSTRALIA

UNISURV REPORT S-57, 2000

A MULTI-PARAMETER RADAR APPROACH TO STAND STRUCTURE AND FOREST BIOMASS ESTIMATION

PETER NILO TIANGCO

Received: June 2000
Accepted: September 2000

SCHOOL OF GEOMATIC ENGINEERING
UNIVERSITY OF NEW SOUTH WALES
UNSW SYDNEY NSW 2052
AUSTRALIA

National Library of Australia

Card No. and ISBN 0 - 7334 - 0786 - 2

FOREWORD

Radar or microwave remote sensing is becoming an increasingly important tool for monitoring the Earth's resources because of its ability to penetrate rain and cloud and to be obtained independently of solar illumination. However the relationship between the measured backscattered radiation, the transmitted signal and the physical characteristics of the target area are extremely complex, and are as much a function of the properties of the Earth surface as the wavelength, polarisation and look angle of the incident radiation. For this reason much of the research in this area has been directed to developing theoretical models that allow the prediction of Earth parameters from multi-polarised and multi-frequency imaging radar systems.

The work that Peter Tiangco undertook for his PhD, was the development of models that allow the prediction of certain forest stand characteristics and the estimation of forest biomass. His work was based on the theoretical consideration that a tree was comprised of two simple parts, the trunk and the canopy (leaves, twigs, branches), and that longer wavelength (P and L) copolarised radiation would have a backscattered response correlated with trunk size due to canopy penetration and ground/trunk double bounce effects, while the backscattered shorter wavelength (C band) crosspolarised radiation would have a higher correlation with the canopy size and density. Thus the their sum should represents a total response from all the biomass contributing elements, and allow for its estimation in tonnes per hectare, while their difference should be a measure of the different trunk/canopy characteristics of the trees. Essentially this theory was proven for measured backscattered reported from northern hemisphere forests, but was not as significant when comparing pine and eucalypt forests in Australia.

Much of the earlier research on the estimation of biomass from radar backscattered response used only single wavelength data, and simple regression models between measured biomass and return signal, and therefore did not incorporate all the biomass impact, as longer wavelength returns tended to be dominated by trunk effects and shorter wavelength by canopy effects. Thus the use of multi-wavelength data as developed in this research has significantly improved the ability to estimate total biomass. In addition different tree species/types can have quite different response/biomass relationships, due to leaf orientation and height and diameter of trunks. This work has also provided an approach to the separation of tree types,

ranging from small trunk/ big canopy trees to large trunk/small canopy trees, with different relationships then being used for biomass prediction.

Tiangco's research has links to other radar research in the School of Geomatic Engineering (UNSW), where similar approaches have been made in discriminating urban land use classes from radar returns, which are also strongly related to double bounce effects and crosspolarised return from urban forest areas, to research into radar speckle filtering for better classification of forest images and other classification procedures, and to research using interferometric radar measures for acquiring digital terrain models, where the top of canopy or bare earth return are a function of radar wavelength and forest coverage. The research is also closely related to work in the School of Geography (UNSW) where major studies on the global estimation of biomass, using both radar and visible/infrared remote sensing approaches, are being undertaken, as part of regional and international joint research efforts, particularly to determine the impact of deforestation on global CO2 levels and global warming.

To this end the University of New South Wales in association with CSIRO, in Australia, and the Jet Propulsion Laboratory and NASA in the USA, have collaborated in acquiring quad-polarised multi-wavelength radar image data (AirSAR), and interferometric data (TopSAR), over many countries of the Asia-Pacific region in two PACRIM projects, the second of which was completed in September 2000. AirSAR data from the first PACRIM project in 1996 was used in this current research project.

Bruce Forster

September 2000

ACKNOWLEDGEMENTS

The author wishes to express his heartfelt gratitude to his research supervisor, Prof. Bruce C. Forster, for his unwavering guidance, expert suggestions and warm friendship. Sincere thanks are also due to Mrs. Cindy Cisneros-Tiangco for her invaluable support and encouragement. Indeed, the selfless assistance extended by these two remarkable individuals throughout the entire course of this study provided the author the strength and inspiration to complete this thesis.

Several individuals and institutions were likewise instrumental in the completion of this work. To them, the author extends his appreciation.

To Messrs. Phil Whiteman, Henry Lieshout, Richard Appleton and Jason Clark of the Australian Paper Plantations Pty. Ltd. for their extraordinary hospitality and tireless assistance during the fieldwork conducted at the Gippsland study site.

To Drs. Armando Apan, Josef Aschbacher, and Yunhan Dong, not only for their technical inputs during the topic identification, model and analysis method formulation phases of the study, but also for their camaraderie. Special thanks to Dr. Apan for constantly sending valuable technical papers and materials and for being always willing to go out of his way and lend a helping hand.

To Ms. Jennifer Pett of the Department of Natural Resources and Environment Corporate Library in Melbourne, Victoria for promptly sending the essential articles and reports on allometric equations, which seemed to be unavailable elsewhere.

To Mr. Leon Daras and Ms. Maria Ponce of the School of Geomatic Engineering, UNSW, for their splendid administrative assistance. Sincere appreciation is also due to Mr. Chon Satirapod of the SNAP group for lending the GPS receiver used during the field data collection.

To NASA/JPL for providing the AIRSAR images of the study sites. Ms. Ellen O'Leary's quick and dependable response to requests for radar data is commendable.

To Ms. Gina Umali for her help during the field data collection activities carried out at the Blue Mountains National Park study site.

To Mr. Norbert Que for his help in the printing of the final copy of this thesis.

To my good friends cum tennis buddies Joel Marciano, Gilbert Santayana, Gilbert Gonzales, Jac Catalan, Norbert and Leilani Que for making my stay in Australia more enjoyable.

To my family back home, especially my brother Paul, for their support and motivation.

To the Australian Agency for International Development (AusAID) for financially supporting the study until the end of February, 1999.

Above all, to Him for making everything possible.

ABSTRACT

The use of radar remote sensing to estimate biomass has been receiving increasing interest in recent years mainly due to the capability of the radar to provide data independent of solar illumination and weather conditions, and the worldwide demand for information on biomass change and its relationship to global warming. With the advent of multi-parameter imaging radar systems and the simultaneous use of different frequency-polarisation combinations, more accurate estimation may now be possible. The theoretical basis behind the inference of target properties from multi-parameter radar data must then be investigated and the extension of the developed methodologies to other investigations explored.

In this research, a Trunk-Canopy Biomass Index (TCBI) and a Trunk-Canopy Morphology Index (TCMI), derived from multi-frequency/multi-polarised radar data as a means of predicting aboveground biomass in different forest species, are proposed. The TCBI, which is the sum of the L-HH and C-HV backscatter, can be a measure of the total aboveground biomass since both trunk and crown layers are considered. Owing to possible morphological variations, the relationship between TCBI and total biomass is however not expected to be unique for a whole forest vegetation. It is important therefore that the stand structure be first considered to allow a more accurate biomass assessment using the TCBI. An index of the relative proportions of the trunk and crown may be indicative of the approximate tree morphology. The TCMI, which is the ratio of the L-HH to C-HV backscatter, may provide a measure of tree structure. Two categories are used to classify stands according to structure: the needle-leaved pines/conifers and the broad-leaved evergreen/deciduous trees. A two-stage procedure for forest biomass estimation is proposed: first using the TCMI and then the TCBI.

The effectiveness of the indices were first assessed by applying them to data interpolated from published research. Stand structure and total aboveground biomass were found to be highly correlated with the TCMI and TCBI, respectively. Further verification was carried out using radar and field data from the Blue

Mountains and Gippsland study sites. Due to the structural similarity between radiata pines and most eucalypts, the average difference between their TCMI values was found to be not as significant as theory proposed. A low correlation between TCBI and total biomass was observed due to the early saturation of radar measurements, caused by high biomass densities in the sampled areas. A new index, the $TCBI_{new}$, produced a much better correlation especially within the 0 - 245 tonnes/ha biomass range. This index also provided the best biomass estimate relative to other bands and band combinations.

TABLE OF CONTENTS

LIST OF FIGURES

LIST OF TABLES

CHAPTER 1

INTRODUCTION

1.1 Background and rationale

The importance of the forest as a multi-purpose resource base is a long recognised fact. It is not only a source of wood, food and other forest products such as tannins, resins and pulp, but also of water and energy. In addition, it serves as habitat for numerous species of flora and fauna and plays an important role in the maintenance of balance in ecosystems and in the preservation of biodiversity. More recently, the global importance of the forest resource is further recognised in its role as a carbon dioxide-consuming entity that could help in the prevention of the so-called greenhouse effect. In a nutshell, the forest thus has three distinctive but independent functions: productive, protective, and regenerative (BIOTROP, 1989).

For the past several decades, however, continuous over-exploitation of forest resources became a common trend worldwide leading to a massive depletion of the same. Forest destruction and its devastating effects led to the growing cognisance of the importance of treating the forest as a valuable asset that should be utilised and developed on a sustained basis. Needless to say, the success of forest management and development schemes depends on the availability of precise and timely information. The conventional methods of data collection and handling, alone, are not very effective for the purpose. The use of remote sensing will provide for a more efficient and accurate acquisition and analysis of the essential data.

Remote sensing is defined as the inference of information about objects through the analysis of data acquired at a distance by electromagnetic energy sensors (Avery and Berlin, 1991). The sensor could either be ground-based, on-board an aircraft, spacecraft or earth-orbiting satellite with the capability of recording information at different dates, different scales, and different portions of the

electromagnetic spectrum. These multi-revisit, multi-stage and multi-spectral qualities make remote sensing a valuable tool for forestry applications.

Radar technology is highly regarded as the solution to the problems associated with the use of optical sensors. The capability of the radar device to operate independent of solar illumination and the prevailing atmospheric conditions are two of the most cited arguments for its use especially in regions with persistent fog or cloud cover such as most areas in the tropics. Moreover, system parameters like incidence angle, frequency/wavelength, and polarisation can be configured depending on the objectives of the study. The radar sensitivity to geometric and dielectric properties of the target provides access to parameters different from those available using optical sensors. These properties highlight the radar's usefulness in providing information to complement those from visible and infrared sensors when such are available.

Being relatively new, however, it is believed that microwave remote sensing has a lot of catching up to do relative to its optical-based counterpart in terms of analysis algorithms and procedures, data archives, and user community size. Optical remote sensing is a mature technology that through several decades has been developing a broad knowledge base thereby leading to well-defined and well-established image interpretation techniques (Gerstl, 1990). Nonetheless, the growing number of researches on radar data applications during the past years is a positive step towards narrowing the technology gap.

The early 70s saw the first demonstration of the usefulness of airborne radar images in the tropics with projects such as NIRAD in Nigeria, Radam in Brazil, and Proradam in Columbia (FAO, 1993). It was not until 1978 that the first spaceborne radar remote sensing system was put into orbit by the United states on board the SEASAT satellite. This was followed by two short-term radar missions, the Shuttle Imaging Radar (SIR) A and B in 1981 and 1984, respectively. Long-term spaceborne radar missions designed for civilian applications started with the launch of the former USSR's ALMAZ-1 in 1987, followed by ALMAZ-2 and Europe's ERS-1 in 1991, Japan's JERS-1 in 1992, and Canada's RADARSAT in 1995. These

radar systems had single frequency band and polarisation. The novelty of the accumulated radar data led to ongoing studies on new image processing and analysis techniques, data calibration, basic research on radar polarimetry, interferometry, backscatter modelling, and other practical applications. The SIR-C/X-SAR 1 and 2 missions in April and October 1994 provided, for the first time, multi-parameter spaceborne radar images (ESA, 1995).

1.2 Definition of problem areas

As not until the launch of remote sensing systems such as SIR-C/X-SAR and AIRSAR that multi-parameter data from a single platform been available, most of the forestry-related radar studies conducted to date have made use of individual frequency-polarisation bands. The majority of the research sites are in temperate forest regions with the vegetation usually dominated by single or few species of coniferous trees. Also, most of these studies concentrated on managed vegetation located in flat areas and only few have been conducted in natural forest environments (Werle, 1989b). Owing to the numerous differences, such as species composition/structure and dielectric conditions, between temperate and tropical forest areas and between cultural and natural vegetation, results from these previous studies cannot be considered applicable to all areas. As such, experiments designed according to the conditions of a specific area are essential. The simultaneous use of different radar frequencies and polarisations has great potential for providing a multi-dimensional set of measurements, akin to shifting from monochrome to colour optical imagery (ESA, 1995), and should be thoroughly looked into.

1.3 Study objective and thesis layout

The main objective of this study is to develop techniques for the assessment and characterisation of Australian forests through the use of multi-parameter radar data. A key concern is the simultaneous use of different radar frequencies and polarisations to optimise the information extraction process. Assessment of forest

resources is carried out through the determination of the general stand structure and estimation of total aboveground biomass.

A review of past and current studies involving the use of radar remote sensing in forestry is presented in Chapter 2. The review, which examines the various methodologies used and the results obtained, provides for the identification of specific research gaps thereby defining the direction for this particular study.

Chapter 3 presents the theoretical basis behind the use of different radar parameters for the determination of morphological structure and total aboveground biomass of forest resources. In here, the manner in which radar parameters such as frequency/wavelength and polarisation react to target properties such as those pertaining to roughness, geometric, and dielectric properties is explored for a clear understanding of the backscatter-target relationship. Consequently, simple backscattering models and indices are formulated for the inference of tree structure and total stand biomass from radar data.

The theories, models and indices introduced in Chapter 3 are applied using measured and modelled data from published similar works of other researchers. The main purpose of this procedure is to test the accuracy of these models and indices in providing estimates of forest biomass and structure against the accuracy of the methods used in other researches. The results of this comparative test are presented and discussed in Chapter 4.

The models and indices are then used to assess the structure and total aboveground biomass of broad-leaved and coniferous forest areas in Australia. Chapter 5 gives a detailed description of the study sites, field data and radar data used. The data analysis and assessment procedures are presented in Chapter 6 while a discussion of the results obtained from the application of these procedures to the radar and field data from the study sites are given in Chapter 7. A general summary, concluding remarks and recommendations for further research form Chapter 8. A glossary of radar terms used in this thesis is provided in Appendix 1.1 for readers not familiar with radar terminology. Some readers may find it easier to read the

chapter on the theoretical basis (Chapter 3) before reading the literature review (Chapter 2).

CHAPTER 2

LITERATURE REVIEW: THE USE OF RADAR REMOTE SENSING IN FORESTRY

2.1 Introduction

The development of remote sensing as a field of study is generally anchored on the developments in photography, dating to the mid-19th and early 20th century, when balloons, kites, pigeons, and airplanes were first used as camera platforms to obtain information at high altitudes over large areas using the visible part of the spectrum. With the invention in the first half of the last century of coloured films, near-infrared and infrared-sensitive photographic emulsions, non-imaging radar and thermal sensors, remote sensing has been extended into the other portions of the electromagnetic spectrum. This allowed the acquisition of information on events and phenomena beyond the range of human vision (Richason, 1978). Studies on the various applications of colour infrared and multi-spectral photography were initiated in the mid-1960s by the National Aeronautics and Space Administration (NASA) which lead to the launch of the first Earth Resources Technology Satellite, later renamed Landsat 1, in 1972 (Elachi, 1987). A rapid growth in remote sensing, especially in non-photographic remote sensing from space, followed the successful launch of Landsat 1 (Fischer et al., 1976).

Radar systems, which operate at the relatively long wavelength part of the spectrum, were first intensively used during World War II to detect and locate targets such as ships and planes. Radar development was kept as a military secret during the War such that codes (e.g., X-band, C-band, L-band) were assigned to the wavelengths used (FAO, 1993). With radar declassification after the War, imaging radars have evolved to be a valuable civilian tool for applications such as in forest resource assessment and monitoring. The usefulness of imaging radars in these types of application is closely tied to the capability of microwaves to penetrate

through clouds, haze and light rain. This is important particularly in frequently cloud-covered forest areas where data acquisition through the use of optical sensors or any other means is not always possible. Moreover, radars provide their own source of energy thus allowing data acquisition independent of solar illumination. As microwaves see forest targets in a different perspective, the information content of radar imageries is therefore different to that of optical data.

In forestry, the general research direction is aimed at providing full understanding of the relationships between the radar backscatter and the biophysical characteristics and processes within forest stands. Some of the major difficulties encountered along this line relate to the complexity of trees and forest stands in terms of geometry and abundance of constituents, the topographic distortions associated with rugged terrain and the presence of speckles in the resulting image. To date, several models, geocoding and filtering algorithms/procedures have been developed to deal with these problems though most of the same are still subjects of current investigations.

In this review, past and current studies on the application of radar remote sensing in forestry are examined to obtain an overview of research results, accomplishments and limitations. Some initiatives involving the use of radar in conjunction with optical data are also included. The objective of this review is thus to consolidate and assess the accumulated knowledge concerning the usefulness to forestry of different radar frequencies, polarisations and look angles so as to identify specific application areas in need of further research. It should be noted that the topics covered in this chapter are generalised; more detailed reviews are presented according to their specific themes in later chapters.

2.2 Basis and methodology

This review is based on the search, collection and analysis of published articles, reports, dissertations and other related literature. Most of the reference materials used were obtained from the main library of the University of New South

Wales in Kensington, NSW, although some were acquired from other sources. The selection and analysis of the materials were directed by the issue of how the different forest biophysical properties relate to varying radar parameters of frequency/wavelength, polarisation and incidence angle. While not every research carried out under this subject was discussed, an effort was made to have key areas represented. As much as possible, the scope was limited to studies involving the airborne and spaceborne active sensors.

2.3 Studies of interest to forestry

2.3.1 Forest biomass estimation

Accurate knowledge of forest biomass is vital to understanding ecosystem processes and their interaction with climate and carbon cycles. Even though the capability of radar signals to penetrate forest canopies has been known for some time, only lately has it been demonstrated that such signals are indeed sensitive to biomass (Way, 1993). Attempts to evaluate the relationships between the forest biomass and radar backscatter have been made in recent studies using both aircraft and satellite data at various wavelengths polarisations and incidence angles. This section is divided according to these two kinds of platforms in the light of the possible differences in the validity and applicability of the findings.

Airborne radar systems

Hussin et al. (1991), using L-band HV-polarised multiple incidence angle aircraft synthetic aperture radar (SAR) data, showed a significant relationship between radar backscatter and stand biomass, basal area, and tree height for 55 slash pine plantations in Florida. Similar results were obtained by Sader (1987), who used L-band quad-polarised data. No significant relationship was noticed between the like-polarised data and forest biomass, canopy structure and species composition.

An investigation of the strong correlation between L- and P-band backscatter and forest biomass observed from earlier analyses of NASA/JPL SAR images of the Landes (France) and Duke (USA) pine forests was conducted by Beaudoin et al. (1994). P-band was found to be the optimal frequency for forest observations and that HH return is physically related to both trunk and crown biomass whereas VV, and particularly HV, are linked to crown biomass alone. Using the same forest areas as study sites, Dobson et al. (1992) examined the dependence of C-, L- and P-band backscatter on aboveground biomass of maritime and loblolly pine stands. Little dispersion in the data between the two conifer species was observed at P-band, which may be ascribed to the similarity in trunk structure of the two species. The L-band backscattering behaviour was similar to that of the P-band. For C-band, however, σ°_{HV} of loblolly pine was found to be 1-3 dB higher than the σ°_{HV} of the maritime pine. The difference in crown structure, such as in the length, diameter and orientation distribution of the needles and small branches, was given as the probable cause of the backscattering discrepancy. Polarisations most sensitive to specular scattering mechanisms by the trunk and the ground surface, viz. HH and HV, showed the highest sensitivity to biomass. Kasischke et al. (1995) studied the relationship between C-, L- and P-band backscatter and loblolly pine biomass at the Duke forest in North Carolina, USA and found significant correlation in all three frequencies. At P- and L-bands, the greatest sensitivity to biomass variations occurred in the HH and VH polarisations while VH showed the greatest sensitivity in the case of C-band. In a related study over a forest in Germany, Rauste et al. (1994) observed a positive correlation between P-HV backscatter and tree biomass at 0-500 tonnes/ha, and between L-band and biomass at 0-70 tonnes/ha, although in the latter case, the backscatter decreased slowly with increasing biomass. Observations of SAR data conducted by Christensen, Jr. et al. (1990) showed a positive relationship between L-HH and L-VV backscatter and biomass for levels less than 100 tonnes/ha. The high effectiveness of long radar wavelengths such as that of the P-band for predicting forest biomass was corroborated by the findings of Israelsson et al. (1994), Rignot et al. (1994b), Beaudoin et al. (1992), and two recent works of Rauste (1992, 1993) and Le Toan et al. (1991, 1992).

In another study, Rignot et al. (1994c) compared biomass levels from forest inventories with those predicted from linearly and circularly polarised P-band radar signals. The measurements were found to be in good agreement except when the phase difference between HH and VV-polarisation was large. Also, at biomass levels greater than 200 tonnes/ha, where the P-band response from the forest saturates, it was shown that polarimetric information allows further characterisation of the vegetation.

Using AIRSAR multi-parameter data of the same area but taken at different dates (and different temperatures and moisture conditions), Moghaddam et al. (1993) analysed the variations of radar backscatter with biomass and other forest parameters in each of the two dates and compared the results. Differences of several dB between the backscatters have been observed causing the authors to infer that radar measurements cannot be used to uniquely obtain the biomass and that inversion algorithms to determine the fundamental scattering properties of forest components should be used instead.

Durden et al. (1991) examined multi-frequency, multi-polarisation and multi-incidence angle AIRSAR images of a forested area near Mt. Shasta, California and found that the C-band cross section averaged over like and cross polarisations is the best parameter for distinguishing between two stands with different biomass at different incidence angles. The average P- and L-band cross sections also appeared correlated with biomass but only at smaller incidence angles; they were not useful for distinguishing the stands with different biomass levels at large incidence angles. The other radar parameters, which measure forest polarisation properties, were not useful in this respect as well.

Imhoff (1993) determined the biomass saturation levels for the C-, L- and P-band images over a tropical evergreen forest composed of broad-leaved trees and a temperate coniferous forest for the purpose of assessing radar applicability to global biomass estimation. SAR signal saturation points for the two forest types were reached at approximately the same levels of biomass. These values were matched with the Matthews' world map of vegetation types and it was found that only 3% of

the world's vegetation could be accounted using C-band (20 tonnes/ha threshold). L-band (40 tonnes/ha threshold) picks up another 3%, plus another 12% for the P-band (100 tonnes/ha threshold). Since most of the world's biomass are beyond the saturation levels of the three bands, the author suggested the use of aids to classification such as data from other sensors, polarimetry techniques, and the possibility of using longer wavelengths and smaller incidence angles to push the saturation point upwards.

As a possible answer to SAR signal saturation with increasing biomass, Saatchi et al (1995) formulated a hybrid technique of image classification, modelling and inversion algorithm. The technique has been tested over a boreal forest in Canada by using the multi-parameter AIRSAR data and was determined to be effective in enhancing biomass estimation. Modification of the technique into more sophisticated forms was recommended for application in tropical forests.

An experimentation of radar image processing methods for mapping standing biomass of a forest in Maine, USA was done by Ranson and Sun (1992 and 1994a). Using AIRSAR multi-parameter data, it was determined that the ratio of HV backscatter between P- or L-band and C-band was a good parameter for total biomass mapping. The ratio was observed to enhance the correlation between image signature and standing biomass ($R = 0.83$ for P/C and $R = 0.79$ for L/C) and was found to be sensitive to biomass levels above 150 tonnes/ha. HH and VV, especially at P-band, were sensitive to changing surface conditions (e.g., ground covered with water or wet ice). Cross-polarised backscatter was seen to originate mainly from multiple scattering within the tree canopy and as such was less influenced by surface conditions. The highest correlation between radar backscatter and forest biomass was obtained using P-HV. The predicted versus measured biomass values had an R^2 value of 0.82 thus indicating a reasonable estimate from SAR data. Further field biomass measurements were suggested by the authors to evaluate the method.

Williams et al. (1994) obtained biomass projections in a boreal forest in Alaska by integrating AIRSAR-based classification of vegetation succession stages, existing biomass measures within successional stages, and knowledge of rates and

processes influencing succession. The projections demonstrated the importance of current vegetation type (and biomass) distribution for prediction of future biomass distributions.

Spaceborne radar systems

Wang et al. (1994) investigated the effects of biomass and soil moisture changes in young (< 15 years old) loblolly pine stands at the Duke forest in North Carolina, USA to ERS-1 (C-band) backscatter. It was found out that ERS-1 backscatter from the pine stands was less than or equal to the backscatter from wet short-grass fields of 0.5 tonnes/ha biomass and there was no significant correlation between the backscatter and biomass (R = 0.19). Under dry soil conditions, there was a 2-3 dB increase in the short-grass backscatter as biomass increased from 0.5 tonnes/ha to about 5 -15 tonnes/ha with a correlation coefficient (R) of 0.46. As the ground changed from dry to wet, the increase in the backscatter from the short-grass field and the stands was 5 and 3 dB, respectively. Based on subsequent modelling and sensitivity analysis of the ERS-1 SAR backscatter from the stands over dry grounds, it was observed that as the surface-soil moisture increased, the major backscatter contributor was changed from the canopy volume scattering to surface backscatter between 4 tonnes/ ha and 10 tonnes/ ha. At biomass levels equal to or more than 13 tonnes/ha, the canopy volume scattering was always the main contributor regardless of the increase in moisture or roughness. It was concluded that ERS-1's applicability to forest monitoring is limited by system's signal saturating at low standing biomass and its high sensitivity to soil moisture conditions.

Pulliainen et al. (1993) and Pulliainen et al. (1995) utilised ERS-1 SAR images for stem/bole volume retrieval in boreal forest areas in Finland. Stem volume estimates obtained from the ERS-1 data were compared with ground-based measurements and good results were obtained from both studies. In the case of the former, the obtained average correlation coefficient between the radar-derived estimates and the ground-based stem volumes was 0.64 with an average rms retrieval error of 94 m^3/ha. Total forest dry biomass (tonnes/ha) was then

approximated by multiplying the stem volume (m^3/ha) by 0.6. The successful use of the C-band ERS-1 data in both studies was attributed to the typically sparse structure of boreal forests that allowed easy penetration of the radar signal through the canopy layer thereby causing the level of backscatter to depend on biomass.

Application of both ERS-1 and JERS-1 data was done by Harrell et al. (1995) to evaluate C- and L-band sensitivity to the biophysical properties of thirty-two boreal forest areas in Alaska. Both bands were responsive to forest biomass, density and height, and the interactions appeared greatest when surface moisture conditions were minimised as a factor. Biomass and backscatter correlation were strongest in the late winter and late summer imageries.

Dobson et al. (1995b, 1995c) devised a three-step process for the estimation of forest biomass from polarimetric SAR data. The process involved the use of SAR data for terrain classification, estimation of basal area, height and dry crown biomass, and the application of a biophysical model to combine the estimates with ancillary information on trunk taper factor and wood density for the determination of trunk biomass. The total biomass was then computed as the sum of the crown and trunk biomass. Using SIR-C images, the methodology was tested in a northern Michigan forest and high correlation was observed between the radar-derived estimates and in-situ data. The incorporation of X-SAR data caused an improvement in the accuracy of the estimates, particularly in the case of crown biomass. The temporal stability of the retrieval procedures was then examined using four SIR-C/X-SAR images of the same site (Dobson et al., 1996b). Date-to-date variations in the algorithm coefficients were found to be related to the surface dielectric properties with the strongest net effects observed from areas of low biomass levels.

SIR-C and X-SAR data over a boreal forest in Saskatchewan, Canada were analysed by Ranson et al. (1995c) for the purpose of generating forest cover type and aboveground woody dry biomass maps. The effect of seasonal changes on radar backscatter was also investigated using SIR-C images of two different dates (April and October 1994). X-band backscattering, which occurred at the upper part of the

canopy, was seen to be sensitive to leaf and branch shapes and orientations. This band was hence concluded to be useful for discrimination between tree types. Highest correlation between backscatter and biomass was obtained with the use of the April data and the L-HV and C-HV ratio. The greater amount of backscattering in the April data (compared to the October data) was attributed to the frozen trees and wetter background during this month. Cross-polarisation signatures had more sensitivity to the crown structure than like-polarised returns. Radar-based biomass estimates were found to be within ± 20 tonnes/ha, at a confidence interval of 95%, of the ground-based measurements.

Ranson et al. (1996) investigated approaches to improve estimates of forest biomass based on the use of forest classification maps of a test site in Canada derived from SIR-C/X-SAR data. A supervised Bayesian classifier was used in the classification procedure to map the area into several non-forest and forest classes (dry conifer, wet conifer, and deciduous). Dry biomass and radar backscatter regression equations for the forest types were developed and applied to the radar data. Each of the best fit equations generated was different from the others indicating the importance of considering forest type on the biomass estimation process. L-HV and C-HV were deemed as the best channels for estimating biomass of conifers while a combination of L-HH, L-HV and C-HV gave the best result for the limited deciduous data available.

The applicability of spaceborne P-band imaging radar to biomass estimation was tested by Rignot et al. (1995) over three boreal/temperate and one tropical rain forest sites. To minimise the effect of the Faraday rotation, a phenomenon that affects long wavelength imaging radars in spaceborne applications, circular polarisation was used. This type of polarisation, however, produced estimation errors that reached 100 % over flooded forests, wet or damaged trees and sparse open tall forests and was thus concluded to be of limited use for measuring biomass. The opposite was found in the case of linear polarisations, which yielded more reliable estimates. At the three temperate sites, combined biomass estimates from P-HH, HV and VV data were within 12 to 27 % of the values computed from allometric equations. Using HV data alone, the radar-based estimates were only 2 to

14 % less accurate. At the tropical site, combined horizontally and vertically polarised P-band data discriminated biomass classes in good agreement with forest inventory estimates. Overall, P-HV signals were found to be dominated by scattering from the larger and lower primary branches and are thus related to fresh branch biomass and the forest type. P-HH was dominated by trunk-ground scattering at high biomass levels and is correlated with fresh stem biomass. Branch scattering was the dominant mechanism at P-VV and the signals were found to be less sensitive to the ground layer conditions.

2.3.2 Forest backscatter modelling and simulation

Scattering models have been formulated during the past years from which specific backscattering characteristics were reasonably predicted (Sun and Simonett, 1991). Two categories may be used to classify these models (Karam et al., 1992c):

(1) *phenomenological models* - are based on the understanding of the relative importance of the different scattering mechanisms; these models are constructed by adding up the contributions of the different forest components considered to be significant.

(2) *physical models* - are based on the electromagnetic wave-forest canopy interaction; the canopy could be treated either as a discrete or as a continuous medium.

Majority of the models developed to date are discrete scattering models based on methods such as the Born approximation, distorted Born approximation, and the Radiative Transfer Theory, where the canopy is viewed as an ensemble of randomly distributed scatterers in one or many layers (Saatchi et al., 1994). Several scattering mechanisms that are usually taken into account were enumerated by Sun and Ranson (1995) as:

(1) *direct crown backscattering*

(2) *direct trunk backscattering*

(3) *direct soil surface backscattering*

(4) *trunk-ground scattering*

(5) *crown-ground scattering*

The suitability and applicability of the models are in general affected by a) the model derivation approaches used, b) the assumptions adopted, c) the forest parameters/components considered, and d) other factors relating to the forest area from which the models were derived.

The Michigan Microwave Canopy Scattering Model (MIMICS) was developed by the University of Michigan based on the Radiative Transfer Theory for predicting backscattering from forest canopies (Ulaby et al. 1990). The canopy is taken as two aboveground horizontal vegetation layers of crowns and trunks representing various classes of tree components modelled as dielectric cylinders or disks. Through this model, the backscattering coefficient for different combinations of polarisation, frequency and incidence angle can be determined. Imhoff (1995) applied this model to simulate forest stands with equivalent aboveground biomass but differing architecture/structure using tropical and subtropical forest biometric data. Backscatter variations of up to 18 dB were predicted for some bands and polarisation thereby indicating the considerable effect of tree structure on the SAR return. Some other works demonstrating the successful use of this model were those of Dobson et al. (1993, 1994), McDonald et al. (1989, 1991), and Seifert et al. (1996).

Ferrazzoli and Guerriero (1995) developed a model based on the Radiative Transfer Theory and the Matrix Doubling algorithm to study radar sensitivity to tree geometry and woody volume. Based on the model computations, P-HV and L-HV backscatter were found to be sensitive to woody volume although branch dimensions and orientation were noted to have a strong influence on the radar response.

There has been a number of other studies on the application of the Radiative Transfer Theory for the interpretation of polarimetric radar backscatter from pines and conifers (Mougin et al. (1989), Karam and Fung (1989a, 1989b, 1989c, 1989d),

Karam et al. (1991,1992a,1992b,1993,1995), Hsu et al. (1992, 1993), Lavalle et al. (1992), Amar et al. (1993), and Souyris et al. (1995)) and from deciduous/broad-leaved stands (Chauhan and Lang (1989), Karam and Fung (1989a, 1989b, 1989c, 1989d, 1990), Wang et al. (1990), Israelsson and Askne (1993), and Karam et al. (1988, 1995)). The canopy constituents such as the branches, leaves and trunks are treated as embedded in layers over a rough ground surface. The leaves are represented as needles, cones or discs and the trunks and branches as finite randomly oriented cylinders. In an innovative study, Karam and Fung (1986) modelled backscatter from defoliated vegetation by considering the latter mainly as a layer of dielectric, finite-length cylinders (without the leafy component) above an irregular ground surface.

Considering the typically thick vegetation covering undisturbed wetland environments and the consequent difficulty in the application of empirical surface models in these areas, Slatton et al. (1996) utilised a discrete scatterer model to account for the dominant scattering mechanisms and aid in the mapping of a herbaceous coastal wetland area in Texas based on AIRSAR data. The Canopy Structure Index (CSI), which is the ratio of the VV and the sum of VV and HH backscatter, and the Volume Scattering Index (VSI), which is a measure of depolarisation relative to the sum of the co-polarised and cross-polarised returns, were also examined to determine the relative influences of surface and vegetation multiple scattering at different locations within the site.

In a study of hemlock trees in Maine, Lang and Chauhan (1990) used the distorted Born approximation to calculate the backscattering coefficients as a function of incidence angle. The modelling suggested that ground conditions do not have an effect on medium to large incident angle C-band returns while in the P- and L-bands, the trunks and the ground produce a strong direct backscatter. The strong influence of surface scattering at P-band was a result of reduced canopy attenuation (Lang, Chauhan, and Ranson, 1991). Lang et al. (1992, 1994) used measurements from a red pine forest in the same area (Maine) to derive a distorted Born approximation model of the stand. Based on subsequent computations, it was revealed that the high P-band HH returns were due to direct-reflected contributions

from the ground. The same model was employed by Chauhan et al. (1991) to obtain the backscatter at P-, L- and C-SAR of a mixed coniferous forest near Howland, Maine. Comparison of results showed model values lower than the calibrated data. The results, however, agreed closely when the ratios of VV to HH and HV to HH were compared. Chauhan et al. (1994) used measurements from young and old aspen and jackpine stands of a Canadian boreal forest in a distorted Born approximation to compute the backscatter coefficients. At L-band, it was shown that large HH backscatter from the old jackpine is due to double-bounce scattering from the trunks while the VV return is directly from the canopy. Also, like and cross polarisation ratios from the same band tracked biomass for old and young jackpine stands. In accordance with this method, Dong et al. (1995) developed a wave approach for predicting forest volume attenuation and backscattering coefficients at L- and P-bands. The orientation of the scatterers was assumed to be uniform given that the foliage is not the dominant layer in modelling at longer wavelengths. The total leaf biomass, mean leaf volume, leaf shape and the dielectric constant have been demonstrated to be the key parameters for the model.

Chuah and Kung (1994) applied the Monte Carlo method to track the scattering and attenuation processes within a given layer of vegetation medium. It was indicated in the simulation results that attenuation coefficients calculated using this multiple scattering model may be different from those generated from single scattering models. A good match was obtained when the calculated results were compared with the measured data. The same method was used by Tsang et al. (1994) to study scattering from a large number of trees with clustering branches/leaves and from vertical dielectric cylinders randomly placed on a dielectric surface. Results from the application of the Monte Carlo technique to investigate electromagnetic scattering from a vegetative medium by Chuah (1994) revealed that at high frequency and large incident angle, volume-volume scattering is the dominant mechanism for backscatter. At low frequency and near-vertical incident angle, direct surface scattering was the main contributor to the main-polarised return while surface-volume interaction was the major mechanism for cross-polarised backscatter. Based on these findings, it was suggested that surface-volume interaction should not be neglected for the L- and C-band frequency range.

Sun et al. (1989, 1991) developed a radar backscatter model for discontinuous canopies of low to medium density forests under the L-band frequency. The backscatter from various forest components were individually calculated and their Stokes matrices added together to get the Stokes matrix of the total backscatter. Appropriate extinction for each of the components was computed by introducing probabilities of radar beam-tree crown intersection. A variant of this model was made by Sun and Simonett (1990) for the same forest conditions but with multi-parameter radar data. Sensitivity analyses and simulation results showed reasonable prediction of backscattering coefficients for multiple wavelengths, multiple polarisations, and multiple incidence angles by the model.

A model of L-band microwave backscatter for the observation of polarisation responses from forested sites was put forward by Durden et al. (1988, 1989). The forest was modelled as consisting of an upper layer of randomly oriented cylinders that represent branches, a lower layer of nearly vertical dielectric cylinders representing tree trunks below which is a rough dielectric surface representing the forest floor. Several scattering mechanisms were identified and the corresponding Stokes matrices were calculated to derive the total Stokes matrix and resulting polarisation signature. Accurate prediction of the polarisation of scattered waves has been observed from the application of the model and additional mechanisms such as the effect of leaves and twigs were considered unnecessary. Two polarisation signature predicting models were developed by Van Zyl and Zebker (1987). The first model predicts the full polarisation signatures of vegetation similar to tall grass, even in cases when the vegetation layers are relatively thin. The second model predicts the polarisation dependence from different tree types. It was concluded that different tree types could be distinguished from the polarisation signatures.

Modelling of L-band conifer backscatter in relation to variations in canopy volume as a function of crown width and canopy depth was conducted by Wang et al. (1992) as part of the sensitivity analyses of the Santa Barbara microwave backscatter model for forests with discontinuous canopies (a thorough description of the model is given by Wang et al., 1993c). Data from a ponderosa pine forest in

California were used though the crown width and depth were varied from ¼ to 4 times the measured values for the purpose. Results showed that at L-band and large incidence angles, modelled backscatter is sensitive to factor-of-two changes in canopy width and depth even in cases of relatively dry soil conditions and average tree water status. This was attributed to the strong effect of ground-trunk interactions at low canopy volumes, as opposed to canopy attenuation and canopy volume scattering at greater canopy widths and depths. In a later study, Wang and Imhoff (1993) applied the Santa Barbara model to predict L-HH radar backscatter from a mangrove forest in Bangladesh. It was shown in the results that the dominant return for non-flooded stands comes from the canopy volume and that double-bounce trunk-ground interaction is enhanced by the presence of water below the trees. For flooded mangroves, the trunk-ground interaction was dominant at small incidence angles though this dominance was reduced as the incidence angle increased. For the delineation of flooding boundaries within mangroves from SIR-B data, the use of small incidence angles was recommended. The same model was applied by Wang et al. (1994), but this time for the investigation of the continuous canopies of the Amazon forest at varying incidence angles. Modelled canopy volume scattering from flooded forest sites dominated the C-HH, C-VV, and L-VV backscatter at 20^0- 60^0 incidence angles. At L-HH and 20^0- 35^0, the modelled canopy-ground and canopy volume returns contributed roughly equally to the total backscatter although some contribution from the trunk-ground interaction was observed. At P-HH and P-VV, the canopy-ground and the trunk-ground were the dominant factors at small and large incidence angles, respectively. The inability of radar systems using C-HH, C-VV, and L-VV parameters to penetrate canopies was ascertained by the dominant canopy volume scattering at these configurations. However, at L-HH, P-HH, and P-VV, when trunk-ground and canopy-ground terms dominated or contributed significantly to the total backscatter, canopy penetration was concluded to have taken place. Wang et al. (1993a) compared P-, L- and C-band SAR data from three ponderosa pine stands in California with data derived from the application of the Santa Barbara backscatter model. Overall, the model made good predictions of the multi-parameter radar backscatter for all the stands. The observed and modelled VV-HH phase difference for two of the stands at P-band were at least -80^0, thus indicating the occurrence of double-bounce scattering.

Woodhouse and Hoekman (1996) used a tree growth model to obtain statistical data for a boreal forest located in Sweden. A radar backscatter model was then applied using the data generated from the use of the tree growth model to predict multi-polarised C-band backscatter from three stands within the area. Comparison of the modelled and simulated backscatter values revealed a difference of 2.5 dB between the like and cross-polarised signals with the observed values higher than the modelled ones.

A comparison of two different modelling techniques for the computation of radar backscatter from red pine and jack pine stands at L-band frequency was undertaken by Lang and Landry (1996). The first technique involved the reconstruction of all branch nodes and the coherent addition of backscatter from the individual branch links while the second technique was the standard statistical approach, where an independent treatment of the branches with prescribed orientation statistics was made. The backscatter values computed using the two techniques showed no difference when trunks were the dominant scatterers. However, a difference of as much as 6 dB was obtained when volume scattering was the dominant scattering mechanism.

In an effort to study the scattering mechanisms in a pine forest in Mt. Shasta, California, Wang and Davis (1996) applied a signal decomposition method based on the backscatter covariance matrix from the target vegetation. Two sets of AIRSAR data taken during a 1991 wet spring and a 1989 dry summer. The different scattering mechanisms identified were scattering with a) odd number of reflections, b) even number of reflections, and c) diffused scattering power.

A procedure for pixel composition determination in microwave remote sensing of forests with sparse canopy has been proposed by Kolawole (1991). He modelled the forest as a collection of spherical canopies containing identically sized and randomly distributed cylindrical elements. From the model, radar backscattering has been shown to be significantly dependent on four primary scattering units, namely, volume, surface, canopy to surface and trunk to surface. Miller et al. (1990) introduced a forest imaging model for SAR where the forest is

represented as an array of labelled cells, each label indicating the physical contents of the cell, which is then used to deduce its single bounce and double bounce scattering properties via appropriate scattering models.

Axelsson (1992) used a model originally developed to estimate polarisation characteristics of double-bounce reflections from semi-transparent disc elements above a rough surface. First, she determined the polarisation matrix of an arbitrarily oriented single disc and then applied a cloud model to estimate backscattering from the canopy. Both single and double bounce reflections from the leaves and the rough surface were considered.

Israelsson and Askne (1993) analysed the effect of leaning trunks on radar backscatter. It was observed that backscattering is not influenced by the leaning at C- and L-band but decreases at P-band particularly at HH polarisation. Apparently, this effect is due to the distortion of the trunk-ground dihedral reflection. In a related vein, Van Zyl (1992, 1993), using a discrete scatterer model, examined the effect of topography on radar scattering. He showed that the dominant scattering mechanism may change drastically when the surface is tilted relative to the horizontal and that topographical effect is more pronounced in the case of longer wavelengths. The effect of ground surface-related scattering on C-band backscatter was investigated by Wang et al. (1996) using data from five loblolly pine stands at the Duke forest in North Carolina. Modest sensitivity to surface-related scattering was detected from C-HH and C-VV returns from 8-year old stands at 20^0 and 30^0 incidence angles as well as from 25-year old stands at 20^o angle of incidence. The maxima of the ratios between the modelled total backscatter and modelled canopy scattering for all stands decrease with increase in the incidence angle. This effect was due to the greater canopy scattering contribution to the total backscatter brought about by the increase in incidence angle.

Richards et al. (1993) examined the nature of backscatter response from Australian native forests and noted the need for deriving models based on an understanding of the scattered electromagnetic fields within the forest, in contrast to the usual application of the Radiative Transfer Theory. It was argued that the

recommended approach has the advantage of producing information on phase difference, which has been shown in recent studies to be possibly an effective means of determining principal scattering elements within the forest. Although particular attention was focused on the parameters obtainable from ERS-1, data from JERS-1 and SIR-B were also used. Another study involving the modelling of Australian vegetation was made by Ahmed (1991), where a backscatter model for arbitrarily oriented pine and eucalyptus stands was developed from SIR-B data.

Wegmuller et al. (1994) applied a theoretical radar backscatter model to simulate ERS-1 SAR sensitivity to temperate forest components. The dominant sources of backscattering at C-band were the crown (especially the small and medium branches) and the ground surface. The needles and broad leaves did not contribute much but acted as absorbers thus limiting crown transmissibility. Needle and broad leaf loss or drying caused the backscatter to increase while freezing conditions caused its sharp decrease. These results were consistent with those obtained by Wang et al. (1993b) in their modelling of L-band radar backscatter for five Alaskan boreal stands under frozen and thawed conditions. It was concluded from the model results that the smaller dielectric constant of the frozen trees was the main cause for the weaker backscatter from these trees. Lopes et al. (1991) related the effect of coniferous tree architecture on radar backscattering. Through the use of a validated theoretical model to interpret data acquired over coniferous stands, tree architecture was shown to have a huge influence on the backscatter signatures. At X-band, however, for which the needles were the main scattering sources and the penetration depth was low, the branches that represent the actual tree architecture did not significantly contribute to the total backscatter.

The backscattering properties of boreal stands in Finland were investigated by Pulliainen et al. (1994) by the use of ERS-1 SAR data and a semi-empirical C- and X-band model. Weather and seasonal conditions were observed to have a huge effect on the radar response to forest volume. Backscatter and biomass correlations were either positive or negative or about zero depending on the same conditions. The highest positive correlation was obtained in case of very dry or wet snow-covered ground while the highest negative relationship was after heavy rain, when

the soil was still wet but the moisture content of the canopy was back to its normal value.

Baker et al. (1994) made use of calibrated, fully polarimetric SAR responses in three frequencies from a Corsican pine forest in the U.K. and related said returns to physical characteristics of the vegetation. The radar backscatter at P- and L-bands, especially the cross-polarised returns, correlated well with volume. Regression models were made and assessed as to their accuracy in predicting timber volume over large areas around the test site. Fuller use of the information from the measured data, such as that relating to HH and VV correlation and to theoretical models that more comprehensibly consider polarimetric backscatter mechanisms was suggested.

A method for estimating scattering by shape-of-revolution objects to model trunks and derive cylinder radius was developed by Robin and Guissard (1994). Trunk biomass-backscatter relationship was then established from the output of the process. Moghaddam (1995) devised an inversion algorithm that uses a parametric model to obtain canopy parameters, which could be utilised as inputs to ecosystem modelling. The algorithm was shown to be useful in monitoring moisture status of the canopy and has great potential as basis for the development of its future versions.

Some other studies involving the modelling and simulation of radar signatures for the prediction of forest characteristics were those of Altman and Schneider (1985), Sun et al. (1988), Mo and Wang (1988), Sun and Simonett (1988), Wang et al. (1989), Chauhan and Lang (1990), Nilson (1991), Kolawole (1992), Sun and Ranson (1993), Luckman and Baker (1993), Moghaddam et al. (1992, 1994), Ranson et al. (1995b, Lang et al. (1993, 1995), and Jin and Huang (1996).

2.3.3 Forest resource monitoring

The forest resource of the world is rapidly being depleted more so in tropical countries. Obviously, the failure to plan and implement effective strategies will lead

to its continued depletion. A careful monitoring of forest areas is needed in order to determine whether the currently applied management schemes are still justified in the light of recent conditions and developments. Spaceborne and airborne radar remote sensing systems are useful tools in this regard due to their synoptic view, cost effectiveness, all-weather and multi-temporal data acquisition capabilities.

The applicability of spaceborne imaging radar for monitoring forest conversion and depletion was investigated by Werle (1989a) through the use of SIR-A images of five tropical sites. It was concluded that L-HH radar data can be used to identify and possibly monitor a variety of conversion and depletion areas such as logging, new settlement, cattle grazing and grassland succession areas. Recent clearings with sizes of 10-15 hectares were easily identified from the 1:250,000 SIR-A images. Sites of commercial logging were pinpointed mainly because of their distinct shapes and cutover boundary size. The backscatter from artificial grazing areas and natural grassland successions provided very sharp tonal and textural contrast relative to the surrounding vegetation.

SEASAT and SIR-B images obtained in 1978 and 1984, respectively, were used by Hoffer and Lee (1989) to assess changes within a forest in Florida. The data sets were geometrically rectified, filtered and registered. Training statistics for "forest change" and "no change" classes were developed from forest inventory data and colour infrared aerial photographs of the area. Results from qualitative and quantitative change classification analysis revealed that reforestation and deforestation sites can be successfully defined and separated from "no change" areas.

Stone and Woodwell (1985) utilised 1981 SIR-A and 1984 SIR-B images to locate and define deforestation in Brazilian Amazonia. Two sites were examined for deforestation using SIR-A and the results were found to be within 10% of Brazilian estimates (maps made from the use of a video camera and a microcomputer). Forest clearings were also identified from the SIR-B images. The results from the two data sets were compared and some differences, such as the much narrower range of tonal contrasts and larger amount of speckle in the SIR-B images, were observed. Also,

the SIR-B imageries showed fewer cleared areas than those of the SIR-A though the latter was taken earlier.

Haas et al. (1996) tested the suitability of SIR-C/X-SAR data for forest monitoring using the Oberpfaffenhofen site in Germany as study area. All of the radar data sets were calibrated to allow a direct comparison of the backscatter values. Ground truth data were obtained from field observations and aerial photographs. Analysis results indicated that structural characteristics such as stand height and density are the more important parameters for radar image-based classification and that typical parameters like tree species or stand composition do not have much influence on the radar backscatter. The X-SAR images provided less information for the classification. Agricultural and wooded areas can not be differentiated using this particular radar band and even the use of multitemporal data sets could not improve the information content of the images. The information extraction process was however enhanced through the use of the multi-frequency and multi-polarisation SIR-C data.

The use of polarisation synthesis techniques for monitoring deforestation was investigated by Souyris et al. (1996) through the analysis of SIR-C/X-SAR images of the Landes forest in France. It was resolved that the best results for the segmentation of forest and non-forest areas could be provided by the degree of coherence at C-band between the HH and VV returns. L-HV turned out to be the most appropriate configuration for the estimation and mapping of forest biomass.

Another study involving the application of SIR-C/X-SAR data for forest resource-related monitoring was that of Bergen et al. (1996). Using multi-date images of the NASA Michigan Forests supersite, three main goals were set for the study, namely; 1) to estimate the amount of carbon stored in the site vegetation; 2) to account for the changes in carbon balance due to human disturbance such as clearcutting and thinning; and 3) to measure the amount of carbon gained from annual forest growth. Forest biomass was estimated using field data and allometric biomass equations. The amount of carbon held by the vegetation was computed based on the allometric rule that biomass is approximately 47 % carbon. A total of

12.82×10^9 kg of carbon has been computed as the amount in storage and an estimated 6.02×10^6 kg of carbon (equivalent to 300 ha of forest) were removed between the April and October 1994 data acquisition dates.

Guided by research experiences with multi-frequency polarimetric AIRSAR data, Keil et al. (1995) employed multi-frequency SIR-C/X-SAR for rainforest monitoring in different sites in Germany and Brazil. In the German sites, deciduous, coniferous, cultures and storm-damaged areas have been successfully separated. The combined use of the three frequencies allowed the differentiation of regrowth and deforested areas. For mountainous areas like those in the Brazilian sites, it was suggested that geocoding and terrain correction of SIR-C data are necessary for further differentiation, specifically in terms of age and crown density. A related forest monitoring study is being conducted in a so-called Oberpfaffenhofen super test site in Germany by Seifert et al. (1995).

Rignot et al. (1992) and Way et al. (1993) assessed the potential of the single-frequency, single-polarisation ERS-1 data in monitoring phenologic and environmental changes within Alaskan forests. Correlation of the significant differences observed from the radar backscatter with ground truth information indicated changes in the soil and vegetation liquid water content due to freeze/thaw events as the main influencing factors. The good potential of C-VV data acquired from AIRSAR to monitor drought and flood situations was confirmed in the study by Rignot et al. but the potential of ERS-1 for detecting phenologic changes and different tree species was concluded to be less promising in both of the studies. A demonstration of the capability of airborne SAR to detect flooding under the vegetation canopy was further demonstrated in a study conducted by Hess et al. (1994). Weydahl (1992) analysed multi-temporal ERS-1 images of a region in Norway for the identification of land cover classes and the assessment of the method's potential in monitoring seasonal changes. He concluded that an increase in the overall classification accuracy could be attained by combining several images taken at different dates over the same area though the result is also influenced by the image combination, number of images, and the speckle filter applied. The increase in accuracy as a consequence of using multi-temporal data was likewise

demonstrated by a study of ERS-1 images of a test site in the Ivory Coast by Conway et al. (1993).

A new method of discriminating forests from deforested areas using multi-temporal ERS-1 images of a tropical rain forest site in South Sumatra was examined by Le Toan et al. (1996). The temporal variation of the radar backscatter, as assessed by the ratio between two images, served as the basis for the method. Results showed that forest and non-forest sites could be accurately discriminated through the use of multi-date data with optimal acquisition periods. A forest/non-forest map, covering a ground area of 60,000 km^2, was produced based on five multi-temporal images of the site.

Ciolkosz et al. (1993) tested the potential of ERS-1 data for forest damage assessment. Multi-temporal ERS-1 images of forest areas in Mt. Sudety, Poland were acquired for the study. It was revealed that classes such as older stands, thickets, clearcuts, sparse vegetation, burned areas, as well as boundaries between forests and arable lands, can be distinguished from the images. However, species delineation and state of damage estimation were not possible. In conclusion, it was suggested that ERS-1 data have very limited application in detailed applications and that they can serve only as an auxiliary source of information in such kinds of endeavour. More encouraging results were obtained by Kuntz and Siegert (1994), who were able to identify several forest types from a single ERS-1 scene of a forest site in Indonesia. The authors concluded that ERS-1 data could serve as a valuable tool for monitoring forest conversion and land use planning in the frequently cloud-covered tropical forest regions.

The applicability of JERS-1 data to monitoring changes in vegetative conditions caused by seasonal changes, flooding and biomass burning was examined by Suga et al. (1996). Regarding biomass burning, the backscattering coefficients before and after a forest fire occurrence were compared and a difference of 3.2 dB was observed. It was deduced that a decrease in biomass due to forest fire can be detected from a decrease in the SAR backscatter. The investigations on the effects of

flooding and seasonal variations were conducted using agricultural crop vegetation and paddy fields as study sites.

Four forested sites in Germany were imaged by AIRSAR at C-, L- and P-bands and four polarisation combinations for the purpose of estimating forest damages (Lahti et al., 1993). Two radar scenes were used for the purpose, one having an incidence angle ranging from 35^0 to 55^0 and the other from 48^0 to 55^0. In both scenes, P-HH was found to be the best in separating forest damage classes though L-HV and C-HV have been found to be useful in the scene with smaller incidence angles. The classification accuracy was computed to be 60% when three health conditions were considered.

Sun and Ranson (1996) made use of a 3-D backscatter model and variogram analysis to study how forest patterns caused by logging are related to the spatial properties of radar images. The model construction entailed the preparation of a stem map for a 3-hectare 70-year old forest stand in Maine, which included information such as the Cartesian stem location, diameter at breast height (dbh), species, and the relative canopy position for each of the stems with a dbh over 3 centimetres. Strip cut patterns of varying azimuth angle orientation relative to the radar range direction were superimposed on the 3-D model and the L-band returns were simulated. The simulated results were in good agreement with AIRSAR data of a managed forest in the same area.

Temporal changes in a forest in Alaska were investigated by Way et al. (1991) by the use of AIRSAR data. Results indicated that phenologic and environmental changes within this type of forest can be monitored and that tree species can be mapped by taking seasonal differences in seasonal signatures into consideration. Dobson et al. (1991) undertook a similar study in Michigan using radar data from the same system and concluded that profound differences in backscatter between forest communities in a single-date or multi-date images are readily observable primarily due to foliation and precipitation factors.

Drieman et al. (1989) used multi-temporal airborne C-SAR images of a forest site in Ontario as a first effort in improving discouraging results from past research carried out in the same study area with single date C-SAR. The multi-temporal colour composites provided a clear distinction among the major forest types and allowed the detection of changes caused by timber harvesting and varying ground water levels. Differentiation of the forest types was not possible using a single image. The use of multi-temporal SAR data as a tool for forest management applications was suggested as having much better potential than the use of single date SAR image.

2.3.4 Forest structure characterisation, vegetation classification and mapping

The discrimination, characterisation and mapping of different forest cover types are essential components of forest resource inventory that, in turn, is a prerequisite for effective forest management. Whenever possible, the use of airborne or spaceborne remote sensing is always recommendable in this regard due to the high efficiency in terms of time and cost of the technology as compared to the conventional ground data collection methods. Notable progress has been made over the past decades on the use of optical sensors in forest inventory. The advent of airborne/spaceborne radar throws a new challenge for its optimum exploitation given its huge potential in enabling forest inventory regardless of solar irradiance, weather, day or night conditions.

Airborne radar systems

AIRSAR multi-band polarimetric images of different forest sites in Latin America were obtained by Van der Sanden and Hoekman (1995) to study the scattering behaviours of primary tropical forests and other vegetation classes (selectively logged forest, secondary forest, and non-forest areas). The tropical forest canopy backscatter was dominant in all frequencies and that trunk-ground interaction in the P-band was very minimal due to obstruction by high canopy biomass. A single C-band was of little value to classification while single L- and P-bands provided for the identification of non-forested areas. Logged, secondary and

primary forest discrimination necessitated the use of two- or three-band composites. Combinations with P-band included performed better than those with L-band. In a comparable research effort, Freeman et al. (1992) demonstrated that multi-parameter radar data can be an effective tool for tropical vegetative cover mapping. Forest class discrimination, and hence the estimation of the areal coverage of each class, was shown to be possible due to the differences in the radar signatures observable from different vegetation types. Backscatter from volume scattering appeared to increase with biomass until a plateau is reached and only the presence of additional scattering mechanisms can increase the backscatter beyond the plateau. Polarisation parameters were considered necessary to detect the presence of non-volume scattering.

Ranson and Sun (1993) used AIRSAR data of a forest in Maine to identify and classify areas with low biomass levels. The classes were classified based on varying tree heights and/or densities that reflect natural and man-made conditions. Non-forest classes were also considered. The following categories of low biomass units were used for the study:

(1) *Grassland* - grass-covered smooth surface, including sparsely planted seedlings 2-3 feet high;
(2) *Bog* - low shrub and moss-covered, with few small trees;
(3) *Regeneration area* - successional area after clear cutting, with dense, young deciduous trees;
(4) *Opening* - lower biomass 'gaps' surrounded by taller mature forests; usually occurring at poorly drained sites;
(5) *Thinned* - also 'gaps' in forests caused by tree felling and thinning instead of soil moisture conditions; trees have similar size as in surrounding area but much lower density (about 100 trees/hectare); and
(6) *Old Cut* - large trees with lower density than category 5 (~40 trees/ha); clear cut areas, where surface is rough, wet with few remaining big trees (usually conifers).

Based on the separabilities between the classes, optimal variables computed from the Stokes matrices of P-, L- and C-band were selected. Image classification was subsequently conducted and the patch number, area, and perimeter were calculated.

Five vegetation types in the Bonanza Creek Experimental Forest in Alaska, namely, 1) white spruce, 2) balsam poplar, 3) black spruce, 4) alder/willow shrubs, and 5) bog/fen/non-forest vegetation, were discriminated by Rignot et al. (1994a) using a *maximum-a-posteriori* Bayesian classifier on multi-temporal AIRSAR data. The results indicated that C-band is more useful than L- or P- for separating forest types and that HV is the best polarisation for forest type mapping at all frequencies. A classification accuracy of 90 % was obtained by combining L-HV and C-HV data acquired during spring. During the dry summer, when leaves are present on the deciduous trees, the classification accuracy for the same radar channel combination was reduced to 62 %. In general, the classification accuracy improved significantly with an increase in the number of looks of the SAR data.

Proisy et al. (1996) assessed the capability of radar systems to retrieve forest structural parameters through the statistical analysis of AIRSAR data acquired over mangrove forest sites at the French Guyana. Multi-polarised backscatter at P-, L- and C-bands were correlated with structural characteristics viz. tree diameter, tree height, stand density, and basal area as well as with aboveground biomass by parts (leaves, branches, and trunks). Overall, the cross-polarised (HV) backscatter at the three frequencies provided the best results, such as an average correlation coefficient (R^2) of 0.89 with tree density. P-VV proved to be the best tree height estimator, producing an R^2 of 0.65. Concerning correlation with total biomass, P-HV had the highest R^2 (0.78) followed by L-HV (0.73) and C-VV (0.68). In general, radar backscatter increased with biophysical quantities except at low biomass levels, where a decrease in P-VV was observed.

An assessment of the biophysical characteristics of two tropical forest sites in a mountainous region in Costa Rica using both raw and topographically corrected NASA-JPL SAR data was undertaken by Wu (1989). Each site contained 81 test

plots where stand data such as tree height, principal species, number of trees, bole height, and diameter-at-breast height were collected from the field. Topographic data were derived from the digital elevation data. Eighteen out of the 81 plots for each site were used in the analyses and results indicated that per plot bole and tree volumes are related to SAR data. No difference was observed between the findings from the topographically corrected and raw SAR data. Further study using all 81 plots had been recommended.

The applicability of NASA-JPL SAR images on the determination of biophysical characteristics over a range of different forest environments was evaluated by Ford and Wickland (1985). The test site, situated on the Atlantic coastal plain of South Carolina, contain varied vegetation associations from swamp and bottomland hardwoods to pine plantations and open fields to upland scrub oak. Swamp showed high DN values in all polarisations while tributary deltas impacted by thermal stress gave low cross-polarisation responses. Open pine stands had relatively high horizontal parallel-polarisation response while dense pine stands gave a dominant cross-polarisation backscatter. The polarisation signatures were related to biophysical properties by comparing the false-colour composite radar images with existing maps of forest stands in the timber compartments. The most useful correlative variables were stand basal area, forest age, site condition index, and forest management type. Another study of the applicability of NASA-JPL L-band multi-polarisation data to forest vegetation characterisation was undertaken by Evans et al. (1986) with Wyoming and South Carolina as test sites. In the Wyoming site, strong cross-polarisation responses denoted the effects of vegetation while local variations in like-polarisation images indicated topographic effects. Forest cover characteristics in the South Carolina site were discriminated by polarisation responses reflecting canopy density and structure as well as the presence or absence of standing water below the canopy. Analysis by Hoffer and Mueller (1985) of X- and L-band multi-polarisation data taken from the same area (South Carolina) resulted in the discrimination of various forest and other cover types. A related study was done by Shinohara et al. (1992) where, through the use of L-HH SAR data, substantial correlation between backscatter, stand density and total breast height area, among other parameters, had been demonstrated.

Lemoine et al. (1991) investigated the separability of forest stands in the Dutch Flevoland site of the MAESTRO-1 campaign using multi-parameter AIRSAR data. Their findings reinforced the conclusions made in other studies by other investigators that polarimetric data, especially the linear cross-polarisation channel (HV), are useful in the delineation of vegetative cover and forest species and that different scattering mechanisms play a role at the respective frequencies. Similar findings were obtained by Beaudoin et al. (1991) in their analysis of SAR polarimetric signatures of pine stands at the Landes area in France during the same MAESTRO-1 campaign. Results from a study of L-band responses conducted at the Flevoland test site by De Matthaeis et al. (1991) pointed to the importance of the trunk-to-soil double bounce in the determination of HH backscattering and of the branches in the determination of VV and HV returns. Israelsson and Askne (1991) and Israelsson and Sylvander (1992), under the same campaign and the same study area, found the P-band as the best wavelength for the discrimination of different forest types mainly due to its strong canopy penetration capability. The similarity in structure of the top layers of the trees in the study site made discrimination by the shorter wavelengths difficult.

Ranson and Sun (1994b) used multi-frequency temporal polarimetric SAR images of an experimental forest in Maine and were able to classify the area into general forest categories such as softwood, hardwood, regeneration, and clearing with more than 80% accuracy. A high accuracy was also obtained in the case of the non-forest categories such as wetland, bog, grassland, and water. Classifications using single-date images gave low accuracies.

Multi-frequency and quad-polarised NASA/JPL data acquired over the Thetford forest in UK were used for forest inventory assessment by Baker et al. (1991). The application of multi-frequency data was concluded to be essential for the effective discrimination between species. The C-band provided information on differences in twig and leaf structure at the outer canopy layers while the longer wavelengths, particularly in the cross-polarised P-band, gave information on the volumetric properties of the canopy. Also, in the case of P-HV/VH, a systematic increase of backscatter cross section with growth stage for a given species was

observed thus aiding in the estimation of biomass. Along the same line, Keil assessed the information content of a forest area in the Harz mountains of Germany and demonstrated the high potential of multi-parameter AIRSAR data for forest classification purposes.

Lopes et al. (1992) related polarisation phase difference and wave attenuation to the structural parameters of vegetation. Using polarimetric data taken from the Landes forest in France, they found that only the HH/VV complex degree of coherence coefficient was significant in the said forest site. Higher magnitude of D_{HHVV} (degree of coherence) was found on clear-cuts due to the dominant effect of single bounce scattering. In contrast, lower correlation values were observed from the forest areas due to multiple scattering. An inverse relationship was noticed between D_{hhvv} and biomass with a lower limit of 100 tonnes/ha.

Ahern and Drieman (1988) tested the accuracy of CCRS C-band SAR in discriminating clearcut areas in a Canadian boreal forest. The radar-derived estimates were compared with those plotted from panchromatic areal photographs and an average error of -11%, with a corresponding boundary placement error of 30 metres, was incurred. These errors were deemed too large for acceptable forest inventory update and several areas for improvement, such as use of multi-temporal and multi-look data sets, have been identified.

Kasischke et al. (1985) analysed X-, C- and L-band multi-polarimetric SAR images of the Duke forest, North Carolina. The 5,000-hectare forest is vegetated by pines (southern, loblolly and Virginia) and hardwoods (beech, poplar, red gum, river birch, sycamore, and oak). The stands range in size from 1 to >50 hectares, and in age from 1 to >100 years. Analysis results indicated that both tree species and general age classes can be distinguished. In an investigation of scattering coefficients from calibrated X- and L-band data of 23 test sites located in the same forest (Duke), Kasischke and Larson (1986) detected correlations between the L-band backscatter (σ^0) and the tree height for the pine stands, L-band σ^0 and stems per acre for the deciduous stands, and X-band σ^0 and basal area for the deciduous stands.

In an effort to determine which stand characteristics are measurable with airborne radar and to what degree of accuracy this can be done, two Finnish forest areas have been evaluated by Hyyppa et al. (1993) using a helicopter-borne scatterometer. The investigated stand parameters were: stem volume/ha, basal area/ha, mean height/ha, dominant height/ha, and average height of the crown base (pine stands). The accuracy of the methods was evaluated for individual sample plots, for forest stands, and for areas combining several stands by calculating the mean squared error of multiple regression models. For the plotwise comparisons, the average R^2 for the stand parameters was 0.84, 0.77 for the compartments, and 0.87 in the case of areas combining several stands. Some other studies involving the use of helicopter-borne scatterometers were those of Hallikainen et al. (1989), Heiska et al. (1992), and Hyyppa et al. (1992, 1994). All of these studies were done in Finnish forest sites and all gave favourable results pertaining to the applicability of airborne radar to forest characterisation in terms of tree height, species, and stand volume, among others.

Hussin and Hoffer (1990) experimented with L-band multi-polarised airborne imaging radar data for the differentiation of a swamp forest in Florida. It was found out that, depending upon the polarisation, at least two swamp vegetation types can be discriminated from each other and from pine stands of varying age and density classes. Like-polarised data was better for forest discrimination than cross-polarised ones and distinctly different radar responses were obtained from forested wetlands at different incidence angles. Wu (1993) extended the scope further by focusing on coastal zone forests. His conclusions were that AIRSAR data are useful in delineating wetlands; C-band can discriminate marsh grasses and shrubs with heights of less than three metres; and that the dynamic range of SAR data can be used to characterise the very high backscatter of the forested wetlands with standing water to the low return of the submerged sediment.

Rignot et al. (1993) explored the applicability of multi-frequency, multi-polarisation, and multi-temporal airborne SAR images on the mapping of taiga forest stands in Alaska and obtained very interesting results. Tree classification accuracy was highest (86%) with the use of fully polarimetric L- and C-band

combined on a date where the forest just recovered from flooding. The most useful frequency and polarisation for tree type mapping were C-band and HV. Combination of multi-date SAR images did not improve the accuracy. Data acquired on different dates and under different environmental conditions produced classification accuracies 16% to 41% lower. Single-frequency and single-polarisation data showed limited mapping capability.

Spaceborne radar systems

Paudyal et al. (1995a) used two ERS-1 images taken at different dates for the identification of mangroves and inland forests in a coastal region of southern Thailand. Mangroves showed within class variation of the order of 2 dB as a function of height and density though their similarity with agricultural areas caused difficulty in the input of this information to an automatic classification system. Majority of the inland forests are located in rugged terrain and were affected by pronounced foreshortening. Forests located in the backslopes of mountains exhibited lower response and were confused with wind-roughened sea surface. In a separate study conducted in two forested sites in West Thailand and involving five-dated ERS-1 data, Paudyal et al. (1995b) detected similar radar responses from evergreen, mixed and bamboo classes but a lower backscatter from the scrub vegetation type. Clearcut areas were also easily discriminated from the images. Use of multi-temporal ERS-1 data (at least three different dates) was recommended for better separation between different classes.

An evaluation on the suitability of ERS-1 SAR images for large-scale inventory of forest resources was made by Tomppo et al. (1994). Out of the 19 summer and autumn SAR images of a test site in South Finland, seven were geometrically rectified, filtered and classified using a k-nearest neighbour algorithm. The performance of the classification was judged by comparing the obtained estimates with existing government data based on ground measurements and aerial photographs. Twice mode-filtered ERS-1 images gave the best results in the standwise comparison while raw multi-temporal ERS-1 images gave the smallest bias and root mean square error.

Freeman et al. (1994) made use of JERS-1 radar images to classify different forest types in the Amazon. The image local mean and standard deviation of texture have been used as inputs to a standard maximum-likelihood classifier. Edge detection and edge-following algorithms were applied to detect rivers and other related features. High classification accuracies were obtained for Palm (91.2%), low texture forests (90%), high texture forests (88%) and medium texture forests (66-88%) but poor accuracy was obtained for low vegetation (48%) due to the confusion of this class with clear cut areas.

A combination of the C-Band ERS-1 and the L-band JERS-1 was utilised by Sugimura et al. (1993) to investigate the capability of this combination in discriminating forest vegetation in Mt. Fuji, Japan. Each of the radar images was projected orthogonally using a digital terrain model. The two data sets were used as input in the analysis of principal components and production of colour composites. It was shown that broad-leaved trees, needle-leaved trees and grasslands could be identified by the method.

SIR-B L-band HH-polarisation data obtained at 41^0 incidence angle was analysed by Anthony (1986) for forest type discrimination. Density slicing and visual interpretation of a single radar image showed no further differentiation than forest/non-forest. When ground inventory data was introduced, five different forest cover types were identified although difficulties were encountered in case of similar stand structure.

Multiple incidence angle SIR-B experiments over forest areas have been conducted by several researchers. Cimino et al. (1986) discriminated various forest types in the Chubut province of Argentina by their relative brightness against incidence angle signatures. The factors observed to have the most influence on radar backscatter were canopy structure, density, and ground cover (particularly the presence of dead branches and trunks). It was resolved that different forest species and the structure of a single species could be discriminated by multiple incidence angle radar data and that the consideration of backscatter variations due to the

incidence angle is important when analysing data collected at different frequencies and polarisations.

SIR-B images obtained at two different incidence angles were analysed by Ford and Casey (1988) for vegetation delineation in the rain forest of Borneo. Three units of forest canopy and two units of open surface cover were discriminated in a coastal lowland within the area. However, in the interior upland, three major species associations with contrasting canopy structures were not discernible in the images. It was deduced that discrimination of different forest canopies in the interior of Borneo necessitates a wider radar response capability possibly obtainable at shorter wavelengths and multi-polarisation states. Imhoff et al. (1986) employed three SIR-B data sets with 26^0, 46^0, 58^0 incidence angles to investigate the effects of these angles on information content and vegetation penetration in the mangrove forests of Southern Bangladesh. Results indicated that significant vegetation penetration is achievable at all angles and that the tree/canopy structural morphology may influence this phenomenon. In a study of a forest site in northern Florida using SIR-B data, Hoffer et al. (1985) were able to identify six different forest cover classes and at least four other land uses as a function of incidence angle. Ahmed and Richards (1989), in an investigation conducted in a pine plantation in Australia, noted that a peaking of forest backscatter occurs at around 35^0 due to double-bounce reflection involving the trunk and the ground. A procedure for providing relative calibration to SIR-B multiple incidence angle backscatter prior to associating them with forest biophysical characteristics has been actualised by Richards and Ahmed (1988).

Ranson et al. (1995a) evaluated the usefulness SIR-C/X-SAR images for forest ecological studies in Maine. A decision tree classifier with 13 channels and trained for nine classes was applied. Non-forested areas were accurately discriminated, ranging from 100% for open water to 79% for wetlands. For the four forest classes, the results were 70% for softwood stands, 57% for hardwood, and below 50% for mixed wood and regeneration areas. Another evaluation of SIR-C/X-SAR for land cover classification was conducted by Stolz and Mauser (1995) in the Bavarian alpine forest area in Germany. The study, however, included an

assessment of agricultural crop-vegetated areas and that forested areas were all put under one class. Nevertheless, of the land cover classes considered, only the class "forest" reached an excellent classification accuracy (92%).

A tropical rain forest area in Brazil was classified and mapped by Freeman (1995) based on SIR-C data. The classes identified were forest, low vegetation, flooded vegetation, water, and unclassified sites. Comparison with ground truth data for accuracy assessment has yet to be done although first indications have shown that the classifications were reasonably accurate.

2.3.5 Synergism of radar and optical data

The synergism of optical and radar data, when both are available, will provide a better assessment of forest resources than the use of a single data source (Aschbacher et al., 1995). This could be ascribed to the differences between microwave and optical sensing, in so far as interactions with the vegetation are concerned, thereby causing the extraction of complementary information. Optical sensors depend on the effects caused by the chlorophyll, leaf structure, the green leaf area and the leaf area content while microwave sensors respond to larger-scale structures of the canopy, plant water content, plant size distributions, and surface soil conditions (Wu, 1985). For example, radar images have potentially richer information about the biomass and structure of forest stands because microwaves, especially at long wavelengths such as P- or L-Band, can easily penetrate forest foliage so that contributors to the total backscatter will include foliage, twigs, branches, trunks, understory and ground surfaces.

For forest vegetation typing

Chen et al. (1988) were among the first to investigate the potential use of co-registered TM and L-band Synthetic Aperture Radar (SAR) images with multiple incidence angles for classifying various forest stands of different densities and structures. A variety of forest stands ranging from clear cut to over-mature stands of ponderosa pine were present along with ponderosa pine plantations of various ages

in the study area in Shasta, California. The SIR-B images with incidence angles 29.7° and 63.8°, smoothed by median filtering, were used as the base images and TM images were registered to the SIR-B images. Relations between radar backscattering and forest structure were then identified and results were compared from radar and TM images by clustering the SIR-B images, TM images and the co-registered SIR-B, TM images. Using a clustering algorithm, the co-registered TM and SIR-B images were classified into 27 clusters. The 27 original clusters were then combined and grouped into five classes. By comparing the five classes to field observation and aircraft infrared colour photos, the type of forest stands the five classes represented were then determined. Results showed that multi-incidence SAR data was useful in delineating a variety of features of forest structure and made possible the derivation of parameters that are well correlated with some important forest characteristics such as height and density, especially for L band radar images at small incidence angles. Furthermore, radar images significantly increased the separation between forest stands with different spatial structures over that obtained from TM images alone. Their work showed that combining radar images with TM images will provide important information for monitoring forest ecosystems and forest inventory.

Pedersen et al. (1991) presented vegetation classification results using C-band polarimetric SAR data combined with Landsat TM data acquired over agricultural areas in selected parts of Europe during the Maestro campaign in 1989. The NASA/JPL DC-8 polarimetric SAR, which operates simultaneously at three frequencies, P-, C-, and L-band, was used in the campaign. Improved classification capability was demonstrated when the C-band HH, VV and HV synthesised images were used together with the TM data. Comparison of SAR co- and cross-polarisation signatures for the main crop types within the test area did not give evidence of unique, separable crop responses.

Nezry et al (1992) used SIR-B and SPOT data acquired over central Sumatra in a supervised classification of vegetation. Assessment of SAR data potentialities was carried out by using SIR-B image alone, and combined SIR-B and SPOT data. Combined filtered SIR-B imagery and SPOT data used jointly in a supervised

classification led to better discrimination of surface units. The results indicated the unique capabilities of combined visible and SAR data for classifying tropical vegetation, especially for forest/non-forest discrimination.

Another study that involved the combination of SAR and optical data was conducted by Pedersen et al. (1993). In here, ERS-1 data were used together with SPOT data for the purpose of mapping a forest area in a Norwegian region. The study showed that younger cutting classes could be separated from the older ones by the use of Landsat bands 3, 4, 5 and SPOT bands 2 and 3 but none of the said classes could be separated through SPOT band 1. There were indications that the oldest class could be separated by the use of SAR data though results were inconclusive due to the limited availability of statistics for this data type. A significant correlation between satellite signal and forest age was observed for TM bands 4 and 5 and SPOT band 3 under the 25-35 years age range.

Similarly, Rignot et al. (1993) combined optical and SAR data for mapping boreal forest areas in Fairbanks, Alaska and concluded that this method is useful for identifying tree species. Biomass estimates from SAR at L-band HV polarisation, NDVI from SPOT red and infrared radiances, and supervised segmentation map of the SAR data facilitated the process of species discrimination.

In the work of Leysen et al. (1994), ERS-1 SAR data over a test site in West Africa were evaluated on their information content for mapping tropical forest ecosystems. Using a multi-temporal ERS-1 SAR data set covering full seasonal cycle and a mono-temporal SPOT panchromatic image, supervised classifications were carried out at reduced pixel spacing (i.e., 100m). Comparable accuracy levels were found when the two classification results were compared on the basis of accuracy tests for forest/non-forest discrimination.

Aschbacher et al. (1994a, 1994b) applied multi-sensor and multi-temporal satellite data to map different classes of mangroves in Phangnga Bay, Southern Thailand. Both visible and infrared (VIR) and synthetic aperture radar data were utilised. SPOT XS, Landsat TM and MOS were selected for the VIR data while

ERS-1 and JERS-1 were chosen for the SAR data. Both visual and digital image analyses were employed although greater emphasis was given to the latter. The computer softwares used for the investigation included ERDAS (Earth Resources Data Analysis System), Easi-pace (for textural analysis) and ARC-INFO (for database digitising). It was found that cloud-free SPOT data is suitable for the discrimination of mangrove and non-mangrove areas. At least four different classes were identified using this data type. Mangrove delineation was also successfully done using combined ERS-1 and TM data. Using TM data only, the presence of clouds and cloud shadows proved to be a severe hindrance to accurate classification. The classification accuracies obtained were 84.80% for SPOT, 87.25% for the combined SPOT and ERS-1, 52.06% for combined ERS-1 and JERS-1, 47.00% for ERS-1 (multi-temporal), and 68.60% for TM. It was concluded that the synergism of VIR and SAR data gives more accurate classification than the use of a single data source. In the case of the radar data, improvement in accuracy was obtained when ERS-1 and JERS-1 data were combined instead of either of them taken separately. VIR data, in combination with ERS-1 data, provided additional information such as the approximate age of the mangrove stands. Logged-over areas, abandoned paddy fields, soil saturated with water and barren lands were also discriminated in the combined imagery.

Shimabukuro et al. (1995) carried out a comparison between the results of vegetation land cover classification using multi-temporal Landsat Thematic mapper (TM) alone, and then in conjunction with a Canadian airborne C-band synthetic aperture radar image gathered as part of the South American Radar Experiment (SAREX '92). The study showed that the addition of radar backscatter and texture information (HH and VV polarisations) to optical data sets significantly increased the separability of classes. For example, VV backscatter was much higher in areas of permanent agriculture versus those of smaller rotational fields. However, the complexity of the radar backscatter information requires sophisticated analytical capabilities that are still in development. The authors believe that synergistic use of active and passive sensors holds a broad promise on solving some of the analytical needs for the global carbon change modelling communities that cannot be solved

with optical data without intensive field validation and/or extensive multi-temporal data sets.

Also during the SAREX '92 experiment, an initial mapping of the mangrove forests of French Guyana using SPOT and ERS-1 data was conducted by Sery et al. (1995), the completion of which involved additional sensors. SPOT, ERS-1, JERS-1, SAREX and AIRSAR polarimetric data were used. To deal with this diversity, a multi-source hierarchical classification method was used. Results showed that AIRSAR polarimetric data, if obtainable regularly from space, would easily replace optical data in the tropical or equatorial region. SAREX is of interest due to its fine ground resolution. A temporal series mixing ERS-1 and JERS-1 seemed to the authors to be the solution for a not too fine classification in the region mentioned. Moreover, the contribution of ERS-1 and JERS-1 data to SPOT images classification proved obvious. Best results were obtained when optical and SAR data were combined.

For forest resource assessment and monitoring

Lee and Hoffer (1990) studied data sets obtained over a forested area in northern Florida by SIR-B and Landsat TM during the period of October 9-12, 1984. The three different incidence angles of SIR-B data and seven bands of TM data were geometrically corrected and digitally registered. The SIR-B and TM data were then transformed through two statistical approaches (principal components and canonical correlation analysis) to integrate the inherent variability within the data. Relationships between forest biomass and the sensor responses were made separately for the SIR-B, TM, and the two transformed data sets. The results showed that the data transformed through the canonical analysis had the highest correlations with forest biomass as compared to either SIR-B or TM data alone. A later study by Lozano-Garcia and Hoffer (1992) used the same SIR-B data combined with Landsat-5 TM data to create a digitally-registered 10-channel optical/microwave data set. Analyses were carried out on the data obtained by the two sensors separately and in combination. The radar data were filtered with a low-pass filter to eliminate the speckle noise. Classifications of the TM, SIR-B and

combined TM and SIR-B data sets were performed with both per-point and contextual classifiers. The results showed that filtered radar data sets can be used to classify accurately major cover types (i.e., pine forest, swamplands and radar smooth targets) and that the contextual classifier provided better classification performance. The combined TM and SIR-B data provided statistically improved classification performances compared to classifications from the SIR-B data of three incidence angles, or the TM data alone. A four-band subset (TM-2, TM-4, TM-5, and SIR-B 28) of the 10 channels of the combined TM and SIR-B data set provided higher classification performance (91% overall performance) than the 10 channel data set (86% overall performance).

Stone et al. (1989) examined forests in the Brazilian Amazon Basin state of Para with Landsat and SIR-A data. The area of primary forest there can be defined with either the combined SIR-A/Landsat data or with the Landsat or SIR-A data alone. It appeared that SIR-A data helped distinguish a greater number of classes within the primary forest. Landsat was sufficient to classify secondary forests with NDVIs (0.60 to 0.69) characteristic of rapidly growing vegetation. L-band radar data proved most helpful in determining primary forest composition but were insufficient in areal coverage to help with the determination of the areas or rates of deforestation.

Wu (1987) used airborne SAR data sets acquired over a tropical forest in Costa Rica to study elevation gradients that affect tropical forest stand characteristics. Digital elevation data were produced after digitising the contour lines on a topographic map of the study area. A rubber sheeting computer program was used to georeference the SAR data sets to the digital elevation data. The TOPO computer program developed at the Earth Resources Laboratory (ERL) at NASA's National Space Technology Laboratories (NSTL) was used to generate the terrain slope and aspect angle data from the terrain elevation data set. A computer program also developed at ERL was then used to compute the local incidence angle of the target/scene as seen by the SAR system, using the slope and aspect data and radar look angles. The computed local incidence angles were used to delete those data areas that were shadowed (incidence angle greater than 90 degrees) and to produce

the local incidence angle data that were not shadowed. The results of the data analysis indicated that SAR data are related to elevation gradient. It is known that tree species, stem frequency, and tree height are related to temperature and precipitation, both of which are influenced by elevation. The results of this study imply that SAR data are related to forest structure as it changes over that elevation gradient.

Lavalle et al. (1993) selected the Black Forest area in South Germany for an experiment on multi-sensor data source for forest monitoring. Numerous sensors, operating from the visible to the microwave regions, were used (AVIRIS, TMS, GER II, AIRSAR). Classical indices derived from optical (NDVI, MSI, GEMI, Red Edge) and radar (backscattered power, polarisation indices) data acquired from the test site were computed. The radiometrically calibrated optical data were first corrected for atmospheric effects using an empirical method for the GER II data and the Atmospheric Removal Procedure for the AVIRIS data. The radar images were calibrated and georeferenced. The various indices were then produced. Previous literature stated that these indices were sensitive to a variety of canopy characteristics such as biomass (leafy and wood), water content and tree growth stage (structure, damage). The retrieved indices were correlated with the available ground information on these variables and their performance was assessed for this particular test site. Results showed a lack of correlation between measured forest parameters and optical indices that was predictably due to the different ground truth characterisation needed for the validation optical data with respect to microwave data. The ground measured quantities (biomass, tree height and perimeter) are linked to the woody structure of the forest, which cannot yet be deduced by optical sensors while its influence on radar measurements seems to be fairly established. The authors concluded that in spite of this, both data types showed similar spatial patterns over images of large forest areas and the use of combined wavelength looked very promising.

Keil et al. (1994) investigated ERS-1 SAR data in combination with Landsat TM data for monitoring tropical rainforest cover and land use change detection in a test site in Acre, Brazil. (Also part of the TREES program). The first or preliminary

results of the study showed that ERS-1 SAR data have a high information content for the discrimination between forest and nonforest areas more so when data acquisition is carried out during the late dry season where there is expected an improvement of the contrast between forest and nonforest areas. Results indicated that differentiation within the rain forest is difficult, especially because of the strong influence of relief. This relief influence can be taken into account by visual interpretation for forest/non-forest separation.

2.3.6 Radar image analysis techniques

Although the analysis methods used for optical images have had some success in radar image analysis, modifications to these methods or the development of new techniques had been found to be necessary and/or more advantageous by a number of researchers owing to the novelty and inherent differences of radar with optical data. The long experience with optical data proved to be very useful as it became the base upon which these new techniques were formulated.

An important concern in radar data analysis is the presence of speckle noises, which degrade the image appearance by making it grainy. Conventional image processing/enhancement techniques used for optical images do not work well with radar images due to the multiplicative nature of the speckles. Ironically, it is often necessary to remove the speckles before the radar image could be effectively used for various applications such as in forestry. Attempts have been made to remove or reduce speckles in the radar image. Lee (1986) classified speckle-suppression techniques into two categories. In the first category are those that improve the SAR image appearance by averaging several frames obtained from a portion of the available azimuth spectral band to reduce the noise variance (i.e., multi-look processing). Techniques in the second category are those which are applied after the images have been formed. The development focus of most past and current speckle suppression techniques is the second category. These techniques (i.e., median filtering, gradient inverse weighted filtering, and local statistics method) are primarily based on the statistical properties of the speckle and are adaptive in the sense that the smoothing function of each pixel depends on the local photometric

statistics (Wu and Maitre, 1990). Some examples of studies conducted in this respect are those of Frost et al. (1982), Lee (1986), Li (1988), Lin and Allebach (1990), Nezry et al. (1990), Wu and Maitre (1990), Lopes et al. (1990a, 1990b, 1990c, 1993), Paudyal and Aschbacher (1993), and Shi and Fung (1994).

Touzi et al. (1988) developed a constant false alarm rate (CFAR) edge detector suitable for radar images based on the ratio between pixel values. The edge detector, for a better and finer detection, operates at all four directions over windows of increasing size. The performance of the operator (probabilities of detection and false alarm) was theoretically assessed using the statistical properties of the speckle. The experimental performance was found to be in good agreement with the theoretical study. It was hinted that a new speckle filter based on this ratio edge detector may give good results for radar images. Quegan et al. (1993) assessed the structural content of ERS-1 images and developed an image segmentation algorithm based on clearly defined edge detection measures and edge credibility probabilities. The properties and usefulness to various application areas of the segmentation tools are currently being studied.

A method to optimise the degree of polarisation of a partially polarised wave from a non-stationary object was devised by Touzi et al. (1992). Analytic computation of the minimum and maximum values of the degree of polarisation and the corresponding transmitted polarisations is possible through the method. A procedure for the optimisation of the scattered wave intensity was also included. In an analysis with JPL data, parameters used for target discrimination such as received intensity extrema, coefficient of variation, fractional polarisation and the span, were deduced from the extreme values of the degree of polarisation and the scattered wave intensity.

An algorithm for the unsupervised classification of scattering behaviour using radar polarimeter data was created by Van Zyl (1989). The algorithm works by comparing polarisation properties of each pixel to simple classes of scattering such as even number of reflections, odd number of reflections, and diffuse scattering. The scattering from clear-cut areas and agricultural fields were found to

be similar to that predicted by the odd number of reflection class while tree-vegetated areas were classified as a mixture of pixels exhibiting characteristics of all three classes, although each pixel was identified with only a single class. These led to the conclusion that numerous scattering mechanisms are present in thickly vegetated areas. With increases in incidence angle, more pixels were classified as diffuse scatterers. The response from an area with dead trees on water-saturated ground was different from that coming from a normal tree-covered area. In areas with lakes surrounded by forests, a strong even number of reflections was observed on the far-range shores.

Several techniques of analysing polarimetric radar data for vegetation discrimination were developed by Evans et al. (1988). The techniques involve the determination of the heterogeneity of scatterers within subregions, the optimisation of the return power from these areas, and the identification of probable scattering mechanisms for each pixel in the radar image. Applying the techniques using NASA/JPL airborne SAR images of a forested area in Maine, it was observed that the contrast between vegetated and clear-cut areas changes dramatically with polarisation and that clear-cut areas previously not discernible on HH and VV images were significantly enhanced. Further, it was noticed that the techniques were very useful in the interpretation of scattering from forested areas since clear-cut and tree-covered sites were classified as having different scattering mechanisms.

Wu (1985) generated three channels of ratioed multi-polarisation NASA/JPL L-band SAR data (VV/HH, VH/HH, and VH/VV) for the delineation of surface features of a test site in Mississippi. VH and HV were assumed to be identical so only the VH polarisation was used. A linear stretching of the ratioed data was done for the derivation of a digital number within the 0-255 range. Results indicated that a better delineation of surface features (e.g., hardwood, young pine, pine, clear cut, flooded marsh swamp) can be achieved by the use of ratioed data. A complementarity between the ratioed data and the original polarisation data had been observed and that the former provided information unavailable from the original three-polarisation data. The polarisation ratio of L-HV to L-VV has been found by Rao and Rao (1996) to be very useful in the discrimination of vegetation in a test

site in Gujarat, India. As discussed in the previous sections of this chapter, the ratioing technique has also been used by a number of investigators (Ranson and Sun (1992,1994a), Ranson et al. (1995c), Slatton et al. (1996), Chauhan et al. (1991, 1994), and Le Toan et al. (1996)) for different forest-related applications.

Ulaby et al. developed a Level-1 automatic classifier and evaluated its accuracy using multi-polarimetric L- and C-band AIRSAR data taken from a 7.5 km x 12.4 km area in Michigan. Four classes; namely, urban, tall vegetation, short vegetation and bare surfaces, were used for the purpose and the classification accuracy attained for each of the classes was at least 95%.

De Grandi et al. (1992) investigated two supervised fully polarimetric classification methods using AIRSAR multi-frequency and multi-polarisation data. The first method was based on the maximum likelihood approach and the other, on a maximum contrast approach. Comparison results indicated a slightly better performance for the first method. It also had clear advantages over a two-channel or a single-channel classifier. In an extension of this investigation, De Grandi et al. (1994) used the same radar data, study area, and classification techniques but focused on the influence of topography on the classification results. Results revealed that the terrain slope angle influences the classification accuracy. The inclusion of prior knowledge of the response of a certain class to slope change was suggested to be a possible strategy to improve the accuracy. The overall classification accuracies for the study are of the order of 70% but higher at P-band.

Pope et al. (1994) analysed fully polarimetric AIRSAR data of forest and wetland ecosystems in Central America based upon four biophysical indices: the volume scattering index (VSI), canopy structure index (CSI), biomass index (BI), and the interaction type index (ITI). ITI was found to be the most important index for level, vegetated terrain; BMI was most useful for differentiating between vegetated and non-vegetated areas and between sloping and level terrain. The relative importance of the indices varied with vegetation type (i.e., PVSI for distinguishing between upland forests and regrowth and PCSI for differentiating swamp forest types). The potentialities of spaceborne SARs for tropical ecosystem

studies were evaluated based on the results of the study but unpromising results were obtained as most of these SARs, at the time of the study, were single channel systems. More significant results were believed to be possible from multi-frequency, fully polarimetric spaceborne SAR systems such as the SIR-C/X-SAR and the forthcoming EOS.

The usefulness of SIR-C data for land cover classification purposes in areas having moderate terrain variations was investigated by Holecz et al. (1996). Firstly, the SIR-C data acquired from a hilly to mountainous area in Switzerland were calibrated, radiometrically and geometrically, with the aid of a Digital Elevation Model (DEM). A supervised and an unsupervised classification method based on a scale-space clustering algorithm and a quadratic classifier, respectively, were then performed on the calibrated data. A comparison between the classification results and digital ground truth data showed that it is possible to achieve an accurate land cover classification even in areas of rugged terrain provided that the SAR data are correctly calibrated and that prior information is available.

A backscatter and textural segmentation method for vegetation and forest delineation was developed by Beaudoin et al. (1990). The method was tested with the use of a 7-look C-VV SAR image of the Thetford forest in UK. Three general land uses (forest, crops, built-up areas) have been texturally discriminated and four forest types (Corsican pine, Scots pine, broad-leaved trees, and young pine plantations) have been radiometrically delineated. A good agreement was obtained between the final segmentation image and land-use map, with the precision computed to be 80%.

A systematic approach based on the observation of the transmit and receive channel combinations, which give rise to backscatter statistics has been applied by Lavalle and Sieber (1993) in the analysis of multi-frequency polarimetric data from the Black Forest site in Germany. The method involves the computation of parameters such as minimum and maximum values of power and contrast by a variable-size moving window. Maps of the transmit/receive configurations that give rise to the extreme values are then produced. It was revealed that at longer

wavelengths, the spatial orientation of the main branches in the forest is related to the maximum return power. Also, the approach increased the contrast of the forest return and thus has great potential in various applications such as boundary mapping.

In recognition of the inadequacy of the conventional approach of image classification, which is the assignment of each pixel to a specific class when the area covered by the pixel may involve more than one class, Du et al. (1993) devised a fuzzy approach for earth terrain cover classification. The methodology utilises a fuzzy c-means clustering algorithm. The algorithm computes the feature covariance matrix for each class and generates a fuzzy partition of the whole image. A defuzzification is then applied to complete the process of image classification. In order to substantiate the fuzzy classification algorithm, multi-look polarimetric AIRSAR data of a part of San Francisco was used. The results were believed to be encouraging and that many other applications in image analysis are deemed to be pursuable with the approach.

Xinghe and Ping (1993) proposed the use of texture for the analysis of remotely-sensed imagery. They suggested that texture, being a measure of the image gradient of grey, will enable the quantitative extraction of two parameters: texture intensity and texture density. The texture intensity is known to be useful in the differentiation of one pixel with its neighbours while the texture density is for the definition of the frequency of changes of grey levels. Under the first, the moving window size is decided based on the type of texture to be enhanced. In the latter approach, the threshold decides the types of textures to be considered for statistics generation. A relative gradient approach, which describes the textural characteristics of the image from the relative grey level changes, was also proposed. It was implied that by the use of this method, textures of bright and dark areas in an image, including those with tiny and blurring textural structures, can be enhanced.

Identification of forest cover types in a site in Guyana based on textural features computed from grey level co-occurrence matrices and grey level difference vectors of X- and C-band airborne SAR data was done by Van der Sanden and

Hoekman (1992). They concluded that the use of radar backscatter offers fewer possibilities. X-band data was observed to be more suited to textural analysis than the C-band data and that VH offers more possibilities than HH or VV. In a related study over a Brazilian forest, Filho et al. (1992) concluded that textural information in C-band SAR data is more useful for land cover discrimination than the average grey level. Luckman et al. (1994) applied texture analysis on a C-band airborne SAR imagery of a tropical forest and were able to discriminate forest age classes that had similar radar responses. As different results were obtained from similar studies of temperate coniferous forests, it was suggested that the texture-age relationship observed in the study is particular only to tropical forests. Ulaby et al. (1986) used SIR-A data from five forested regions (two tropical and three temperate forests) to assess the importance of texture to image classification. The use of textural information in combination with tone in a multi-dimensional classification method improved the classification accuracy among the five forest types from 75% (based on tone alone) to 93%. Holecz et al. (1989) demonstrated the application of a methodology on the analysis of Seasat image over areas with rugged terrain. The methodology involved geocoding, normalisation of the radiometric information according to local topography, and the textural analysis of the image data. More descriptions and applications of some computable textural features based on grey-tone relationships were given in the studies of Haralick et al. (1973), Frost et al. (1984), and Weishampel et al. (1994).

Wang et al. (1995) devised a line-preserving post-processing method for the maximum likelihood classification of radar images. The technique involves the detection of misclassified pixels, a common consequence of maximum likelihood classifications of SAR images due to the presence of speckles, and the subsequent reclassification of said pixels to the classes of neighbouring pixels. The SAR image used for the study was the CCRS C-band with HH, VV and HV polarisations. Results indicated that the procedure is indeed efficient in the reduction of misclassified pixels while preserving lines, corners and boundaries.

Expert classification systems that uses classification rules derived from a spectral knowledge base are viable alternatives to traditional parametric classifiers

(Wharton, 1989). In this regard, Hess et al. (1994) designed tree-based models for the mapping of floodplain inundation in Georgia using multi-frequency polarimetric JPL SAR. Five vegetation categories namely, woody flooded (flooded forests), woody non-flooded (pines and oaks), herbaceous flooded (marsh), herbaceous or bare non-flooded (clearcut, pasture, road) and open water (river, pond, ocean), and thirteen radar variables (combinations of the different frequencies, polarisation, angle and the phase difference) were used. Classification trees for the five cover classes were produced from the radar variables and a rules-based classifier was constructed based on the trees. Error rate was computed based on the number of misclassified pixels when the tree was applied to the training data. Eight trees with different number of nodes were constructed and each was found to have a different error rate and degree of robustness.

A knowledge-based, hierarchical classifier is being developed by Pierce et al. (1995) in line with the availability of multi-parameter data from spaceborne radar sensors and the perceived need for classification algorithms that are robust to variability in seasonal variations, weather, and local vegetation species. Preliminary results from the use of this classifier on a SIR-C/X-SAR single image (with hardwood, upland conifer, lowland conifer, aspen, short vegetation and flat area as classes) yielded an average accuracy of 93.5%. Dobson et al. (1996a) and Pierce et al. (1994) classified land cover classes in a Michigan test area by incorporating a knowledge-based conceptual model into a classifier that uses hierarchical decision rules to differentiate vegetation classes. The radar data utilised were from ERS-1 and JERS-1 composites. Two levels of classification were produced by the classifier. At level-1, the area is divided into man-made features (urban), bare surface, short vegetation, and tall vegetation. The tall vegetation is differentiated further at level-2 based on the stem and foliage architecture such as excurrent (i.e., pines), decurrent (i.e., oaks), and columnar (i.e., palm). The overall classification accuracies produced from the use of the composite classifier were all in excess of 90%. These results were better compared to an unsupervised classification applied on multi-temporal AVHRR data of the same area, even when supplemented with prior information on elevation, climate, and ecoregion.

Yamagata and Yasuoka (1993) analysed ERS-1 and JERS-1 data for the classification of wetland vegetation types in the Kushimo mire, Japan. Texture analysis using the co-occurrence matrix was applied. Results showed that textural parameters such as sum variance, sum average, and sum entropy are useful for the delineation of wetland vegetation. Bogs and the wetland fen vegetation were effectively discriminated from JERS-1 data while the swamp forests were differentiated from the fen vegetation by ERS-1 data. The development of much faster supervised textural classification applicable to full scene images was insinuated as necessary.

A comparison of the results of two image classification techniques, the maximum likelihood as applied to the first order statistics of the measured signals, and the minimum distance as applied to the second order statistics, was undertaken by Van Zyl and Burnette (1989). Both single-frequency and multi-polarisation radar data of various land covers had been used. The comparison showed a similarity in the results from the two algorithms though the minimum distance method had an advantage of using less computer time. More accurate results were obtained from the use of full three-frequency data set than with the use of any of the single-frequency images. Kurvonen et al. (1996) analysed the textural information content of multi-data ERS-1 data with first and second order statistical measures for the purpose of separating the different forest types and land-use classes in a boreal forest in Finland. The derivable textural information was expected to be low at the onset due to the resampling and averaging procedures done on the images. Nonetheless, the accuracy of the forest type/land-use classification was significantly improved by the application of the textural parameters. The simultaneous use of multi-date images had been deemed essential as the textural and/or intensity information generated was not adequate for a satisfactory classification if only one image was used at a time.

A new method, previously demonstrated as a topographic mapping technique, was investigated by Askne and Hagberg (1993) for its potential in the discrimination of land surfaces. The method involves the construction of coherence maps and analysis of coherence texture from interferometric radar images acquired

by INSAR. Different coherence values were observed from different kinds of surface properties. The scattering centre of the forest seemed to be the major branches relatively independent from wind. The separation of forest and open fields based on backscatter was difficult but was easy using coherence. It was suggested that clear cuts or forest fires, where little change will be expected from the backscatter, could be identified using coherence measurements due to the drastic variations in the coherence properties of the said phenomena. In a related study, SAR interferometric analysis of repeat-pass ERS-1 data was conducted by Wegmuller et al. (1995) for mapping forest stands in an area in Switzerland. As interferometric correlation is known to be dependent on the amount of volume scattering and temporal change, forest areas were identified on the basis of low interferometric correlation, medium to high backscatter intensity, and low temporal backscatter intensity change. The shapes, sizes and locations of the forest stands identified through this interferometric approach were in good agreement with those within a cloud- free optical image of the same area.

2.4 Conclusions

The applicability of radar images from airborne and spaceborne platforms for forestry applications such as in biomass estimation, damage appraisal, flooding detection, structure characterisation, species discrimination, inventory and mapping, monitoring of forest conversion, depletion, and reforestation has been investigated in a number of studies. The combined use of radar and optical data for forest resource assessment and the development of backscatter models for the prediction of forest characteristics have been explored as well. Comparison of the accuracy of the results is nevertheless made difficult by the inherent differences in the remote sensors used, calibration methods applied, levels of detail and accuracy assessment methods employed.

Most of the researches were conducted in temperate forest regions and while encouraging results were obtained, the methodologies developed may not be necessarily appropriate to semi-tropical and tropical forest zones considering the

differences in species, tree geometry, species diversity, stand structure, biomass, moisture, and applied management practices between these environments. As most tropical/semi-tropical forests, or most naturally forested areas for that matter, have rugged terrain, it is deemed that important consideration should be given to the topographical effects.

Secondary forests, whether natural or artificial, should be important targets for further research in view of the massive depletion of primary forests, intensifying reforestation and forest protection efforts, and thus the eventual succession of the first as the major vegetation type especially in the tropical regions.

As the main focus of the researches was the unraveling of the relationships between forest biophysical properties and the different radar parameters such as those pertaining to frequency and polarisation, and given the unavailability of multi-parameter data from a single sensor until several years ago, it is easily understandable that the majority of the studies involved the use of single frequency-polarisation combination bands. An examination of the procedures and algorithms developed in the light of the availability of multi-parameter radar data is necessary.

It is envisioned that the operational application of radar data to forest management by the public and the private sectors will be realised as sensors with better capabilities become available, as more practical data processing and analysis algorithms are developed, and as more cost-effective computers and analysis equipment become accessible.

CHAPTER 3

THEORETICAL BASIS

3.1 Introduction

The amount and quality of information that can be inferred from radar data depend on the characteristics of the target and the radar system. Important factors under the former relate to the roughness, geometric and dielectric properties of the imaged surface, while under the latter are the microwave frequency/wavelength, polarisation and incidence angle used in the data acquisition process. Accurate inference of target properties results from the formulation of a well-established relationship between the target and the radar parameters. Being well established implies that such relationship is based on a complete recognition of the different scattering mechanisms present and a clear understanding of how these mechanisms relate to the radar parameters.

The target is characterised by a parameter σ°, which is the radar cross section per unit of the target surface. Commonly called the radar backscattering coefficient, σ° is a function of both the surface and radar viewing parameters. σ° is a dimensionless parameter but is usually expressed in decibels ($\sigma^\circ_{dB} = 10 \log \sigma^\circ$) as it is associated to a high dynamic range, of the order of 10^5 (FAO, 1993). The degree of success of various radar applications relies on the sensitivity of σ° to the specific target components. Determination of the desired sensitivities are made through the application of theoretical backscattering models and the conduct of empirical studies intended at establishing a relationship between σ° and the physical properties of the target (Ulaby, 1982).

In the field of forestry, specifically in the area of forest biomass and stand structure assessment, numerous empirical investigations aimed at correlating σ°

with stand biomass and morphology have been reported with high degrees of success as discussed in Chapter 2. Best estimates are usually obtained when all available radar wavebands, polarisations, and incidence angles are utilised, either singly or in combination, and linked with data on stand height, stand density, canopy depth and thickness, crown closure, trunk/branch and leaf dimensions, vegetation and soil moisture content, undergrowth vegetation, and site topography, among other variables. The main drawback of this type of approach, however, is the lack of understanding of the reasons behind the generated relationships. This problem highlights the need to explore on the theoretical basis for a more holistic comprehension of the backscattering processes involved and thus a more universal application of the methodologies that will be developed along the course of a particular study.

3.2 Parameters influencing radar backscattering from forests

As stated above, the radar backscattering coefficient σ° is a function of both the target and radar viewing parameters. These parameters and their effects on σ° are enumerated and briefly discussed below.

3.2.1 Wavelength/Frequency

The wavelengths used in imaging radar system applications normally range from 1 centimetre to 1 metre or frequencies 30 GHz to 0.3 GHz. Each band is defined as a single frequency although it in fact covers a narrow range of frequencies. The relationship between wavelength and frequency can be illustrated by the formula:

$$f = c/\lambda \qquad (3.1)$$

where f is the frequency in Hertz, c is the speed of light (equivalent to 3 x 10^8 metres/second), and λ is the wavelength in metres.

For ease in computation, frequency (f) could be related to wavelength (λ) by the equation $f = 30/\lambda$, where the unit of f is in GHz (10^9 Hz = 1 GHz) and λ in centimetres.

The varying levels of electromagnetic energy, as measured by frequency and wavelength, are arranged in an ordered array called the electromagnetic spectrum. This array and the band names assigned to the microwave portions commonly used by imaging radars are presented in Figures 3.1 and 3.2.

The depth of target penetration by the incident radar energy is contingent upon the wavelength employed. The longer the wavelength, the deeper the penetration. Assuming a single band is used, the penetration depth will likewise be influenced by the degree of attenuation imposed by the components of the target. Provided that the density of the scattering centres is constant with depth, the loss in the forward energy can be expressed by the formula (from UNSW course notes, 1996)

$$P_{(Z)} = P_{(0)}\, e^{-ke\,Z} \qquad (3.2)$$

where $P_{(Z)}$ is the power density at depth (or path length) Z, $P_{(0)}$ the power density at the surface of the target, and k_e the extinction coefficient for the medium. The extinction (or penetration) depth (δ), which is equivalent to $1/k_e$, is the depth at which the power density has fallen off to 1/e of its value at the surface. Determination of the value of k_e is, however, made difficult by the fact that it is made up of both a scattering term (k_s) and an absorption term (k_a) such that

$$k_e = k_s + k_a \qquad (3.3)$$

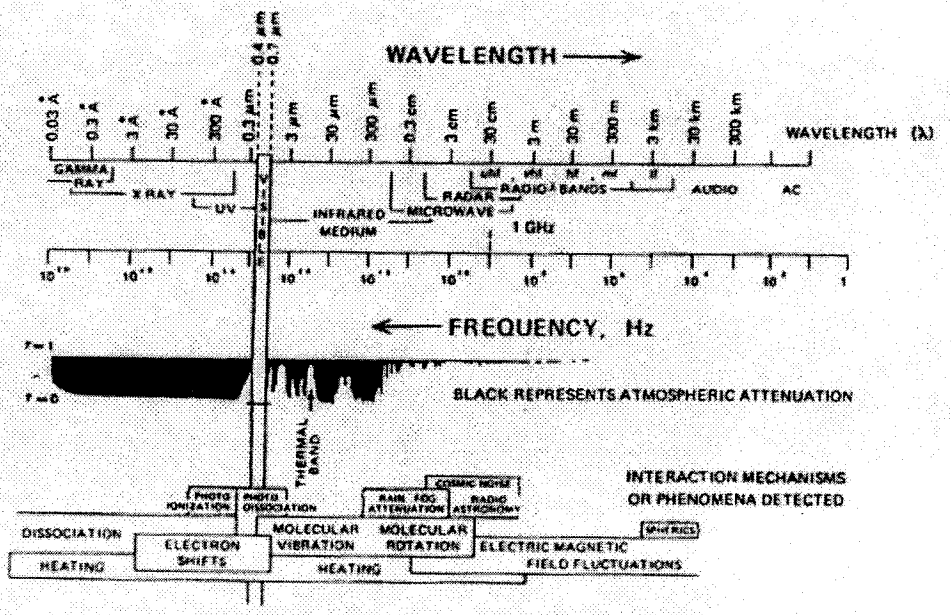

Figure 3.1. The electromagnetic spectrum (from ASPRS, 1983)

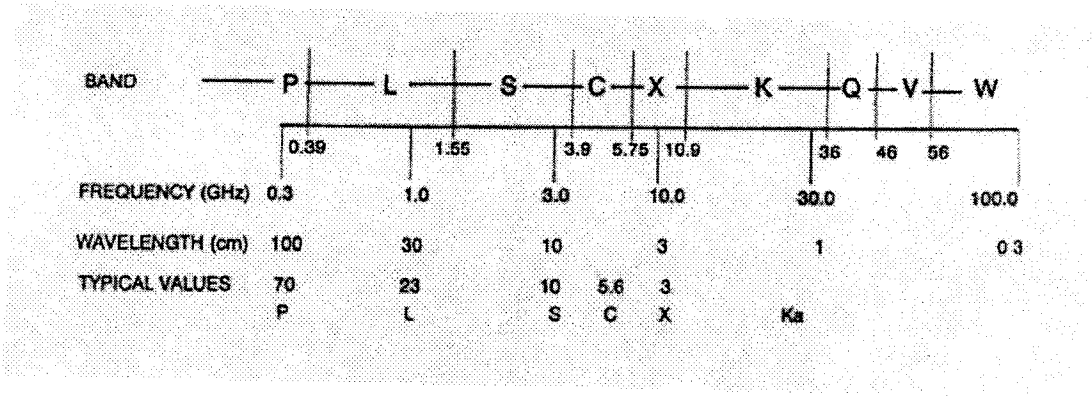

Figure 3.2. The different radar bands along the microwave spectrum (from ASPRS, 1983)

where k_s results from energy loss in the forward direction resulting from the scattering of energy away from that direction while k_a is a consequence of energy loss due to absorption by the target components.

The degree of penetration in forests determines the level of information that could be provided by the radar. With the relatively short wavelengths of the X- (3 cm) and C- (5.6 cm) bands, penetration will be confined to the upper portion of the crown. In some cases, the C-band radiation may reach the middle and perhaps the lower portion of the crown, depending on the density and dimensions of the leaves and branches. It follows therefore that the information content of images taken with these bands is related to the upper layer of the canopy. With the L-band (23 cm), the radiation is expected to penetrate the leaves and small branches and the image information content could thus be related to the branches and eventually the tree trunks. These different degrees of microwave penetration are illustrated in Figure 3.3. A deeper penetration of the canopy can be achieved by the use of the P-band (70 cm). In this case, the σ° could be a result of the tree trunks as well as the undergrowth, the ground surface, and even the subsurface.

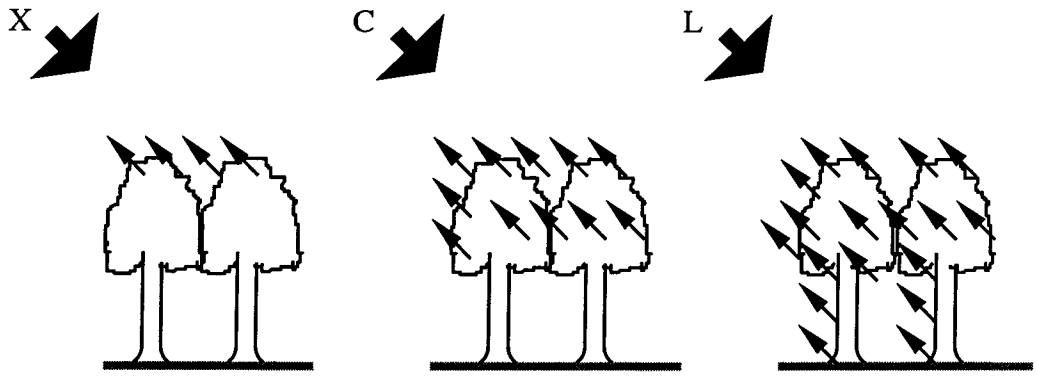

Figure 3.3. Backscatter of forest vegetation in X-, C- and L-bands (after NASA, 1989).

3.2.2 Polarisation

The orientation of the electric field vector of the electromagnetic wave transmitted and received by the radar sensor is referred to as polarisation. Radar systems can be configured to have different polarisations although the linear

combinations viz. HH, HV, VV and VH are the most commonly utilised. The first letter refers to the polarisation of the transmitted wave while the second corresponds to the received wave. HH, for example, denotes a horizontal transmission and a horizontal reception. Some researchers, however, use the opposite such that the first letter refers to the polarisation of the received wave and the second to that of the transmitted energy. When the polarisation of the emitted and received waves are the same, the waves are said to be like-polarised or co-polarised. Cross-polarisation is the case when the incident and the backscattered radiation are of opposite polarity eg. HV. A radar system configured to simultaneously transmit in two orthogonal polarisation states and receive in the same two polarisation modes, such as the AirSAR of NASA/JPL, is called a quadrature polarisation or *quad pol* radar (FAO, 1993). Besides linear polarisation, the other polarisation types used by radar systems are the circular and elliptical, where the wave plane rotates as the waves propagate. The direction of the rotation may be either clockwise or counterclockwise, hence the terms *right-hand polarised* and *left-hand polarised* waves (Ulaby et al., 1981).

Information on the different components of the forest can be inferred from polarisation. The way in which the wave reacts to different shapes, form and orientation of leaves, twigs and other scattering elements within the canopy is influenced by polarisation. Vertically polarised waves interact more strongly with the vertically oriented canopy components than the horizontally polarised pulses. This leads to differences in canopy penetration depth and backscattered power between the two polarisation types. Multiple-bounce backscattering brought about by corner reflection from trunks and canopy volume scattering, and scattering from sufficiently rough surfaces (i.e., diffuse surfaces) tend to cause depolarisation. Although not often evident in the radar imagery due to the use of increased receiver gains, cross-polarised returns are generally lower than the corresponding co-polarised backscatter (UNSW course notes, 1996).

With the differences in the sensitivities of the polarisation types, parameters such as the *polarisation index* (HH/VV) and *linear depolarisation ratio* (HV/VV), in addition to the individual co-polarised and cross-polarised backscattering

coefficients, can be used to determine the nature of backscattering, identify the various scattering mechanisms and estimate the biophysical properties of a given forest stand. The difference in the phase of the horizontal and vertical signals, called *polarisation phase difference*, has also been demonstrated in recent studies to be useful in the identification and understanding of the dominant scattering elements and processes (Dong et al., 1995, 1996).

3.2.3 Incidence angle

The incidence angle is defined by the angle formed between the radar illumination and the normal to the imaged surface. Even within an image, there will be a change in the incidence angle from the near range to the far range with the degree of change depending on the altitude of the radar platform. An image taken at a relatively low altitude, as that from airborne platforms, will have a less uniform illumination across the entire swath compared to that taken by satellite-based systems. This causes a difference in viewing geometry and thus in the geometric distortions associated with side-looking imaging radars. In areas of high relief variations, there will be a brightening and foreshortening of the slopes facing the radar, and elongating and shadowing of slopes positioned away from the radar. On the optimistic side, shadows on the radar image can be a source of useful image and system information while topographic distortions could be partly compensated for by the use of digital elevation models. Shadows, for example, give a good visual representation of relief, aid in the determination of object height, serve as a reliable indicator of the radar illumination direction in the absence of annotation, and can provide information regarding the radar (i.e., determination of system noise).

The backscattering coefficient of most targets varies with the angle of incidence mainly as a consequence of the difference in slant range. Looking at a particular forested area, the backscatter contribution from the canopy component is expected to increase with incidence angle due to the corresponding increase in slant path through the volume. The increase in incidence angle causes greater attenuation by the tree crown due to the longer distance within the crown through which the wave must pass. A radar looking at a relatively steep angle has a better chance of

seeing through the canopy than one looking at a more oblique angle from the nadir (ESA, 1995).

The distortions brought about by differences in topography emphasise the importance of undertaking geometric corrections in images of forest areas located in mountainous regions.

3.2.4 Moisture content

A target's ability to absorb and reflect microwave radiation depends on its electrical properties. A measure of the electrical properties of the target material is provided by the complex dielectric constant. The relationship between dielectric constant and target reflectivity can be illustrated by taking the case of a perfectly smooth and lossless (zero conductivity) ground surface. Here, the reflected power can be represented by the power reflection coefficient or reflectivity, R,

$$R = |\rho|^2 \tag{3.4}$$

where ρ is the Fresnel reflection coefficient. Assuming a normal incidence,

$$\rho = 1 - (\varepsilon_r)^{1/2} \; / \; 1 + (\varepsilon_r)^{1/2} \tag{3.5}$$

where ε_r is the relative dielectric constant of the ground. So, if the dielectric constant of the ground is low, only a small percentage of the incident energy will be reflected and the majority will be transmitted into the ground. For example, if ε_r is 2, then R will be less than 10 % for most radar wavelengths and so more than 90 % of the incident radiation will penetrate the ground.

In dry conditions, the dielectric constant of most natural targets in the microwave region ranges from 3 to 8 (FAO, 1993). Water, on the other hand, has a dielectric constant in the vicinity of 80. This is the reason why a change in the water content of the target results in a corresponding change in the dielectric properties.

An increase in the target's water content, and hence an increase in its dielectric constant, causes greater radar reflectivity and less penetration. Assuming all other factors are constant, identical targets with different moisture contents will appear to be different. A wet diffuse scattering target will usually appear brighter in the image than a dry target although radar penetration will be deeper in the latter. Depending on the radar wavelength, the radiation may completely penetrate very dry materials resulting in backscatter from subsurface features.

The moisture content of the forest vegetation, considering its effect on the reflectivity and depth of penetration, thus has a strong influence on the information that can be determined from the backscattering coefficient. With C-band, canopy volume scattering may dominate when the crown is dry. Backscattering in this band, however, may be confined to the surface component if the moisture content of the crown is high.

3.2.5 Surface roughness

The definition of surface roughness is based on the root mean square (RMS) of surface height and the surface correlation length. A surface is considered to be smooth if the height and length variations are small compared to the incident wavelength and rough if the surface dimension variations and the wavelength are at least comparable. The Rayleigh's criterion sets the boundary between smooth and rough surfaces. According to this criterion, a surface is said to be smooth when

$$h < \lambda / 8 \cos \theta \tag{3.6}$$

and could be considered as rough if

$$h > \lambda / 8 \cos \theta \tag{3.7}$$

where h is the RMS surface height, λ is the wavelength, and θ is the incidence angle.

The shorter the wavelength, the rougher a given surface will appear to be. Using a single wavelength, an increase in the incidence angle will cause the surface to appear smoother.

In general, a rough surface will produce a greater amount of backscattering, and thus will appear brighter on the radar image, than a smooth surface of the same material. A good example is the bright appearance that could be observed from a rough or wind-stressed body of water relative to the dark tonality which will be exhibited by a calm surface. This phenomenon is due to the so-called specular and diffuse reflectance, which are both related to surface roughness. Horizontally aligned smooth surfaces are called specular targets (from the Latin word *speculum*, which means *mirror*) since they reflect almost all of the incident radiation away from the radar. Specular objects thus appear dark on the radar image. On the other hand, rough surfaces reflect the incoming energy in a manner known as diffuse scattering, where the incident wave is reflected in various directions thereby causing the surface to appear bright on the radar imagery. These two types of reflectance patterns are presented in Figures 3.4a and 3.4b.

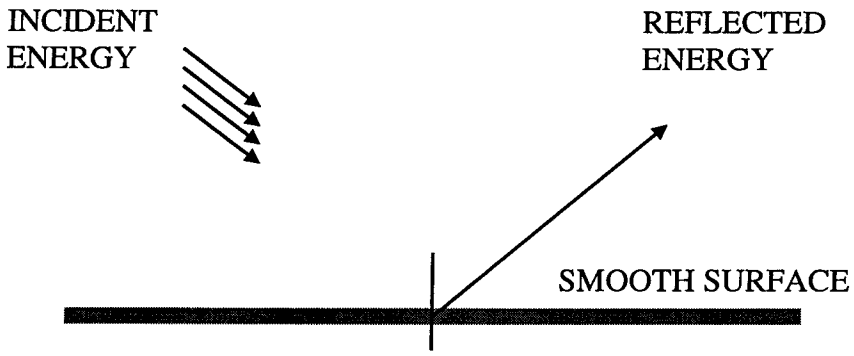

Figure 3.4a Specular surface reflectance pattern

The effect of surface roughness on the backscatterred energy can be useful in the determination of canopy structure and classification of forest stands. With the long wavelengths, information on the presence of undergrowth vegetation, debris and decaying organic matter, as well as other ground features could be inferred from

the reflected radiation. Detection and mapping of flooded vegetation is another important area of application.

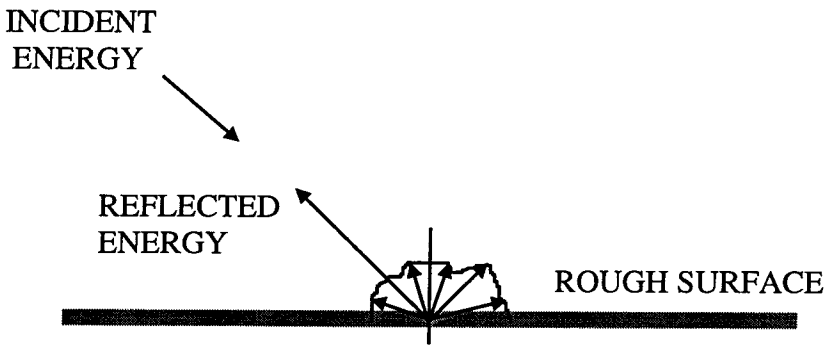

Figure 3.4b. Diffuse surface reflectance pattern

3.3 Synergism of radar parameters for optimum information extraction

The advent of multi-parameter imaging radars extricated investigators from the limitations of using mono-band radar data in carrying out forest-related research. The opportunity lies in the simultaneous use of all the parameters of the radar for optimum extraction of information from radar imagery. It is believed that a better assessment of forest resources could be achieved by utilising a combination of the parameters. The theoretical basis for this premise and the different combinations will be presented in the following topics. This research will focus on the more controllable radar system-based components such as wavelength and polarisation with forest aboveground biomass and stand structure assessment as the particular areas of application.

3.3.1 Forest aboveground biomass estimation

Combined wavelength and polarisation estimation

The total forest aboveground biomass is the summation of the biomass of the crown and bole components of all the trees in the area under consideration.

Obviously, to derive an estimate of this quantity from radar data, information on both the crown and the bole should be available. A simple model of the total biomass could then be given as

$$B_{total} = B_t + B_c \tag{3.8}$$

where B_{total} represents the total aboveground biomass, B_t the trunk biomass, and B_c the crown biomass.

The C-band, with its relatively shorter wavelength, is sensitive to the upper layer of the vegetation such as the leaves, twigs and small branches of the crown. The more penetrative wavelength of the L-band can pass through a greater volume of the canopy and interacts with bigger structures at the lowermost canopy portion and more regularly, with the trunk and big branches. Most of the returns from the latter are from tree-ground double bounce backscattering that occurs mainly due to the vertical orientation of the trunk with respect to the ground thus forming a corner reflector-like structure. Thus,

$$\sum_{n=1}^{N} (\sigma^O) = i_n\sigma^O_{L\text{-}} + j_n\sigma^O_{C\text{-}} \tag{3.9}$$

where $\sum_{n=1}^{N} (\sigma^O)$ is the backscattering coefficient sum correlated with the total aboveground biomass; i and j are the unit vectors in x and y axes in the xy coordinate system corresponding to the backscattering coefficients of the L- and C-band, respectively. This relationship is illustrated in Figure 3.5. Also portrayed in the figure are the differences in sensitivity between C- and L-band to the different stand components (i.e., crown versus trunk) as a consequence of differences in penetration. Illustrated schematically in the diagram are trees with large trunks and small crowns, and those with large crowns and small trunks. This concept will be more thoroughly explained in Section 3.3.2.

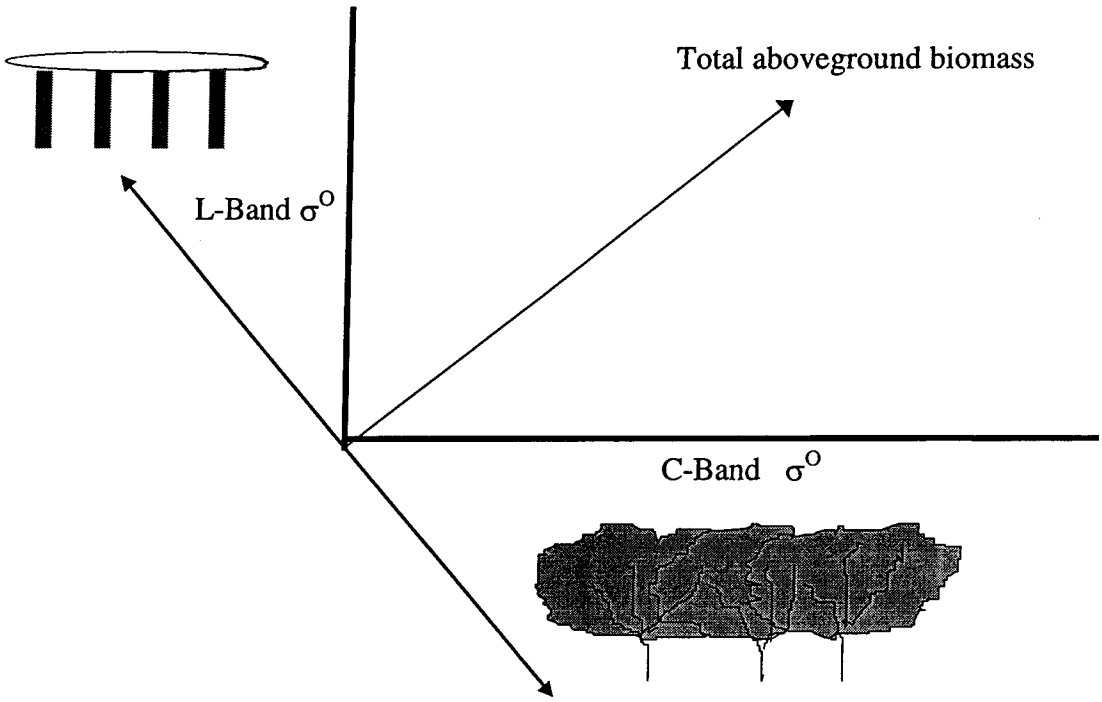

Figure 3.5. Total aboveground biomass as a function of L- and C-band backscatter

The type of polarisation employed determines the radar response to the various shapes and orientations of the scattering mechanisms within the canopy. Backscatter from cross-polarised waves tends to be related to the canopy volume rather than the lower components such as the soil and as such may be an indicator of crown biomass (ESA, 1995). Incoming vertically polarised waves readily interact with the vertical components of the canopy. Due to the nature of its orientation, horizontally polarised radiation tends to have a deeper degree of penetration and is less likely to be affected by canopy attenuation. The highest correlations between radar backscatter and total biomass are obtained using waves with HV- and HH-polarisation: VV-polarised waves are more sensitive to the components of the crown and tend to saturate at lower total biomass levels (Dobson et al.,1995a).

Integrating the theories pertaining to the sensitivities of the different radar wavelengths and polarisations, we can deduce the following relationships:

$$\sigma^{O}(B_{t+lb}) \approx \sigma^{O}_{L\text{-}HH} \quad (3.10)$$

$$\sigma^{O}(B_{L+b}) \approx \sigma^{O}_{C\text{-}HV} \quad (3.11)$$

where B_{t+lb} refers to the biomass of the trunk and lower branches, B_{L+b} is the biomass of the leaves and most of the branches, while $\sigma^{O}_{L\text{-}HH}$ and $\sigma^{O}_{C\text{-}HV}$ are the L-HH and C-HV backscattering coefficients, respectively.

Considering the above relationships, equation 3.9 could then be written as

$$\sum_{n=1}^{N} (\sigma^{O}) = i_n\sigma^{O}_{L\text{-}HH} + j_n\sigma^{O}_{C\text{-}HV} \quad (3.12)$$

where $i\,\sigma^{O}_{L\text{-}HH} + j\,\sigma^{O}_{C\text{-}HV}$ is called the Trunk-Canopy Biomass Index (TCBI). To avoid possible overestimation of total aboveground biomass, other polarisation combinations of the L- and C-bands were not included in the equation as the biomass values they represent are already included in the $\sigma^{O}_{L\text{-}HH}$ and $\sigma^{O}_{C\text{-}HV}$ backscatter.

The co-polarised component (HH or VV) is generally higher than that of the cross-polarised component (HV). This is because the former is the result of first-order scattering while the latter is a result of second-order scattering. In order to take the influence of the cross-polarised component into account, equation (3.12) could also be written as $TCBI = a\,\sigma^{O}_{co} + b\,\sigma^{O}_{cro}$, where a and b are weighing factors for the co-polarised and cross-polarised component, respectively. This formula can be further extended to a general form: $TCBI = \sum_i a_i\sigma^{O}_{coi} + \sum_j b_j\sigma^{O}_{croj.}$, where all available multi-frequency and multi-polarisation measures are included. For simplicity, $a = b = 1$, have been used in this research.

Saturation of radar measurements

The amount or density of the scattering components within the crown, in addition to wavelength and dielectric constant, also influences the penetration depth achieved by the transmitted energy. The influence stems from the changes in path length and the degree of attenuation imposed by the crown components on the incident radiation. As the energy travels through the canopy, it is gradually depleted by the scattering caused by dielectric discontinuities in the different canopy layers such that there is less energy available to the next layer (UNSW course notes, 1996). If we assume a continuous increase in the dimensions and amount of canopy components from left to right of a forest profile, there will be a point in the profile wherein even the longer wavelength of the L-band would no longer be able to pass through the crown layer due to attenuation. This concept is illustrated in Figure 3.6.

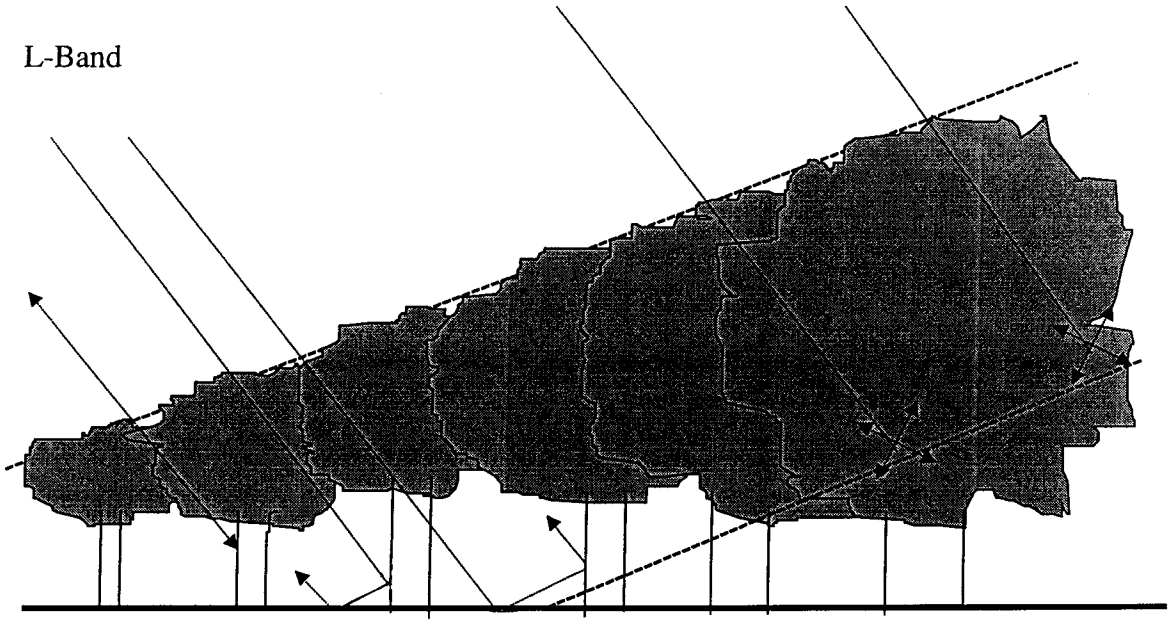

Figure 3.6. Illustration of the penetration of L-band as a function of increasing canopy components.

The first three L-band waves in Figure 3.6 are able to penetrate through the crown and can be used to derive information on the trunk biomass. The last two waves, however, are completely attenuated by the crown and thus cease to provide

information on the trunk component. If one's interest also includes the components underneath the canopy, using L-band, as in the case of the last two waves, will lead to inaccurate results.

The increase in the dimensions, amount or density of the different tree components is generally directly correlated with an increase in the total aboveground biomass. That is, as the total biomass increases in value, lesser canopy penetration is expected from the forward radiation. With L-band, the amount of biomass at which the energy no longer passes through the canopy is called the saturation level for that band. Since the type of polarisation also exerts influence on the penetration depth, the same band with different polarisations will also have different levels of saturation. These influences are illustrated in Figure 3.7.

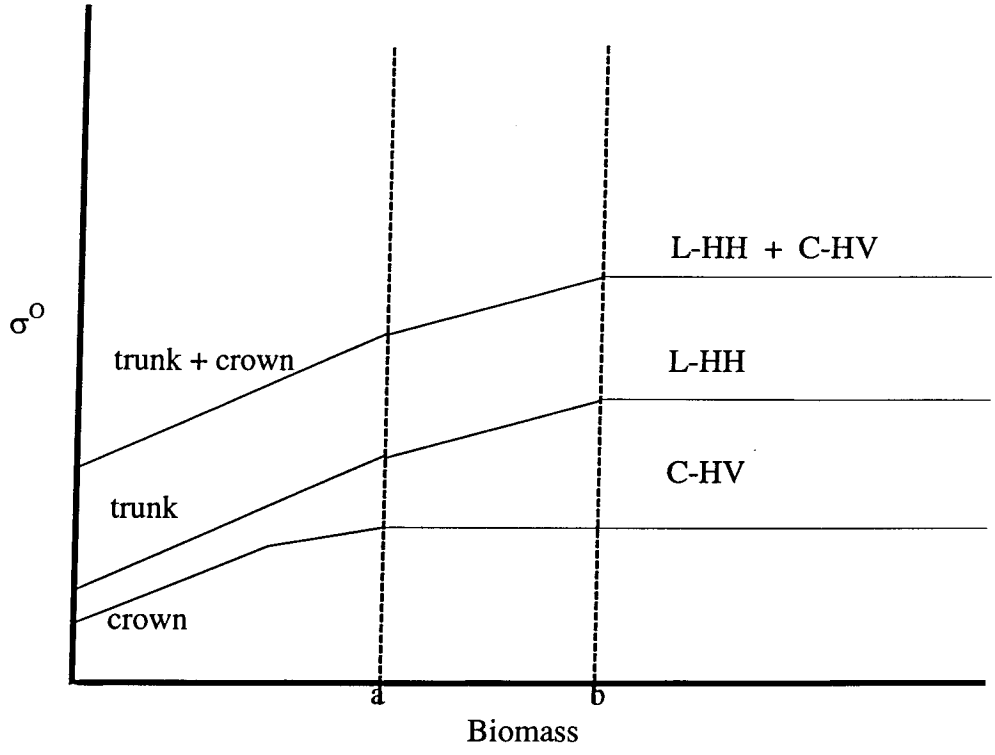

Figure 3.7. Sensitivities to forest components and theoretical saturation levels for C-HV, L-HH, and LHH + C-HV

Point b in Figure 3.7 corresponds to the amount of biomass where the sensitivity of both the L-HH and LHH + C-HV backscattering to biomass measurements becomes saturated. The saturation point for C-HV is represented by

point a. The flattening of the lines beyond these points indicates that the backscattering coefficients no longer respond to an increase in biomass of the forest components. Thus, any derived relationship between biomass and backscatter would no longer be valid.

This notion of saturation has important implications for the application of radar to forest areas of high biomass. Returning to figure 3.7, it can be deduced that equation 3.12 is no longer applicable to biomass levels to the right of b. Theoretically, the $\sigma^{O}_{L\text{-}HH} + \sigma^{O}_{C\text{-}HV}$ corresponding to the amount of biomass in excess of the saturation level could be added into equation 3.12 to come up with $\sigma^{O}(B_T)$ at that point. For example, if the saturation for $\sigma^{O}_{L\text{-}HH} + \sigma^{O}_{C\text{-}HV}$ is at 150 tonnes/ha and the total biomass of the forest under consideration is 200 tonnes/ha, then the sum of the $\sigma^{O}_{L\text{-}HH} + \sigma^{O}_{C\text{-}HV}$ at 150 tonnes/ha and the $\sigma^{O}_{L\text{-}HH} + \sigma^{O}_{C\text{-}HV}$ at 50 tonnes/ha could be used to give $\sigma^{O}(B_T)$. However, while theoretically possible, it is not a practical solution given that the biomass values are not known beforehand and the intention is to derive biomass estimates from radar data without prior knowledge.

A possible solution for the estimation of biomass at ranges beyond the $\sigma^{O}_{L\text{-}HH} + \sigma^{O}_{C\text{-}HV}$ saturation point is the use of bands with longer wavelengths. Equation 3.12 could then be modified to

$$\sum_{n=1}^{N} (\sigma^{O}) = \sigma^{O}_{P\text{-}HH} + \sigma^{O}_{L\text{-}HV} \qquad (3.13)$$

In here, P-HH (instead of L-HH) and L-HV (instead of C-HV) are used for the sensing of the trunk and crown components. In some cases, such as when the total biomass is remarkably high, the use of P-HV (instead of L-HV) could also be explored. This is shown in Figure 3.8.

The impact of topography on trunk and canopy backscattering

The overall effect of the slope of the underlying ground on the radar backscatter is influenced by the radar and vegetation parameters. At forest biomass

levels below the L-band saturation point, topographic variations, though insignificant to the canopy volume scattering term, will affect the double-bounce scattering involving the trunk and the forest floor such that an increase in the L-band backscatter is normally expected as the ground tilts towards the radar sensor. In view of this situation, inconsistencies can be expected from the L-band measurements thereby necessitating the application of appropriate techniques to correct the problem. This is not the case with the C-band backscatter as it is generally related to the canopy components only, except in the case of sparsely vegetated areas, where the σ^{o}_{C} may be affected as well. The effect of slope variations on the radar return is illustrated in Figure 3.9.

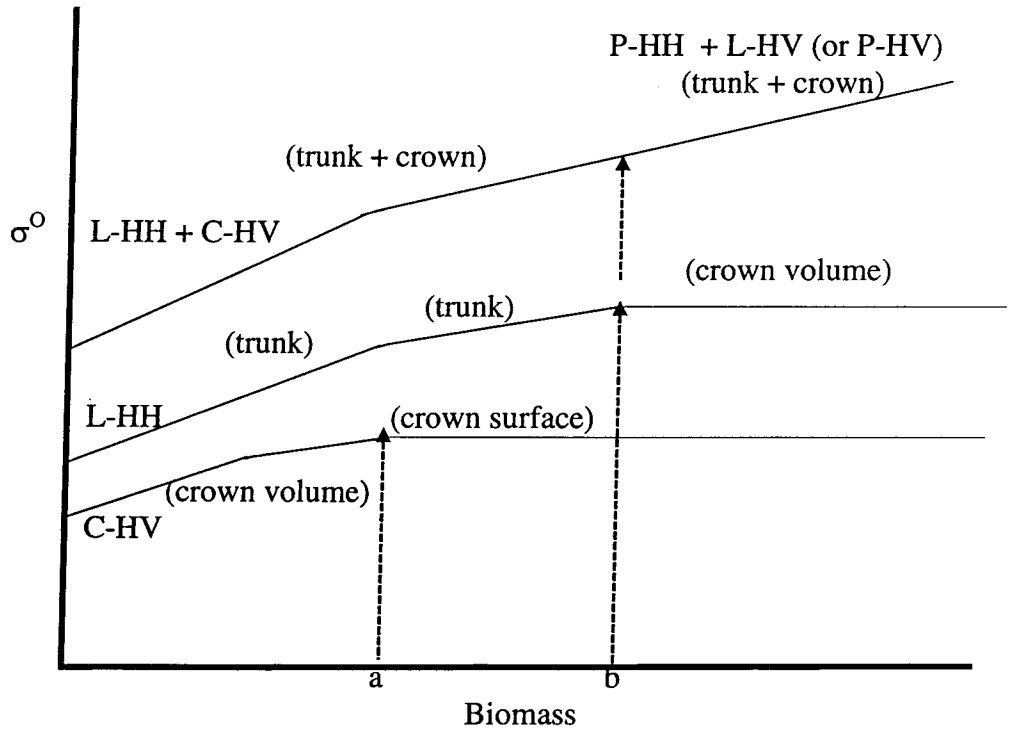

Figure 3.8. Use of P-HH and L-HV (or P-HV) backscatter to derive biomass estimates at levels above the L-HH + C-HV saturation point

3.3.2 Stand morphology/structure determination

In this study, two general categories are used to differentiate stands according to morphology: those composed of needle-leaved pines/conifers and

broad-leaved deciduous/evergreen trees. The cross-section appearance of the two categories are depicted in Figure 3.10. Trees under the former are characterised by an excurrent branching pattern, where the bole outgrows the lateral branches thus resulting in a well-defined cylindrical trunk and a usually conical crown. The lateral branches extend up to the relatively lower portion of the central stem producing a narrow and deep crown but the bole is visible almost throughout the entire tree height due to the small size and density of the branches and the needle-like leaves. Trees under the latter are characterised by a less-pronounced trunk but bigger and more voluminous leaves, as well as a wider and thicker crown compared to that of the former. The branching pattern is usually decurrent, where the lateral branches grow at the same rate, or even faster, than the bole and the definition of the bole can be completely lost due to repeated forking (Dobson et al., 1995a). Some broad-leaved species have an excurrent branching pattern during the early development stage and change to the decurrent type as they mature.

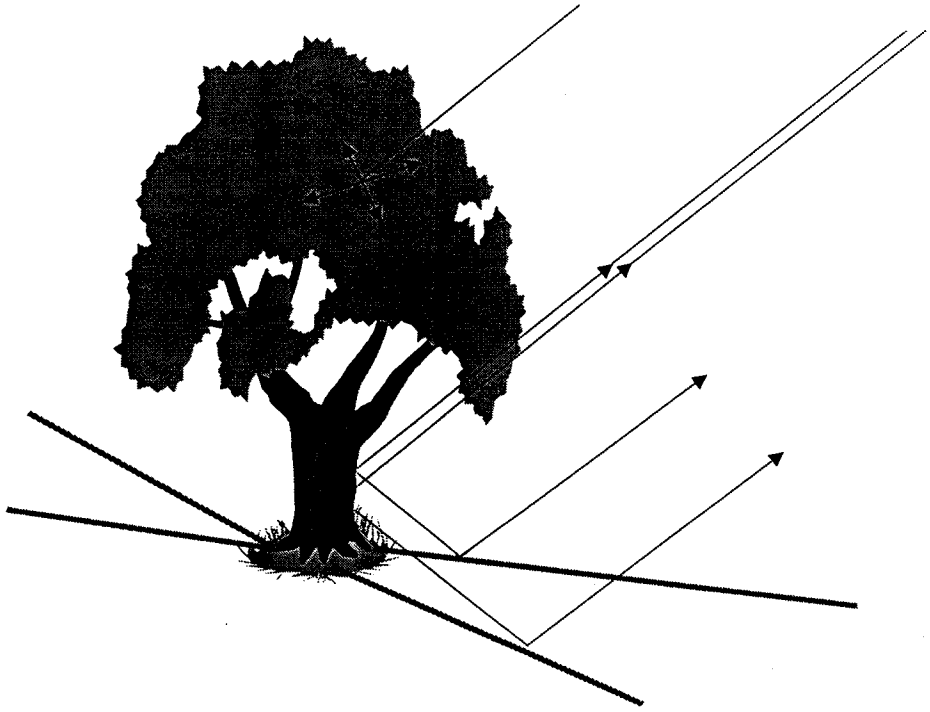

Figure 3.9. Illustration of trunk-ground backscattering as affected by tilts in the ground surface.

Figure 3.10. Cross-section representation of the broad-leaved and needle-leaved tree categories.

As radar backscattering behaviour is directly influenced by the geometric properties of the target, it follows that the backscattering from stands of varying structural attributes will be relatively different. A stand of needle-leaved trees, with the small size and density of the leaves and branches as well as the long trunks of the trees, will have a strong L-HH return. On the other hand, the greater attenuation imposed by the bigger and more dense foliage components, coupled with the less conspicuous trunks, will result in a lower L-HH but higher C-HV backscatter from stands of broad-leaved trees. This change could also be related to, say, big-trunked trees and mallee or scrub type vegetation, or mangroves and trees with more conspicuous trunks. This theory is illustrated in Figure 3.11.

It is suggested that the above theory can be useful in the determination of tree structure. Given that the sensitivity of the L-HH and C-HV σ^{O} is a function of the trunk and crown components, respectively, then the true ratio of these two backscattering coefficients is a possible measure of tree morphology. This could be illustrated by the expression

$$\frac{\sigma^{o}_{L\text{-}HH}}{\sigma^{o}_{C\text{-}HV}} \approx \frac{\text{trunk}}{\text{crown}} = \text{TCMI} \qquad (3.14)$$

where TCMI is the Trunk-Canopy Morphology Index. A high TCMI implies a tree structure with more trunk and less crown component while a low TCMI indicates the opposite. When the biomass levels are particularly high, the L-HH and C-HV backscatter, as discussed above in the case of the TCBI, could also be substituted with P-HH and L-HV (or P-HV) measurements, respectively.

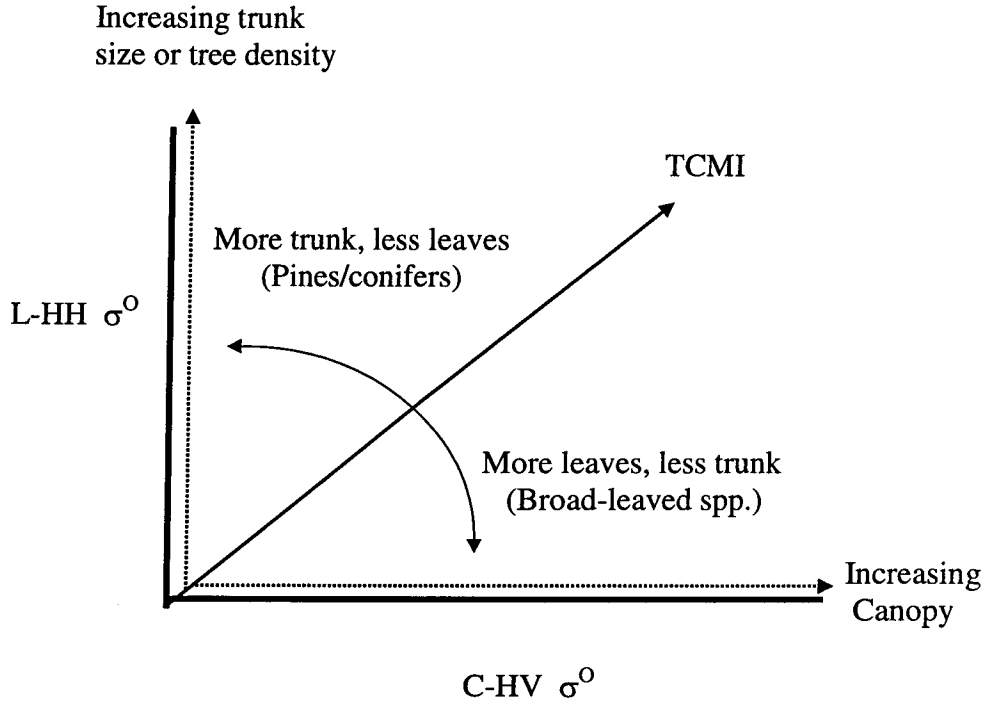

Figure 3.11. Sensitivity of L-HH and C-HH σ^{o} to stand structure properties

3.3.3 TCMI as indicator of leaf properties

Since the two general categories used to differentiate stand structure (i.e., needle-leaved and broad-leaved) are also indicative of the leaf type, TCMI can then be used to deduce leaf characteristics. A high TCMI value typifies a stand made up of trees with thin elongated leaves and hence a low leaf area. A low TCMI value

indicates broad but relatively shorter leaves. Nevertheless, the leaf area in the latter case is expected to be higher compared to that in the former.

3.4 Summary and conclusions

The capability of microwave energy to penetrate forest vegetation makes possible the extraction of information on both the foliar and woody components from radar data. The depth of penetration, and hence the type of derivable information, is dependent upon parameters relating to both the radar sensor and the target such as the wavelength, polarisation and incidence angle used, as well as the geometric and dielectric properties of the target vegetation.

At C-band, the backscattered energy is correlated mainly with the crown constituents such as the leaves, twigs and small branches. Information on the other components beneath the canopy can be sensed through the use of bands with longer wavelengths such as the L- or P-band. The sensitivity of co-polarised and cross-polarised waves to the shapes and orientation of the different tree constituents provide an added advantage in the information extraction procedure. Given the relatively greater degree of penetration by horizontally polarised waves and the strong interaction of the vertically polarised energy with the vertically oriented canopy parts, different wavelength-polarisation combinations can be then used to suit the purpose of the study. In the field of forest biomass estimation, the Trunk-Canopy Biomass Index (TCBI), which is the sum of the L-HH and C-HV backscatter, can be a measure of the total aboveground biomass as both the crown and trunk layers are taken into consideration. The relationship between TCBI and biomass, however, is not expected to be unique for a whole forest vegetation owing to possible variations in morphological structure of the stands within the area. It is important therefore that stand structure be first considered to allow a more accurate biomass assessment by the TCBI parameter.

In this study, two categories are used to classify stands according to structure: the needle-leaved pines/conifers and the broad-leaved

deciduous/evergreen trees. Under the first category are trees having a long main stem and a usually deep, narrow and cone-shaped crown composed of needles and small branches that exhibit an excurrent pattern. Trees under the latter have a less-pronounced trunk, a wider and thicker crown with more voluminous leaves and a generally decurrent branching pattern. Consequently, an index of the relative proportions of the crown and the trunk may be indicative of the approximate tree morphology. It is believed that the Trunk-Canopy Morphology Index (TCMI), which is the ratio of the L-HH to C-HV backscatter, provides a measure of tree structure.

A two-stage procedure for forest biomass estimation is therefore proposed. The first stage involves the determination of the stand structure category based on the TCMI. Once the structure is known, a specific structure-dependent TCBI could then be applied for the biomass estimation process.

CHAPTER 4

APPLICATION OF RADAR THEORY TO PUBLISHED RELATED RESEARCH

4.1 Introduction

The importance of quantifying and monitoring forest vegetation, given the vital productive, protective, and regenerative functions of this natural resource, is undeniable. Information on the amount and extent of vegetation provides an insight on what or how much to expect from a specific forest area in terms of these functions. From another perspective, the information can be useful in determining whether or not forest rehabilitation or other appropriate actions are needed in consideration of these three major functions.

Forest aboveground biomass, or the quantity of vegetative material per unit area, is one of the parameters recognised as a good indicator of forest condition. The use of radar remote sensing to provide estimates of this parameter has been receiving increasing interest over recent years. This is mainly due to the ability of the radar to provide data independent of solar illumination and weather conditions. In addition, radar waves, depending on the wavelength/frequency, can be employed to scope different sections of the vegetation profile. Information on crown layer components (e.g., foliage) can be inferred from the radar backscatter at high frequency bands such as C- and X- while information pertaining to the trunks and lower branches can be obtained through the longer and more penetrative wavelengths of L- and P- bands.

The availability of multi-parameter radar sensors made feasible the estimation of both the foliar and woody biomass using a single radar system. Since the backscattering coefficient is influenced not only by the quantity of biomass but by how the individual components are oriented and distributed throughout the entire

tree length, it is also possible to determine the general tree/stand structure based on the radar data. In fact, as suggested in the previous chapter, the determination of the general tree/stand structure must precede biomass estimation and that radar data-based biomass equations should be formulated based on the structure. Otherwise, erroneous results will most likely be produced as it is possible to obtain different backscatter readings from two stands containing the same amount of biomass but are structurally different.

In this chapter, the effectiveness of the theories, models and indices presented in Chapter 3 in providing measures of forest aboveground biomass and stand structure is assessed and demonstrated by applying them to actual and modelled data from published related works of other investigators. Summaries of the studies considered have been given in Chapter 2 while a more detailed discussion of the results is presented here. As most of the data and results are reported in the form of graphs, interpolation was done to obtain measurements for the backscattering coefficients and the corresponding forest biomass levels.

4.2 Data sources

Listed and individually described in Table 4.1 are the different studies used in the assessment of the theories and concepts previously presented. All but two of the studies involved the use of either SIR-C/X-SAR or AIRSAR system. In all of these, the HV and VH polarisations were regarded as identical and only the HV data were hence included in the analysis. The incidence angles utilised ranged from 19° - 50° and varying but closely related saturation limits were observed. Ranson et al. (1995), for example, noted a saturation level of 100 tonnes/ha for C- band, 200 tonnes/ha for L-band and beyond 200 tonnes/ha for P-band while saturation levels of 100 and 200 tonnes/ha were reported for the L and P- bands, respectively, by Dobson et al. (1992).

Author/s	Radar System	Band/s Used	Polarisation	Incidence Angle	Study Site/s	Dominant Vegetation	Saturation Limits (t/ha)	Remarks
1. Imhoff, 1993	JPL SAR (AIRSAR)	P-, L-, C-	HH,VV,HV	40° - 50°	a) Hawaii b)North America & Europe	a)Tropical broad-leaved evergreen b) Conifers	C- = 20 L- = 40 P- = 100	HV and VH treated as the same
2. Souyris et al.,1995	SIR-C/X-SAR	a) L-, C- b) X-	a) HH,VV,HV b) HH, VV	26.4°	Les Landes Forest, France	Pines/conifers	50	-do-
3. Dobson et al., 1995a	SIR-C/X-SAR	a) L-, C- b) X-	a) HH,VV,HV b) HH, VV	31°	Raco Supersite, Michigan, USA	Broad-leaved hardwoods and conifers	(multi-step approach accurate up to 250 t/ha)	-do-
4. Dobson et al., 1995b	SIR-C/X-SAR	L-	HH, VV, HV	19° - 47°	Raco Supersite, Michigan, USA	Broad-leaved hardwoods & conifers	——	-do-
5. Hsu et al., 1993	AIRSAR	P-, L-, C-	HH, VV, HV	45°	Les Landes Forest, France	Pines/conifers	——	-do-
6. Dobson et al.,1992	AIRSAR	P-, L-, C-	HH, VV, HV	40° - 50°	a)Les Landes forest, France b)Duke forest, USA	Pines/Conifers	P- = 200 L- = 100	-do-
7. Karam et al., 1995	AIRSAR	P-, L-, C-	HH, VV, HV			Pines/conifers	——	-do-
8. Harrel et al., 1995	JERS-1 & ERS-1	L- & C-	HH & VV	45°	Les Landes forest, France	Pines/conifers(White and black spruce)	——	
9. Christensen et al. 1990	Airborne SAR (P-3)	L-	HH, VV	42° - 49°	Duke Forest, USA	Pines/conifers	100	
10. Moghaddam et al., 1994	AIRSAR	P-, L-, C-	HH, VV, HV	35° - 50°	Oregon, USA	Mixed hardwoods and conifers	200(for 40°-50°) 300(for °35) 150 (for 50°)	L-HH data not available from report
11. Ranson & Sun, 1994	AIRSAR	P-, L-, C-	HH, VV, HV	25°,35°,50°	Maine, USA	Mixed hardwoods and conifers	157	L-HH data not available
12. Ranson et al., 1995	AIRSAR	P-, L-, C-	HH, VV, HV	25°,35°,45°	Maine, USA	Mixed hardwoods and conifers	C-=100, L-=200 P- = > 200	C-HV data not available

Table 4.1. List and description of the different studies used in the assessment of Chapter 3 concepts and theories

4.3 Radar backscatter versus forest biomass

All of the studies considered here, and most of the research so far reported in the literature, have correlated radar backscatter with forest biomass using single radar wavelength and polarisation combinations. Although some of the forests investigated are composed of broad-leaved and mixed broad-leaved/needle-leaved species, the majority of the sites are vegetated by managed, even-aged and mono-specific coniferous stands located in temperate zones. Due to known difficulties associated with rugged topography, the different forest areas selected as study sites are located in flat to moderately sloping areas.

Figures 4.1 to 4.4 show the interpolated data and results from the different studies. The data are presented in two main categories, one each for pines/conifers and broad-leaved stands. Here, only the L-HH and C-HV backscattering data are taken into account owing to the concepts discussed in Chapter 3. This qualification limited the number of cases considered, as only a few of the related investigations have used either or both of the L-HV and C-HV backscattering data. A maximum of 300 tonnes/ha was used in view of the typical saturation of radar measurements at all bands beyond this biomass level. For both L-HH and C-HV, σ° was observed to increase linearly with biomass until the saturation level for each of these wavelength-polarisation combinations is reached.

The TCBI and TCMI data corresponding to those plotted in Figures 4.1 to 4.4 are given in Tables 4.2 to 4.4. For easier visual comparison of the results, the data are likewise presented as graphs in Figures 4.5 and 4.6. The TCB and TCM indices were computed based on the intensity (or true) values of the individual backscattering data i.e., not decibels. The σ° values were converted into intensity values through the formula

$$x = 10^{\sigma^\circ/10} \qquad (4.1)$$

where x is the intensity or true value and σ° the backscattering coefficient (in decibel). No significant variation was observed between the TCBI and TCMI values within the same stand structure category from the different investigations. The similarity in the values of these indices occurred over the entire biomass range, except for some cases at low biomass levels, where inconsistent results were obtained. Factors such as strong influence of terrain/ground conditions on the radar backscatter due to low stand/crown component volume and density, may have caused these results. In general, at biomass levels below the radar saturation limits, positive linear relationships between total aboveground biomass and the two indices were observed. In comparing these index values, and all other results presented in this chapter, the effects on the data of factors such as dissimilarities in the radar systems used (e.g., viewing angle and platform altitude), discrepancies in the applied calibration methods, terrain variations, stand morphology, density and composition differences, and the possible errors introduced during the interpolation of the backscattering data and biomass levels, should however be noted.

The correlation between forest biomass and L-HH, C-HV and TCBI are presented in Table 4.5.

4.3.1 TCBI and total forest aboveground biomass

Table 4.5 indicates that in the case of C-HV, the use of TCBI (L-HH + C-HV) brought about a better correlation between radar backscatter and total forest biomass. On the other hand, in the case of L-HH, mixed results were obtained. Although much is still to be desired regarding both the number of cases and data considered, this finding is generally in support of the theory presented in the previous chapter (see equation 3.12).

Following are biomass equations derived based on linear regression analysis performed on the TCBI and biomass data from the various studies. The equations

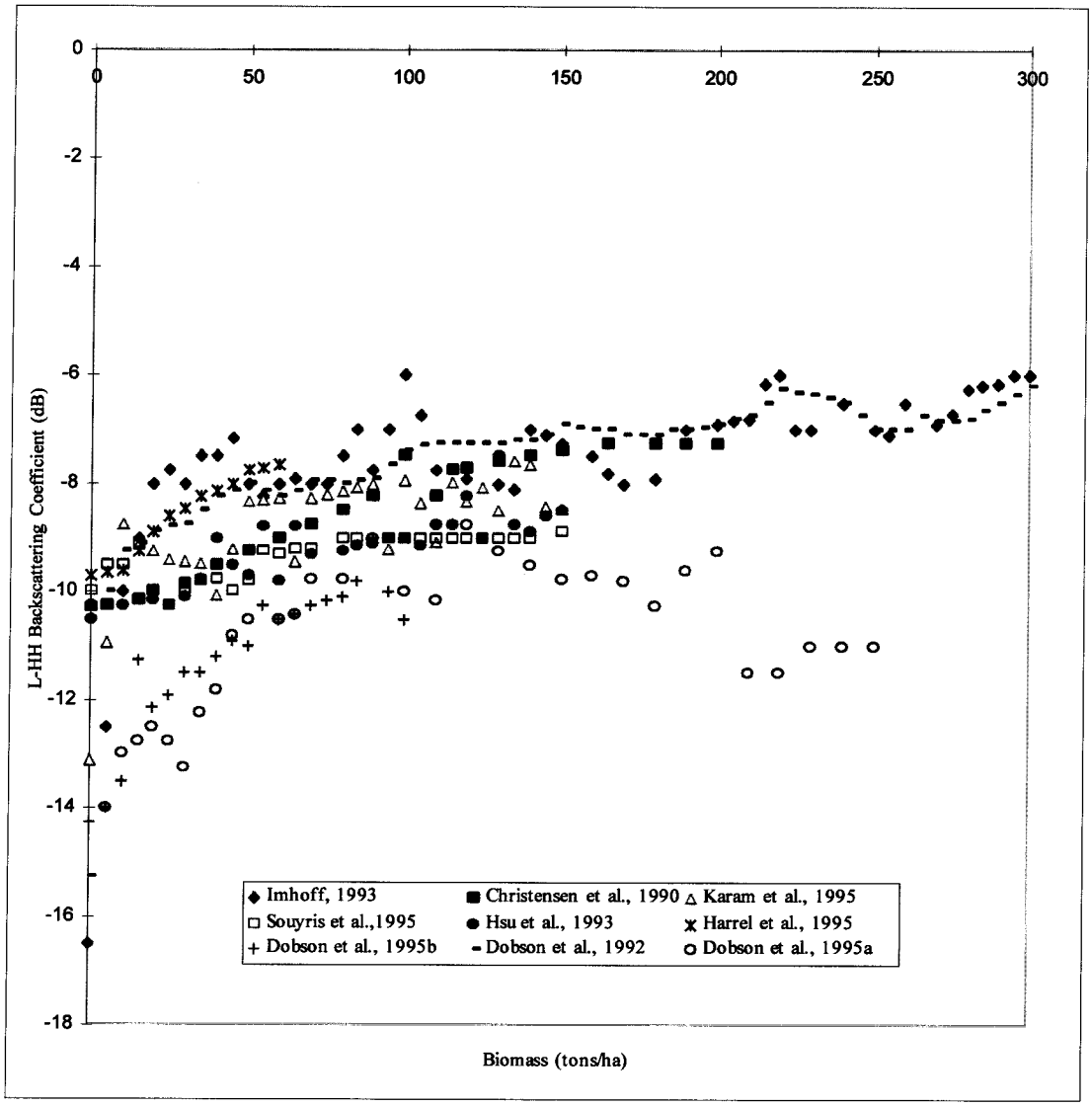

Figure 4.1 L-HH backscattering data for pines/conifers as interpolated from published research

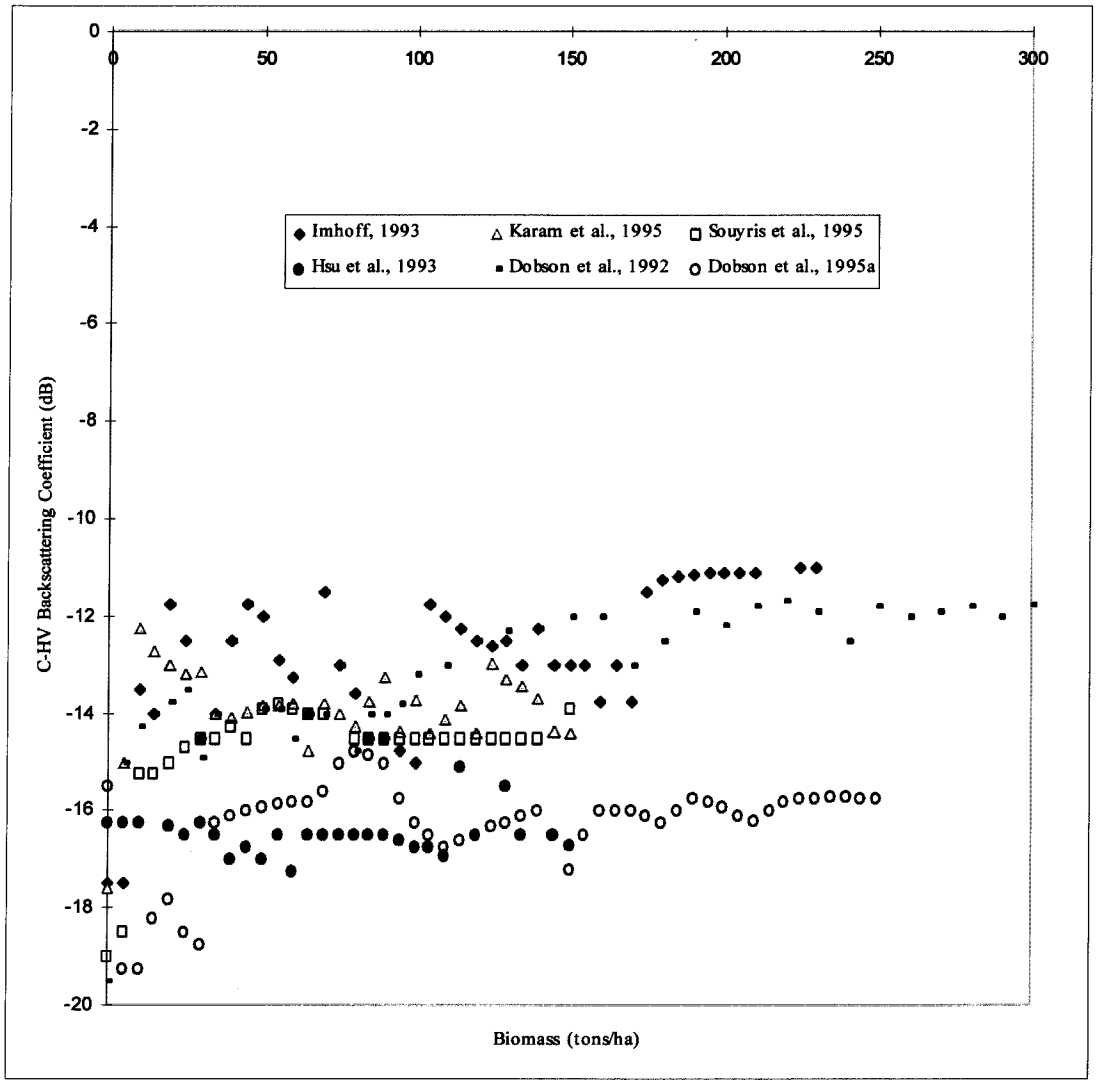

Figure 4.2 Interpolated C-HV data for pines/conifers

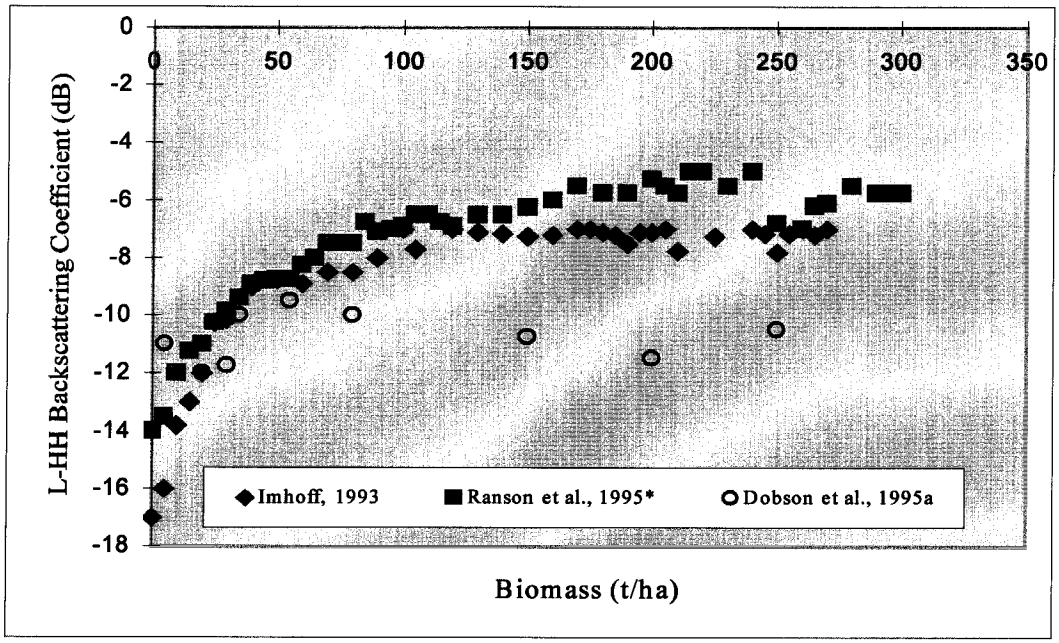

Figure 4.3 Interpolated L-HH data for broad-leaved evergreen/deciduous and mixed* stands

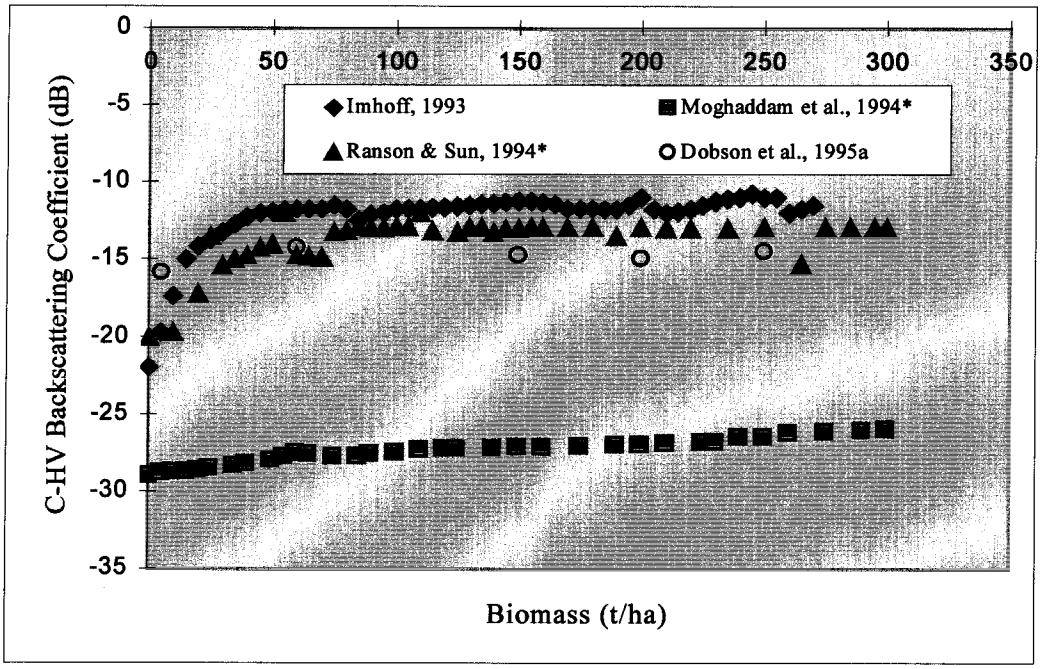

Figure 4.4 Interpolated C-HV data for broad-leaved and mixed* stands

BIOMASS (t/ha)	TCBI (L-HH + C-HV) : PINES/CONIFERS					
	Imhoff, 1993	Karam et al., 1995	Hsu et al., 1993	Souyris et al., 1995	Dobson et al., 1992	Dobson et al., 1995a
0	0.0402	0.0661	0.1128	0.1126	0.0411	0.1226
5	0.0740	0.1120		0.1263	0.1316	0.0517
10	0.1447	0.1923	0.1181	0.1421	0.1564	0.0620
15	0.1657	0.1765		0.1529	0.1628	0.0682
20	0.2253	0.1687	0.1200	0.1316	0.1710	0.0728
25	0.2241	0.1624	0.1168	0.1283	0.1765	0.0672
30	0.1940	0.1618	0.1214	0.1355	0.1657	0.0607
35	0.2176	0.1523	0.1283	0.1402	0.1811	0.0833
40	0.2341	0.1373	0.1458	0.1435	0.2059	0.0906
45	0.2596	0.1602	0.1333	0.1355	0.2199	0.1083
50	0.2216	0.1884	0.1271	0.1455	0.1992	0.1148
55	0.2009	0.1894	0.1542	0.1605	0.1938	
60	0.2058	0.1904	0.1235	0.1582	0.1851	0.1154
65	0.2020	0.1471	0.1542	0.1600	0.1929	0.1175
70	0.2293	0.1911	0.1399	0.1600	0.2001	0.1335
75	0.2086	0.1915			0.2104	
80	0.2215	0.1913	0.1412	0.1614	0.1920	0.1394
85	0.2350	0.1980	0.1440	0.1614	0.2001	
90	0.2034	0.2054	0.1454		0.2020	0.1575
95	0.2330	0.1566	0.1478	0.1614	0.2135	
100	0.2828	0.2028	0.1470	0.1614	0.2298	0.1237
105	0.2782	0.1825	0.1428	0.1614		
110	0.2310	0.1623	0.1538	0.1614	0.2385	0.1177
115		0.2004	0.1643	0.1614		
120	0.2184	0.1829	0.1720	0.1614	0.2446	0.1557
125		0.2062	0.1259	0.1614		
130	0.2147	0.1886	0.2060	0.1614	0.2472	0.1426
135	0.2050	0.2204	0.1557	0.1614		
140	0.2591	0.2150	0.1288	0.1614	0.2501	0.1373
145	0.2451	0.1804	0.1604			
150	0.2385	0.1785	0.1626	0.1696	0.2673	0.1250
155						
160	0.2200				0.2626	0.1323
165	0.2161					
170	0.2007				0.2451	0.1298
175						
180	0.2372				0.2512	0.1181
185						
190	0.2763				0.2641	0.1363
195						
200	0.2818				0.2644	0.1446
205	0.2842					
210	0.2866				0.2774	0.0948
215						
220					0.3047	0.0971
225	0.2790					
230	0.2790				0.2963	0.1060
235						
240					0.2801	0.1063
245						
250					0.2656	0.1060
255						
260					0.2626	
265						
270					0.2711	
275						
280					0.2750	
285						
290					0.2870	
295						
300					0.3067	

Table 4.2 TCBI values for pines/conifers from results of related research

BIOMASS (t/ha)	TCMI (L-HH / C-HV) : PINES/CONIFERS					
	Imhoff, 1993	Karam et al., 1995	Hsu et al., 1993	Souyris et al., 1995	Dobson et al., 1992	Dobson et al., 1995a
0	1.2589	2.8054	3.7584	7.9433	2.6607	3.3497
5	3.1623	2.5410		7.9433	3.1623	3.3497
10	2.2387	2.2284	3.9811	3.7584	3.1623	4.2170
15	3.1623	2.3014		4.1210	3.0903	3.5075
20	2.3714	2.3659	4.1210	3.1623	3.0549	3.3884
25	2.9854	2.3768	4.2170	2.7861	2.9512	3.7584
30	4.4668	2.3496	4.1210	2.8184	4.1210	3.5481
35	4.4668	2.8445	4.7315	2.9512	3.5481	2.5119
40	3.1623	2.5293	6.3096	2.8184	2.6607	2.6915
45	2.8840	3.0061	5.3088	2.8184	2.2909	3.3113
50	2.5119	3.5727	5.3703	2.5704	3.8905	3.4674
55	2.9174	3.5645	5.8884	2.8510	3.7584	
60	3.3497	3.5563	5.5590	2.8840	4.2170	3.3884
65	4.0738	3.4119	5.8884	3.0200	3.8459	3.4674
70	2.2387	3.5727	5.2481	3.0200	4.0272	3.8459
75	3.1623	3.8107			3.1989	
80	4.0738	4.1020	5.3088	3.5481	4.7315	3.1623
85	5.6234	3.7068	5.4325	3.5481	4.0272	
90	4.7315	3.3420	5.4954		4.0738	3.9811
95	5.9566	3.2734	5.7544	3.5481	4.1210	
100	7.9433	3.7757	5.9566	3.5481	3.8019	4.2170
105	3.1623	4.0272	5.7544	3.5481		
110	2.6607	3.1915	6.5313	3.5481	3.7584	4.5709
115		3.8637	4.3152	3.5481		
120	2.8840	4.0365	6.6834	3.5481	3.3497	5.9566
125		3.0761		3.5481		
130	2.8184	3.0409	6.3096	3.5481	3.1989	5.0119
135	3.0903	3.8548	5.9566	3.5481		
140	3.3497	4.0179		3.5481	3.1989	4.4668
145	3.8905	3.9355	6.1660			
150	3.7584	3.9174	6.6069	3.1623	3.2359	5.5590
155						
160	4.2170				3.1623	4.2658
165	3.3113					
170	3.7584				3.8905	4.1687
175						
180	2.1627				3.4674	3.9811
185						
190	2.6002				3.0903	4.1210
195						
200	2.6303				3.3884	4.6238
205	2.6607					
210	2.6915				3.1989	2.9512
215						
220					3.5075	2.6915
225	2.5119					
230	2.5119				3.5892	2.9854
235						
240					3.9811	2.9512
245						
250					3.0200	2.9854
255						
260					3.1623	
265						
270					3.1989	
275						
280					3.1623	
285						
290					3.5481	
295						
300					3.5892	

Table 4.3 TCMI values for pines/conifers from results of related research

BIOMASS (t/ha)	BROAD-LEAVED EVERGREEN/DECIDUOUS			
	TCBI (L-HH + C-HV)		TCMI (L-HH / C-HV)	
	Imhoff, 1993	Dobson et al., 1995a	Imhoff, 1993	Dobson et al., 1995a
0	0.0263		3.1623	
5	0.0357	0.1051	2.3714	3.0903
10	0.0600		2.2803	
15	0.0817		1.5849	
20	0.1016		1.6406	
25	0.1366		2.2387	
30	0.1439		2.0417	
35				
40	0.1855		2.1135	
45				
50	0.1979		2.0654	
55				
60	0.1957		1.9275	
65				
70	0.2081		2.1135	
75				
80	0.2081		2.1135	
85				
90	0.2201		2.5704	
95				
100	0.2664		2.9854	
105	0.2371		2.5235	
110				
115				
120	0.2687		2.8840	
125				
130	0.2658		2.7542	
135				
140	0.2652		2.6607	
145				
150	0.2634	0.1176	2.5119	2.5119
155				
160	0.2638		2.6002	
165				
170	0.2671		2.9512	
175	0.2671		2.9512	
180	0.2623		2.8973	
185	0.2574		2.8510	
190	0.2447		2.6607	
195	0.2658		2.7542	
200	0.2744	0.1024	2.4547	2.2387
205	0.2664		2.9854	
210	0.2310		2.6607	
215				
220				
225	0.2592		2.6607	
230				
235				
240	0.2790		2.5119	
245	0.2769		2.2909	
250	0.2454	0.1246	2.0893	2.5119
255	0.2722		2.4266	
260	0.2626		3.1623	
265	0.2574		2.8510	
270	0.2703		2.8184	
275				
280				
285				
290				
295				
300				

Table 4.4 TCBI and TCMI for broad-leaved stands from results of related research

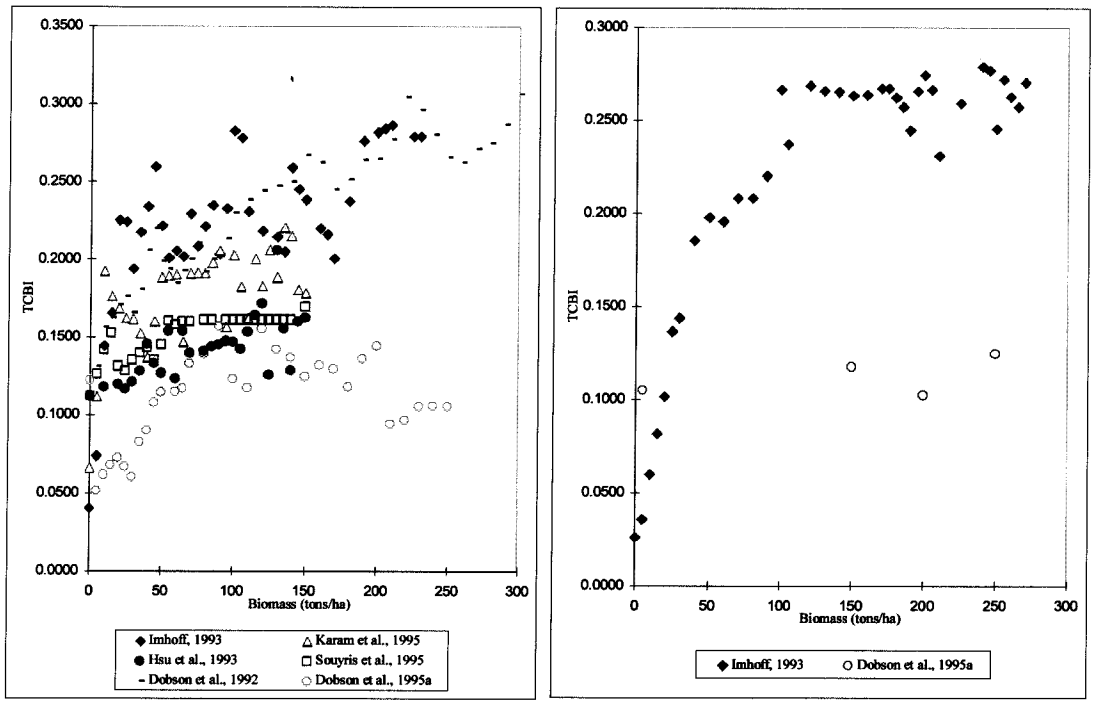

Figure 4.5 TCBI values against total aboveground biomass as computed from related studies for pines/conifers (left) and broad-leaved stands (right)

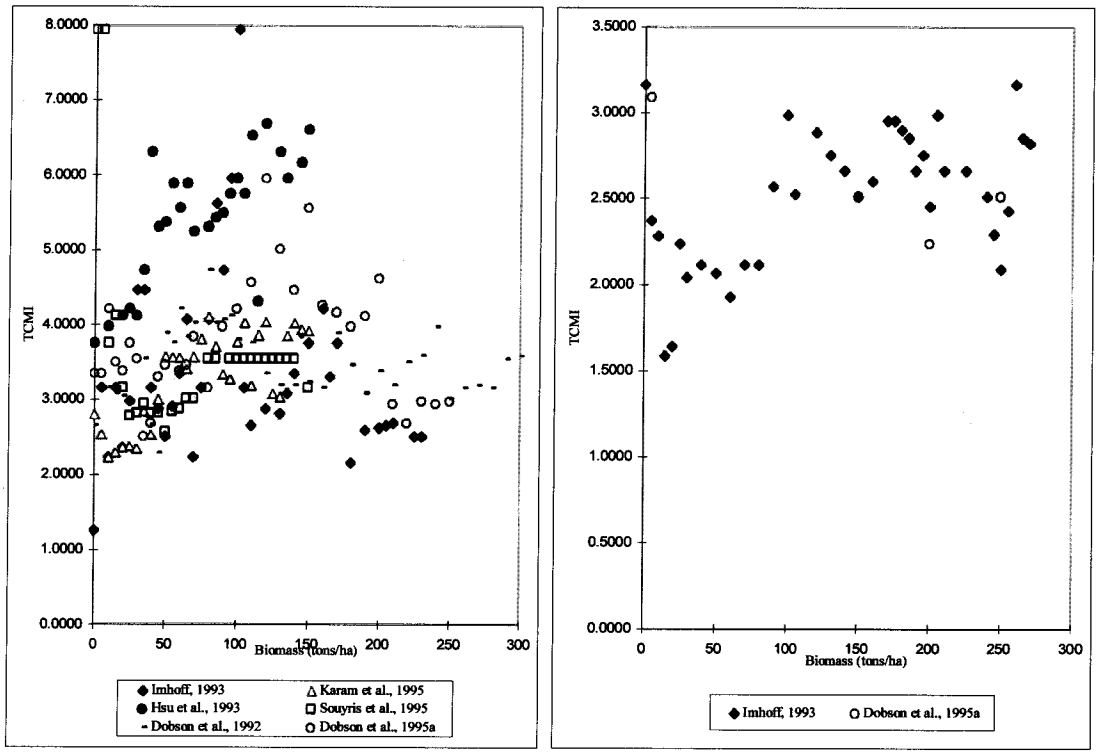

Figure 4.6 TCMI values for pines/conifers (left) and broad-leaved stands (right) plotted against total aboveground biomass

INVESTIGATOR/S	SAR Backscatter	CORRELATION COEFFICIENT			
		PINE / CONIFER		BROAD LEAF	
		Biomass (t/ha)		Biomass (t/ha)	
		0 - 300	20 - 150	0 - 300	20 - 150
1. IMHOFF, M.L.(1993)	L-HH	0.7354	0.3140	0.8219	0.9321
	C-HV	0.6378	0.0051	0.6801	0.7926
	L-HH+ C-HV	0.6579	0.3002	0.8134	0.9326
2. KARAM, M.A. ET AL. (1995)	L-HH	0.7004	0.6347		
	C-HV	-0.0369	-0.2083		
	L-HH+ C-HV	0.5990	0.5571		
3. HSU, C.C. ET AL. (1993)	L-HH	0.8086	0.7581		
	C-HV	0.1037	0.2417		
	L-HH+ C-HV	0.6792	0.6131		
4. SOUYRIS, J.C. ET AL. (1995)	L-HH	0.7907	0.8764		
	C-HV	0.4919	-0.0020		
	L-HH+ C-HV	0.8268	0.8289		
5. DOBSON, M.C. ET AL.(1992)	L-HH	0.8731	0.9705		
	C-HV	0.7952	0.4900		
	L-HH+ C-HV	0.8769	0.8996		
6. DOBSON, M.C. ET AL.(1995a)	L-HH	0.4037	0.8320	0.0182	0.2317
	C-HV	0.3737	0.1329	0.4431	
	L-HH+ C-HV	0.4320	0.7759	0.5345	0.7759
7. DOBSON, M.C. ET AL. (1995b)	L-HH		0.7999		
8. HARREL, P.A. ET AL. (1995)	L-HH	0.9888	0.9879		
9. CHRISTENSEN ET AL. (1990)	L-HH	0.9665	0.9659		
10. MOGHADDAM, ET AL.(1994)	C-HV*			0.9744	
11. RANSON & SUN (1994)	C-HV*			0.5113	0.6393
12. RANSON ET AL. (1995)	L-HH*			0.8544	0.9557

Note: * = Mixed pine and broad-leaved forest vegetation

Table 4.5 Correlation between forest biomass and L-HH, C-HV and L-HH + C-HV backscatter

are specific to the stand structural class and are thus grouped into two categories, one set each for needle-leaved and broad-leaved stands.

PINES/CONIFERS

Imhoff, 1993 : Biomass = 866.75 TCBI - 89.69 (4.2)
R = 0.6580; Std. Error = 51.4997

Karam et al., 1995 : Biomass = 873.28 TCBI - 78.78 (4.3)
R = 0.5990; Std. Error = 37.0253

Hsu et al., 1993 : Biomass = 1476.90 TCBI - 131.00 (4.4)
R = 0.6792; Std. Error = 33.1052

Souyris et al., 1995 : Biomass = 2609.60 TCBI - 323.09 (4.5)
R = 0.8267; Std. Error = 26.2516

Dobson et al., 1992 : Biomass = 1495.00 TCBI - 209.59 (4.6)
R = 0.8769; Std. Error = 44.3426

Dobson et al., 1995a : Biomass = 1176.20 TCBI - 22.57 (4.7)
R = 0.4320; Std. Error = 71.9721

BROAD-LEAVED STANDS

Imhoff, 1993 : Biomass = 973.50 TCBI - 74.48 (4.8)
R = 0.8134; Std. Error = 51.4492

Dobson et al., 1995a : Biomass = 5396.50 TCBI - 455.58 (4.9)
R = 0.5345; Std. Error = 109.4144

While the regression equation for pines/conifers generated from the results of Souyris et al. (1995) had a somewhat higher multiplicative coefficient, similarities could be observed between the equations from Imhoff (1993) and Karam et al. (1995), and from Hsu et al. (1993), Dobson et al. (1992) and Dobson et al. (1995a). The discrepancies between these groups of equations could be attributed to radar system differences and other reasons specified in Section 4.3. The differences in the equations generated for broad-leaved stands from Imhoff (1993) and Dobson et al. (1995a) are significant. However, it should be noted that the latter equation was based on four biomass values only. The highest correlation with biomass (0.8769) was exhibited by that from Dobson et al. (1992), with the equation explaining 77 % of the biomass variation.

Given in Table 4.6 are the TCBI values averaged over the entire biomass range for each of the studies. A comparison of the average biomass between coniferous stands from the different studies, and between coniferous and broad-leaved stands, could be made by using these values as inputs to the corresponding biomass formulas given in equations 4.2 to 4.9.

It can be discerned from the table below that the TCBI values from the results of Imhoff (1993) and Dobson et al. (1995a) for pines/conifers and broad-leaved stands are nearly identical. This was most probably caused by the averaging process, which took into consideration the extreme values within the 0 -300 tonnes/ha biomass range. Moreover, in the case of Dobson et al. (1995a), the insufficiency of available data may also have contributed to the similarity of the averaged results.

4.4 Radar backscatter versus forest stand structure

Radar backscatter is mainly influenced by the geometric properties of the target. As stated above, forest stands with the same biomass but dissimilar morphology may produce different backscatter readings. Hence, radar data-based equations to estimate total aboveground biomass should be tailored according to the

general structure of the forest stand under consideration. Although the importance of determining the stand structure prior to generating radar-derived estimates of forest biomass was emphasised in some of the studies (e.g., Imhoff, 1993; Dobson et al.,1995a), not one of the investigations reviewed here have considered stand structure determination through the use of radar backscattering data. In the absence of prior information on stand structure, radar data-based techniques, such as the application of TCMI, is deemed essential.

Author/s	Average TCBI Value	
	Pines/conifers	Broad-leaved stands
1. Imhoff, 1993	0.2224	0.2187
2. Karam et al., 1995	0.1761	
3. Hsu et al., 1993	0.1426	
4. Souyris et al., 1995	0.1514	
5. Dobson et al., 1992	0.2242	
6. Dobson et al., 1995a	0.1106	0.1125

Table 4.6. Average TCBI values for coniferous and broad-leaved stands as computed from interpolated results of different studies

4.4.1 TCMI and stand structure

The applicability of TCMI, which is the true ratio between the L-HH and C-HV backscatter, as a possible measure of stand morphology is premised on the differences in the sensitivity of the two wavelength-polarisation combinations to the various tree components. Higher TCMI values are expected for conifers given their bigger trunk and smaller crown component volume compared to their broad-leaved counterpart. This theory has been proven to be generally true based on the test applied using interpolated backscatter and biomass values from related

investigations albeit an overlapping of some of the values was observed. The overlaps between the conifer and broad-leaved stand TCMI points, as can be seen from Tables 4.2 to 4.3 and Figure 4.7, occur at the lower and higher part of the biomass range. This is quite expected due to the minor differences in vegetation structure at low biomass levels and the saturation of radar measurements at high amounts of biomass. The usefulness of TCMI is thus at its optimum when there is a distinct difference in structure between the broad-leaved and needle-leaved trees and the backscattering data are taken at biomass levels below the radar saturation limits.

To further illustrate the usefulness of the TCMI in accounting for the difference in structure between broad-leaved and needle-leaved stands, given in Figure 4.8 are the graphs corresponding to those in Figure 4.7 but with the L-HH and C-HV data limited to those taken within a biomass range of 20 to 150 tonnes/ha. By adjusting the lower and higher ends of the biomass range to these levels, the probability that the broad-leaved and needle-leaved trees are more structurally defined, and that the radar measurements are less affected by saturation limits, is increased - and so is the effectiveness of the TCMI. As can be discerned from the figure, the overlapping TCMI points that exist in Figure 4.7 have been eliminated in the case of the lower graph (Dobson's) and were greatly reduced in the case of the upper chart (Imhoff's). For a similar purpose, given below are the average TCMI values within the 0 to 300 tonnes/ha and 20 to 150 tonnes/ha biomass range for the different studies. The 20 to 150 tonnes/ha range caused a higher dynamic range between the TCMI values, and hence a better separation, of the pine and broad-leaved stands. Interestingly, the average TCMI values generated from the different investigations for pines/conifers, except those from Hsu et al. (1993), are similar though the data were taken from different study sites and conditions. The same observation holds true in the case of the values from the broad-leaved stands.

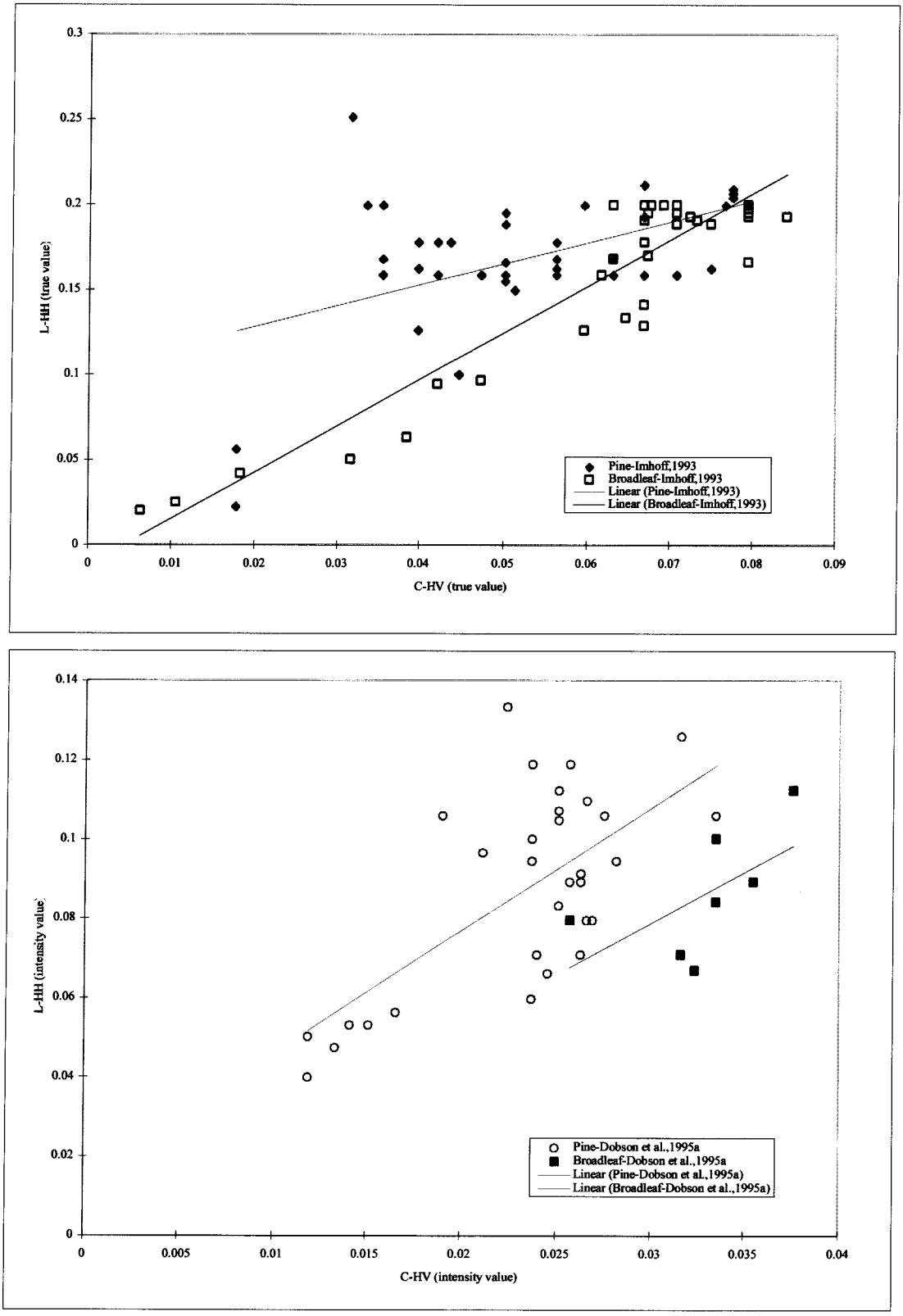

Figure 4.7 Stand structure determination based on the TCMI values interpolated from Imhoff, 1993 (top) and Dobson et al., 1995a (bottom)

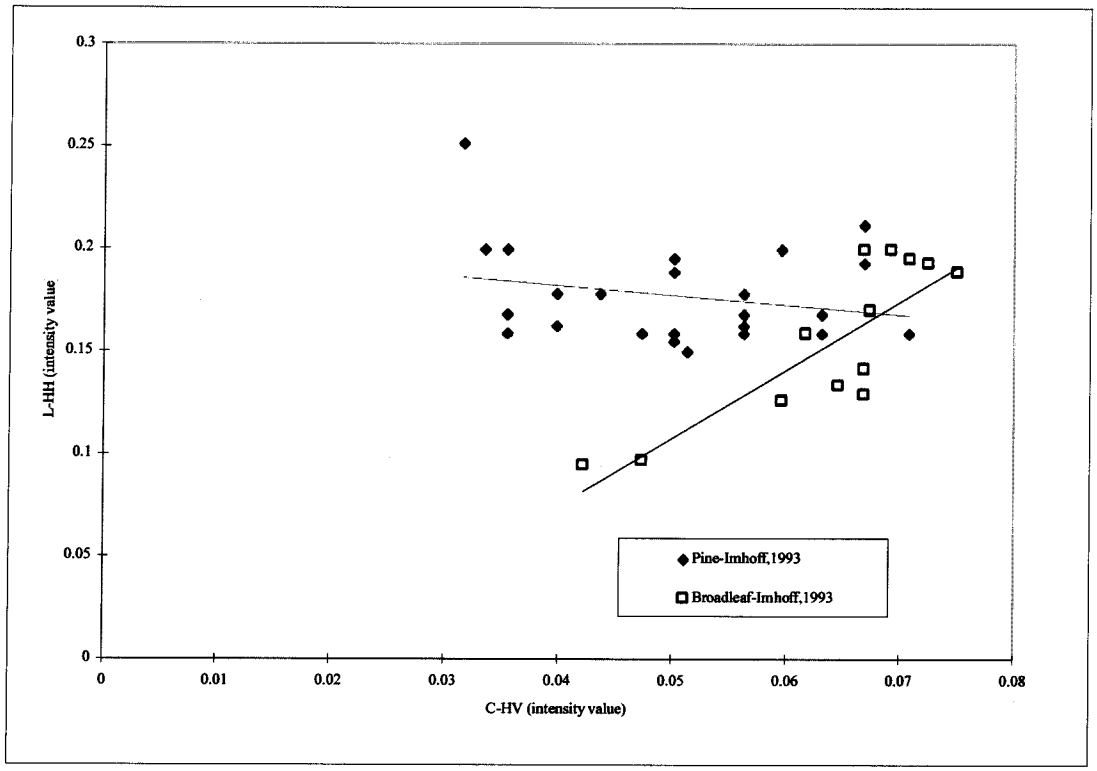

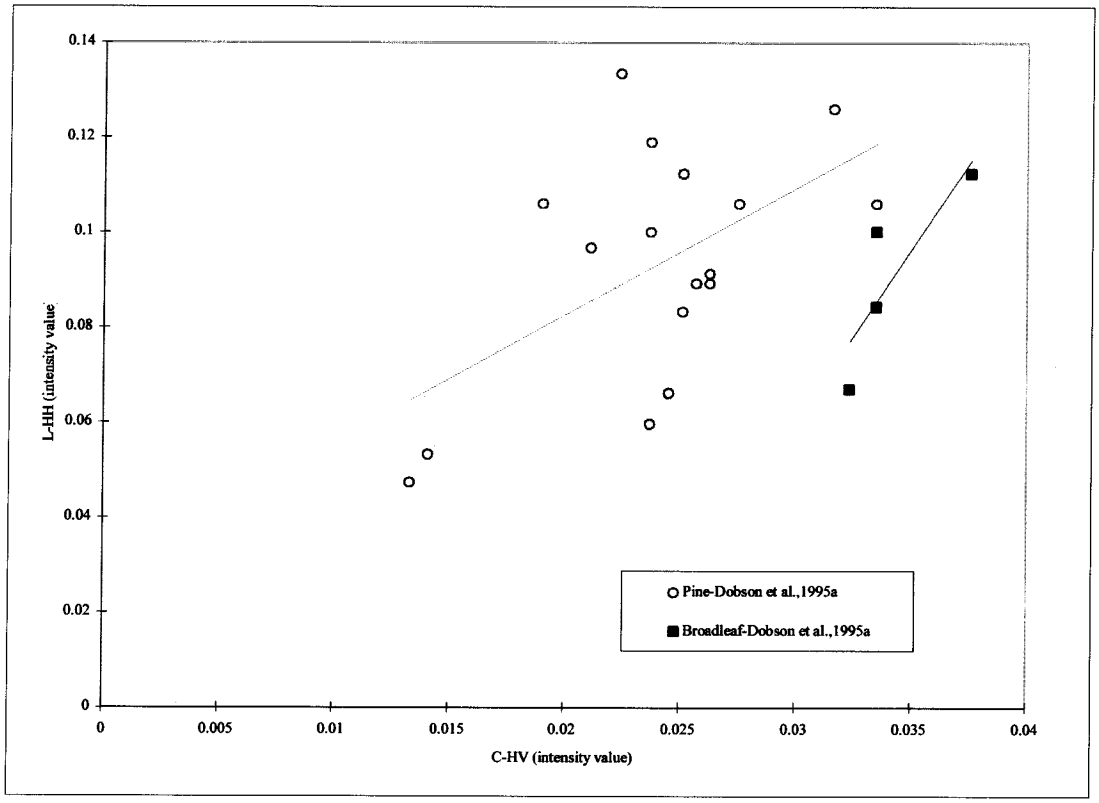

Figure 4.8 Stand structure determination based on the TCMI values within a 20 to 150 t/ha biomass range from Imhoff, 1993 (top) and Dobson et al.,1995a (bottom)

4.5 Relating stand age to TCBI and TCMI

The quantity and distribution of biomass within a tree are related to its age. When young, the total aboveground biomass is expected to be low and there is not much difference between the amounts of foliar and woody biomass. The structure is not yet defined and it is very difficult to differentiate between needle-leaved and broad-leaved trees based on radar data. The total aboveground biomass increases with age until a species-dependent maturity age is reached. Also, the structure becomes more defined with age. The increase in woody biomass is much greater than foliar biomass such that at maturity, the former typically accounts for more than 90% of the total aboveground biomass (Dobson et al., 1992). Relating these concepts with TCBI and TCMI, it can then be concluded that a) TCBI has a positive linear correlation with age, until the saturation limit is reached, at which the value of TCBI becomes constant, and b) TCMI varies with age except during the young and mature stages of the stand, where the value of the TCMI remains relatively constant. It should be emphasised, however, that these conclusions more specifically apply to even-aged stands.

Author/s	Average TCMI Value			
	Pines/conifers		Broad-leaved stands	
	0 - 300	20 - 150	0 - 300	20 - 150
1. Imhoff, 1993	3.3695	3.7013	2.5168	2.3430
2. Karam et al., 1995	3.2902	3.4119		
3. Hsu et al., 1993	5.4144	5.5431		
4. Souyris et al., 1995	3.6145	3.2267		
5. Dobson et al., 1992	3.4657	3.5937		
6. Dobson et al., 1995a	3.7642	3.9058	2.5882	2.5119

Table 4.7. Average TCMI values within biomass ranges of 0 to 300 t/ha and 20 to 150 t/ha for the different studies

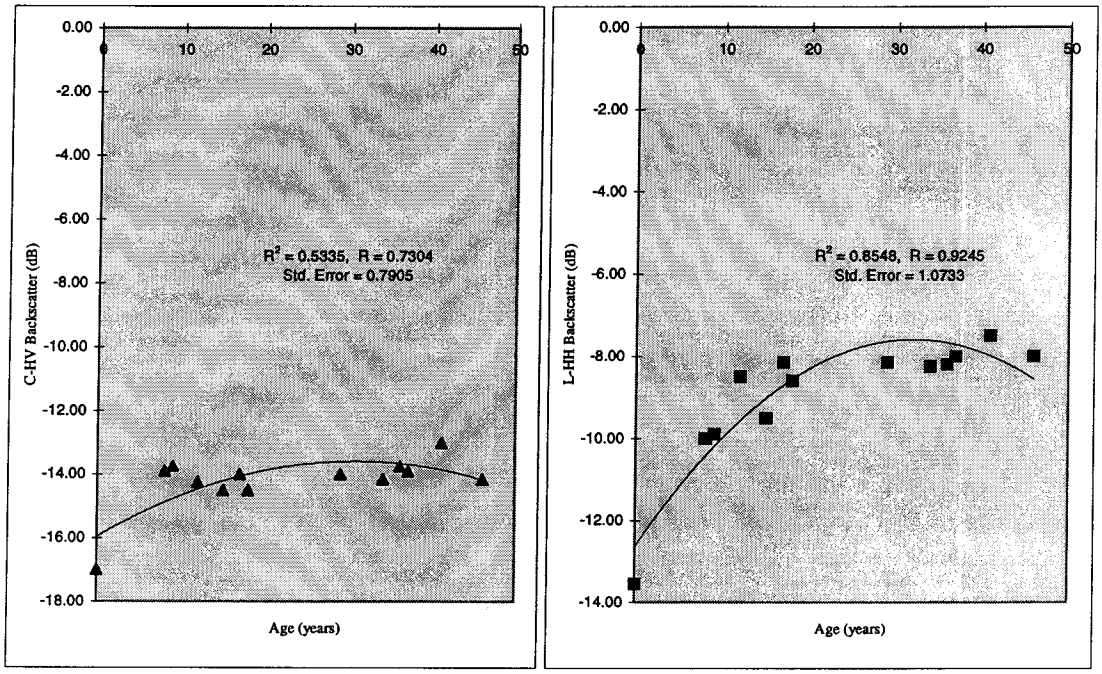

Figure 4.9 Measured C-HV (left) and L-HH (right) backscatter as a function of coniferous stand age (from Karam et al., 1995)

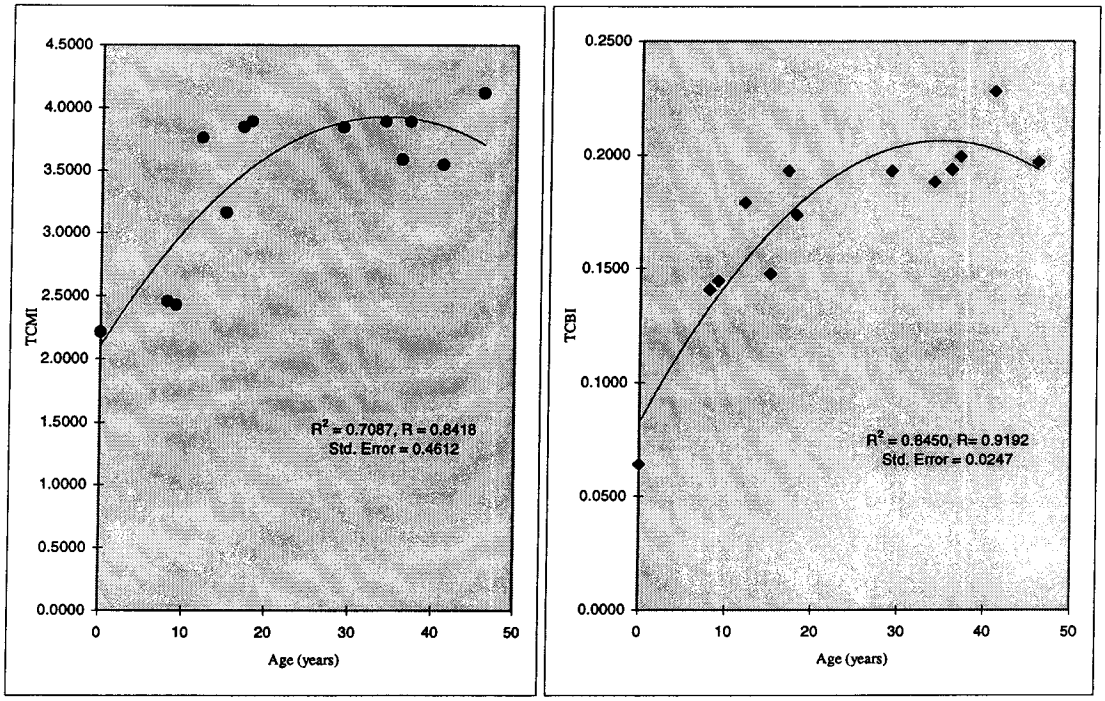

Figure 4.10 TCMI (left) and TCBI value (right) computed from the Fig. 4.9 graphs and plotted against stand age

4.6 Summary and conclusions

The assessment of the effectiveness of previously introduced theories carried out in this chapter based on interpolated data from published research produced promising results. TCMI has been found to provide a good measure of the general stand structure that is deemed necessary prior to the application of biomass estimation techniques. The overlapping of the TCMI values of the needle-leaved and broad-leaved stands, which occurred at both ends of the forest biomass range could be explained by the near homogeneity in structure of the stands at low biomass levels and the saturation of radar measurements at high amounts of biomass. In terms of biomass estimation, a higher correlation between TCBI and forest biomass was achieved compared to that of C-HV in all of the studies considered but mixed results were obtained in the case of L-HH. TCBI and TCMI have been shown to have a positive relationship with stand age until the values remain relatively constant due to either stand maturity or radar measurement saturation. Comparison of the results is made difficult by the limitations both in the number of related studies reported in the literature and in the amount of data available from each of the studies, inherent differences in the radar systems used, differences in the applied calibration techniques, in-situ variations (i.e., in terms of stand structure and composition, topography and other terrain features) and possible interpolation-related errors. Nevertheless, given all of these limitations, the results support the theories proposed in Chapter 3.

CHAPTER 5

STUDY SITES AND EXPERIMENTAL DATA

5.1 Introduction

Further testing of the validity of the radar concepts introduced and applied in the previous chapters and the conduct of supplementary forest vegetation-radar backscatter analysis necessitate the use of more comprehensive data from independent study sites. For these purposes, a portion of the Blue Mountains National Park in New South Wales and a pine plantation in the Gippsland Region in Victoria, both in Australia, were selected. These sites were used for correlating radar backscatter with broad-leaved and needle-leaved vegetation parameters, respectively. Besides vegetation structure and composition, other criteria used in the selection of the test sites include the availability of radar images, terrain conditions, and accessibility. Validation and additional analysis of the relationship between vegetation and radar backscatter were carried out using field measurements, allometric equations, and the corresponding AIRSAR quadpolarised radar data for the study areas.

Section 5.2 describes the study sites in terms of area and location, geology, topography, landform, climate, flora and fauna. Also described in this section are the specific forest parameters measured in the field, the data collection procedures applied, and the radar data utilised for the investigation. Details pertaining to the ancillary information sources employed to facilitate data analysis are given in Section 5.3.

5.1.1 The NASA/JPL AIRSAR

The Airborne Synthetic Aperture Radar (AIRSAR) is a side-looking imaging radar system developed by the Jet Propulsion Laboratory of the National Aeronautics and Space Administration in Pasadena, California. The all-weather radar system, carried aboard a DC-8 aircraft, is capable of operating at P-band (68 cm), L-band (24 cm) and C-band (5.6 cm) in full polarimetric mode (i.e., HH, VV, HV, and VH). These capabilities provide for the acquisition of data at different frequency and polarisation transmit-receive combinations, called radar bands or channels, for a wide variety of applications. The aircraft flies at a nominal altitude of 8000 m and a nominal velocity of 250 m per second. The data is in a compressed Stokes matrix format. Each pixel has 10 bytes of data and spacing between pixels is usually at 10 m in both the range and azimuth direction. All the radar data bands are concurrently recorded by the sensor and are later processed as coregistered images.

5.2 Description of study site 1 : Blue Mountains National Park, New South Wales, Australia

5.2.1 Location

One of the two areas used for the study lies at the eastern edge of the Lower Blue Mountains National Park, a park well-known for its spectacular sandstone cliffs, gorges, densely wooded valleys and mountains, that when viewed from a distance exhibit a blue haze which changes with light and weather. The study site is located about 65 kilometres west of Sydney in New South Wales, Australia. It is bounded by UTM (Australian Map Grid) coordinates 6255000 - 6261000 North and 279000 - 282000 East (33^0 49' 26'' to 33^0 46' 13'' North and 150^0 36' 43'' to 150^0 38' 45'' East), covering an area of around 1,800 hectares (3 km x 6 km). Roughly 60 - 70 % of the area is forested while the rest is composed of grasslands/clearings, water bodies, walking tracks, barren cliffs and gorges. The location map for the area is given in Figure 5.1.

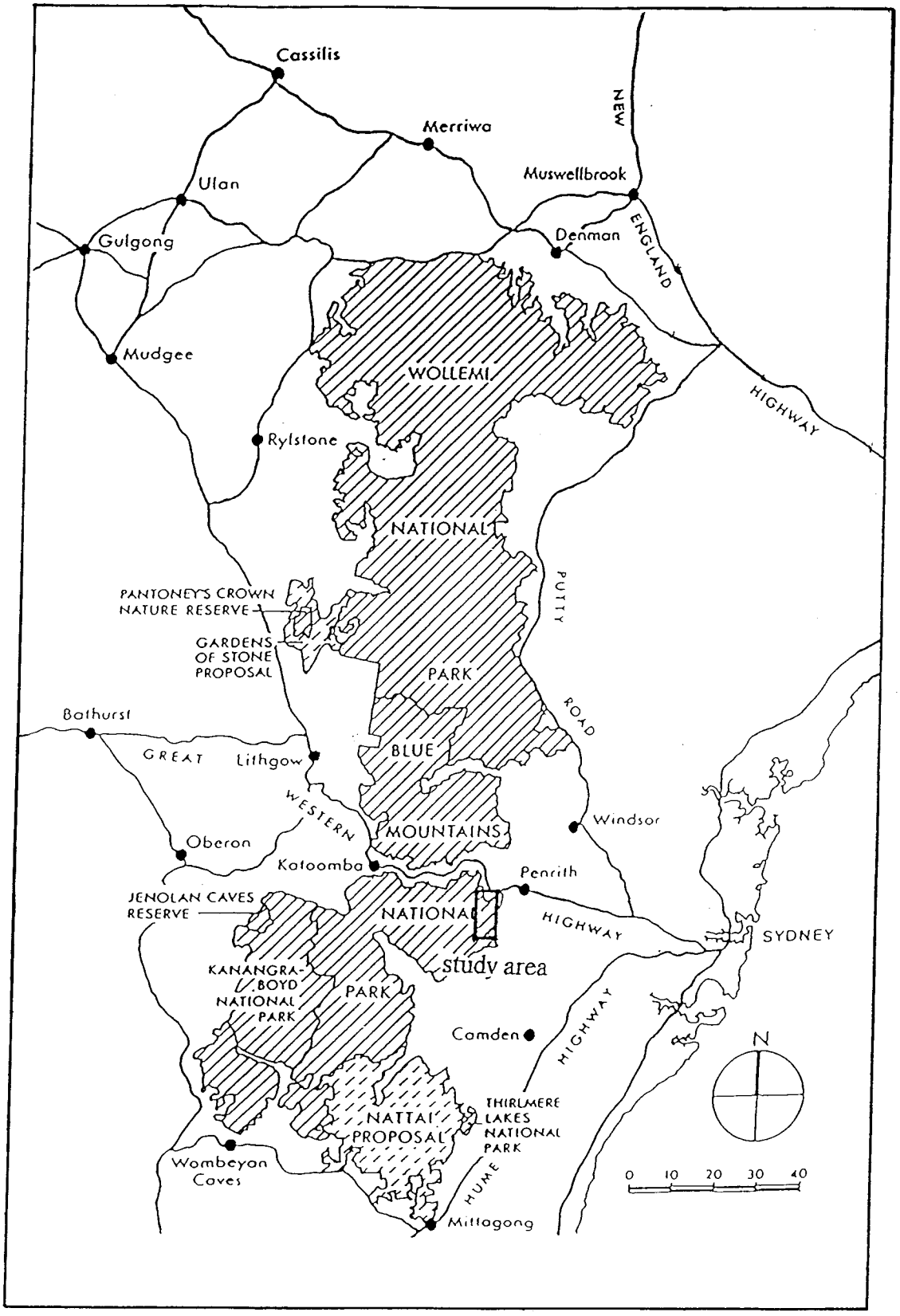

Figure 5.1 Location of study site 1

5.2.2 Geology, landform and topography

The Blue Mountains is basically a huge landscape of plateau surfaces, cliffs and valleys, capped by thick layers of brown and yellow sandstone with thin stratum of red and grey shale embedded in between. The predominant plateau surfaces, especially those draped by shale or basalt, are generally broad though a considerable amount of relief and stepped profiles resulting from erosion of sandstone and claystone measures could be observed (Mosley, 1989). The relatively high weathering resistance of limestone and karst rocks, coupled with fracturing along joint places, brought about the formation of splendid-looking cliffs that contain numerous caves. Rocks beneath the cliffs are of the softer and finer-grained type and are made up of grey and pink shales with random sandstone beds and coal seams (BMRTO,1997). The appearance and composition of the valleys vary depending primarily on the type/s of rocks and minerals the rivers and streams come in contact with. Mosley (1989), for example, noted the "V" cross-section of the Hawkesbury Sandstone compared to the characteristic benched profile of the alternating sandstone and claystone of the Narrabeen Group. He also pointed differences in width between the two areas, with the valleys under the latter reaching a width of up to three kilometres compared to the downstream valleys under the former that are just about 500 metres wide. In general, the common materials lining the rivers and valleys are sandstone blocks and gravelly sand.

Except for a few steep inclines along Mt. Portal and both sides of the Nepean River and its tributaries, the study site is generally characterised by a flat to undulating land surface with gentle slopes. The average elevation is from 160 to 180 metres above sea level with the ridges forming Mt. Portal and the water channel sides rising to a maximum height of 236 to 242 metres.

5.2.3 Climate

The Blue Mountains has a more temperate climate compared to that of the lower Sydney region. In the winter months of June, July and August, the average temperature in the Upper Blue Mountains is about 5^0 C. This drops to around 18^0 C

during the summer months of December, January and February. Given in Figure 5.2 are the average temperatures in the Upper and Lower Blue Mountains region while in Figure 5.3 are the average maximum and minimum monthly temperatures within Katoomba, a city within the Blue Mountains region. As can be seen from the figures, the climate in the Lower Blue Mountains, where the study site is located, is much warmer than in the Upper Blue Mountains area. In here, the average temperature is 16^0 C during winter and 29^0 C in summer. Katoomba, being within the Upper area, has lower mean temperatures, with winter and summer averaging at 6.9^0 C and 17.7^0 C, respectively.

The continual contact between the uplifting air masses and the mountains contributes to a higher incidence of rainfall within the Blue Mountains than in Sydney. An average rainfall of around 1050 mm/year and 850 mm/year are recorded for the Upper and Lower Blue Mountains, respectively. Shown in the graphs below are the average monthly rainfall (Figure 5.4) and average number of rain days per month (Figure 5.5) in the city of Katoomba. The city receives an average rainfall of 97 mm/month in winter and 153 mm/month in summer. The average number of rain days per month during winter and summer are 9 and 12, respectively. Despite the cool temperatures, there are only around 5 snow days per year in the upper mountains and it is very uncommon to see snow at the lower areas (Blue Mountains Web, 1998).

5.2.4 Natural vegetation and fauna

The area's main vegetation is the open eucalypt forest although a great diversity of plant species is present. Among the dominant tree species are the Red Ironbark (*Eucalyptus sideroxylon*), Broad-leaved Red Ironbark (*Eucalyptus siderophloia*), Narrow-leaved Red Ironbark (*Eucalyptus creba*), Grey Ironbark (*Eucalyptus paniculata*), Red Mahogany (*Eucalyptus resinifera*), Scribbly Gum (*Eucalyptus micrantha*), Manna Gum (*Eucalyptus viminalis*), Spotted Gum (*Eucalyptus maculata*), Turpentine (*Syncarpia glomulifera*), Paperbark (Malaleuca

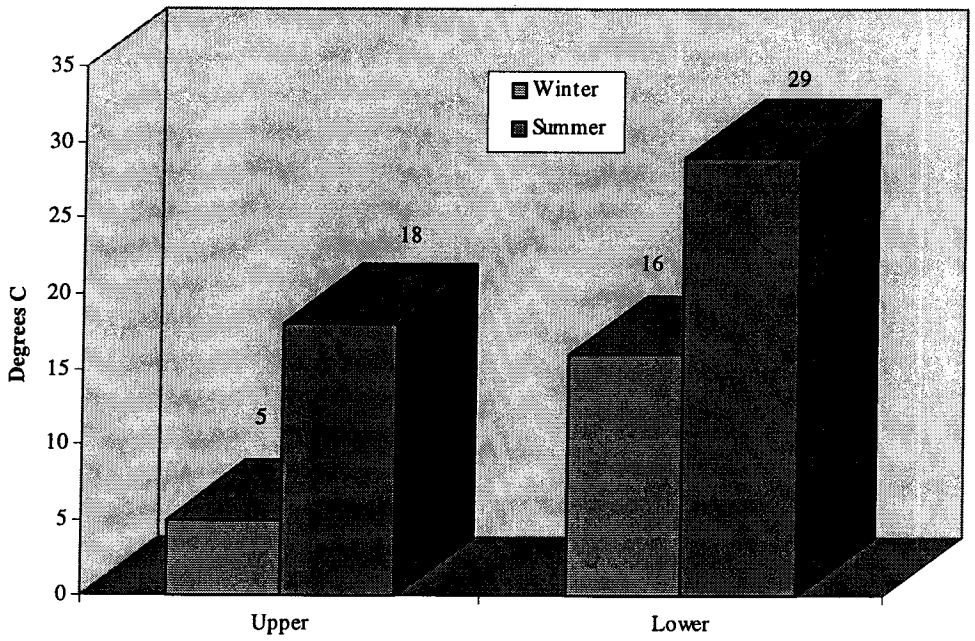

Figure 5.2 Average temperature in the Upper and Lower Blue Mountains
Source: http://www.bluemts.com.au/

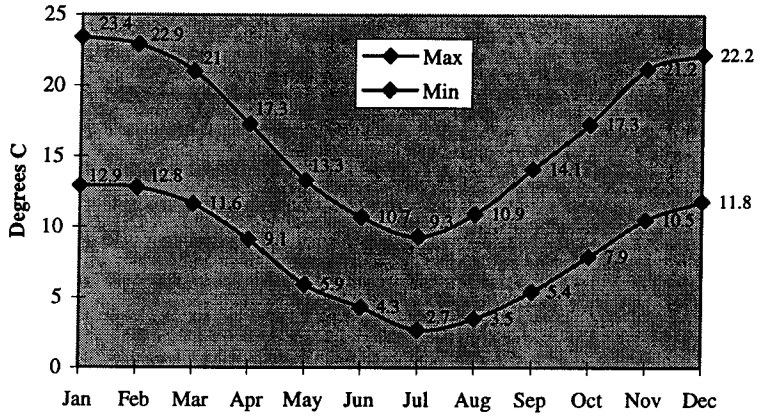

Figure 5.3 Average maximum and minimum monthly temperatures in Katoomba
Source: http://www.bluemts.com.au/

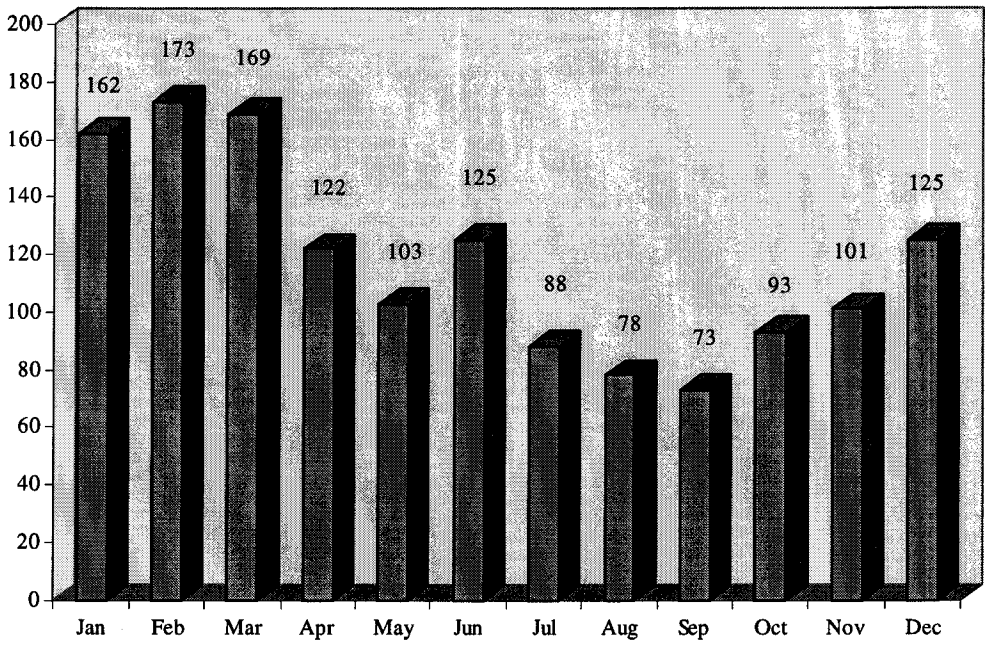

Figure 5.4 Average rainfall (in mm) for each month of the year in Katoomba
Source: http://www.bluemts.com.au/

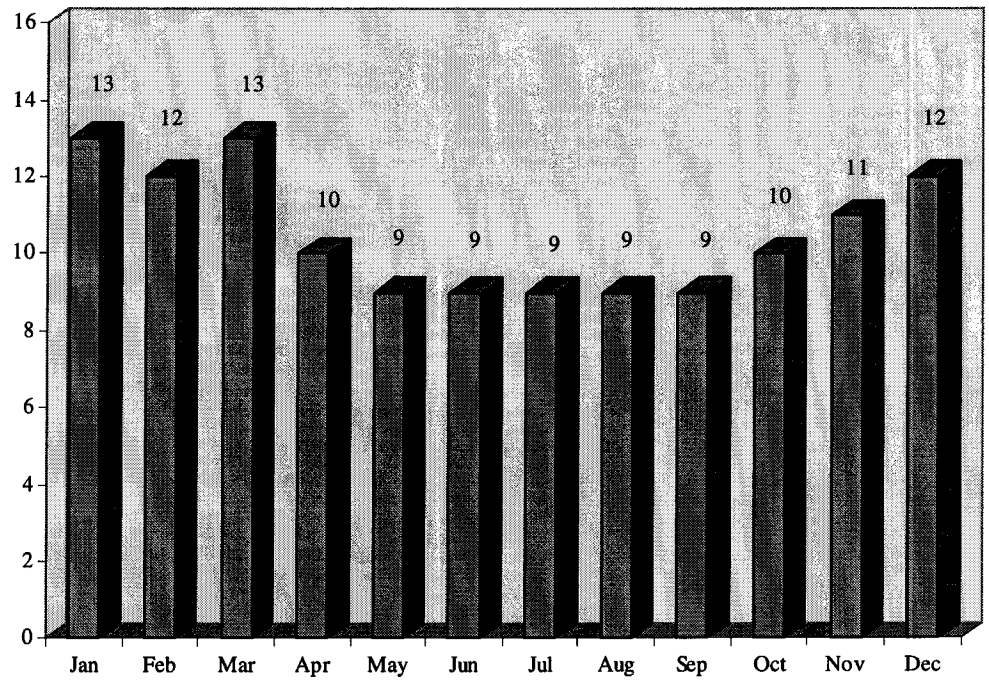

Figure 5.5 Average number of rain days for each month of the year in Katoomba
Source: http://www.bluemts.com.au/

linariifolia), Woollybutt (*Eucalyptus longifolia*), Red Bloodwood (*Eucalyptus gummifera*), Forest Red Gum (*Eucalyptus tereticornis*), Black Box (*Eucalyptus largiflorens*), Narrow-leaved Peppermint (*Eucalyptus robertsoni*), Paperbark (*Melaleuca linariifolia*), Swamp Gum (*Eucalyptus ovata*), River Red Gum (*Eucalyptus camaldulensis*), Sydney Blue Gum (Eucalyptus saligna), and the White Cypress Pine (*Callitris hugelii*). Various species of shrubs grow intermittently at the understory level and in sites where trees are absent either due to low soil nutrient and moisture, as well as in low anchorage sites such as rock ridge tops and cliff edges . These include the Waratah (*Telopea speciosissima*), Wattles (*Acacia spp.*), Sundrews (*Drosera spp.*), Bladderworts (*Utricularia spp.*), Mountain Devil (*Lambertia formosa*), She Oak (*Casuarina distyla*), Heath Banksia (*Banksia ericifolia*), Blue Mountains Mallee Ash (*Eucalyptus stricta*), and the Stunted She Oak (*Casuarina nana*).

With the rich flora, and the noted close association between vegetation and animals, comes a wide variety of fauna. The majority of the animals that thrive in the area feed on plant components such as leaves, fruits, lichens, nectar and seeds, though few carnivores have been observed. Some of the examples identified by Mosley (1989) are the a) fruit-eating Gang-gang and Yellow-tailed Black Cockatoo, Grey-headed and Little Red flying fox, Mountain Bushtail Possum, King Parrot, Crimson Rosella, and Wonga Pigeon; b) leaf-eating Koalas, Greater Glider, Eastern Grey Kangaroo, Red-necked Wallaby, Wallaroo, Common Wombat, and the Mountain Brushtail Possum (with some of these feeding on fruits and lichens as well); c) nectar-eating New Holland Honeyeater, White-eared Honeyeater, Lewin Honeyeater, Eastern Pygmy Possum, Feather-tailed Glider, Sugar Glider, and the Squirrel Glider; d) leaf litter-eating Superb Lyrebird, Bell miner and the Eastern Whipbird; e) ant-eating Long-nosed Bandicoot and the Short-beaked Echidna; f) seed-eating Tawny Grassbird and the beautiful Firetail; g) insect eating White-throated Treecreeper and the Striated Thornbill; and g) few carnivores such as the Wedge-tailed Eagle, Peregrine Falcon, Tiger Cat, several species of owl (Tawny Frogmouth, Bobook, Masked, Sooty, Powerful, and Barking), frogs, snakes (Red-bellied Black snake, Brown Tree Snake, and the Broad-headed Snake), other reptiles

such as the Eastern Water Dragon, Goanna, Bearded Dragon, Diamond Python, and the rare Pink-tongued lizard.

5.3 Experimental data for study site 1

5.3.1 Multi-frequency quadpolarised radar data

On November 8, 1996, the NASA/JPL AIRSAR system recorded quadpolarised synthetic aperture radar data at P-, L- and C- bands over the western part of Sydney, with near and far incidence angles of 22.4^0 and 62.1^0, respectively. Taken at an altitude of 8,055.6 m, the radar scene has a cross-track swath of 8.5 km and an along-track swath of 59.5 km with the centre coordinates at latitude 33.79^0 North and longitude 150.98^0 East. The data set was processed at NASA/JPL on July 16, 1997. Included in the procedure is the multi-looking of the image to 18 looks in the azimuth direction to reduce the occurrence of speckles and the calibration of the data. A calibration factor of -108.35 dB was applied on both the HH and VH while a factor of -108.50 dB was used on HV and VV data.

5.3.2 Field data

Intensive fieldwork was conducted during the months of September and October, 1998 to obtain in situ data for the vegetation-radar backscatter analysis. Prior to the conduct of the fieldwork, geo-referenced TCBI, TCMI and other radar images of various frequency-polarisation combinations were generated using the ENVI software and were visually analysed for orientation, identification of landmarks and familiarisation with other recognisable features within the study site. The procedure also allowed preliminary partitioning of the vegetated sites into different segments or strata based on backscatter and colour variations. Stratum boundaries and their approximate coordinates were likewise defined based on these variations. Sample plots were then randomly fixed in each of the representative segments making sure that the plots are well within the limits of the segments. Using the same software, the location coordinates of the centres of the different

sample plots were individually derived and noted. This stratified random method of sampling was used in view of it being a more efficient scheme in forest areas which are not completely uniform (i.e., in terms of stand age, species composition, and site conditions) compared to the simple random and systematic sampling methods (Shiver and Borders, 1996).

A total of twenty five sample plots were identified. The sample plots were circular with a radius of 10 m, except for the first plot, which had a radius of 20 m. The reduction in plot size was made in consideration of the relatively uniform distribution of the trees, and hence the small variation among sample plots, within each stratum. Circular plots were used since these are less time-consuming to establish on the ground compared with the square and rectangular ones. Moreover, with the potentially large nonsampling errors associated with the omission or inclusion of trees near plot edges, the use of circular plots is preferable considering that the amount of edge on a circle is minimum compared to any other shape (Shiver and Borders, 1996).

Navigation and location of the pre-identified sample plots within the site were facilitated by the use of a Global Positioning System (GPS) instrument, topographic maps, and hard copies of Landsat TM and AIRSAR images. A differential GPS unit was used for the first five sample plots while a hand-held unit was utilised for the balance of the plots due to the unavailability of the radio beacon and external antenna after the first week of ground truth data collection. In some cases, minor adjustment in the location of sample plots in the field had to be made in consideration of factors such as accessibility, terrain and other ground conditions. Generally, efforts were made to ensure that the plots had relatively flat terrain and were relatively homogeneous with regard to species in the surrounding area within the same segment. Communication with Han (1998) reveals a positional accuracy of up to 5 m for the differential GPS and about 100 m (with a standard deviation of 25 m) for the hand-held unit. However, with the sample plots established within relatively large homogeneous segments, it was assumed that minor shifts in plot positions as a consequence of inaccuracies inherent in the GPS receivers, along with adjustments due to existing ground conditions, will not have a great effect on the

analysis results. Data pertaining to tree attributes that have an important effect on the amount of radar backscatter, as enumerated below, were collected from each sample plot:

a) species;
b) trunk diameter at breast height (dbh) over bark;
c) crown width/coverage;
d) total tree height;
e) trunk height;
f) crown height;
g) tree density;
h) number of branches per tree;
i) average branch diameter;
j) average branch length; and
k) average branch angle from the vertical.

Data on trunk circumference at breast height (cbh) over bark and crown width/coverage were obtained with the use of 5m- and 30m- steel tapes. The dbh over bark was later computed from the cbh using the formula dbh = cbh / π. Crown width/coverage was taken as the average of two perpendicular measurements of the crown extent. The crown extent measurements were obtained by laying the 30 m steel tape straight on the ground with each end of the tape positioned parallel to the corresponding crown edge. The total tree, trunk and crown heights were calculated based on clinometer readings obtained at a 10-m distance from the base of the trunk.

Species composition

A total of 1,313 trees belonging to 19 species were inventoried from the 25 sample plots. Trees from the Ironbark group (Red, Grey, Narrow-leaved and Broad-leaved) and the Gum group (River Red, Spotted, Scribbly, Swamp, Forest Red, Sydney Blue, and Manna) accounted for 39.15 % and 10.36 % of the total, respectively. Other dominant species are the Red Mahogany (12.11 %), Turpentine (12.72 %), White Cypress Pine (11.35 %), Woollybutt (6.47 %), and Paper bark

(4.72 %). A complete list of the different trees measured from all the plots, including the number of trees per species and the corresponding percentage of the total, is given in Table 5.1.

Scientific name	Common Name	Tally	% of Total
Eucalyptus sideroxylon	Red Ironbark	256	19.50
Eucalyptus creba	Narrow-leaved Red Ironbark	144	10.97
Eucalyptus paniculata	Grey Ironbark	80	6.09
Eucalyptus siderophloia	Broad-leaved Red Ironbark	34	2.59
Eucalyptus micrantha	Scribbly Gum	45	3.43
Eucalyptus saligna	Sydney Blue Gum	26	1.98
Eucalyptus maculata	Spotted Gum	27	2.06
Eucalyptus tereticornis	Forest Red Gum	20	1.52
Eucalyptus ovata	Swamp Gum	10	0.76
Eucalyptus viminalis	Manna Gum	3	0.23
Eucalyptus camaldulensis	River Red Gum	5	0.38
Eucalyptus resinifera	Red Mahogany	159	12.11
Syncarpia glomulifera	Turpentine	167	12.72
Callitris hugelii	White Cypress Pine	149	11.35
Eucalyptus longifolia	Woollybutt	85	6.47
Malaleuca linariifolia	Paperbark	62	4.72
Eucalyptus largiflorens	Black Box	25	1.90
Eucalyptus robertsoni	Narrow-leaved Peppermint	15	1.14
Eucalyptus gummifera	Red Bloodwood	1	0.07

Table 5.1 List of all tree species measured in study site 1 including corresponding frequency and percentage of the total

Trunk diameter and total tree height

The biggest tree trunk diameter was measured at 88.17 centimetres from a Scribbly Gum while the smallest was at 1.91 centimetres from a Woollybutt. The

trunk diameter was taken over the bark at about 1.4 metres (breast height) from the ground. The tallest tree, a Red Mahogany, stood at 42.12 metres and the shortest at 1.91 metres were two paperbarks and a Woollybutt.

Shown in Figure 5.6 is the tree distribution by dbh, Figure 5.7 is the distribution by total height, and Figure 5.8 is the total tree height as a function of dbh for six of the most dominant species in the study site. In terms of distribution by dbh, majority of the trees measured are included in the small diameter classes. Of the 1,313 trees sampled, 568 (43.26 %) belong to the 0.00 - 9.99 cm dbh class, 440 (33.51 %) to the 10.00 -19.99 cm class, 183 (13.94 %) to the 20.00 -29.99 cm class, 59 (4.49 %) to the 30.00 - 39.99 cm class, and the remaining 63 (4.80 %) distributed among the last five dbh classes (40.00 - 89.99 cm). The same trend holds true in the case of tree distribution by total height, where 90.86 % of the trees are in the first four height classes (0.00 - 19.99 m). Regression analysis performed on the data from the six most dominant species produced a modest correlation between dbh and total height. The highest correlation (R = 0.8122) was obtained from the Woollybutt data while the lowest (R = 0.6308) was computed from the Red Mahogany dbh over bark and total height measurements.

Tree density and crown width/cover

An average density of about 15 trees per pixel (10 m x 10 m) was computed based on the total number of trees inventoried and total area sampled although the density per sample plot varied from 25 to 6 trees per pixel. Turpentines were observed to grow in clumps hence increasing the tree density in plots where they are present. In some of the plots, large numbers of juvenile trees, characterised by long slender trunks and thin/transparent crowns, were found to be present. Individual crown widths/coverages ranged from 0.62 m to 17.95 m although the general forest canopy could be described as being relatively open, with about 30 percent of the sky visible from the ground under the trees.

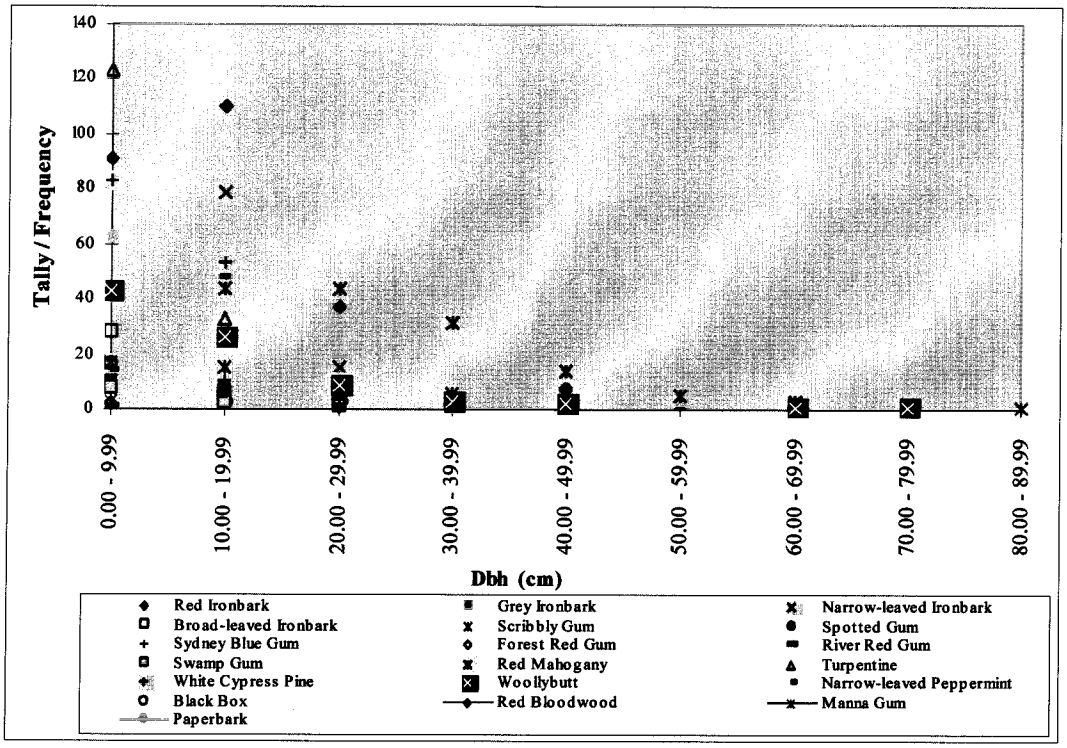

Figure 5.6 Tree distribution by dbh over bark in the Blue Mountains study site

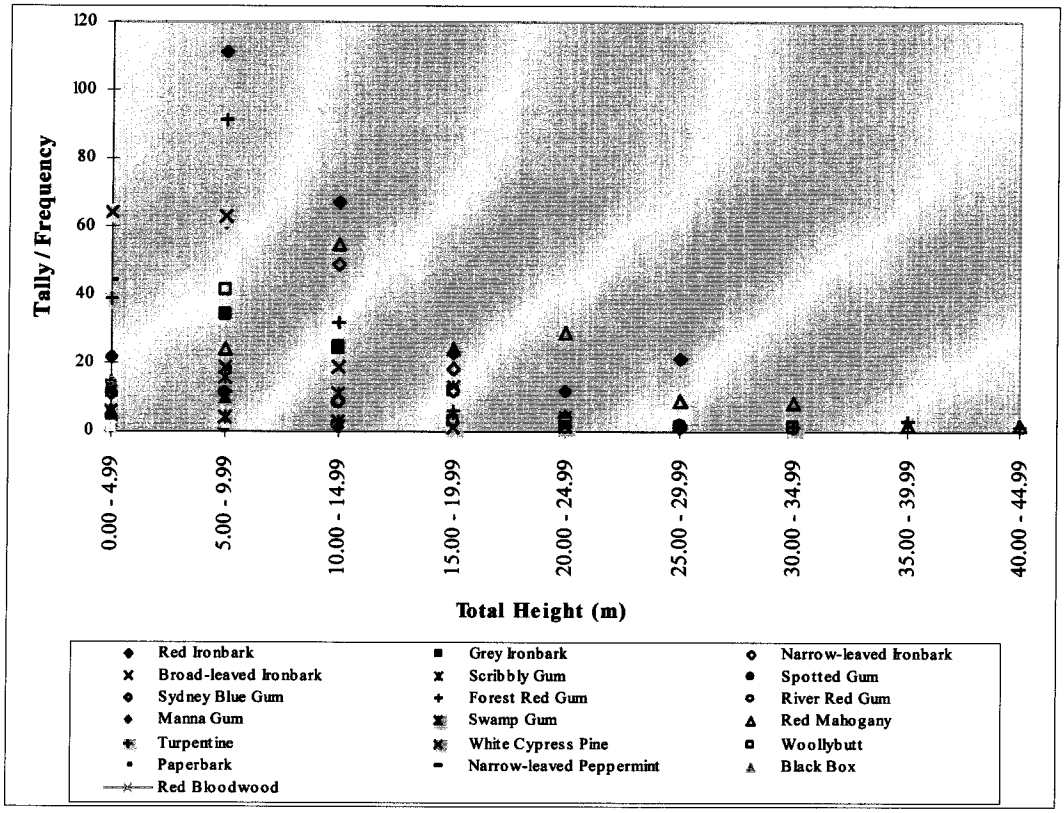

Figure 5.7 Tree distribution by total height in the Blue Mountains study site

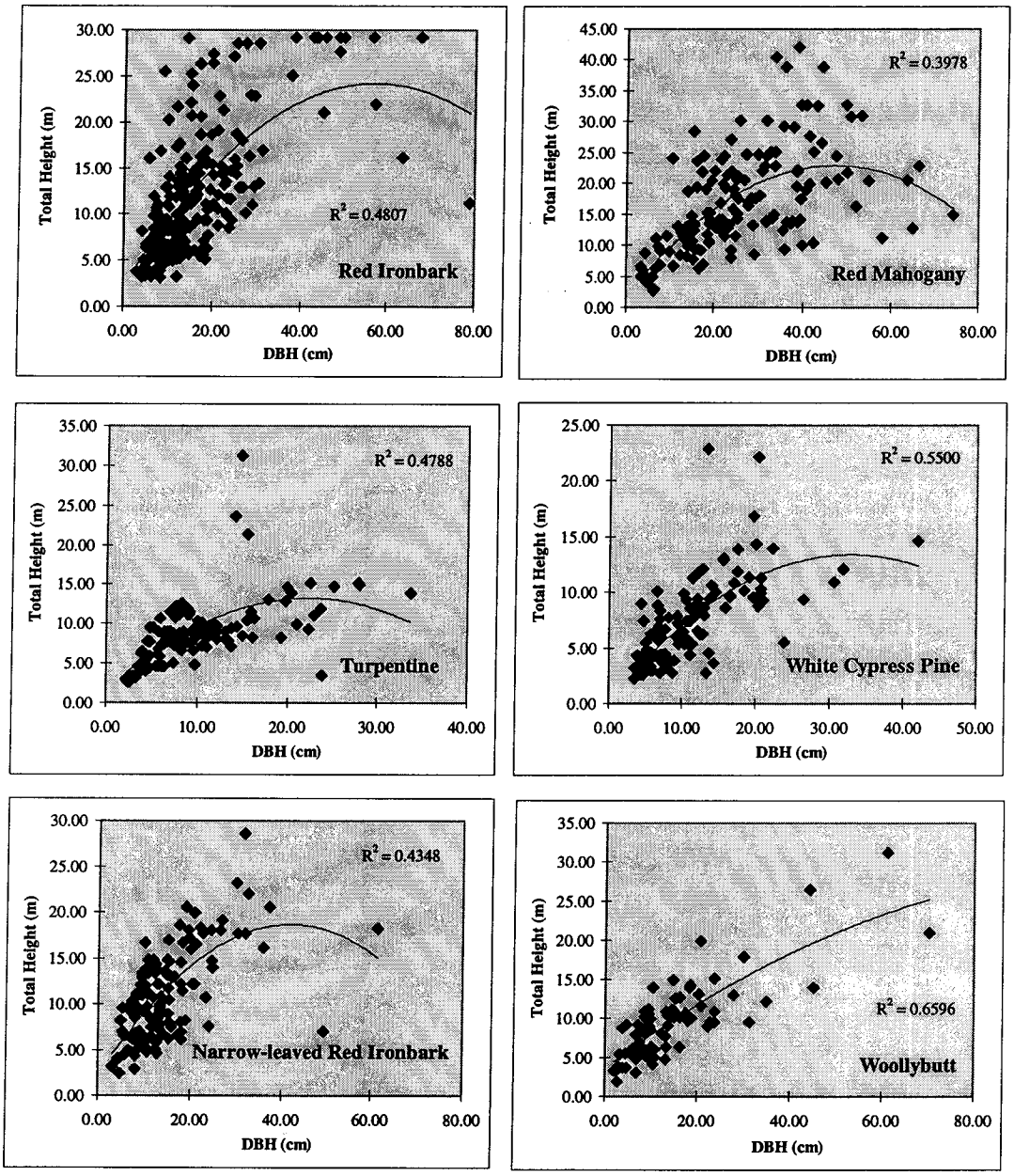

Figure 5.8 DBH versus total tree height for six of the most dominant species in the Blue Mountains National Park study site

Shown in Figure 5.9 is the crown width distribution for all the trees measured. Majority of the trees have small crown coverages with 385 (29.32 %) trees having crown widths 1.99 m and below, 549 (41.81 %) with crowns within the 2.00 - 3.99 m class, 225 (17.14 %) in the 4.00 - 5.99 m group, and 74 (5.64 %) in the 6.00 - 7.99 m class.

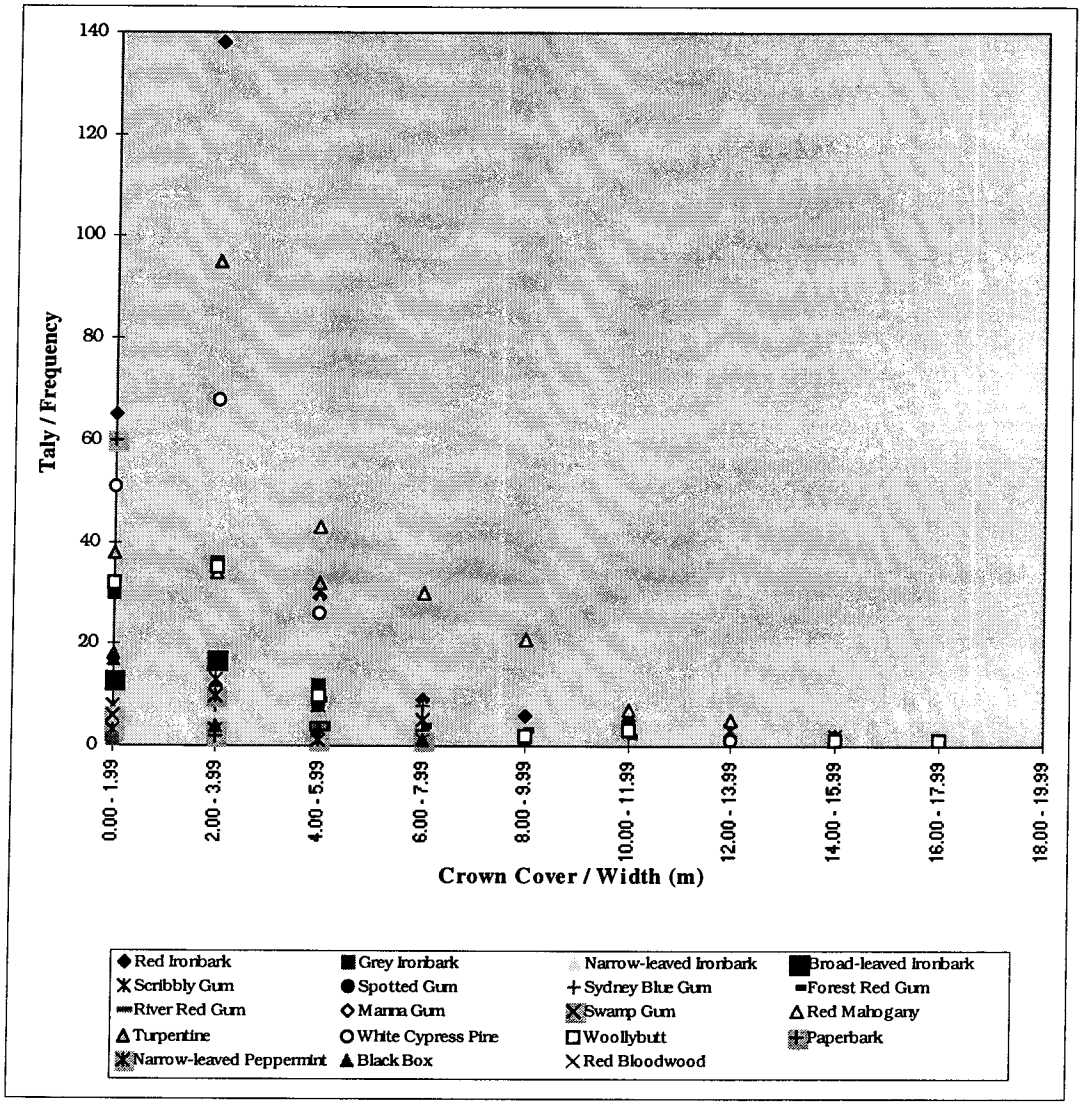

Figure 5.9 Crown cover/width distribution for trees in the Blue Mountains study site

Branch parameters

The different tree branch-related measurements taken in the field were the number of branches per tree, average branch diameter, average branch length, and the average branch angle from the vertical. Data for these parameters were generated based on ocular estimation and are presented in Figures 5.10 and 5.11. The White Cypress Pines and the Turpentines had the most number of branches. Also, as can be seen from the figures, these two species have the highest branch angles among the dominant species owing to their near-horizontal branching pattern.

However, being mostly composed of juvenile trees (which have an undeveloped general structure), these species had the least average branch diameter and relatively short branch lengths. It is for the same reason why branch angles of about 40^0 to 50^0 were also measured from some trees belonging to these species. For the balance of the trees, the branches were observed to be generally oriented at around 45^0.

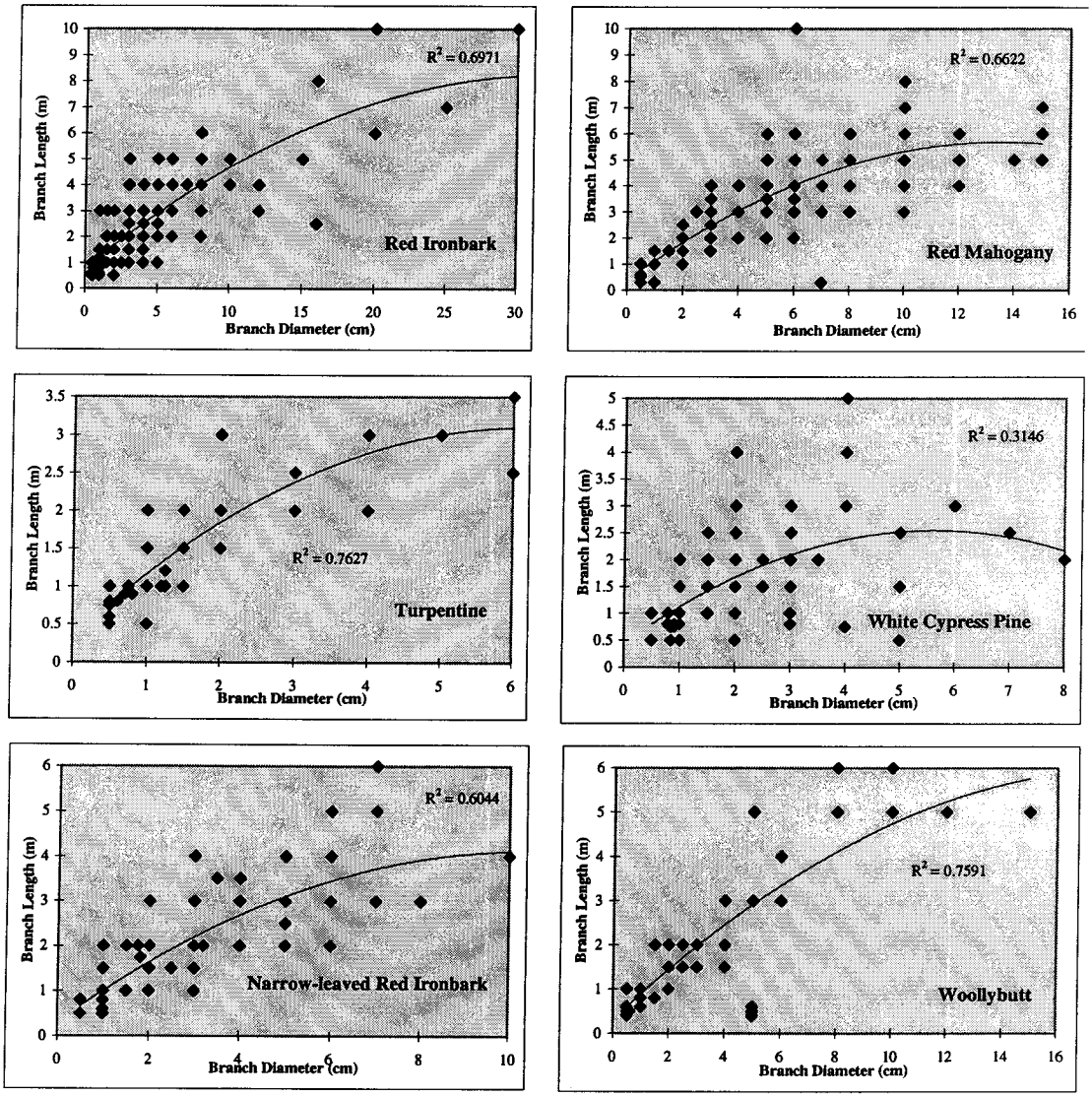

Figure 5.10 Branch diameter versus branch length for the six most dominant species in the Blue Mountains National Park study site

A good correlation between branch diameter and branch length was observed from Turpentine (R = 0.87), Red Mahogany (R = 0.81), Red Ironbark (R = 0.83),

Woollybutt (R = 0.87), and Narrow-leaved Red Ironbark (R = 0.78) data. For the White Cypress Pines, however, the correlation between these parameters was relatively low (R = 0.56). Except for the White Cypress Pines, which had a low R value of 0.68, there was practically no correlation between the average branch angle and average number of branches for all the trees belonging to the enumerated species.

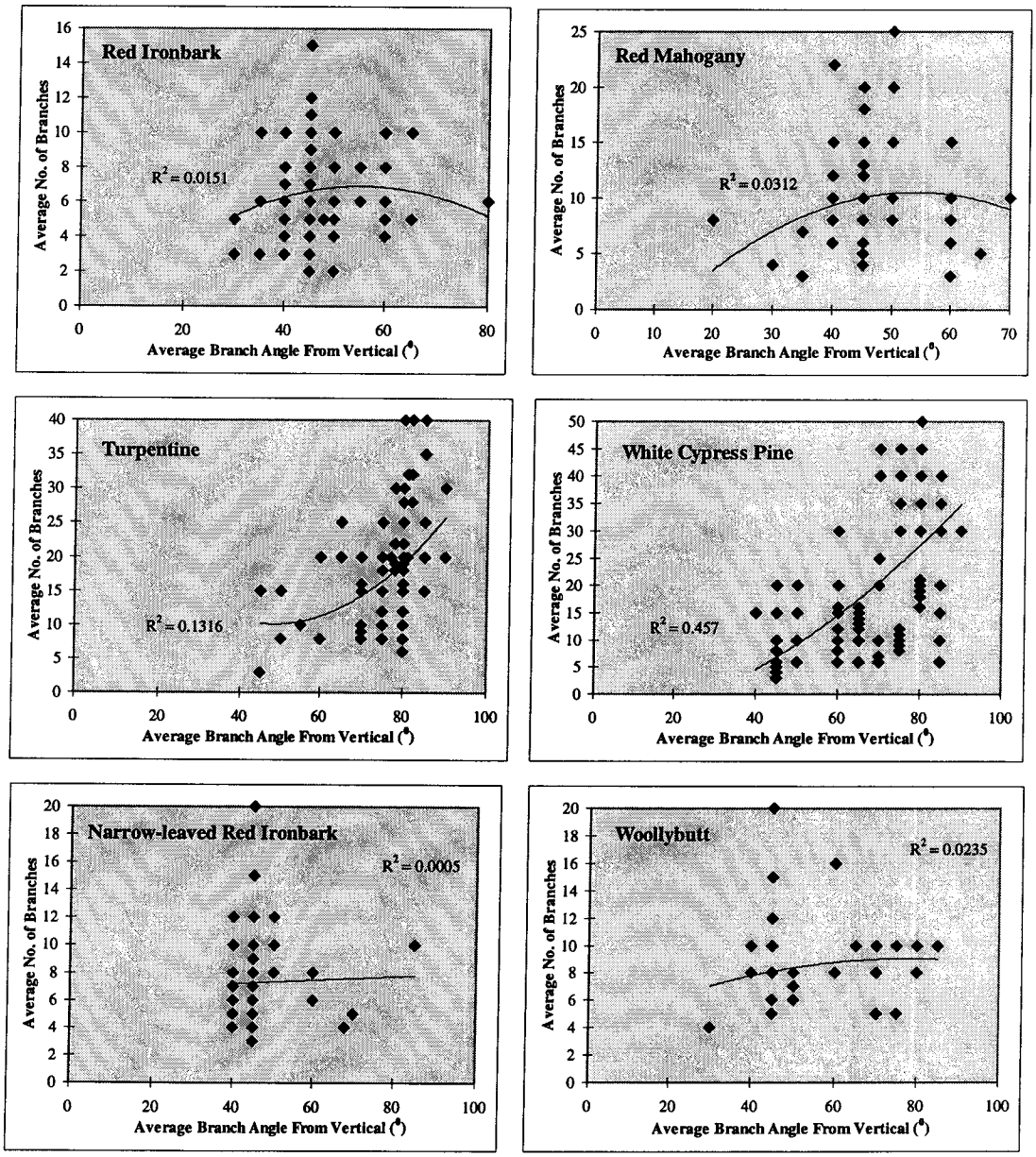

Figure 5.11 Average branch angle from the vertical against average number of branches for the six most dominant species in the Blue Mountains National Park site

5.4 Description of study site 2 : Gippsland Region, Victoria, Australia

5.4.1 Location

The site used for investigating the relationship between radar backscatter and needle-leaved vegetation characteristics is located in Stockdale, a small township in the Gippsland region of the State of Victoria, Australia (Figure 5.12). The area, bounded by UTM (Australian Map Grid) coordinates 5809000 - 5817000 North and 514000 - 518000 East (37^0 52' 00'' to 37^0 47' 40'' North and 147^0 09' 30'' to 147^0 12' 15'' East), is part of the Stockdale plantation of the Australian Paper Plantations Pty. Ltd. (APPPL). On the western side of the plantation are the eucalypt-dominated natural stands of the State Forests of Victoria.

The following information on geology, landform, and climate, unless otherwise specified, were drawn from Poutsma and Turvey (1979).

5.4.2 Geology, landform and topography

The APPPL plantations in Gippsland encompass a variety of landforms, from the mountainous, steeply dissected Strzelecki Ranges, to the flat flood plain of the Latrobe River and wind-ridged and sand-covered relict marine terraces of Stradbroke and Glencoe. As variable is the lithology of the parent material, which indicates an extended and active tectonic history. Included are consolidated and unconsolidated siliceous materials of alluvial and aeolian origin, basalt, metamorphosed rocks, and calcareous marine rocks. The age of these materials ranges from 10,000 years old for the alluvial materials in the Latrobe River flood plains to 440 million years old for rocks formed during the Silurian epoch.

Stockdale is part of the tectonic structure called the Gippsland Basin, where the Cretaceous sediments were covered with alluvial deposits and older volcanic basalt flows during the early Tertiary times. In the Oligocene era, some 25 to 40 million years ago, the Basin subsided and was covered with up to 1200 m of terrestrial materials such as the brown coal deposits.

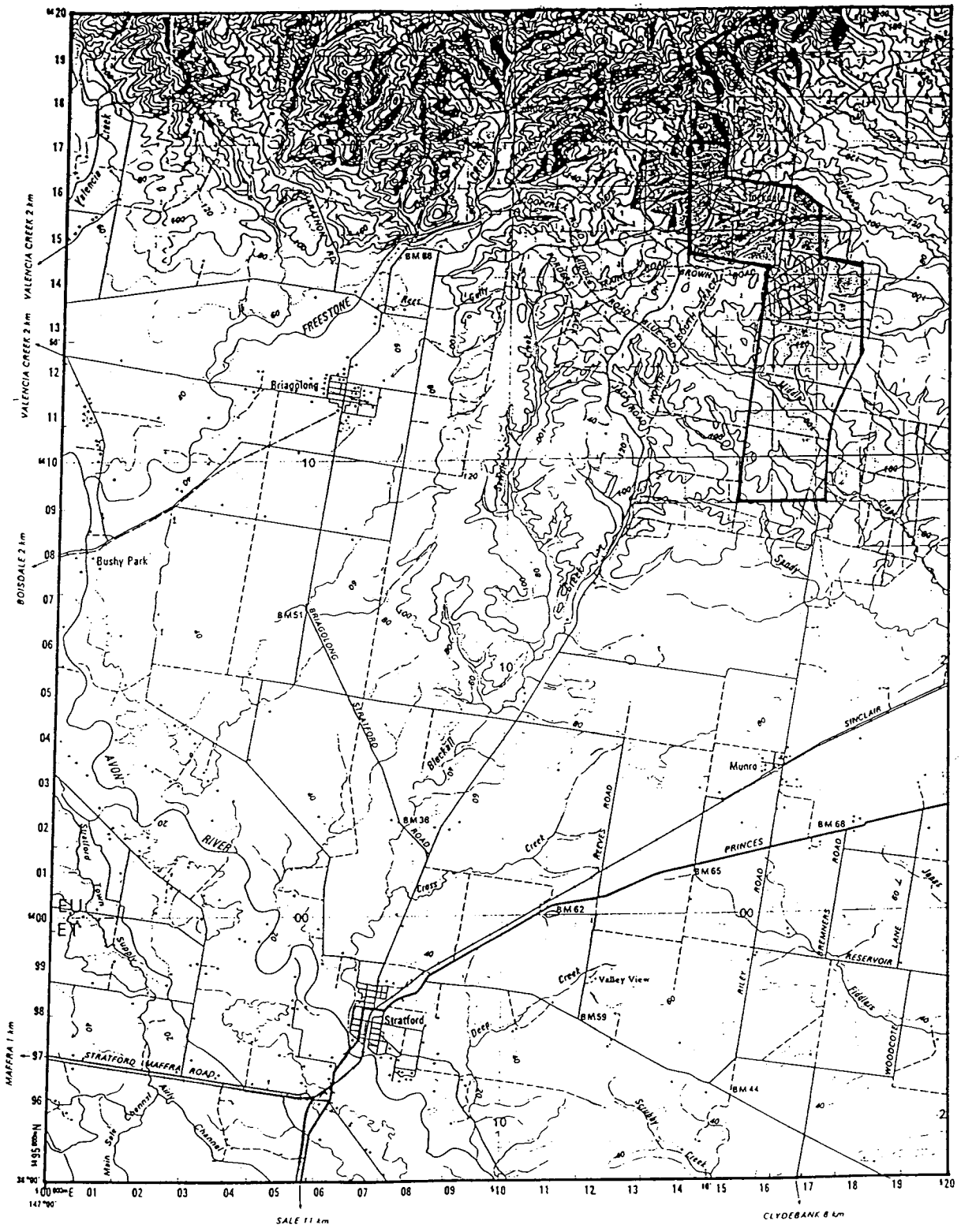

Figure 5.12 Location of study site 2

In the Miocene period, the sea encroached the eastern part of the Basin thereby depositing calcareous and other materials. These deposits were further coated with clays, sands and gravel in the Pliocene period (2 to 4 million years ago) thus forming a higher level plain of alluvial fans and flood plain deposits that make up the parent material for the present day soils over a large part of the area. These deposits were regionally raised and locally warped in the mid-Pleistocene period consequently joining the South Gippsland and the Central Highlands. In portions of the area where this older land surface is still intact, the topography is gently undulating. Erosion and dissection by local drainage ways have caused other portions, particularly those in raised area adjacent to the Highlands, to have a rolling and locally hilly topography.

The study area, being characterised by a flat to gently undulating topography, is believed to be a part of the older land surface formation. The elevation is from 100 to 160 metres above sea level although about 90 % of the study area is within the 110 to 120 metre elevation range. The average slope is from 2 to 5 degrees. Navigation inside the plantation is facilitated by an asphalted main road and a number of gravel roads, which dissect the area. Moreover, each of the plantation compartments is surrounded by fire lanes capable of vehicle access.

5.4.3 Climate

Generally, the climate is controlled by cyclonic depressions that move from west to east parallel to the southern coast of Australia. The path of these depressions moves closer to Australia during the winter season thus bringing more rain to the southern part of the country. Depressions forming off the east coast also influences the weather, bringing in heavy rains to the eastern parts of the area, at any time of the year. Over all the APPPL's Gippsland plantation sites, however, the average annual rainfall varies from more than 1400 mm (56 inches) on the Strzelecki Ranges and the Central Highlands to the north, to around 700 mm (28 inches) on the eastern section, where the study area is located. This huge reduction in the amount of rainfall is an effect of the marked rain shadow cast by the Strzelecki Ranges.

Compared to the wetter, higher plantation sites, where rainfall is moderate in winter and peaks in spring, rainfall in the study area is in general evenly spread throughout the year. Figure 5.13 shows the average monthly and annual rainfall in the study site, as computed over a 10-year period.

Gippsland has a mild temperate climate of four distinct seasons that are normally free of extreme temperatures (ATN, 1998). The average temperature differences between and within seasons, however, tend to be more variable in the study site. For example, as recorded at a meteorological station in the nearby township of Stratford, mean daily maximum and minimum temperatures during the peak winter and summer months could vary from 14.2^0 C to 2.4^0 C and 27.5^0 C to 12.4^0 C, respectively (Table 5.2).

5.4.4 Vegetation and fauna

Apart from few small and widely separated eucalypt stands, the study area is basically a mono-specific plantation of radiata pines (*Pinus radiata*). The entire plantation is subdivided into compartments of varying sizes, each of which being separated by fire lanes of about 4 to 5 metres in width. The pines in the compartments are of varying age, depending on the year of stand establishment subsequent to timber harvesting. Thinning operations start 14 to 15 years after planting and the rotation period is from 25 to 30 years, depending upon the tree size (Appleton, 1999, personal communication). To facilitate the passage of machinery for later age weed control, plant spacing was changed in 1984 from a square 3.0 m by 3.0 m to 3.6 m inter-row by 3.0 m intra-row thereby reducing the stocking density from 1750 to 1400 seedlings per hectare. In 1986, with the introduction of cuttings- based planting, stocking was further reduced to 1000 seedlings per hectare (Lieshout et al., 1996).

A number of animals have been observed in the Stockdale plantation, the most common being kangaroos, emus, dingoes, squirrels, possums, and various species of birds such as cockatoos, parrots and pigeons.

5.5 Experimental data for study site 2

5.5.1 Multi-frequency quadpolarised radar data

Quadpolarised P-, L- and C- band SAR data were acquired over the eastern Gippsland area by the AIRSAR system on September 8, 1993. The radar scene was taken from an altitude of 7,956.5 m with centre coordinates of 36.17^0 North latitude and 147.16^0 East longitude and near and far look angles of 22.4^0 and 62.3^0, respectively. Prior to processing, the P-band data were filtered to remove radio frequency interference. The image was then processed to 18 looks in the azimuth direction to reduce the amount of speckles. An amplitude calibration factor of -95.79 dB was applied to HH, -92.54 dB to HV, -95.39 dB to VH, and -92.84 dB to VV data. The scene was subset at NASA/JPL to include only the study site, which is located at the top right part of the georeferenced image.

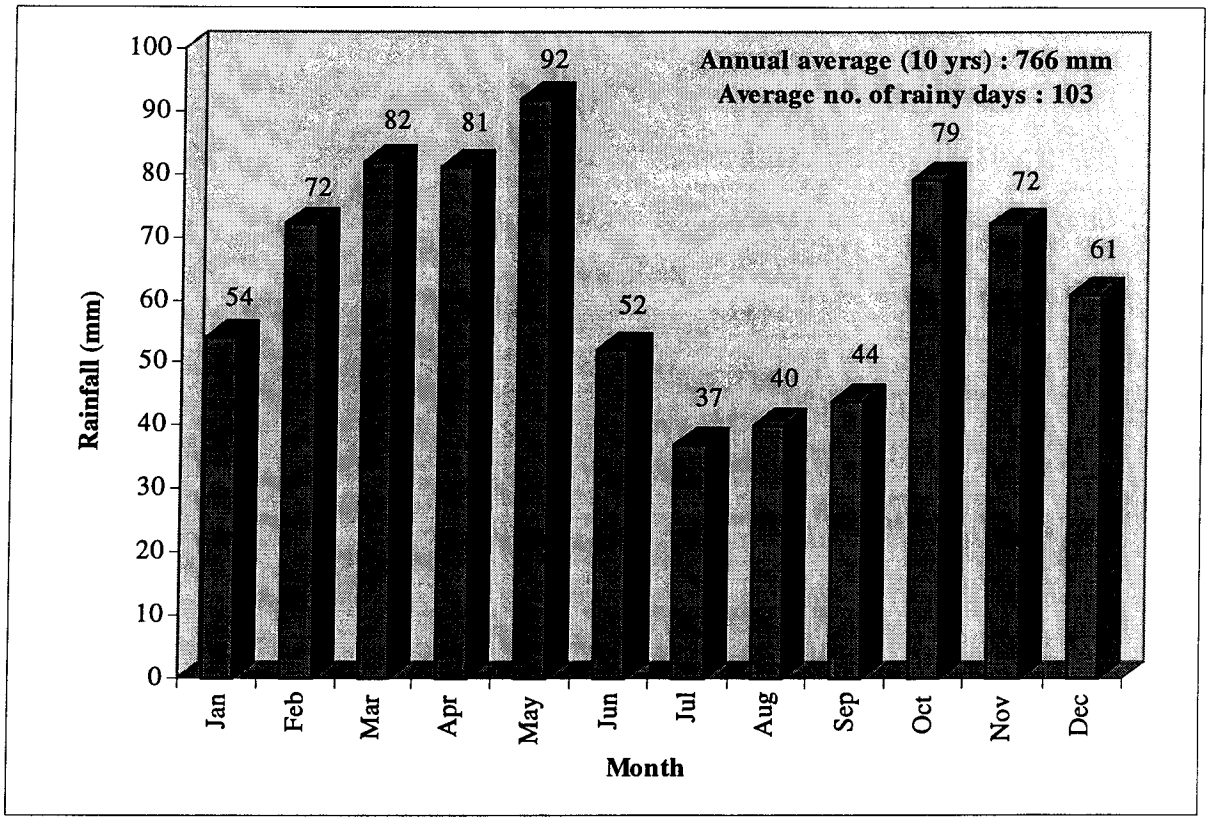

Figure 5.13 Average monthly and annual rainfall in the Stockdale (Gippsland) site
Source: Poutsma and Turvey, 1979

	Jan	Feb	Mar	Apr	May	Jun	Jul	Aug	Sep	Oct	Nov	Dec
Max	27.5	26.5	24.4	21.9	18.0	15.2	14.2	16.2	18.3	21.0	23.6	26.3
Min	12.4	12.3	10.6	7.8	5.5	3.8	2.4	3.2	5.4	6.6	8.6	10.6

Note: Plant growth is retarded at mean temperatures lower than 10^0 C and arrested at temperatures below 5^0 C (Poutsma and Turvey, 1979)

Table 5.2 Mean daily maximum and minimum temperatures (in degrees Celsius) as recorded in Stratford, a township near the study site. Source: Bureau of Meteorology, 1999

5.5.2 Field data

Field data collection was conducted in the plantation stands in February, 1999. Similar to the Blue Mountains study site, visual analysis of multi-parameter radar images and topographic maps was first undertaken, before the fieldwork, for orientation and familiarisation purposes. The different strata were identified based on the established plantation compartments. With the varying stand ages and the fire lanes surrounding each of the compartments, stratum boundaries were easily defined.

As the radar image was taken in 1993, it is expected that much has changed in terms of the tree dimensions. It was considered that using current field data obtained from the corresponding compartments would result in inaccurate backscatter-stand parameter relationships. To remedy the situation, measurements from nearby stands with ages the same as those imaged in 1993 were used as surrogate data for the latter. Given the similarity in plantation establishment and maintenance practices, topography, geology, climate, etc., between the imaged and substitute stands, this is considered a better approach than trying to compute and adjust the current field data to 1993 figures. The compartment maps and plantation

records provided by APPPL prior to the conduct of fieldwork, coupled with the technical inputs from APPPL personnel, were instrumental in the selection of the representative sample plots within the compartments.

To conform with the shape of the compartments and to be consistent with the size of the Blue Mountains sample plots, rectangular plots of 15 m by 21 m were established. Twenty five plots were used, from each of which data pertaining to tree species, dbh over bark, crown width/coverage, trunk/total height, density, average number of branches per tree, average branch diameter, average branch length, and average branch angle from the vertical, were gathered using the same methods applied in the Blue Mountains study area. Trees along the compartment boundaries were observed to generally have trunk and branch dimensions much greater than the rest of the trees in the stand. This is due to the so called "edge effect", where the presence of more favourable conditions along the edges (e.g., more sunlight for photosynthesis) causes better tree growth. As this is the case, efforts were made to avoid taking data from trees along the compartment boundaries so as not to obtain higher than actual averages.

Trunk diameter and total height

Given in Table 5.3 are the average dbh over bark and average total height for trees in the different age classes. Due to the morphological characteristics of conifers/pines, as described in Chapter 3, the total height, trunk height and crown height were treated as one parameter. The highest average dbh of 31.34 cm and average total height of 27.16 m were both obtained from 27 year old stands. As shown in Figures 5.14 (a) to 5.14 (c), a positive relationship exists between stand age and average trunk diameter (R = 0.94), stand age and trunk height (R = 0.99), along with average diameter and trunk height (R = 0.96).

Tree density and crown width/cover

As indicated earlier, seedling spacing was changed in 1984 from 3.0 m by 3.0 m to 3.0 m by 3.6 m for better access to later age weed control machines.

Thinning starts 14-15 years after planting and a stand normally undergoes 3-4 thinning operations prior to harvesting. Higher stocking density is thus expected of stands below 14 years old compared to those above this particular age. Then again, for those 14 -15 years old and above, stands with ages closer to harvest time normally have less stocking density than the younger ones as they already have undergone more thinning. In the different 21 m by 15 m sampling plots, the number of trees ranged from 30 to 46. Crown widths ranged from 3.85 m to 6.75 m with the visibility of the sky from the ground varying from 10 - 50 %.

Branch parameters

The tree branch-related data acquired were similar to those from the Blue Mountains study area. This time, however, only one set of measurements was taken for each stand considering the homogeneity in the branch dimensions of the mono-specific trees making up each compartment. The measurements, as presented in Table 5.3, were obtained from representative trees that best approximate the average branch proportions for each of the compartments. The average number of branches per tree ranged from 50 to 80 with the average branch diameter and branch length at 4.16 cm and 3.44 m, respectively. The branches are angled at 80 - 90^0 from the vertical and are arranged in whorls of 6-10 branches. The whorls are 1-2 feet apart with the first located approximately 12 cm from the ground.

5.6 Ancillary information sources

To facilitate field data collection and analysis, secondary data sources such as topographic maps, plantation compartment maps, road maps and plantation records were used.

Age	Ave. Diameter (cm)	Total Ht. (m)	Ave. Branch Diameter (cm)	Ave. Branch Length (m)	Cover (m)	Sky Visibility (%)	No. of Trees in Plot
5	13.43	9.80	4.30	2.80	4.80	20 - 30	43
5	13.55	10.40	4.00	2.60	4.60	20 - 30	41
5	14.09	10.72	4.10	2.70	4.65	20 - 30	40
6	14.43	12.25	3.80	2.40	4.85	20 - 30	43
6	15.58	11.36	5.20	3.78	5.20	10 - 20	38
6	15.22	11.27	3.30	2.36	3.90	30 -50	39
9	17.39	12.87	5.00	2.30	5.20	10 - 15	34
9	16.86	13.81	4.00	4.00	3.90	25 - 30	38
10	16.46	16.30	5.60	4.30	5.20	30 - 40	43
10	17.55	14.44	3.90	3.70	6.25	10 - 15	40
10	17.47	13.55	3.80	4.20	6.00	30 - 50	39
19	22.04	18.05	3.60	3.50	4.65	10 -15	30
19	20.81	19.75	3.80	2.20	4.00	40	35
19	18.90	19.74	4.20	3.60	4.80	30 - 40	44
22	21.46	21.34	3.50	2.40	4.05	20 - 25	36
22	19.30	21.53	5.20	4.80	5.45	10 - 15	46
22	20.69	21.72	3.50	4.05	3.85	10 - 15	40
22	21.65	21.34	3.70	4.00	6.75	10 - 15	36
24	22.23	22.60	3.50	4.05	4.90	10 -1 5	38
24	23.05	23.18	4.90	4.20	5.25	10 - 15	35
24	23.08	21.96	5.00	4.20	5.60	10 -15	35
26	29.51	25.31	4.00	3.75	4.20	10 - 20	32
26	28.76	24.20	3.50	3.50	4.50	15 - 20	31
27	31.34	26.52	4.50	3.50	5.00	15 - 20	31
27	29.86	27.16	4.20	3.20	4.35	10 - 20	34

Table 5.3 Average dbhob, total height, branch diameter, branch length, crown coverage and age classes for the trees in the different sample plots in the Gippsland study site

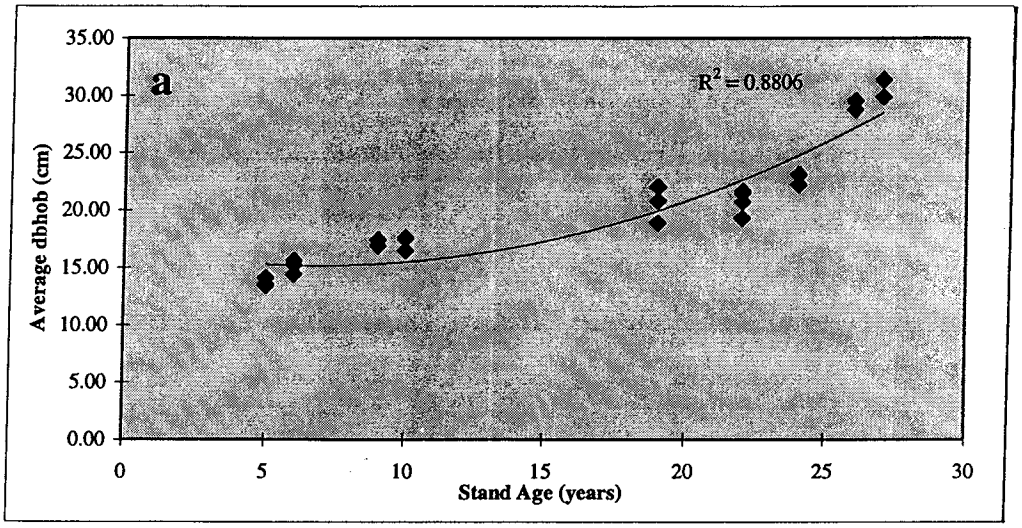

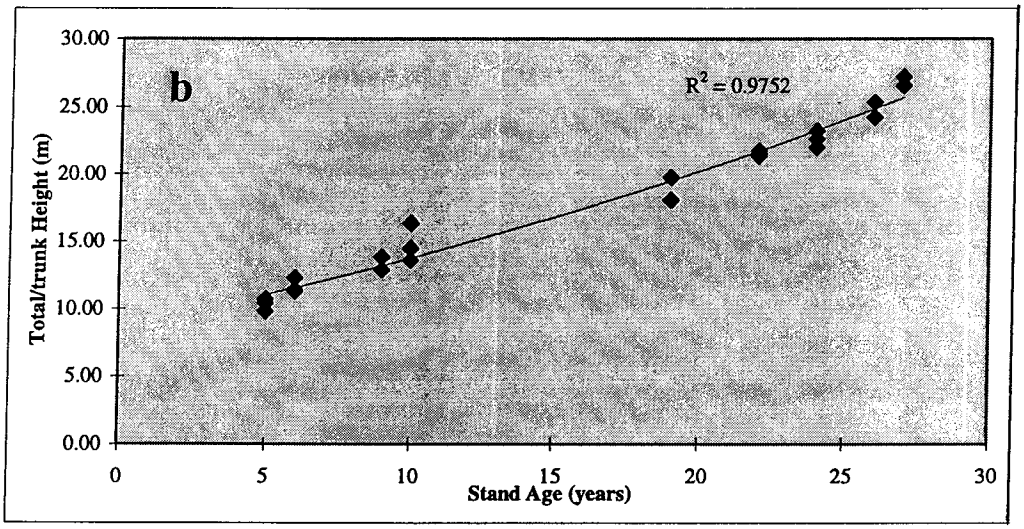

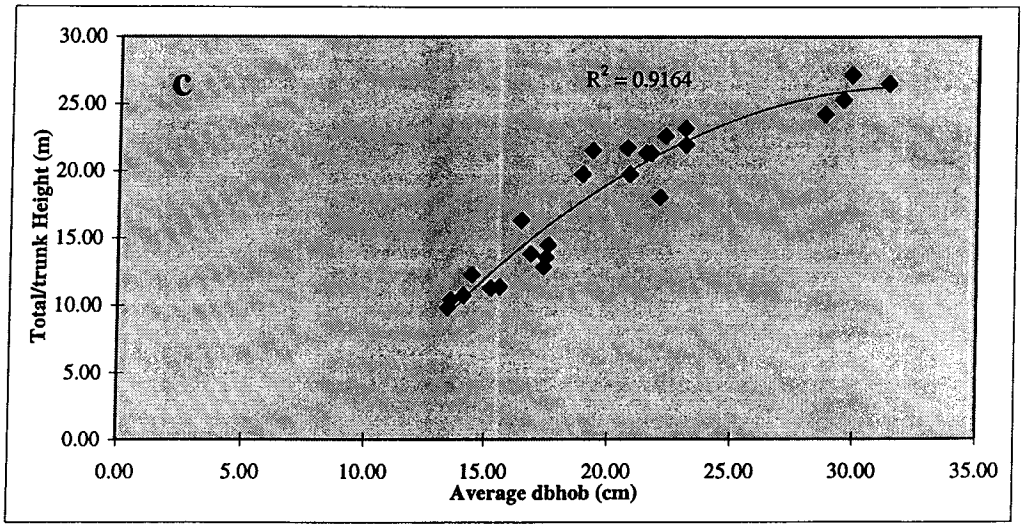

Figure 5.14 Relationships between stand age and average dbh over bark (a), stand age and total/trunk height (b), and average dbh over bark and total/trunk height (c) in the Gippsland study site

For both the study sites, topographic maps at a scale of 1:100,000, printed in 1983 by the Division of National Mapping (NATMAP) of the Commonwealth government, were utilised. These maps have a contour interval of 20 metres with the horizontal datum based on the Australian geodetic datum of 1966 and the vertical datum on the Australian height datum of 1971. For more details, 1:25,000 and 1:10,000 scaled topographic maps printed by the Central Mapping Authority of New South Wales in 1983 and 1981, respectively, were also used for the Blue Mountains site while 1:25,000 topographic maps printed in 1982 by the Department of Crown Lands and Survey of Victoria were procured for the Gippsland site. The 1:25,000 maps have a contour interval of 10 metres while the 1:10,000 maps have an interval of 4 metres.

A map identifying the compartment number of the stands and a document containing detailed historical plantation records were given by APPPL for the Gippsland study site. These provided, among others, the information required for the identification of the representative plots such as the current stand age and the age of the stands imaged in 1993. Also supplied was a plantation road map, which made travelling inside the study area much easier.

CHAPTER 6

DATA ANALYSIS METHODOLOGY

6.1 Introduction

The process of determining stand structure and estimating total aboveground biomass based on radar data involves establishing relationships between the ground truth data and the amount of backscatter. Establishing forest parameter-radar backscatter relationships requires careful analysis of both the radar and ground truth data so as to obtain correct estimates. In this chapter, the different data processing and analysis methods used are enumerated and individually discussed. These procedures, however, should not be assumed to be a strict list of steps for every radar remote sensing application. The analysis techniques to be applied, in general, should depend on the purpose of the study or the amount and nature of information required from the radar data. Presented in Section 6.2 are the preprocessing, image enhancement, and image segmentation procedures employed, while in Section 6.3 are the operations devoted to ground-truth data analysis. Included in Section 6.4 are the allometric equations adopted to obtain estimates of total forest aboveground biomass. This is followed by a description of the image segmentation procedures used in Section 6.5, an account of the accuracy assessment methods employed in Section 6.6, a synopsis of the main data analysis steps applied in Section 6.7, and the general summary and conclusions in Section 6.8.

6.2 Radar data analysis

6.2.1 Preprocessing operations

Remotely sensed data contain systematic and nonsystematic errors or distortions that are normally introduced during the image acquisition process. These errors degrade image quality and may impact the accuracy of image analysis results.

It is thus necessary that the errors be removed prior to further data manipulation. Procedures to correct or compensate for these errors or distortions are called preprocessing operations as they are applied before primary data manipulation and analysis to extract information from the image.

Preprocessing operations normally applied to remotely sensed data sets include *radiometric* and *geometric* correction. For radar data, radiometric calibration is performed to establish the relationship between the detector output and input radiation intensity thus making comparison of data values between images possible (Rees, 1990). Geometric correction is done to adjust the image spatial coordinates to their true spatial coordinates on the earth's surface. Both of these procedures are aimed at improving image quality and data analysis accuracy through the production of images that are both geometrically and radiometrically correct.

For the AIRSAR data sets used in this study, amplitude and phase calibration, deskewing, and other procedures to compensate for systematic errors were carried out by NASA/JPL. Correction for the random errors, as explained below, was undertaken at the Remote Sensing Laboratory of the University of New South Wales in Sydney.

Geometric correction and image spatial subsetting

Due to a number of factors such as platform altitude and velocity variations, earth curvature, and relief displacement, remotely sensed images contain geometric distortions that need to be compensated before the images will have the geometric integrity of a map. Geometric correction involves the transformation of a remotely sensed image so that it has map-like scale and projection properties (Mather, 1987). This procedure is necessary so that field sampled areas can be accurately related to their image equivalent locations. Lillesand and Kiefer (1987) identified two types of distortions that need to be addressed in the transformation process; the systematic, or predictable and the random, or unpredictable. They pointed out that systematic distortions are well understood and easily correctable through the application of mathematical formulas. An example of this is the eastward rotation of the earth

beneath a satellite sensor during imaging thereby causing each sweep to cover an area slightly to the west of the previous sweep. This error, known as skew distortion, is corrected by a technique called as deskewing, where each successive scan line is offset slightly to the west. Random or unpredictable errors, according to them, could be corrected by the use of well-distributed ground control points (GCPs). GCPs are features that could be easily identified and accurately located both on the digital image and the map of the area. According to the same authors, the rectification process is performed by using the position coordinates of the GCPs on the image (in row and column numbers) and on the map (in UTM or latitude-longitude) as inputs to a least-squares regression analysis to determine coefficients for two coordinate transformation equations that can be applied to relate the geometrically correct map coordinates and the distorted image coordinates. Distorted image coordinates for any map position could then be precisely estimated once the coefficients for these equations are known. However, this method does not account for errors due to terrain height variation.

Figure 6.1 illustrates how a distorted input grid is geometrically rectified and supplied with brightness values. In here, the location coordinates and pixel values in the output grid are computed from the input grid using coordinate transform coefficients that model the distortions in the original scene. As the coordinates in the input grid are non-integers, an intensity interpolation technique is applied to obtain the exact brightness value for the output pixel.

How well the coefficients derived from the GCPs account for the geometric distortions in the original image could be gauged by the use of the root mean square error (RMS_{error}). The RMS_{error} denotes an accuracy rating for the GCPs in the image. The higher the RMS_{error} value, the higher amount of distortion not compensated for by the rectification procedure. For each of the control points, RMS_{error} is computed using the formula

$$RMS_{error} = \sqrt{(x' - x_{orig})^2 + (y' - y_{orig})^2} \qquad (6.1)$$

where x' and y' are the computed image coordinates while x_{orig} and y_{orig} are the row and column coordinates in the original image. The total RMS_{error} is then computed by getting the sum of the individual RMS_{error} values. In practice, a user-specified upper limit for the total RMS_{error} is usually set. If this limit is exceeded, GCPs with high individual RMS_{error} are usually deleted one at a time until a total RMS_{error} below the threshold is reached (Jensen, 1986). The second stage of the geometric correction process, which involves the interpolation or transfer of the pixel values from the original image into the rectified output image matrix, is subsequently performed. This procedure, otherwise known as *resampling*, could be undertaken in different approaches, such as, nearest neighbour, bilinear interpolation, and cubic convolution. In the nearest neighbour method, the value of the closest input pixel is assigned to the output pixel. Bilinear interpolation assigns a value to the output pixel based on a weighted average of the values from the four nearest input pixels. In cubic convolution, the same principle of weighted averaging is used. In this method, however, the weighted values from 16 surrounding input pixels are used to compute the value of the output pixel.

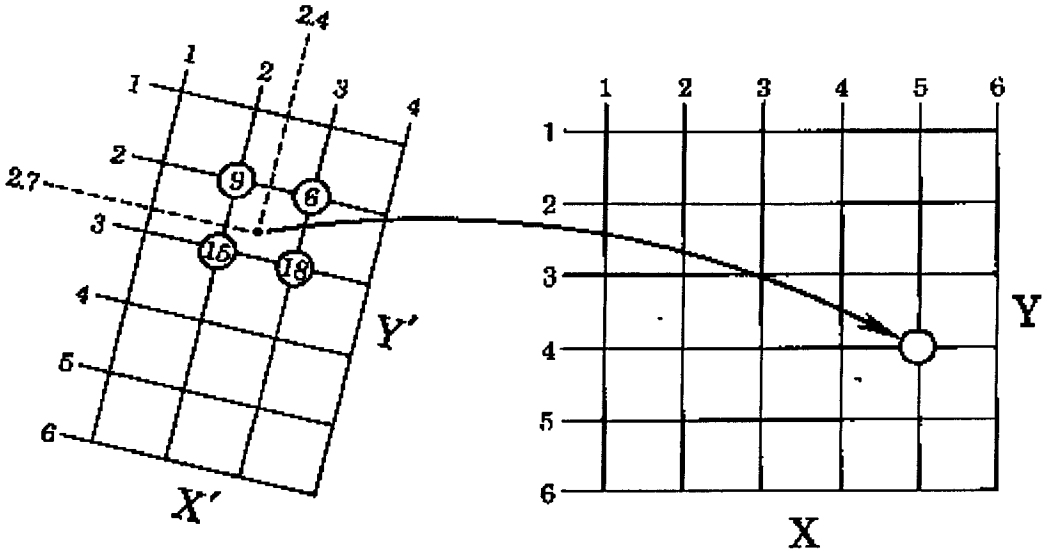

Figure 6.1 Image Rectification : derivation of location and brightness values from a geometrically distorted input grid to a rectified output grid (from Jensen, 1986)

In selecting GCPs, it is important not to choose features that are subject to change such as points on coastlines or agricultural field boundaries especially in cases where there is a big time difference between the image acquisition and the last map revision. Examples of features that make good GCPs are intersections of roads or highways, airport runways, edges of land parcels, isolated buildings and the like. Aside from being easily discernible on the image and the corresponding map, these features are permanent, or unlikely to change in position. Other factors to be considered in GCP selection pertain to the spatial distribution and the number of control points needed. In principle, the GCPs should be evenly distributed over the image area, with good coverage near the edges and in the centre. In terms of GCP number, it is obviously another case of the more, the better although the accuracy may actually decrease with an increase in number because the analyst chooses the best points first (Campbell, 1987). According to Bernstein (1983), 16 GCPs may be an acceptable number provided each control point can be located with an accuracy of one-third of a pixel. More GCPs are needed if the points are poorly distributed or if accurate placement is difficult.

Since the original data sets used in this study are in a compressed Stokes Matrix format, they were first decompressed/synthesised in order to generate multi-parameter floating point images for subsequent processing. The resulting images were geo-referenced to a UTM and latitude-longitude map projections using a first order polynomial and resampled with the nearest neighbour method. A total of 51 GCPs was used for the Blue Mountains site while 20 GCPs were utilised for the Gippsland site. In both cases, the GCPs were identified with the aid of topographic maps of different scales. In as much as the forest areas of interest occupy less than a quarter of the images, spatial subsetting was performed to reduce the volume of data and thus facilitate subsequent data handling, processing and analysis procedures. For the Gippsland site, geometric correction was performed on the subset image using intersections of compartment boundaries, roads and fire lanes within the pine plantations as GCPs. For the Blue Mountains site, geometric correction was conducted prior to image spatial subsetting since it was difficult to select good GCP locations within the forested areas of the Blue Mountains National Park. Thus, for an easier and more accurate identification of GCPs, and consequently a better

geometric correction result, the whole of the radar scene was used in the geometric correction process. The subset images extracted from the two radar scenes to constitute the Blue Mountains and the Gippsland study site cover approximately 1,800 ha and 2,000 ha of forest areas, respectively. Residual error after registration for the two sites was approximately half a pixel, which was within the accuracy required for the project, as sample plots were more than 300 m^2 in area.

The range of elevation across most of the areas covered by the subset images were 100 to 160 metres above sea level for the Blue Mountains site and 110 to 120 metres above sea level for the Gippsland site. In the case of the Blue Mountains site, however, almost all of the GCPs were located within the flat areas below the mountains with an almost uniform elevation of 60 metres above sea level. A height displacement error is thus expected to occur because of the difference in the residual level used for the geo-referencing process, as represented by the elevation of the GCPs, and the actual elevation of the study site. With an AirSAR look angle of 22.4^0 to 62.1^0 from the near to far range, the height displacement is given by the formula

$$s = \Delta h / \tan \theta \qquad (6.2)$$

where s is the height displacement, Δh the terrain height difference above datum, and θ is the look angle. This error is compensated for during the data analysis by adjusting the locations of the sample plots in the image in the direction towards the antenna (North to South) with the magnitude of the adjustment equivalent to the height displacement. To derive the look angle for each sample plot, an incidence angle image was generated and then linked to the input radar image using one of the functions under the radar tool menu of the ENVI software. Given in Table 6.1 are the data on elevation, radar look angle and height displacement for the different sample plots. For the Gippsland study site, as discussed in Section 5.5.2 of the previous chapter, the measurements taken from the randomly placed sample plots were only used as surrogate data for the stand compartments of comparable age

identified in the image using updated plantation maps and other relevant data. For this reason, it was thus considered unnecessary to apply the adjustment.

Map projection

Due to shape of the earth, remotely sensed images of the planet's resources are basically acquired over a spherical surface. A system of representation of all or part of these images of the earth on a plane map surface is called a map projection (Sanchez and Canton, 1999). Accuracy errors in the representation on maps of features derived from the spherical earth, which can be expected to occur because of the inherent differences between the two surfaces, may be confined to a few distortions relating to shape, direction, area, or size of the features, or may be minimal in certain portions of the map (Campbell, 1987).

The radar images in this study were formatted using the Universal Transverse Mercator (UTM) projection, and in particular the Australian Map Grid Zone 55 for the Gippsland site and Zone 56 for the Blue Mountains site. This projection was developed by the U.S Army in 1947 for the production of maps at a worldwide scale. It is an offshoot of the system introduced in 1569 by Gerhard Kramer, a Dutch cartographer who preferred to be called by the equivalent of his name in Latin, Gerardus Mercator. In its most popular version, the earth is divided into sixty longitude zones, which are six degrees apart. The zones are numbered successively in an easterly direction from the first zone, which encompasses 6^0 east of the meridian at 180^0 longitude. For each UTM zone, the central meridian is at 3^0 from the zone's east boundary and the latitude, which originates from the equator, covers the area from 84^0 North to 80^0 South. A false northing of 10,000,000 m is added to the southern hemisphere latitudes and a false easting of 500,000 m is used for all of the central meridians to avoid obtaining negative values. The UTM system also assigns letters C through X to eight-degree zones along the parallels, though this designation is ordinarily waived in civilian maps (Sanchez and Canton, 1999).

Sample Plot	UTM Coordinates (m)	Elevation (m)	Look Angle (^{0})	Height Displacement (m)
1	6258340 N, 279463 E	120	44.95	70.36
2	6260249 N, 280737 E	140	52.44	74.10
3	6258314 N, 279826 E	120	44.33	71.77
4	6258043 N, 279650 E	120	43.20	74.41
5	6258757 N, 280359 E	160	46.20	112.71
6	6259156 N, 280947 E	160	47.87	106.92
7	6258815 N, 280628 E	160	46.45	11.82
8	6257495 N, 279124 E	120	40.93	80.10
9	6257351 N, 278937 E	120	40.31	81.77
10	6259303 N, 279190 E	120	48.50	62.90
11	6259380 N, 279066 E	100	48.80	41.54
12	6258192 N, 279214 E	120	43.82	72.95
13	6257585 N, 281344 E	100	41.30	52.76
14	6255598 N, 279679 E	100	32.61	71.14
15	6255167 N, 279538 E	100	31.18	75.03
16	6258388 N, 281333 E	100	44.65	47.36
17	6256572 N, 280542 E	100	37.05	60.80
18	6256366 N, 280529 E	100	36.20	62.60
19	6255054 N, 280050 E	100	30.72	76.36
20	6255260 N, 280299 E	100	31.56	73.97
21	6255301 N, 280231 E	100	31.73	73.50
22	6255802 N, 280305 E	100	33.83	68.05
23	6258141 N, 281219 E	100	43.61	48.96
24	6257063 N, 281212 E	100	39.10	56.72
25	6258189 N, 281519 E	100	43.05	49.85

Table 6.1 Location, elevation, radar look angle and height displacement for the sample plots in study site 1

Effects on classification accuracy

Preprocessing operations intended to rectify geometric and radiometric errors may themselves introduce characteristics that may lead to subsequent inaccuracies in

the data analysis results (Campbell, 1983). This is because preprocessing causes changes in the data. Campbell (1987) specified the mean values for each band, the variances and covariances, and the correlations between bands as some examples of data that are altered, to some extent, from their original form after preprocessing. He cited a study made by Kovalick in 1983, where the effects of resampling and destriping on image classification accuracies were investigated. In this study, it was found that resampling causes an increase in variance but a reduction in the class means of the training data. He thus pointed out that although preprocessing procedures are essential in most remote sensing applications, there can be no list of standard preprocessing steps. That rather, the preprocessing techniques should be tailored according to the data at hand and the project needs and that only those operations that are essential to achieve a given purpose should be used. Because radar images have resulted from coherent return signals, they show a considerable amount of "speckle" (i.e., variations in backscatter response) from one resolution element to another, even for the same surface material. Thus, per pixel based classification is inappropriate and will lead to high classification errors. For this reason, classification was applied to the average backscatter derived from various techniques including segmentation.

6.2.2 Image enhancement

Image enhancement procedures are applied to facilitate visual interpretation by highlighting differences among image features of varying characteristics in a scene. The purpose is to create enhanced images from the original image data that will bring about greater amounts of visually interpretable image information. The enhanced images could be interactively displayed on the computer monitor or printed in a hard copy format in monochrome or colour (Lillesand and Kiefer, 1987). With respect to image restoration, Campbell (1987) specified two main differences. Firstly, he noted the objectivity of image restoration as opposed to the subjectivity of image enhancement. According to him, image restoration is conducted based on a specific knowledge of the causes of the distortions and the nature of the transformation algorithms applied to correct the faults. The effects of such correction procedures could be observed and are even measurable. Image

enhancement, on the other hand, is carried out without a full understanding of the causes for image appearance changes. The analyst judges the success of the procedure based on the resulting image's visual appearance and manual interpretability. The second difference he identified relates to the purpose of each procedure. That is, image restoration is employed as a preliminary step to digital (and visual) analysis while image enhancement is solely for subsequent visual interpretation. Hence, while statistical effects on image data are very important in image restoration, they are of little significance in image enhancement.

For both images of the areas used in this study, image enhancement routines under ENVI were applied. Among these are the contrast enhancement and spatial filtering routines. On the basis of differences in brightness/backscatter, several zones or classes in the image were identified and marked for comparison with the field data. The following theories and principles behind these specific image enhancement techniques, unless otherwise specified, were sourced from Campbell (1987), Jensen (1986), Mather (1987), and Richards (1993).

Contrast manipulation

In remote sensing, contrast relates to the range of digital numbers (DNs) or brightness values within an image. An increase in contrast effects a better visual discrimination of the different features in the image by the human observer. Contrast is improved by widening the original range of brightness values to make full use of the capabilities of the output or display device. Although the process entails the replacement of the pixel values in the original image by new values that matches the broader dynamic range of the display medium, the information content of the image is unaltered. In other words, only the lookup tables are modified to accentuate image features and the digital values stored in the computer memory remain unchanged. In this study, the different contrast manipulation techniques employed include the Linear, Histogram, and Gaussian stretch, which present different options of changing the contrast stretch of the displayed image.

Linear stretch

Linear stretch uses a new data distribution in the transformation of original DNs with new minimum and maximum data values set. The old minimum and maximum values are then adjusted according to the new data limits, with the intermediate values scaled proportionately between them. The main drawback of this method stems from its uniform assignment of display levels to the image pixel values regardless of their frequency of occurrence.

Histogram equalisation

An image histogram is a graph of the frequency distribution of the digital values of the different features in an image. Histogram equalisation is a method of assigning and stretching the image values to corresponding values in the display based on their frequency of occurrence so as to improve radiometric detail. The idea is to make each class in the output display have an equal number of pixel values thus generating an almost uniform output histogram. The best improvement in contrast will be among image features which have the highest frequency.

Gaussian stretch

This contrast enhancement technique involves the fitting of the histogram of the image pixel values to a normal or Gaussian histogram. This frequency distribution graph, as illustrated in Figure 6.2, is characterised by a bell-shaped curve where the mean is zero and about 61 % of the variable values are within one standard deviation from the mean. A proportional decrease in the frequency or probability values, as could be observed from the figure, occurs at both sides of the mean.

In some cases, a specific extent of image values may be exclusively dedicated to the entire display device for a more detailed analysis of the features within that image value range. If the purpose, for example, is to analyse a specific

forest stand which is represented in a small range of image values, then better results may be achieved by expanding this range according to the full display capability.

Spatial filtering

Similar to contrast manipulation, spatial filtering techniques are intended to facilitate data analysis by improving image interpretability. However, rather than simply modifying the lookup tables, these techniques alter the image data. In addition, unlike contrast manipulation methods which act on individual pixels without reference to the spatial context, spatial filters make use of spatial frequency information (Rees, 1990). Spatial frequency pertains to the number of changes in the digital values per unit distance. Image portions exhibiting high variability in these values over short distances are termed as *high frequency* areas. *Low frequency* areas are those having relatively few changes in the digital values over a given distance. Filters that emphasise fine details and edges in the image features are thus called *high frequency* filters while those that suppress detail and tend to smoothen the image are labelled as *low frequency* filters.

Most of the *low frequency* filters could be classified into three types: the *moving-average*, the *median*, and the *adaptive* filters. *Moving-average* filters utilise the mean of the pixels within a moving window that is passed from the left to the right of the image to remove or suppress sharply fluctuating data values consequently reducing the overall image variability. *Median* filters use the median of the of the pixels within the filter window. In both types of filter, a fixed set of weights is applied to all parts of the image covered by the moving window. The use of the median is deemed better than that of the mean since this parameter is less sensitive to errors or to extreme data values. While such abnormally high values, which usually represent noise, are considered in the averaging process used by *moving-average* filters, they are removed by the *median* filters. Feature edges are also preserved better by *median* filters compared to *moving-average* filters, which tend to blur or smoothen the pixels surrounding the central pixel. The trade-off, however, is that it takes more time to filter an image using the *median* instead of the *moving average*. *Adaptive* filters differ from the *median* and the *moving-average*

filters in terms of the smoothing method applied. In adaptive filtering, the weights are computed per window position and are based on the mean and variance of the values within the window. This filter type was the one used in this study to reduce the amount of speckles in the radar images.

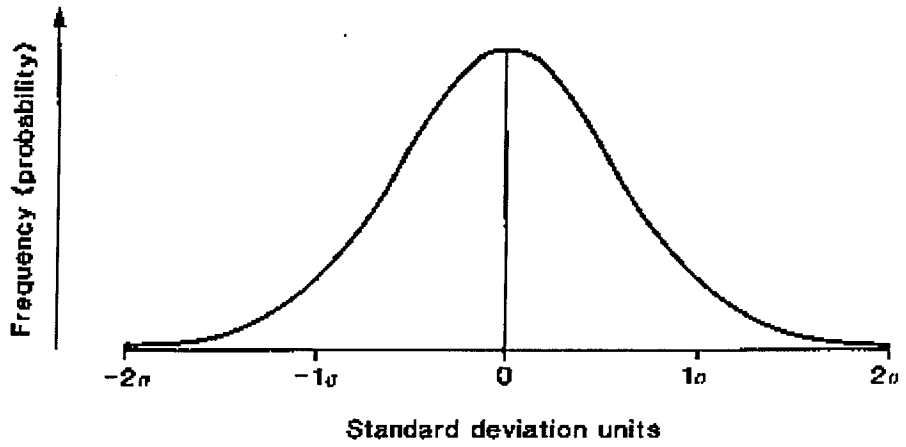

Figure 6.2 Standard Normal or Gaussian distribution (from Mather, 1987)

In contrast to *low frequency* filters, *high frequency* filters de-blur the image by eliminating low spatial frequencies and emphasising high frequency information or local spatial detail. An example of a simple high frequency filtering technique is the so called *image subtraction* method, which involves the pixel-by-pixel subtraction of a *low frequency* filtered output image from the original, unfiltered image. Other *high frequency* filtering methods, like the use of the *Laplacian* operator, are mainly based on the application of the concept of the derivative to determine the rate and direction of changes in backscatter values over the image space. Image portions exhibiting abrupt or sharp change in backscatter values represent high frequency areas and could be identified by their high gradient or the first derivative. The second derivative, which has a zero value when the gradient (first derivative) is constant, can be useful in the identification of minimum and maximum points in a slope of backscatter values. One technique to exaggerate the high frequency components is to add to the original image a multiple of the gradient

values at each pixel location hence amplifying areas with sharp variations in backscatter values.

For the delineation of vegetation boundaries in the study sites, *edge enhancement*, which is an extension of the technique of *high frequency* filtering (or image sharpening) was used. In this method, not only are the edges of the features enhanced but the low frequency information contained in the original image are preserved as well. The method is discussed further in a later section.

Speckle suppression

A consequence of the coherent nature of the synthetic aperture radar imaging process is the occurrence of "speckle". Speckle is a form of noise resulting from the interference imposed by several scattering centres of the different resolution cells making up the target. This interference, either positive or negative, on the elementary returns from the scattering centres produces light or dark image brightness thus creating a grainy texture and a "salt and pepper" appearance for the radar image (FAO, 1993). The presence of speckles raises a degree of uncertainty on the backscattered signals from the resolution cells thus adversely affecting data analysis results. There are two approaches to mitigate the effects of this problem: multi-looking of the radar image and the application of speckle filters. The first technique involves the averaging of the backscatter response from two or more independent images (or looks) to reduce the random variations caused by the speckles. The second approach entails the use of adaptive (low frequency) filters which compute and adopt the average brightness of adjacent cells within a moving window of specified size (e.g., 3 x 3 pixels). Speckle reduction through both methods, however, has the corresponding effect of reducing the spatial resolution. As this is the case, a trade-off between the permissible amount of speckle and spatial resolution has to be established.

As the images have already been processed to 18-looks in the azimuth direction, an acceptable level of speckle is observed. Additional multi-looking of the subset images were nonetheless performed to determine whether further

improvement could be achieved. Adaptive filters were then applied to both the original and multi-looked images.

Edge enhancement

As the name of the method implies, the aim of edge enhancement is to intensify the visible boundaries between areas in the image with contrasting brightness. Coarse resolution, the presence of noise, and other similar factors generally blur the edges between adjacent parcels in the image. To facilitate visual separation of the parcels, the edges of the parcels are made sharper. This is typically accomplished through the use of a moving window, which is systematically run through the image and centred successively on each pixel. The local average of the values within the window is computed and the value of the central pixel is compared with this average. The value is altered if it surpasses a specified difference from the computed average, thus highlighting the difference in brightness between the two sections.

For the images used in this study, edge enhancement was performed to facilitate identification of the boundaries between different parcels for the random placement of sample plots and subsequent data analysis. In consideration of minor positioning inaccuracies inherent in the GPS and radar imaging system, plots were placed well inside the parcels and those located at or close to parcel boundaries were not included in the field data collection. Stand structure and total biomass models were then developed and assessed based on the field and radar statistical data from the various parcels.

Monochrome to colour representation

Much of the time spent on image interpretation and processing, even in those activities that are quantitative in nature, is in performing display operations (Sanchez and Canton, 1999). Apart from better image resolution and wider brightness range, another factor that can improve visual discrimination of image features is the use of the available display colour range in the representation of the features instead of

merely using the monochrome display range. This is because the human eye can differentiate a limited range of discrete colours but an even more restricted range of grey values between black and white (Harrison and Jupp, 1990). As previously discussed, a multi-parameter radar scene is composed of a set of data values representing the backscatter intensities, as recorded in different frequency and polarisation combinations. For the radar system used in this study, the data contain information from the C-, L-, and P- bands with HH, VV, VH, and HV polarisation. Similar to the case of scene data taken by sensors operating in the visible and infrared portions of the electromagnetic spectrum, these different frequency-polarisation combinations were thus displayed three at a time using the red, green and blue (RGB) colour guns of the computer monitor for better visual discrimination. For every pixel in the radar image, the intensity of each of the RGB components is proportional to the amount of backscatter measured in the frequency-polarisation band assigned to each colour gun. All possible frequency-polarisation band and colour gun assignments were tested to find the combination/s that best highlights the colour differences among the forest stands in both study areas.

6.2.3 Visual image segmentation based on interpretation elements

Manual delineation of the different forest stands in the radar images of both study sites was undertaken based on the application of image interpretation elements such as tone, texture, size, shape, pattern, site, and association, which are separately defined below. This process was conducted with the awareness of the differences in sensitivities between the optical and radar signal, and how images taken by these two types of sensors should be interpreted accordingly.

Tone

Tone relates to the lightness or darkness of image features. It is depicted in shades of grey (e.g., light grey, medium grey, or dark grey/black) in black and white images and is described in terms of the specific colour of the feature (e.g., light red, medium red, or dark red) in colour images. Visible tonal variations occur among targets due to differences in their backscatter values. High backscatter intensities

produce light tones while low intensity signals generate dark tones on the radar image. Areas covered with tall vegetation, due to the presence of multiple bounce and volume scatterers within these sites, usually generate a relatively high backscatter intensity. Conversely, water bodies and open areas such as flat grasslands generally produce a low response mainly due to the specular reflectance of the radar signal. As a result, forested areas appear in light grey to medium grey tones while the second group of features generally occur in shades of dark grey to black on the radar image.

Texture

Texture can be defined as the degree of roughness or smoothness caused by spatial variations in backscatter between different targets within an image. It could be classified into different categories based on scale. Laur (1989) identified three texture types according to the number of resolution cells involved: micro-texture, meso-texture, and macro-texture. Micro-texture could be seen as a collection of grains of random brightness the size of which comparable to one resolution cell. Speckle is representative of this category. It differs from the two other types in the sense that it is system-inherent and as such could not be related to the real variation between the resolution cells in the radar scene. Meso-texture pertains to the natural variation in radar backscatter from features consisting several resolution cells. This category, also called "scene texture", is the most useful among the three types in the interpretation of the radar image (FAO, 1993). Spatial variation on a scale of numerous resolution cells is classified under macro-texture, or scene "structure". Some examples under this type are forest boundaries and linear features such as roads and streams.

Size

Size can be divided into two categories, relative and absolute, both of which are useful in visual image interpretation. The size of a target relative to known image objects provides a basis for the approximation of the image scale and the subsequent size estimation and identification of the target and other unknown

features. A main road, for example, could be confused with a walking track until a comparison of their sizes is made. Absolute measurements allow the extraction of quantitative information such as those pertaining to lengths, areas, or volumes of the imaged features. These information, among other factors, can aid in the confirmation of the target identity especially if the target dimensions are so distinctive that they form definitive criteria for specific objects or class of objects (Campbell, 1987). Information on the size of the different forest stands was also useful in the random selection and placement of sample plots. As much as possible, plots were located within stands large enough to allow for possible GPS-based placement errors.

Shape

The form or shape of the feature outline provides useful clues towards the identification of the target. Quite often, separation between natural and man-made targets can be made based solely on shape. Forest plantations, for example, usually appear in square or rectangular blocks that are separated by straight tracks for fire control and equipment access. Natural stands, on the other hand, are typically irregular in shape. Another example are roads or rail tracks, which generally appear as straight lines of uniform width with gentle curves, as opposed to the meandering streams or rivers, which usually have varying widths throughout their entire length. Although due to orientation at right angles to the incoming radar, certain features can have distorted or over exaggerated size and shape.

Pattern

Pattern refers to the repetitive spatial arrangement of related objects in a region within the image. This is more common in man-made features, where pattern is intentionally established according to a certain purpose or purposes. Typical examples along this line are the orderly arrangement of houses in a village/subdivision and of individual trees in a plantation or orchard. In both cases, the spacing between the houses and trees are set to improve the environmental conditions and to permit better accessibility within the sites.

Site

The geographic or topographic position of the target with respect to other image objects can be helpful in feature identification or in the fine tuning of the identification process. For example, mangrove species are not expected to be found in high elevations as trees belonging to this vegetation type thrive in low areas adjacent to water bodies. This information thus provides the basis for the re-identification of forest stands located on mountain tops, which were previously identified as belonging to such species.

Association

Association pertains to the typical simultaneous occurrence of objects minus the strict spatial arrangement denoted by pattern (Campbell, 1987). Some image features may be identified based mainly on their association with known objects. This is true in the case of natural or man-made features which are so closely interrelated that the identification of one feature tends to indicate or confirm the presence of the other (Henderson and Xia, 1998). This could be illustrated by a forest plantation being classified as such based on the presence of adjacent forest nurseries.

6.3 Field data analysis

Data on species, total and trunk height, bole diameter at breast height over bark, branching pattern, and other tree-associated parameters that affect the radar backscatter intensity were collected from the sites, organised, analysed and related to the backscatter data in different frequency-polarisation combinations. Other parameters such as topography and moisture conditions were also considered for a more holistic analysis. The analysis procedures, carried out using appropriate computer softwares, were guided by whether the stand structure and total aboveground biomass could be estimated from radar data through the application of models and indices. These models/indices were formulated based on a regression

analysis performed on the field measurements and biomass values that were obtained using appropriate allometric equations. Results from these operations are presented and discussed in the next chapter.

6.4 Allometric equations

6.4.1 For pines/conifers

The allometric equation formulated by Stewart and Flinn (1981) for the calculation of the total dry weight of all tree components was used to estimate the aboveground biomass of the pine stands. The equation was based on the results of a study conducted on 15-year old *Pinus radiata* stands in Gippsland, Victoria, Australia. In this investigation, 16 plots, each with an area of 0.16 hectare, were established in a seven hectare plantation. All trees in the sample plots were measured and divided into five diameter classes, each having an equal number of trees. Two trees were subjectively selected from near to mid point of each diameter class for the purpose of biomass sampling. The dbhob of each of the ten trees were measured and the dead branches from the ground level to the base of the crown were removed. The diameters and heights above ground level of all dead branches were simultaneously measured. Two branches were randomly selected from the whorls and the components classified as either dead branch wood or dead foliage. The trees were then felled and measurements pertaining to tree height, height to the green crown, stem diameter over bark at the base of the green crown, and the diameters and heights above ground level of all remaining branches were taken. Cones and stem foliage were collected prior to removing the branches from the main stem. The fresh and dry weights of the different components were then taken. The fresh weights of the wood and bark were measured by dividing the stem into 1.5 m sections, cutting discs of 5 cm thickness from the midpoint of each section, and separately weighing the wood and the bark. The dry weights were determined by oven-drying the tree constituents to constant weight at 80^0 C and calculating the dry weights from the section fresh weights, fresh weight ratios of the wood and bark from each disc, and the fresh weight-dry weight ratio of the disc components.

Equations for biomass prediction based on branch diameter and dbhob measurements were obtained through regression analysis. As the scatter diagrams generated for the different components exhibited curvilinearity, the data were fitted to the allometric function $Y = AX^B$. The data were then logarithmically transformed and the parameters of the function determined by linear regression techniques. The resulting allometric equation used for predicting the dry weights of the tree components is given below.

$$\log_{10} Y = \log_{10} A + B \log_{10} X \qquad (6.3)$$

where Y is the dependent variable, X the independent variable, and A and B are the parameters of the function.

The equation from the logarithmic regression of total foliage weight and branch diameter was solved for all branches in each of the five sections per tree to calculate the foliage weight per section of each tree and hence, the total foliage weight. Regression analyses involving branch diameter and branch wood weight in the green crown, as well as foliage and branch wood weight in the dead crown, were performed and the resulting equations solved for the green and dead crown branch diameters to obtain crown component weights per tree. Regressions were then fitted for these weights against dbhob. These regressions, along with those relating stem component weights against dbhob, were solved using tree dbhob data from the 16 sample plots to derive land area estimates of tree components weights. A correction factor, computed using the following formula, was applied to account for the systematic bias due to logarithmic transformation:

$$Y_i \text{ (corrected)} = \text{antilog } (Y_i + \tfrac{1}{2} S^2_{YX}) \qquad (6.4)$$

where Y is the dependent variable, X the independent variable, and S^2_{YX} the mean square about the regression.

The allometric regression parameter coefficients used for the prediction of crown and stem component weights are presented in Table 6.2. The individual

allometric regressions were all significant ($P < 0.001$). The total aboveground biomass computed for the stand was 162.20 +/- 5.10 tonnes/ha, broken down as follows: stem wood 67 %, stem bark 8.6 %, dead and living foliage 6.8 %, and branch wood plus cones 16.4 %. The aboveground biomass estimates for the different tree components obtained in the study compared favourably with results reported by other researchers for *P. radiata* stands of the same age. Considering allowance for stand age, the biomass amounts computed were similar to that obtained from a 12-year old stand in Tumut, New South Wales, Australia but was less than that in an 18-year old stand in New Zealand (269.30 tonnes/ha). The difference in the latter case was attributed to the more favourable growing conditions such as more fertile soils and evenly distributed precipitation of 1500 mm per annum in New Zealand. In all of these studies, foliage accumulation and shedding was found to be in equilibrium between 10 and 18 years old and that foliage weight was independent of the site index.

Component (Y, kg)	Dimension (X, cm)	n	$\log_{10} A$	B	S_{YX} ($\log_{10}$ units)	C.F.
Dead branch wood	Branch diameter	114	-1.5508	2.7380	0.1626	1.0726
Dead foliage	Branch diameter	114	-2.4567	0.6450	0.5126	2.0069
Living branch wood	Branch diameter	372	-1.7627	2.9856	0.2164	1.1322
Living foliage	Branch diameter	372	-1.6190	2.0491	0.2394	1.1641
Dead branch wood	Dbhob	10	-2.5232	2.5149	0.1498	1.0613
Dead foliage	Dbhob	10	-0.9254	0.4454	0.0917	1.0226
Living branch wood	Dbhob	10	-2.9973	3.1679	0.0889	1.0212
Living foliage	Dbhob	10	-1.8614	2.2039	0.0622	1.0103
Cones	Dbhob	10	-2.1543	2.1940	0.2422	1.1683
Stem wood	Dbhob	10	-0.6655	2.0680	0.0564	1.0085
Stem bark	Dbhob	10	-1.5969	2.0981	0.0608	1.0099
Total	Dbhob	10	-0.6198	2.1615	0.0497	1.0066

Y = dependent variable, X = independent variable, n = no. of samples, A = regression intercept, B = regression slope, S_{YX} = standard deviation of regression, and C.F. = correction factor for logarithmic bias.

Table 6.2 Allometric regressions for the prediction of tree component dry weights of *Pinus radiata* stands (from Stewart and Flinn, 1981).

6.4.2 For broad-leaved stands

Biomass prediction for the broad-leaved stands was carried out using allometric equations developed by Stewart, Flinn and Aeberli (1979) for an uneven-aged mixed eucalypt forest in Eastern Victoria, Australia. Only three sets of equations (allometric and linear) were developed from the study inasmuch as 78 % of the total eucalypt vegetation in the sampling area is comprised of three species namely, *E. agglomerata*, *E. muellerana*, and *E. sieberi* and it was deemed impractical to harvest trees from the five species comprising the remaining 22 % of the population. The biomass estimates for the trees from the five species, *E. sideroxylon*, *E. consideniana*, *E. globoidea*, *E. goniocalyx*, and *E. bridgesiana*, were obtained from the equations formulated for the three dominant species.

Tree component measurements were taken from 17 sample plots, each 0.1 ha in area, within a contiguous tract of 1500 x 400 m. A total of 31 trees, divided into three diameter classes (large, medium, and small), were sampled. Of this number, 11 are *E. muellerana* and 10 trees each of *E. agglomerata* and *E. sieberi*. After measuring dbhob, the trees were felled and data on stem diameter over bark measured at the base of the crown, total length, crown length, branch diameter measured eight cm from the intersection of the branch and the stem, and the branch height above the base of the stem were recorded. The branches were separated into leaves (including petiole), twigs (including buds and capsules), wood and bark and their fresh weights measured. The stem was cut into sections and cross sectional discs five cm thickness were sawn from the midpoint of each section. The stem wood and bark were then separated and their fresh weights taken. The dry weight and moisture content of the different branch and stem constituents were determined from representative sub-samples subsequently taken from the branch and cross sectional disc components. Regression analysis was then performed for each species to derive equations for the prediction of the dry weights of branch and stem components from branch diameter and dbhob measurements. The S_{YX} (standard deviation of the regression) and R^2 (coefficient of determination) values were used to evaluate the precision of the regression equations. Land area estimates of the aboveground biomass were computed by applying the appropriate equations using

branch and stem dimensions of the individual trees and summing the predicted weights for each sample plot. The total aboveground biomass estimated for the forest area was 344 tonnes/ha with stem wood constituting 60.1 % of this total, stem bark 15.8 %, branch wood 16.5 %, branch bark 3.9 %, twigs 2.0 %, and leaves 1.7 %.

The allometric equations for the three species of eucalypts are in the same form as in equation 6.3 with the regression parameter coefficients given in Table 6.3. The correction factor formula presented in equation 6.4 is also applied in all cases to eliminate bias during the conversion of the logarithmic estimates into arithmetic units.

Similar to what was done by Stewart et al. (1979) in the application of the regression equations, the biomass amounts for all the broad-leaved species in the Blue Mountains site of this particular study were estimated using either of the three equations. The selection of the equation to be used for a specific species in the study site depended on the resemblance of the species to either of the three eucalypt species with available equations. The closest resemblance in terms of general tree structure, composition, morphology and growth pattern of the stem and branch components determine the choice of equation. Listed in Table 6.4 are the broad-leaved tree species in the Blue Mountains study site categorised according to the equation used for biomass prediction. The biomass of the trees included in the first group had been estimated using the equation for *E. agglomerata* while the biomass of those in the second and third groups has been predicted using the equations for *E. sieberi* and *E. muellerana*, respectively. Not included in the list is the White Cypress Pine (*Callitris hugelii*) since the biomass of the trees of this species had been estimated using the allometric equation for *Pinus radiata*.

Unlike in the case of *Pinus radiata*, no allometric equation for the direct prediction of the total dry biomass was developed for the broad-leaved species. Instead, the total biomass is derived by summing up the biomass of the individual tree components computed from allometric equations which use either the branch diameter or dbhob as the independent variable. As some of the branch diameter data for the trees in the Blue mountains study site were collected using ocular estimation

it was decided that the dbhob values, which were all obtained from actual measurement of the stem diameters, be exclusively used instead.

Component (Y, kg)	Dimension (X, cm)	n	$\log_{10}$ A	B	S_{YX}	R^2	C.F.
Eucalyptus agglomerata							
Leaves	Branch diameter	42	-1.2240	1.6678	0.1528	0.911	1.0272
Twigs	Branch diameter	42	-1.2898.	1.7729	0.1275	0.943	1.0189
Branch wood	Branch diameter	42	-1.9513	2.8435	0.2006	0.946	1.0474
Branch bark	Branch diameter	42	-2.4176	2.7816	0.1902	0.949	1.0425
Stem wood	dbhob	10	-0.9407	2.3156	0.07605	0.980	1.0067
Stem bark	dbhob	10	-1.3879	2.2365	0.07575	0.978	1.0066
Eucalyptus sieberi							
Leaves	Branch diameter	38	-0.8018	1.3273	0.2172	0.781	1.0558
Twigs	Branch diameter	38	-0.8777	1.4506	0.1804	0.861	1.0382
Branch wood	Branch diameter	38	-1.7180	2.8260	0.1854	0.957	1.0404
Branch bark	Branch diameter	38	-2.5940	2.8774	0.1482	0.973	1.0256
Stem wood	dbhob	10	-1.0373	2.3867	0.07103	0.976	1.0058
Stem bark	dbhob	10	-2.1434	2.7344	0.08243	0.976	1.0079
Eucalyptus muellerana							
Leaves	Branch diameter	52	-1.1547	1.5265	0.1865	0.874	1.0409
Twigs	Branch diameter	52	-1.1258	1.5231	0.1521	0.912	1.0270
Branch wood	Branch diameter	52	-2.1885	3.0690	0.2047	0.959	1.0494
Branch bark	Branch diameter	52	-2.6478	2.8632	0.1873	0.960	1.0412
Stem wood	dbhob	11	-1.2827	2.5199	0.08609	0.975	1.0086
Stem bark	dbhob	11	-1.1425	1.9912	0.1032	0.944	1.0123

$\log_{10}Y = \log_{10}A + B \log_{10}X$ where Y = dependent variable, X = independent variable, n = no. of samples, A = regression intercept, B = regression slope, S_{YX} = standard deviation of regression, R^2 = coefficient of determination and C.F. = correction factor for logarithmic bias.

Table 6.3 Regressions for the prediction of branch and stem component dry weights of *E. agglomerata*, *E. sieberi* and *E. muellerana* (from Stewart et al., 1979)

Hence, for each broad-leaved tree, the total biomass was estimated by first computing for the stem wood (or stem bark) dry biomass and then using this value to calculate for the biomass of the other components. This process was based on the percentages derived by Stewart et al. (1979) for the different tree components (i.e., stem wood constituting 60.1 % of the total, 15.8% for stem bark, 16.5 % for branch wood, 3.9 % for branch bark, 2.0 % for twigs and 1.7 % for leaves).

Group I (E. agglomerata)	Group II (E. sieberi)	Group III (E.muellerana)
E. maculata	E. sideroxylon	E. robertsoni
E. micrantha	E. creba	
E. saligna	E. paniculata	
E. tereticornis	E. siderophloia	
E. ovata	E. resinifera	
E. viminalis	E. longifolia	
E. camaldulensis	S. glomulifera	
E. largiflorens		
E. gummifera		
M. linariifolia		

Table 6.4 List of all broad-leaved tree species in the Blue Mountains study site categorised according to the allometric equation used to estimate total biomass

6.5 Image classification

Classification is a process whereby images are divided into regions or classes of similar properties. It is different from visual image segmentation in the sense that the criteria used in the assignment of pixels to different classes are quantitative in nature. In VIR images, for example, classification is commonly performed based on the DNs of the pixels composing the image. The underlying principle is that pixels with similar DNs generally represent surfaces with similar properties or characteristics. The classified image is then presented as a mosaic of uniform parcels, each represented by a colour code or symbol (Campbell, 1987).

In this study, the classification of the images of the study sites is made in accordance with the objectives of the investigation. That is, the separation between

classes is based on predicted stand structure and total aboveground biomass. Below are the specific procedures undertaken for the purpose.

6.5.1 Computation of TCMI and TCBI

As discussed in Chapter 3, stand structure and total aboveground biomass could be determined based on the TCMI and TCBI. For each study site, the TCMI and TCBI values from the different sample plots were calculated from image backscatter measures. Biomass estimation models were then generated based on these index values and the total aboveground biomass of the stands, as computed using appropriate allometric equations.

In consideration of the coherent nature of the radar signal, the backscatter value for each sample plot was obtained not only from one but a number of pixels. The average value obtained from the backscatter values of the central and neighbouring pixels is recorded. The total number of pixels used in each process is around 100 pixels, this being the average amount in which the backscatter value stabilises based on plots of backscatter against the number of pixels.

6.5.2 Relating forest parameters with other frequency-polarisation combinations

Apart from the TCBI and the TCMI, other radar frequency-polarisation combinations were explored in terms of their relationship with forest parameters such as stand structure and total aboveground biomass. This step is in line with the intention of validity testing, that is, on whether the concepts and indices introduced in Chapter 3 provide for the best radar data-based estimates of forest properties. The relationships between the various frequency-polarisation combinations and total biomass were derived in consideration of the biomass saturation limits for each of the bands (see Section 3.3.1 of Chapter 3). The individual saturation levels were ascertained by plotting the various bands against increasing amounts of biomass. The point in the graph in which the backscattering coefficient no longer responds to any increase in biomass denotes the saturation limit for the band.

6.5.3 Production of derived images and maps

Results from the above procedures were presented in the form of derived images/maps and their potential assessed. These include TCMI, TCBI, and biomass distribution images/maps for the study areas.

6.6 Accuracy assessment

Prior knowledge of the general structure of the stands in the different sample plots, as obtained from the field data collection activities conducted in the study sites, was used as the basis for the assessment of the accuracy of the TCMI-based stand structure estimates. For reasons previously discussed, higher TCMI values are expected from coniferous stands relative to broad-leaved vegetation. To allow testing of the accuracy of each stand structure-specific biomass model in providing measures of total aboveground biomass, some sample plots were not used in the model formulation process but were assigned as model validation (test) sites. Using the field data from these test sites, accuracy assessment was then carried out based on a comparison of the biomass values derived from the application of the models and those computed from the appropriate allometric equations.

6.7 Integrated data analysis

The various field and radar data analysis methods employed for the estimation of the general structure and total aboveground biomass of the broad-leaved and needle-leaved stands in study sites 1 and 2 are summarised in Figure 6.3.

Visual image segmentation for study site 1 was undertaken based on the application of image interpretation elements on different radar band combination images enhanced using various image enhancement methods. As previously discussed, differences in tone and colour of the various stands due to backscatter variations in different band and polarisation combinations denote vegetation

diversity in terms of species, tree morphology and total aboveground biomass. Stand structure and biomass models/equations were consequently developed utilising backscatter measurements and total aboveground biomass levels calculated from appropriate allometric equations as inputs. The accuracy of the models in providing estimates of general structure and total biomass was assessed using the same allometric equations, radar backscatter and ground truth data from test plots set aside for the purpose. Although 149 of the 1313 trees sampled are White Cypress Pines, they were classified under the broad-leaved category. This is because majority of these trees are in the sapling stage and thus exhibit little difference in terms of structure relative to the broad-leaved trees. Moreover, these pines are so completely intermixed with the broad-leaved trees that it is not possible to discriminate them in the radar image.

Visual classification of the study site 2 image was relatively easier due to the following reasons: a) the vegetation is mono-specific; b) the availability of detailed compartment maps and plantation data for every compartment; and c) the various compartments can be clearly identified on the radar image. The methods employed to obtain measures and estimates of stand structure and total aboveground biomass for the needle-leaved conifers are the same as those applied to the broad-leaved stands. Similar to what was done in study site 1, the accuracy of the derived biomass estimation model/equation was assessed using the pine allometric equation, field and radar data from five previously designated test plots.

6.8 Summary and conclusions

There is a wide range of data analysis procedures that can be applied to radar data. Although standard analysis methods exist, additional techniques may be introduced to the whole data analysis process. Conversely, some of the procedures considered as parts of the standard method may be considered unnecessary and thus disregarded. Generally, the analysis methods to be applied depend on the quality of available data and the purposes or uses to which these data are to be put. As such, there should be no fixed or standardised menu of procedures for each and every

application. Rather, the analyst must be cognisant of the qualities of the data at hand and be able to identify and schedule the appropriate rectification and analysis techniques to achieve the study objective.

The specific data analysis procedures covered in this chapter have been organised for the purpose of developing a system of methodologies that will enable the determination of the general stand structure and total forest aboveground biomass from multi-parameter radar data. These procedures could be included under the categories of either preprocessing, image enhancement, and image segmentation or classification.

Preprocessing is a necessary phase in most, if not all, remote sensing applications. The steps under this category are designed to correct or compensate for the systematic and non-systematic errors introduced during the image acquisition process so as to make radiometric and geometric characteristics of the image as close as possible to what the image is supposed to have. These steps are termed as preprocessing operations since they are applied prior to primary data analysis. For the radar data used in this study, only the corrections for random errors were performed as systematic error compensation was already done by NASA/JPL.

Subsequent to preprocessing operations are the application of image enhancement techniques that include contrast manipulation, spatial filtering and monochrome to colour representation. These techniques are intended to facilitate interpretation by improving the visual interpretability of the image (e.g., by the removal or reduction of noise and other unwanted effects) and highlighting differences among features that are of interest to the user. Visual feature discrimination and image segmentation were carried out with the aid of information provided by image interpretation elements such as tone, texture, size, shape, pattern, site and association.

Based on the information gathered from the fieldwork, corresponding allometric equations were selected from published research and used to estimate the total aboveground biomass of the different forest stands. The biomass estimates

were then related with the TCBI values for the formulation of stand structure-specific equations or models for radar data-based biomass estimation operations. Additionally, other frequency-polarisation combinations were also tested for their applicability in providing estimates of stand structure and forest biomass. The accuracy of these models and indices were assessed using field data from randomly selected test sites. Results obtained from these procedures are presented in the next chapter.

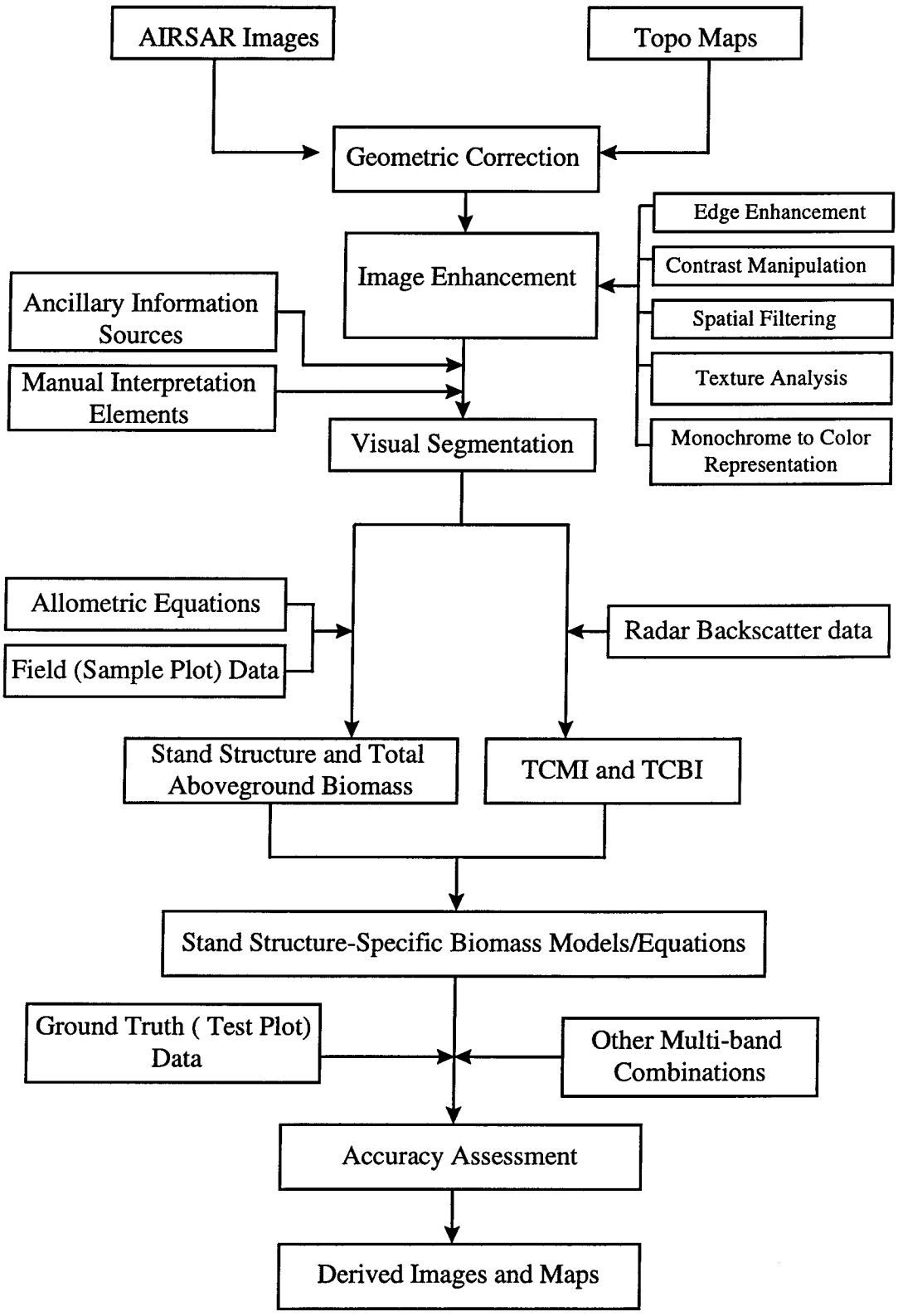

Figure 6.3 Methodology for the estimation of stand structure and total aboveground biomass of the broad-leaved and needle-leaved vegetation in study sites 1 and 2

CHAPTER 7

APPLICATION OF MORPHOLOGY AND BIOMASS RADAR MODELS TO FIELD SAMPLED DATA

7.1 Introduction

In Chapter 4, promising results were obtained from the application of the theories and indices to interpolated data from published research. Stand structure and total aboveground biomass, for example, were found to be highly correlated with the TCMI and TCBI, respectively. With these results, however, are potential problems caused by factors such as the limitation in the amount of data available from the published studies, the comparability of the data from different researchers, and the possible errors introduced during the interpolation process. In order to verify the validity of the results, further application of the theories, models and indices based on an adequate amount of actual measured values from independent study sites is thus necessary. This chapter presents the outcome of the application of the models and indices to field and experimental data for broad-leaved and needle-leaved stands in the Blue Mountains and Gippsland study sites with the field data being collected using the methods described in the previous chapter. Apart from validity testing, it is believed that a better understanding of the radar backscatter-vegetation component interactions will be obtained from the application of the methods given the relatively more complete amount of data from the study sites as compared to the research data from Chapter 4.

7.2 Relating radar data to field data

Given in Tables 7.1 and 7.2 are the backscatter in different bands for the sample plots in the Blue Mountains and Gippsland study sites used for the development of stand structure and biomass models. In each of the two sites, radar

and field data from 20 sample plots, randomly chosen from a total of 25, were used for the model formulation with the data from the other five plots used for post-testing of the accuracy of the derived models. The backscatter amounts are in intensity values and can be converted to decibels using the formula given in equation 4.1.

7.2.1 Radar data-based indices against stand structure and forest biomass

Presented in Table 7.3 are the total aboveground dry biomass, TCMI and TCBI values for the model development plots in the two study sites. The total aboveground dry biomass for each plot was computed from field measurements and the allometric equations described in the previous chapter.

TCMI and stand structure

The TCMI values for the broad-leaved stands range from 3.10 to 7.03, with a mean value of 4.65, and the values for the needle-leaved pines are from 3.46 to 6.72, with a mean value of 4.81. These results are generally in agreement with the theories introduced in Chapter 3, and the results presented in Chapter 4, which suggest lower values for the broad-leaved stands relative to those of the needle-leaved pines. Although this is the case, the average difference between the two sets of values is not sufficiently significant for the TCMI to be considered a good measure of stand morphology. This deviation from the good results presented in Chapter 4 could be ascribed to the close similarity in structure among most eucalypts and the radiata pines. Compared to most broad-leaved species in the northern hemisphere and the tropics, eucalypts generally have narrower and less voluminous leaves, less defined crown, relatively longer and more cylindrical trunk, and with a branching pattern more closely resembling that of the pines (see Appendices 5.1 and 5.2). It should be noted, however, that the L-HH and C-HV plot (Figure 7.1) clearly separates the two tree species.

Plot #	C-HH	C-VV	C-HV	L-HH	L-VV	L-HV	P-HH	P-VV	P-HV
1	0.1044	0.0828	0.0232	0.1053	0.0867	0.0247	0.0754	0.0843	0.0125
2	0.1047	0.0594	0.0176	0.0872	0.0876	0.0281	0.0515	0.0861	0.0136
4	0.1300	0.1013	0.0271	0.1124	0.1006	0.0318	0.0654	0.1010	0.0127
5	0.0915	0.0763	0.0174	0.0820	0.0741	0.0216	0.0513	0.0744	0.0096
6	0.1594	0.1074	0.0305	0.1069	0.1000	0.0377	0.0470	0.0865	0.0150
7	0.1083	0.0800	0.0212	0.0961	0.0868	0.0261	0.0431	0.0810	0.0113
8	0.1198	0.0962	0.0250	0.0998	0.1043	0.0297	0.0460	0.0722	0.0110
9	0.0947	0.0748	0.0192	0.0841	0.0862	0.0216	0.0430	0.0790	0.0113
10	0.1133	0.0712	0.0201	0.0874	0.0843	0.0288	0.0416	0.0820	0.0149
11	0.0927	0.0540	0.0154	0.0901	0.0597	0.0170	0.0399	0.0617	0.0096
13	0.1332	0.0942	0.0226	0.1412	0.0867	0.0246	0.0970	0.0825	0.0120
14	0.1467	0.1336	0.0341	0.1056	0.1173	0.0294	0.1034	0.0986	0.0089
16	0.1045	0.0764	0.0182	0.0996	0.0735	0.0233	0.0523	0.0743	0.0120
17	0.1468	0.1130	0.0294	0.1193	0.0934	0.0327	0.0587	0.0791	0.0135
18	0.1350	0.1010	0.0274	0.1241	0.0833	0.0269	0.0546	0.0677	0.0093
20	0.1939	0.1961	0.0447	0.1533	0.1145	0.0329	0.0910	0.0915	0.0098
22	0.1198	0.1054	0.0237	0.1027	0.0887	0.0215	0.0422	0.0671	0.0079
23	0.1034	0.0704	0.0174	0.1223	0.0814	0.0240	0.0858	0.1033	0.0123
24	0.1230	0.1010	0.0300	0.1435	0.0914	0.0268	0.0659	0.0801	0.0121
25	0.1051	0.0807	0.0213	0.1075	0.0782	0.0267	0.0539	0.0790	0.0122

Table 7.1 Backscatter (in intensity values) in different bands for the sample plots in the Blue Mountains study site used for the development of stand structure and biomass models

Plot #	C-HH	C-VV	C-HV	L-HH	L-VV	L-HV	P-HH	P-VV	P-HV
2	0.3708	0.3595	0.0764	0.3185	0.2440	0.0587	0.1238	0.1482	0.0205
3	0.3449	0.3203	0.0846	0.3545	0.2781	0.0824	0.1538	0.2014	0.0274
4	0.2035	0.1596	0.0527	0.3148	0.2109	0.0620	0.1821	0.1955	0.0173
5	0.2521	0.2690	0.0598	0.4018	0.2628	0.0700	0.2045	0.2349	0.0347
8	0.1907	0.1721	0.0522	0.3286	0.2563	0.0967	0.2479	0.2099	0.0398
9	0.1454	0.1587	0.0518	0.3348	0.2429	0.0809	0.2749	0.2599	0.0533
10	0.1608	0.1420	0.0550	0.3085	0.2086	0.0835	0.3027	0.1895	0.0488
12	0.1808	0.1724	0.0603	0.3652	0.2320	0.1021	0.2921	0.2679	0.0600
13	0.2389	0.1805	0.0664	0.3343	0.2223	0.0870	0.3601	0.1585	0.0547
15	0.2396	0.1998	0.0712	0.2881	0.2397	0.0885	0.3768	0.1779	0.0546
14	0.2756	0.1920	0.0675	0.3284	0.2390	0.0777	0.3722	0.1669	0.0593
16	0.1904	0.1813	0.0629	0.2379	0.1594	0.0578	0.3776	0.1661	0.0550
17	0.2405	0.2126	0.0625	0.2781	0.1872	0.0707	0.3846	0.1802	0.0681
18	0.2356	0.2251	0.0795	0.2752	0.2202	0.0750	0.4184	0.2112	0.0748
19	0.1875	0.1900	0.0633	0.2783	0.1967	0.0807	0.3750	0.1776	0.0834
21	0.2125	0.2267	0.0713	0.2723	0.2048	0.0819	0.3324	0.1766	0.0909
23	0.1978	0.1515	0.0538	0.2314	0.1726	0.0644	0.2562	0.1171	0.0488
22	0.2452	0.1905	0.0671	0.2569	0.1966	0.0747	0.2196	0.1018	0.0380
24	0.2409	0.1983	0.0666	0.2758	0.2173	0.0739	0.2317	0.1082	0.0435
25	0.2170	0.1670	0.0590	0.2670	0.1841	0.0674	0.2246	0.1107	0.0407

Table 7.2 Backscatter (in intensity values) in different bands for the 20 model development sample plots in the Gippsland study site

Study Site 1 (Blue Mountains)				Study Site 2 (Gippsland)				
Plot	Biomass (t/ha)	TCMI	TCBI	Plot	Age	Biomass (t/ha)	TCMI	TCBI
2	96.19	4.95	0.1048	2	5	89.27	4.17	0.3949
25	131.30	5.05	0.1288	3	5	94.53	4.19	0.4391
10	148.31	4.35	0.1075	4	6	108.84	5.97	0.3675
13	222.42	6.25	0.1638	5	6	112.12	6.72	0.4616
23	240.03	7.03	0.1397	8	9	129.44	6.30	0.3808
20	242.44	3.43	0.1980	9	9	131.79	6.46	0.3866
24	246.35	4.78	0.1735	10	10	141.79	5.61	0.3635
16	267.80	5.47	0.1178	12	10	149.66	6.06	0.4255
1	276.98	4.54	0.1285	13	19	193.10	5.03	0.4007
17	288.25	4.06	0.1487	15	19	196.84	4.05	0.3593
18	294.42	4.53	0.1515	14	19	199.80	4.87	0.3959
5	297.52	4.71	0.0994	16	22	212.99	3.78	0.3008
6	331.31	3.50	0.1374	17	22	214.00	4.45	0.3406
22	369.10	4.33	0.1264	18	22	216.53	3.46	0.3547
14	374.43	3.10	0.1397	19	24	241.25	4.40	0.3416
4	386.40	4.15	0.1395	21	24	243.95	3.82	0.3436
9	422.53	4.38	0.1033	23	26	353.10	4.30	0.2852
8	518.67	3.99	0.1248	22	26	377.40	3.83	0.3240
7	557.51	4.53	0.1173	24	27	413.32	4.14	0.3424
11	583.98	5.85	0.1055	25	27	442.05	4.53	0.3260

Table 7.3 Total aboveground dry biomass, TCMI and TCBI values for the sample plots in study sites 1 and 2 (Blue Mountains and Gippsland)

TCBI and total aboveground dry biomass

Given in Figure 7.2 is a graph of the TCBI values against the total aboveground dry biomass for both the broad-leaved and needle-leaved stands in the two study sites. Easily discernible from the figure are the low to medium R values for both stand categories (0.4577 for broad-leaved stands and 0.7620 for pines) thus indicating a weak to moderate relationship between TCBI and total biomass. This is most likely due to the early saturation of the C-HV and L-HH signals (therefore rendering the TCBI ineffective) as a consequence of the high amounts of forest biomass in the study areas.

The pine data curve is very similar to that of Dobson et al. 1995a, where there is a decline in the TCBI beyond the 90 tonnes/ha biomass range. This negative correlation between TCBI and total biomass above this range is primarily due to the radiata pine canopy becoming very closed as biomass increases hence causing less and less radar signal penetration. Thus, departing from what the TCBI theory is based on, it is only the crown component which is being sensed by the C-HV and most of the L-HH signals, at biomass levels above 90 tonnes/ha. Additional field data collection from sample plots with low tree density (total biomass of 100 tonnes/ha or less) could have been undertaken except they do not truly represent real working forests. The data curve for the broad-leaved stands, on the other hand, does not exhibit a similar trend. This is because of the relatively less dense canopy and a higher amount of undergrowth biomass (i.e., from small trees) in the eucalypt-dominated stands.

7.2.2 Saturation of radar measurements

Different levels of saturation, or the amount of biomass in which the backscatter no longer responds to any further increase in biomass, were observed for the different bands. The saturation level for the C-, L- and P- bands are generally about <100 tonnes/ha, 140 tonnes/ha, and 245 tonnes/ha, respectively.

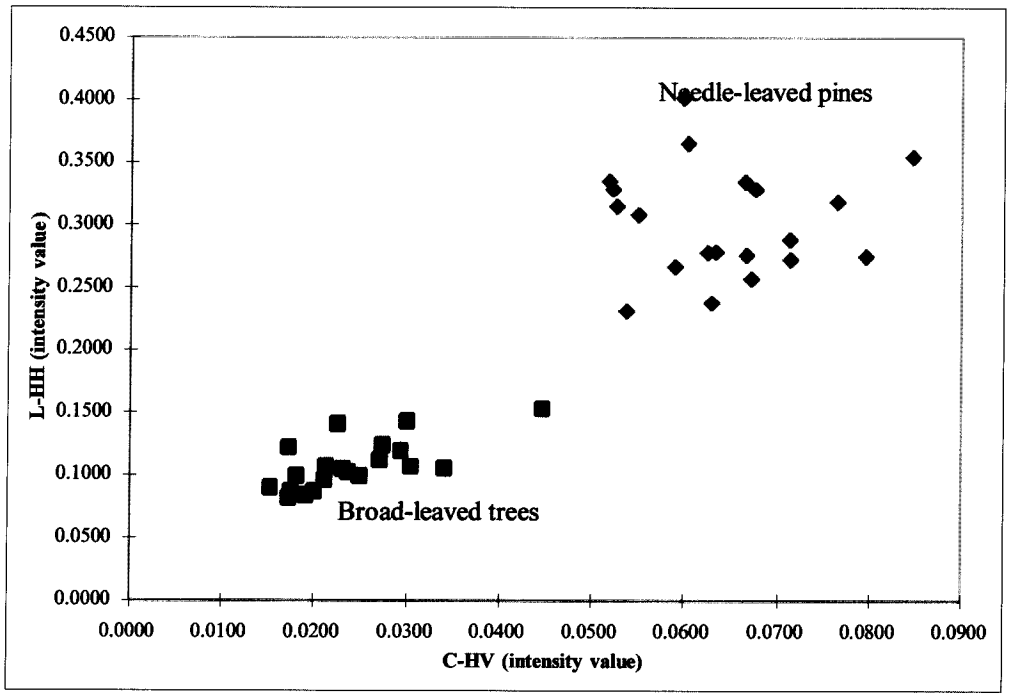

Figure 7.1 Separation of broad-leaved and needle-leaved stands by TCMI

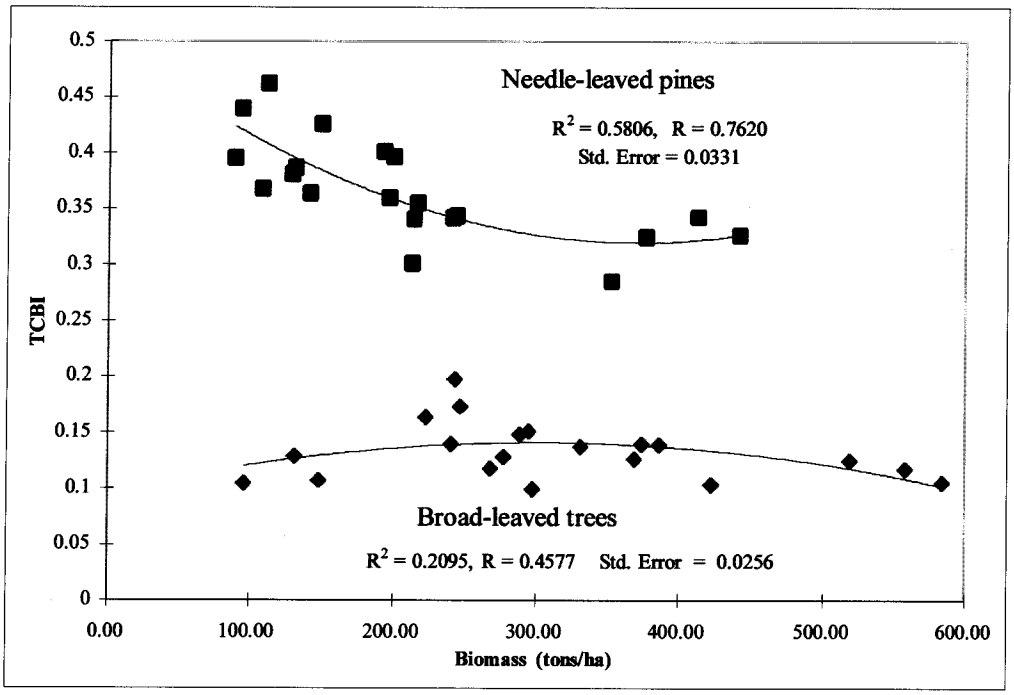

Figure 7.2 TCBI against broad-leaved and needle-leaved stand biomass

To illustrate the effect of radar signal saturation on the effectiveness of the indices, Figure 7.3 graphs the TCMI values for both pines and the eucalypt-dominated stands, while plotted in Figure 7.4 are the TCBI values versus the total aboveground dry biomass with the total biomass in both cases confined to the 0 - 245 tonnes/ha range. Such limitation in the biomass range caused a slightly better separation between the broad-leaved and needle-leaved trees by the TCMI. This also produced a much higher correlation between the TCBI and total aboveground dry biomass for the broad-leaved stands, where the value of R increased from 0.4577 to 0.8271. In the case of the radiata pines, however, no improvement in the TCBI-total biomass correlation was observed (the R was in fact reduced from 0.7620 to 0.6716). As discussed above, this is because of the saturation of the C-HV and L-HH signals beyond the 90 tonnes/ha range as a consequence of the pine canopy closing up such that the TCBI then becomes negatively correlated with biomass.

7.2.3 Use of bands with deeper penetration

Increases in the total biomass (i.e., crown and trunk) usually mean less and less penetration by the radar waves up to a point of saturation where penetration is no longer possible. Compared to the forest data from other researchers presented in Chapter 4, the vegetation in both the Blue Mountains and Gippsland study sites contain much higher amounts of biomass. As a result, the C-HV and L-HH data become saturated thus resulting to a low correlation between the total aboveground biomass and the radar data-based biomass index (TCBI). Clearly, this also has an impact on the TCMI-stand structure correlation due to the failure of the radar waves to provide measures of both the crown and trunk components.

As stated above, confining the field data collection to sample plots with low biomass is not a solution as these are not typical of real forest areas. A better option, as discussed in Chapter 3, would be to explore the possibility of extending the radar data-based stand structure and biomass estimation approach by using the deeper-penetrating P-HH (in lieu of L-HH) and P-HV (in lieu of C-HV) backscatter

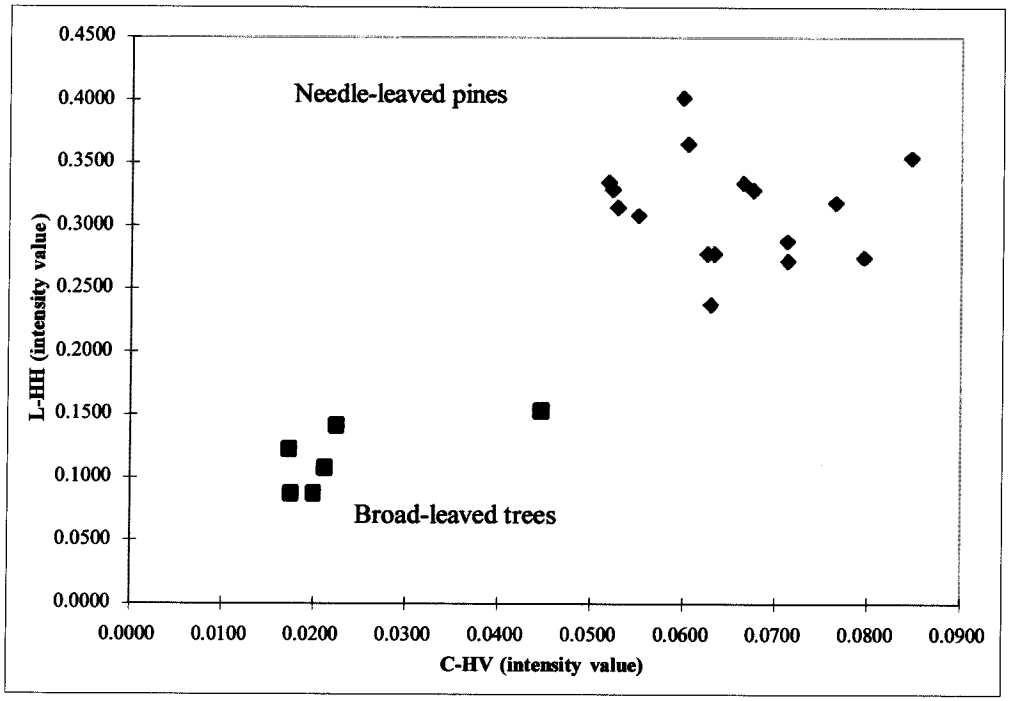

Figure 7.3 TCMI values for broad-leaved and needle-leaved stands within a 0 - 245 t/ha total aboveground biomass range

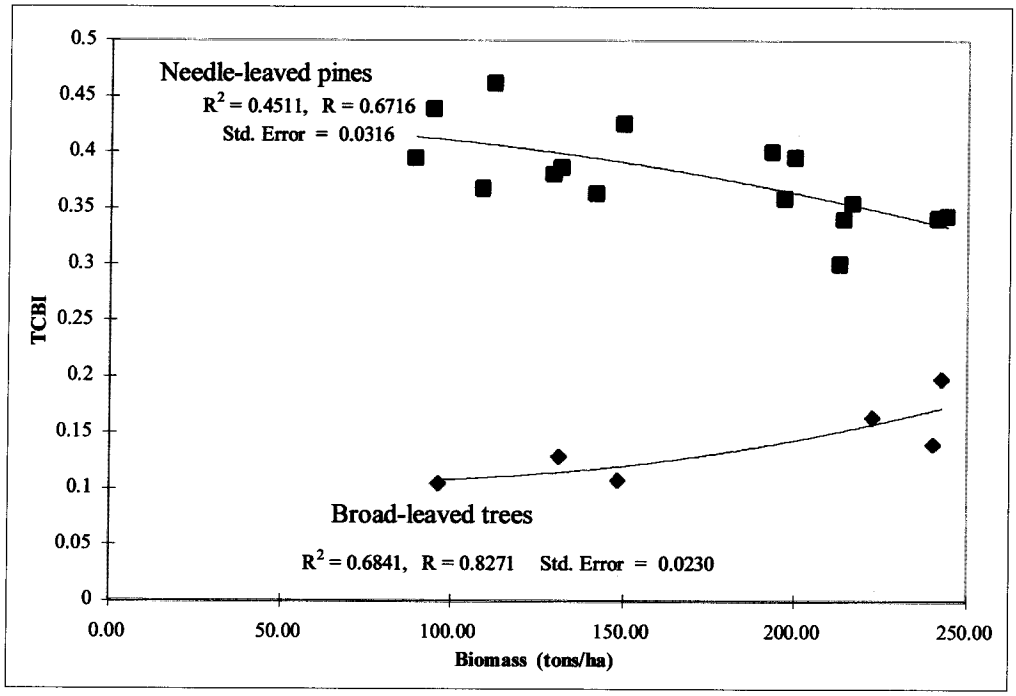

Figure 7.4 TCBI against broad-leaved and needle-leaved stand biomass within a 0 - 245 t/ha total aboveground biomass range

for the TCM and TCB indices. The equations for these new indices can be written as

$$TCBI_{new} = \sigma^{O}_{P\text{-}HH} + \sigma^{O}_{PHV} \quad (7.1)$$

$$TCMI_{new} = \sigma^{O}_{P\text{-}HH} / \sigma^{O}_{P\text{-}HV} \quad (7.2)$$

Shown opposite the total aboveground dry biomass amounts in Table 7.4 are the computed $TCMI_{new}$ and $TCBI_{new}$ values for the various sample plots in the two study sites. These data are likewise presented in the form of graphs in Figures 7.5 and 7.6. A number of observations and conclusions can be made from the data presented in these table and graphs. Firstly, the use of the $TCMI_{new}$ brought about only a minor improvement in the separation between the broad-leaved and needle-leaved stands. Compared to the previous (TCMI) data, the difference between the mean $TCMI_{new}$ value of the eucalypt-dominated stands (5.40) and the pines (5.92) is slightly bigger. This again could be related to the similarity in morphology between the eucalypts and the pines. Secondly, $TCBI_{new}$ has a higher correlation with total biomass compared to TCBI. In the case of the radiata pines, the improvement in the value of R was from 0.7620 to 0.9159. Although an increase in the R value could also be observed from the eucalypt data (from 0.4577 to 0.4813), the final value of R is still low. This is because the total biomass amounts in the majority of the sample plots in the Blue Mountains site are so high that they are beyond the saturation level even of the P-band.

Again, to examine the effect of radar signal saturation, plotted in Figure 7.7 are the $TCMI_{new}$ values for both stand categories while in Figure 7.8 are the $TCBI_{new}$ values against total aboveground dry biomass with the total biomass in both cases limited to the 0 - 245 tonnes/ha range. As can be seen from these figures, there was almost no improvement in the separation between the two stand structure

Study Site 1 (Blue Mountains)				Study Site 2 (Gippsland)			
Plot	**Biomass (t/ha)**	**$TCMI_{new}$**	**$TCBI_{new}$**	**Plot**	**Biomass (t/ha)**	**$TCMI_{new}$**	**$TCBI_{new}$**
2	96.19	3.79	0.0651	2	89.27	6.04	0.1443
25	131.30	4.42	0.0661	3	94.53	5.61	0.1812
10	148.31	2.79	0.0565	4	108.84	10.53	0.1994
13	222.42	8.08	0.1090	5	112.12	5.89	0.2392
23	240.03	6.98	0.0981	8	129.44	6.23	0.2877
20	242.44	9.29	0.1008	9	131.79	5.16	0.3282
24	246.35	5.45	0.0780	10	141.79	6.20	0.3515
16	267.80	4.36	0.0643	12	149.66	4.87	0.3521
1	276.98	6.03	0.0879	13	193.10	6.58	0.4148
17	288.25	4.35	0.0722	15	196.84	6.90	0.4314
18	294.42	5.87	0.0639	14	199.80	6.28	0.4315
5	297.52	5.34	0.0609	16	212.99	6.87	0.4326
6	331.31	3.13	0.0620	17	214.00	5.65	0.4527
22	369.10	5.34	0.0501	18	216.53	5.59	0.4932
14	374.43	11.62	0.1123	19	241.25	4.50	0.4584
4	386.40	5.15	0.0781	21	243.95	3.66	0.4233
9	422.53	3.81	0.0543	23	353.10	5.25	0.3050
8	518.67	4.18	0.0570	22	377.40	5.78	0.2576
7	557.51	3.81	0.0544	24	413.32	5.33	0.2752
11	583.98	4.16	0.0495	25	442.05	5.52	0.2653

Table 7.4 Total aboveground dry biomass, $TCMI_{new}$ and $TCBI_{new}$ values for the sample plots in study sites 1 and 2 (Blue Mountains and Gippsland)

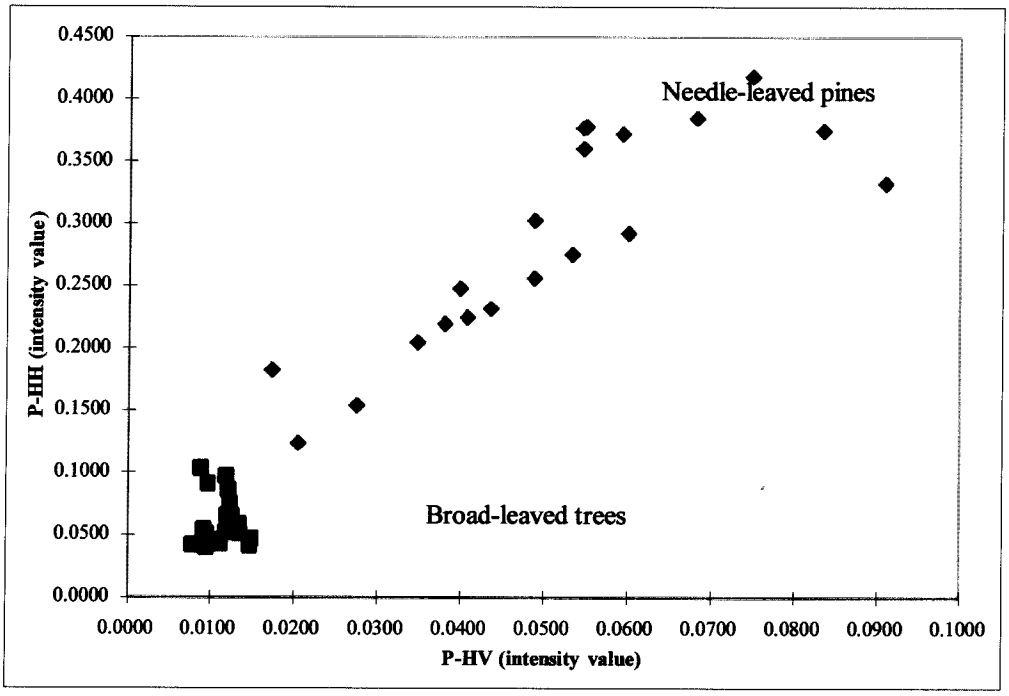

Figure 7.5 $TCMI_{new}$ values for broad-leaved and needle-leaved stands

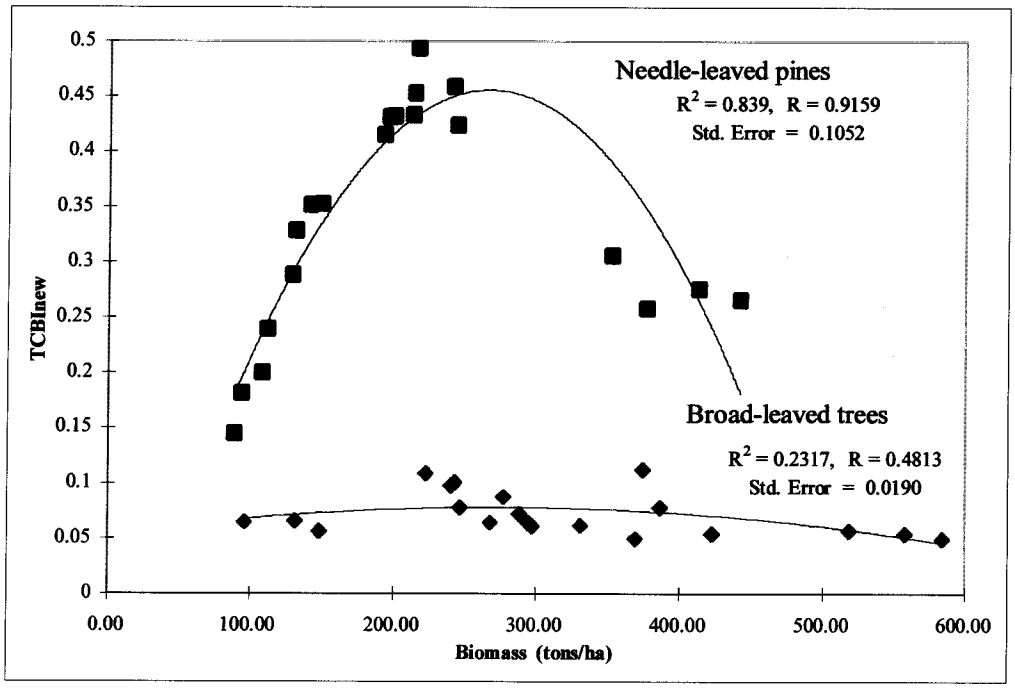

Figure 7.6 $TCBI_{new}$ versus total aboveground dry biomass

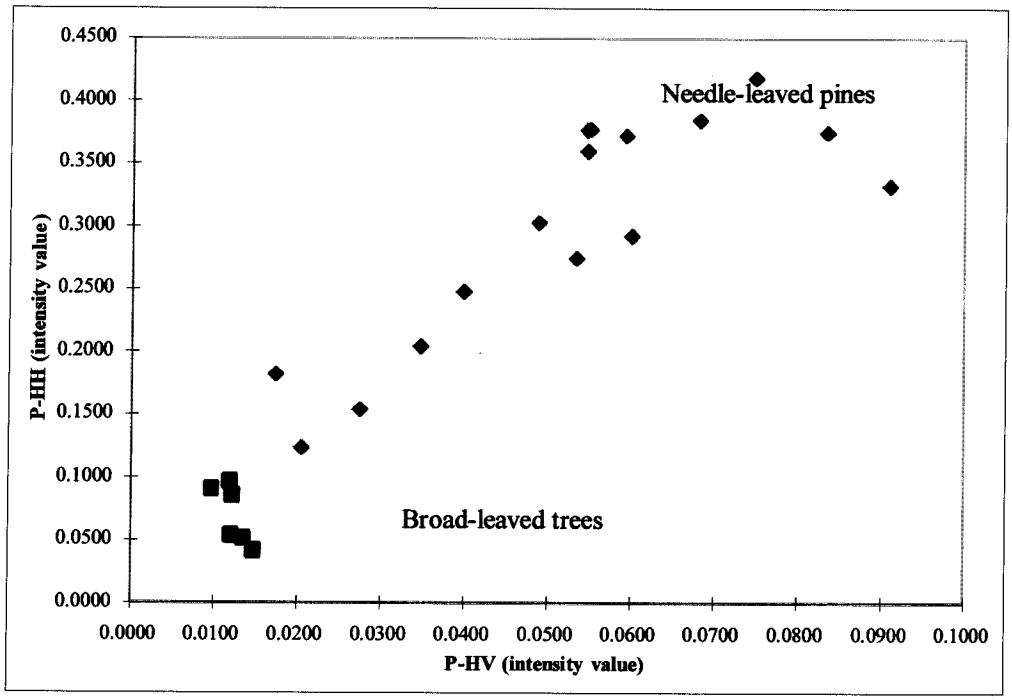

Figure 7.7 $TCMI_{new}$ values for broad-leaved and needle-leaves stands within a 0 - 245 t/ha total biomass range

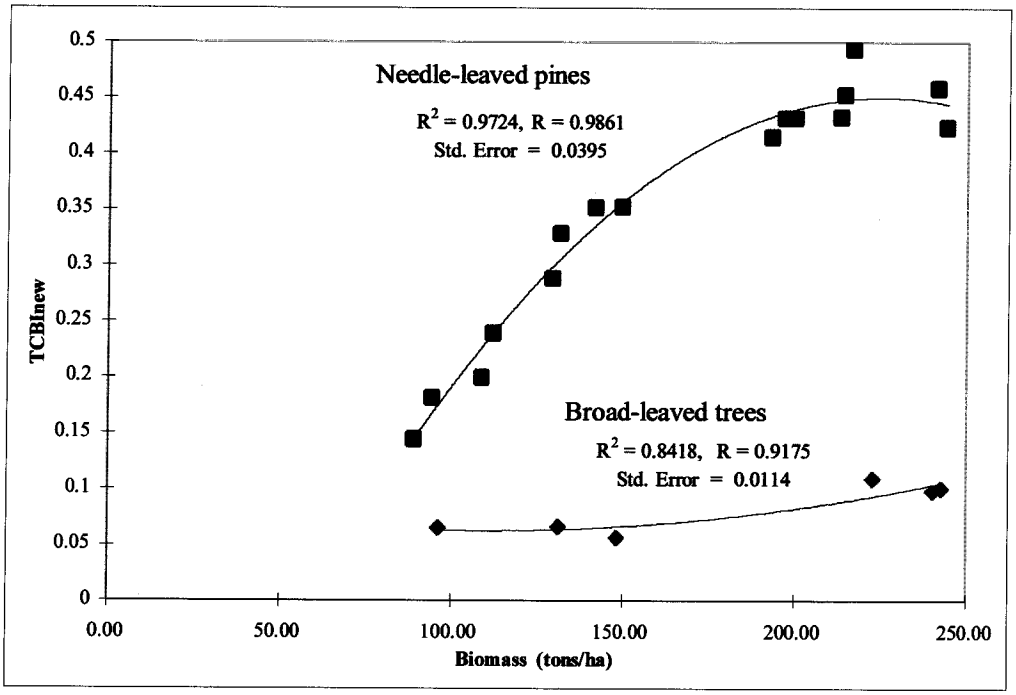

Figure 7.8 $TCBI_{new}$ values against total aboveground dry biomass within a 0 -245 t/ha total biomass range

categories by the $TCMI_{new}$ but a large increase in correlation between the $TCBI_{new}$ and total biomass. The R value for the eucalypt-dominated stands increased from 0.4813 to 0.9175 and that of the pines moved from 0.9159 to 0.9861.

Below are the equations for the estimation of total aboveground dry biomass based on $TCBI_{new}$ for each structural category. These equations were derived by plotting the two sets of variables against each other and fitting lines which best approximate the relationship. Since the purpose is for the prediction of total biomass from $TCBI_{new}$ values, the latter was treated as the independent variable (x axis). The choice of the best equation was based on the line which gives the highest R^2 or R value. This is illustrated in Figure 7.9. For the two stand categories, the equations that have the highest R are given below:

$$\text{Total Biomass (Broad-leaf)} = 11698.00\ TCBI_{new}^2 + 550.74\ TCBI_{new} + 49.88 \quad (7.3)$$
$$R = 0.8912; \quad \text{Standard Error} = 31.9445$$

$$\text{Total Biomass (Needle-leaf)} = 823.03\ TCBI_{new}^2 - 74.96\ TCBI_{new} + 82.59 \quad (7.4)$$
$$R = 0.9499; \quad \text{Standard Error} = 18.9750$$

However, it should be noted that the above equations were derived based on a total aboveground dry biomass range of from 0 to 245 tonnes/ha only. As such, these are not expected to be accurate in sites with biomass levels significantly above this range. It should also be noted that equation 7.3 is now only based on six samples.

7.3 Accuracy Assessment

The accuracies of the derived models/indices were assessed based on field and experimental data from previously designated model validation plots for each of the study sites. The general stand structure and total aboveground dry biomass within each plot were predicted using the $TCMI_{new}$ and structure-specific biomass

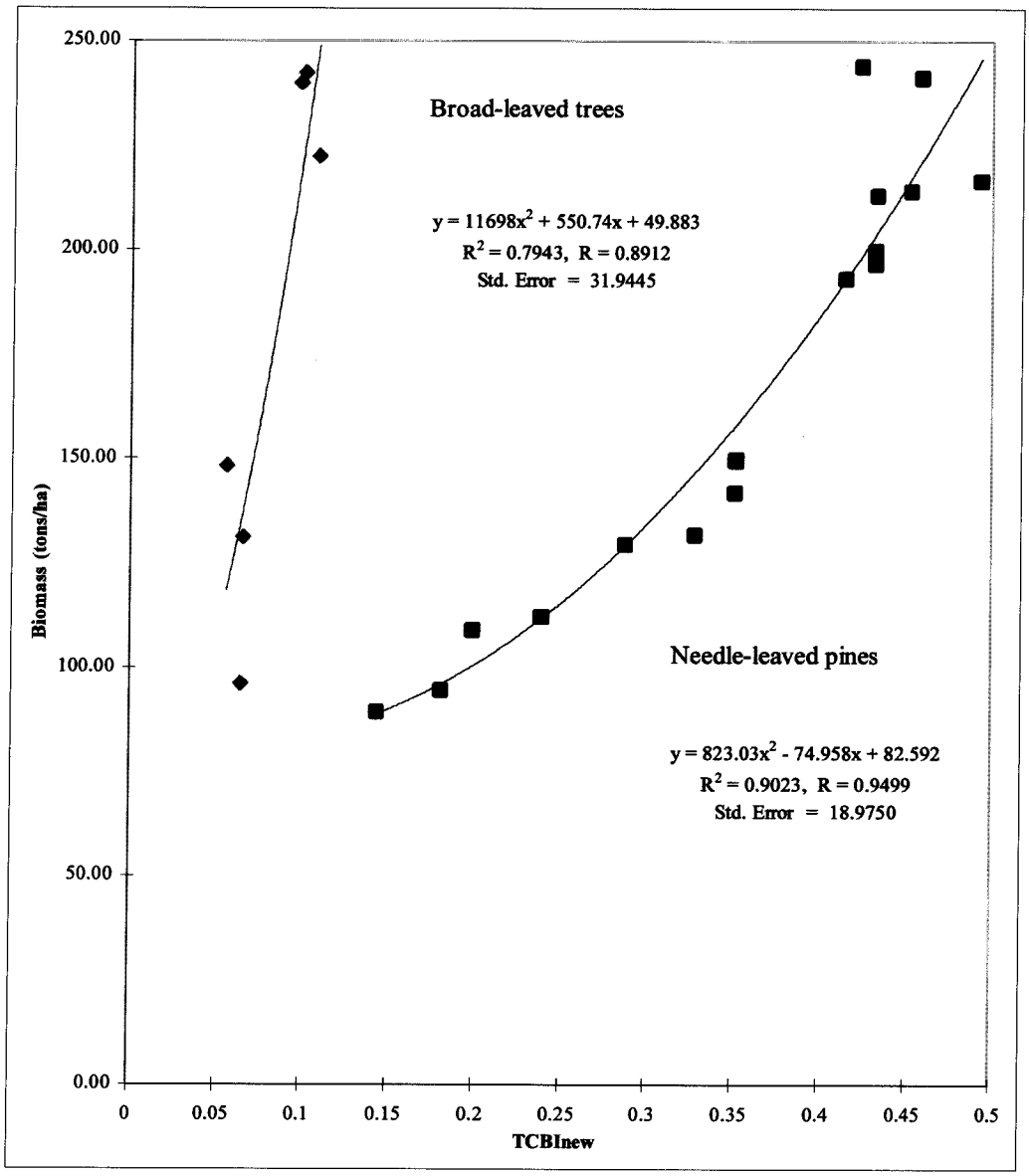

Figure 7.9 Derivation of biomass equations based on the total aboveground dry biomass - $TCBI_{new}$ relationship

equations. $TCMI_{new}$ results were evaluated based on *a priori* information on tree structure, as gathered during the field work, and in comparison with the $TCMI_{new}$ values computed from the model development plots. The accuracies of the $TCBI_{new}$-based equations were evaluated by comparing the resulting biomass estimates with the "actual" total aboveground dry biomass of the trees in each plot. In the absence of "actual" biomass data, biomass values calculated based on actual field

measurements and the allometric equations described in Chapter 6 were used instead.

The backscatter in different bands, $TCMI_{new}$, $TCBI_{new}$, "actual" and predicted biomass values for the model validation plots in each study site are presented in Tables 7.5 and 7.6. The $TCMI_{new}$ values for the five test plots in study site 2, which range from 4.77 to 9.80 (with a mean value of 6.56), are well within the value range for needle-leaved stands previously computed from the model development plots. Except for test plots 12 and 19, however, unusually high $TCMI_{new}$ values were obtained from the test plots in the first study site and no adequate reasons can be suggested for this effect. The average accuracy of the biomass estimates for the broad-leaved and needle-leaved stand categories are 72% and 87%, respectively. In general, the accuracy is relatively high at low biomass levels and declines with increases in biomass. This trend could be attributed to the saturation of radar measurements, and hence the reduction in the effectiveness of the $TCBI_{new}$, at high amounts of biomass, as previously discussed.

7.4 Biomass versus individual bands and band combinations

Shown in Figures 7.3.1 to 7.3.6 in Appendix 7.3 are graphs of total biomass and the different individual bands including the corresponding equations with the highest R or R^2 values for both sites. For study site 1, the best correlation with biomass was obtained with the C-VV (R = 0.4713) while the lowest was with the L-HV (R = 0.3087). For study site 2, P-HH provided the highest correlation coefficient of 0.9058 followed by P-HV at 0.8450. The lowest correlation with pine biomass was observed from the C-HV backscatter (R = 0.0854). Various band combinations other than those used in the TCBI and $TCBI_{new}$ were also tested for correlation with biomass (see Figures 7.3.7 to 7.3.14 in Appendix 7.3). The best correlation for the broad-leaved stands was observed from the sum of P-HH, P-VV and P-HV backscatter (R = 0.4748) while the sum of P-HH and L-HV gave the highest R value (0.8953) for the pines. The band combinations which gave the lowest correlation with total biomass were L-HV + P-HV (R = 0.3396) for study site

1 and C-HH + P-HV (R = 0.1140) for study site 2. The higher correlation between total aboveground dry biomass and $TCBI_{new}$ in both study sites, as can be seen from these results, highlight the advantage of using this index over other bands and band combinations to derive estimates of total biomass from multi-parameter radar data.

7.5 Radar backscatter and stand age

The relationship of stand age with the total aboveground dry biomass, $TCMI_{new}$ and $TCBI_{new}$ were investigated for the even-aged radiata pines within the various compartments of the APPPL Gippsland plantations covered by the radar image. Stand age was found to be highly correlated with biomass with the value of R at 0.9864. Very low R values, however, were obtained for the stand age-$TCMI_{new}$ (0.3643) and stand age-$TCBI_{new}$ (0.5515) relationships (see Figure 7.4.1 in Appendix 7.4). When the amount of total aboveground biomass was limited to the 0 to 245 tonnes/ha range, the R values for the stand age-biomass and stand age - $TCBI_{new}$ relationships improved to 0.9917 and 0.9539, respectively (Figure 7.4.2, Appendix 7.4). No improvement in correlation between stand age and $TCMI_{new}$ was observed. Prediction of the age of radiata pines in even-aged plantation compartments based on radar data, as suggested by these results, could thus be best made using the $TCBI_{new}$. This can be represented by the model given below. However, as in the case of equations 7.3 and 7.4, it should be noted that this model/equation is most accurate within a biomass range of 0 to 245 tonnes/ha.

$$\text{Stand age (in years)} = 178.69\ TCBI_{new}^2 - 51.464\ TCBI_{new} + 8.4221 \qquad (7.5)$$

$$R = 0.9539; \quad \text{Standard Error} = 2.9135$$

Sample Plot	C-HH	C-VV	C-HV	L-HH	L-VV	L-HV	P-HH	P-VV	P-HV	$TCMI_{new}$	$TCBI_{new}$	Actual Biomass (t/ha)	Predicted Biomass (t/ha)	Accuracy (%)
15	0.1208	0.1021	0.0225	0.0981	0.0568	0.0089	0.0823	0.0736	0.0049	16.7959	0.0872	220.59	186.85	0.85
12	0.1350	0.1028	0.0266	0.1070	0.1087	0.0294	0.0764	0.0839	0.0140	5.4571	0.0904	247.66	195.27	0.79
21	0.1703	0.1625	0.0418	0.1573	0.1108	0.0306	0.0935	0.1002	0.0109	8.5780	0.1044	311.95	234.88	0.75
19	0.2124	0.2080	0.0455	0.1674	0.1312	0.0390	0.0794	0.1040	0.0124	6.4032	0.0918	319.43	199.02	0.62
3	0.1107	0.0862	0.0233	0.1258	0.0899	0.0229	0.0967	0.1059	0.0109	8.8716	0.1076	410.23	244.58	0.60

Table 7.5 Radar backscatter (intensity values) in different bands, $TCMI_{new}$, $TCBI_{new}$, actual and predicted total aboveground dry biomass for the model validation (test) plots in study site 1

Sample Plot	C-HH	C-VV	C-HV	L-HH	L-VV	L-HV	P-HH	P-VV	P-HV	$TCMI_{new}$	$TCBI_{new}$	Actual Biomass (t/ha)	Predicted Biomass (t/ha)	Accuracy (%)
1	0.3517	0.3482	0.0751	0.3116	0.2825	0.0683	0.1201	0.1381	0.0201	5.9751	0.1402	92.80	88.26	0.95
6	0.2561	0.2131	0.0538	0.3555	0.2274	0.0578	0.1735	0.1709	0.0177	9.8023	0.1912	112.71	98.35	0.87
11	0.1490	0.1284	0.0501	0.2782	0.2086	0.0749	0.2527	0.2067	0.0406	6.2241	0.2933	153.64	131.41	0.86
7	0.2371	0.2199	0.0733	0.2707	0.2021	0.0703	0.3342	0.2093	0.0700	4.7743	0.4042	215.49	186.75	0.87
20	0.1810	0.1945	0.0645	0.2526	0.1860	0.0669	0.3594	0.1803	0.0599	6.0000	0.4193	242.46	195.86	0.81

Table 7.6 Radar backscatter (intensity values) in different bands, $TCMI_{new}$, $TCBI_{new}$, actual and predicted total aboveground dry biomass for the model validation (test) plots in study site 2

The accuracy of the above model for stand age prediction was tested using the data from the five model validation plots in study site 2 (Gippsland). The accuracies of the stand age estimates, as presented in Table 7.7 below, ranged from 94% to 76%. Similar to the results obtained from the testing of the biomass estimation model, accuracy is at its highest at the lowest biomass level and generally declines as biomass increases.

Test Plot	Biomass (t/ha)	Actual Age (years)	Predicted Age (years)	Accuracy (%)
1	92.80	5	4.72	94
6	112.71	6	5.12	85
11	153.64	10	8.70	87
31	215.49	22	16.81	76
20	242.46	24	18.26	76

Table 7.7 Accuracy of the $TCBI_{new}$ - based stand age estimates

7.6 Summary and conclusions

Success in forest monitoring and regulation is dependent on the timely and accurate quantification of the resource base. Exploring the potential of radar remote sensing in providing estimates of total forest aboveground biomass is highly justified given the known advantages of this technology over the more conventional methods and the importance of the total aboveground biomass as a good measure of forest condition. The models and indices introduced in Chapter 3 have been shown to provide good measures of the general stand structure and total biomass when applied to interpolated data from related published research. The concern on whether these favourable results will hold true when more extensive data sets from independent study sites are used has been addressed in this chapter.

In accordance with the theories presented in Chapter 3, generally higher TCMI values were obtained for the needle-leaved pines compared to those of the broad-leaved stands. However, the average difference between these sets of values is not significant enough for the TCMI to be considered a good measure of stand morphology. This is mainly due to the similarity in structure between most eucalypts and the radiata pines. Hence, even the use of bands with longer wavelength (i.e., in $TCMI_{new}$) did not cause a major improvement in the separability of the structural classes. A low correlation between TCBI and total aboveground dry biomass has been observed. This is because of the early saturation of the C-HV and L-HH backscatter as a consequence of high biomass levels. Application of the deeper-penetrating P-band produced a much better correlation between $TCBI_{new}$ and total aboveground dry biomass especially within the 0 - 245 tonnes/ha biomass range. The use of the $TCBI_{new}$ has been demonstrated to provide the best estimate of biomass relative to other radar bands and band combinations. Given these results, and the good correlation between biomass and stand age, the age of radiata pines in even-aged plantation stands can also be accurately predicted based on the $TCBI_{new}$.

CHAPTER 8

CONCLUSIONS AND RECOMMENDATIONS

8.1 Summary and conclusions

The forest, with its protective, productive, and regenerative functions, is an important resource which needs to be managed on a sustained basis. The availability of accurate, timely and an adequate amount of information on the quantity and extent of forest vegetation is a vital factor for successful management. Remote sensing can provide a more efficient alternative to the conventional methods of data collection and handling especially in distantly located and inaccessible forest areas.

Forest biomass, or the quantity of vegetative material per unit area, is one of the recognised indicators of forest condition. The increasing popularity over the recent years of the use of radar remote sensing to obtain biomass estimates is mainly due to the ability of the radar to provide data independent of solar illumination and prevailing atmospheric conditions. Along with the advent of multi-parameter imaging radar systems are the potential advantages from the simultaneous use of different frequency-polarisation combinations to derive more accurate estimates. However, it is imperative that the theoretical basis behind the inference of forest properties from multi-parameter radar be first explored. Apart from giving a clear understanding of the backscattering processes involved, this step is expected to provide for a more universal application of the developed methodologies.

The total forest aboveground biomass is the summation of the biomass of the crown and trunk components of all the trees in the area under consideration. The capability of microwave energy to penetrate forest vegetation makes possible the extraction of information on both components. At C-band, the backscattered energy is correlated mainly with the crown constituents such as the leaves, twigs, and small

branches. Information on the other tree parts below the canopy can be sensed through the use of bands with longer wavelengths such as the L- and P-band. The sensitivity of the co-polarised and cross-polarised waves to the shapes and orientation of the various tree constituents provide an added advantage in the information extraction procedure. Given the relatively greater degree of penetration by horizontally-polarised waves and the strong interaction of the vertically-polarised energy with the vertically-oriented parts of the vegetation, different wavelength-polarisation combinations can be applied for the estimation of parameters such as total forest aboveground biomass.

The Trunk-Canopy Biomass Index (TCBI), which is the sum of the L-HH and C-HV backscatter, was proposed as a measure of the total aboveground biomass as both the trunk and crown layers are taken into consideration. Nonetheless, owing to possible morphological variations, the relationship between TCBI and total biomass is not expected to be unique for a whole forest vegetation. It is important therefore that the stand structure be first considered to allow a more accurate biomass assessment using the TCBI. An index of the relative proportions of the trunk and crown may be indicative of the approximate tree morphology. It is believed that the Trunk-Canopy Morphology Index (TCMI), which is the ratio of the L-HH to C-HV backscatter, provides a measure of the tree structure. In this study, two categories are used to classify stands according to structure: the needle-leaved pines/conifers and the broad-leaved evergreen/deciduous trees. Higher TCMI values are expected for conifers given their bigger trunk and smaller crown component volume compared to their broad-leaved counterpart. A two-stage procedure of forest biomass estimation is thus proposed. The first stage involves the determination of the stand structure category based on the TCMI. Once the structure is known, a specific structure-dependent TCBI could then be applied for the biomass estimation process.

The effectiveness of these indices was assessed by applying them to actual and modelled data interpolated from published works of other investigators. Stand structure and total aboveground biomass were found to be highly correlated with the TCMI and TCBI, respectively. With these results, however, are potential problems

caused by factors such as the limitation in the amount of data available from the published studies, comparability of the data from the different researchers, and the possible errors introduced during the interpolation process. In order to verify the validity of these results, further application of the theories, models and indices was conducted using radar and field data from two study sites, one located in the Blue Mountains National Park in New South Wales and the other in the Gippsland Region in Victoria, both in Australia. Generally higher TCMI values were obtained for the needle-leaved radiata pines in Gippsland compared to those of the eucalypt-dominated broad-leaved stands in the Blue Mountains. However, the average difference between the sets of values was not significant enough for the TCMI to be considered a good measure of stand morphology. This is mainly because of the similarity in structure between most eucalypts and the radiata pines such that even the use of bands with longer wavelength (P-HH/P-HV, called $TCMI_{new}$) did not cause a major improvement in the separability of the structural classes. Due to the early saturation of the C-HV and L-HH backscatter, a low correlation between TCBI and total aboveground biomass has been observed. Application of the deeper-penetrating P-band produced a much better correlation between $TCBI_{new}$ (P-HH+P-HV) and total aboveground biomass especially within the 0 - 245 tonnes/ha biomass range. The use of the $TCBI_{new}$ has been demonstrated to provide the best estimate of biomass relative to other radar bands and band combinations.

Stand structure-specific equations for the estimation of biomass based on the $TCBI_{new}$ were derived. The accuracies of the derived equations were assessed using field and experimental data from previously designated model validation plots for each of the study sites. The average accuracy of the biomass estimates for the needle-leaved and broad-leaved stands were 87% and 72%, respectively. The accuracy was observed to be generally high at low biomass levels and declines with increases in biomass. This trend could be attributed to the saturation of radar measurements, and hence the reduction in the effectiveness of $TCBI_{new}$, at high amounts of biomass.

The relationship of stand age with the total aboveground biomass and the new indices were investigated for the radiata pines in the Gippsland study site.

Results showed a high correlation between stand age and biomass, as well as stand age and $TCBI_{new}$ at biomass levels within the 0 -245 tonnes/ha range. An age-predicting equation based on the $TCBI_{new}$ was derived and then tested using the data from the model validation plots. The accuracies of the equation-based estimates ranged from 94% to 76% with the accuracy observed to be at its highest at the lowest biomass level and declines as biomass increases.

8.2 Recommendations for future research

It is recommended that the methodology developed in this study be tested and extended to other application sites such as those with broad-leaved vegetation typical of tropical and northern hemisphere species. The use of more extensive data sets in terms of both field and radar data is proposed in this regard. Since the majority of natural forests are in mountainous locations, effective techniques and methods for terrain correction and geocoding need to be developed. This is to minimise, if not eliminate, obstacles to accurate inference of forest properties from radar data such as the occurrence of radar shadow, foreshortening, layover as well as topography-based backscatter variations.

BIBLIOGRAPHY

Ahern, F.J., and J.A. Drieman, 1988. Assessment of clearcut mapping accuracy with C-band SAR data. *Proceedings of the International Geoscience and Remote Sensing Symposium,* Edinburgh, Scotland, 13-16 September, 3:1335-1337.

Ahmed, Z., and J.A. Richards, 1989. Multiple incidence angle SIR-B forest observations. *IEEE Transactions on Geoscience and Remote Sensing* 27(5):586-591.

Ahmed, Z., 1991. Radar backscatter modelling of forested regions containing arbitrarily oriented woody structures. Ph.D. Dissertation, Univ. of New South Wales, Kensington, Australia.

Altman, F.J., and A. Schneider, 1985. Biophysical characterization of trees. *Proceedings of the International Geoscience and Remote Sensing Symposium,* Amherst, Massachusetts, 7-9 October, pp. 183-188.

Amar, F., A.K. Fung, G. De Grandi, C. Lavalle, and A. Sieber. 1993. Backscattering from forest canopies over slanted terrain. *Proceedings of the International Geoscience and Remote Sensing Symposium,* Tokyo, Japan, 18-21 August, pp.576-579.

American Society of Photogrammetry and Remote Sensing, 1983. *Manual of Remote Sensing*, Vols. I and II, Sheridan Press.

Anthony, D.A., 1986. Forest cover analysis using SIR-B data. *Proceedings of the International Geoscience and Remote Sensing Symposium,* Zurich, Switzerland, 8-11 September, 3:1683-1687.

Appleton, R. 1999. Personal communication.

Aschbacher, J., C.P. Giri, R.S. Ofren, P.N. Tiangco, J-P. Delsol, T.B. Suselo, S. Vibulsresth, and T. Charuppat, 1994a. Tropical mangrove vegetation mapping using advanced remote sensing and GIS technology. *Executive Summary*, Asian Institute of Technology, Bangkok, Thailand, 16 pp.

Aschbacher, J., C.P. Giri, R.S. Ofren, P.N. Tiangco, J-P. Delsol, T.B. Suselo, S. Vibulsresth, and T. Charuppat, 1994b. Tropical mangrove vegetation mapping using advanced remote sensing and GIS technology. *Final Report* , Asian Institute of Technology, Bangkok, Thailand, 90 pp.

Aschbacher, J., P.N. Tiangco, C.P. Giri, R.S. Ofren, D.R. Paudyal, and Y.K. Ang, 1995. Comparison of different sensors and analysis techniques for tropical mangrove mapping. *Proceedings of the International Geoscience and Remote Sensing Symposium,* Florence, Italy, 3:2109-2111.

Askne, J., and J.Q. Hagberg, 1993. Potential of interferometric SAR for classification of land surfaces. *Proceedings of the International Geoscience and Remote Sensing Symposium,* Tokyo, Japan, 18-21 August, pp.985-987.

Avery, T.E., and G.L. Berlin, 1991. Fundamentals of remote sensing and airphoto interpretation. 5th ed. Maxwell Mcmillan International, 372 pp.

Axelsson, S.R.J., 1992. Two-bounce scattering of mm-waves from a semi-transparent vegetation canopy. *Proceedings of the International Geoscience and Remote Sensing Symposium,* Houston, Texas, 26-29 May, 1:526-529.

Australian Tourism Net, 1998. Gippsland, *http://www.atn.com.au/vic/east*

Baker, J.A., R.A. Cordey, G.B. Groom, P.L. Mitchell, and J.J. Settle, 1991. Forest inventory using polarimetric multi-frequency radar. *Proceedings of the International Geoscience and Remote Sensing Symposium,* Espoo, Finland, 3-6 June, 2:693.

Baker, J.R., P.L. Mitchell, R.A. Cordey, G.B. Broom, J.J. Settle, and M.R. Stileman, 1994. Relationships between physical characteristics and polarimetric radar backscatter for Corsican pine stands in Thetford forest, U.K. *International Journal of Remote Sensing* 15(14):2827-2849.

Beaudoin, A., T. Le Toan, A. Lopes, and H. Laur, 1990. Forest and land-use segmentation of SAR images using backscatter and textural information. . *Proceedings of the International Geoscience and Remote Sensing Symposium,* Maryland, USA, 20-24 May, 1:871-874.

Beaudoin, A., T. Le Toan, and S. Goze, 1991. Analysis of SAR polarimetric signatures of pine forests. *Proceedings of the International Geoscience and Remote Sensing Symposium,* Espoo, Finland, 3-6 June, 2:701.

Beaudoin, A., T. Le Toan, S. Goze, E. Nezry, A. Lopes, C.C. Hsu, H.C. Han, J.A. Kong, and R.T. Shin, 1994. Retrieval of forest biomass from SAR data. *International Journal of Remote Sensing* 15(14):2777-2796.

Beaudoin, A., and T. Le Toan, 1992. Simulation of forest backscatter as a function of forest and ground parameters. *Proceedings of the International Geoscience and Remote Sensing Symposium,* Houston, Texas, 26-29 May, 2:1212-1214.

Bergen, K.M., M.C. Dobson, and L.E. Pierce, 1996. Carbon dynamics in northern forests using SIR-C/X-SAR imagery. *Proceedings of the International Geoscience and Remote Sensing Symposium,* Lincoln, Nebraska, 27-31 May, pp.580-582.

Bernstein, R., (ed.), 1983. Image geometry and rectification. *Manual of Remote Sensing*, 2nd Edition. American Society of Photogrammetry, pp. 873-922.

BIOTROP, 1989. Mangrove management: its ecological and economic considerations. *SEAMO-BIOTROP*, Bogor, Indonesia, 353 pp.

Blue Mountains Regional Tourism Organization, 1997. Blue mountains region, *http://www.lisp.com.au/~bmrto.*

Blue Mountains Web, 1998. Tourist site, *http://www.bluemts.com.au/tourist.*

Bureau of Meteorology, 1999. Climate averages, *http://www.bom.gov.au/climate.*

Campbell, J. B., 1987. Introduction to remote sensing. The Guilford Press, New York. 551 pp.

Campbell, J. B., 1983. Mapping the land: aerial imagery for land use information. *Resource Publications in Geography.* Commercial Printing Inc., Pennsylvania. 97 pp.

Chauhan, N.S., and R.H. Lang, 1990. Boreal forest characterization for radar modeling. *Proceedings of the International Geoscience and Remote Sensing Symposium,* Maryland, USA, 1:865-869.

Chauhan, N.S., R.H. Lang, J. Ranson, and O. Kilic, 1994. Multi-stand radar modeling from a boreal forest: results from the BOREAS intensive field campaign. *Proceedings of the International Geoscience and Remote Sensing Symposium,* Pasadena, California, 8-12 August, 1:235-237.

Chauhan, N.S., and R.H. Lang, 1991. Radar modeling of a boreal forest. *IEEE Transactions on Geoscience and Remote Sensing* 29(4):627-638.

Chauhan, N.S., and R.H. Lang, 1989. X-band backscatter modeling of orchard canopy. *Proceedings of the International Geoscience and Remote Sensing Symposium,* Vancouver, Canada, 10-14 July, 4:2501.

Chen, J., D.S. Simonett, and G. Sun, 1988. Computer-aided interpretation of coniferous forest radar images. *Proceedings of the International Geoscience and Remote Sensing Symposium,* Edinburgh, Scotland, 13-16 September, 3:1368.

Christensen, N.L., E.S. Kasischke, and M.C. Dobson, 1990. SAR-derived estimates of aboveground biomass in forested landscapes. *Proceedings of the International Geoscience and Remote Sensing Symposium,* Maryland, USA, 20-24 May, 2:1209-1212.

Chuah, H.T., 1994. A study of backscattering mechanisms from a vegetative medium. *Remote Sensing Reviews,* vol. 10, pp. 217-244.

Chuah, H.T., and W.L. Kung, 1994. A microwave propagation model for estimation of effective attenuation coefficients in a vegetation canopy. *Remote Sensing of Environment* 50:212-220.

Cimino, J.B., A. Brandani, D. Casey, J. Rabassa, and S.D. Wall, 1986. Multiple incidence angle SIR-B experiment over Argentina: mapping of forest units. *IEEE Transactions on Geoscience and Remote Sensing* GE-24(4):498-509.

Cimino, J.B., S. Wall, and D. Casey, 1985. Vegetation mapping using multiple incidence angle SIR-B data over the Chubut region of Argentina. *Proceedings of the International Geoscience and Remote Sensing Symposium,* Amherst, Massachusetts, 7-9 October, p.575.

Ciolkosz, A., T. Zawila-Niedzwiecki, and Z. Bochenek, 1993. The application of ERS-1 images for forest damage assessment. *Proceedings of the 2nd ERS-1 Symposium - Space at the Service of our Environment,* Hamburg, Germany, 11-14 October, pp. 453-458.

Cobb, D., J. Mynhier, C. Stinson, and C. Kinata, 1991. Running Microsoft Excel. Microsoft Press, Washington, USA. 766 pp.

Conway, J.A., M. Leysen, and A.J. Sieber, 1993. Evaluating multi-temporal ERS-1 data for tropical forest mapping: data selection, processing and target identification. *Proceedings of the 2nd ERS-1 Symposium - Space at the Service of our Environment,* Hamburg, Germany, 11-14 October, pp. 441-446.

Dallemand, J.F., J. Lichtenegger, R.K. Raney, and R. Schumann, 1993. Radar imagery: theory and interpretation lecture notes. *RSC Series No. 67,* FAO, Rome, Italy,103 pp.

De Grandi, G., G. Lemoine, and A. Sieber, 1992. Supervised fully polarimetric classification: an experimental study on the MAESTRO1 Freiburg data set. *Proceedings of the International Geoscience and Remote Sensing Symposium,* Houston, Texas, 26-29 May, 1:782-785.

De Grandi, G., G. Lemoine, H. De Groof, C. Lavalle, and A.J. Sieber, 1994. Fully polarimetric classification of the Black Forest MAESTRO-1 AIRSAR data. *International Journal of Remote Sensing* 15(14):2755-2775.

De Matthaeis, P., P. Ferrazzoli, L. Guerriero, G. Schiavon, D. Solimini, and P. Tognolatti, 1991. Radar response to vegetation parameters: comparison between theory and MAESTRO-1 results. *Proceedings of the International Geoscience and Remote Sensing Symposium,* Espoo, Finland, 3-6 June, 2:685-688.

Dobson, M.C., E. Wilcox, and F.T. Ulaby, 1993. Effects of forest structure on radar response to forest biomass. *Proceedings of the International Geoscience and Remote Sensing Symposium,* Tokyo, Japan, 18-21 August, 1:383.

Dobson, M.C., F.T. Ulaby, L.E. Pierce, T.L. Sharik, K.M. Bergen, J. Kellndorfer, J.R. Kendra, E. Li, Y.C. Lin, A. Nashashibi, K. Sarabandi, and P. Siqueira, 1995a. Estimation of forest biophysical characteristics in Northern Michigan with SIR-C/X-SAR. *IEEE Transactions on Geoscience and Remote Sensing* 33(4):877-894.

Dobson, M.C., F.T. Ulaby, T. Le Toan, A. Beaudoin, E.S. Kasischke, and N. Christensen, 1992. Dependence of radar backscatter on coniferous forest biomass. *IEEE Transactions on Geoscience and Remote Sensing* 30(2):412-415.

Dobson, M.C., L. Pierce, and F. Ulaby, 1996a. Knowledge-based land-cover classification using ERS-1/JERS-1 SAR composites. *IEEE Transactions on Geoscience and Remote Sensing* 34(1):83-99.

Dobson, M.C., L. Pierce, and F. Ulaby, 1994. Semi-empirical method for estimation of forest biophysical properties from multifrequency polarimetric SAR. *Proceedings of the International Geoscience and Remote Sensing Symposium,* Pasadena, California, 8-12 August, 4:2466.

Dobson, M.C., L.E. Pierce, K.M. Bergen, and F.T. Ulaby, 1996b. Temporal stability of northern forest biophysical retrievals using SIR-C/X-SAR. *Proceedings of the International Geoscience and Remote Sensing Symposium,* Lincoln, Nebraska, 27-31 May, p.1092.

Dobson, M.C., L. Pierce, K. Bergen, J. Kellndorfer, and F.T. Ulaby, 1995b. Retrieval of above-ground biomass and detection of forest disturbance using SIR-C/X-SAR. *Proceedings of the International Geoscience and Remote Sensing Symposium,* Florence, Italy, 2:987-989.

Dobson, M.C., L. Pierce, K. McDonald, and T. Sharik, 1991. Seasonal change in radar backscatter from mixed conifer and hardwood forests in northern Michigan. . *Proceedings of the International Geoscience and Remote Sensing Symposium,* Espoo, Finland, 3-6 June, 3:1121-1124.

Dong, Y., J.A. Richards, and J. Cashman, 1995. A model of volume attenuation and backscattering by foliage at L- and P-bands. *International journal of Remote Sensing* 16(7):1231-1247.

Dong, Y. and B.C. Forster, 1996. Understanding of partial polarisation in polarimetric SAR data. *International journal of Remote Sensing* 17(12):2467-2475.

Drieman, J.A., D.G. Leckie, and F.J. Ahern, 1989. Multitemporal C-SAR for forest typing in eastern Ontario. *Proceedings of the International Geoscience and Remote Sensing Symposium,* Vancouver, Canada, 10-14 July, 3:1376-1378.

Du, L., J.S. Lee, and S.A. Mango, 1993. Fuzzy classification of earth terrain covers using multi-look polarimetric SAR images. *Proceedings of the International Geoscience and Remote Sensing Symposium,* Tokyo, Japan, 18-21 August, 4:1602-1604.

Durden, S.L., H.A. Zebker, and J. Van Zyl, 1988. Application of radar polarimetry to forestry. *Proceedings of the International Geoscience and Remote Sensing Symposium,* Edinburgh, Scotland, 13-16 September, 2:1003-1004.

Durden, S.L., J.D. Klein, and H.A. Zebker, 1991. Polarimetric radar measurements of a forested area near Mt. Shasta. *IEEE Transactions on Geoscience and Remote Sensing* 29(3):444-450.

Durden, S.L., J.J. Van Zyl, and H.A. Zebker, 1989. Modeling and observation of the radar polarization signature of forested areas. *IEEE Transactions on Geoscience and Remote Sensing* 27(3):290-301.

Elachi, C., 1987. Introduction to the physics and techniques of remote sensing. John Wiley and Sons, Inc. 413 pp.

ENVI, 1995. User's manual for ENVI version 2.0, October 1995 edition. Better Solutions Consulting Limited Liability Company, Colorado, USA.

Estes, J.E., E.J. Hajic, and L.R. Tinney, 1983. Fundamentals of image analysis: analysis of visible and thermal infrared data. *Manual of Remote Sensing.* Chapter 24, Vol. 1, pp. 1039 - 1040.

European Space Agency, 1995. Satellite radar in agriculture: experience with ERS-1. *ESA SP-1185,* ESA Publications Division, Noordwijk, The Netherlands.

Evans, D.L., 1992. Current status and future developments in radar remote sensing. *ISPRS Journal of Photogrammetry and Remote Sensing* 47:79-99.

Evans, D.L., T.G. Farr, J.J. Van Zyl, and H.A. Zebker, 1988. Radar polarimetry: analysis tools and applications. *IEEE Transactions on Geoscience and Remote Sensing* 26(6):774-789.

Evans, D.L., T.G. Farr, J.P. Ford, T.W. Thompson, and C.L. Werner, 1986. Multipolarization radar images for geologic mapping and vegetation discrimination. *IEEE Transactions on Geoscience and Remote Sensing* GE-24(2):246-257.

Ferrazzoli, P., and L. Guerriero, 1995. Radar sensitivity to tree geometry and woody volume: a model analysis. *IEEE Transactions on Geoscience and Remote Sensing,* 33(2):360-371.

Filho, P.H., L.V. Dutra, K. Grover, S. Amaral, and S. Quegan, 1994. Land cover discrimination using Sarex data. *Proceedings of the International Geoscience and Remote Sensing Symposium,* Pasadena, California, 8-12 August, 2:1074-1075.

Fischer, W.A., W.R. Hemphill, and A. Kover, 1976. Progress in remote sensing : 1972-1976. *Photogrammetria*, 32:33-72.

Food and Agriculture Organization, 1993. *Radar Imagery: Theory and Interpretation Lecture Notes*, Remote Sensing Centre, Research and Technology Development Division, Agriculture Department, Rome, Italy.

Ford, J.P., and D.E. Wickland, 1985. Forest discrimination with multipolarization imaging radar. *Proceedings of the International Geoscience and Remote Sensing Symposium,* Amherst, Massachusetts, 7-9 October, pp. 462-465.

Ford, J.P., and D.J. Casey, 1988. Shuttle radar mapping with diverse incidence angles in the rainforest of Borneo. *International Journal of Remote Sensing* 9(5):927-943.

Freeman, A., 1995. Mapping vegetation types using SIR-C data. *Proceedings of the International Geoscience and Remote Sensing Symposium,* Florence, Italy, 2:921-923.

Freeman, A., C. Kramer, and B. Chapman, 1994. Classification of the Amazon rain forest using JERS-1 data. *Proceedings of the International Geoscience and Remote Sensing Symposium,* Pasadena, California, 8-12 August, 3:1595-1597.

Freeman, A., S. Durden, and R. Zimmerman, 1992. Mapping sub-tropical vegetation using multi-frequency, multi-polarization SAR data. *Proceedings of the International Geoscience and Remote Sensing Symposium,* Houston, Texas, 26-29 May, 2:1686-1689.

Frost, V.S., J.A. Stiles, K.S. Shanmugan, and J.C. Holtzman, 1982. A model for radar images and its application to adaptive digital filtering of multiplicative noise. *IEEE Transactions on Pattern Analysis and Machine Intelligence,* PAMI-4(2): 157-165.

Frost, V.S., K.S. Shanmugan, and J.C. Holtzman, 1984. The influence of sensor and flight parameters on texture in radar images. *IEEE Transactions on Geoscience and Remote Sensing* GE-22(5):440-448.

Gerstl, S.A.W., 1990. Physics concepts of optical and reflectance signatures: a summary review. *International Journal of Remote Sensing* 11(7):1109-1117.

Hallikainen, M., T. Tares, J. Hyppa, and E. Somersalo, 1989. Classification of forest types by microwave scatterometer. *Proceedings of the International Geoscience and Remote Sensing Symposium,* Vancouver, Canada, 10-14 July, 4:2378-2381.

Han, S., 1998. Personal communication.

Haralick, R.M., K. Shanmugam, and I. Dinstein, 1973. Textural features for image classification. *IEEE Transactions on Systems, Man, and Cybernetics*, SMC-3:610-621.

Harrel, P.A., L.L. Bourgeau-Chavez, E.S. Kasischke, N.H.F. French, and N.L. Christensen, Jr., 1995. Sensitivity of ERS-1 radar data to biomass and stand structure in Alaskan boreal forest. *Remote Sensing of Environment* 54:247-260.

Harrison, B.A. and D.L.B. Jupp, 1990. Introduction to image processing: part II of MicroBRIAN resource manual. CSIRO, Canberra, Australia.

Hass, A., B. Forster, and U. Ammer, 1996. The suitability of multifrequency, multipolarimetric and multitemporal radar data for forest monitoring. *Proceedings of the International Geoscience and Remote Sensing Symposium,* Lincoln, Nebraska, 27-31 May, pp.1080-1082.

Heiska, K., M. Hallikainen, and J. Hyyppa, 1992. Backscattering behaviour of forest at C- and X-band under winter conditions. *Proceedings of the International Geoscience and Remote Sensing Symposium,* Houston, Texas, 26-29 May, 1:536-538.

Henderson, F.M. and Z. Xia, 1998. Radar applications in urban analysis, settlement detection and population estimation. In Henderson and Lewis (Eds.), *Principles and Applications of Imaging Radar,* pp. 733 - 763.

Hess, L.L., J.M. Melack, and D.S. Simonett, 1990. Radar detection of flooding beneath the forest canopy: a review. *International Journal of Remote Sensing,* 11(7): 1313-1325.

Hess, L.L., J.M. Melack, and F.W. Davis, 1994. Mapping of floodplain inundation with multi-frequency polarimetric SAR: use of a tree-based model. *Proceedings of the International Geoscience and Remote Sensing Symposium,* Pasadena, California, 8-12 August, 2:1072-1073.

Hoffer, R.M., and Kyu-Sung Lee, 1989. Forest change classification using SEASAT and SIR-B satellite SAR data. *Proceedings of the International Geoscience and Remote Sensing Symposium,* Vancouver, Canada, 10-14 July, 3:1372-1375.

Hoffer, R.M., P.W. Mueller, and D.F. Lozano-Garcia, 1985. Assessing forest resources using multiple incidence angle SIR-B data. *Proceedings of the International Geoscience and Remote Sensing Symposium,* Amherst, Massachusetts, 7-9 October, p. 572.

Hoffer, R.M., and P.W. Mueller, 1985. Use of multiple polarization X- and L-band SAR data for identifying forest cover types. *Proceedings of the International Geoscience and Remote Sensing Symposium,* Amherst, Massachusetts, 7-9 October, p. 676.

Holecz, F., E. Meier, C. Graf, and D. Nuesch, 1989. Textural analysis applied to geocoded SAR images. *Proceedings of the International Geoscience and Remote Sensing Symposium,* Vancouver, Canada, 10-14 July, 5:2789-2793.

Holecz, F., T.R. Michel, and M. Keller, 1996. Calibration and classification of SIR-C data in moderate slope areas. *Proceedings of the International Geoscience and Remote Sensing Symposium,* Lincoln, Nebraska, 27-31 May, pp.248-250.

Hsu, C.C., H.C. Han, R.T. Shin, J.A. Kong, A. Beaudoin, and T. Le Toan, 1992. Radiative transfer theory for polarimetric remote sensing of pine forest. *Proceedings of the International Geoscience and Remote Sensing Symposium,* Houston, Texas, 26-29 May, 2:1129-1131.

Hsu, C.C., R.T. Shin, J.A. Kong, A. Beaudoin, and T. Le Toan, 1993. Application of theoretical model for microwave remote sensing of forest. *Proceedings of the International Geoscience and Remote Sensing Symposium,* Tokyo, Japan, 18-21 August, 2:595-597.

Hussin Y.A., and R.M. Hoffer, 1990. Swamp forest differentiation with multipolarized and multiple incidence angle L-band radar data. *Proceedings of the International Geoscience and Remote Sensing Symposium,* Maryland, USA, 1:573-575.

Hussin Y.A., R.M. Reich, and R.M. Hoffer, 1991. Estimating Slash Pine biomass using radar backscatter. *IEEE Transactions on Geoscience and Remote Sensing* 29(3):427-431.

Hyyppa, J., J. Pulliainen, K. Heiska, and M. Hallikainen, 1994. Statistics of backscattering source distribution of boreal coniferous forest at C- and X-band. *Proceedings of the International Geoscience and Remote Sensing Symposium,* Pasadena, California, 8-12 August, 1:241-242.

Hyyppa, J., M. Hallikainen, and H. Hyyppa, 1992. Forest inventory using forest canopy profiles. *Proceedings of the International Geoscience and Remote Sensing Symposium,* Houston, Texas, 26-29 May, 2:1216-1219.

Hyyppa, J., M. Hallikainen, and J. Pulliainen, 1993. Accuracy of forest inventory based on radar-derived stand profile. *Proceedings of the International Geoscience and Remote Sensing Symposium,* Tokyo, Japan, 18-21 August, 2:391-393.

Imhoff, M.L., 1995. A theoretical analysis of the effect of forest structure on synthetic aperture radar backscatter and the remote sensing of biomass. *IEEE Transactions on Geoscience and Remote Sensing,* 33(2):341-352.

Imhoff, M.L., M. Story, C. Vermillion, F. Khan, and F. Polcyn, 1986. Forest canopy characterization and vegetation penetration assessment with space-borne radar. *IEEE Transactions on Geoscience and Remote Sensing* GE-24(4):535-542.

Imhoff, M.L., 1993. Radar backscatter/biomass saturation: observations and implications for global biomass assessment. *Proceedings of the International Geoscience and Remote Sensing Symposium,* Tokyo, Japan, 18-21 August, 1:43-45.

Israelsson, H., and J. Askne, 1991. Analysis of polarimetric SAR observations of forested areas as part of the MAESTRO-1 program. *Proceedings of the International Geoscience and Remote Sensing Symposium,* Espoo, Finland, 3-6 June, 2:703-705.

Israelsson, H., J. Askne, and R. Sylvander, 1994. Potential of SAR for forest bole volume estimation. *International Journal of Remote Sensing* 15(14):2809-2826.

Israelsson, H., and J. Askne, 1993. The effect of leaning trunks on forest radar backscattering. *Proceedings of the International Geoscience and Remote Sensing Symposium,* Tokyo, Japan, 18-21 August, 1:57-59.

Israelsson, H., and R. Sylvander, 1992. Estimation of forest parameters using polarimetric multi-frequency SAR data. *Proceedings of the International Geoscience and Remote Sensing Symposium,* Houston, Texas, 26-29 May, 1:786-788.

Jensen, J. R., 1986. Introductory digital image processing: a remote sensing perspective. Prentice-Hall, N.J. 379 p.

Jin, Ya-Qiu, and Xing-Zhong Huang, 1996. Correlation of temporal variations of active and passive microwave signatures from vegetation canopy. *IEEE Transactions on Geoscience and Remote Sensing,* 34(1):257-263.

Karam, M.A., and A.K. Fung, 1990. A canopy scattering model and its application to a deciduous forest. *Proceedings of the International Geoscience and Remote Sensing Symposium,* Maryland, USA, 20-24 May, 1:137-140.

Karam, M.A., and A.K. Fung, 1989a. A first order backscattering model for a forested canopy with a volume-fraction profile. *Proceedings of the International Geoscience and Remote Sensing Symposium,* Vancouver, Canada, 10-14 July, 5:2836-2839.

Karam, M.A., A.K. Fung, A.J. Blanchard, and C.E. Nance, 1988. The extinction properties of forest components. *Proceedings of the International Geoscience and Remote Sensing Symposium,* Edinburgh, Scotland, 13-16 September, 2:999-1002.

Karam, M.A., A.K. Fung, A. Lopes, and E. Mougin, 1991. A fully polarimetric scattering model for a coniferous forest. *Proceedings of the International Geoscience and Remote Sensing Symposium,* Espoo, Finland, 3-6 June, 1:19-22.

Karam, M.A., and A.K. Fung, 1986. A scattering model for defoliated vegetation. *Proceedings of the International Geoscience and Remote Sensing Symposium,* Zurich, Switzerland, 8-11 September, 2:879-881.

Karam, M.A., and A.K. Fung, 1989b. Electromagnetic wave extinction within a forested canopy. *Proceedings of the International Geoscience and Remote Sensing Symposium,* Vancouver, Canada, 10-14 July, pp.2502-2505.

Karam, M.A., and A.K. Fung, F. Amar, E. Mougin, A. Lopes, and A. Beaudoin, 1992a. Polarimetric signatures of a coniferous forest canopy based on vector radiative transfer theory. *Proceedings of the International Geoscience and Remote Sensing Symposium,* Houston, Texas, 26-29 May, 1:773-775.

Karam, M.A., and A.K. Fung, G. De Grandi, C. Lavalle, and A. Sieber, 1992b. Properties of radar backscatter of forests measured with a multifrequency polarimetric SAR. *Proceedings of the International Geoscience and Remote Sensing Symposium,* Houston, Texas, 26-29 May, 1:533-535.

Karam, M.A., and A.K. Fung, G. De Grandi, C. Lavalle, and A. Sieber, 1993. Backscattering from forest canopies over slanted terrain. *Proceedings of the International Geoscience and Remote Sensing Symposium,* Tokyo, Japan, 18-21 August, 2:576-579.

Karam, M.A., D.M. LeVine, F. Amar, and A.K. Fung, 1993. Understanding the relation between the forest biomass and the radar backscattered signals. *Proceedings of the International Geoscience and Remote Sensing Symposium,* Tokyo, Japan, 18-21 August, 2:573-575.

Karam, M.A., F. Amar, A.K. Fung, E. Mougin, A. Lopes, D.M. Le Vine, and A. Beaudoin, 1995. A microwave polarimetric scattering model for forest canopies based on vector radiative transfer theory. *Remote Sensing of Environment* 53:16-30.

Karam, M.A., and A.K. Fung, 1989c. Leaf-shape effects in electronic wave scattering from vegetation. *IEEE Transactions on Geoscience and Remote Sensing* 27(6):687-697.

Karam, M.A., and A.K. Fung, 1989d. Radiative transfer theory for active remote sensing of a forested canopy. *Proceedings of the International Geoscience and Remote Sensing Symposium,* Vancouver, Canada, 10-14 July, 4:2493-2496.

Karam, M.A., and A.K. Fung, R.H. Lang, and N.S. Chauhan, 1992c. A microwave scattering model for layered vegetation. *IEEE Transactions on Geoscience and Remote Sensing,* 30(4):767-784.

Kasischke, E.S., and J.C. Clinthorne, 1985. Analysis of a southern pine forest using X-, C- and L-band, dual polarized SAR imagery. *Proceedings of the International Geoscience and Remote Sensing Symposium,* Amherst, Massachusetts, 7-9 October, p. 174.

Kasischke, E.S., N.L. Christensen, Jr., and L.L. Bourgeau-Chavez, 1995. Correlating radar backscatter with components of biomass in Loblolly pine forests. *IEEE Transactions on Geoscience and Remote Sensing,* 33(3):643-658.

Kasischke, E.S., and R.W. Larson, 1986. Calibrated X- and L-band scattering coefficients from a southern U.S. forest. *Proceedings of the International Geoscience and Remote Sensing Symposium,* Zurich, Switzerland, 8-11 September, 2:895-900.

Keil, L., D. Scales, and R. Winter, 1995. Investigation of forest areas in Germany and Brazil using SAR data of the SIR-C/X-SAR and other SAR missions. *Proceedings of the International Geoscience and Remote Sensing Symposium,* Florence, Italy, 2:997-999.

Keil, M., J. Raupenstrauch, T. Tares, and R. Winter, 1993. Investigations of forest information content of polarimetric AIRSAR data in the Harz mountains. *Proceedings of the 25th International Symposium on Remote Sensing and Global Environmental Change,* Graz, Austria, 4-8 April, 1:339-349.

Keil, M., R. Winter, and H. Honsch, 1993. Tropical rainforest investigation in Brazil using ERS-1 SAR data. *Proceedings of the 2nd ERS-1 Symposium - Space at the Service of our Environment,* Hamburg, Germany, 11-14 October, pp. 481-485.

Kolawole, M.O., 1991. A sparse canopy forest backscatter model. *Proceedings of the International Geoscience and Remote Sensing Symposium,* Espoo, Finland, 3-6 June, 1:5-9.

Kolawole, M.O., 1992. On the relationships between attenuation and volume scattering coefficients, and vegetation canopy characteristics. *Proceedings of the 6th Australasian Remote Sensing Conference,* Wellington, New Zealand, 2-6 November, 2:217-225.

Kuntz, S., and F. Siegert, 1994. Evaluation of ERS-1 SAR data for tropical rainforest monitoring. *Earth Observation Quarterly,* ESA Publications Division, ESTEC, Noordwijk, The Netherlands, September, 45:1-16.

Kurvonen, L., J. Pulliainen, M. Hallikainen, and P. Mikkela, 1996. Retrieval of forest parameters from multitemporal spaceborne SAR data. *Proceedings of the International Geoscience and Remote Sensing Symposium,* Lincoln, Nebraska, 27-31 May, pp.1759-1762.

Lahti, K., Y. Rauste, and M. Holm, 1993. Relationships between C-, L-, and P-band SAR data and forest damages. In Winkler (Ed.), *Remote Sensing for Monitoring the Changing Environment of Europe,* pp. 61-67.

Lang, R.H., N. Chauhan, and J. Ranson, 1991. Comparison of Howland forest SAR data and model predictions. *Proceedings of the International Geoscience and Remote Sensing Symposium,* Espoo, Finland, 3-6 June, 1:3.

Lang, R.H., and N. Chauhan, 1990. Radar sensitivity to forest stand parameters. *Proceedings of the International Geoscience and Remote Sensing Symposium,* Maryland, USA, 20-24 May, 1:481.

Lang, R.H., O. Kilic, N. Chauhan, and J. Ranson, 1992. Modeling of SAR returns from a red pine stand. *Proceedings of the International Geoscience and Remote Sensing Symposium,* Houston, Texas, 26-29 May, 2:1138-1140.

Lang, R.H., and R. Landry, 1996. Forest backscatter modeling: simulation versus discrete random media approach. *Proceedings of the International Geoscience and Remote Sensing Symposium,* Lincoln, Nebraska, 27-31 May, pp.726-727.

Lang, R.H., R. Landry, O. Kavakhoglu, and J.C. Deguise, 1995. Simulation of microwave backscatter from a red pine stand. In Mougin, E., K.J. Ranson, and J.A. Smith (Eds.), *Multispectral and Microwave Sensing of Forestry, Hydrology and Natural Resources,* Proceedings, SPIE 2314, pp.538-548.

Lang, R.H., R. Landry, O. Kilic, N. Chauhan, N. Khadr, and D. Leckie, 1993. Effect of species structure and dielectric constant on C-band forest backscatter. *Proceedings of the International Geoscience and Remote Sensing Symposium,* Tokyo, Japan, 18-21 August, 2:583-586.

Lang, R.H., N.S. Chauhan, K.J. Ranson, and O. Kilic, 1994. Modeling P-band SAR returns from a red pine stand. *Remote Sensing of Environment* 47:132-141.

Laur, H., T. Le Toan, and A. Lopes, 1989. Textural segmentation of SAR images using first order statistical parameters. *Proceedings of the International Geoscience and Remote Sensing Symposium,* Ann Arbor, Michigan, 18 - 21 May.

Lavalle, C., and A.J. Sieber, 1993. Forest backscattering observations by using particular polarimetric states. *Proceedings of the 25th International Symposium on Remote Sensing and Global Environmental Change,* Graz, Austria, 4-8 April, 1:310-315.

Lavalle, C., G. De Grandi, I. Champion, A.J. Sieber, A. Fung, M. Karam, and F. Amar, 1992. Influence of the terrain topography and vegetation parameters on the polarimetric scattering cross sections: modeling and experimental verification for the MAESTRO1 Freiburg data set. *Proceedings of the International Geoscience and Remote Sensing Symposium,* Houston, Texas, 26-29 May, 1:239-241.

Lavalle, C., G. Schmuck, J.R. Verdebout, A.J. Sieber, G. Andreoli, and B.D. Hosgood, 1993. Microwave and optical techniques for forest monitoring: the Black Forest experiment. *Proceedings of the Topical Symposium on Combined Optical-Microwave Earth and Atmosphere Sensing,* Albuquerque, New Mexico, 22-25 March, pp.56-59.

Lee, J.S., 1986. Speckle suppression and analysis for synthetic aperture radar. *Optical Engineering,* 25(45): 636-643.

Lee, K.S., and R.M. Hoffer, 1990. Analysis of combined SIR-B and TM data for assessing forest biomass. *Proceedings of the International Geoscience and Remote Sensing Symposium,* Maryland, USA, 20-24 May, 2:1227-1230.

Lemoine, G.G., D.H. Hoekman, and H.J.C. van Leeuwen, 1991. Separability of agricultural fields and forest stands using multi-frequency polarimetric SAR data of the Flevoland site. *Proceedings of the International Geoscience and Remote Sensing Symposium,* Espoo, Finland, 3-6 June, 2:681-684.

Le Toan, T., A. Beaudoin, J. Riom, and D. Guyon, 1992. Relating forest biomass to SAR data. *IEEE Transactions on Geoscience and Remote Sensing* 30(2):403-411.

Le Toan, T., and A. Beaudoin, 1991. Relating forest parameters to SAR data. *Proceedings of the International Geoscience and Remote Sensing Symposium,* Espoo, Finland, 3-6 June, 2:689-692.

Le Toan, T., F. Ribbes, T. Hahn, N. Floury, and U.R. Wasrin, 1996. Use of ERS-1 SAR data for forest monitoring in South Sumatra. *Proceedings of the International Geoscience and Remote Sensing Symposium,* Lincoln, Nebraska, 27-31 May, pp.842-844.

Leysen, M., J.A. Conway, and A.J. Sieber, 1993. Evaluating multi-temporal ERS-1 data for tropical forest mapping: regional mapping and change detection applications. *Proceedings of the 2nd ERS-1 Symposium - Space at the Service of our Environment,* 11-14 October, pp. 447-452.

Lillesand, T.M. and R.W. Kiefer, 1987. Remote sensing and image interpretation. 2nd Edition. John Wiley and Sons. 721 pp.

Li, C., 1988. Two adaptive filters for speckle reduction in SAR images by using the variance ratio. *International Journal of Remote Sensing* 9(4):641-653.

Lin, Q., and J.P. Allebach, 1990. Combating speckle in SAR images: vector filtering and sequential classification based on a multiplicative noise model. *IEEE Transactions on Geoscience and Remote Sensing,* 28(4): 647-653.

Lopes, A., E. Mougin, A. Beaudoin, and M.A. Karam, 1991. Relating the microwave signatures of trees to their structure: results of an experimental/theoretical approach. *Proceedings of the International Geoscience and Remote Sensing Symposium,* Espoo, Finland, 3-6 June, 1:11-14.

Lopes, A., E. Mougin, A. Beaudoin, S. Goze, E. Nezry, R. Touzi, M.A. Karam, and A.K. Fung, 1992. Phase difference statistics related to sensor and forest parameters. *Proceedings of the International Geoscience and Remote Sensing Symposium,* Houston, Texas, 26-29 May, 1:779-781.

Lopes, A., E. Nezry, R. Touzi, and H. Laur, 1990a. Maximum a posteriori speckle filtering and first order texture models in SAR images. *Proceedings of the International Geoscience and Remote Sensing Symposium,* Maryland, USA, 20-24 May, pp. 2409-2412.

Lopes, A., E. Nezry, R. Touzi, and H. Laur, 1993. Structure detection and statistical adaptive speckle filtering in SAR images. *International Journal of Remote Sensing,* 14(9): 1735-1758.

Lopes, A., H. Laur, and E. Nezry, 1990b. Statistical distribution and texture in multilook and complex SAR images. *Proceedings of the International Geoscience and Remote Sensing Symposium,* Maryland, USA, 20-24 May, pp. 2427-2430.

Lopes, A., R. Touzi, and E. Nezri, 1990c. Adaptive speckle filters and scene heterogeneity. *IEEE Transactions on Geoscience and Remote Sensing,* 28(6):160-168.

Lozano-Garcia, D.F., and R.M. Hoffer, 1993. Synergistic effects of combined Landsat-TM and SIR-B data for forest resource assessment. *International Journal of Remote Sensing* 14(14):2677-2694.

Luckman, A.J., G. Groom, and J. Baker, 1994. Forest age discrimination from texture measures of SAR imagery. *Proceedings of the International Geoscience and Remote Sensing Symposium,* Pasadena, California, 8-12 August, 1:104-107.

Luckman, A.J., and J.R. Baker, 1993. AIRSAR observations of a temperate forest and modelling of topographic effects. *Proceedings of the 25th International Symposium on Remote Sensing and Global Environment Change,* Graz, Austria, 4-8 April, 1:316-326.

Mather, Paul M., 1987. Computer processing of remotely-sensed images: an introduction. John Wiley and Sons. 352 pp.

McDonald, K.C., M.C. Dobson, and F.T. Ulaby, 1991. Modeling multi-frequency diurnal backscatter from a walnut orchard. . *Proceedings of the International Geoscience and Remote Sensing Symposium,* Espoo, Finland, 3-6 June, 3:1125-1128.

McDonald, K.C., M.C. Dobson, and F.T. Ulaby, 1989. Using MIMICS to model microwave backscatter from tree canopies. *Proceedings of the International Geoscience and Remote Sensing Symposium,* Vancouver, Canada, 10-14 July, 4:2491.

Miller, R.J., L.M.J. Brown, and A.J. Sieber, 1990. Principles of high resolution forest imaging model for SAR. *Proceedings of the International Geoscience and Remote Sensing Symposium,* Maryland, USA, 20-24 May, 1:491-494.

Mo, T., and J.R. Wang, 1988. Modelling of SAR polarization phase difference from trees. *Proceedings of the International Geoscience and Remote Sensing Symposium,* Edinburgh, Scotland, 13-16 September, 1:55-58.

Moghaddam, M., 1995. Retrieval of forest canopy parameters for OTTER using an optimization technique. In Mougin, E., K.J. Ranson, and J.A. Smith (Eds.), *Multispectral and Microwave Sensing of Forestry,* Proceedings, SPIE 2314, pp.549-558.

Moghaddam, M., S. Durden, and H. Zebker, 1993. Effects of environmental change on radar backscatter in the Oregon transect. *Proceedings of the International Geoscience and Remote Sensing Symposium,* Tokyo, Japan, 18-21 August, 1:580-582.

Moghaddam, M., S. Durden, H. Zebker, and J. Klein, 1992. Radar measurement of forested areas during OTTER. *Proceedings of the International Geoscience and Remote Sensing Symposium,* Houston, Texas, 26-29 May, 2:1135-1137.

Moghaddam, M., S. Durden, and H. Zebker, 1994. Radar measurement of forested areas during OTTER. *Remote Sensing of Environment* 47:154-166.

Mosley, G., 1989. Blue mountains for world heritage. Colong Foundation for Wilderness, Sydney, Australia, 135 p.

Mougin, E., A. Lopes, and M.A. Karam, 1989. Interpretation of microwave signatures of vegetation by a cylinder theoretical scattering model. *Proceedings of the International Geoscience and Remote Sensing Symposium,* Vancouver, Canada, 10-14 July, 5:2840-2842.

National Aeronautics and Space Administration, 1989. *SAR Synthetic Aperture Radar, Earth Observing System, Instrument Panel Report,* Vol. IIf, Washington, D.C.

Nezry, E., A. Lopes, and R. Touzi, 1991. Detection of structural and textural features for SAR images filtering. *Proceedings of the International Geoscience and Remote Sensing Symposium,* Espoo, Finland, 3-6 June, pp. 2169-2172.

Nezry, E., E. Mougin, A. Lopes, J.P. Gastellu-Etchegorry, F. Zagolski, and Y. Laumonier, 1992. Tropical vegetation mapping with combined visible and SAT spaceborne data. *Proceedings of the International Geoscience and Remote Sensing Symposium,* Houston, Texas, 26-29 May, 2:989-991.

Nezry, E., E. Mougin, A. Lopes, J.P. Gastellu-Etchegorry, and Y. Laumonier, 1993. Tropical vegetation mapping with combined visible and SAR spaceborne data. *International Journal of Remote Sensing* 14(11):2165-2184.

Nilson, T., 1991. A forest canopy reflectance model. *Proceedings of the International Geoscience and Remote Sensing Symposium,* Espoo, Finland, 3-6 June, 3:1559-1560.

Paris, J.F., and R. Woodruff, 1991. Results from four years of field research with a C-band (6-cm) field microwave scatterometer in cultural and natural vegetation sites. *Proceedings of the International Geoscience and Remote Sensing Symposium,* Espoo, Finland, 3-6 June, 4:2255-2256.

Paudyal, D.R., and J. Aschbacher, 1993. Land-cover suitability studies of filtered ERS-1 SAR images in the tropics. *Proceedings of the International Geoscience and Remote Sensing Symposium,* Tokyo, Japan, 18-21 August, pp.1216-1218.

Paudyal, D.R., P.N. Tiangco, J. Aschbacher, and Y. Ang, 1995a. Assessment of multi-temporal ERS-1 SAR data for tropical forest discrimination and mapping in South Thailand. TREES ERS-1 '94 Final Meeting, JRC, Ispra, Italy, 23-24 February 1995.

Paudyal, D.R., P.N. Tiangco, J. Aschbacher, and Y. Ang, 1995b. Assessment of multi-temporal ERS-1 SAR data for tropical forest discrimination and mapping in West Thailand. TREES ERS-1 '94 Final Meeting, JRC, Ispra, Italy, 23-24 February 1995.

Person, R. and M. Campbell, 1988. Using Excel: IBM version. Que Corporation, Carmel, Indiana. 808 pp.

Pedersen, J.P., H. Johnsen, T. Guneriussen, B. Johansen, and M. Rosengren, 1991. Vegetation and forestry mapping in Thetford (UK) using combined MAESTRO SAR and Landsat/Thematic Mapper data. *Proceedings of the International Geoscience and Remote Sensing Symposium,* Espoo, Finland, 3-6 June, 2:697-700.

Pedersen, J.P., T. Guneriussen, and B. Johansen, 1993. Application of ERS-1 data in combination with Landsat and SPOT data for forestry mapping in a Norweigian forest region. *Proceedings of the International Geoscience and Remote Sensing Symposium,* Tokyo, Japan, 18-21 August, 1:46-48.

Pierce, L.E., K. Bergen, M.C. Dobson, and F.T. Ulaby, 1995. Land-cover classification using SIR-C/X-SAR data. *Proceedings of the International Geoscience and Remote Sensing Symposium,* Florence, Italy, 2:918-920.

Pierce, L.E., M.C. Dobson, and F.T. Ulaby, 1994. Knowledge-based land-cover classification using ERS-1/JERS-1 composites. *Proceedings of the International Geoscience and Remote Sensing Symposium,* Pasadena, California, 8-12 August, 3:1599-1601.

Pope, K.O., J.M. Rey-Benayas, and J.F. Paris, 1994. Radar remote sensing of forest and wetland ecosystems in the Central American tropics. *Remote Sensing of Environment* 48:205-219.

Poutsma, T. and N.D. Turvey, 1979. A survey of the soils on the Gippsland property of APM Forests Pty. Ltd.: a factual soil framework for silvicultural decisions. Amcor Plantations technical report.

Proisy, C., E. Mougin, and F. Fromard, 1996. Investigating correlations between radar data and mangrove forest characteristics. *Proceedings of the International Geoscience and Remote Sensing Symposium,* Lincoln, Nebraska, 27-31 May, pp.733-735.

Pulliainen, J., K. Heiska, J. Hyyppa, and M. Hallikainen, 1993. Backscattering properties of boreal forests at C- and X-bands. *Proceedings of the International Geoscience and Remote Sensing Symposium,* Tokyo, Japan, 18-21 August, 2:388-390.

Pulliainen, J., P. Mikkela, K. Heiska, J. Koskinen, and M. Hallikainen, 1994. Seasonal effects on C- and X-band backscattering properties of Finnish boreal forests. *Proceedings of the International Geoscience and Remote Sensing Symposium,* Pasadena, California, 8-12 August, 1:238-240.

Pulliainen, J., P. Mikkela, M. Hallikainen, and E. Tomppo, 1995. Estimation of forest biomass and soil moisture in boreal forests employing ERS-1 SAR data. *Proceedings of the International Geoscience and Remote Sensing Symposium,* Florence, Italy, 3:2035-2037.

Quegan, S., R.G. Caves, and R.G. White, 1993. The structural content of ERS-1 images and its implications. *Proceedings of the 2nd ERS-1 Symposium - Space at the Service of our Environment,* Hamburg, Germany, 11-14 October, pp. 623-628.

Ranson, K.J., G. Sun, B. Montgomery, and R.H. Lang, 1996. Mapping of boreal forest biomass using SAR. *Proceedings of the International Geoscience and Remote Sensing Symposium,* Lincoln, Nebraska, 27-31 May, pp.577-579.

Ranson, K.J., G. Sun, J.F. Weishampel, and R.G. Knox. 1995a. An evaluation of AIRSAR and SIR-C/X-SAR images for northern forest ecological studies in Maine, USA. *Proceedings of the International Geoscience and Remote Sensing Symposium,* Florence, Italy, 2:994-996.

Ranson, K.J., G. Sun, J.F. Weishampel, and R.G. Knox. 1995b. Interfacing forest succession and radar backscatter models for forest ecosystem studies. In Mougin, E., K.J. Ranson, and J.A. Smith (Eds.), *Multispectral and Microwave Sensing of Forestry, Hydrology and Natural Resources,* Proceedings, SPIE 2314, pp.526-536.

Ranson, K.J., and G. Sun, 1992. Mapping biomass for a northern forest ecosystem using multi-frequency SAR data. *Proceedings of the International Geoscience and Remote Sensing Symposium,* Houston, Texas, 26-29 May, 2:1220-1222.

Ranson, K.J., and G. Sun, 1994a. Mapping biomass of a northern forest using multifrequency SAR data. *IEEE Transactions on Geoscience and Remote Sensing,* 32(2):388-396.

Ranson, K.J., and G. Sun, 1994b. Northern forest classification using temporal multifrequency and multipolarimetric SAR images. *Remote Sensing of Environment* 47:142-153.

Ranson, K.J., and G. Sun, 1993. Retrieval of forest spatial patterns from SAR images. *Proceedings of the International Geoscience and Remote Sensing Symposium,* Tokyo, Japan, 18-21 August, 3:1213-1215.

Ranson, K.J., S. Saatchi, and G. Sun, 1995c. Boreal forest ecosystem characterization with SIR-C/X-SAR. *IEEE Transactions on Geoscience and Remote Sensing,* 33(4):867-876.

Rao, K.S., and Y.S. Rao, 1996. Potential of SIR-C data to study vegetation over Gujarat test site, India. *Proceedings of the International Geoscience and Remote Sensing Symposium,* Lincoln, Nebraska, 27-31 May, pp.201-203.

Rauste, Y., 1992. Estimation of biomass in mixed forests using polarimetric SAR data. *Proceedings of the International Geoscience and Remote Sensing Symposium,* Houston, Texas, 26-29 May, 1:789- 791.

Rauste, Y., 1993. Multitemporal analysis of forest biomass using AIRSAR data. *Proceedings of the 25th International Symposium on Remote Sensing and Global Environmental Change,* Graz, Austria, 4-8 April, 1:328-336.

Rauste, Y., T. Hame, J. Pulliainen, K. Heiska, and M. Hallikainen, 1994. Radar-based forest biomass estimation. *International Journal of Remote Sensing* 15(14):2797-2808.

Rees, W.G., 1990. Physical principles of remote sensing. Cambridge University Press. Cambridge. 247 pp.

Richards, J.A., 1990. Radar backscatter modelling of forests: a review of current trends. *International Journal of Remote Sensing* 11(7):1299-1312.

Richards, J.A., 1993. Remote sensing digital image analysis: an introduction. 2nd Ed. Springer-Verlag Berlin, Germany. 340 pp.

Richards, J.A., Y. Dong, and J.D. Cashman, 1993. SAR observations and backscatter modelling of Australian native forests. *Proceedings of the 2nd ERS-1 Symposium - Space at the Service of our Environment,* Hamburg, Germany, 11-14 October, pp. 463-467.

Richards, J.A., and Z. Ahmed, 1988. Association of radar backscatter with biophysical characteristics of Australian forests. *Proceedings of the International Geoscience and Remote Sensing Symposium,* Edinburgh, Scotland, 13-16 September, 3:1363-1365.

Richason, B.F., Jr., 1978. Remote sensing: an overview. In Richason, B.F., Jr. (Ed.), *Introduction to Remote Sensing of the Environment.* Kendall/Hunt Publishing Company, Iowa, USA, pp. 1-13.

Rignot, E., C. Williams, J.B. Way, and L.A. Viereck, 1994a. Mapping of forest types in Alaskan boreal forests using SAR imagery. *IEEE Transactions on Geoscience and Remote Sensing,* 32(5):1051-1058.

Rignot, E., C. Williams, and J.B. Way, 1993. Mapping of taiga forest units using AIRSAR data and/or optical data, and retrieval of forest parameters. *Proceedings of the International Geoscience and Remote Sensing Symposium,* Tokyo, Japan, 18-21 August, 1:49-51.

Rignot, E., J.B. Way, C. Williams, L.Viereck, and J. Yarie, 1994b. P-band radar mapping of forest biomass in boreal forests of interior Alaska. *Proceedings of the International Geoscience and Remote Sensing Symposium,* Pasadena, California, 8-12 August, 3:1853-1855.

Rignot, E., J.B. Way, K. McDonald, L. Viereck , and P. Adams, 1992. Monitoring of environmental conditions in the Alaskan forests using ERS-1 SAR data. *Proceedings of the International Geoscience and Remote Sensing Symposium,* Houston, Texas, 26-29 May, 1:530-532.

Rignot, E., J. Van Zyl, and R. Zimmermann, 1994c. Inference of forest biomass using P-band circular-polarized radar signals. *Proceedings of the International Geoscience and Remote Sensing Symposium,* Pasadena, California, 8-12 August, 4:2467-2469.

Rignot, E., R. Zimmermann, and J. Van Zyl, 1995. Spaceborne applications of P band imaging radars for measuring forest biomass. *IEEE Transactions on Geoscience and Remote Sensing,* 33(5):1162-1169.

Robin, E., and A. Guissard, 1994. A parametric study of the trunk-ground corner effect in forest remote sensing. *Proceedings of the International Geoscience and Remote Sensing Symposium,* Pasadena, California, 8-12 August, 1:100-102.

Saatchi, S., and M. Moghaddam, 1995. Biomass distribution in boreal forest using SAR imagery. In Mougin, E., K.J. Ranson, and J.A. Smith (Eds.), *Multispectral and Microwave Sensing of Forestry, Hydrology and Natural Resources,* Proceedings, SPIE 2314, pp.437-447.

Saatchi, S., M. Moghaddam, K. McDonald, and S. Durden, 1994. Microwave scattering from forest canopies. *Proceedings of the International Geoscience and Remote Sensing Symposium,* Pasadena, California, 8-12 August, 1:547.

Sader, S.A., 1987. Forest biomass, canopy structure, and species composition relationships with multipolarization L-band synthetic aperture radar data. *Photogrammetric Engineering and Remote Sensing* 53(2):193-202.

Sanchez, J. and M. P. Canton, 1999. Space image processing. CRC Press. Boca Raton, Florida. 424 pp.

Seifert, F.M., H. Kietzmann, and M. Zink, 1995. Forest monitoring with SIR-C/X-SAR. *Proceedings of the International Geoscience and Remote Sensing Symposium,* Florence, Italy, 2:1067-1068.

Seifert, F.M., H. Kietzmann, and M. Zink, 1996. Multifrequency and polarimetric analysis of forests with SIR-C/X-SAR data. *Proceedings of the International Geoscience and Remote Sensing Symposium,* Lincoln, Nebraska, 27-31 May, pp.1086-1088.

Sery, F., D.D. Gambart, E. Mougin, F. Fromard, and J.P. Rudant, 1995. Mapping on mangrove forest using multisource data. *Proceedings of the International Geoscience and Remote Sensing Symposium,* Florence, Italy, 2:1222-1224.

Shi, Z., and K.B. Fung, 1994. A comparison of digital speckle filters. *Canadian Crown Copyright,* pp. 2129-2133.

Shimabukuro, Y.E., W.T. Lawrence, and F.J. Ahern, 1995. Tropical vegetation analysis with Landsat Thematic Mapper and Canadian synthetic aperture radar data. In Mougin, E., K.J. Ranson, and J.A. Smith (Eds.), *Multispectral and Microwave Sensing of Forestry, Hydrology and Natural Resources,* Proceedings, SPIE 2314, pp.255-260.

Shinohara, H., T. Homma, H. Nohmi, H. Hirosawa, and T. Tagawa, 1992. Relation between L-band microwave penetration/backscattering characteristics and state of trees. *Proceedings of the International Geoscience and Remote Sensing Symposium,* Houston, Texas, 26-29 May, 1:539-541.

Shiver, B.D. and B.E. Borders, 1996. Sampling techniques for forest resource inventory. John Wiley and Sons, Inc. 356 pp.

Skidmore, A.K., 1989. Extracting forest resource information from remotely sensed and ancillary data: use of an expert system. Ph.D. Dissertation, Australian National University, Canberra, Australia.

Slatton, K.C., M.M. Crawford, J.C. Gibeaut, and R. Gutierrez, 1996. Modeling wetland vegetation using polarimetric SAR. *Proceedings of the International Geoscience and Remote Sensing Symposium,* Lincoln, Nebraska, 27-31 May, pp.263-265.

Souyris, J.C., and T. Le Toan, 1995. Inversion of Landes forest biomass using SIR-C/X-SAR data: experiment and theory. *Proceedings of the International Geoscience and Remote Sensing Symposium,* Florence, Italy, 2:1201-1203.

Souyris, J.C., T. Le Toan, N. Floury, L. Thomasson, C.C. Hsu, and J.A. Kong, 1996. Use of polarization synthesis for deforestation studies based on SIR-C/X-SAR data analysis. *Proceedings of the International Geoscience and Remote Sensing Symposium,* Lincoln, Nebraska, 27-31 May, pp.836-838.

Stewart, H.T.L., and D.W. Flinn, 1981. Above-ground biomass of *Pinus radiata* in South Gippsland, Victoria. Research Branch Report No. 174, For. Comm. Victoria (unpubl).

Stewart, H.T.L., D.W. Flinn, and B.C. Aeberli, 1979. Above-ground biomass of a mixed eucalypt forest in Eastern Victoria. *Australian Journal of Botany* 27: 725-740.

Stolz, R., and W. Mauser, 1995. First evaluations of shuttle SIR-C X-SAR data for landcover classifications. *Proceedings of the International Geoscience and Remote Sensing Symposium,* Florence, Italy, 2:1058-1060.

Stone, T.A., 1985. Analysis of deforestation in Amazonia using shuttle-imaging radar. *Proceedings of the International Geoscience and Remote Sensing Symposium,* Amherst, Massachusetts, 7-9 October, p.574.

Stone, T.A., G.M. Woodwell, and R.A. Houghton, 1989. Tropical deforestation in Para, Brazil: analysis with Landsat and Shuttle Imaging Radar-A. *Proceedings of the International Geoscience and Remote Sensing Symposium,* Vancouver, Canada, 10-14 July, 1:192-195.

Suga, Y., S. Takeuchi, and H. Tsu, 1996. Monitoring of the change of vegetative conditions using multitemporal SAR data. *Proceedings of the International Geoscience and Remote Sensing Symposium,* Lincoln, Nebraska, 27-31 May, pp.1763-1765.

Sugimura, T., A. Inanaga, Y. Nakayama, S. Tanaka, and H. Nishikawa, 1993. Observation of vegetation around Mt. Fuji using ERS-1 and JERS-1 SAR data. *Proceedings of the 25th International Symposium on Remote Sensing and Global Environmental Change,* Graz, Austria, 4-8 April, 2:521-531.

Sun, G., and D.S. Simonett, and A.H. Strahler, 1991. A radar backscattering model for discontinuous coniferous forests. *IEEE Transactions on Geoscience and Remote Sensing* 29(4):639-650.

Sun, G., and D.S. Simonett, and A.H. Strahler, 1989. A radar backscattering model for discontinuous forest canopies. *Proceedings of the International Geoscience and Remote Sensing Symposium,* Vancouver, Canada, 10-14 July, 5:2832-2835.

Sun, G., and D.S. Simonett, and J. Chen, 1988. Simulation of the radar signature of sparse Ponderosa pine forest. *Proceedings of the International Geoscience and Remote Sensing Symposium,* Edinburgh, Scotland, 13-16 September, 3:1367.

Sun, G., and D.S. Simonett, 1990. Polarimetric radar backscatter modeling for discontinuous canopies. *Proceedings of the International Geoscience and Remote Sensing Symposium,* Maryland, USA, 20-24 May, 1:483-486.

Sun, G., and D.S. Simonett, 1988. Simulation of L-HH microwave backscattering from a coniferous forest stands: a comparison with SIR-B data. *International Journal of Remote Sensing* 9(5):907-925.

Sun, G., and K.J. Ranson, 1993. Modeling of radar responses to forest physical parameters. *Proceedings of the International Geoscience and Remote Sensing Symposium,* Tokyo, Japan, 18-21 August, 2:384-386.

Sun, G., and K.J. Ranson, 1996. Radar modeling of forest spatial structure. *Proceedings of the International Geoscience and Remote Sensing Symposium,* Lincoln, Nebraska, 27-31 May, pp. 1096-1098.

Sun, G., and K.J. Ranson, 1995. Spatially explicit modeling of radar backscatter from forest canopies. In Mougin, E., K.J. Ranson, and J.A. Smith (Eds.), *Multispectral and Microwave Sensing of Forestry, Hydrology and Natural Resources,* Proceedings, SPIE 2314, pp.559-570.

Thompson, M.D., and R. Dams, 1990. Forest and land cover mapping from SAR: a summary of recent tropical studies. *Proceedings of the 23rd International Symposium on Remote Sensing of Environment,* Bangkok, Thailand, 19-25 April, pp. 509-515.

Tiangco, P.N. and B.C. Forster, 1998. Development of trunk-canopy biomass and morphology indices from quadpolarized radar data. *Proceedings of the 9th Australasian Remote Sensing Photogrammetry Conference,* Sydney, Australia, 20 - 24 July, 1998. Vol. 1, paper no. 220.

Tomppo, E., P. Mikkela, H. Henttonen, M. Katila, M. Hallikainen, J. Hyyppa, J. Pulliainen, K. Heiska, T. Tares, and G. Vass, 1994. Application of ERS-1 SAR data in large area forest inventory. *Proceedings of the International Geoscience and Remote Sensing Symposium,* Pasadena, California, 8-12 August, 4:2474-2476.

Touzi, R., S. Goze, T. Le Toan, A. Lopes, and E. Mougin, 1992. Polarimetric discriminators for SAR images. *IEEE Transactions on Geoscience and Remote Sensing* 30(5):973-980.

Tsang, L., Z. Chen, K.H. Ding, C. Hsu, and G. Zhang, 1994. Collective scattering effects in vegetation canopies at microwave frequencies based on the Monte Carlo simulations. *Proceedings of the International Geoscience and Remote Sensing Symposium,* Pasadena, California, 8-12 August, 1:548-550.

Ulaby, F.T., F. Kouyate, B. Brisco, and T.H. Lee Williams, 1986. Textural information in SAR images. *IEEE Transactions on Geoscience and Remote Sensing* GE-24:235-245.

Ulaby, F.T., K. Sarabandi, K. McDonald, M. Whitt, and M.C. Dobson, 1990. Michigan microwave scattering model. *International Journal of Remote Sensing,* 11:1223-1253.

Ulaby, F.T., 1982. Radar signatures of terrain: useful monitors of renewable resources. *Proceedings of the IEEE* 70(12):1410-1427.

Ulaby, F.T., R.K. Moore, and A.K. Fung, 1981. Microwave remote sensing: active and passive. Vol. I: Microwave remote sensing fundamentals and radiometry. Addison-Wesley Publishing Co., Mass., 456 pp.

UNSW Centre for Remote Sensing, 1996. *Microwave Remote Sensing Course Notes*, First Session, School of Geomatic Engineering, The Univ. of New South Wales, Kensington, Australia.

Van der Sanden, J.J., and D.H. Hoekman, 1993. Identification of tropical forest cover types using X-band and C-band airborne SAR data. *SAREX-92 Final Workshop,* ESA-HQ, Frascati, Italy, 6-8 December 1993.

Van der Sanden, J.J., and D.H. Hoekman, 1995. Multiband polarimetric SAR in support of tropical forest resource assessment. *Proceedings of the International Geoscience and Remote Sensing Symposium,* Florence, Italy, 2:1207-1209.

Van Zyl, J.J., and C.F. Burnette, 1989. Classification of earth terrain cover using multifrequency imaging radar polarization data. *Proceedings of the International Geoscience and Remote Sensing Symposium,* Vancouver, Canada, 10-14 July, 1:29.

Van Zyl, J.J., and H.A. Zebker, 1987. Radar polarization signatures of vegetated areas. *Proceedings of the International Geoscience and Remote Sensing Symposium,* Ann Arbor, Michigan, 18-21 May, 2:835-837.

Van Zyl, J.J., 1993. The effect of topography on radar scattering from vegetated areas. *IEEE Transactions on Geoscience and Remote Sensing* 31(1):153-160.

Van Zyl, J.J., 1992. The effect of topography on radar scattering from vegetated areas. *Proceedings of the International Geoscience and Remote Sensing Symposium,* Houston, Texas, 26-29 May, 2:1132-1134.

Van Zyl, J.J., 1989. Unsupervised classification of scattering behavior using radar polarimetry data. *IEEE Transactions on Geoscience and Remote Sensing* 27(1):36-45.

Wang, Y., D.C. He, and G.B. Benie, 1995. A line-preserving post-processing technique for maximum likelihood classification of SAR images. *International Journal of Remote Sensing* 16(11):2081-2087.

Wang, Y., D.S. Simonett, and M. Imhoff, 1990. A multiple polarization layered radar model for mangal forests. *Proceedings of the International Geoscience and Remote Sensing Symposium,* Maryland, USA, 20-24 May, 1:487-490.

Wang, Y., E.S. Kasischke, J.M. Melack, F.W. Davis, and N.L. Christensen, Jr., 1994. The effects of changes in Loblolly pine biomass and soil moisture on ERS-1 backscatter. *Remote Sensing of Environment* 49:25-31.

Wang, Y., F.W. Davis, and J.M. Melack, 1992. Modeled response of L-band radar backscatter from conifer woodland to changes in tree canopy volume. *Proceedings of the International Geoscience and Remote Sensing Symposium,* Houston, Texas, 26-29 May, 1:776-778.

Wang, Y., F.W. Davis, and J.M. Melack, 1993a. Simulated and observed backscatter at P-, L-, and C-bands from Ponderosa pine stands. *IEEE Transactions on Geoscience and Remote Sensing,* 31(4):871-879.

Wang, Y., and F.W. Davis, 1996. Radar backscatter components from ponderosa pine forests. *Proceedings of the International Geoscience and Remote Sensing Symposium,* Lincoln, Nebraska, 27-31 May, pp.1077-1079.

Wang, Y., J.L. Day, F.W. Davis, and J.M. Melack, 1993b. Modeling L-band radar backscatter of Alaskan boreal forest. *IEEE Transactions on Geoscience and Remote Sensing,* 31(6):1146-1153.

Wang, Y., J.L. Day, and F.W. Davis, 1996. Sensitivity of modeled C-band backscatter from loblolly pine forests to surface soil roughness and moisture. *Proceedings of the International Geoscience and Remote Sensing Symposium,* Lincoln, Nebraska, 27-31 May, pp.1083-1085.

Wang, Y., J. Day, and G. Sun, 1993c. Santa Barbara microwave backscattering model for woodlands. *International Journal of Remote Sensing* 14(8):1477-1493.

Wang, Y., L.L. Hess, S. Filoso, and J.M. Melack, 1994. Canopy penetration studies: modeled radar backscatter from Amazon floodplain forests at C-, L-, and P-band. *Proceedings of the International Geoscience and Remote Sensing Symposium,* Pasadena, California, 8-12 August, 2:1060-1062.

Wang, Y., and M.L. Imhoff, and D.S. Simonett, 1989. Radar modeling of tropical mangal forest stands. *Proceedings of the International Geoscience and Remote Sensing Symposium,* Vancouver, Canada, 10-14 July, 4:2497-2500.

Wang, Y., and M.L. Imhoff, 1993. Simulated and observed L-HH radar backscatter from tropical mangrove forests. *International Journal of Remote Sensing* 14(15):2819-2828.

Way, J.B., E. Rignot, K. McDonald, L. Viereck, C. Williams, and P. Adams, 1993. Monitoring seasonal change in taiga forests using ERS-1 SAR data. *Proceedings of the International Geoscience and Remote Sensing Symposium,* Tokyo, Japan, 18-21 August, 1:52.

Way, J.B., and E. Rignot, 1991. Monitoring temporal change in Alaskan forests using AIRSAR data. *Proceedings of the International Geoscience and Remote Sensing Symposium,* Espoo, Finland, 3-6 June, 3:1117-1119.

Way, J.B., 1993. Sensitivity of forest biomass based on the analysis of scattering mechanism. *Proceedings of the International Geoscience and Remote Sensing Symposium,* Tokyo, Japan, 18-21 August, 2:387.

Wegmuller U., C.L. Werner, D. Nuesch, and M. Borgeaud, 1995. Forest mapping using ERS-1 SAR repeat-pass interferometry. *Earth Observation Quarterly*, ESA Publications Division, ESTEC, Noordwijk, The Netherlands, September, 49:4-7.

Wegmuller, U., F. Holecz, Y. Wang, and G. Kattenborn, 1994. Theoretical sensitivity of ERS-1 SAR backscatter over forest. *Proceedings of the International Geoscience and Remote Sensing Symposium,* Pasadena, California, 8-12 August, 4:2477-2479.

Weishampel, J.F., G. Sun, K.J. Ranson, K.D. LeJeune, and H.H. Shugart, 1994. Forest textural properties from simulated microwave backscatter: the influence of spatial resolution. *Remote Sensing of Environment* 47:120-131.

Werle, D., 1989a. Potential application of imaging radar for monitoring the depletion of tropical forests. *Proceedings of the International Geoscience and Remote Sensing Symposium,* Vancouver, Canada, 10-14 July, 3:1383-1386.

Werle, D., 1989b. Radar remote sensing for application in forestry: a literature review for investigators and potential users of SAR data in Canada. Canada Centre for Remote Sensing, Ontario, Canada. 42 pp.

Weydahl, D.J., 1992. Multitemporal analysis of ERS-1 images over land areas. *Proceedings of the 2nd Scandinavian SAR Symposium,* September 1992.

Wharton, S.W., 1989. Knowledge-based spectral classification of remotely sensed image data. In G. Asrar (Ed.), *Theory and Applications of Optical Remote Sensing,* John Wiley and Sons, New York.

Williams, C., E. Rignot, K. McDonald, L. Viereck, A. Balser, and J.B. Way, 1994. An ecological approach to radar mapping of biomass in interior Alaskan boreal forests. *Proceedings of the International Geoscience and Remote Sensing Symposium,* Pasadena, California, 8-12 August, 3:1856-1859.

Woodhouse, I.H., and D.H. Hoekman, 1996. Modeling of microwave backscatter using a tree-growth model for boreal forests within the NOPEX test site. *Proceedings of the International Geoscience and Remote Sensing Symposium,* Lincoln, Nebraska, 27-31 May, pp.260-262.

Wooding, M., E. Attema, J. Aschbacher, M. Borgeaud, R. Cordey, H. De Groof, J. Harms, J. Lichtenegger, G. Niewenhuis, C. Schmullius, and A. Zmuda, 1995. Satellite radar in agriculture: experience with ERS-1. *ESA SP-1185,* ESA Publications division, Noordwijk, The Netherlands, 71 pp.

Wu, S.T., 1985. A preliminary report on the measurements of forest canopies with C-band radar scatterometer at NASA/NSTL. *Proceedings of the International Geoscience and Remote Sensing Symposium,* Amherst, Massachusetts, 7-9 October, pp. 168-173.

Wu, S.T., 1989. Assessment of tropical forest biophysical characteristics with multipolarization SAR data acquired over a mountainous region in Costa Rica. *Proceedings of the International Geoscience and Remote Sensing Symposium,* Vancouver, Canada, 10-14 July, 3:1379-1382.

Wu, S.T., 1987. Integration of topographic data with synthetic aperture radar data for determining forest properties in mountainous terrain. *Proceedings of the International Geoscience and Remote Sensing Symposium,* Ann Arbor, Michigan, 18-21 May, 2:1499-1503.

Wu, S.T., 1985. Multipolarization SAR data for surface feature delineation. *Proceedings of the International Geoscience and Remote Sensing Symposium,* Amherst, Massachusetts, 7-9 October, pp. 678-683.

Wu, S.T., 1993. P-, L- and C-band polarimetric radar measurements of coastal zone forest and other surface covers. *Proceedings of the International Geoscience and Remote Sensing Symposium,* Tokyo, Japan, 18-21 August, 3:1219-1221.

Wu, Y., and H. Maitre, 1990. A speckle suppression method for SAR images using maximum homogeneous region filter. *Proceedings of the International Geoscience and Remote Sensing Symposium,* Maryland, USA, 3: 2413-2416.

Xinghe, S., and Q. Ping, 1993. Texture analysis for remotely sensed imagery. *Proceedings of the 9th Thematic Conference on Geologic Remote Sensing,* Pasadena, California, 8-11 February, pp. 311-321.

Yamagata, Y. and Y. Yasuoka, 1993. Classification of wetland vegetation by texture analysis methods using EDRS-1 and JERS-1 images. *Proceedings of the International Geoscience and Remote Sensing Symposium,* Tokyo, Japan, 18-21 August, 4:1614-1616.

Zoughi, R., and R.K. Moore, 1985. Identification of primary contributors to the backscatter from pine, pin oak, black walnut, American sycamore, sugar maple and creeping juniper at 10 GHZ. *Proceedings of the International Geoscience and Remote Sensing Symposium,* Amherst, Massachusetts, 7-9 October, p.175.

APPENDICES

Appendix 1.1 Glossary (from FAO, 1993)

Absorption: Reduction in the electromagnetic wave strength, as determined by the dielectric properties of the medium where the wave propagates.

Almaz: Synthetic aperture radar (S-band) satellite launched by the USSR in May 1991 and operated until October 1992.

Along-track: Dimension parallel to the path of the radar, also called the azimuth or cross range direction.

Amplitude: Measure of signal strength, particularly the strength or "height" of an electromagnetic wave (units of voltage).

Antenna: Device to transmit and receive electromagnetic energy by a radar. Polarisation on transmit and on receive is determined by the antenna.

Attenuation: Decrease in the signal strength, commonly caused by factors such as absorption and volume scattering in a medium as the wave passes through.

Azimuth: The relative position of an object within the field of view of an antenna in the plane intersecting the radar's line of flight.

Backscatter: The microwave signal reflected by elements of an illuminated scene back to the radar, as recorded by the sensor.

Backscattering coefficient (σ^0): The conventional measure of the strength of the radar signals reflected by a distributed scatterer, usually expressed in dB. It is a normalised dimensionless number, comparing the strength observed to that expected from an area of one square metre.

Brightness: Property of radar image where the observed strength of the radar reflectivity is expressed as being proportional to a digital number or to a grey scale, which, for a photographic positive, shows "bright" as "white".

Calibration: Process which enables one to relate digital numbers describing an image to physical quantities such as reflectivity, geometry (position or size), or phase.

C-band: Microwave band in which the wavelengths are at or near 5.6 cm.

CCT: Computer compatible tape. Akin to a floppy disk in personal computers, it functions as storage medium for image files.

Conductivity: Property of an object to allow the flow of electrical current with very little loss. In general, conductivity is increased with increased moisture content.

Decibel (dB): Measurement of signal strength, properly applied to a ratio of powers, used in radar as measure of reflectivity where the dynamic range may span several factors of ten.

Dielectric constant: Fundamental (complex) parameter, also known as the "complex permittivity", that describes the electrical properties of a lossy medium.

Digital number (DN): Numerical number between zero and 255 assigned to each spatial grid position in the file to represent the brightness levels of an image.

Dynamic range: Refers to the variety of signal amplitudes or power levels available in a system or data file.

Electromagnetic wave: A wave propagating at the speed of light in free space (i.e., normal atmospheric conditions) and described by variations in electric and magnetic fields.

ERS-1: Synthetic aperture radar (C-band) satellite launched by the European Space Agency in July 1991.

Foreshortening: Spatial distortion where the terrain slopes facing the side-looking radar's illumination appear to be shorter than their true size. This effect is more pronounced for steeper slopes and incidence angles.

Frequency: Rate of oscillation of a wave. For electromagnetic waves, the product of wavelength and frequency is equal to the speed of propagation, which, in free space, is the speed of light.

Ground range: Range direction of a side-looking radar image as projected onto the nominally horizontal reference plane, similar to the spatial display of conventional maps.

Histogram: Graph which plots numbers of samples against digital number (the statistical distribution of brightness) of data selected from a region of an actual image file.

Image: Mapping of the observed radar reflectivity of a scene.

Incidence angle: Angle between the radar line of sight to an element of an imaged scene, and a vertical direction characteristic of the scene.

Intensity: Strength of a field or of a distribution, such as an image file, proportional to magnitude squared.

JERS-1: Synthetic aperture radar (L-band) satellite launched by Japan in February 1992.

Layover: Extreme form of foreshortening, where the top of a reflecting object (e.g. mountain) is closer to the radar than the lower parts of the object. Such feature appears to have fallen towards the radar. This effect is more pronounced for radars with smaller incidence angle.

L-band: Microwave band in which the wavelengths are at or near 23.5 cm.

Looks: Each of the sub-images used to form the output summed image, implemented in the SAR processor. The averaging process (multi-looking) reduces the occurrence of speckles thus facilitating image interpretation.

Magnitude: The amplitude of the wave irrespective of the phase.

Microwave: An electromagnetic wavelength in (or near) the span 1 - 100 cm.

Nadir: Point on the earth's surface which is directly below the radar.

Noise: Any unwanted or contaminating signal competing with the desired signal.

P-band: Microwave band in which the wavelengths are at or near 70 cm.

Penetration depth: The depth in which the microwave enters a medium such as dry sand or forest canopy. It is, in general, proportional to the wavelength and inversely proportional to the loss tangent.

Phase: The angle of a complex number.

Pixel: Derived from "picture element". It indicates the spatial position of a sample of a digital image file which consist of a spatial array of digital numbers. An ensemble of pixels forms the geometric grid on which an image is built.

Polarisation: Orientation of the electric field vector of the electromagnetic wave, either "horizontal" (H) or "vertical" (V) in conventional imaging radar systems. It is established by the antenna, which may be adjusted to be different on transmit and on receive. Possible polarisation states include all E vector angular and time varying orientations leading to elliptical and circular polarisations.

Post-processing: Steps applied to digital radar data to adjust selected attributes of an image, such as geometric or radiometric corrections, speckle reduction, and contrast enhancement.

Power: For a given signal, proportional to the magnitude squared.

Processing: Sometimes called "preprocessing", it is the means of converting the received reflected signal into an image.

Pulse: Group of waves with a distribution confined to a short interval of time.

Quadrature: Signal component that is 90^0 out of phase with respect to the reference frequency.

Radar: Derived from Radio Detection And Ranging. The basic components are the transmitter, the antenna, the receiver, and the data handling equipment.

Radiation: Act of giving off electromagnetic energy, particularly by the antenna of a radar when excited by the transmitter.

Range: Line of sight distance between the radar and each illuminated scatterer. This term is also applied to the dimension of an image away from the line of flight of the radar.

Reflectivity: Property of illuminated objects to reradiate a portion of the incident energy. For side-looking radars, the observable portion of the reflected energy is called backscatter.

Resolution: Refers to the ability of a system to differentiate two image features corresponding to two closely spaced objects in the illuminated scene.

Roughness: Variation of surface height within an imaged resolution cell.

SAR: Synthetic Aperture Radar, so-called because azimuth resolution is achieved through computer operations on a set of signals such that the processor is able to function like a large antenna aperture in computer memory, therefore realising azimuth resolution improvement in proportion to azimuth size.

S-band: Microwave band in which the wavelengths are at or near 10 cm.

Scene: Object space illuminated by the radar.

Shadow: A region hidden behind an elevated feature in the scene and is thus not visible in the resulting radar image.

Signal: Generalised terminology used to signify a mathematical description of a wave, pulse or other sequence of interest.

Signal-to-noise ratio: Quantitative basis for comparing the relative level of a desired signal to unwanted elements, traditionally taken to be additive noise.

SIR-A and SIR-B: NASA sponsored radar missions (at L-band) in the Space Shuttle, each lasting about one week.

SIR-C/X-SAR: Shuttle radar built for missions which started in 1993. It carries a quadrature polarimetric SAR at C-, L- and X-bands, offering a variety of incidence angles, wavelength bands, resolution and polarisation modes.

Speckle: Statistical fluctuation or uncertainty associated with the brightness of each pixel in the image of a scene. This gives the image a "salt and pepper" like appearance thereby degrading image quality.

Speed of light: Approximately 300,000 kilometres per second, the speed of light in "free space", a condition typical of electromagnetic propagation through most atmospheric conditions.

Tone: First order spatial average of image brightness.

Transmission: Signal or energy sent by the radar, normally in the form of a sequence of pulses, to illuminate a scene of interest.

Volume scattering: Multiple scattering events occurring inside a medium which is neither dense nor having a large loss tangent, such as a forest canopy.

Wavelength: Distance between two events of a recurring feature in a periodic sequence, such as the crests in the waves.

X-band: Microwave band with wavelengths at or near 3 cm.

Appendix 4.1

DEVELOPMENT OF TRUNK-CANOPY BIOMASS AND MORPHOLOGY INDICES FROM QUADPOLARISED RADAR DATA

Peter N. Tiangco and Bruce C. Forster
School of Geomatic Engineering
University of New South Wales
Sydney, NSW 2052, Australia
email: z2146531@student.unsw.edu.au
B.Forster@unsw.edu.au

Abstract - The capability of microwave energy to penetrate forest vegetation makes possible the extraction of information on both the crown and trunk components from radar data. At C-band, the backscattered energy is correlated mainly with the crown constituents such as the leaves, twigs and small branches. Information on the other components beneath the canopy can be sensed through the use of bands with longer wavelengths such as the L- or P-band. The sensitivity of co-polarised and cross-polarised waves to the shapes and orientation of different tree constituents provide an added advantage in the information extraction procedure. The Trunk-Canopy Biomass Index (TCBI), which is the sum of the L-HH and C-HV backscatter, can be a measure of the total aboveground biomass as both the crown and trunk layers are taken into consideration. Owing to possible morphological variations, the relationship between TCBI and biomass is however not expected to be unique for a whole forest vegetation. It is important therefore that stand structure be first considered to allow a more accurate biomass assessment by the TCBI. An index of the relative proportions of the crown and trunk may be indicative of the approximate tree morphology. It is believed that the Trunk-Canopy Morphology Index (TCMI), which is the ratio of the L-HH to C-HV backscatter, provides a measure of tree structure. In this study, two categories are used to classify stands according to structure: the needle-leaved pines/conifers and the broad-leaved deciduous/evergreen trees. A two-stage procedure of forest biomass estimation is therefore proposed. The first stage involves the determination of the stand structure category based on the TCMI. Once the structure is known, a specific structure-dependent TCBI could then be applied for the biomass estimation process. The effectiveness of these indices is assessed by applying them to actual and modelled data interpolated from published works of other investigators. Stand structure and total aboveground biomass were found to be highly correlated with TCMI and TCBI, respectively. Comparison of the results is made difficult by the limitations in the amount of data available from the published studies and the possible errors introduced during the interpolation process. In order to verify the validity of these results, further application of these indices using AIRSAR images and adequate amount of actual and measured values from an independent study site in the Blue Mountains area in New South Wales, Australia will be conducted.

1. INTRODUCTION

The importance of quantifying and monitoring forest vegetation, given the vital productive, protective, and regenerative functions of this natural resource, is undeniable. Information on the amount and extent of vegetation provides an insight on what or how much to expect from a specific forest area in terms of these functions. From another perspective, the information can be useful in determining whether or not forest rehabilitation or other appropriate actions are needed in consideration of these three major functions.

Forest aboveground biomass, or the quantity of vegetative material per unit area, is one of the parameters recognised as a good indicator of forest condition. The use of radar remote sensing to provide estimates of this parameter has been receiving increasing interest over recent years. This is mainly due to the ability of the radar to provide data independent of solar illumination and weather conditions. In addition, radar waves, depending on the wavelength/frequency, can be employed to scope different sections of the vegetation profile. Information on crown layer components (e.g.

foliage) can be inferred from the radar backscatter at high frequency bands such as C- and X- while information pertaining to the trunks and lower branches can be obtained through the longer and more penetrative wavelengths of L- and P- bands.

Since the backscattering coefficient is influenced not only by the quantity of biomass but by how the individual components are oriented and distributed throughout the entire tree length, it is also possible to determine the general tree/stand structure based on the radar data. In fact, due to possible morphological variations between stands within a given forest area, it is recommended that the determination of the general tree/stand structure must precede biomass estimation and that radar data-based biomass equations should be formulated based on the structure. This is to avoid erroneous results will most likely be produced as it is possible to obtain different backscatter readings from two stands containing the same amount of biomass but are structurally-different.

2. SYNERGISM OF RADAR PARAMETERS FOR OPTIMUM INFORMATION EXTRACTION

The amount and quality of information which can be inferred from radar data depend on the characteristics of the target and the radar system. Important factors under the former relate to the roughness, geometric and dielectric properties of the imaged surface while under the latter are the microwave frequency/wavelength, polarisation and incidence angle used in the data acquisition process. Accurate inference of vegetation properties results from the formulation of a well-established relationship between the target and the radar parameters. Being well-established implies that such a relationship is based on a complete recognition of the different scattering mechanisms present and a clear understanding of how these mechanisms relate to the radar parameters.

The advent of multi-parameter imaging radars extricated investigators from the limitations of using mono-band radar data in carrying out forest-related research. The opportunity lies in the simultaneous use of the radar parameters for optimum extraction of information from radar imagery. It is believed that a better assessment of forest resources could be achieved by utilising a combination of the parameters. The theoretical basis for this premise and the different combinations will be presented in the following topics. Focus will be on the more controllable radar system-based components such as wavelength and polarisation, with forest aboveground biomass and stand structure assessment as the particular areas of application.

2.1. Forest aboveground biomass assessment

2.1.1. Combined wavelength and polarisation estimation

The total forest aboveground biomass is the summation of the biomass of the crown and bole components of all the trees in the area under consideration. Obviously, to derive an estimate of this quantity from radar data, information on both the crown and the bole should be available. A simple model of the total biomass could then be given as

$$B_{total} = B_t + B_c \quad (1)$$

where B_{total} represents the total aboveground biomass, B_t the trunk biomass, and B_c the crown biomass.

The C-band, with its relatively shorter wavelength, is sensitive to the upper layer of the vegetation such as the leaves, twigs and small branches of the crown. The more penetrative wavelength of the L-band can pass through a greater volume of the canopy and interacts with bigger structures at the lowermost canopy portion and more regularly, with the trunk and big branches. Most of the returns from the latter is from tree-ground double bounce backscattering which occurs mainly due to the vertical orientation of the trunk with respect to the ground hence forming a corner reflector-like structure. Thus,

$$\sum_{n=1}^{N} (\sigma^{O}) = i_n\sigma^{O}_{L-} + j_n\sigma^{O}_{C-} \quad (2)$$

where $\sum_{n=1}^{N} (\sigma^{O})$ is the backscattering coefficient sum correlated with the total aboveground biomass; i and j are the unit vectors in x and y axes in the xy coordinate system corresponding to the backscattering coefficients of the L- and C-band, respectively.

The type of polarisation employed determines the radar response to the various shapes and orientations of the scattering mechanisms within the canopy. Backscatter from cross-polarised waves tends to be related to the canopy volume rather than the lower components such as the soil and as such may be an indicator of crown biomass (ESA, 1995). Incoming vertically-polarised waves readily interact with the vertical components of the canopy. Due to the nature of its orientation, horizontally-polarised radiation tends to have a deeper degree of penetration and is less likely to be affected by canopy attenuation. The highest correlations between radar backscatter and total biomass are obtained using waves with HV- and HH- polarisation: VV-polarised waves are more sensitive to the components of the crown and tend to saturate at lower total biomass levels (Dobson et al.,1995a).

Integrating the theories pertaining to the sensitivities of the different radar wavelengths and polarisations, we can deduce the following relationships:

$$\sigma^{O}(B_{t+lb}) \approx \sigma^{O}_{L\text{-}HH} \quad (3)$$

$$\sigma^{O}(B_{L+b}) \approx \sigma^{O}_{C\text{-}HV} \quad (4)$$

where B_{t+lb} refers to the biomass of the trunk and lower branches, B_{L+b} is the biomass of the leaves and most of the branches, while $\sigma^{O}_{L\text{-}HH}$ and $\sigma^{O}_{C\text{-}HV}$ are the L-HH and C-HV backscattering coefficients, respectively. Considering the above relationships, equation (2) could then be written as

$$\sum_{n=1}^{N} (\sigma^{O}) = i_n\sigma^{O}_{L\text{-}HH} + j_n\sigma^{O}_{C\text{-}HV} \quad (5)$$

where $i\,\sigma^{O}_{L\text{-}HH} + j\,\sigma^{O}_{C\text{-}HV}$ is called the Trunk-Canopy Biomass Index (TCBI). To avoid possible overestimation of total aboveground biomass, other polarisation combinations of the L- and C-bands were not included in the equation as the biomass values they represent are already included in the $\sigma^{O}_{L\text{-}HH}$ and $\sigma^{O}_{C\text{-}HV}$ backscatter.

2.1.2. Saturation of radar measurements

The amount or density of the scattering components within the crown, in addition to wavelength and dielectric constant, also influences the penetration depth achieved by the transmitted energy. The influence stems from the changes in path length and the degree of attenuation imposed by the crown components on the incident radiation. As the energy travels through the canopy, it is gradually depleted by the scattering caused by dielectric discontinuities in the different canopy layers such that there is less energy available to the next layer (UNSW course notes, 1996). If we assume a continuous increase in the dimensions and amount of canopy components from left to right of a forest profile, there will be a point in the profile wherein even the longer wavelength of the L-band would no longer be able to pass through the crown layer due to attenuation.

The increase in the dimensions, amount or density of the different tree components is generally directly correlated with an increase in the total aboveground biomass. That is, as the total biomass increases in value, lesser canopy penetration is expected from the forward radiation. With L-band, the amount of biomass at which the energy no longer passes through the canopy is called the saturation level for that band. Since the type of polarisation also exerts influence on the penetration

depth, the same band with different polarisations will also have different levels of saturation. These influences are illustrated in Figure 1.

Point b in Figure 1 corresponds to the amount of biomass where the sensitivity of both the L-HH and LHH + C-HV backscattering to biomass measurements becomes saturated. The saturation point for C-HV is represented by point a. The flattening of the lines beyond these points indicates that the backscattering coefficients no longer respond to an increase in biomass of the forest components. Thus, any derived relationship between biomass and backscatter would no longer be valid.

This notion of saturation has important implications for the application of radar to forest areas of high biomass. Returning to figure 1, it can be deduced that equation (5) is no longer applicable to biomass levels to the right of b. A possible solution for the estimation of biomass at ranges beyond the $\sigma^{O}_{L\text{-}HH}$ + $\sigma^{O}_{C\text{-}HV}$ saturation point is the inclusion of the backscattering from a band with a longer wavelength. Equation (5) could then be modified to

$$\sum_{n=1}^{N} (\sigma^{O}) = i_n \sigma^{O}_{L\text{-}HH} + j_n \sigma^{O}_{C\text{-}HV} + k_n \sigma^{O}_{P\text{-}HH} \qquad (6)$$

where k is the unit vector corresponding to P-band with HH polarisation backscattering coefficient, $\sigma^{O}_{P\text{-}HH}$.

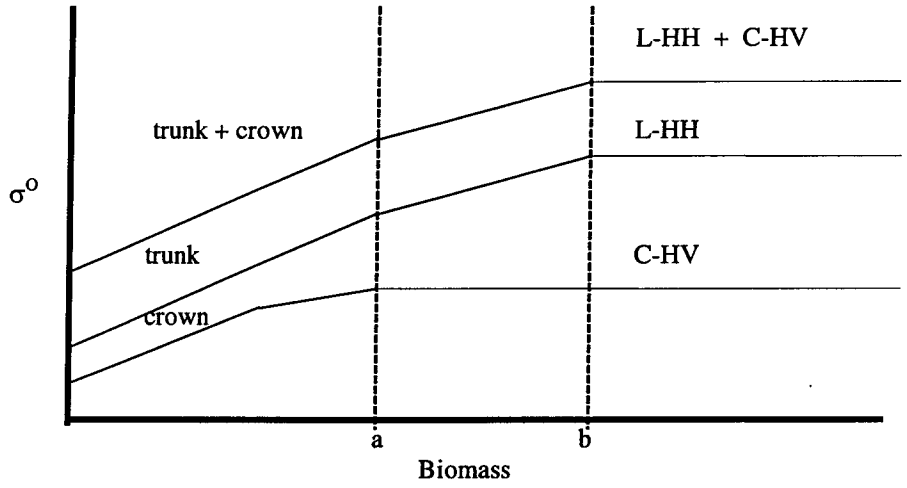

Figure 1. Sensitivities to forest components and theoretical saturation levels for C-HV, L-HH, and LHH + C-HV

2.2. Stand morphology/structure determination

In this study, two general categories are used to differentiate stands according to morphology: those composed of needle-leaved pines/conifers and broad-leaved deciduous/evergreen trees. Pines/conifers are characterised by a pattern where the bole outgrows the lateral branches thus resulting in a well-defined cylindrical trunk and a usually conical crown. The lateral branches extend up to the relatively lower portion of the central stem producing a narrow and deep crown but the bole is visible almost throughout the entire tree height due to the small size and density of the branches and the needle-like leaves. Broad-leaved trees are characterised by a less-pronounced trunk but bigger and more voluminous leaves, as well as a wider and thicker crown compared to that of the conifers. The lateral branches grow at the same rate, or even faster, than the bole and the definition of the bole can be completely lost due to repeated forking (Dobson et al., 1995a).

As radar backscattering behaviour is directly influenced by the geometric properties of the target, it follows that the backscattering from stands of varying structural attributes will be relatively different. A stand of needle-leaved trees, with the small size and density of the leaves and branches as well as

the long trunks of the trees, will have a strong L-HH return. On the other hand, the greater attenuation imposed by the bigger and more dense foliage components, coupled with the less conspicuous trunks, will result in a lower L-HH but higher C-HV backscatter from stands of broad-leaved trees. This change could also be related to, say, big-trunked trees and mallee or scrub type vegetation, or mangroves and trees with more conspicuous trunks. This theory is illustrated in Figure 2.

It is suggested that the above theory can be useful in the determination of tree structure. Given that the sensitivity of the L-HH and C-HV σ^o is a function of the trunk and crown components, respectively, then the true ratio of these two backscattering coefficients is a possible measure of tree morphology. This could be illustrated by the expression

$$\frac{i_n \sigma^o_{\text{L-HH}}}{j_n \sigma^o_{\text{C-HV}}} \approx \frac{\text{trunk}}{\text{crown}} = \text{TCMI} \qquad (7)$$

where TCMI is the Trunk-Canopy Morphology Index. A high TCMI implies a tree structure with more trunk and less crown component while a low TCMI indicates the opposite.

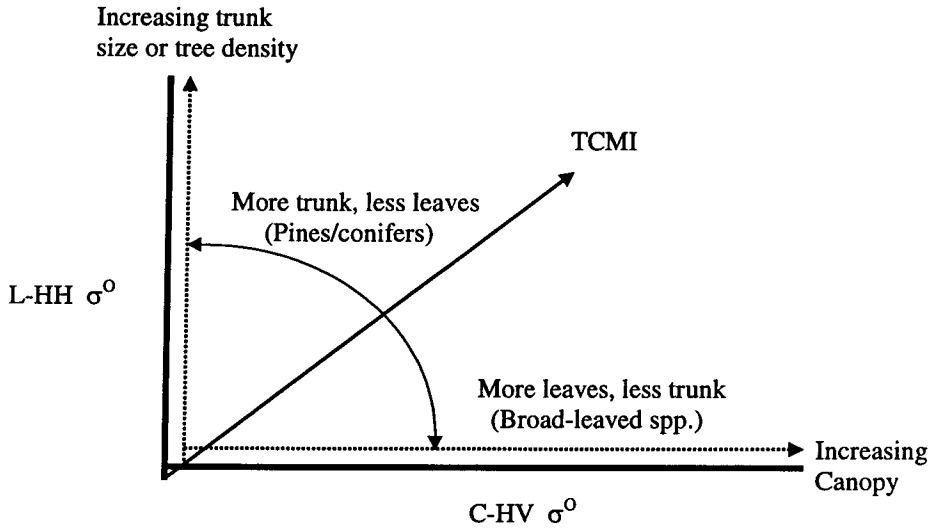

Figure 2. Sensitivity of L-HH and C-HH σ^o to stand structure properties

3. APPLICATION OF RADAR THEORY TO PUBLISHED RESEARCH

The effectiveness of the earlier presented theories, models and indices in providing measures of forest aboveground biomass and stand structure is assessed and demonstrated by applying them to actual and modelled data from published related works of other investigators. As most of the data and results from the published papers are reported in the form of graphs, interpolation was done to obtain measurements for the backscattering coefficients and the corresponding forest biomass levels.

3.1. Data Sources

Listed and individually described in Table 1 are the different studies used in the assessment of the theories and concepts previously presented. All but two of the studies involved the use of either SIR-C/X-SAR or AIRSAR system. In all of these, the HV and VH polarisations were regarded as identical and only the HV data were hence included in the analysis. The incidence angles utilised ranged from 19° - 50° and varying but closely related saturation limits were observed.

3.2. Radar backscatter versus forest biomass

All of the studies considered here, and most of the research so far reported in the literature, have correlated radar backscatter with forest biomass using single radar wavelength and polarisation

combinations. Although some of the forests investigated are composed of broad-leaved and mixed broad-leaved/needle-leaved species, the majority of the sites are vegetated by managed, even-aged and mono-specific coniferous stands located in temperate zones. Due to known difficulties associated with rugged topography, the different forests areas selected as study sites are located in flat to moderately-sloping areas.

In the interpolation of data from the different studies, only the L-HH and C-HV backscattering data were taken into account owing to the concepts discussed earlier. This qualification limited the number of cases considered, as only a few of the related investigations have used either or both of the L-HV and C-HV backscattering data. A maximum of 300 t/ha was used in view of the typical saturation of radar measurements at all bands beyond this biomass level. For both L-HH and C-HV, σ° was observed to increase linearly with biomass until the saturation level for each of these wavelength-polarisation combinations is reached. The TCB and TCM indices were computed based on the intensity (or true) values of the individual backscattering data i.e. not decibels. The σ° values were converted into intensity values through the formula

$$x = -\log (\sigma^\circ/10) \quad (8)$$

where x is the intensity or true value and σ° the backscattering coefficient (in decibel). No significant variation was observed between the TCBI and TCMI values within the same stand structure category from the different investigations. The similarity in the values of these indices occurred over the entire biomass range, except for some cases at low biomass levels, where inconsistent results were obtained. Factors such as strong influence of terrain/ground conditions on the radar backscatter due to low stand/crown component volume and density, may have caused these results. In general, at biomass levels below the radar saturation limits, positive linear relationships between total aboveground biomass and the two indices were observed. In comparing these index values, the effects on the data of factors such as dissimilarities in the radar systems used (e.g. viewing angle and platform altitude), discrepancies in the applied calibration methods, terrain variations, stand morphology, density and composition differences, and the possible errors introduced during the interpolation of the backscattering data and biomass levels, should however be noted.

The correlation between forest biomass and L-HH, C-HV and TCBI are presented in Table 2.

3.2.1. TCBI and total forest aboveground biomass

Table 2 indicates that in the case of C-HV, the use of TCBI (L-HH + C-HV) brought about a better correlation between radar backscatter and total forest biomass. On the other hand, in the case of L-HH, mixed results were obtained. Although much is still to be desired regarding both the number of cases and data considered, this finding is generally in support of the theory presented above (see equation (5)). Following are biomass equations derived based on linear regression analysis performed on the TCBI and biomass data from the various studies.

Author/s	Radar System	Band/s Used	Polarisation	Incidence Angle	Study Site/s	Dominant Vegetation	Saturation Limits (t/ha)	Remarks
1. Imhoff, 1993	JPL SAR (AIRSAR)	P-, L-, C-	HH,VV,HV	40° - 50°	a) Hawaii b)North America & Europe	a)Tropical broad-leaved evergreen b) Conifers	C- = 20 L- = 40 P- = 100	HV and VH treated as the same
2. Souyris et al.,1995	SIR-C/X-SAR	a) L-, C- b) X-	a) HH,VV,HV b) HH, VV	26.4°	Les Landes Forest, France	Pines/conifers	50	-do-
3. Dobson et al., 1995a	SIR-C/X-SAR	a) L-, C- b) X-	a) HH,VV,HV b) HH, VV	31°	Raco Supersite, Michigan, USA	Broad-leaved hardwoods and conifers	(multi-step approach accurate up to 250 t/ha)	-do-
4. Dobson et al., 1995b	SIR-C/X-SAR	L-	HH, VV, HV	19° - 47°	Raco Supersite, Michigan, USA	Broad-leaved hardwoods & conifers	——	-do-
5. Hsu et al., 1993	AIRSAR	P-, L-, C-	HH, VV, HV	45°	Les Landes Forest, France	Pines/conifers	——	-do-
6. Dobson et al.,1992	AIRSAR	P-, L-, C-	HH, VV, HV	40° - 50°	a)Les Landes forest, France b)Duke forest, USA	Pines/Conifers	P- = 200 L- = 100	-do-
7. Karam et al., 1995	AIRSAR	P-, L-, C-	HH, VV, HV			Pines/conifers	——	-do-
8. Harrel et al., 1995	JERS-1 & ERS-1	L- & C-	HH & VV	45°	Les Landes forest, France	Pines/conifers(White and black spruce)	——	
9. Christensen et al. 1990	Airborne SAR (P-3)	L-	HH, VV	42° - 49°	Duke Forest, USA	Pines/conifers	100	
10. Moghaddam et al., 1994	AIRSAR	P-, L-, C-	HH, VV, HV	35° - 50°	Oregon, USA	Mixed hardwoods and conifers	200(for 40°-50°) 300(for °35) 150 (for 50°)	L-HH data not available from report
11. Ranson & Sun, 1994	AIRSAR	P-, L-, C-	HH, VV, HV	25°,35°,50°	Maine, USA	Mixed hardwoods and conifers	157	L-HH data not available
12. Ranson et al., 1995	AIRSAR	P-, L-, C-	HH, VV, HV	25°,35°,45°	Maine, USA	Mixed hardwoods and conifers	C-=100, L-=200 P- = > 200	C-HV data not available

Table 1. List and description of the different studies used in the assessment of concepts and theories

INVESTIGATOR/S	SAR Backscatter	CORRELATION COEFFICIENT			
		PINE / CONIFER Biomass (t/ha)		BROADLEAF Biomass (t/ha)	
		0 - 300	20 - 150	0 - 300	20 - 150
1. IMHOFF, M.L. (1993)	L-HH	0.7354	0.3140	0.8219	0.9321
	C-HV	0.6378	0.0051	0.6801	0.7926
	L-HH+ C-HV	0.6579	0.3002	0.8134	0.9326
2. KARAM, et al. (1995)	L-HH	0.7004	0.6347		
	C-HV	-0.0369	-0.2083		
	L-HH+ C-HV	0.5990	0.5571		
3. HSU, C.C. et al. (1993)	L-HH	0.8086	0.7581		
	C-HV	0.1037	0.2417		
	L-HH+ C-HV	0.6792	0.6131		
4. SOUYRIS, et al. (1995)	L-HH	0.7907	0.8764		
	C-HV	0.4919	-0.0020		
	L-HH+ C-HV	0.8268	0.8289		
5. DOBSON, et al.(1992)	L-HH	0.8731	0.9705		
	C-HV	0.7952	0.4900		
	L-HH+ C-HV	0.8769	0.8996		
6. DOBSON, et al.(1995a)	L-HH	0.4037	0.8320	0.0182	0.2317
	C-HV	0.3737	0.1329	0.4431	
	L-HH+ C-HV	0.4320	0.7759	0.5345	0.7759
7. DOBSON, et al. (1995b)	L-HH		0.7999		
8. HARREL, et al. (1995)	L-HH	0.9888	0.9879		
9.CHRISTENSEN et al.(1990)	L-HH	0.9665	0.9659		
10.MOGHADDAM, et al.('94)	C-HV*			0.9744	
11. RANSON & SUN (1994)	C-HV*			0.5113	0.6393
12. RANSON et al. (1995)	L-HH*			0.8544	0.9557

Note: * = Mixed pine and broad-leaved forest vegetation

Table 2. Correlation between forest biomass and L-HH, C-HV, and L-HH + C-HV backscatter

PINES/CONIFERS

Imhoff, 1993 : Biomass = 866.75 TCBI - 89.69 (9)
r^2 = *0.4329*

Karam et al., 1995 : Biomass = 873.28 TCBI - 78.78 (10)
r^2 = *0.3588*

Hsu et al., 1993 : Biomass = 1476.90 TCBI - 131.00 (11)
r^2 = *0.4613*

Souyris et al., 1995 : Biomass = 2609.60 TCBI - 323.09 (12)
r^2 = *0.6835*

Dobson et al., 1992 : Biomass = 1495.00 TCBI - 209.59 (13)
r^2 = *0.7689*

Dobson et al., 1995a : Biomass = 1176.20 TCBI - 22.57 (14)
$r^2 = 0.1866$

BROAD-LEAVED STANDS

Imhoff, 1993 : Biomass = 973.50 TCBI - 74.48 (15)
$r^2 = 0.6616$

Dobson et al., 1995a : Biomass = 5396.50 TCBI - 455.58 (16)
$r^2 = 0.2857$

While the regression equation for pines/conifers generated from the results of Souyris et al. (1995) had a somewhat higher multiplicative coefficient, similarities could be observed between the equations from Imhoff (1993) and Karam et al. (1995), and from Hsu et al. (1993), Dobson et al. (1992) and Dobson et al. (1995a). The discrepancies between these groups of equations could be attributed to radar system differences and other reasons specified in Section 3.2. The differences in the equations generated for broad-leaved stands from Imhoff (1993) and Dobson et al. (1995a) are significant. However, it should be noted that the latter equation was based on four biomass values only. The highest correlation with biomass was exhibited by that from Dobson et al. (1992), with the equation explaining 77% of the biomass variation.

Given in Table 3 are the TCBI values averaged over the entire biomass range for each of the studies. A comparison of the average biomass between coniferous stands from the different studies, and between coniferous and broad-leaved stands, could be made by using these values as inputs to the corresponding biomass formulas given in equations (9) to (16).

It can be discerned from the table below that the TCBI values from the results of Imhoff (1993) and Dobson et al. (1995a) for pines/conifers and broad-leaved stands are nearly identical. This was most probably caused by the averaging process, which took into consideration the extreme values within the 0 - 300 t/ha biomass range. Moreover, in the case of Dobson et al. (1995a), the insufficiency of available data may also have contributed to the similarity of the averaged results.

Author/s	Average TCBI Value	
	Pines/conifers	Broad-leaved stands
1. Imhoff, 1993	0.2224	0.2187
2. Karam et al., 1995	0.1761	
3. Hsu et al., 1993	0.1426	
4. Souyris et al., 1995	0.1514	
5. Dobson et al., 1992	0.2242	
6. Dobson et al., 1995a	0.1106	0.1125

Table 3. Average TCBI values for coniferous and broad-leaved stands as computed from interpolated results of different studies

3.3. Radar backscatter versus forest stand structure

Radar backscatter is mainly influenced by the geometric properties of the target. As stated above, forest stands with the same biomass but dissimilar morphology may produce different backscatter readings. Hence, radar data-based equations to estimate total aboveground biomass should be tailored according to the general structure of the forest stand. Although the importance of determining the stand structure prior to generating radar-derived estimates of forest biomass was emphasised in some of the studies (e.g. Imhoff, 1993; Dobson et al.,1995a), not one of the investigations reviewed here have considered stand structure determination through the use of radar backscattering data. In the absence of *a priori* information on stand structure, radar data-based techniques, such as the application of TCMI, is deemed essential.

3.3.1. TCMI and stand structure

The applicability of TCMI, which is the true ratio between the L-HH and C-HV backscatter, as a possible measure of stand morphology is premised on the differences in the sensitivity of the two wavelength-polarisation combinations to the various tree components. Higher TCMI values are expected for conifers given their bigger trunk and smaller crown component volume compared to their broad-leaved counterpart. This theory has been proven to be generally true based on the test applied using interpolated backscatter and biomass values from related investigations albeit an overlapping of some of the values was observed. The overlaps between the conifer and broad-leaved stand TCMI points, as can be seen from Figure 3, occur at the lower and higher part of the biomass range. This is quite expected due to the minor differences in vegetation structure at low biomass levels and the saturation of radar measurements at high amounts of biomass. The usefulness of TCMI is thus at its optimum when there is a distinct difference in structure between the broad-leaved and needle-leaved trees and the backscattering data are taken at biomass levels below the radar saturation limits.

To further illustrate the usefulness of the TCMI in accounting for the difference in structure between broad-leaved and needle-leaved stands, given in Figure 3b are the graphs corresponding to those in Figure 3a but with the L-HH and C-HV data limited to those taken within a biomass range of 20 to 150 t/ha. By adjusting the lower and higher ends of the biomass range to these levels, the probability that the broad-leaved and needle-leaved trees are more structurally defined, and that the radar measurements are less affected by saturation limits, is increased - and so is the effectiveness of the TCMI. As can be discerned from the figure, the overlapping TCMI points which exist in Figure 3a have been eliminated in the case of Dobson (1995a) and were greatly reduced in the case of Imhoff (1993). For a similar purpose, given below are the average TCMI values within the 0 to 300 t/ha and 20 to 150 t/ha biomass range for the different studies. The 20 to 150 t/ha range caused a higher dynamic range between the TCMI values, and hence a better separation, of the pine and broad-leaved stands. Interestingly, the average TCMI values generated from the different investigations for pines/conifers, except those from Hsu et al. (1993), are similar though the data were taken from different study sites and conditions. The same observation holds true in the case of the values from the broad-leaved stands.

Author/s	Average TCMI Value			
	Pines/conifers		Broad-leaved stands	
	0 - 300	20 - 150	0 - 300	20 - 150
1. Imhoff, 1993	3.3695	3.7013	2.5168	2.3430
2. Karam et al., 1995	3.2902	3.4119		
3. Hsu et al., 1993	5.4144	5.5431		
4. Souyris et al., 1995	3.6145	3.2267		
5. Dobson et al., 1992	3.4657	3.5937		
6. Dobson et al., 1995a	3.7642	3.9058	2.5882	2.5119

Table 4. Average TCMI values within biomass ranges of 0 to 300 t/ha and 20 to 150 t/ha for the different studies

4. SUMMARY AND CONCLUSIONS

The capability of microwave energy to penetrate forest vegetation makes possible the extraction of information on both the foliar and woody components from radar data. The depth of penetration, and hence the type of derivable information, is dependent upon parameters relating to both the radar sensor and the target such as the wavelength, polarisation and incidence angle used, as well as the geometric and dielectric properties of the target vegetation.

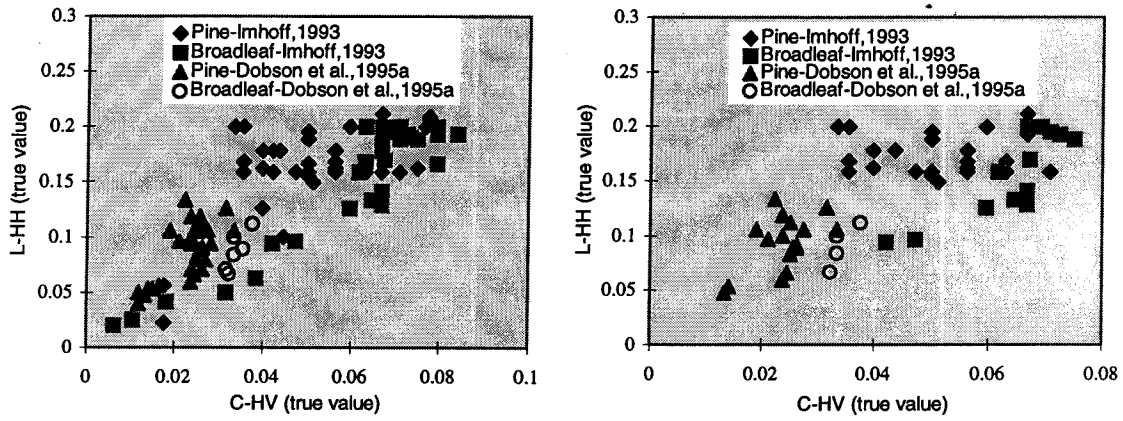

Figure 3. TCMI values within 0 -300 t/ha (a) and 20 - 150 t/ha (b) biomass ranges based on interpolated data from Imhoff, 1993 and Dobson et al. 1995a.

At C-band, the backscattered energy is correlated mainly with the crown constituents such as the leaves, twigs and small branches. Information on the other components beneath the canopy can be sensed through the use of bands with longer wavelengths such as the L- or P-band. The sensitivity of co-polarised and cross-polarised waves to the shapes and orientation of the different tree constituents provide an added advantage in the information extraction procedure. Given the relatively greater degree of penetration by horizontally-polarised waves and the strong interaction of the vertically-polarised energy with the vertically-oriented canopy parts, different wavelength-polarisation combinations can be then used to suit the purpose of the study. In the field of forest biomass estimation, the Trunk-Canopy Biomass Index (TCBI), which is the sum of the L-HH and C-HV backscatter, can be a measure of the total aboveground biomass as both the crown and trunk layers are taken into consideration. The relationship between TCBI and biomass, however, is not expected to be unique for a whole forest vegetation owing to possible variations in morphological structure of the stands within the area. It is important therefore that stand structure be first considered to allow a more accurate biomass assessment by the TCBI parameter.

In this study, two categories are used to classify stands according to structure: the needle-leaved pines/conifers and the broad-leaved deciduous/evergreen trees. Under the first category are trees having a long main stem and a usually deep, narrow and cone-shaped crown composed of needles and small branches. Trees under the latter have a less-pronounced trunk, a wider and thicker crown with more voluminous leaves. Consequently, an index of the relative proportions of the crown and the trunk may be indicative of the approximate tree morphology. It is believed that the Trunk-Canopy Morphology Index (TCMI), which is the ratio of the L-HH to C-HV backscatter, provides a measure of tree structure.

A two-stage procedure for forest biomass estimation is therefore proposed. The first stage involves the determination of the stand structure category based on the TCMI. Once the structure is known, a specific structure-dependent TCBI could then be applied for the biomass estimation process.

The assessment of the effectiveness of the introduced theories carried out based on interpolated data from published research produced promising results. TCMI has been found to provide a good measure of the general stand structure which is deemed necessary prior to the application of biomass estimation techniques. The overlapping of the TCMI values of the needle-leaved and broad-leaved stands which occurred at both ends of the forest biomass range could be explained by the near homogeneity in structure of the stands at low biomass levels and the saturation of radar measurements at high amounts of biomass. In terms of biomass estimation, a higher correlation between TCBI and forest biomass was achieved compared to that of C-HV in all of the studies considered but mixed results were obtained in the case of L-HH. Comparison of the results is made difficult by the limitations both in the number of related studies reported in the literature and in the

amount of data available from each of the studies, inherent differences in the radar systems used, differences in the applied calibration techniques, in-situ variations (i.e., in terms of stand structure and composition, topography and other terrain features) and possible interpolation-related errors. Nevertheless, given all of these limitations, the results support the theories proposed.

To further verify the validity of the results, subsequent application of the TCB and TCM indices using extensive field data and AIRSAR images of an independent study site in the edge of the Blue Mountains National Park in New South Wales, Australia will be made.

5. REFERENCES

Dobson, M.C., F.T. Ulaby, L.E. Pierce, T.L. Sharik, K.M. Bergen, J. Kellndorfer, J.R. Kendra, E. Li, Y.C. Lin, A. Nashashibi, K. Sarabandi, and P. Siqueira, 1995a. Estimation of forest biophysical characteristics in Northern Michigan with SIR-C/X-SAR. *IEEE Transactions on Geoscience and Remote Sensing* 33(4):877-894.

Dobson, M.C., F.T. Ulaby, T. Le Toan, A. Beaudoin, E.S. Kasischke, and N. Christensen, 1992. Dependence of radar backscatter on coniferous forest biomass. *IEEE Transactions on Geoscience and Remote Sensing* 30(2):412-415.

European Space Agency, 1995. Satellite radar in agriculture : experience with ERS-1. *ESA SP-1185*, ESA Publications Division, Noordwijk, The Netherlands, 71 p.

Hsu, C.C., R.T. Shin, J.A. Kong, A. Beaudoin, and T. Le Toan, 1993. Application of theoretical model for microwave remote sensing of forest. *Proceedings of the International Geoscience and Remote Sensing Symposium,* Tokyo, Japan, 18-21 August, 2:595-597.

Imhoff, M.L., 1993. Radar backscatter/biomass saturation: observations and implications for global biomass assessment. *Proceedings of the International Geoscience and Remote Sensing Symposium,* Tokyo, Japan, 18-21 August, 1:43-45.

Karam, M.A., F. Amar, A.K. Fung, E. Mougin, A. Lopes, D.M. Le Vine, and A. Beaudoin, 1995. A microwave polarimetric scattering model for forest canopies based on vector radiative transfer theory. *Remote Sensing of Environment* 53:16-30.

Souyris, J.C., and T. Le Toan, 1995. Inversion of Landes forest biomass using SIR-C/X-SAR data: experiment and theory. *Proceedings of the International Geoscience and Remote Sensing Symposium,* Florence, Italy, 2:1201-1203.

UNSW Centre for Remote Sensing, 1996. *Microwave Remote Sensing Course Notes*, First Session, School of Geomatic Engineering, The Univ. of New South Wales, Kensington, Australia.

Appendix 5.1

Presented in this appendix are photographs of the broad-leaved trees in some of the sample plots in the Blue Mountains National Park study site.

Figure 5.1.1 Ironbark -dominated vegetation

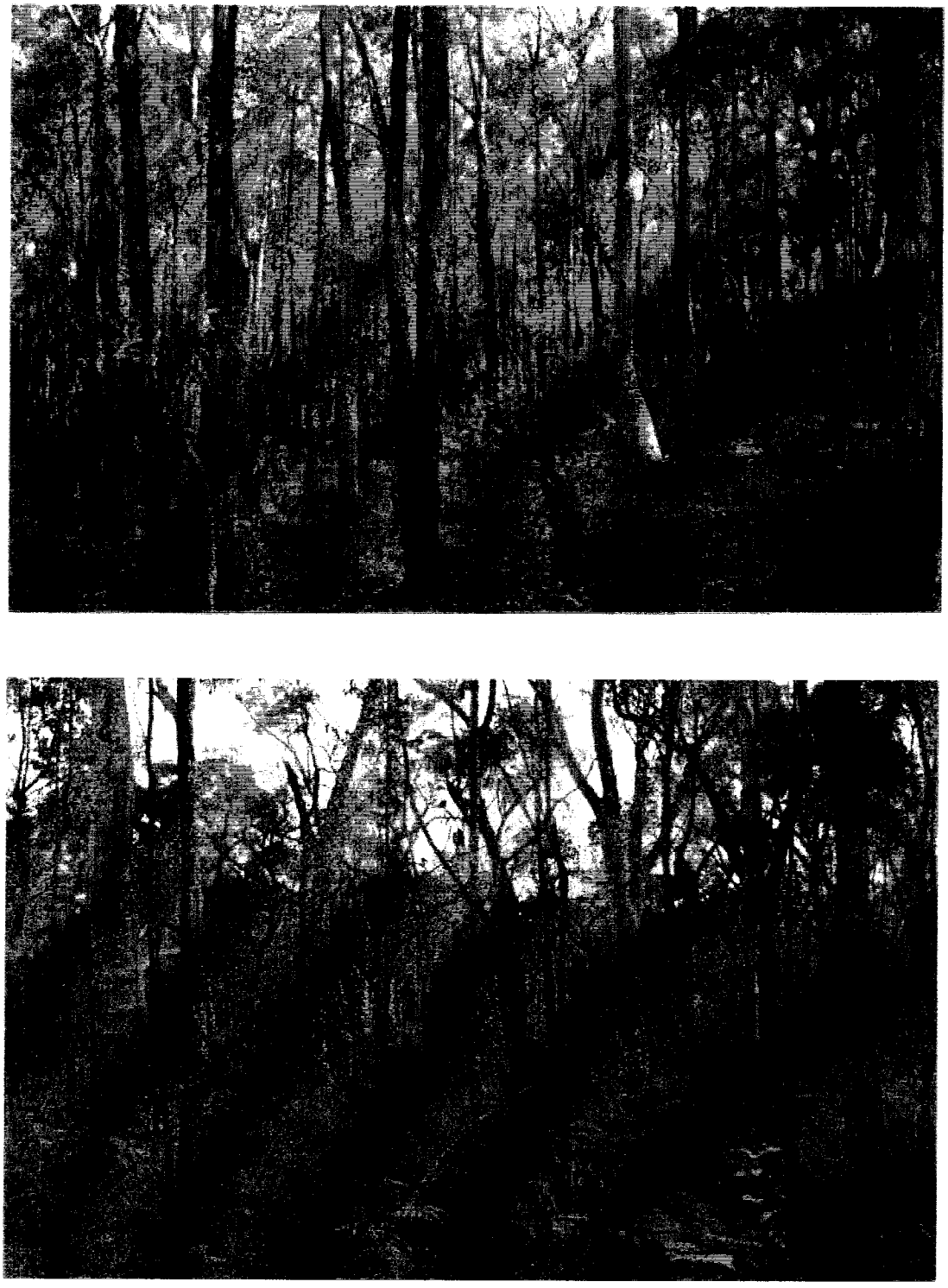

Figure 5.1.2 Scribbly gum - dominated vegetation

Figure 5.1.3 Mixed vegetation composed of turpentines, ironbarks, and gum

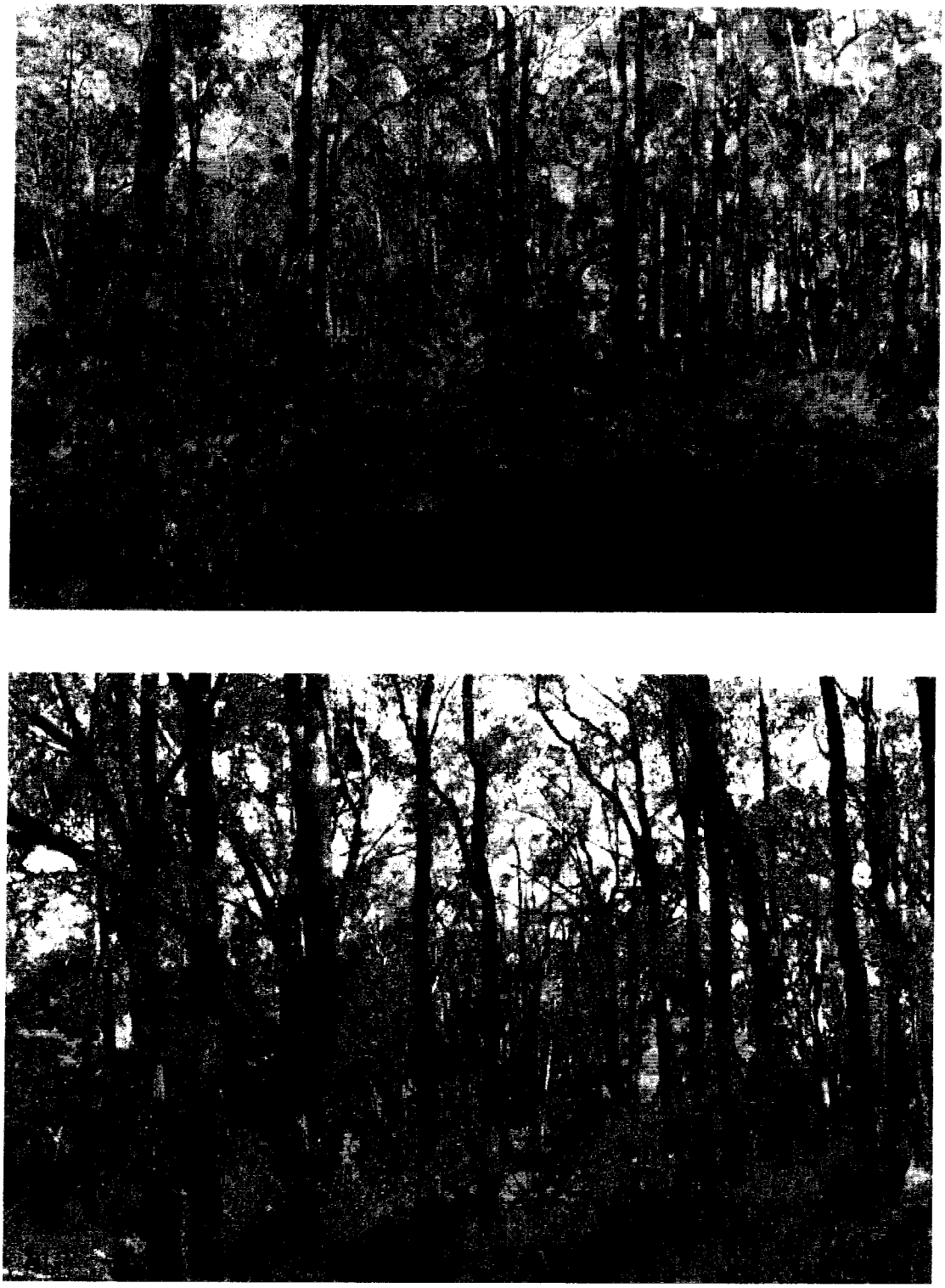

Figure 5.1.4 Mixed stand with medium to dense undergrowth vegetation

Appendix 5.2

Given in this appendix are photographs of the needle-leaved radiata pines in some of the sample plots in the Gippsland study site.

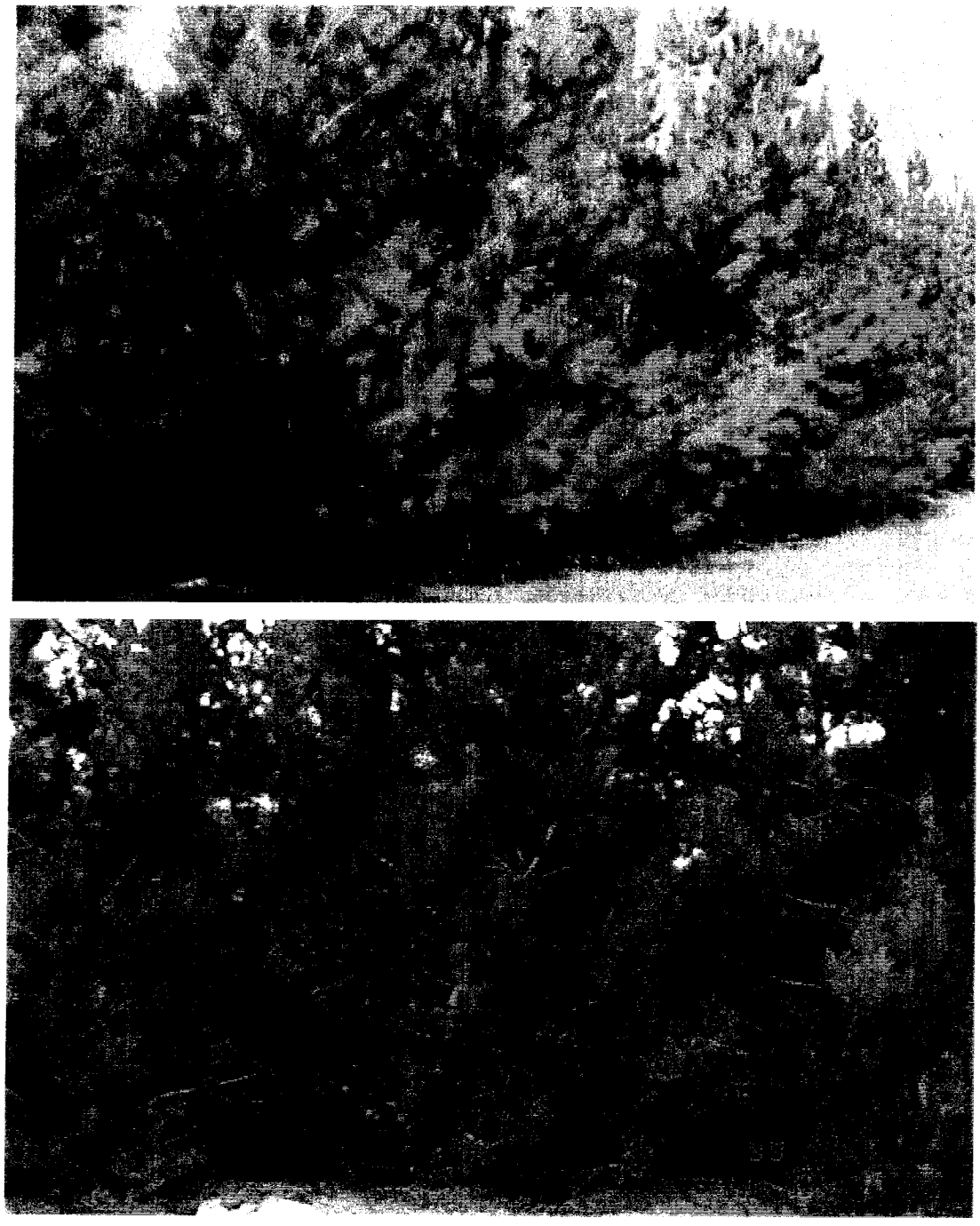

Figure 5.2.1 Five (top) and six (bottom) - year old radiata pine stands

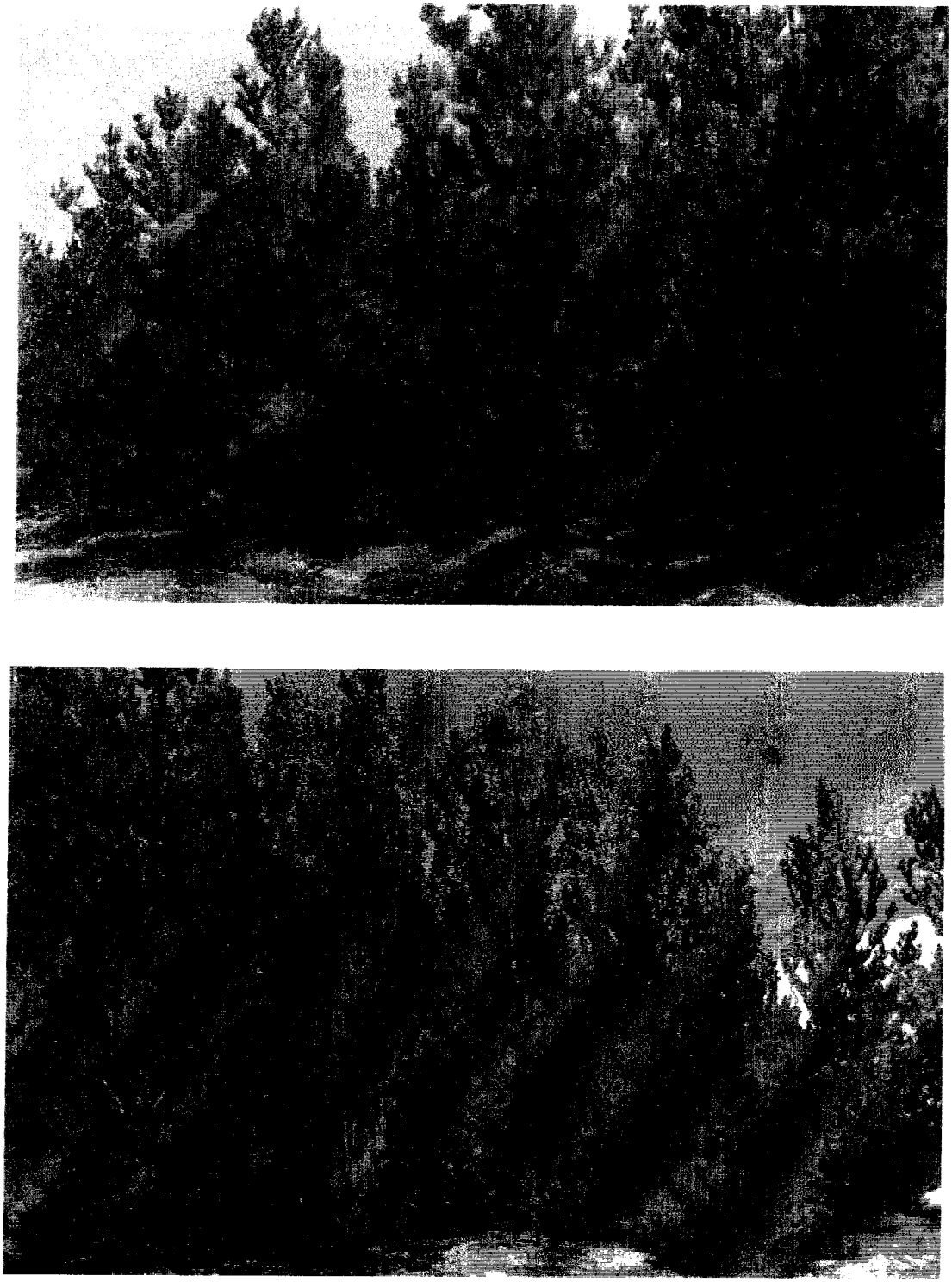

Figure 5.2.2 Nine (top) and ten (bottom) - year old stands

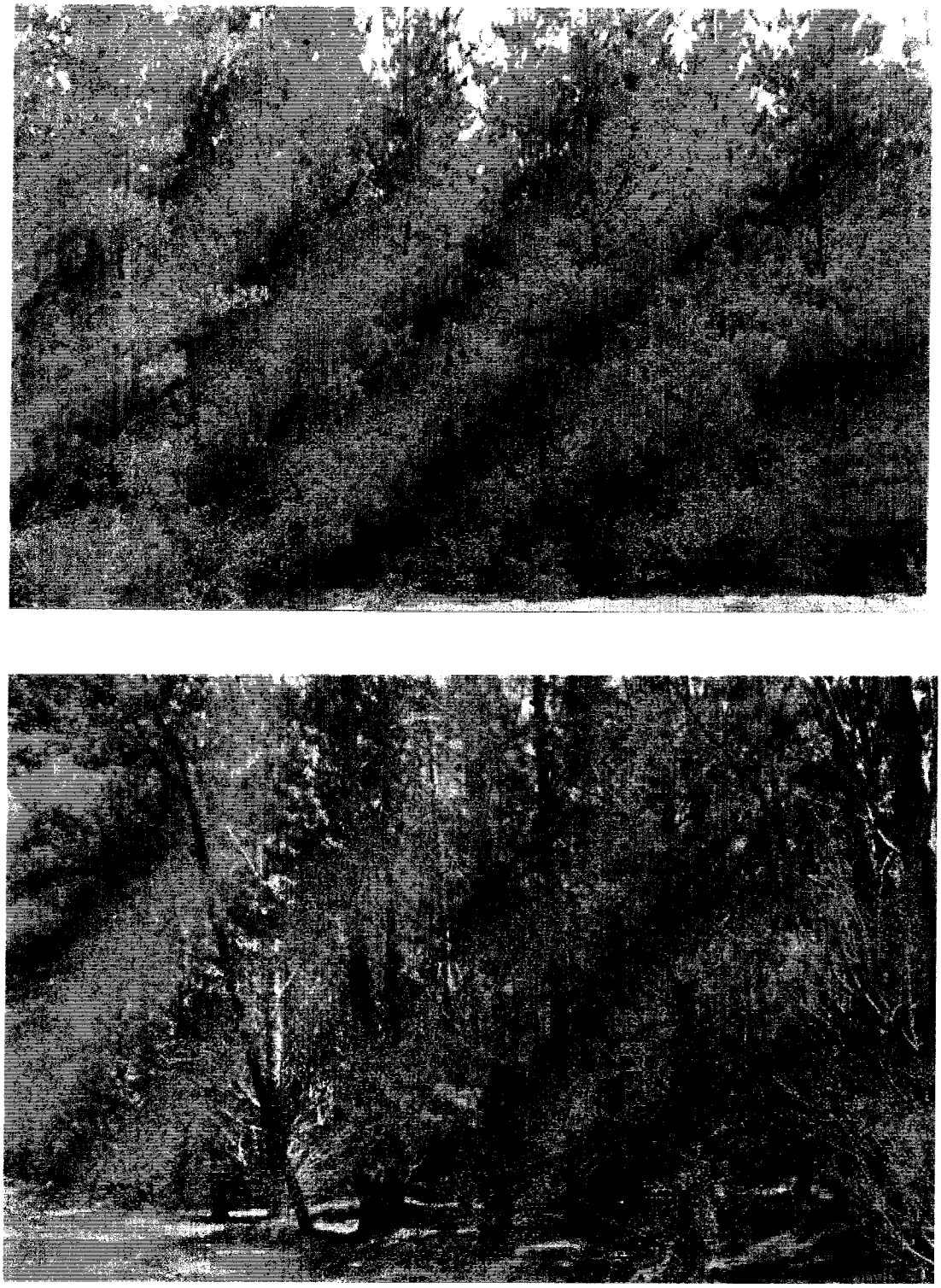

Figure 5.2.3 Nineteen (top) and twenty two (bottom) - year old radiata pine stands

Figure 5.2.4 Twenty four - year old pine stands

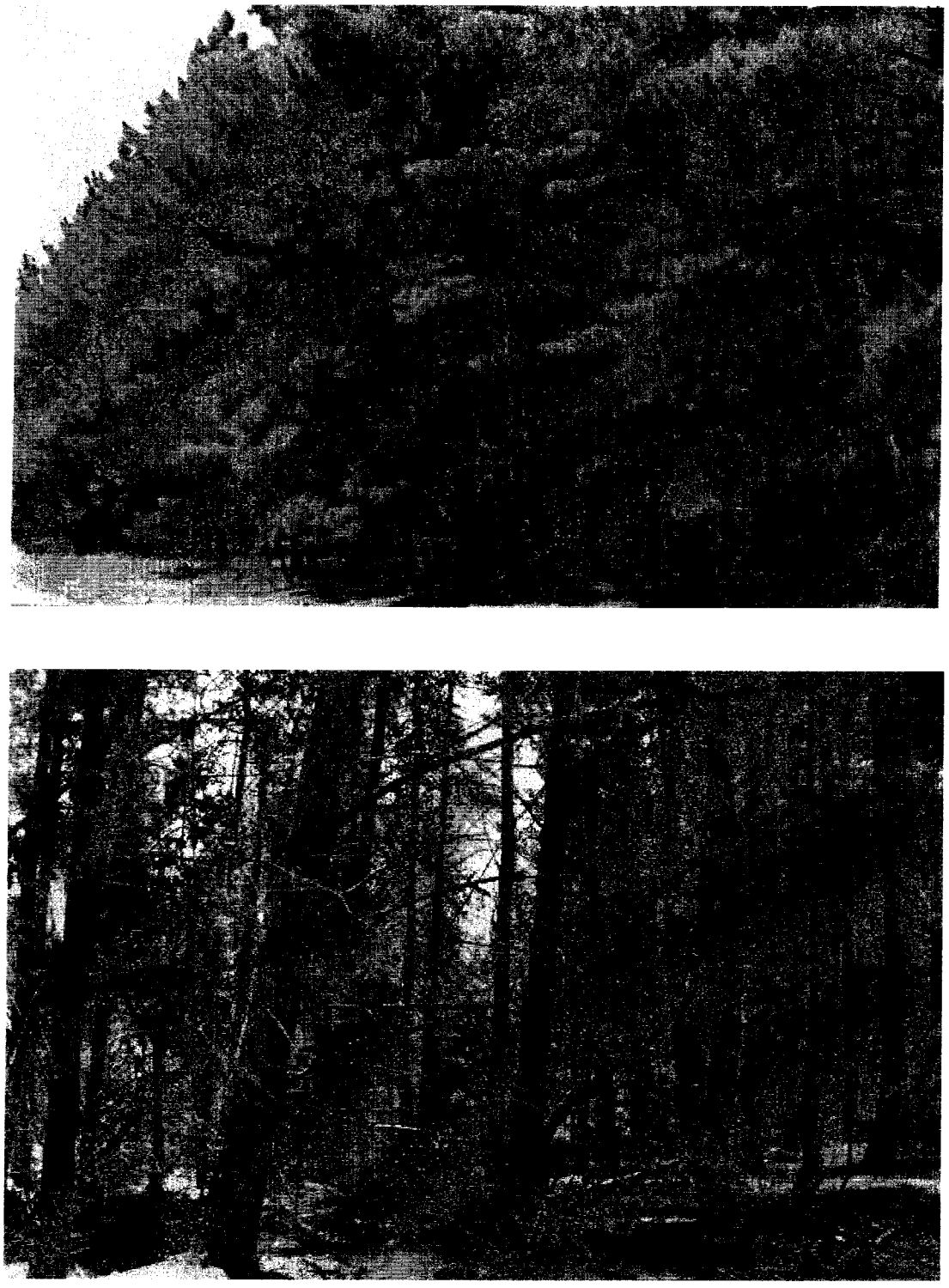

Figure 5.2.5 Twenty six (top) and twenty seven (bottom) - year old stands

Appendix 6.1

This appendix presents details on the two computer softwares used for the analysis of field and radar data for the Blue Mountains and Gippsland study sites. The information pertaining to these softwares, as given below, were obtained from Cobb et al. (1991), Person and Campbell (1988) and the ENVI Version 2.0 User's Manual, October 1995 edition.

6.1.1 Microsoft Excel

Microsoft Excel features three work environments, namely, spreadsheets, graphics, and macros. These features, all integrated into a user-friendly software package, enable Microsoft Excel to handle a wide range of analysis tasks for different areas of application. The graphical user interface (GUI) it uses is provided either by MS-DOS or Windows '95/'98 under the Microsoft Windows environment. This set-up results in an environment with an easy to learn and use menu structure that permits multitasking and the exchange of data among different programs.

As a spreadsheet program, Excel allows the input of texts, numbers, and formulas into a grid of cells which is 256 columns wide and 16,384 rows deep. It also works as a database manager, where raw data, data analysis and projection results could be stored for future retrieval and manipulation. Besides performing mathematical computations based on the data and formulas entered, Excel could be set to automatically create charts in different predefined formats. Depending on the user, customised two or three dimensional charts in varying angles of view or chart perspectives could be produced as well, along with other high quality graphics. Graphic objects could be drawn with the use of the tool bar buttons, or can be imported from the Windows Clipboard, to be pasted onto the worksheet. These charts and graphics can be displayed, stored or printed as separate documents or embedded in the worksheet data. With Excel, user-defined scripts (called macros) can be created to automate routine tasks or write sophisticated application programs in the spreadsheet. Aside from allowing the creation of personalised menus and

dialog boxes, user-defined functions could also be devised and added to Excel's library of built-in functions.

Microsoft Excel was used for the analysis of the experimental and field data from the two study sites. This includes the input of all data and allometric equations into a spread sheet for subsequent biomass estimation, regression analyses to derive new stand structure and total aboveground biomass models, testing for the significance of the analyses, and the preparation of charts and diagrams.

6.1.2 ENVI

ENVI, or the Environment for Visualising Images, is an easy to use yet powerful image processing software for the multi-spectral analysis of spaceborne and airborne remote sensor data of any size and type on a wide range of computing platforms. The software is written in the Interactive Data Language (IDL), an array-based programming language that features an integrated image processing and display capabilities, as well as a user-friendly Graphical User Interface (GUI) toolkit. ENVI utilises a combined file and band-based approach to image processing thus allowing the analysis of entire image files, individual bands, or both. Just as each of the spectral bands becomes available to all system functions when an input file is opened, bands from different files can also be selected and processed simultaneously after opening multiple input files. In addition to a variety of tools, such as those which make possible the extraction of spectral signatures, use of spectral libraries, and the analysis of high spectral resolution images (e.g., AVIRIS, GERIS and GEOSCAN), ENVI also supports functions for the analysis of multi-parameter radar data.

In this study, ENVI was used for the loading, processing and analysis of the radar images. Included under these procedures are image synthesis, geometric correction and spatial subsetting, contrast manipulation, speckle suppression, edge enhancement, display of monochrome and colour images, image classification, computation of image statistical data, and the production of derived images and maps.

Appendix 7.1

This appendix presents the details of the field data from the sample plots in study site 1 (Blue Mountains National Park).

Sample Plot No. 1		Plot Size: 20 m radius	Collection Date: 13/09/98				Location: LL 33 47 31.6 N, 150 37 03 E			
							UTM 0279463 E, 6258340 N			
Tree #	Scientific Name	Common Name	Dbh (cm)	Total ht (m)	Cover (m)	ANBT	ABD (cm)	ABL (m)	ABAV (deg)	Total Tree Weight (kg)
1	Eucalyptus sideroxylon	Red Ironbark	48.70	27.70	7.02	15.00	16.00	2.50	45	1636.79
2	Eucalyptus sideroxylon	Red Ironbark	67.80	29.20	12.14	10.00	30.00	10.00	40	3605.23
3	Eucalyptus sideroxylon	Red Ironbark	45.20	21.06	8.20	6.00	12.00	4.00	45	1369.80
4	Eucalyptus sideroxylon	Red Ironbark	43.61	29.20	14.55	6.00	10.00	5.00	45	1257.48
5	Eucalyptus siderophloia	Broad-leaved Red Ironbark	22.92	13.28	4.15	3.00	10.00	3.00	35	270.82
6	Eucalyptus sideroxylon	Red Ironbark	56.66	29.20	12.78	10.00	15.00	5.00	45	2348.91
7	Eucalyptus sideroxylon	Red Ironbark	28.33	22.92	8.35	6.00	10.00	4.00	45	449.16
8	Eucalyptus sideroxylon	Red Ironbark	45.52	29.20	9.30	4.00	25.00	7.00	40	1392.93
9	Eucalyptus sideroxylon	Red Ironbark	26.58	18.02	5.04	3.00	8.00	2.00	35	385.73
10	Eucalyptus sideroxylon	Red Ironbark	37.88	25.11	8.35	6.00	12.00	4.00	40	898.46
11	Eucalyptus sideroxylon	Red Ironbark	43.45	29.20	9.35	9.00	12.00	4.00	45	1246.55
12	Eucalyptus sideroxylon	Red Ironbark	48.70	29.20	14.03	10.00	16.00	8.00	45	1636.79
13	Eucalyptus sideroxylon	Red Ironbark	38.52	29.20	6.30	8.00	12.00	4.00	40	934.92
14	Eucalyptus sideroxylon	Red Ironbark	25.15	18.71	3.34	10.00	5.00	2.00	45	337.95
15	Eucalyptus sideroxylon	Red Ironbark	42.65	29.20	10.30	8.00	15.00	5.00	40	1192.75
16	Eucalyptus sideroxylon	Red Ironbark	21.33	12.10	3.55	4.00	6.00	2.00	45	228.08
17	Eucalyptus sideroxylon	Red Ironbark	49.97	29.20	7.25	4.00	12.00	3.00	45	1740.78
18	Eucalyptus resinifera	Red Mahogany	38.52	19.44	8.75	18.00	6.00	4.00	45	934.92
19	Eucalyptus resinifera	Red Mahogany	36.29	13.71	9.65	20.00	8.00	4.00	50	810.97
20	Eucalyptus resinifera	Red Mahogany	23.24	12.87	5.45	4.00	6.00	10.00	30	279.89
21	Eucalyptus resinifera	Red Mahogany	35.65	29.20	7.25	22.00	10.00	4.00	40	777.42
22	Eucalyptus resinifera	Red Mahogany	42.34	25.11	10.25	13.00	12.00	5.00	45	1171.62
23	Eucalyptus resinifera	Red Mahogany	18.78	10.72	5.20	6.00	6.00	5.00	40	168.38
24	Eucalyptus resinifera	Red Mahogany	21.49	16.77	5.38	6.00	8.00	5.00	40	232.16
25	Eucalyptus resinifera	Red Mahogany	39.47	32.69	9.33	12.00	10.00	5.00	40	991.19
26	Eucalyptus resinifera	Red Mahogany	41.38	27.70	9.25	10.00	10.00	6.00	40	1109.53
27	Eucalyptus resinifera	Red Mahogany	24.83	21.06	4.20	3.00	10.00	6.00	35	327.83
28	Eucalyptus resinifera	Red Mahogany	24.83	18.02	6.89	8.00	10.00	8.00	20	327.83
29	Eucalyptus resinifera	Red Mahogany	40.74	32.69	9.85	10.00	12.00	4.00	45	1069.22
30	Eucalyptus resinifera	Red Mahogany	33.74	25.11	6.88	18.00	6.00	4.00	45	681.69
31	Eucalyptus resinifera	Red Mahogany	49.66	32.69	8.75	12.00	8.00	5.00	40	1714.43
32	Eucalyptus resinifera	Red Mahogany	50.61	30.85	10.00	15.00	8.00	5.00	40	1794.17
33	Eucalyptus resinifera	Red Mahogany	23.87	21.96	6.23	7.00	10.00	8.00	35	298.54
34	Eucalyptus resinifera	Red Mahogany	17.19	21.96	3.75	5.00	6.00	4.00	45	136.30
35	Eucalyptus creba	Narrow-leaved Red Ironbark	8.91	11.04	3.90	8.00	3.00	2.00	40	28.43
36	Eucalyptus siderophloia	Broad-leaved Red Ironbark	6.37	6.58	2.00	5.00	2.00	1.00	45	12.73
37	Eucalyptus creba	Narrow-leaved Red Ironbark	8.59	11.04	4.25	5.00	3.00	1.50	45	26.06
38	Eucalyptus sideroxylon	Red Ironbark	7.00	6.79	3.00	10.00	2.00	1.00	40	15.99
39	Eucalyptus sideroxylon	Red Ironbark	13.37	14.16	3.86	10.00	2.00	2.00	35	74.82
40	Eucalyptus sideroxylon	Red Ironbark	6.84	8.44	2.74	11.00	2.00	1.00	45	15.13
41	Eucalyptus sideroxylon	Red Ironbark	9.55	9.51	3.43	6.00	2.00	1.00	45	33.51
42	Eucalyptus sideroxylon	Red Ironbark	6.37	7.01	1.69	8.00	1.00	0.50	45	12.73
43	Eucalyptus creba	Narrow-leaved Red Ironbark	8.12	9.80	4.46	8.00	3.00	2.00	45	22.74
44	Eucalyptus sideroxylon	Red Ironbark	12.57	15.13	3.61	6.00	2.00	1.00	40	64.62
45	Eucalyptus creba	Narrow-leaved Red Ironbark	6.37	9.51	2.97	5.00	1.00	0.50	40	12.73
46	Eucalyptus creba	Narrow-leaved Red Ironbark	5.25	7.01	2.55	5.00	1.00	0.50	40	8.05
47	Eucalyptus creba	Narrow-leaved Red Ironbark	7.64	10.09	3.98	7.00	2.00	2.00	40	19.68
48	Eucalyptus creba	Narrow-leaved Red Ironbark	9.39	12.87	4.75	8.00	2.00	2.00	40	32.20
49	Eucalyptus creba	Narrow-leaved Red Ironbark	5.25	9.51	2.53	6.00	1.00	0.50	40	8.05
50	Eucalyptus creba	Narrow-leaved Red Ironbark	4.93	8.19	2.40	5.00	1.00	0.50	40	6.93
51	Eucalyptus creba	Narrow-leaved Red Ironbark	8.28	11.04	3.42	6.00	1.00	1.00	40	23.82
52	Eucalyptus sideroxylon	Red Ironbark	9.39	12.87	2.30	6.00	2.00	1.00	35	32.20
53	Eucalyptus sideroxylon	Red Ironbark	9.87	12.87	2.23	5.00	1.00	1.00	30	36.24
54	Eucalyptus sideroxylon	Red Ironbark	8.28	9.51	2.87	6.00	2.00	1.00	40	23.82
55	Eucalyptus siderophloia	Broad-leaved Red Ironbark	6.68	7.01	2.64	4.00	3.00	1.00	40	14.31
56	Eucalyptus sideroxylon	Red Ironbark	5.25	3.54	2.15	4.00	1.00	0.50	40	8.05
57	Eucalyptus sideroxylon	Red Ironbark	14.16	11.04	3.80	6.00	3.00	1.50	45	85.89
58	Eucalyptus siderophloia	Broad-leaved Red Ironbark	6.53	6.79	1.93	5.00	2.00	1.00	45	13.51
59	Eucalyptus siderophloia	Broad-leaved Red Ironbark	6.68	5.96	1.75	5.00	2.00	1.00	45	14.31
60	Eucalyptus siderophloia	Broad-leaved Red Ironbark	5.57	5.96	1.77	5.00	2.00	1.00	45	9.26

Sample Plot No. 1		Plot Size: 20 m radius	Collection Date: 13/09/98				Location: LL 33 47 31.6 N, 150 37 03			
							UTM 0279463 E, 6258340 N			
Tree #	**Scientific Name**	**Common Name**	**Dbh (cm)**	**Total ht (m)**	**Cover (m)**	**ANBT**	**ABD (cm)**	**ABL (m)**	**ABAV (deg)**	**Total Tree Weight (kg)**
61	Eucalyptus siderophloia	Broad-leaved Red Ironbark	4.93	3.89	1.32	5.00	1.00	1.00	40	6.93
62	Eucalyptus siderophloia	Broad-leaved Red Ironbark	4.46	4.98	1.85	6.00	1.00	1.00	40	5.44
63	Eucalyptus sideroxylon	Red Ironbark	5.89	4.98	1.85	6.00	1.00	1.00	40	10.57
64	Eucalyptus siderophloia	Broad-leaved Red Ironbark	8.75	5.96	1.94	5.00	1.00	1.00	45	27.23
65	Eucalyptus siderophloia	Broad-leaved Red Ironbark	5.41	5.17	1.53	6.00	1.00	1.00	45	8.64
66	Eucalyptus siderophloia	Broad-leaved Red Ironbark	6.37	5.36	2.18	6.00	1.00	1.00	60	12.73
67	Eucalyptus siderophloia	Broad-leaved Red Ironbark	3.66	2.34	1.75	6.00	1.00	1.00	50	3.40
68	Eucalyptus siderophloia	Broad-leaved Red Ironbark	4.93	3.19	2.35	7.00	2.00	1.00	50	6.93
69	Eucalyptus siderophloia	Broad-leaved Red Ironbark	4.93	3.19	2.26	5.00	2.00	1.00	45	6.93
70	Eucalyptus siderophloia	Broad-leaved Red Ironbark	5.09	3.19	1.53	6.00	2.00	1.00	45	7.48
71	Eucalyptus sideroxylon	Red Ironbark	7.96	8.19	3.67	6.00	2.00	1.00	45	21.69
72	Eucalyptus siderophloia	Broad-leaved Red Ironbark	5.09	4.06	3.13	5.00	2.00	1.00	45	7.48
73	Eucalyptus sideroxylon	Red Ironbark	6.37	6.58	2.63	5.00	3.00	1.00	40	12.73
74	Eucalyptus sideroxylon	Red Ironbark	5.89	7.01	1.76	5.00	2.00	1.00	45	10.57
75	Eucalyptus sideroxylon	Red Ironbark	11.30	7.01	3.56	6.00	2.00	1.00	50	50.09
76	Eucalyptus siderophloia	Broad-leaved Red Ironbark	8.12	6.37	3.56	4.00	3.00	2.00	40	22.74
77	Eucalyptus siderophloia	Broad-leaved Red Ironbark	6.05	3.19	2.50	7.00	2.00	1.00	40	11.27
78	Eucalyptus creba	Narrow-leaved Red Ironbark	3.18	3.19	1.37	10.00	0.50	0.50	85	2.43
79	Eucalyptus creba	Narrow-leaved Red Ironbark	5.89	6.58	2.37	8.00	1.00	1.00	45	10.57
80	Eucalyptus siderophloia	Broad-leaved Red Ironbark	9.55	8.44	3.56	6.00	2.00	1.00	50	33.51
81	Eucalyptus sideroxylon	Red Ironbark	7.48	7.01	1.92	6.00	1.00	0.50	80	18.71
82	Eucalyptus sideroxylon	Red Ironbark	7.64	7.01	1.83	6.00	1.00	1.00	60	19.68
83	Eucalyptus sideroxylon	Red Ironbark	7.80	7.01	1.99	6.00	0.50	0.50	60	20.67
84	Eucalyptus sideroxylon	Red Ironbark	7.32	6.58	1.87	6.00	1.00	1.00	60	17.78
85	Eucalyptus sideroxylon	Red Ironbark	9.23	6.79	2.88	6.00	2.00	1.00	50	30.91
86	Eucalyptus sideroxylon	Red Ironbark	4.14	3.19	2.24	5.00	2.00	1.00	40	4.55
	Total Dry Weight (kg)									34806.66
	Total Biomass (tons/ha)									276.98

Where: Dbh = Diameter at breast height (over bark)

ANBT = Average Number of Branches per Tree

ABT = Average Branch Diameter

ABL = Average Branch Length

ABAV = Average Branch Angle from the Vertical

Sample Plot No. 2		Plot Size: 10 m radius	Collection Date: 14/09/98			Location: LL 33 46 31 N, 150 37 55.7 E UTM 0280737 E, 6260249 N				
Tree #	Scientific Name	Common Name	Dbh (cm)	Tht (m)	Cover (m)	ANBT	ABD (cm)	ABL (m)	ABAV (deg)	Total Tree Weight (kg)
1	Callitris hugelii	White Cypress Pine	18.46	10.17	5.55	40	2.00	2.50	80	131.86
2	Eucalyptus resinifera	Red Mahogany	10.82	6.67	3.68	10	4.00	2.00	45	45.18
3	Callitris hugelii	White Cypress Pine	12.25	11.78	3.75	50	2.00	2.50	80	54.38
4	Callitris hugelii	White Cypress Pine	11.46	11.28	3.76	40	2.00	2.50	85	47.03
5	Callitris hugelii	White Cypress Pine	10.19	9.89	3.82	40	1.50	2.50	75	36.46
6	Callitris hugelii	White Cypress Pine	7.64	6.67	2.91	35	2.00	2.00	85	19.58
7	Callitris hugelii	White Cypress Pine	8.12	7.72	3.07	40	1.50	2.00	80	22.32
8	Callitris hugelii	White Cypress Pine	6.68	6.67	3.41	40	1.50	2.00	80	14.67
9	Callitris hugelii	White Cypress Pine	6.84	6.92	3.05	35	1.50	1.50	80	15.44
10	Callitris hugelii	White Cypress Pine	7.16	5.95	2.81	30	1.00	1.50	85	17.03
11	Eucalyptus resinifera	Red Mahogany	16.39	9.35	4.72	10	5.00	3.00	40	121.72
12	Callitris hugelii	White Cypress Pine	10.19	6.46	3.26	40	3.00	1.00	75	36.46
13	Callitris hugelii	White Cypress Pine	5.73	4.61	2.29	35	1.00	1.00	80	10.51
14	Eucalyptus resinifera	Red Mahogany	21.80	12.42	3.45	6	6.00	2.00	40	240.45
15	Eucalyptus resinifera	Red Mahogany	14.01	9.86	3.45	6	5.00	2.00	40	83.60
16	Eucalyptus resinifera	Red Mahogany	18.94	14.10	9.50	10	8.00	4.00	45	171.80
17	Callitris hugelii	White Cypress Pine	7.00	6.10	3.20	35	1.00	1.00	80	16.22
18	Callitris hugelii	White Cypress Pine	5.73	6.26	2.69	35	1.00	1.00	85	10.51
19	Callitris hugelii	White Cypress Pine	5.73	6.26	2.08	30	1.00	1.00	80	10.51
20	Eucalyptus creba	Narrow-leaved Red Ironbark	7.48	9.03	2.26	20	0.50	0.50	45	18.71
21	Eucalyptus creba	Narrow-leaved Red Ironbark	5.57	6.55	1.34	20	0.50	0.50	45	9.26
22	Callitris hugelii	White Cypress Pine	12.73	8.67	4.35	25	2.50	1.50	70	59.06
23	Callitris hugelii	White Cypress Pine	9.23	7.87	2.50	35	2.00	1.50	75	29.47
24	Callitris hugelii	White Cypress Pine	11.78	7.87	4.33	40	3.00	2.00	75	49.90
25	Callitris hugelii	White Cypress Pine	22.28	13.98	4.31	45	5.00	1.50	70	197.99
26	Callitris hugelii	White Cypress Pine	9.23	5.95	3.84	45	2.00	2.00	80	29.47
27	Callitris hugelii	White Cypress Pine	23.87	5.49	2.51	30	1.00	1.00	75	229.83
28	Callitris hugelii	White Cypress Pine	12.41	6.26	4.34	30	2.00	2.00	75	55.92
29	Callitris hugelii	White Cypress Pine	26.42	9.37	4.05	30	3.00	1.50	80	286.12
30	Callitris hugelii	White Cypress Pine	11.14	8.58	3.95	30	1.00	1.50	75	44.26
31	Callitris hugelii	White Cypress Pine	16.55	9.72	4.53	45	1.50	1.50	80	104.14
32	Callitris hugelii	White Cypress Pine	11.78	8.48	3.64	45	2.00	2.00	70	49.90
33	Callitris hugelii	White Cypress Pine	13.69	9.45	3.83	40	1.00	1.50	80	69.06
34	Callitris hugelii	White Cypress Pine	10.50	9.35	4.24	45	2.00	1.50	75	38.97
35	Callitris hugelii	White Cypress Pine	11.78	8.86	3.16	45	1.00	1.50	75	49.90
36	Callitris hugelii	White Cypress Pine	7.00	6.69	2.81	35	1.00	1.50	75	16.22
37	Callitris hugelii	White Cypress Pine	7.64	4.47	2.83	30	1.00	1.50	75	19.58
38	Callitris hugelii	White Cypress Pine	12.10	9.41	4.00	45	2.50	2.00	80	52.87
39	Callitris hugelii	White Cypress Pine	7.00	7.58	2.14	40	2.00	1.00	75	16.22
40	Callitris hugelii	White Cypress Pine	11.78	8.33	4.03	40	2.00	2.00	80	49.90
41	Callitris hugelii	White Cypress Pine	7.00	8.33	3.87	35	1.00	2.00	80	16.22
42	Eucalyptus resinifera	Red Mahogany	4.46	5.01	1.49	8	0.50	0.50	45	5.44
43	Syncarpia glomulifera	Turpentine	9.23	7.51	3.31	35	1.00	0.50	85	30.91
44	Syncarpia glomulifera	Turpentine	15.44	10.41	3.98	40	2.00	1.50	85	105.47
45	Syncarpia glomulifera	Turpentine	14.32	9.61	4.11	40	2.00	1.50	85	88.21
46	Syncarpia glomulifera	Turpentine	6.68	7.72	3.10	20	1.00	1.00	85	14.31
47	Syncarpia glomulifera	Turpentine	7.32	7.30	2.73	20	1.00	1.00	85	17.78
48	Syncarpia glomulifera	Turpentine	5.73	6.10	2.48	20	1.00	1.00	85	9.90
49	Eucalyptus creba	Narrow-leaved Red Ironbark	13.37	9.21	2.56	6	1.00	1.50	45	74.82
50	Eucalyptus creba	Narrow-leaved Red Ironbark	13.37	9.47	1.89	6	1.00	1.00	45	74.82
	Total Dry Weight (kg)									3022.29
	Total Biomass (tons/ha)									96.19

Sample Plot No. 3		Plot Size: 10 m radius	Collection Date: 18/09/98			Location: LL 33 47 35.2 N, 150 37 18.7 E				
						UTM 0279826 E, 6258314 N				
Tree #	**Scientific Name**	**Common Name**	**Dbh (cm)**	**Tht (m)**	**Cover (m)**	**ANBT**	**ABD (cm)**	**ABL (m)**	**ABAV (deg)**	**Total Tree Weight (kg)**
1	Eucalyptus micrantha	Scribbly Gum	50.93	21.72	7.09	8.00	20.00	5.00	45	1721.81
2	Eucalyptus micrantha	Scribbly Gum	37.56	20.12	7.90	10.00	15.00	10.00	45	850.70
3	Eucalyptus micrantha	Scribbly Gum	21.96	16.17	5.05	8.00	8.00	4.00	40	245.56
4	Eucalyptus micrantha	Scribbly Gum	26.74	13.44	4.65	6.00	7.00	4.00	40	387.25
5	Eucalyptus micrantha	Scribbly Gum	73.85	21.68	10.93	25.00	20.00	10.00	45	4070.51
6	Eucalyptus micrantha	Scribbly Gum	44.88	19.44	6.56	10.00	15.00	7.00	40	1284.86
7	Eucalyptus micrantha	Scribbly Gum	37.24	18.02	6.14	6.00	10.00	5.00	45	834.10
8	Eucalyptus micrantha	Scribbly Gum	31.83	21.98	8.06	6.00	9.00	8.00	40	579.86
9	Eucalyptus micrantha	Scribbly Gum	21.49	16.17	3.05	5.00	6.00	3.00	40	233.38
10	Eucalyptus micrantha	Scribbly Gum	36.92	14.97	6.45	6.00	7.00	5.00	45	817.68
11	Eucalyptus micrantha	Scribbly Gum	23.87	11.72	9.50	6.00	8.00	6.00	50	297.86
12	Eucalyptus micrantha	Scribbly Gum	10.50	10.09	2.29	4.00	4.00	4.00	30	44.50
13	Eucalyptus micrantha	Scribbly Gum	4.30	5.76	0.62	8.00	0.50	0.30	45	5.62
14	Eucalyptus micrantha	Scribbly Gum	15.60	16.19	1.98	8.00	7.00	5.00	45	111.16
15	Eucalyptus creba	Narrow-leaved Red Ironbark	18.94	8.19	3.73	8.00	7.00	6.00	40	171.80
16	Eucalyptus creba	Narrow-leaved Red Ironbark	12.73	8.19	2.83	5.00	5.00	3.00	40	66.59
17	Syncarpia glomulifera	Turpentine	9.55	6.58	2.33	25.00	0.50	0.50	85	33.51
18	Syncarpia glomulifera	Turpentine	19.89	14.63	2.33	25.00	0.50	0.50	85	193.20
19	Syncarpia glomulifera	Turpentine	15.92	10.72	1.97	25.00	0.50	0.50	85	113.43
20	Syncarpia glomulifera	Turpentine	10.50	7.24	3.21	25.00	0.50	0.50	85	42.08
21	Syncarpia glomulifera	Turpentine	6.05	7.47	1.94	25.00	0.50	0.50	85	11.27
22	Syncarpia glomulifera	Turpentine	12.10	8.96	2.53	25.00	0.50	0.50	85	58.92
23	Syncarpia glomulifera	Turpentine	7.96	6.79	1.59	25.00	0.50	0.50	85	21.69
24	Syncarpia glomulifera	Turpentine	13.05	8.96	1.65	25.00	0.50	0.50	85	70.64
25	Syncarpia glomulifera	Turpentine	10.98	8.19	1.72	25.00	0.50	0.50	85	46.78
26	Eucalyptus sideroxylon	Red Ironbark	9.71	11.04	2.66	6.00	4.00	2.00	45	34.86
27	Eucalyptus sideroxylon	Red Ironbark	10.19	10.72	2.11	6.00	2.00	2.00	45	39.10
28	Eucalyptus sideroxylon	Red Ironbark	13.37	12.48	1.66	4.00	2.00	2.00	45	74.82
29	Eucalyptus sideroxylon	Red Ironbark	14.64	13.87	2.33	5.00	3.00	3.00	40	92.96
30	Eucalyptus sideroxylon	Red Ironbark	8.12	16.85	2.42	6.00	2.00	2.00	45	22.74
31	Eucalyptus sideroxylon	Red Ironbark	7.96	8.96	1.73	5.00	3.00	2.00	40	21.69
32	Eucalyptus sideroxylon	Red Ironbark	4.46	4.98	0.75	3.00	3.00	3.00	30	5.44
33	Eucalyptus sideroxylon	Red Ironbark	7.64	11.04	1.63	3.00	1.00	1.00	40	19.68
34	Eucalyptus sideroxylon	Red Ironbark	5.09	6.37	1.60	5.00	1.00	1.00	45	7.48
35	Eucalyptus sideroxylon	Red Ironbark	12.10	13.55	2.93	7.00	3.00	2.00	45	58.92
36	Eucalyptus sideroxylon	Red Ironbark	7.32	10.29	1.53	5.00	1.00	1.00	45	17.78
37	Eucalyptus sideroxylon	Red Ironbark	6.21	7.34	1.35	4.00	1.00	1.00	40	11.99
38	Eucalyptus sideroxylon	Red Ironbark	8.59	8.85	1.55	4.00	1.00	1.00	40	26.06
39	Eucalyptus sideroxylon	Red Ironbark	7.00	6.79	1.46	5.00	1.00	1.00	40	15.99
40	Eucalyptus micrantha	Scribbly Gum	5.73	6.79	1.56	5.00	1.00	1.00	40	10.94
41	Eucalyptus micrantha	Scribbly Gum	7.32	10.72	1.53	5.00	0.50	0.50	40	19.29
42	Eucalyptus micrantha	Scribbly Gum	6.37	4.98	0.81	2.00	0.50	0.50	40	13.96
43	Eucalyptus sideroxylon	Red Ironbark	13.21	7.40	3.07	7.00	3.00	5.00	40	72.71
	Total Dry Weight (kg)									12889.42
	Total Biomass (tons/ha)									410.23

Sample Plot No. 4		Plot Size: 10 m radius	Collection Date: 24/10/98			Location: LL 33 47 40.1 N, 150 37 15.3 E				
						UTM 0279650 E, 6258043 N				
Tree #	**Scientific Name**	**Common Name**	**Dbh (cm)**	**Tht (m)**	**Cover (m)**	**ANBT**	**ABD (cm)**	**ABL (m)**	**ABAV (deg)**	**Total Tree Weight (kg)**
1	Eucalyptus creba	Narrow-leaved Red Ironbark	31.83	17.68	4.45	8.00	5.00	3.00	40	593.18
2	Callitris hugelii	White Cypress Pine	14.64	9.99	3.50	16.00	2.00	1.00	60	79.89
3	Eucalyptus creba	Narrow-leaved Red Ironbark	37.24	20.51	6.31	12.00	6.00	4.00	50	862.84
4	Eucalyptus creba	Narrow-leaved Red Ironbark	32.47	21.96	6.85	10.00	7.00	5.00	50	621.89
5	Eucalyptus sideroxylon	Red Ironbark	23.24	11.73	5.35	10.00	5.00	2.00	45	279.89
6	Eucalyptus sideroxylon	Red Ironbark	23.87	14.70	3.50	8.00	5.00	3.00	40	298.54
7	Eucalyptus sideroxylon	Red Ironbark	12.41	7.29	2.69	5.00	3.00	2.00	45	62.69
8	Eucalyptus creba	Narrow-leaved Red Ironbark	15.92	12.87	2.64	8.00	2.00	1.50	60	113.43
9	Eucalyptus creba	Narrow-leaved Red Ironbark	18.14	11.45	4.95	8.00	3.00	1.50	45	155.07
10	Eucalyptus creba	Narrow-leaved Red Ironbark	30.24	17.62	5.80	10.00	7.00	3.00	45	524.83
11	Eucalyptus creba	Narrow-leaved Red Ironbark	18.94	20.51	3.65	8.00	3.00	2.00	45	171.80
12	Eucalyptus resinifera	Red Mahogany	24.35	19.01	3.65	10.00	2.00	2.00	45	312.99
13	Callitris hugelii	White Cypress Pine	19.10	11.36	5.88	35.00	2.00	2.00	80	141.89
14	Eucalyptus creba	Narrow-leaved Red Ironbark	29.92	23.18	7.15	10.00	4.00	3.00	45	511.75
15	Eucalyptus creba	Narrow-leaved Red Ironbark	31.51	28.53	6.05	6.00	5.00	4.00	45	579.12
16	Callitris hugelii	White Cypress Pine	20.21	22.08	5.90	30.00	2.00	2.00	80	160.38
17	Eucalyptus creba	Narrow-leaved Red Ironbark	26.42	18.05	5.55	8.00	5.00	3.00	50	380.24
18	Callitris hugelii	White Cypress Pine	15.60	13.03	4.55	30.00	2.00	1.50	90	91.59
19	Callitris hugelii	White Cypress Pine	17.51	13.87	3.75	30.00	1.00	1.00	90	117.56
20	Eucalyptus robertsoni	Narrow-leaved Peppermint	9.07	9.90	4.95	12.00	2.00	2.50	60	22.67
21	Eucalyptus resinifera	Red Mahogany	63.66	20.51	7.80	10.00	7.00	4.00	45	3102.11
22	Eucalyptus sideroxylon	Red Ironbark	57.30	21.96	9.35	10.00	8.00	4.00	45	2412.40
23	Callitris hugelii	White Cypress Pine	20.69	11.29	3.15	20.00	3.00	3.00	60	168.69
24	Callitris hugelii	White Cypress Pine	15.92	8.61	4.00	16.00	1.00	1.50	80	95.67
25	Callitris hugelii	White Cypress Pine	20.69	9.98	4.00	30.00	3.00	2.00	60	168.69
26	Callitris hugelii	White Cypress Pine	11.14	4.38	3.45	10.00	1.00	2.00	70	44.26
27	Eucalyptus robertsoni	Narrow-leaved Peppermint	5.41	7.88	3.05	8.00	1.00	1.50	50	6.17
28	Eucalyptus robertsoni	Narrow-leaved Peppermint	5.73	7.65	2.75	10.00	1.00	1.50	50	7.12
29	Eucalyptus robertsoni	Narrow-leaved Peppermint	4.77	7.58	2.40	8.00	0.80	1.30	48	4.50
30	Eucalyptus robertsoni	Narrow-leaved Peppermint	5.09	7.88	2.93	8.00	0.80	1.40	47	5.29
31	Eucalyptus robertsoni	Narrow-leaved Peppermint	5.41	7.43	3.00	9.00	1.00	1.30	49	6.17
32	Eucalyptus robertsoni	Narrow-leaved Peppermint	5.41	7.50	3.03	9.00	1.00	1.60	50	6.17
33	Eucalyptus robertsoni	Narrow-leaved Peppermint	5.25	7.50	3.05	9.00	0.75	1.50	50	5.72
34	Eucalyptus robertsoni	Narrow-leaved Peppermint	4.77	7.88	3.08	8.00	0.75	1.50	52	4.50
35	Eucalyptus robertsoni	Narrow-leaved Peppermint	5.73	7.28	2.85	8.00	1.00	1.25	49	7.12
36	Eucalyptus robertsoni	Narrow-leaved Peppermint	5.41	7.88	3.10	8.00	1.00	1.50	50	6.17
	Total Dry Weight (kg)									12140.68
	Total Biomass (tons/ha)									386.40

Sample Plot No. 5		Plot Size: 10 m radius	Collection Date: 24/10/98				Location: LL 33 47 19.8 N, 150 37 40 E			
							UTM 0280359 E, 6258757 N			
Tree #	**Scientific Name**	**Common Name**	**Dbh (cm)**	**Tht (m)**	**Cover (m)**	**ANBT**	**ABD (cm)**	**ABL (m)**	**ABAV (deg)**	**Total Tree Weight (kg)**
1	Eucalyptus paniculata	Grey Ironbark	25.94	20.22	4.50	12.00	3.00	2.00	45	364.04
2	Eucalyptus paniculata	Grey Ironbark	29.92	12.87	5.75	10.00	4.00	4.00	45	511.75
3	Eucalyptus camaldulensis	River Red Gum	17.19	22.81	5.05	12.00	2.00	2.00	45	139.21
4	Eucalyptus camaldulensis	River Red Gum	16.07	22.81	5.70	8.00	3.00	2.00	45	119.20
5	Eucalyptus maculata	Spotted Gum	26.42	27.43	4.65	10.00	4.00	3.00	40	376.65
6	Syncarpia glomulifera	Turpentine	10.50	10.12	2.70	30.00	1.00	1.00	90	42.08
7	Syncarpia glomulifera	Turpentine	5.09	9.56	2.35	20.00	1.00	1.00	90	7.48
8	Syncarpia glomulifera	Turpentine	4.77	9.56	2.30	20.00	1.00	1.00	90	6.41
9	Syncarpia glomulifera	Turpentine	5.09	9.56	2.13	20.00	1.00	1.00	90	7.48
10	Eucalyptus resinifera	Red Mahogany	21.96	19.87	9.70	20.00	8.00	4.00	45	244.66
11	Eucalyptus paniculata	Grey Ironbark	29.76	10.94	7.75	12.00	4.00	4.00	50	505.27
12	Eucalyptus paniculata	Grey Ironbark	12.41	10.07	1.95	6.00	1.00	1.00	45	62.69
13	Eucalyptus siderophloia	Broad-leaved Red Ironbark	20.05	10.45	6.15	8.00	4.00	3.00	50	196.91
14	Eucalyptus siderophloia	Broad-leaved Red Ironbark	24.67	9.98	3.90	8.00	4.00	3.00	45	322.84
15	Callitris hugelii	White Cypress Pine	6.68	4.32	2.63	6.00	2.00	1.00	50	14.67
16	Callitris hugelii	White Cypress Pine	6.37	4.32	2.38	6.00	2.00	1.00	50	13.20
17	Callitris hugelii	White Cypress Pine	6.68	4.32	2.38	6.00	2.00	1.00	50	14.67
18	Eucalyptus resinifera	Red Mahogany	57.93	11.21	9.05	6.00	6.00	4.00	45	2476.86
19	Eucalyptus paniculata	Grey Ironbark	20.69	5.91	4.15	8.00	2.00	2.00	45	212.16
20	Eucalyptus maculata	Spotted Gum	28.01	11.58	8.45	12.00	5.00	3.00	40	431.29
21	Eucalyptus maculata	Spotted Gum	24.03	10.19	8.55	10.00	5.00	3.00	45	302.48
22	Syncarpia glomulifera	Turpentine	8.28	8.78	4.60	20.00	1.00	1.00	80	23.82
23	Syncarpia glomulifera	Turpentine	8.28	8.53	4.70	19.00	1.00	1.00	78	23.82
24	Syncarpia glomulifera	Turpentine	7.96	8.53	4.13	19.00	1.00	1.00	80	21.69
25	Syncarpia glomulifera	Turpentine	7.32	8.78	4.10	20.00	1.00	1.00	75	17.78
26	Syncarpia glomulifera	Turpentine	7.32	8.63	4.30	15.00	0.80	0.90	75	17.78
27	Syncarpia glomulifera	Turpentine	7.96	8.13	4.30	15.00	0.80	0.90	80	21.69
28	Syncarpia glomulifera	Turpentine	8.28	7.73	4.35	20.00	1.00	1.00	80	23.82
29	Syncarpia glomulifera	Turpentine	8.28	7.73	4.35	20.00	1.00	1.00	80	23.82
30	Syncarpia glomulifera	Turpentine	7.96	8.78	4.05	20.00	1.00	1.00	81	21.69
31	Syncarpia glomulifera	Turpentine	7.96	8.78	4.00	20.00	1.00	1.00	81	21.69
32	Syncarpia glomulifera	Turpentine	7.96	8.63	3.88	20.00	1.00	1.00	75	21.69
33	Syncarpia glomulifera	Turpentine	8.28	8.78	3.85	18.00	0.75	1.00	78	23.82
34	Syncarpia glomulifera	Turpentine	7.96	8.63	3.85	18.00	0.75	1.00	80	21.69
35	Syncarpia glomulifera	Turpentine	8.59	8.78	4.08	20.00	1.00	1.00	77	26.06
36	Syncarpia glomulifera	Turpentine	8.28	8.78	3.95	20.00	1.00	1.00	80	23.82
37	Eucalyptus resinifera	Red Mahogany	38.52	21.96	8.05	10.00	6.00	3.00	45	934.92
38	Eucalyptus maculata	Spotted Gum	11.78	8.26	2.70	6.00	1.00	2.00	50	58.00
39	Eucalyptus paniculata	Grey Ironbark	7.00	5.61	1.05	10.00	0.50	0.50	50	15.99
40	Eucalyptus resinifera	Red Mahogany	31.83	13.81	2.65	8.00	4.00	3.00	45	593.18
41	Syncarpia glomulifera	Turpentine	9.07	11.53	3.20	30.00	1.00	1.00	80	29.65
42	Syncarpia glomulifera	Turpentine	8.59	11.53	3.20	30.00	1.00	1.00	80	26.06
43	Syncarpia glomulifera	Turpentine	8.91	11.13	3.20	25.00	0.80	0.90	75	28.43
44	Syncarpia glomulifera	Turpentine	8.91	11.13	3.25	25.00	0.80	0.90	75	28.43
45	Syncarpia glomulifera	Turpentine	9.07	11.18	3.25	25.00	1.00	1.00	80	29.65
46	Syncarpia glomulifera	Turpentine	7.96	11.18	3.00	28.00	1.20	1.00	82	21.69
47	Syncarpia glomulifera	Turpentine	7.64	11.53	3.00	28.00	1.20	1.00	80	19.68
48	Syncarpia glomulifera	Turpentine	7.64	12.21	3.15	30.00	1.00	1.00	80	19.68
49	Syncarpia glomulifera	Turpentine	7.96	12.21	2.90	30.00	1.00	1.00	80	21.69
50	Syncarpia glomulifera	Turpentine	8.28	12.59	2.88	30.00	1.00	1.00	78	23.82
51	Syncarpia glomulifera	Turpentine	8.91	11.89	3.03	30.00	1.00	1.00	78	28.43
52	Syncarpia glomulifera	Turpentine	7.32	11.89	3.03	32.00	1.25	1.20	82	17.78
53	Syncarpia glomulifera	Turpentine	7.96	11.53	3.03	32.00	1.25	1.00	81	21.69
54	Syncarpia glomulifera	Turpentine	7.00	11.53	2.70	30.00	1.00	1.00	78	15.99
55	Syncarpia glomulifera	Turpentine	8.59	11.53	3.00	30.00	1.00	1.00	78	26.06
56	Eucalyptus resinifera	Red Mahogany	24.19	15.94	5.00	10.00	3.00	3.00	45	308.13
57	Eucalyptus paniculata	Grey Ironbark	14.32	10.93	1.70	8.00	1.00	1.00	50	88.21
58	Syncarpia glomulifera	Turpentine	6.37	9.03	2.70	20.00	0.50	0.80	80	12.73
59	Syncarpia glomulifera	Turpentine	5.73	9.03	2.70	20.00	0.50	0.80	80	9.90
60	Syncarpia glomulifera	Turpentine	5.73	9.03	2.63	18.00	0.50	0.75	78	9.90
61	Syncarpia glomulifera	Turpentine	6.37	9.03	2.63	18.00	0.50	0.75	75	12.73
62	Syncarpia glomulifera	Turpentine	7.00	9.03	2.63	22.00	0.70	0.90	80	15.99
63	Syncarpia glomulifera	Turpentine	6.37	9.03	2.38	22.00	0.70	0.90	80	12.73
64	Syncarpia glomulifera	Turpentine	6.68	9.03	2.38	22.00	0.60	0.80	78	14.31
65	Syncarpia glomulifera	Turpentine	7.00	8.49	2.13	20.00	0.50	0.80	80	15.99
66	Syncarpia glomulifera	Turpentine	6.37	8.49	2.63	20.00	0.50	0.80	80	12.73
67	Syncarpia glomulifera	Turpentine	6.37	8.49	2.70	20.00	0.50	0.80	80	12.73
68	Syncarpia glomulifera	Turpentine	17.83	13.03	4.35	16.00	2.00	2.00	70	148.66
	Total Dry Weight (kg)									9348.08
	Total Biomass (tons/ha)									297.52

Sample Plot No. 6		Plot Size: 10 m radius	Collection Date: 19/09/98			Location: LL 33 47 05 N, 150 38 03 E UTM 0280947 E, 6259156 N				
Tree #	**Scientific Name**	**Common Name**	**Dbh (cm)**	**Tht (m)**	**Cover (m)**	**ANBT**	**ABD (cm)**	**ABL (m)**	**ABAV (deg)**	**Total Tree Weight (kg)**
1	Eucalyptus longifolia	Woollybutt	14.96	11.04	1.85	10.00	1.00	0.60	45	97.86
2	Eucalyptus resinifera	Red Mahogany	39.31	14.16	4.53	8.00	7.00	0.30	45	981.68
3	Eucalyptus longifolia	Woollybutt	8.91	5.15	2.12	10.00	0.50	0.50	45	28.43
4	Eucalyptus longifolia	Woollybutt	2.86	3.47	0.85	6.00	0.50	0.60	45	1.89
5	Eucalyptus longifolia	Woollybutt	4.77	3.65	1.37	6.00	0.50	0.60	45	6.41
6	Eucalyptus longifolia	Woollybutt	3.82	8.75	1.84	20.00	1.00	0.60	45	3.76
7	Eucalyptus longifolia	Woollybutt	2.86	3.82	0.67	5.00	0.50	0.50	45	1.89
8	Callitris hugelii	White Cypress Pine	6.68	4.17	1.23	10.00	1.00	0.50	60	14.67
9	Eucalyptus longifolia	Woollybutt	4.46	5.45	1.16	10.00	0.50	0.50	85	5.44
10	Eucalyptus longifolia	Woollybutt	16.23	6.30	2.46	8.00	4.00	1.50	45	118.92
11	Eucalyptus longifolia	Woollybutt	16.23	10.14	3.29	6.00	3.00	2.00	45	118.92
12	Eucalyptus longifolia	Woollybutt	14.96	10.14	1.96	5.00	2.00	1.50	45	97.86
13	Eucalyptus longifolia	Woollybutt	3.82	3.68	1.31	8.00	0.50	0.50	70	3.76
14	Eucalyptus longifolia	Woollybutt	10.03	6.30	1.55	10.00	0.50	0.50	75	37.65
15	Eucalyptus longifolia	Woollybutt	1.91	3.28	0.74	5.00	5.00	0.40	75	0.72
16	Eucalyptus longifolia	Woollybutt	7.16	4.97	1.52	10.00	0.50	0.40	75	16.87
17	Eucalyptus longifolia	Woollybutt	2.71	1.91	1.01	5.00	5.00	0.50	75	1.65
18	Callitris hugelii	White Cypress Pine	4.30	4.19	1.07	8.00	5.00	0.50	75	5.65
19	Callitris hugelii	White Cypress Pine	6.21	4.38	2.14	15.00	0.50	1.00	45	12.50
20	Eucalyptus resinifera	Red Mahogany	49.97	21.72	6.78	15.00	10.00	5.00	45	1740.78
21	Eucalyptus longifolia	Woollybutt	3.18	5.42	1.07	5.00	0.50	0.50	70	2.43
22	Eucalyptus longifolia	Woollybutt	8.91	8.07	2.12	10.00	1.00	1.00	70	28.43
23	Eucalyptus sideroxylon	Red Ironbark	14.96	8.69	3.64	6.00	2.00	1.50	50	97.86
24	Eucalyptus resinifera	Red Mahogany	15.44	12.48	3.64	10.00	3.00	2.00	45	105.47
25	Syncarpia glomulifera	Turpentine	10.19	8.66	3.48	20.00	2.00	1.50	60	39.10
26	Syncarpia glomulifera	Turpentine	7.96	8.15	2.70	20.00	2.00	1.50	60	21.69
27	Syncarpia glomulifera	Turpentine	9.87	8.40	3.45	20.00	2.00	1.50	60	36.24
28	Eucalyptus resinifera	Red Mahogany	74.17	14.92	8.75	10.00	8.00	3.00	45	4466.40
29	Syncarpia glomulifera	Turpentine	8.91	7.66	2.46	40.00	1.00	1.50	80	28.43
30	Syncarpia glomulifera	Turpentine	9.55	9.26	2.13	40.00	1.00	2.00	82	33.51
31	Syncarpia glomulifera	Turpentine	9.23	8.97	2.14	40.00	1.00	2.00	80	30.91
32	Syncarpia glomulifera	Turpentine	8.44	8.97	2.00	40.00	1.00	2.00	80	24.93
33	Eucalyptus resinifera	Red Mahogany	13.53	12.98	3.07	8.00	3.00	2.00	45	76.96
34	Syncarpia glomulifera	Turpentine	10.03	10.31	3.54	40.00	1.00	1.50	80	37.65
35	Syncarpia glomulifera	Turpentine	4.77	4.42	1.35	40.00	1.00	1.00	80	6.41
36	Syncarpia glomulifera	Turpentine	3.82	6.22	1.25	40.00	1.00	1.00	80	3.76
37	Syncarpia glomulifera	Turpentine	3.82	5.00	1.04	40.00	1.00	1.00	80	3.76
38	Syncarpia glomulifera	Turpentine	11.78	8.76	2.77	40.00	1.00	1.00	80	55.29
39	Eucalyptus longifolia	Woollybutt	9.71	9.03	2.53	5.00	2.00	1.00	45	34.86
40	Syncarpia glomulifera	Turpentine	4.14	4.39	1.27	3.00	1.00	0.50	45	4.55
41	Syncarpia glomulifera	Turpentine	10.19	9.12	2.63	25.00	1.00	1.50	75	39.10
42	Syncarpia glomulifera	Turpentine	12.10	9.69	2.58	25.00	1.00	1.50	75	58.92
43	Syncarpia glomulifera	Turpentine	11.78	9.99	2.59	25.00	1.00	1.50	75	55.29
44	Syncarpia glomulifera	Turpentine	3.82	6.22	1.30	20.00	1.00	1.00	75	3.76
45	Syncarpia glomulifera	Turpentine	4.14	5.00	1.25	20.00	1.00	1.00	75	4.55
46	Callitris hugelii	White Cypress Pine	8.91	3.83	2.54	6.00	3.00	1.50	45	27.32
47	Callitris hugelii	White Cypress Pine	5.41	3.79	1.45	8.00	3.00	1.00	45	9.29
48	Callitris hugelii	White Cypress Pine	5.25	3.60	1.43	5.00	2.00	1.00	45	8.71
49	Callitris hugelii	White Cypress Pine	8.44	3.79	1.56	8.00	3.00	1.00	45	24.26
50	Eucalyptus longifolia	Woollybutt	10.50	4.12	2.16	10.00	1.00	0.60	65	42.08
51	Eucalyptus longifolia	Woollybutt	8.59	10.12	1.93	8.00	0.50	1.00	60	26.06
52	Eucalyptus resinifera	Red Mahogany	7.32	9.80	1.86	8.00	0.50	1.00	60	17.78
53	Eucalyptus longifolia	Woollybutt	13.21	4.81	1.62	10.00	1.00	0.60	65	72.71
54	Eucalyptus longifolia	Woollybutt	8.75	8.61	1.91	10.00	0.60	0.50	45	27.23
55	Eucalyptus longifolia	Woollybutt	7.16	9.15	1.56	10.00	0.50	0.50	70	16.87
56	Eucalyptus resinifera	Red Mahogany	12.73	11.47	2.15	6.00	2.00	1.50	60	66.59
57	Eucalyptus longifolia	Woollybutt	14.80	14.91	2.15	8.00	2.00	1.50	50	95.39
58	Eucalyptus longifolia	Woollybutt	6.68	7.91	1.72	8.00	5.00	0.60	50	14.31
59	Eucalyptus longifolia	Woollybutt	8.59	10.84	1.69	8.00	0.50	0.60	50	26.06
60	Eucalyptus creba	Narrow-leaved Red Ironbark	24.51	18.04	4.29	8.00	6.00	2.00	45	317.89
61	Eucalyptus longifolia	Woollybutt	30.08	17.83	4.80	10.00	5.00	3.00	45	518.27
62	Eucalyptus longifolia	Woollybutt	7.64	6.99	1.98	10.00	0.50	1.00	75	19.68
63	Eucalyptus longifolia	Woollybutt	23.87	10.84	3.55	10.00	1.00	1.00	75	298.54
64	Eucalyptus longifolia	Woollybutt	6.68	5.74	2.17	10.00	0.50	1.00	70	14.31
65	Eucalyptus longifolia	Woollybutt	9.87	8.61	2.27	10.00	1.00	1.00	70	36.24
66	Eucalyptus longifolia	Woollybutt	2.86	3.69	1.30	5.00	2.00	2.00	70	1.89
67	Eucalyptus longifolia	Woollybutt	13.69	9.13	2.37	10.00	1.00	1.00	70	79.14
68	Eucalyptus longifolia	Woollybutt	7.48	6.29	1.37	10.00	1.00	0.80	80	18.71
69	Eucalyptus longifolia	Woollybutt	6.68	6.07	1.32	10.00	1.00	0.80	80	14.31
70	Eucalyptus longifolia	Woollybutt	6.21	5.19	1.55	10.00	1.00	0.60	80	11.99
	Total Dry Weight (kg)									10409.76
	Total Biomass (tons/ha)									331.31

Sample Plot No. 7		Plot Size: 10 m radius	Collection Date: 19/09/98				Location: LL 33 47 16.3 N, 150 37 50 E			
							UTM 0280628 E, 6258815 N			
Tree #	**Scientific Name**	**Common Name**	**Dbh (cm)**	**Tht (m)**	**Cover (m)**	**ANBT**	**ABD (cm)**	**ABL (m)**	**ABAV (deg)**	**Total Tree Weight (kg)**
1	Eucalyptus resinifera	Red Mahogany	39.95	9.98	7.81	15.00	8.00	4.00	45	1020.05
2	Eucalyptus resinifera	Red Mahogany	35.97	9.30	8.83	15.00	10.00	6.00	45	794.09
3	Eucalyptus resinifera	Red Mahogany	64.94	12.84	9.47	15.00	8.00	4.00	45	3252.25
4	Eucalyptus resinifera	Red Mahogany	23.87	9.28	6.75	8.00	8.00	4.00	45	298.54
5	Eucalyptus creba	Narrow-leaved Red Ironbark	61.43	18.18	9.20	12.00	10.00	4.00	45	2849.24
6	Eucalyptus longifolia	Woollybutt	61.12	31.23	10.92	12.00	15.00	5.00	45	2814.13
7	Eucalyptus longifolia	Woollybutt	4.77	9.23	9.03	5.00	1.00	1.00	45	6.41
8	Eucalyptus gummifera	Red Bloodwood	21.96	21.65	6.05	6.00	6.00	3.00	45	245.56
9	Eucalyptus resinifera	Red Mahogany	6.68	11.12	1.94	6.00	2.00	1.50	45	14.31
10	Eucalyptus resinifera	Red Mahogany	3.50	6.10	1.14	6.00	1.00	1.00	45	3.06
11	Eucalyptus resinifera	Red Mahogany	3.34	6.50	1.24	6.00	1.00	1.00	45	2.74
12	Eucalyptus resinifera	Red Mahogany	33.74	40.47	7.15	18.00	10.00	5.00	45	681.69
13	Eucalyptus resinifera	Red Mahogany	44.25	38.91	13.50	15.00	12.00	6.00	50	1301.74
14	Eucalyptus resinifera	Red Mahogany	17.51	24.41	4.15	12.00	5.00	3.00	45	142.40
15	Eucalyptus resinifera	Red Mahogany	31.83	30.23	7.07	12.00	8.00	5.00	45	593.18
16	Eucalyptus resinifera	Red Mahogany	35.97	38.91	8.64	6.00	10.00	5.00	45	794.09
17	Eucalyptus longifolia	Woollybutt	7.32	6.18	2.88	10.00	1.00	1.00	85	17.78
18	Eucalyptus longifolia	Woollybutt	7.64	5.74	1.94	10.00	1.00	1.00	80	19.68
19	Eucalyptus longifolia	Woollybutt	9.87	6.22	2.18	10.00	1.00	1.00	80	36.24
20	Eucalyptus resinifera	Red Mahogany	6.68	6.29	1.32	10.00	0.50	0.60	60	14.31
21	Eucalyptus resinifera	Red Mahogany	6.05	4.97	1.33	10.00	0.50	0.60	60	11.27
22	Eucalyptus resinifera	Red Mahogany	3.34	4.97	1.08	3.00	0.50	0.50	60	2.74
23	Eucalyptus resinifera	Red Mahogany	4.30	8.69	0.97	5.00	0.50	0.30	65	4.98
24	Eucalyptus resinifera	Red Mahogany	10.35	24.02	2.02	10.00	0.50	0.50	70	40.57
25	Eucalyptus resinifera	Red Mahogany	15.28	28.38	3.14	10.00	2.00	1.00	50	102.90
26	Eucalyptus resinifera	Red Mahogany	7.64	6.79	1.76	10.00	0.50	0.50	60	19.68
27	Eucalyptus resinifera	Red Mahogany	54.75	20.45	10.89	12.00	15.00	6.00	45	2164.34
28	Eucalyptus longifolia	Woollybutt	20.69	19.90	4.90	6.00	10.00	5.00	45	212.16
29	Eucalyptus sideroxylon	Red Ironbark	3.02	3.80	1.36	5.00	0.50	0.50	60	2.15
30	Eucalyptus sideroxylon	Red Ironbark	10.66	5.61	2.28	10.00	0.50	0.50	60	43.61
	Total Dry Weight (kg)									17516.96
	Total Biomass (tons/ha)									557.51

Sample Plot No .8		Plot Size: 10 m radius	Collection Date: 21/09/98				Location: LL 33 47 58.5 N, 150 36 50.6 E			
							UTM 0279124 E, 6257495 N			
Tree #	**Scientific Name**	**Common Name**	**Dbh (cm)**	**Tht (m)**	**Cover (m)**	**ANBT**	**ABD (cm)**	**ABL (m)**	**ABAV (deg)**	**Total Tree Weight (kg)**
1	Eucalyptus tereticornis	Forest Red Gum	41.70	14.97	8.23	12.00	6.00	3.50	40	1083.62
2	Eucalyptus tereticornis	Forest Red Gum	41.70	18.17	4.76	12.00	7.00	3.00	35	1083.62
3	Eucalyptus tereticornis	Forest Red Gum	24.35	12.47	4.65	12.00	5.00	3.00	40	311.84
4	Eucalyptus tereticornis	Forest Red Gum	42.97	27.70	6.83	10.00	7.00	5.00	40	1161.79
5	Eucalyptus tereticornis	Forest Red Gum	26.10	15.64	4.49	10.00	5.00	3.50	40	366.23
6	Eucalyptus tereticornis	Forest Red Gum	18.94	15.76	4.23	8.00	5.00	5.00	35	174.26
7	Eucalyptus tereticornis	Forest Red Gum	26.10	21.06	4.67	8.00	5.00	4.50	35	366.23
8	Eucalyptus tereticornis	Forest Red Gum	21.01	15.13	4.75	8.00	5.00	4.50	40	221.54
9	Eucalyptus tereticornis	Forest Red Gum	29.92	24.55	7.05	8.00	6.00	5.00	40	502.46
10	Eucalyptus tereticornis	Forest Red Gum	43.93	25.42	5.10	10.00	7.00	6.00	35	1222.45
11	Eucalyptus tereticornis	Forest Red Gum	38.83	17.44	9.98	8.00	7.00	7.00	45	918.97
12	Eucalyptus tereticornis	Forest Red Gum	14.64	3.02	0.95	2.00	6.00	1.00	85	96.03
13	Eucalyptus resinifera	Red Mahogany	53.16	31.03	12.10	20.00	10.00	6.00	50	2017.19
14	Eucalyptus resinifera	Red Mahogany	13.37	10.85	5.05	6.00	3.00	4.00	45	74.82
15	Eucalyptus tereticornis	Forest Red Gum	49.66	38.98	6.25	12.00	12.00	7.00	35	1623.77
16	Eucalyptus tereticornis	Forest Red Gum	42.97	41.61	7.23	12.00	10.00	8.00	35	1161.79
17	Eucalyptus tereticornis	Forest Red Gum	56.98	39.36	10.55	12.00	8.00	7.00	40	2232.71
18	Eucalyptus tereticornis	Forest Red Gum	21.33	19.39	4.07	6.00	5.00	5.00	35	229.40
19	Eucalyptus tereticornis	Forest Red Gum	47.11	38.94	10.05	8.00	8.00	6.00	40	1437.42
	Total Dry Weight (kg)									16296.61
	Total Biomass (tons/ha)									518.67

Sample Plot No. 9		Plot Size: 10 m radius	Collection Date: 21/09/98				Location: LL 33 48 02.9 N, 150 36 43.1 E			
							UTM 0278937 E, 6257351 N			
Tree #	**Scientific Name**	**Common Name**	**Dbh (cm)**	**Tht (m)**	**Cover (m)**	**ANBT**	**ABD (cm)**	**ABL (m)**	**ABAV (deg)**	**Total Tree Weight (kg)**
1	Eucalyptus resinifera	Red Mahogany	66.21	22.85	7.50	10.00	8.00	3.00	45	3406.52
2	Eucalyptus resinifera	Red Mahogany	39.47	17.44	5.70	20.00	10.00	6.00	45	991.19
3	Eucalyptus resinifera	Red Mahogany	51.88	16.34	12.00	15.00	10.00	8.00	60	1903.78
4	Eucalyptus resinifera	Red Mahogany	42.34	10.36	10.00	15.00	10.00	7.00	60	1171.62
5	Eucalyptus resinifera	Red Mahogany	31.83	24.50	5.35	10.00	8.00	6.00	45	593.18
6	Eucalyptus sideroxylon	Red Ironbark	17.03	26.35	2.85	5.00	4.00	2.50	45	133.31
7	Eucalyptus sideroxylon	Red Ironbark	8.91	25.48	1.30	5.00	0.50	0.50	45	28.43
8	Eucalyptus sideroxylon	Red Ironbark	9.71	20.28	2.29	5.00	1.00	1.00	60	34.86
9	Eucalyptus sideroxylon	Red Ironbark	7.32	10.69	3.10	6.00	1.50	1.50	45	17.78
10	Callitris hugelii	White Cypress Pine	4.46	8.95	2.38	7.00	1.00	1.00	70	6.11
11	Eucalyptus sideroxylon	Red Ironbark	6.68	9.80	1.79	5.00	1.00	1.00	50	14.31
12	Eucalyptus sideroxylon	Red Ironbark	30.24	28.53	7.50	8.00	7.00	4.00	45	524.83
13	Eucalyptus sideroxylon	Red Ironbark	15.12	20.68	2.85	5.00	1.00	3.00	40	100.36
14	Eucalyptus creba	Narrow-leaved Red Ironbark	10.50	13.57	3.27	7.00	2.00	2.00	45	42.08
15	Eucalyptus sideroxylon	Red Ironbark	5.09	6.73	2.06	5.00	5.00	1.00	48	7.48
16	Eucalyptus sideroxylon	Red Ironbark	4.46	5.04	1.55	5.00	1.00	1.00	45	5.44
17	Callitris hugelii	White Cypress Pine	6.53	10.12	3.38	20.00	1.50	2.50	85	13.93
18	Eucalyptus sideroxylon	Red Ironbark	6.21	5.50	1.85	6.00	1.00	1.00	45	11.99
19	Eucalyptus sideroxylon	Red Ironbark	7.64	5.96	2.74	6.00	1.00	1.00	40	19.68
20	Eucalyptus sideroxylon	Red Ironbark	11.94	9.90	1.37	6.00	1.00	1.00	45	57.09
21	Callitris hugelii	White Cypress Pine	10.50	5.64	4.05	20.00	2.00	2.00	85	38.97
22	Eucalyptus tereticornis	Forest Red Gum	3.82	3.59	1.97	5.00	1.00	1.00	45	4.28
23	Eucalyptus sideroxylon	Red Ironbark	19.58	10.77	3.83	5.00	5.00	4.00	45	185.91
24	Eucalyptus sideroxylon	Red Ironbark	6.68	11.88	2.27	5.00	1.00	1.00	45	14.31
25	Callitris hugelii	White Cypress Pine	6.68	8.83	2.55	15.00	1.00	1.50	85	14.67
26	Callitris hugelii	White Cypress Pine	4.14	4.01	1.54	10.00	1.00	1.00	85	5.20
27	Eucalyptus sideroxylon	Red Ironbark	11.30	8.70	3.60	5.00	1.00	1.00	50	50.09
28	Eucalyptus resinifera	Red Mahogany	5.89	4.81	2.72	5.00	1.00	1.00	45	10.57
29	Eucalyptus resinifera	Red Mahogany	4.62	3.98	1.63	6.00	1.00	1.50	45	5.91
30	Callitris hugelii	White Cypress Pine	5.25	4.84	2.40	6.00	1.00	1.50	85	8.71
31	Eucalyptus sideroxylon	Red Ironbark	11.30	5.60	3.78	6.00	4.00	2.00	50	50.09
32	Eucalyptus tereticornis	Forest Red Gum	57.61	13.06	8.20	12.00	12.00	8.00	45	2290.90
33	Eucalyptus sideroxylon	Red Ironbark	16.07	6.09	3.47	6.00	6.00	3.00	40	116.15
34	Eucalyptus tereticornis	Forest Red Gum	6.21	4.02	4.25	6.00	2.00	2.00	55	13.16
35	Eucalyptus resinifera	Red Mahogany	13.69	8.26	4.05	6.00	3.00	3.00	45	79.14
36	Eucalyptus sideroxylon	Red Ironbark	10.03	6.75	2.64	5.00	4.00	3.00	40	37.65
37	Eucalyptus sideroxylon	Red Ironbark	17.35	5.50	2.86	5.00	4.00	2.00	45	139.33
38	Eucalyptus sideroxylon	Red Ironbark	9.23	8.70	1.74	5.00	1.00	1.00	45	30.91
39	Eucalyptus sideroxylon	Red Ironbark	7.80	5.36	1.62	5.00	1.00	1.00	45	20.67
40	Eucalyptus sideroxylon	Red Ironbark	7.80	5.36	1.62	5.00	1.00	1.00	45	20.67
41	Eucalyptus sideroxylon	Red Ironbark	5.09	4.80	0.99	5.00	1.00	1.00	45	7.48
42	Eucalyptus sideroxylon	Red Ironbark	12.57	14.45	1.79	5.00	2.00	1.50	45	64.62
43	Eucalyptus sideroxylon	Red Ironbark	24.51	27.10	6.15	8.00	8.00	5.00	50	317.89
44	Eucalyptus sideroxylon	Red Ironbark	29.44	22.82	4.50	6.00	10.00	4.00	45	492.47
45	Callitris hugelii	White Cypress Pine	4.77	7.45	2.53	10.00	3.00	3.00	45	7.09
46	Callitris hugelii	White Cypress Pine	4.77	7.45	2.53	10.00	3.00	3.00	45	7.09
47	Eucalyptus sideroxylon	Red Ironbark	13.37	9.28	2.33	8.00	2.00	2.00	45	74.82
48	Eucalyptus sideroxylon	Red Ironbark	13.37	9.28	2.33	8.00	2.00	2.00	45	74.82
	Total Dry Weight (kg)									13275.89
	Total Biomass (tons/ha)									422.53

Sample Plot No.10		Plot Size: 10 m radius	Collection Date: 23/09/98				Location: LL 33 46 58.6 N, 150 36 55.2 E			
							UTM 0279190 E, 6259303 N			
Tree #	**Scientific Name**	**Common Name**	**Dbh (cm)**	**Tht (m)**	**Cover (m)**	**ANBT**	**ABD (cm)**	**ABL (m)**	**ABAV (deg)**	**Total Tree Weight (kg)**
1	Eucalyptus micrantha	Scribbly Gum	11.46	9.28	2.36	8.00	4.00	2.00	35	54.44
2	Eucalyptus micrantha	Scribbly Gum	10.50	7.58	1.48	8.00	4.00	2.00	35	44.50
3	Eucalyptus micrantha	Scribbly Gum	15.12	9.01	2.73	8.00	4.00	2.00	40	103.44
4	Eucalyptus micrantha	Scribbly Gum	7.00	6.00	1.25	6.00	2.00	2.00	40	17.40
5	Eucalyptus largiflorens	Black Box	15.12	5.48	4.28	8.00	6.00	2.50	60	103.44
6	Eucalyptus micrantha	Scribbly Gum	15.12	8.03	2.08	6.00	4.00	3.00	45	103.44
7	Eucalyptus largiflorens	Black Box	14.32	4.34	3.17	10.00	1.50	1.00	70	91.26
8	Eucalyptus micrantha	Scribbly Gum	11.14	8.75	2.17	8.00	2.50	2.00	50	51.00
9	Eucalyptus sideroxylon	Red Ironbark	8.28	3.16	1.89	5.00	2.00	0.50	50	23.82
10	Eucalyptus micrantha	Scribbly Gum	9.55	7.15	1.87	8.00	0.50	1.00	45	35.69
11	Eucalyptus sideroxylon	Red Ironbark	16.55	9.50	2.74	10.00	4.00	2.00	45	124.56
12	Eucalyptus micrantha	Scribbly Gum	8.28	7.73	2.88	10.00	1.00	0.60	50	25.62
13	Malaleuca linariifolia	Paperbark	3.50	2.25	1.54	3.00	1.00	1.00	70	3.50
14	Eucalyptus largiflorens	Black Box	6.37	2.77	1.32	2.00	2.00	1.00	70	13.96
15	Eucalyptus largiflorens	Black Box	5.73	2.71	1.54	8.00	1.00	0.40	70	10.94
16	Malaleuca linariifolia	Paperbark	3.82	2.56	1.13	8.00	1.00	0.40	70	4.28
17	Malaleuca linariifolia	Paperbark	5.09	2.59	1.46	10.00	1.00	0.50	70	8.33
18	Eucalyptus largiflorens	Black Box	4.77	2.77	1.25	8.00	1.00	0.50	70	7.17
19	Eucalyptus micrantha	Scribbly Gum	17.19	8.50	3.97	8.00	6.00	4.00	45	139.21
20	Eucalyptus sideroxylon	Red Ironbark	18.14	7.07	3.87	8.00	5.00	5.00	60	155.07
21	Eucalyptus largiflorens	Black Box	22.92	6.00	5.50	12.00	7.00	3.00	60	271.00
22	Eucalyptus micrantha	Scribbly Gum	14.96	5.32	3.66	6.00	4.00	3.00	45	100.93
23	Eucalyptus sideroxylon	Red Ironbark	14.16	6.36	3.77	6.00	4.00	3.00	45	85.89
24	Eucalyptus micrantha	Scribbly Gum	17.83	7.15	5.30	8.00	6.00	3.00	60	151.44
25	Eucalyptus largiflorens	Black Box	22.60	5.83	3.40	10.00	4.00	2.00	60	262.36
26	Eucalyptus largiflorens	Black Box	21.01	6.48	4.26	12.00	4.00	15.00	60	221.54
27	Eucalyptus largiflorens	Black Box	7.16	2.64	1.88	8.00	2.00	1.00	60	18.33
28	Eucalyptus robertsoni	Narrow-leaved Peppermint	6.05	2.64	1.86	4.00	1.00	0.50	45	8.16
29	Eucalyptus micrantha	Scribbly Gum	17.35	11.45	3.44	8.00	4.00	3.00	75	142.21
30	Eucalyptus micrantha	Scribbly Gum	12.73	8.03	3.92	8.00	3.00	2.00	60	69.48
31	Malaleuca linariifolia	Paperbark	3.82	2.08	1.48	10.00	1.00	0.60	80	4.28
32	Malaleuca linariifolia	Paperbark	3.82	2.08	1.48	10.00	1.00	0.60	80	4.28
33	Malaleuca linariifolia	Paperbark	6.05	2.43	1.85	10.00	1.00	0.60	80	12.39
34	Malaleuca linariifolia	Paperbark	6.05	2.43	1.85	10.00	1.00	0.60	80	12.39
35	Eucalyptus micrantha	Scribbly Gum	15.92	10.38	5.35	5.00	7.00	4.00	50	116.48
36	Eucalyptus micrantha	Scribbly Gum	20.53	11.72	4.38	8.00	6.00	3.00	60	210.06
37	Eucalyptus largiflorens	Black Box	9.23	3.47	1.36	3.00	2.00	0.50	70	33.00
38	Malaleuca linariifolia	Paperbark	5.41	1.91	1.22	5.00	1.00	0.50	70	9.58
39	Malaleuca linariifolia	Paperbark	5.41	1.91	1.22	5.00	1.00	0.50	70	9.58
40	Eucalyptus largiflorens	Black Box	10.03	2.77	1.55	8.00	1.00	0.60	85	39.96
41	Eucalyptus ovata	Swamp Gum	5.73	2.77	1.21	10.00	1.00	0.50	60	10.94
42	Eucalyptus largiflorens	Black Box	8.28	2.08	1.35	8.00	1.00	0.50	85	25.62
43	Eucalyptus largiflorens	Black Box	7.80	2.77	1.25	10.00	1.00	0.50	80	22.33
44	Malaleuca linariifolia	Paperbark	4.30	2.41	1.00	4.00	1.00	0.50	45	5.62
45	Malaleuca linariifolia	Paperbark	4.14	4.12	1.64	6.00	1.00	0.50	80	5.15
46	Malaleuca linariifolia	Paperbark	4.14	4.12	1.64	6.00	1.00	0.50	80	5.15
47	Eucalyptus largiflorens	Black Box	7.32	3.02	1.41	6.00	1.00	0.50	80	19.29
48	Eucalyptus largiflorens	Black Box	7.64	5.36	1.88	6.00	1.00	0.60	60	21.29
49	Eucalyptus largiflorens	Black Box	7.80	7.02	1.63	6.00	2.00	1.00	60	22.33
50	Eucalyptus largiflorens	Black Box	5.57	3.46	1.39	6.00	1.00	0.60	50	10.24
51	Eucalyptus ovata	Swamp Gum	8.28	3.53	1.37	8.00	1.00	0.50	60	25.62
52	Eucalyptus largiflorens	Black Box	4.93	2.59	1.39	6.00	1.00	0.60	60	7.73
53	Eucalyptus largiflorens	Black Box	6.37	3.46	1.66	6.00	1.00	0.60	50	13.96
54	Eucalyptus largiflorens	Black Box	10.66	5.27	2.66	10.00	3.00	1.00	60	46.08
55	Eucalyptus sideroxylon	Red Ironbark	13.69	13.14	2.33	8.00	4.00	1.50	40	79.14
56	Eucalyptus largiflorens	Black Box	6.05	3.79	1.46	6.00	3.00	1.00	35	12.39
57	Eucalyptus largiflorens	Black Box	19.74	6.73	7.00	10.00	8.00	3.00	60	191.68
58	Eucalyptus micrantha	Scribbly Gum	42.34	14.31	10.49	20.00	10.00	5.00	70	1122.32
59	Eucalyptus largiflorens	Black Box	9.39	3.71	1.97	6.00	4.00	1.00	60	34.33
60	Eucalyptus sideroxylon	Red Ironbark	12.73	5.17	4.58	8.00	2.50	2.00	50	66.59
61	Malaleuca linariifolia	Paperbark	3.98	2.85	2.22	3.00	1.00	0.50	60	4.70
	Total Dry Weight (kg)									4659.90
	Total Biomass (tons/ha)									148.31

Sample Plot No.11		Plot Size: 10 m radius	Collection Date: 23/09/98				Location: LL 33 46 57 N, 150 36 49 E			
							UTM 0279066 E, 6259380 N			
Tree #	**Scientific Name**	**Common Name**	**Dbh (cm)**	**Tht (m)**	**Cover (m)**	**ANBT**	**ABD (cm)**	**ABL (m)**	**ABAV (deg)**	**Total Tree Weight (kg)**
1	Eucalyptus micrantha	Scribbly Gum	75.12	19.57	14.00	20.00	15.00	7.00	80	4234.87
2	Eucalyptus micrantha	Scribbly Gum	24.83	19.90	4.19	20.00	10.00	5.00	50	326.18
3	Eucalyptus micrantha	Scribbly Gum	18.62	18.18	3.09	12.00	8.00	3.00	50	167.55
4	Eucalyptus micrantha	Scribbly Gum	18.46	19.63	3.60	12.00	8.00	3.00	50	164.26
5	Malaleuca linariifolia	Paperbark	5.09	5.49	1.63	10.00	0.50	0.50	75	8.33
6	Malaleuca linariifolia	Paperbark	5.41	5.24	1.70	12.00	0.45	0.70	75	9.58
7	Malaleuca linariifolia	Paperbark	4.93	5.33	1.73	11.00	0.50	0.65	75	7.73
8	Malaleuca linariifolia	Paperbark	4.14	3.04	1.70	10.00	0.50	0.65	75	5.15
9	Malaleuca linariifolia	Paperbark	5.25	5.49	1.43	10.00	0.40	0.50	75	8.94
10	Malaleuca linariifolia	Paperbark	4.62	5.49	1.65	10.00	0.55	0.50	75	6.63
11	Malaleuca linariifolia	Paperbark	4.77	2.82	1.51	12.00	0.50	0.50	75	7.17
12	Malaleuca linariifolia	Paperbark	5.09	5.76	1.72	12.00	0.60	0.50	75	8.33
13	Malaleuca linariifolia	Paperbark	5.41	5.66	1.43	11.00	0.45	0.50	75	9.58
14	Malaleuca linariifolia	Paperbark	4.77	5.49	1.55	11.00	0.45	0.50	75	7.17
15	Eucalyptus largiflorens	Black Box	8.44	5.81	2.00	6.00	2.00	1.00	70	26.78
16	Eucalyptus largiflorens	Black Box	10.03	6.13	1.79	6.00	3.00	1.00	70	39.96
17	Malaleuca linariifolia	Paperbark	3.34	4.86	1.04	6.00	1.00	0.50	85	3.14
18	Malaleuca linariifolia	Paperbark	3.50	2.55	1.12	8.00	0.95	0.60	80	3.50
19	Malaleuca linariifolia	Paperbark	2.86	5.15	1.13	8.00	1.00	0.50	85	2.20
20	Malaleuca linariifolia	Paperbark	3.02	4.94	1.20	8.00	1.00	0.50	85	2.49
21	Malaleuca linariifolia	Paperbark	3.12	4.86	1.23	6.00	1.00	1.00	85	2.68
22	Malaleuca linariifolia	Paperbark	3.50	4.68	1.45	6.00	1.00	1.00	85	3.50
23	Malaleuca linariifolia	Paperbark	3.37	5.83	1.45	6.00	1.00	1.00	85	3.21
24	Malaleuca linariifolia	Paperbark	3.42	5.04	1.44	8.00	1.00	1.00	85	3.31
25	Malaleuca linariifolia	Paperbark	3.25	4.86	1.30	8.00	0.90	1.00	85	2.94
26	Malaleuca linariifolia	Paperbark	3.26	4.86	1.35	8.00	0.90	0.75	85	2.97
27	Malaleuca linariifolia	Paperbark	3.31	4.86	1.30	8.00	0.88	0.75	85	3.07
28	Malaleuca linariifolia	Paperbark	3.34	4.86	1.14	7.00	0.88	0.75	80	3.14
29	Malaleuca linariifolia	Paperbark	3.34	4.86	1.10	7.00	0.90	0.75	80	3.14
30	Malaleuca linariifolia	Paperbark	3.50	4.86	1.30	7.00	0.95	0.60	80	3.50
31	Malaleuca linariifolia	Paperbark	3.57	4.86	1.27	7.00	0.95	0.60	80	3.64
32	Malaleuca linariifolia	Paperbark	3.44	4.86	1.58	7.00	0.95	0.60	80	3.35
33	Malaleuca linariifolia	Paperbark	3.37	4.86	1.32	7.00	0.85	0.60	80	3.21
34	Malaleuca linariifolia	Paperbark	3.37	5.32	1.35	7.00	0.85	1.00	80	3.21
35	Malaleuca linariifolia	Paperbark	3.12	5.32	1.45	5.00	0.80	1.00	80	2.68
36	Malaleuca linariifolia	Paperbark	3.10	5.06	1.13	5.00	0.80	1.00	80	2.64
37	Malaleuca linariifolia	Paperbark	3.26	5.42	1.15	5.00	0.80	0.98	75	2.97
38	Malaleuca linariifolia	Paperbark	3.26	4.93	1.12	5.00	0.80	0.95	75	2.97
39	Malaleuca linariifolia	Paperbark	3.50	2.82	1.29	8.00	1.00	0.75	80	3.50
40	Malaleuca linariifolia	Paperbark	3.82	5.13	1.37	8.00	1.00	0.75	75	4.28
41	Malaleuca linariifolia	Paperbark	3.82	4.86	1.78	8.00	1.00	0.75	80	4.28
42	Malaleuca linariifolia	Paperbark	4.14	4.81	1.25	8.00	1.00	1.00	85	5.15
43	Malaleuca linariifolia	Paperbark	4.04	4.86	1.15	8.00	1.00	1.00	85	4.88
44	Eucalyptus sideroxylon	Red Ironbark	11.78	21.65	1.09	5.00	1.50	1.00	50	55.29
45	Eucalyptus sideroxylon	Red Ironbark	15.28	24.02	2.33	5.00	1.00	1.00	50	102.90
46	Eucalyptus micrantha	Scribbly Gum	32.63	18.18	4.41	5.00	5.00	6.00	30	613.98
47	Eucalyptus micrantha	Scribbly Gum	43.61	19.90	12.50	10.00	6.00	5.00	50	1202.03
48	Eucalyptus sideroxylon	Red Ironbark	10.03	8.14	1.73	6.00	2.00	2.00	40	37.65
49	Eucalyptus micrantha	Scribbly Gum	42.97	18.77	11.05	10.00	8.00	7.00	55	1161.79
50	Eucalyptus sideroxylon	Red Ironbark	11.78	6.99	1.82	8.00	1.00	1.00	60	55.29
51	Eucalyptus sideroxylon	Red Ironbark	10.19	5.15	1.85	5.00	2.50	2.00	65	39.10
52	Malaleuca linariifolia	Paperbark	8.28	3.45	1.44	5.00	2.00	1.00	65	25.62
53	Malaleuca linariifolia	Paperbark	7.32	3.11	1.13	6.00	1.75	1.00	65	19.29
54	Malaleuca linariifolia	Paperbark	7.96	3.37	1.28	6.00	1.75	1.25	65	23.40
55	Malaleuca linariifolia	Paperbark	8.59	3.41	1.43	5.00	2.00	1.50	55	27.96
56	Malaleuca linariifolia	Paperbark	8.67	3.45	1.25	5.00	2.00	1.00	50	28.57
57	Malaleuca linariifolia	Paperbark	8.34	3.45	1.15	5.00	2.25	1.00	70	26.08
58	Malaleuca linariifolia	Paperbark	8.44	3.46	1.23	6.00	2.20	1.00	70	26.78
59	Malaleuca linariifolia	Paperbark	8.05	3.10	1.18	6.00	2.00	1.00	70	24.05
60	Malaleuca linariifolia	Paperbark	8.40	3.45	1.85	5.00	2.50	2.00	65	26.55
61	Malaleuca linariifolia	Paperbark	8.28	3.29	1.44	5.00	2.00	1.00	65	25.62
62	Eucalyptus micrantha	Scribbly Gum	58.89	12.04	13.00	16.00	12.00	6.00	60	2409.84
63	Eucalyptus micrantha	Scribbly Gum	40.11	7.57	13.00	12.00	12.00	7.00	60	990.25
64	Eucalyptus robertsoni	Narrow-leaved Peppermint	8.91	3.27	1.42	8.00	1.00	0.60	60	21.68
65	Eucalyptus robertsoni	Narrow-leaved Peppermint	6.68	2.42	1.55	8.00	1.00	6.00	60	10.50
66	Eucalyptus ovata	Swamp Gum	8.28	2.08	1.49	20.00	1.00	0.50	80	25.62
67	Eucalyptus micrantha	Scribbly Gum	88.17	15.26	15.00	8.00	16.00	7.00	45	6136.65
68	Eucalyptus sideroxylon	Red Ironbark	14.64	5.64	3.76	6.00	3.00	2.00	60	92.96
	Total Dry Weight (kg)									18348.65
	Total Biomass (tons/ha)									583.98

Sample Plot No.12		Plot Size: 10 m radius	Collection Date: 23/09/98				Location: LL 33 47 35.7 N, 150 36 55 E			
							UTM 0279214 E, 6258192 N			
Tree #	**Scientific Name**	**Common Name**	**Dbh (cm)**	**Tht (m)**	**Cover (m)**	**ANBT**	**ABD (cm)**	**ABL (m)**	**ABAV (deg)**	**Total Tree Weight (kg)**
1	Eucalyptus resinifera	Red Mahogany	44.09	26.52	9.15	10.00	10.00	5.00	45	1290.59
2	Eucalyptus resinifera	Red Mahogany	26.74	20.51	4.25	10.00	6.00	5.00	45	391.26
3	Eucalyptus resinifera	Red Mahogany	14.64	10.61	2.42	10.00	4.00	3.00	45	92.96
4	Eucalyptus siderophloia	Broad-leaved Red Ironbark	8.59	8.32	4.33	6.00	3.00	3.00	60	26.06
5	Eucalyptus maculata	Spotted Gum	13.37	12.73	4.48	6.00	3.00	3.00	50	77.79
6	Eucalyptus siderophloia	Broad-leaved Red Ironbark	7.64	7.11	2.29	5.00	2.00	2.00	45	19.68
7	Eucalyptus siderophloia	Broad-leaved Red Ironbark	8.44	7.58	1.87	6.00	2.00	2.00	45	24.93
8	Eucalyptus sideroxylon	Red Ironbark	7.00	7.82	2.60	6.00	2.00	1.50	45	15.99
9	Eucalyptus siderophloia	Broad-leaved Red Ironbark	7.16	6.01	4.07	6.00	2.00	1.50	45	16.87
10	Eucalyptus resinifera	Red Mahogany	38.83	22.23	10.25	12.00	15.00	7.00	45	953.46
11	Eucalyptus sideroxylon	Red Ironbark	12.57	12.73	3.50	6.00	3.00	3.00	45	64.62
12	Eucalyptus creba	Narrow-leaved Red Ironbark	17.83	12.20	4.88	10.00	5.00	4.00	45	148.66
13	Eucalyptus sideroxylon	Red Ironbark	8.91	5.82	3.61	8.00	2.00	2.00	45	28.43
14	Eucalyptus sideroxylon	Red Ironbark	12.73	6.95	4.95	6.00	6.00	3.00	60	66.59
15	Eucalyptus siderophloia	Broad-leaved Red Ironbark	6.37	4.97	2.16	4.00	1.00	0.60	45	12.73
16	Eucalyptus creba	Narrow-leaved Red Ironbark	24.83	13.94	4.23	8.00	4.00	3.00	45	327.83
17	Eucalyptus sideroxylon	Red Ironbark	7.96	4.97	2.44	6.00	1.00	1.00	45	21.69
18	Eucalyptus sideroxylon	Red Ironbark	8.28	4.89	2.35	6.00	1.00	1.00	45	23.82
19	Eucalyptus maculata	Spotted Gum	8.59	7.80	2.79	8.00	1.50	2.00	75	27.96
20	Eucalyptus creba	Narrow-leaved Red Ironbark	4.30	4.03	1.28	4.00	1.50	2.00	68	4.98
21	Eucalyptus creba	Narrow-leaved Red Ironbark	4.46	3.96	1.37	5.00	1.00	0.50	70	5.44
22	Eucalyptus sideroxylon	Red Ironbark	8.12	8.50	2.58	8.00	1.00	1.00	55	22.74
23	Eucalyptus sideroxylon	Red Ironbark	7.96	8.03	2.75	8.00	3.00	2.50	60	21.69
24	Eucalyptus sideroxylon	Red Ironbark	8.28	8.50	2.57	8.00	2.00	1.50	60	23.82
25	Eucalyptus sideroxylon	Red Ironbark	12.10	9.01	3.97	8.00	2.00	1.50	50	58.92
26	Eucalyptus siderophloia	Broad-leaved Red Ironbark	12.41	6.66	3.37	8.00	3.00	2.00	45	62.69
27	Eucalyptus siderophloia	Broad-leaved Red Ironbark	7.00	5.69	3.15	5.00	2.00	1.50	45	15.99
28	Eucalyptus sideroxylon	Red Ironbark	13.37	7.29	3.29	6.00	3.00	2.00	45	74.82
29	Eucalyptus siderophloia	Broad-leaved Red Ironbark	6.68	4.94	2.82	6.00	2.00	1.50	45	14.31
30	Eucalyptus sideroxylon	Red Ironbark	4.46	4.13	1.97	6.00	1.00	1.00	45	5.44
31	Eucalyptus resinifera	Red Mahogany	27.69	16.96	4.93	12.00	8.00	4.00	45	425.44
32	Eucalyptus resinifera	Red Mahogany	41.38	19.87	9.30	10.00	12.00	6.00	45	1109.53
33	Eucalyptus resinifera	Red Mahogany	45.20	20.22	4.62	12.00	15.00	5.00	45	1369.80
34	Eucalyptus resinifera	Red Mahogany	32.79	25.11	6.55	10.00	12.00	6.00	45	636.54
35	Eucalyptus sideroxylon	Red Ironbark	11.78	17.25	4.35	8.00	4.00	3.00	45	55.29
36	Eucalyptus resinifera	Red Mahogany	22.60	19.25	4.67	10.00	10.00	3.00	45	261.93
	Total Dry Weight (kg)									7781.48
	Total Biomass (tons/ha)									247.66

Sample Plot No.13		Plot Size: 10 m radius	Collection Date: 25/10/98				Location: LL 33 47 58.1 N, 150 38 17.5 E			
							UTM 0281344 E, 6257585 N			
Tree #	**Scientific Name**	**Common Name**	**Dbh (cm)**	**Tht (m)**	**Cover (m)**	**ANBT**	**ABD (cm)**	**ABL (m)**	**ABAV (deg)**	**Total Tree Weight (kg)**
1	Eucalyptus creba	Narrow-leaved Red Ironbark	26.74	19.07	5.85	12.00	6.00	3.00	45	391.26
2	Eucalyptus creba	Narrow-leaved Red Ironbark	12.25	14.03	3.20	8.00	3.00	1.50	45	60.79
3	Eucalyptus saligna	Sydney Blue Gum	32.15	17.67	6.80	12.00	5.00	3.00	40	593.38
4	Eucalyptus creba	Narrow-leaved Red Ironbark	14.80	13.15	4.55	10.00	3.00	2.00	45	95.39
5	Eucalyptus creba	Narrow-leaved Red Ironbark	14.32	13.62	4.13	10.00	3.20	2.00	45	88.21
6	Eucalyptus creba	Narrow-leaved Red Ironbark	14.96	13.15	4.43	9.00	3.00	2.00	45	97.86
7	Eucalyptus creba	Narrow-leaved Red Ironbark	10.19	13.79	3.50	8.00	2.00	2.00	45	39.10
8	Eucalyptus creba	Narrow-leaved Red Ironbark	10.50	13.79	3.55	8.00	2.00	2.00	45	42.08
9	Eucalyptus creba	Narrow-leaved Red Ironbark	9.55	13.32	3.35	7.00	1.80	1.75	45	33.51
10	Eucalyptus creba	Narrow-leaved Red Ironbark	10.82	13.79	3.53	7.00	1.75	2.00	45	45.18
11	Eucalyptus creba	Narrow-leaved Red Ironbark	10.82	13.32	3.35	8.00	2.00	2.00	45	45.18
12	Eucalyptus creba	Narrow-leaved Red Ironbark	19.42	18.02	4.95	10.00	5.00	3.00	45	182.32
13	Eucalyptus creba	Narrow-leaved Red Ironbark	10.19	11.98	3.08	6.00	3.00	2.00	45	39.10
14	Eucalyptus creba	Narrow-leaved Red Ironbark	10.66	14.81	2.68	8.00	3.00	2.00	40	43.61
15	Eucalyptus creba	Narrow-leaved Red Ironbark	8.59	9.22	2.57	8.00	1.00	1.00	45	26.06
16	Eucalyptus saligna	Sydney Blue Gum	15.76	15.92	3.45	8.00	2.00	2.00	45	113.80
17	Eucalyptus saligna	Sydney Blue Gum	14.64	17.17	2.70	8.00	2.00	2.00	40	96.03
18	Eucalyptus creba	Narrow-leaved Red Ironbark	9.55	10.90	2.65	6.00	2.00	2.00	45	33.51
19	Eucalyptus creba	Narrow-leaved Red Ironbark	18.14	16.70	5.40	12.00	5.00	3.00	45	155.07
20	Eucalyptus creba	Narrow-leaved Red Ironbark	15.28	14.64	3.38	10.00	4.00	2.00	45	102.90
21	Eucalyptus saligna	Sydney Blue Gum	28.97	19.33	6.20	12.00	3.00	4.00	45	466.10
22	Eucalyptus creba	Narrow-leaved Red Ironbark	20.05	15.92	3.60	12.00	3.00	3.00	45	196.91
23	Eucalyptus creba	Narrow-leaved Red Ironbark	7.48	6.12	1.74	6.00	1.00	1.00	45	18.71
24	Eucalyptus creba	Narrow-leaved Red Ironbark	15.12	16.90	2.88	10.00	3.00	2.00	45	100.36
25	Eucalyptus saligna	Sydney Blue Gum	14.96	17.67	2.71	6.00	4.00	2.00	40	100.93
26	Eucalyptus creba	Narrow-leaved Red Ironbark	12.25	13.79	2.75	8.00	3.00	3.00	45	60.79
27	Eucalyptus creba	Narrow-leaved Red Ironbark	12.25	13.32	2.63	8.00	3.00	3.00	45	60.79
28	Eucalyptus creba	Narrow-leaved Red Ironbark	11.78	13.79	2.40	7.00	3.50	3.50	45	55.29
29	Eucalyptus creba	Narrow-leaved Red Ironbark	11.78	14.81	2.68	8.00	3.00	3.00	45	55.29
30	Eucalyptus creba	Narrow-leaved Red Ironbark	12.41	14.29	2.63	8.00	3.00	3.00	45	62.69
31	Eucalyptus creba	Narrow-leaved Red Ironbark	12.41	13.79	2.75	8.00	3.00	3.00	45	62.69
32	Eucalyptus creba	Narrow-leaved Red Ironbark	20.69	19.89	6.35	10.00	4.00	3.00	45	212.16
33	Eucalyptus saligna	Sydney Blue Gum	11.46	11.81	3.70	10.00	3.00	3.00	40	54.44
34	Eucalyptus saligna	Sydney Blue Gum	6.37	10.26	1.18	3.00	2.00	1.00	45	13.96
35	Eucalyptus creba	Narrow-leaved Red Ironbark	7.32	4.77	2.70	4.00	3.00	1.50	45	17.78
36	Eucalyptus creba	Narrow-leaved Red Ironbark	20.37	12.18	4.80	8.00	3.00	2.00	45	204.46
37	Eucalyptus creba	Narrow-leaved Red Ironbark	20.69	12.18	4.63	8.00	3.00	2.00	45	212.16
38	Eucalyptus creba	Narrow-leaved Red Ironbark	17.51	18.56	5.55	8.00	5.00	3.00	45	142.40
39	Eucalyptus creba	Narrow-leaved Red Ironbark	10.66	11.25	2.40	6.00	2.00	2.00	45	43.61
40	Eucalyptus saligna	Sydney Blue Gum	26.74	19.07	5.45	8.00	5.00	3.00	45	387.25
41	Eucalyptus saligna	Sydney Blue Gum	17.51	9.67	2.45	8.00	4.00	3.00	45	145.25
42	Eucalyptus saligna	Sydney Blue Gum	30.08	16.53	7.15	10.00	6.00	6.00	40	508.67
43	Eucalyptus creba	Narrow-leaved Red Ironbark	21.17	16.53	6.80	15.00	5.00	3.00	45	224.04
44	Eucalyptus creba	Narrow-leaved Red Ironbark	10.50	9.70	2.83	8.00	4.00	2.00	45	42.08
45	Eucalyptus saligna	Sydney Blue Gum	18.14	16.70	4.20	10.00	3.00	3.00	45	157.77
46	Eucalyptus creba	Narrow-leaved Red Ironbark	17.83	14.54	4.10	8.00	5.00	3.00	45	148.66
47	Eucalyptus creba	Narrow-leaved Red Ironbark	21.96	18.30	5.95	10.00	5.00	2.50	45	244.66
48	Eucalyptus creba	Narrow-leaved Red Ironbark	22.60	17.67	6.55	12.00	4.00	3.00	45	261.93
49	Eucalyptus saligna	Sydney Blue Gum	27.06	16.27	6.20	10.00	4.00	3.00	45	398.00
	Total Dry Weight (kg)									6988.43
	Total Biomass (tons/ha)									222.42

Sample Plot No.14		Plot Size: 10 m radius	Collection Date: 26/09/98				Location: LL 33 49 02.4 N, 150 37 13.4 E			
							UTM 0279679 E, 6255598 N			
Tree #	**Scientific Name**	**Common Name**	**Dbh (cm)**	**Tht (m)**	**Cover (m)**	**ANBT**	**ABD (cm)**	**ABL (m)**	**ABAV (deg)**	**Total Tree Weight (kg)**
1	Eucalyptus resinifera	Red Mahogany	43.13	32.65	6.55	12.00	12.00	5.00	45	1224.87
2	Eucalyptus maculata	Spotted Gum	14.64	14.91	3.94	6.00	5.00	5.00	45	96.03
3	Eucalyptus maculata	Spotted Gum	13.21	15.38	4.21	6.00	5.00	5.00	45	75.66
4	Eucalyptus maculata	Spotted Gum	16.87	28.09	4.73	6.00	6.00	5.00	45	133.31
5	Syncarpia glomulifera	Turpentine	5.89	10.69	3.99	12.00	2.00	2.00	80	10.57
6	Syncarpia glomulifera	Turpentine	15.44	21.36	5.60	12.00	4.00	3.00	75	105.47
7	Eucalyptus maculata	Spotted Gum	4.77	8.14	2.26	6.00	1.00	0.50	45	7.17
8	Syncarpia glomulifera	Turpentine	4.30	5.36	2.31	8.00	1.00	1.00	75	4.98
9	Syncarpia glomulifera	Turpentine	5.73	6.79	2.93	8.00	1.00	1.00	75	9.90
10	Syncarpia glomulifera	Turpentine	3.02	3.34	2.28	8.00	1.00	1.00	80	2.15
11	Syncarpia glomulifera	Turpentine	2.55	2.62	1.78	8.00	0.50	1.00	80	1.43
12	Syncarpia glomulifera	Turpentine	2.55	2.62	1.60	8.00	0.50	1.00	80	1.43
13	Syncarpia glomulifera	Turpentine	2.55	2.62	1.68	8.00	0.50	1.00	80	1.43
14	Syncarpia glomulifera	Turpentine	2.55	2.62	1.75	8.00	0.50	1.00	80	1.43
15	Syncarpia glomulifera	Turpentine	2.48	2.62	1.65	8.00	0.50	1.00	80	1.35
16	Syncarpia glomulifera	Turpentine	2.39	2.62	1.68	8.00	0.50	1.00	80	1.23
17	Syncarpia glomulifera	Turpentine	2.50	2.62	1.69	8.00	0.50	1.00	80	1.37
18	Syncarpia glomulifera	Turpentine	2.51	2.62	1.70	8.00	0.50	1.00	80	1.39
19	Syncarpia glomulifera	Turpentine	2.55	2.62	1.83	8.00	0.50	1.00	80	1.43
20	Syncarpia glomulifera	Turpentine	2.55	2.62	1.78	8.00	0.50	1.00	80	1.43
21	Syncarpia glomulifera	Turpentine	2.51	2.62	1.84	8.00	0.50	1.00	80	1.39
22	Syncarpia glomulifera	Turpentine	2.51	2.62	1.78	8.00	0.50	1.00	80	1.39
23	Syncarpia glomulifera	Turpentine	7.00	8.90	4.32	8.00	1.50	2.00	80	15.99
24	Eucalyptus maculata	Spotted Gum	6.37	3.80	2.53	6.00	1.00	1.00	60	13.96
25	Eucalyptus maculata	Spotted Gum	4.62	9.68	4.95	10.00	8.00	5.00	45	6.63
26	Eucalyptus resinifera	Red Mahogany	35.65	12.45	5.94	12.00	10.00	5.00	45	777.42
27	Eucalyptus sideroxylon	Red Ironbark	11.94	6.26	4.45	8.00	5.00	3.00	45	57.09
28	Eucalyptus sideroxylon	Red Ironbark	13.05	7.40	3.20	6.00	4.00	4.00	40	70.64
29	Eucalyptus resinifera	Red Mahogany	37.56	13.94	5.05	8.00	14.00	5.00	40	880.54
30	Eucalyptus resinifera	Red Mahogany	22.44	11.45	4.78	6.00	8.00	5.00	45	257.55
31	Eucalyptus sideroxylon	Red Ironbark	18.62	9.30	4.27	6.00	7.00	4.00	45	164.99
32	Callitris hugelii	White Cypress Pine	5.57	3.45	1.75	12.00	1.00	1.00	75	9.89
33	Callitris hugelii	White Cypress Pine	4.46	2.93	1.93	12.00	1.00	1.00	75	6.11
34	Eucalyptus paniculata	Grey Ironbark	14.32	7.91	2.78	6.00	4.00	4.00	45	88.21
35	Eucalyptus paniculata	Grey Ironbark	14.96	8.13	3.90	6.00	4.00	4.00	45	97.86
36	Eucalyptus sideroxylon	Red Ironbark	23.87	11.66	3.87	8.00	6.00	3.00	45	298.54
37	Eucalyptus resinifera	Red Mahogany	31.83	13.81	6.95	8.00	8.00	5.00	45	593.18
38	Eucalyptus sideroxylon	Red Ironbark	30.56	13.33	5.40	8.00	8.00	6.00	45	538.12
39	Eucalyptus sideroxylon	Red Ironbark	26.26	12.88	4.70	10.00	8.00	4.00	45	374.79
40	Callitris hugelii	White Cypress Pine	3.98	3.28	1.51	10.00	0.50	0.50	75	4.78
41	Eucalyptus resinifera	Red Mahogany	38.83	13.81	5.88	25.00	10.00	5.00	50	953.46
42	Syncarpia glomulifera	Turpentine	3.18	3.11	2.25	12.00	1.00	1.00	75	2.43
43	Callitris hugelii	White Cypress Pine	3.50	2.25	1.63	12.00	0.80	1.00	75	3.63
44	Eucalyptus sideroxylon	Red Ironbark	63.66	16.12	10.15	10.00	20.00	10.00	65	3102.11
45	Eucalyptus resinifera	Red Mahogany	22.28	24.50	5.58	10.00	6.00	4.00	45	253.21
46	Eucalyptus resinifera	Red Mahogany	47.43	24.50	7.75	12.00	8.00	4.00	45	1536.50
	Total Dry Weight (kg)									11764.59
	Total Biomass (tons/ha)									374.43

Sample Plot No.15		Plot Size: 10 m radius	Collection Date: 26/09/98				Location: LL 33 49 14.5 N, 150 37 04.5 E			
							UTM 0279538 E, 6255167 N			
Tree #	**Scientific Name**	**Common Name**	**Dbh (cm)**	**Tht (m)**	**Cover (m)**	**ANBT**	**ABD (cm)**	**ABL (m)**	**ABAV (deg)**	**Total Tree Weight (kg)**
1	Syncarpia glomulifera	Turpentine	28.01	14.92	5.08	30.00	6.00	2.50	80	437.21
2	Syncarpia glomulifera	Turpentine	3.50	3.66	2.35	8.00	1.00	1.50	80	3.06
3	Syncarpia glomulifera	Turpentine	23.87	3.47	1.32	8.00	1.00	1.00	80	298.54
4	Syncarpia glomulifera	Turpentine	3.34	3.47	2.23	8.00	1.50	1.50	80	2.74
5	Eucalyptus maculata	Spotted Gum	29.28	16.70	5.60	10.00	8.00	3.00	45	478.05
6	Eucalyptus paniculata	Grey Ironbark	14.32	14.70	3.51	8.00	2.00	1.50	50	88.21
7	Eucalyptus viminalis	Manna Gum	7.32	10.14	3.35	8.00	2.00	1.50	50	19.29
8	Eucalyptus viminalis	Manna Gum	3.82	7.02	1.75	6.00	1.00	1.00	50	4.28
9	Eucalyptus viminalis	Manna Gum	3.82	7.02	1.75	6.00	1.00	1.00	50	4.28
10	Syncarpia glomulifera	Turpentine	5.89	5.85	2.32	12.00	1.00	1.50	75	10.57
11	Syncarpia glomulifera	Turpentine	5.89	5.85	2.45	12.00	1.00	1.50	75	10.57
12	Syncarpia glomulifera	Turpentine	2.39	2.97	1.49	10.00	0.50	0.50	70	1.23
13	Syncarpia glomulifera	Turpentine	2.55	2.97	1.48	9.00	0.50	0.60	70	1.43
14	Syncarpia glomulifera	Turpentine	2.39	2.97	1.53	10.00	0.50	0.60	70	1.23
15	Syncarpia glomulifera	Turpentine	2.23	2.97	1.55	10.00	0.50	0.60	70	1.04
16	Eucalyptus paniculata	Grey Ironbark	16.07	15.88	3.94	8.00	5.00	3.00	45	116.15
17	Syncarpia glomulifera	Turpentine	3.98	6.46	2.03	8.00	1.00	1.00	60	4.15
18	Syncarpia glomulifera	Turpentine	3.98	6.46	2.15	8.00	1.00	1.00	60	4.15
19	Callitris hugelii	White Cypress Pine	5.09	5.51	2.56	5.00	3.00	0.80	45	8.15
20	Eucalyptus paniculata	Grey Ironbark	33.74	28.53	7.35	10.00	8.00	6.00	45	681.69
21	Callitris hugelii	White Cypress Pine	3.82	4.30	1.51	8.00	1.00	1.00	45	4.38
22	Eucalyptus paniculata	Grey Ironbark	22.92	12.87	3.77	8.00	4.00	3.00	45	270.82
23	Eucalyptus sideroxylon	Red Ironbark	21.01	19.07	5.95	8.00	5.00	4.00	40	220.04
24	Syncarpia glomulifera	Turpentine	4.30	4.01	1.60	8.00	0.50	1.00	60	4.98
25	Syncarpia glomulifera	Turpentine	2.55	3.30	1.41	8.00	0.50	0.60	60	1.43
26	Syncarpia glomulifera	Turpentine	2.86	3.30	1.39	8.00	0.50	0.80	60	1.89
27	Eucalyptus paniculata	Grey Ironbark	15.44	10.93	2.64	10.00	4.00	3.00	45	105.47
28	Eucalyptus ovata	Swamp Gum	4.14	2.00	1.15	5.00	1.00	1.00	45	5.15
29	Eucalyptus sideroxylon	Red Ironbark	4.93	3.30	1.73	6.00	0.60	0.80	45	6.93
30	Eucalyptus paniculata	Grey Ironbark	9.55	5.45	3.75	8.00	2.00	2.00	45	33.51
31	Eucalyptus sideroxylon	Red Ironbark	29.28	13.03	6.60	10.00	6.00	4.00	45	486.14
32	Eucalyptus longifolia	Woollybutt	35.01	12.20	11.35	15.00	12.00	5.00	45	744.70
33	Eucalyptus maculata	Spotted Gum	21.33	7.58	5.15	10.00	8.00	4.00	45	229.40
34	Eucalyptus maculata	Spotted Gum	7.64	7.13	2.85	8.00	1.00	1.50	45	21.29
35	Eucalyptus maculata	Spotted Gum	5.73	4.63	1.83	8.00	1.00	1.50	45	10.94
36	Eucalyptus maculata	Spotted Gum	7.80	6.45	2.39	8.00	1.00	1.50	45	22.33
37	Eucalyptus resinifera	Red Mahogany	29.13	8.50	5.65	8.00	12.00	5.00	45	479.86
38	Eucalyptus resinifera	Red Mahogany	33.42	14.97	7.50	10.00	12.00	5.00	45	666.44
39	Eucalyptus resinifera	Red Mahogany	31.83	13.94	5.80	10.00	12.00	5.00	45	593.18
40	Eucalyptus resinifera	Red Mahogany	21.33	12.60	8.15	8.00	10.00	5.00	45	228.08
41	Eucalyptus longifolia	Woollybutt	31.35	9.50	14.00	8.00	10.00	6.00	45	572.17
42	Callitris hugelii	White Cypress Pine	4.14	3.16	1.40	15.00	1.00	0.80	65	5.20
43	Callitris hugelii	White Cypress Pine	3.82	3.16	1.63	12.00	1.00	0.80	65	4.38
44	Callitris hugelii	White Cypress Pine	4.14	3.16	1.43	16.00	0.85	0.50	65	5.20
45	Callitris hugelii	White Cypress Pine	3.50	3.16	1.48	14.00	0.85	0.75	65	3.63
46	Callitris hugelii	White Cypress Pine	4.14	3.16	1.30	13.00	0.90	0.75	65	5.20
47	Callitris hugelii	White Cypress Pine	4.46	3.16	1.55	15.00	0.90	0.80	65	6.11
48	Callitris hugelii	White Cypress Pine	4.30	3.16	1.38	12.00	1.00	0.80	65	5.65
49	Callitris hugelii	White Cypress Pine	4.46	3.16	1.45	15.00	1.00	0.80	65	6.11
	Total Dry Weight (kg)									6930.94
	Total Biomass (tons/ha)									220.59

Sample Plot No. 16		Plot Size: 10 m radius	Collection Date: 25/10/98				Location: LL 33 47 31.9 N, 150 38 16.9 E			
							UTM 0281333 E, 6258388 N			
Tree #	**Scientific Name**	**Common Name**	**Dbh (cm)**	**Tht (m)**	**Cover (m)**	**ANBT**	**ABD (cm)**	**ABL (m)**	**ABAV (deg)**	**Total Tree Weight (kg)**
1	Eucalyptus longifolia	Woollybutt	10.50	14.00	3.30	6.00	2.00	2.00	50	42.08
2	Eucalyptus saligna	Sydney Blue Gum	13.05	14.24	4.65	6.00	2.00	2.50	50	73.57
3	Eucalyptus longifolia	Woollybutt	5.73	5.63	1.70	6.00	1.00	1.00	45	9.90
4	Eucalyptus resinifera	Red Mahogany	25.46	17.44	6.50	8.00	7.00	3.00	45	348.25
5	Eucalyptus sideroxylon	Red Ironbark	12.10	12.98	2.45	8.00	0.50	1.00	50	58.92
6	Eucalyptus resinifera	Red Mahogany	30.24	18.05	7.55	8.00	8.00	3.00	45	524.83
7	Eucalyptus sideroxylon	Red Ironbark	13.05	12.58	3.15	8.00	1.00	1.50	45	70.64
8	Eucalyptus resinifera	Red Mahogany	25.31	14.31	6.85	10.00	7.00	3.00	45	343.08
9	Eucalyptus longifolia	Woollybutt	6.21	6.16	1.55	8.00	1.00	0.80	80	11.99
10	Eucalyptus resinifera	Red Mahogany	12.41	12.09	3.45	10.00	1.50	1.50	45	62.69
11	Eucalyptus resinifera	Red Mahogany	12.73	11.72	3.38	10.00	1.50	1.50	45	66.59
12	Eucalyptus resinifera	Red Mahogany	12.41	12.09	3.40	10.00	1.50	1.50	45	62.69
13	Eucalyptus resinifera	Red Mahogany	12.41	12.09	3.00	10.00	1.50	1.50	45	62.69
14	Eucalyptus longifolia	Woollybutt	9.87	9.99	2.60	8.00	2.00	1.50	45	36.24
15	Eucalyptus longifolia	Woollybutt	9.87	9.99	2.38	8.00	2.00	1.50	45	36.24
16	Eucalyptus longifolia	Woollybutt	9.55	11.18	2.54	8.00	2.00	1.50	45	33.51
17	Eucalyptus longifolia	Woollybutt	9.55	10.53	2.45	8.00	2.00	1.50	45	33.51
18	Eucalyptus sideroxylon	Red Ironbark	8.12	9.81	2.20	8.00	1.00	1.00	45	22.74
19	Eucalyptus sideroxylon	Red Ironbark	8.12	9.81	2.20	8.00	1.00	1.00	45	22.74
20	Eucalyptus sideroxylon	Red Ironbark	7.96	8.96	2.15	8.00	1.00	1.00	45	21.69
21	Eucalyptus sideroxylon	Red Ironbark	7.96	8.96	2.30	8.00	1.00	1.00	45	21.69
22	Eucalyptus sideroxylon	Red Ironbark	7.96	9.39	2.30	8.00	1.00	1.00	45	21.69
23	Eucalyptus sideroxylon	Red Ironbark	7.96	8.96	2.28	8.00	1.00	1.00	45	21.69
24	Eucalyptus sideroxylon	Red Ironbark	8.28	7.71	2.30	8.00	1.00	1.00	45	23.82
25	Eucalyptus sideroxylon	Red Ironbark	7.64	7.71	2.30	8.00	1.00	1.00	45	19.68
26	Eucalyptus sideroxylon	Red Ironbark	8.28	7.71	2.20	8.00	1.00	1.00	45	23.82
27	Eucalyptus sideroxylon	Red Ironbark	8.28	7.71	2.20	8.00	1.00	1.00	45	23.82
28	Eucalyptus sideroxylon	Red Ironbark	7.64	9.81	2.38	8.00	1.00	1.00	45	19.68
29	Eucalyptus sideroxylon	Red Ironbark	7.00	9.81	2.20	8.00	1.00	1.00	45	15.99
30	Eucalyptus sideroxylon	Red Ironbark	7.00	9.81	2.20	8.00	1.00	1.00	45	15.99
31	Eucalyptus sideroxylon	Red Ironbark	7.32	9.81	2.25	8.00	1.00	1.00	45	17.78
32	Eucalyptus sideroxylon	Red Ironbark	7.32	9.50	2.25	8.00	1.00	1.00	45	17.78
33	Eucalyptus sideroxylon	Red Ironbark	7.32	9.50	2.25	8.00	1.00	1.00	45	17.78
34	Eucalyptus sideroxylon	Red Ironbark	7.64	9.50	2.30	8.00	1.00	1.00	45	19.68
35	Eucalyptus sideroxylon	Red Ironbark	7.64	8.76	2.30	8.00	1.00	1.00	45	19.68
36	Eucalyptus sideroxylon	Red Ironbark	7.64	8.76	2.38	8.00	1.00	1.00	45	19.68
37	Eucalyptus sideroxylon	Red Ironbark	7.64	8.76	2.35	8.00	1.00	1.00	45	19.68
38	Eucalyptus sideroxylon	Red Ironbark	7.96	8.76	2.38	8.00	1.00	1.00	45	21.69
39	Eucalyptus sideroxylon	Red Ironbark	7.96	9.81	2.20	8.00	1.00	1.00	45	21.69
40	Eucalyptus sideroxylon	Red Ironbark	7.96	9.81	2.20	8.00	1.00	1.00	45	21.69
41	Eucalyptus sideroxylon	Red Ironbark	7.64	9.81	2.20	8.00	1.00	1.00	45	19.68
42	Eucalyptus sideroxylon	Red Ironbark	7.96	9.81	2.20	8.00	1.00	1.00	45	21.69
43	Eucalyptus resinifera	Red Mahogany	18.14	19.07	5.20	10.00	3.00	2.50	45	155.07
44	Eucalyptus sideroxylon	Red Ironbark	16.23	11.89	1.65	6.00	3.00	2.50	40	118.92
45	Eucalyptus sideroxylon	Red Ironbark	17.19	16.17	4.65	6.00	5.00	3.00	40	136.30
46	Eucalyptus longifolia	Woollybutt	44.25	26.39	8.80	10.00	8.00	5.00	45	1301.74
47	Eucalyptus resinifera	Red Mahogany	31.51	22.81	8.85	12.00	6.00	3.50	45	579.12
48	Eucalyptus sideroxylon	Red Ironbark	15.60	14.70	4.00	8.00	3.00	2.50	45	108.09
49	Eucalyptus sideroxylon	Red Ironbark	15.12	11.12	1.95	8.00	2.00	3.00	40	100.36
50	Eucalyptus resinifera	Red Mahogany	20.21	22.03	2.95	10.00	3.00	2.50	45	200.66
51	Eucalyptus resinifera	Red Mahogany	27.37	24.64	7.35	10.00	6.00	3.00	45	413.86
52	Eucalyptus resinifera	Red Mahogany	21.01	13.81	4.00	6.00	3.00	2.00	45	220.04
53	Eucalyptus resinifera	Red Mahogany	24.51	19.07	6.70	10.00	5.00	3.50	45	317.89
54	Eucalyptus resinifera	Red Mahogany	25.15	21.19	6.70	10.00	4.00	4.00	45	337.95
55	Eucalyptus resinifera	Red Mahogany	29.92	24.64	12.75	12.00	6.00	3.50	45	511.75
56	Eucalyptus resinifera	Red Mahogany	19.42	20.45	4.85	10.00	5.00	3.00	40	182.32
57	Eucalyptus saligna	Sydney Blue Gum	22.12	22.03	6.45	19.00	5.00	3.00	45	249.70
58	Eucalyptus resinifera	Red Mahogany	16.07	19.39	4.70	6.00	5.00	4.00	45	116.15
59	Eucalyptus sideroxylon	Red Ironbark	12.57	13.39	1.50	10.00	1.00	0.80	50	64.62
60	Eucalyptus resinifera	Red Mahogany	14.01	18.63	3.80	12.00	3.00	2.00	45	83.60
61	Eucalyptus resinifera	Red Mahogany	23.71	27.10	6.20	10.00	3.00	2.50	45	293.81
62	Eucalyptus longifolia	Woollybutt	23.87	15.17	4.65	8.00	5.00	3.00	45	298.54
63	Eucalyptus sideroxylon	Red Ironbark	12.89	11.95	2.45	10.00	1.00	1.00	45	68.60
64	Eucalyptus resinifera	Red Mahogany	15.44	13.44	2.45	10.00	2.00	2.00	45	105.47
65	Eucalyptus sideroxylon	Red Ironbark	11.62	11.83	1.50	8.00	2.00	3.00	45	53.52
	Total Dry Weight (kg)									8414.28
	Total Biomass (tons/ha)									267.80

Sample Plot No. 17		Plot Size: 10 m radius	Collection Date: 27/09/98				Location: LL 33 48 29.6 N, 150 37 44.3 E			
							UTM 0280542 E, 6256572 N			
Tree #	**Scientific Name**	**Common Name**	**Dbh (cm)**	**Tht (m)**	**Cover (m)**	**ANBT**	**ABD (cm)**	**ABL (m)**	**ABAV (deg)**	**Total Tree Weight (kg)**
1	Eucalyptus sideroxylon	Red Ironbark	22.60	13.13	3.02	6.00	6.00	5.00	40	261.93
2	Syncarpia glomulifera	Turpentine	9.71	8.66	3.59	15.00	2.00	2.00	85	34.86
3	Syncarpia glomulifera	Turpentine	13.37	7.82	3.28	15.00	2.00	2.00	80	74.82
4	Syncarpia glomulifera	Turpentine	22.44	15.17	4.15	15.00	5.00	3.00	50	257.55
5	Eucalyptus sideroxylon	Red Ironbark	21.96	15.17	2.16	4.00	4.00	3.00	45	244.66
6	Eucalyptus sideroxylon	Red Ironbark	22.92	10.12	4.04	3.00	1.50	3.00	45	270.82
7	Eucalyptus paniculata	Grey Ironbark	14.64	21.19	2.83	8.00	6.00	3.00	45	92.96
8	Callitris hugelii	White Cypress Pine	10.82	5.74	3.63	6.00	6.00	3.00	45	41.57
9	Eucalyptus robertsoni	Narrow-leaved Peppermint	39.95	24.64	7.65	8.00	8.00	5.00	50	950.06
10	Syncarpia glomulifera	Turpentine	25.15	14.78	5.65	30.00	4.00	3.00	80	337.95
11	Syncarpia glomulifera	Turpentine	3.82	4.58	2.40	8.00	1.00	1.50	50	3.76
12	Syncarpia glomulifera	Turpentine	3.66	4.58	2.63	8.00	1.00	1.50	50	3.40
13	Syncarpia glomulifera	Turpentine	3.82	4.58	2.48	8.00	1.00	1.50	50	3.76
14	Syncarpia glomulifera	Turpentine	3.50	4.58	2.28	8.00	1.00	1.50	50	3.06
15	Syncarpia glomulifera	Turpentine	3.82	4.58	2.40	8.00	1.00	1.50	50	3.76
16	Syncarpia glomulifera	Turpentine	3.50	4.58	2.40	8.00	1.00	1.50	50	3.06
17	Syncarpia glomulifera	Turpentine	4.77	7.71	3.03	12.00	1.00	1.50	80	6.41
18	Syncarpia glomulifera	Turpentine	4.46	7.71	3.15	12.00	1.00	1.50	80	5.44
19	Syncarpia glomulifera	Turpentine	4.77	7.71	3.03	12.00	1.00	1.50	80	6.41
20	Syncarpia glomulifera	Turpentine	4.62	7.71	2.85	12.00	1.00	1.50	80	5.91
21	Syncarpia glomulifera	Turpentine	4.70	7.71	3.00	12.00	1.00	1.50	80	6.16
22	Syncarpia glomulifera	Turpentine	7.48	10.78	3.02	12.00	1.50	1.50	80	18.71
23	Syncarpia glomulifera	Turpentine	10.98	9.19	3.40	12.00	1.50	1.50	80	46.78
24	Eucalyptus sideroxylon	Red Ironbark	16.87	14.45	3.28	6.00	4.00	2.00	45	130.35
25	Eucalyptus sideroxylon	Red Ironbark	18.46	15.38	3.51	6.00	4.00	2.50	45	161.65
26	Eucalyptus sideroxylon	Red Ironbark	22.92	13.55	5.60	10.00	5.00	4.00	45	270.82
27	Eucalyptus sideroxylon	Red Ironbark	25.15	14.31	6.95	8.00	5.00	4.00	45	337.95
28	Callitris hugelii	White Cypress Pine	7.80	4.05	3.38	6.00	5.00	2.50	45	20.47
29	Eucalyptus sideroxylon	Red Ironbark	13.85	8.61	3.90	6.00	3.00	3.00	45	81.35
30	Eucalyptus sideroxylon	Red Ironbark	23.71	8.49	10.65	8.00	5.00	4.00	45	293.81
31	Eucalyptus sideroxylon	Red Ironbark	24.19	9.32	10.75	8.00	5.00	4.00	45	308.13
32	Syncarpia glomulifera	Turpentine	22.92	11.04	4.45	15.00	4.00	2.00	80	270.82
33	Syncarpia glomulifera	Turpentine	33.74	13.87	6.65	15.00	4.00	3.00	80	681.69
34	Syncarpia glomulifera	Turpentine	23.71	11.89	4.80	15.00	4.00	2.00	80	293.81
35	Callitris hugelii	White Cypress Pine	14.01	10.60	3.50	20.00	1.50	1.50	45	72.58
36	Syncarpia glomulifera	Turpentine	19.74	12.87	3.38	15.00	2.00	1.50	45	189.54
37	Eucalyptus sideroxylon	Red Ironbark	15.92	9.01	2.94	8.00	4.00	4.00	45	113.43
38	Syncarpia glomulifera	Turpentine	27.85	15.13	6.05	20.00	4.00	3.00	65	431.30
39	Syncarpia glomulifera	Turpentine	4.46	5.96	2.59	10.00	1.50	1.50	80	5.44
40	Syncarpia glomulifera	Turpentine	4.30	5.96	2.70	10.00	1.50	1.50	80	4.98
41	Syncarpia glomulifera	Turpentine	4.77	5.96	2.88	10.00	1.50	1.50	80	6.41
42	Syncarpia glomulifera	Turpentine	4.46	5.96	2.70	10.00	1.50	1.50	80	5.44
43	Syncarpia glomulifera	Turpentine	4.77	5.96	2.70	10.00	1.50	1.50	80	6.41
44	Eucalyptus resinifera	Red Mahogany	25.15	15.13	5.95	10.00	6.00	5.00	45	337.95
45	Eucalyptus resinifera	Red Mahogany	28.81	13.28	6.05	10.00	8.00	6.00	45	467.44
46	Syncarpia glomulifera	Turpentine	20.37	13.87	5.95	10.00	6.00	3.50	75	204.46
47	Syncarpia glomulifera	Turpentine	15.92	11.53	4.80	15.00	6.00	3.50	75	113.43
48	Syncarpia glomulifera	Turpentine	16.23	10.61	4.65	15.00	3.00	2.50	80	118.92
49	Callitris hugelii	White Cypress Pine	31.83	12.10	8.20	20.00	4.00	5.00	50	428.02
50	Callitris hugelii	White Cypress Pine	21.01	9.28	12.85	15.00	6.00	3.00	40	174.35
51	Eucalyptus sideroxylon	Red Ironbark	28.97	11.02	4.85	6.00	8.00	3.00	45	473.62
52	Eucalyptus sideroxylon	Red Ironbark	12.41	7.51	2.98	6.00	5.00	3.00	45	62.69
53	Callitris hugelii	White Cypress Pine	12.73	6.26	4.19	6.00	3.00	2.50	45	59.06
54	Callitris hugelii	White Cypress Pine	6.68	5.69	1.80	6.00	1.00	2.00	45	14.67
55	Eucalyptus paniculata	Grey Ironbark	10.50	6.37	2.43	6.00	1.50	2.50	45	42.08
56	Callitris hugelii	White Cypress Pine	6.84	6.79	2.44	8.00	1.00	1.50	45	15.44
57	Callitris hugelii	White Cypress Pine	20.69	10.29	5.75	20.00	4.00	4.00	50	168.69
	Total Dry Weight (kg)									9056.82
	Total Biomass (tons/ha)									288.25

Sample Plot No. 18		Plot Size: 10 m radius	Collection Date: 27/09/98				Location: LL 33 48 36.4 N, 150 37 44.1 E			
							UTM 0280529 E, 6256366 N			
Tree #	**Scientific Name**	**Common Name**	**Dbh (cm)**	**Tht (m)**	**Cover (m)**	**ANBT**	**ABD (cm)**	**ABL (m)**	**ABAV (deg)**	**Total Tree Weight (kg)**
1	Eucalyptus paniculata	Grey Ironbark	12.41	6.26	3.90	4.00	5.00	3.00	45	62.69
2	Eucalyptus paniculata	Grey Ironbark	14.32	5.44	4.00	5.00	6.00	3.00	45	88.21
3	Eucalyptus paniculata	Grey Ironbark	19.42	7.83	4.00	6.00	6.00	3.00	45	182.32
4	Eucalyptus paniculata	Grey Ironbark	16.55	6.44	4.13	6.00	6.00	3.00	45	124.56
5	Eucalyptus paniculata	Grey Ironbark	13.69	6.81	4.10	5.00	6.00	3.00	45	79.14
6	Eucalyptus sideroxylon	Red Ironbark	19.10	7.69	4.65	6.00	5.00	3.00	45	175.27
7	Eucalyptus creba	Narrow-leaved Red Ironbark	10.50	5.13	2.70	4.00	4.00	2.00	45	42.08
8	Eucalyptus paniculata	Grey Ironbark	8.91	4.53	1.37	5.00	1.00	1.50	45	28.43
9	Eucalyptus creba	Narrow-leaved Red Ironbark	13.21	7.26	3.47	6.00	4.00	3.00	45	72.71
10	Eucalyptus paniculata	Grey Ironbark	14.32	7.91	2.92	6.00	3.00	3.00	45	88.21
11	Callitris hugelii	White Cypress Pine	8.75	2.78	3.15	6.00	3.00	2.00	65	26.28
12	Callitris hugelii	White Cypress Pine	7.80	3.27	3.40	6.00	3.00	2.00	60	20.47
13	Callitris hugelii	White Cypress Pine	14.32	3.62	4.65	8.00	3.50	2.00	60	76.19
14	Eucalyptus sideroxylon	Red Ironbark	18.46	11.10	5.35	8.00	4.00	3.00	45	161.65
15	Eucalyptus sideroxylon	Red Ironbark	20.05	11.10	5.35	8.00	4.00	3.00	45	196.91
16	Eucalyptus sideroxylon	Red Ironbark	21.33	8.75	5.25	8.00	4.00	3.00	45	228.08
17	Eucalyptus creba	Narrow-leaved Red Ironbark	11.78	7.51	2.05	5.00	2.00	2.00	45	55.29
18	Eucalyptus creba	Narrow-leaved Red Ironbark	8.12	6.86	1.51	5.00	1.00	2.00	45	22.74
19	Eucalyptus creba	Narrow-leaved Red Ironbark	10.35	5.96	1.10	5.00	2.00	2.00	45	40.57
20	Eucalyptus creba	Narrow-leaved Red Ironbark	8.59	6.45	1.15	5.00	2.00	2.00	45	26.06
21	Eucalyptus creba	Narrow-leaved Red Ironbark	7.32	9.01	1.23	5.00	2.00	2.00	45	17.78
22	Eucalyptus creba	Narrow-leaved Red Ironbark	11.78	10.72	1.44	5.00	2.00	2.00	45	55.29
23	Eucalyptus creba	Narrow-leaved Red Ironbark	15.12	11.73	4.15	5.00	2.00	2.00	45	100.36
24	Eucalyptus creba	Narrow-leaved Red Ironbark	13.53	8.96	2.58	5.00	2.00	2.00	45	76.96
25	Eucalyptus creba	Narrow-leaved Red Ironbark	15.92	7.47	4.00	5.00	2.00	2.00	45	113.43
26	Eucalyptus creba	Narrow-leaved Red Ironbark	13.37	7.73	3.50	5.00	2.00	2.00	45	74.82
27	Eucalyptus creba	Narrow-leaved Red Ironbark	13.69	6.45	3.30	5.00	2.00	2.00	45	79.14
28	Eucalyptus creba	Narrow-leaved Red Ironbark	15.28	6.26	3.80	5.00	2.00	2.00	45	102.90
29	Eucalyptus creba	Narrow-leaved Red Ironbark	9.23	6.26	2.00	5.00	2.00	2.00	45	30.91
30	Eucalyptus creba	Narrow-leaved Red Ironbark	9.07	6.75	2.05	5.00	2.00	2.00	45	29.65
31	Eucalyptus creba	Narrow-leaved Red Ironbark	10.03	6.29	1.05	5.00	2.00	1.00	45	37.65
32	Eucalyptus creba	Narrow-leaved Red Ironbark	8.59	6.29	0.85	5.00	2.00	1.00	45	26.06
33	Callitris hugelii	White Cypress Pine	5.73	3.33	1.31	8.00	1.50	1.00	45	10.51
34	Eucalyptus creba	Narrow-leaved Red Ironbark	13.21	12.20	3.15	4.00	3.00	2.00	45	72.71
35	Eucalyptus creba	Narrow-leaved Red Ironbark	9.55	12.20	3.15	4.00	3.00	1.00	45	33.51
36	Eucalyptus creba	Narrow-leaved Red Ironbark	11.46	8.33	3.15	4.00	3.00	1.00	45	51.79
37	Eucalyptus creba	Narrow-leaved Red Ironbark	10.50	11.12	3.15	4.00	3.00	1.00	45	42.08
38	Eucalyptus creba	Narrow-leaved Red Ironbark	15.28	8.05	3.15	4.00	3.00	1.00	45	102.90
39	Eucalyptus sideroxylon	Red Ironbark	9.87	9.19	1.88	6.00	1.50	1.00	45	36.24
40	Eucalyptus paniculata	Grey Ironbark	19.42	15.66	2.30	6.00	5.00	3.00	45	182.32
41	Eucalyptus paniculata	Grey Ironbark	10.82	8.05	1.40	6.00	1.00	1.00	45	45.18
42	Eucalyptus sideroxylon	Red Ironbark	22.28	14.31	5.20	8.00	5.00	4.00	45	253.21
43	Eucalyptus sideroxylon	Red Ironbark	14.96	13.44	3.10	6.00	4.00	3.00	45	97.86
44	Eucalyptus paniculata	Grey Ironbark	19.10	15.17	2.90	6.00	5.00	3.00	45	175.27
45	Eucalyptus paniculata	Grey Ironbark	18.14	13.81	2.23	6.00	3.00	2.00	45	155.07
46	Eucalyptus paniculata	Grey Ironbark	10.76	7.24	1.13	5.00	1.00	0.60	45	44.55
47	Callitris hugelii	White Cypress Pine	7.32	3.90	1.39	6.00	3.00	1.00	45	17.86
48	Eucalyptus paniculata	Grey Ironbark	13.21	10.12	2.80	10.00	3.00	3.00	40	72.71
49	Callitris hugelii	White Cypress Pine	10.35	5.36	1.80	4.00	3.00	1.00	45	37.71
50	Callitris hugelii	White Cypress Pine	9.55	5.36	1.83	4.00	3.00	1.00	45	31.72
51	Callitris hugelii	White Cypress Pine	10.82	5.36	1.80	4.00	3.00	1.00	45	41.57
52	Callitris hugelii	White Cypress Pine	11.46	5.36	1.78	4.00	3.00	1.00	45	47.03
53	Callitris hugelii	White Cypress Pine	11.14	5.36	1.80	4.00	3.00	1.00	45	44.26
54	Eucalyptus creba	Narrow-leaved Red Ironbark	10.82	8.83	1.78	6.00	3.00	2.00	45	45.18
55	Eucalyptus creba	Narrow-leaved Red Ironbark	9.71	9.15	2.48	5.00	3.00	2.00	45	34.86
56	Eucalyptus creba	Narrow-leaved Red Ironbark	11.46	6.46	1.85	6.00	2.00	1.00	45	51.79
57	Eucalyptus sideroxylon	Red Ironbark	22.28	21.28	2.34	6.00	5.00	2.00	45	253.21
58	Eucalyptus resinifera	Red Mahogany	30.88	22.08	5.00	10.00	3.00	4.00	45	551.59
59	Eucalyptus resinifera	Red Mahogany	37.88	29.13	8.20	10.00	5.00	3.00	45	898.46
60	Eucalyptus sideroxylon	Red Ironbark	21.33	22.82	5.40	10.00	4.00	3.00	45	228.08

Sample Plot No. 18		Plot Size: 10 m radius	Collection Date: 27/09/98				Location: LL 33 48 36.4 N, 150 37 44.1 E			
							UTM 0280529 E, 6256366 N			
Tree #	**Scientific Name**	**Common Name**	**Dbh (cm)**	**Tht (m)**	**Cover (m)**	**ANBT**	**ABD (cm)**	**ABL (m)**	**ABAV (deg)**	**Total Tree Weight (kg)**
61	Eucalyptus creba	Narrow-leaved Red Ironbark	15.60	12.98	2.16	8.00	5.00	4.00	45	108.09
62	Eucalyptus creba	Narrow-leaved Red Ironbark	12.73	12.20	3.00	6.00	3.00	2.00	45	66.59
63	Eucalyptus creba	Narrow-leaved Red Ironbark	8.44	10.78	1.52	6.00	3.00	2.00	45	24.93
64	Eucalyptus creba	Narrow-leaved Red Ironbark	11.46	7.47	2.40	5.00	2.00	1.00	45	51.79
65	Eucalyptus sideroxylon	Red Ironbark	25.15	28.53	2.11	8.00	6.00	3.00	45	337.95
66	Eucalyptus sideroxylon	Red Ironbark	19.74	27.43	2.45	8.00	5.00	3.00	45	189.54
67	Eucalyptus sideroxylon	Red Ironbark	19.74	26.39	2.95	8.00	4.00	3.00	45	189.54
68	Eucalyptus sideroxylon	Red Ironbark	18.14	15.99	2.50	6.00	5.00	3.00	45	155.07
69	Eucalyptus sideroxylon	Red Ironbark	14.01	15.99	2.15	6.00	4.00	3.00	45	83.60
70	Eucalyptus sideroxylon	Red Ironbark	10.35	11.88	1.78	6.00	4.00	3.00	45	40.57
71	Eucalyptus sideroxylon	Red Ironbark	12.41	17.60	1.73	4.00	5.00	4.00	40	62.69
72	Eucalyptus resinifera	Red Mahogany	38.83	42.12	15.95	12.00	8.00	6.00	45	953.46
73	Eucalyptus resinifera	Red Mahogany	25.78	30.17	8.30	12.00	6.00	5.00	45	358.73
74	Eucalyptus resinifera	Red Mahogany	21.65	23.87	4.90	12.00	6.00	4.00	45	236.29
75	Eucalyptus paniculata	Grey Ironbark	10.82	12.99	1.95	6.00	3.00	1.50	45	45.18
76	Eucalyptus creba	Narrow-leaved Red Ironbark	7.80	8.53	1.23	5.00	3.00	1.50	45	20.67
77	Eucalyptus creba	Narrow-leaved Red Ironbark	9.07	12.04	1.89	4.00	3.00	1.00	45	29.65
78	Callitris hugelii	White Cypress Pine	11.14	8.52	3.93	4.00	3.00	1.00	45	44.26
79	Callitris hugelii	White Cypress Pine	11.14	8.52	3.90	4.00	3.00	1.00	45	44.26
	Total Dry Weight (kg)									9250.68
	Total Biomass (tons/ha)									294.42

Sample Plot No. 19		Plot Size: 10 m radius	Collection Date: 28/09/98				Location: LL 33 49 18.8 N, 150 37 24.4 E			
							UTM 0280050 E, 6255054 N			
Tree #	**Scientific Name**	**Common Name**	**Dbh (cm)**	**Tht (m)**	**Cover (m)**	**ANBT**	**ABD (cm)**	**ABL (m)**	**ABAV (deg)**	**Total Tree Weight (kg)**
1	Eucalyptus sideroxylon	Red Ironbark	78.94	11.20	11.93	12.00	20.00	6.00	45	5183.55
2	Eucalyptus sideroxylon	Red Ironbark	12.10	3.25	3.65	6.00	2.00	1.50	45	58.92
3	Eucalyptus paniculata	Grey Ironbark	15.92	4.02	1.20	6.00	4.00	1.50	35	113.43
4	Callitris hugelii	White Cypress Pine	7.64	3.09	2.40	6.00	1.00	1.00	70	19.58
5	Eucalyptus paniculata	Grey Ironbark	15.92	4.17	2.25	5.00	3.00	2.00	50	113.43
6	Eucalyptus sideroxylon	Red Ironbark	5.73	3.98	0.85	6.00	1.00	0.60	45	9.90
7	Eucalyptus sideroxylon	Red Ironbark	7.64	4.24	1.42	6.00	1.00	1.00	45	19.68
8	Callitris hugelii	White Cypress Pine	13.37	2.76	3.82	10.00	2.00	0.50	50	65.63
9	Callitris hugelii	White Cypress Pine	7.00	2.77	3.03	10.00	1.00	1.00	50	16.22
10	Eucalyptus longifolia	Woollybutt	22.44	8.95	5.00	10.00	6.00	3.00	45	257.55
11	Eucalyptus creba	Narrow-leaved Red Ironbark	24.03	7.58	4.90	10.00	6.00	4.00	45	303.31
12	Eucalyptus sideroxylon	Red Ironbark	17.98	6.36	4.19	6.00	4.00	2.00	45	151.85
13	Eucalyptus paniculata	Grey Ironbark	13.69	7.94	2.94	6.00	3.00	2.00	45	79.14
14	Eucalyptus paniculata	Grey Ironbark	28.97	8.72	3.96	15.00	4.00	4.00	40	473.62
15	Eucalyptus sideroxylon	Red Ironbark	27.53	10.14	6.00	8.00	5.00	3.00	50	419.63
16	Eucalyptus longifolia	Woollybutt	6.84	3.02	2.33	6.00	2.00	1.00	50	15.13
17	Eucalyptus ovata	Swamp Gum	7.80	2.08	1.96	3.00	5.00	1.00	50	22.33
18	Eucalyptus paniculata	Grey Ironbark	13.05	4.56	2.97	8.00	2.00	2.00	50	70.64
19	Eucalyptus longifolia	Woollybutt	9.55	5.00	2.95	6.00	2.00	1.50	45	33.51
20	Callitris hugelii	White Cypress Pine	4.77	2.78	1.78	10.00	0.80	0.80	50	7.09
21	Eucalyptus longifolia	Woollybutt	15.28	12.58	4.76	8.00	4.00	2.00	45	102.90
22	Eucalyptus sideroxylon	Red Ironbark	3.82	3.40	1.64	6.00	0.50	0.60	60	3.76
23	Eucalyptus resinifera	Red Mahogany	13.85	13.03	3.78	10.00	5.00	4.00	50	81.35
24	Eucalyptus sideroxylon	Red Ironbark	4.14	8.14	2.13	6.00	2.00	2.00	50	4.55
25	Eucalyptus longifolia	Woollybutt	7.96	6.23	1.86	6.00	2.00	1.50	45	21.69
26	Eucalyptus creba	Narrow-leaved Red Ironbark	35.81	16.17	5.30	10.00	10.00	4.00	40	785.73
27	Eucalyptus creba	Narrow-leaved Red Ironbark	24.67	14.70	4.00	10.00	8.00	3.00	40	322.84
28	Eucalyptus sideroxylon	Red Ironbark	17.19	20.58	1.74	6.00	5.00	3.00	40	136.30
29	Malaleuca linariifolia	Paperbark	4.46	9.37	1.20	4.00	1.00	5.00	45	6.11
30	Eucalyptus creba	Narrow-leaved Red Ironbark	13.21	7.31	2.14	8.00	3.00	2.00	45	72.71
31	Eucalyptus longifolia	Woollybutt	18.62	14.24	5.13	8.00	5.00	3.00	50	164.99
32	Eucalyptus creba	Narrow-leaved Red Ironbark	16.39	12.98	3.59	10.00	6.00	3.00	45	121.72
33	Eucalyptus creba	Narrow-leaved Red Ironbark	9.23	5.51	1.74	6.00	1.00	0.80	60	30.91
34	Eucalyptus paniculata	Grey Ironbark	12.10	11.53	3.15	6.00	2.50	2.00	45	58.92
35	Eucalyptus sideroxylon	Red Ironbark	15.76	11.89	3.30	6.00	6.00	3.00	45	110.74
36	Eucalyptus siderophloia	Broad-leaved Red Ironbark	14.64	9.90	3.99	6.00	6.00	3.00	45	92.96
37	Eucalyptus longifolia	Woollybutt	13.21	7.71	2.50	7.00	2.50	2.00	50	72.71
38	Eucalyptus siderophloia	Broad-leaved Red Ironbark	7.64	4.24	2.71	6.00	1.50	1.50	50	19.68
39	Eucalyptus siderophloia	Broad-leaved Red Ironbark	3.50	2.26	1.16	4.00	1.00	0.60	50	3.06
40	Eucalyptus sideroxylon	Red Ironbark	21.17	10.61	4.48	8.00	6.00	3.00	45	224.04
41	Eucalyptus longifolia	Woollybutt	15.44	10.53	3.12	8.00	3.00	2.00	45	105.47
42	Eucalyptus paniculata	Grey Ironbark	5.57	5.36	1.37	4.00	1.00	0.80	45	9.26
43	Eucalyptus longifolia	Woollybutt	8.91	5.99	2.33	6.00	2.50	1.50	45	28.43
44	Eucalyptus longifolia	Woollybutt	6.84	4.81	2.08	5.00	2.00	1.00	45	15.13
	Total Dry Weight (kg)									10036.49
	Total Biomass (tons/ha)									319.43

Sample Plot No. 20		Plot Size: 10 m radius	Collection Date: 28/09/98				Location: LL 33 49 15.4 N, 150 37 36.5 E			
							UTM 0280299 E, 6255260 N			
Tree #	**Scientific Name**	**Common Name**	**Dbh (cm)**	**Tht (m)**	**Cover (m)**	**ANBT**	**ABD (cm)**	**ABL (m)**	**ABAV (deg)**	**Total Tree Weight (kg)**
1	Eucalyptus sideroxylon	Red Ironbark	18.78	10.45	2.13	3.00	4.00	2.00	45	168.38
2	Eucalyptus sideroxylon	Red Ironbark	18.14	9.28	1.18	6.00	1.50	1.00	50	155.07
3	Eucalyptus creba	Narrow-leaved Red Ironbark	17.98	6.09	2.43	4.00	5.00	3.00	40	151.85
4	Eucalyptus sideroxylon	Red Ironbark	4.77	3.76	1.53	4.00	2.00	1.50	45	6.41
5	Eucalyptus paniculata	Grey Ironbark	13.69	10.21	2.25	4.00	3.00	3.00	45	79.14
6	Eucalyptus paniculata	Grey Ironbark	12.10	13.44	1.28	4.00	3.00	3.00	45	58.92
7	Eucalyptus paniculata	Grey Ironbark	3.82	2.61	1.15	8.00	0.40	0.40	45	3.76
8	Eucalyptus paniculata	Grey Ironbark	7.16	7.61	1.56	4.00	1.50	1.50	45	16.87
9	Eucalyptus creba	Narrow-leaved Red Ironbark	12.73	8.61	1.79	6.00	2.50	1.50	45	66.59
10	Eucalyptus resinifera	Red Mahogany	9.23	11.47	1.54	6.00	2.00	2.00	40	30.91
11	Eucalyptus paniculata	Grey Ironbark	15.60	17.25	2.49	6.00	2.00	1.50	40	108.09
12	Eucalyptus paniculata	Grey Ironbark	10.82	17.05	0.96	4.00	1.00	1.00	45	45.18
13	Eucalyptus sideroxylon	Red Ironbark	10.19	14.05	1.79	4.00	1.00	1.00	45	39.10
14	Eucalyptus creba	Narrow-leaved Red Ironbark	7.32	10.23	1.33	6.00	1.00	0.80	45	17.78
15	Eucalyptus sideroxylon	Red Ironbark	14.16	29.15	2.73	6.00	2.00	2.00	45	85.89
16	Eucalyptus creba	Narrow-leaved Red Ironbark	10.03	16.63	1.48	6.00	1.00	1.00	40	37.65
17	Eucalyptus resinifera	Red Mahogany	33.10	14.44	4.78	10.00	6.00	5.00	45	651.39
18	Eucalyptus sideroxylon	Red Ironbark	14.32	8.50	2.57	6.00	2.00	1.00	45	88.21
19	Eucalyptus paniculata	Grey Ironbark	12.10	7.07	1.83	2.00	4.00	4.00	40	58.92
20	Eucalyptus paniculata	Grey Ironbark	10.19	8.70	1.81	4.00	2.00	0.60	45	39.10
21	Eucalyptus creba	Narrow-leaved Red Ironbark	7.96	4.32	1.37	6.00	1.00	0.60	45	21.69
22	Eucalyptus paniculata	Grey Ironbark	6.05	4.02	1.32	4.00	1.50	1.50	45	11.27
23	Eucalyptus micrantha	Scribbly Gum	30.56	8.52	11.85	10.00	5.00	5.00	45	527.56
24	Eucalyptus paniculata	Grey Ironbark	11.78	6.55	1.30	4.00	1.50	2.00	40	55.29
25	Eucalyptus resinifera	Red Mahogany	7.80	9.28	1.90	6.00	2.00	2.00	45	20.67
26	Eucalyptus paniculata	Grey Ironbark	14.32	8.75	1.30	6.00	1.50	1.50	40	88.21
27	Eucalyptus sideroxylon	Red Ironbark	28.17	16.30	7.65	10.00	5.00	3.00	45	443.16
28	Eucalyptus resinifera	Red Mahogany	21.80	14.21	3.89	10.00	7.00	5.00	45	240.45
29	Eucalyptus paniculata	Grey Ironbark	10.03	6.86	1.43	6.00	1.50	1.50	40	37.65
30	Eucalyptus sideroxylon	Red Ironbark	23.24	9.88	2.78	6.00	3.00	3.00	45	279.89
31	Eucalyptus resinifera	Red Mahogany	12.25	8.44	2.50	6.00	2.50	3.00	45	60.79
32	Eucalyptus paniculata	Grey Ironbark	12.10	10.94	1.60	6.00	2.00	2.00	45	58.92
33	Eucalyptus sideroxylon	Red Ironbark	11.46	5.31	2.73	4.00	2.00	2.00	45	51.79
34	Eucalyptus sideroxylon	Red Ironbark	7.32	3.56	1.70	2.00	3.00	1.00	45	17.78
35	Eucalyptus sideroxylon	Red Ironbark	11.14	4.90	1.65	2.00	5.00	2.50	50	48.42
36	Eucalyptus resinifera	Red Mahogany	6.37	2.92	1.70	4.00	2.00	1.00	45	12.73
37	Eucalyptus sideroxylon	Red Ironbark	8.28	3.83	1.78	2.00	4.00	1.00	45	23.82
38	Eucalyptus creba	Narrow-leaved Red Ironbark	17.98	6.96	3.10	3.00	5.00	2.00	45	151.85
39	Eucalyptus sideroxylon	Red Ironbark	12.10	5.14	2.34	4.00	2.00	1.00	45	58.92
40	Eucalyptus sideroxylon	Red Ironbark	8.75	4.38	1.23	6.00	1.00	0.50	55	27.23
41	Eucalyptus sideroxylon	Red Ironbark	18.78	6.28	2.32	3.00	5.00	3.00	40	168.38
42	Eucalyptus sideroxylon	Red Ironbark	10.19	4.93	1.80	2.00	2.00	1.00	45	39.10
43	Eucalyptus sideroxylon	Red Ironbark	6.21	3.23	1.56	4.00	2.00	0.50	50	11.99
44	Eucalyptus sideroxylon	Red Ironbark	13.37	5.76	2.41	3.00	4.00	2.50	45	74.82
45	Callitris hugelii	White Cypress Pine	7.00	2.77	2.45	3.00	4.00	0.75	45	16.22
46	Eucalyptus sideroxylon	Red Ironbark	17.83	5.65	4.05	9.00	1.00	1.20	45	148.66
47	Eucalyptus sideroxylon	Red Ironbark	18.46	5.15	3.98	5.00	5.00	3.00	45	161.65
48	Eucalyptus sideroxylon	Red Ironbark	14.01	6.96	3.90	3.00	6.00	3.00	45	83.60
49	Eucalyptus resinifera	Red Mahogany	6.21	2.73	2.15	5.00	1.00	0.30	45	11.99
50	Eucalyptus sideroxylon	Red Ironbark	5.57	15.99	1.93	6.00	2.50	1.00	45	9.26
51	Eucalyptus ovata	Swamp Gum	7.32	7.79	1.59	20.00	0.50	1.00	55	19.29
52	Eucalyptus sideroxylon	Red Ironbark	27.37	28.53	3.89	8.00	5.00	5.00	45	413.86
53	Eucalyptus sideroxylon	Red Ironbark	14.80	25.27	2.15	8.00	3.00	3.00	45	95.39
54	Eucalyptus sideroxylon	Red Ironbark	14.80	22.08	1.61	8.00	2.00	2.00	40	95.39
55	Eucalyptus resinifera	Red Mahogany	22.92	21.34	3.95	8.00	6.00	6.00	45	270.82
56	Eucalyptus resinifera	Red Mahogany	24.99	20.51	3.85	8.00	6.00	4.00	45	332.87
57	Eucalyptus sideroxylon	Red Ironbark	14.01	11.04	2.07	8.00	3.00	2.50	45	83.60
58	Eucalyptus paniculata	Grey Ironbark	6.05	7.82	1.15	6.00	1.00	1.00	45	11.27
59	Eucalyptus sideroxylon	Red Ironbark	9.23	8.76	1.29	6.00	1.00	1.00	45	30.91
60	Eucalyptus creba	Narrow-leaved Red Ironbark	10.19	6.29	1.56	6.00	2.00	1.00	45	39.10
61	Eucalyptus resinifera	Red Mahogany	15.44	13.28	2.52	10.00	3.00	3.50	45	105.47
62	Eucalyptus resinifera	Red Mahogany	9.87	8.96	1.61	10.00	2.00	2.00	45	36.24
63	Eucalyptus creba	Narrow-leaved Red Ironbark	6.53	4.98	1.17	5.00	1.50	1.00	45	13.51
64	Eucalyptus sideroxylon	Red Ironbark	16.23	12.48	1.66	6.00	3.00	3.00	35	118.92
65	Eucalyptus paniculata	Grey Ironbark	15.60	11.02	1.85	6.00	2.00	2.00	40	108.09
66	Eucalyptus micrantha	Scribbly Gum	22.92	13.03	4.40	10.00	5.00	5.00	50	271.00
67	Eucalyptus resinifera	Red Mahogany	14.32	11.73	3.23	6.00	3.00	1.50	45	88.21
68	Eucalyptus paniculata	Grey Ironbark	4.46	5.99	1.20	4.00	1.00	1.00	60	5.44
69	Eucalyptus sideroxylon	Red Ironbark	21.90	14.45	2.56	6.00	4.00	4.00	45	242.98
70	Eucalyptus sideroxylon	Red Ironbark	9.23	8.58	0.94	4.00	0.50	0.60	60	30.91
71	Eucalyptus siderophloia	Broad-leaved Red Ironbark	9.23	8.85	0.98	6.00	1.00	1.00	45	30.91
72	Eucalyptus longifolia	Woollybutt	13.37	10.93	3.50	8.00	1.50	2.00	70	74.82
73	Eucalyptus siderophloia	Broad-leaved Red Ironbark	12.10	11.18	0.85	2.00	4.00	4.00	20	58.92
74	Eucalyptus sideroxylon	Red Ironbark	18.46	16.85	3.63	8.00	5.00	4.00	45	161.65
	Total Dry Weight (kg)									7617.46
	Total Biomass (tons/ha)									242.44

Sample Plot No. 21		Plot Size: 10 m radius	Collection Date: 28/09/98				Location: LL 33 49 10.5 N, 150 37 32.5 E			
							UTM 0280231 E, 6255301 N			
Tree #	Scientific Name	Common Name	Dbh (cm)	Tht (m)	Cover (m)	ANBT	ABD (cm)	ABL (m)	ABAV (deg)	Total Tree Weight (kg)
1	Eucalyptus longifolia	Woollybutt	70.19	20.89	17.95	20.00	5.00	5.00	45	3915.64
2	Eucalyptus paniculata	Grey Ironbark	12.41	11.84	1.37	8.00	2.00	3.00	45	62.69
3	Eucalyptus paniculata	Grey Ironbark	9.07	6.14	1.75	6.00	1.50	2.00	45	29.65
4	Eucalyptus paniculata	Grey Ironbark	12.41	12.21	2.45	8.00	3.00	3.00	45	62.69
5	Eucalyptus creba	Narrow-leaved Red Ironbark	12.57	5.80	2.05	6.00	2.00	2.00	45	64.62
6	Eucalyptus creba	Narrow-leaved Red Ironbark	17.83	7.98	3.99	8.00	4.00	2.00	45	148.66
7	Callitris hugelii	White Cypress Pine	5.89	2.95	1.53	6.00	1.50	1.00	45	11.15
8	Callitris hugelii	White Cypress Pine	5.73	2.95	1.55	6.00	1.50	1.00	45	10.51
9	Callitris hugelii	White Cypress Pine	6.05	2.95	1.55	6.00	1.50	1.00	45	11.82
10	Callitris hugelii	White Cypress Pine	5.89	2.95	1.55	6.00	1.50	1.00	45	11.15
11	Callitris hugelii	White Cypress Pine	5.89	2.95	1.63	6.00	1.50	1.00	45	11.15
12	Eucalyptus creba	Narrow-leaved Red Ironbark	14.01	6.72	2.38	6.00	2.50	1.50	45	83.60
13	Eucalyptus paniculata	Grey Ironbark	9.07	8.90	2.63	4.00	1.50	1.50	45	29.65
14	Eucalyptus paniculata	Grey Ironbark	9.55	7.51	2.75	4.00	1.50	1.50	45	33.51
15	Eucalyptus sideroxylon	Red Ironbark	19.58	18.63	3.53	6.00	1.50	2.00	45	185.91
16	Eucalyptus sideroxylon	Red Ironbark	13.37	14.00	2.90	6.00	1.50	2.00	45	74.82
17	Eucalyptus creba	Narrow-leaved Red Ironbark	8.91	6.99	1.67	4.00	2.00	1.50	40	28.43
18	Eucalyptus sideroxylon	Red Ironbark	13.37	10.47	2.29	4.00	2.00	1.50	45	74.82
19	Eucalyptus sideroxylon	Red Ironbark	16.87	12.98	4.89	6.00	4.00	4.00	45	130.35
20	Eucalyptus creba	Narrow-leaved Red Ironbark	8.75	5.13	2.37	6.00	1.50	1.00	40	27.23
21	Callitris hugelii	White Cypress Pine	3.98	3.12	1.44	5.00	1.00	1.00	45	4.78
22	Callitris hugelii	White Cypress Pine	3.98	3.12	1.45	6.00	1.00	1.00	45	4.78
23	Callitris hugelii	White Cypress Pine	3.82	3.12	1.45	4.00	1.00	1.00	45	4.38
24	Callitris hugelii	White Cypress Pine	4.14	3.12	1.40	5.00	1.00	1.00	45	5.20
25	Callitris hugelii	White Cypress Pine	4.06	3.12	1.46	5.00	1.00	1.00	45	4.99
26	Callitris hugelii	White Cypress Pine	10.82	7.42	3.00	10.00	2.00	2.00	75	41.57
27	Callitris hugelii	White Cypress Pine	10.50	7.42	3.00	12.00	2.00	2.00	75	38.97
28	Callitris hugelii	White Cypress Pine	10.98	7.42	3.05	11.00	2.00	2.00	75	42.90
29	Callitris hugelii	White Cypress Pine	10.82	7.42	3.03	8.00	2.00	2.00	75	41.57
30	Callitris hugelii	White Cypress Pine	11.14	7.42	3.03	9.00	2.00	2.00	75	44.26
31	Callitris hugelii	White Cypress Pine	10.74	7.42	3.10	10.00	2.00	2.00	75	40.91
32	Callitris hugelii	White Cypress Pine	10.50	7.42	3.00	10.00	2.00	2.00	75	38.97
33	Eucalyptus sideroxylon	Red Ironbark	25.94	12.87	3.90	6.00	5.00	3.00	45	364.04
34	Eucalyptus longifolia	Woollybutt	28.01	13.03	4.35	8.00	5.00	3.00	45	437.21
35	Eucalyptus longifolia	Woollybutt	13.37	6.36	1.74	6.00	1.00	1.00	45	74.82
36	Eucalyptus sideroxylon	Red Ironbark	25.46	15.21	4.50	6.00	5.00	4.00	45	348.25
37	Eucalyptus longifolia	Woollybutt	10.82	6.06	2.01	5.00	1.50	0.80	70	45.18
38	Callitris hugelii	White Cypress Pine	7.00	4.38	1.54	20.00	1.00	1.00	80	16.22
39	Callitris hugelii	White Cypress Pine	7.32	4.38	1.60	21.00	1.00	1.00	80	17.86
40	Callitris hugelii	White Cypress Pine	7.16	4.38	1.53	19.00	1.00	1.00	80	17.03
41	Callitris hugelii	White Cypress Pine	7.64	4.38	1.55	18.00	1.00	1.00	80	19.58
42	Callitris hugelii	White Cypress Pine	7.32	4.38	1.50	20.00	1.00	1.00	80	17.86
43	Callitris hugelii	White Cypress Pine	7.00	4.38	1.53	20.00	1.00	1.00	80	16.22
44	Eucalyptus sideroxylon	Red Ironbark	20.21	14.21	2.70	8.00	3.00	5.00	40	200.66
45	Eucalyptus ovata	Swamp Gum	7.64	3.17	2.19	5.00	4.00	1.50	45	21.29
46	Eucalyptus paniculata	Grey Ironbark	21.33	14.63	5.45	10.00	5.00	3.00	45	228.08
47	Eucalyptus paniculata	Grey Ironbark	25.62	16.19	5.70	10.00	5.00	3.00	45	353.47
48	Eucalyptus paniculata	Grey Ironbark	9.55	13.57	2.93	8.00	2.00	2.00	45	33.51
49	Eucalyptus paniculata	Grey Ironbark	22.44	17.25	4.13	8.00	5.00	3.00	50	257.55
50	Callitris hugelii	White Cypress Pine	13.05	7.91	2.51	10.00	3.00	3.00	45	62.30
51	Eucalyptus longifolia	Woollybutt	7.32	8.21	1.71	6.00	1.00	1.00	45	17.78
52	Eucalyptus longifolia	Woollybutt	7.48	8.21	1.70	6.00	1.00	1.00	45	18.71
53	Eucalyptus longifolia	Woollybutt	7.32	8.21	1.73	6.00	1.00	1.00	45	17.78
54	Eucalyptus resinifera	Red Mahogany	33.74	22.81	12.05	20.00	5.00	4.00	45	681.69
55	Eucalyptus camaldulensis	River Red Gum	9.87	9.50	1.39	6.00	2.00	3.00	40	38.51
56	Eucalyptus paniculata	Grey Ironbark	7.64	7.22	2.35	6.00	1.50	1.50	45	19.68
57	Eucalyptus sideroxylon	Red Ironbark	19.74	15.38	3.19	10.00	5.00	2.50	45	189.54
58	Eucalyptus sideroxylon	Red Ironbark	13.05	14.91	2.83	8.00	2.00	2.00	45	70.64
59	Eucalyptus paniculata	Grey Ironbark	18.78	7.80	3.15	8.00	2.00	2.00	40	168.38
60	Eucalyptus camaldulensis	River Red Gum	28.01	10.61	5.03	8.00	8.00	6.00	40	431.29
61	Eucalyptus camaldulensis	River Red Gum	23.55	13.55	4.70	8.00	8.00	6.00	40	288.75
	Total Dry Weight (kg)									9801.47
	Total Biomass (tons/ha)									311.95

Sample Plot No. 22		Plot Size: 10 m radius	Collection Date: 28/09/98				Location: LL 33 48 53.8 N, 150 37 34.7 E			
							UTM 0280305 E, 6255802 N			
Tree #	**Scientific Name**	**Common Name**	**Dbh (cm)**	**Tht (m)**	**Cover (m)**	**ANBT**	**ABD (cm)**	**ABL (m)**	**ABAV (deg)**	**Total Tree Weight (kg)**
1	Eucalyptus resinifera	Red Mahogany	28.49	17.68	7.05	10.00	6.00	5.00	45	455.20
2	Eucalyptus resinifera	Red Mahogany	27.69	16.49	6.80	8.00	5.00	5.00	45	425.44
3	Eucalyptus resinifera	Red Mahogany	37.24	13.55	10.65	10.00	6.00	5.00	45	862.84
4	Eucalyptus creba	Narrow-leaved Red Ironbark	12.89	8.49	3.93	8.00	5.00	2.00	45	68.60
5	Eucalyptus sideroxylon	Red Ironbark	17.19	18.63	2.30	6.00	4.00	2.00	45	136.30
6	Eucalyptus longifolia	Woollybutt	14.64	11.08	2.20	6.00	3.00	1.50	45	92.96
7	Eucalyptus longifolia	Woollybutt	16.23	12.72	2.98	6.00	4.00	2.00	45	118.92
8	Eucalyptus sideroxylon	Red Ironbark	6.84	5.42	1.41	4.00	1.00	1.00	45	15.13
9	Eucalyptus longifolia	Woollybutt	12.41	8.07	2.88	8.00	2.00	2.00	45	62.69
10	Eucalyptus resinifera	Red Mahogany	29.28	17.68	7.30	10.00	6.00	4.00	45	486.14
11	Eucalyptus resinifera	Red Mahogany	15.60	9.40	3.58	6.00	4.00	2.00	45	108.09
12	Eucalyptus resinifera	Red Mahogany	40.74	19.01	11.15	10.00	10.00	6.00	45	1069.22
13	Eucalyptus ovata	Swamp Gum	21.33	8.07	3.21	8.00	2.00	1.00	70	229.40
14	Eucalyptus ovata	Swamp Gum	11.46	5.53	3.65	8.00	2.00	1.00	70	54.44
15	Eucalyptus ovata	Swamp Gum	17.51	8.82	4.45	8.00	2.00	1.00	70	145.25
16	Eucalyptus sideroxylon	Red Ironbark	26.74	12.87	3.55	8.00	5.00	3.00	45	391.26
17	Eucalyptus paniculata	Grey Ironbark	11.14	5.13	1.55	4.00	2.00	1.50	45	48.42
18	Eucalyptus creba	Narrow-leaved Red Ironbark	10.50	4.81	2.35	4.00	2.00	1.00	45	42.08
19	Eucalyptus sideroxylon	Red Ironbark	13.05	8.28	3.20	6.00	2.00	1.50	45	70.64
20	Eucalyptus sideroxylon	Red Ironbark	14.96	8.50	1.99	6.00	2.00	2.00	45	97.86
21	Eucalyptus creba	Narrow-leaved Red Ironbark	7.96	2.88	1.45	6.00	1.00	1.50	45	21.69
22	Eucalyptus sideroxylon	Red Ironbark	31.19	16.96	5.80	8.00	7.00	4.00	45	565.26
23	Eucalyptus creba	Narrow-leaved Red Ironbark	49.34	7.07	9.95	12.00	6.00	5.00	45	1688.32
24	Eucalyptus paniculata	Grey Ironbark	19.10	8.25	1.60	6.00	4.00	3.00	40	175.27
25	Eucalyptus creba	Narrow-leaved Red Ironbark	13.37	9.90	3.84	6.00	5.00	4.00	40	74.82
26	Eucalyptus creba	Narrow-leaved Red Ironbark	13.05	8.95	3.35	6.00	4.00	3.50	45	70.64
27	Eucalyptus creba	Narrow-leaved Red Ironbark	12.73	4.60	2.54	6.00	3.00	2.00	45	66.59
28	Eucalyptus creba	Narrow-leaved Red Ironbark	15.12	8.96	3.85	6.00	4.00	3.00	45	100.36
29	Callitris hugelii	White Cypress Pine	4.30	2.60	1.94	8.00	1.00	1.00	60	5.65
30	Callitris hugelii	White Cypress Pine	4.46	2.60	1.95	8.00	1.00	1.00	60	6.11
31	Callitris hugelii	White Cypress Pine	4.14	2.60	1.95	8.00	1.00	1.00	60	5.20
32	Callitris hugelii	White Cypress Pine	4.77	2.60	2.60	8.00	1.00	1.00	60	7.09
33	Callitris hugelii	White Cypress Pine	4.46	2.60	2.00	8.00	1.00	1.00	60	6.11
34	Callitris hugelii	White Cypress Pine	4.14	2.60	1.94	8.00	1.00	1.00	60	5.20
35	Callitris hugelii	White Cypress Pine	4.30	2.60	1.95	8.00	1.00	1.00	60	5.65
36	Eucalyptus longifolia	Woollybutt	23.87	9.51	6.00	16.00	6.00	4.00	60	298.54
37	Eucalyptus creba	Narrow-leaved Red Ironbark	4.77	2.43	1.07	4.00	1.00	0.60	45	6.41
38	Eucalyptus creba	Narrow-leaved Red Ironbark	5.57	4.39	1.38	4.00	0.50	0.80	45	9.26
39	Eucalyptus sideroxylon	Red Ironbark	15.92	13.55	2.45	6.00	2.00	2.00	45	113.43
40	Eucalyptus sideroxylon	Red Ironbark	13.69	13.44	1.79	4.00	2.00	2.00	45	79.14
41	Eucalyptus creba	Narrow-leaved Red Ironbark	8.59	5.80	1.22	3.00	3.00	1.00	45	26.06
42	Eucalyptus sideroxylon	Red Ironbark	11.14	7.94	2.88	6.00	2.00	2.00	45	48.42
43	Callitris hugelii	White Cypress Pine	13.69	4.50	3.00	6.00	7.00	2.50	45	69.06
44	Eucalyptus sideroxylon	Red Ironbark	12.73	7.82	3.15	6.00	4.00	2.00	45	66.59
45	Callitris hugelii	White Cypress Pine	7.32	3.66	1.30	6.00	2.00	1.50	50	17.86
46	Eucalyptus longifolia	Woollybutt	45.20	13.99	10.05	4.00	8.00	6.00	30	1369.80
47	Eucalyptus creba	Narrow-leaved Red Ironbark	17.35	6.66	2.89	8.00	6.00	2.00	45	139.33
48	Eucalyptus resinifera	Red Mahogany	47.75	20.68	9.35	8.00	15.00	6.00	45	1561.23
	Total Dry Weight (kg)									11597.12
	Total Biomass (tons/ha)									369.10

Sample Plot No. 23		Plot Size: 10 m radius	Collection Date: 25/10/98				Location: LL 33 47 39.4 N, 150 38 11.5 E			
							UTM 0281219 E, 6258141 N			
Tree #	**Scientific Name**	**Common Name**	**Dbh (cm)**	**Tht (m)**	**Cover (m)**	**ANBT**	**ABD (cm)**	**ABL (m)**	**ABAV (deg)**	**Total Tree Weight (kg)**
1	Callitris hugelii	White Cypress Pine	42.02	14.63	14.25	20	8.00	2.00	70	779.99
2	Eucalyptus sideroxylon	Red Ironbark	13.85	11.82	1.50	8.00	2.00	2.00	45	81.35
3	Eucalyptus paniculata	Grey Ironbark	22.60	13.81	3.50	8.00	5.00	2.50	45	261.93
4	Eucalyptus resinifera	Red Mahogany	24.83	11.45	5.30	10.00	4.00	3.00	45	327.83
5	Eucalyptus resinifera	Red Mahogany	16.87	9.22	4.50	6.00	5.00	2.00	45	130.35
6	Eucalyptus maculata	Spotted Gum	41.86	18.02	14.20	8.00	10.00	6.00	45	1093.23
7	Eucalyptus paniculata	Grey Ironbark	23.87	16.34	4.65	8.00	4.00	4.00	45	298.54
8	Eucalyptus resinifera	Red Mahogany	22.44	12.47	4.60	10.00	5.00	3.00	45	257.55
9	Eucalyptus maculata	Spotted Gum	28.97	12.09	5.90	8.00	8.00	3.50	45	466.10
10	Eucalyptus sideroxylon	Red Ironbark	17.19	15.42	2.20	8.00	3.00	3.00	45	136.30
11	Eucalyptus maculata	Spotted Gum	9.71	8.70	2.10	6.00	3.00	2.00	45	37.08
12	Eucalyptus resinifera	Red Mahogany	23.40	13.30	6.55	8.00	4.00	3.00	45	284.48
13	Eucalyptus resinifera	Red Mahogany	20.37	12.87	5.25	8.00	4.00	3.00	45	204.46
14	Eucalyptus resinifera	Red Mahogany	14.96	10.69	1.20	8.00	3.00	3.00	45	97.86
15	Eucalyptus resinifera	Red Mahogany	14.32	11.72	1.10	8.00	2.00	1.50	45	88.21
16	Eucalyptus resinifera	Red Mahogany	21.01	14.16	4.35	8.00	5.00	3.00	45	220.04
17	Eucalyptus resinifera	Red Mahogany	19.10	15.21	3.20	8.00	3.00	3.00	45	175.27
18	Eucalyptus paniculata	Grey Ironbark	18.46	14.63	2.70	8.00	5.00	3.00	45	161.65
19	Eucalyptus paniculata	Grey Ironbark	24.19	15.21	3.90	8.00	4.00	3.00	45	308.13
20	Eucalyptus resinifera	Red Mahogany	18.46	15.21	5.80	12.00	4.00	3.00	45	161.65
21	Eucalyptus maculata	Spotted Gum	9.23	7.51	1.65	10.00	1.00	1.00	45	33.00
22	Eucalyptus resinifera	Red Mahogany	21.96	13.74	2.80	10.00	4.00	3.00	45	244.66
23	Eucalyptus saligna	Sydney Blue Gum	20.37	16.34	4.70	8.00	5.00	4.00	45	206.31
24	Eucalyptus paniculata	Grey Ironbark	20.69	15.21	2.59	6.00	4.00	3.00	45	212.16
25	Eucalyptus sideroxylon	Red Ironbark	16.55	12.09	3.20	6.00	3.00	2.00	45	124.56
26	Eucalyptus paniculata	Grey Ironbark	22.28	14.44	4.50	6.00	5.00	3.00	45	253.21
27	Eucalyptus paniculata	Grey Ironbark	28.01	16.34	2.55	12.00	4.00	3.00	45	437.21
28	Eucalyptus sideroxylon	Red Ironbark	24.83	15.94	3.90	10.00	4.00	4.00	45	327.83
29	Eucalyptus sideroxylon	Red Ironbark	14.80	11.61	2.23	6.00	3.00	2.00	45	95.39
30	Callitris hugelii	White Cypress Pine	9.39	7.19	2.44	20.00	1.00	1.00	80	30.58
	Total Dry Weight (kg)									7541.74
	Total Biomass (tons/ha)									240.03

Sample Plot No. 24		Plot Size: 10 m radius	Collection Date: 21/10/98				Location: LL 33 48 14.1 N, 150 38 11 E			
							UTM 0281212 E, 6257063 N			
Tree #	**Scientific Name**	**Common Name**	**Dbh (cm)**	**Tht (m)**	**Cover (m)**	**ANBT**	**ABD (cm)**	**ABL (m)**	**ABAV (deg)**	**Total Tree Weight (kg)**
1	Syncarpia glomulifera	Turpentine	14.01	23.60	4.25	20.00	1.00	1.50	70	83.60
2	Syncarpia glomulifera	Turpentine	14.64	31.23	4.45	25.00	2.00	2.00	65	92.96
3	Callitris hugelii	White Cypress Pine	13.37	22.82	4.24	15.00	2.00	4.00	60	65.63
4	Eucalyptus paniculata	Grey Ironbark	11.62	20.68	1.55	3.00	2.00	2.00	30	53.52
5	Eucalyptus resinifera	Red Mahogany	15.92	23.60	4.94	8.00	2.00	2.50	50	113.43
6	Callitris hugelii	White Cypress Pine	15.60	12.87	3.86	15.00	3.00	2.00	50	91.59
7	Eucalyptus saligna	Sydney Blue Gum	23.24	24.64	4.90	10.00	4.00	5.00	40	279.79
8	Callitris hugelii	White Cypress Pine	20.05	14.31	2.00	10.00	0.50	0.50	50	157.67
9	Callitris hugelii	White Cypress Pine	19.74	16.85	4.76	8.00	4.00	4.00	45	152.31
10	Callitris hugelii	White Cypress Pine	17.51	11.89	4.72	15.00	2.00	1.50	60	117.56
11	Eucalyptus paniculata	Grey Ironbark	13.69	15.13	1.60	8.00	2.00	3.00	45	79.14
12	Eucalyptus saligna	Sydney Blue Gum	14.96	12.10	1.95	8.00	4.00	3.00	45	100.93
13	Eucalyptus paniculata	Grey Ironbark	13.53	11.02	2.18	6.00	1.00	0.80	45	76.96
14	Syncarpia glomulifera	Turpentine	8.59	7.51	2.60	10.00	2.00	2.00	75	26.06
15	Syncarpia glomulifera	Turpentine	11.46	9.28	4.70	10.00	1.50	1.50	70	51.79
16	Eucalyptus resinifera	Red Mahogany	14.96	14.63	3.35	6.00	3.00	3.00	40	97.86
17	Eucalyptus saligna	Sydney Blue Gum	18.78	16.19	2.55	6.00	3.00	4.00	40	170.89
18	Eucalyptus maculata	Spotted Gum	20.37	14.97	2.84	8.00	5.00	4.00	45	206.31
19	Eucalyptus maculata	Spotted Gum	9.87	11.10	1.71	5.00	2.00	2.00	45	38.51
20	Callitris hugelii	White Cypress Pine	16.55	9.55	4.12	20.00	3.00	3.00	70	104.14
21	Eucalyptus sideroxylon	Red Ironbark	19.42	12.60	4.50	4.00	4.00	3.00	45	182.32
22	Eucalyptus maculata	Spotted Gum	12.73	10.14	2.05	6.00	3.00	4.00	40	69.48
23	Syncarpia glomulifera	Turpentine	21.01	9.98	3.88	10.00	2.00	2.00	80	220.04
24	Syncarpia glomulifera	Turpentine	9.71	4.82	5.20	10.00	1.00	1.50	55	34.86
25	Callitris hugelii	White Cypress Pine	30.56	10.94	5.35	40.00	4.00	3.00	70	391.87
26	Eucalyptus paniculata	Grey Ironbark	8.59	6.00	2.55	6.00	0.50	0.50	70	26.06
27	Callitris hugelii	White Cypress Pine	12.10	6.55	3.48	10.00	2.00	1.50	65	52.87
28	Eucalyptus saligna	Sydney Blue Gum	27.69	12.88	6.60	12.00	4.00	4.00	45	420.03
29	Eucalyptus sideroxylon	Red Ironbark	16.23	11.66	1.35	6.00	3.00	3.00	45	118.92
30	Syncarpia glomulifera	Turpentine	14.96	8.50	4.50	20.00	2.00	2.00	60	97.86
31	Syncarpia glomulifera	Turpentine	19.26	8.26	4.90	20.00	3.00	2.00	80	178.77
32	Eucalyptus saligna	Sydney Blue Gum	19.74	9.98	2.85	8.00	3.00	3.00	45	191.68
33	Syncarpia glomulifera	Turpentine	7.32	4.97	2.30	8.00	1.00	1.50	80	17.78
34	Syncarpia glomulifera	Turpentine	7.00	7.88	2.30	8.00	1.00	1.00	70	15.99
35	Syncarpia glomulifera	Turpentine	22.28	9.30	5.35	20.00	2.00	2.00	80	253.21
36	Syncarpia glomulifera	Turpentine	13.05	8.03	3.75	10.00	1.50	2.00	80	70.64
37	Syncarpia glomulifera	Turpentine	6.37	7.42	1.60	6.00	2.00	2.00	80	12.73
38	Eucalyptus saligna	Sydney Blue Gum	22.92	16.34	6.20	8.00	5.00	5.00	45	271.00
39	Eucalyptus maculata	Spotted Gum	19.10	9.30	3.20	8.00	4.00	3.00	45	177.67
40	Eucalyptus paniculata	Grey Ironbark	24.19	10.16	2.95	10.00	4.00	3.00	45	308.13
41	Eucalyptus maculata	Spotted Gum	9.71	7.40	0.79	6.00	2.00	2.00	40	37.08
42	Callitris hugelii	White Cypress Pine	20.37	8.77	6.30	20.00	4.00	4.00	60	163.13
43	Callitris hugelii	White Cypress Pine	13.05	8.61	3.05	16.00	3.00	3.00	60	62.30
44	Syncarpia glomulifera	Turpentine	6.21	4.56	0.78	10.00	1.00	1.00	80	11.99
45	Syncarpia glomulifera	Turpentine	5.73	4.56	1.10	10.00	1.00	1.00	80	9.90
46	Syncarpia glomulifera	Turpentine	6.05	4.56	0.80	10.00	1.00	1.00	80	11.27
47	Syncarpia glomulifera	Turpentine	5.41	4.56	1.00	10.00	1.00	1.00	80	8.64
48	Syncarpia glomulifera	Turpentine	6.37	4.56	0.78	10.00	1.00	1.00	80	12.73
49	Eucalyptus saligna	Sydney Blue Gum	21.96	10.28	5.60	8.00	5.00	4.00	50	245.56
50	Syncarpia glomulifera	Turpentine	12.10	8.00	3.65	15.00	1.00	1.50	75	58.92
51	Eucalyptus sideroxylon	Red Ironbark	18.78	9.30	2.40	6.00	4.00	4.00	45	168.38
52	Syncarpia glomulifera	Turpentine	8.28	6.59	2.20	16.00	1.00	1.00	80	23.82
53	Syncarpia glomulifera	Turpentine	13.69	7.15	3.30	15.00	1.50	2.00	80	79.14
54	Eucalyptus saligna	Sydney Blue Gum	21.01	13.81	5.60	8.00	4.00	4.00	45	221.54
55	Eucalyptus paniculata	Grey Ironbark	11.78	6.62	1.20	6.00	2.00	2.00	45	55.29
56	Syncarpia glomulifera	Turpentine	10.98	7.00	3.00	12.00	1.50	1.00	80	46.78
57	Eucalyptus saligna	Sydney Blue Gum	23.87	13.31	6.20	6.00	4.00	3.00	45	297.86
58	Syncarpia glomulifera	Turpentine	16.07	8.28	4.40	15.00	2.00	3.00	70	116.15
59	Eucalyptus maculata	Spotted Gum	7.00	4.97	1.65	6.00	2.00	2.00	40	17.40
60	Eucalyptus saligna	Sydney Blue Gum	22.92	13.81	4.25	8.00	4.00	4.00	45	271.00
61	Callitris hugelii	White Cypress Pine	19.74	9.55	4.85	12.00	4.00	3.00	60	152.31
62	Callitris hugelii	White Cypress Pine	12.73	12.10	1.50	20.00	2.00	2.00	60	59.06
63	Eucalyptus sideroxylon	Red Ironbark	16.23	12.47	1.20	4.00	3.00	4.00	45	118.92
64	Syncarpia glomulifera	Turpentine	13.69	9.40	4.00	15.00	2.00	2.00	80	79.14
65	Syncarpia glomulifera	Turpentine	8.28	7.06	1.70	10.00	1.50	1.50	80	23.82
66	Callitris hugelii	White Cypress Pine	17.03	10.85	4.95	20.00	2.00	3.00	70	110.74
	Total Dry Weight (kg)									7740.32
	Total Biomass (tons/ha)									246.35

Sample Plot No. 25		Plot Size: 10 m radius	Collection Date: 21/10/98				Location: LL 33 47 42.4 N, 150 38 24.7 E			
							UTM 0281519 E, 6258189 N			
Tree #	**Scientific Name**	**Common Name**	**Dbh (cm)**	**Tht (m)**	**Cover (m)**	**ANBT**	**ABD (cm)**	**ABL (m)**	**ABAV (deg)**	**Total Tree Weight (kg)**
1	Malaleuca linariifolia	Paperbark	8.59	6.26	3.13	8.00	1.00	1.00	70	27.96
2	Eucalyptus saligna	Sydney Blue Gum	8.91	8.68	3.30	8.00	2.00	2.00	45	30.42
3	Eucalyptus creba	Narrow-leaved Red Ironbark	13.05	8.76	4.35	10.00	2.00	2.00	45	70.64
4	Eucalyptus longifolia	Woollybutt	21.01	11.61	5.00	10.00	4.00	3.00	45	220.04
5	Eucalyptus longifolia	Woollybutt	20.37	13.13	3.80	12.00	4.00	2.00	45	204.46
6	Eucalyptus resinifera	Red Mahogany	22.92	12.87	6.70	8.00	5.00	4.00	45	270.82
7	Eucalyptus longifolia	Woollybutt	18.46	13.99	2.80	8.00	4.00	3.00	45	161.65
8	Eucalyptus creba	Narrow-leaved Red Ironbark	14.96	14.78	3.50	8.00	3.00	4.00	45	97.86
9	Eucalyptus resinifera	Red Mahogany	18.78	13.44	3.15	10.00	2.00	2.00	45	168.38
10	Eucalyptus resinifera	Red Mahogany	11.62	13.03	1.50	8.00	2.00	2.00	45	53.52
11	Eucalyptus creba	Narrow-leaved Red Ironbark	19.74	17.25	5.05	10.00	4.00	3.00	45	189.54
12	Eucalyptus creba	Narrow-leaved Red Ironbark	13.37	9.69	2.00	8.00	2.00	2.00	40	74.82
13	Eucalyptus creba	Narrow-leaved Red Ironbark	15.28	10.45	3.65	8.00	3.00	2.00	40	102.90
14	Eucalyptus creba	Narrow-leaved Red Ironbark	13.53	10.77	1.85	8.00	3.00	4.00	40	76.96
15	Eucalyptus resinifera	Red Mahogany	15.12	10.69	3.15	10.00	3.00	2.00	40	100.36
16	Eucalyptus resinifera	Red Mahogany	18.78	10.38	5.65	10.00	5.00	6.00	40	168.38
17	Eucalyptus creba	Narrow-leaved Red Ironbark	23.24	10.69	6.95	12.00	4.00	3.00	40	279.89
18	Eucalyptus resinifera	Red Mahogany	16.55	6.26	4.60	8.00	3.00	2.00	45	124.56
19	Eucalyptus resinifera	Red Mahogany	17.51	6.96	4.65	12.00	3.00	3.00	45	142.40
20	Eucalyptus resinifera	Red Mahogany	23.87	8.00	6.90	12.00	5.00	5.00	40	298.54
21	Eucalyptus resinifera	Red Mahogany	15.28	7.77	4.05	6.00	5.00	3.00	40	102.90
22	Eucalyptus creba	Narrow-leaved Red Ironbark	12.41	5.03	2.90	8.00	2.00	2.00	45	62.69
23	Eucalyptus longifolia	Woollybutt	18.78	10.07	3.55	10.00	2.00	2.00	45	168.38
24	Eucalyptus resinifera	Red Mahogany	18.46	11.73	4.55	10.00	4.00	3.00	40	161.65
25	Eucalyptus longifolia	Woollybutt	17.51	10.69	3.55	8.00	2.00	2.00	40	142.40
26	Eucalyptus longifolia	Woollybutt	22.92	9.55	5.45	10.00	3.00	2.00	40	270.82
27	Eucalyptus longifolia	Woollybutt	10.82	4.99	2.75	8.00	2.00	1.50	45	45.18
28	Eucalyptus creba	Narrow-leaved Red Ironbark	13.05	8.61	1.55	6.00	2.00	3.00	40	70.64
29	Eucalyptus longifolia	Woollybutt	13.69	10.40	3.65	8.00	2.00	2.00	45	79.14
30	Eucalyptus longifolia	Woollybutt	18.14	9.78	5.70	8.00	3.00	2.00	45	155.07
	Total Dry Weight (kg)									4125.45
	Total Biomass (tons/ha)									131.30

Appendix 7.2

This appendix presents in detail the data collected from the sample plots in study site 2 (Gippsland).

Sample Plot No. 1		Plot Size: 21 m x 15 m		Collection Date: 02/02/99				Time: 12:00 noon	
Tree #	**Scientific Name**	**Common Name**	**Dbh (cm)**	**Tht (m)**	**Cover (m)**	**ABD (cm)**	**ABL (m)**	**Total Dry Weight (kg)**	**Remarks**
1	Pinus radiata	Radiata Pine	12.41	9.80	4.80	4.30	2.80	55.92	Branching Pattern: 6 -8
2	Pinus radiata	Radiata Pine	14.32					76.19	branches encircling the
3	Pinus radiata	Radiata Pine	11.78					49.90	stem about 6 in. from
4	Pinus radiata	Radiata Pine	9.55					31.72	the ground to the top
5	Pinus radiata	Radiata Pine	14.32					76.19	of the tree.
6	Pinus radiata	Radiata Pine	12.10					52.87	:branches/whorls
7	Pinus radiata	Radiata Pine	13.37					65.63	approximately
8	Pinus radiata	Radiata Pine	14.32					76.19	1-2 ft. apart;
9	Pinus radiata	Radiata Pine	15.28					87.59	:20 - 30 % sky visibility
10	Pinus radiata	Radiata Pine	13.37					65.63	:5 yrs. old
11	Pinus radiata	Radiata Pine	12.73					59.06	:Total ht., cover, ave.
12	Pinus radiata	Radiata Pine	11.14					44.26	branch diameter, and
13	Pinus radiata	Radiata Pine	13.69					69.06	average branch length
14	Pinus radiata	Radiata Pine	12.41					55.92	generally the same for
15	Pinus radiata	Radiata Pine	12.10					52.87	each tree.
16	Pinus radiata	Radiata Pine	13.69					69.06	
17	Pinus radiata	Radiata Pine	12.57					57.48	
18	Pinus radiata	Radiata Pine	10.66					40.26	
19	Pinus radiata	Radiata Pine	15.28					87.59	
20	Pinus radiata	Radiata Pine	16.55					104.14	
21	Pinus radiata	Radiata Pine	15.92					95.67	
22	Pinus radiata	Radiata Pine	12.10					52.87	
23	Pinus radiata	Radiata Pine	16.55					104.14	
24	Pinus radiata	Radiata Pine	19.10					141.89	
25	Pinus radiata	Radiata Pine	17.19					112.99	
26	Pinus radiata	Radiata Pine	12.10					52.87	
27	Pinus radiata	Radiata Pine	13.69					69.06	
28	Pinus radiata	Radiata Pine	10.82					41.57	
29	Pinus radiata	Radiata Pine	12.41					55.92	
30	Pinus radiata	Radiata Pine	12.41					55.92	
31	Pinus radiata	Radiata Pine	14.01					72.58	
32	Pinus radiata	Radiata Pine	11.14					44.26	
33	Pinus radiata	Radiata Pine	13.05					62.30	
34	Pinus radiata	Radiata Pine	13.05					62.30	
35	Pinus radiata	Radiata Pine	11.46					47.03	
36	Pinus radiata	Radiata Pine	15.68					92.60	
37	Pinus radiata	Radiata Pine	16.23					99.86	
38	Pinus radiata	Radiata Pine	12.73					59.06	
39	Pinus radiata	Radiata Pine	12.10					52.87	
40	Pinus radiata	Radiata Pine	12.73					59.06	
41	Pinus radiata	Radiata Pine	13.37					65.63	
42	Pinus radiata	Radiata Pine	13.69					69.06	
43	Pinus radiata	Radiata Pine	14.32					76.19	
	Total Dry Weight (kg)							2923.19	
	Total Biomass (tons/ha)							92.80	

Where: Dbh = Diameter at breast height (over bark)

Tht = Total tree height

ANBT = Average Number of Branches per Tree

ABT = Average Branch Diameter

ABL = Average Branch Length

Sample Plot No. 2		Plot Size: 21 m x 15 m		Collection Date: 02/02/99				Time: 3:00 p.m.	
Tree #	**Scientific Name**	**Common Name**	**Dbh (cm)**	**Tht (m)**	**Cover (m)**	**ABD (cm)**	**ABL (m)**	**Total Dry Weight (kg)**	**Remarks**
1	Pinus radiata	Radiata Pine	13.37	10.40	4.60	4.00	2.60	65.63	Branching Pattern: 6 -8
2	Pinus radiata	Radiata Pine	11.46					47.03	branches encircling the
3	Pinus radiata	Radiata Pine	13.69					69.06	stem about 6 in. from
4	Pinus radiata	Radiata Pine	11.14					44.26	the ground to the top
5	Pinus radiata	Radiata Pine	13.69					69.06	of the tree.
6	Pinus radiata	Radiata Pine	14.64					79.89	:branches/whorls
7	Pinus radiata	Radiata Pine	13.37					65.63	approximately
8	Pinus radiata	Radiata Pine	11.78					49.90	1-2 ft. apart;
9	Pinus radiata	Radiata Pine	15.92					95.67	:20 - 30 % sky visibility
10	Pinus radiata	Radiata Pine	13.37					65.63	:5 yrs. old
11	Pinus radiata	Radiata Pine	14.32					76.19	:Total ht., cover, ave.
12	Pinus radiata	Radiata Pine	13.37					65.63	branch diameter, and
13	Pinus radiata	Radiata Pine	14.01					72.58	average branch length
14	Pinus radiata	Radiata Pine	12.10					52.87	generally the same for
15	Pinus radiata	Radiata Pine	12.10					52.87	each tree.
16	Pinus radiata	Radiata Pine	12.73					59.06	
17	Pinus radiata	Radiata Pine	13.69					69.06	
18	Pinus radiata	Radiata Pine	13.53					67.33	
19	Pinus radiata	Radiata Pine	14.32					76.19	
20	Pinus radiata	Radiata Pine	13.37					65.63	
21	Pinus radiata	Radiata Pine	15.60					91.59	
22	Pinus radiata	Radiata Pine	11.94					51.37	
23	Pinus radiata	Radiata Pine	16.55					104.14	
24	Pinus radiata	Radiata Pine	17.83					122.23	
25	Pinus radiata	Radiata Pine	12.41					55.92	
26	Pinus radiata	Radiata Pine	14.01					72.58	
27	Pinus radiata	Radiata Pine	12.10					52.87	
28	Pinus radiata	Radiata Pine	13.05					62.30	
29	Pinus radiata	Radiata Pine	15.60					91.59	
30	Pinus radiata	Radiata Pine	14.96					83.70	
31	Pinus radiata	Radiata Pine	12.41					55.92	
32	Pinus radiata	Radiata Pine	12.10					52.87	
33	Pinus radiata	Radiata Pine	15.60					91.59	
34	Pinus radiata	Radiata Pine	13.69					69.06	
35	Pinus radiata	Radiata Pine	14.32					76.19	
36	Pinus radiata	Radiata Pine	12.25					54.38	
37	Pinus radiata	Radiata Pine	11.30					45.63	
38	Pinus radiata	Radiata Pine	13.69					69.06	
39	Pinus radiata	Radiata Pine	13.53					67.33	
40	Pinus radiata	Radiata Pine	12.45					56.23	
41	Pinus radiata	Radiata Pine	14.32					76.19	
	Total Dry Weight (kg)							2811.88	
	Total Biomass (tons/ha)							89.27	

Sample Plot No. 3		Plot Size: 21 m x 15 m		Collection Date: 02/02/99				Time: 3:45 p.m.	
Tree #	**Scientific Name**	**Common Name**	**Dbh (cm)**	**Tht (m)**	**Cover (m)**	**ABD (cm)**	**ABL (m)**	**Total Dry Weight (kg)**	**Remarks**
1	Pinus radiata	Radiata Pine	14.01	10.72	4.65	4.10	2.70	72.58	Branching Pattern: 6 -8
2	Pinus radiata	Radiata Pine	12.10					52.87	branches encircling the
3	Pinus radiata	Radiata Pine	13.69					69.06	stem about 6 in. from
4	Pinus radiata	Radiata Pine	13.05					62.30	the ground to the top
5	Pinus radiata	Radiata Pine	13.37					65.63	of the tree.
6	Pinus radiata	Radiata Pine	12.41					55.92	:branches/whorls
7	Pinus radiata	Radiata Pine	14.01					72.58	approximately
8	Pinus radiata	Radiata Pine	13.69					69.06	1-2 ft. apart;
9	Pinus radiata	Radiata Pine	12.41					55.92	:20 - 30 % sky visibility
10	Pinus radiata	Radiata Pine	14.01					72.58	:5 yrs. old
11	Pinus radiata	Radiata Pine	14.96					83.70	:Total ht., cover, ave.
12	Pinus radiata	Radiata Pine	14.32					76.19	branch diameter, and
13	Pinus radiata	Radiata Pine	12.73					59.06	average branch length
14	Pinus radiata	Radiata Pine	13.37					65.63	generally the same for
15	Pinus radiata	Radiata Pine	12.10					52.87	each tree.
16	Pinus radiata	Radiata Pine	13.05					62.30	
17	Pinus radiata	Radiata Pine	14.01					72.58	
18	Pinus radiata	Radiata Pine	14.64					79.89	
19	Pinus radiata	Radiata Pine	14.64					79.89	
20	Pinus radiata	Radiata Pine	13.05					62.30	
21	Pinus radiata	Radiata Pine	15.12					85.63	
22	Pinus radiata	Radiata Pine	13.21					63.96	
23	Pinus radiata	Radiata Pine	13.37					65.63	
24	Pinus radiata	Radiata Pine	17.51					117.56	
25	Pinus radiata	Radiata Pine	17.83					122.23	
26	Pinus radiata	Radiata Pine	13.05					62.30	
27	Pinus radiata	Radiata Pine	14.32					76.19	
28	Pinus radiata	Radiata Pine	13.69					69.06	
29	Pinus radiata	Radiata Pine	14.32					76.19	
30	Pinus radiata	Radiata Pine	12.41					55.92	
31	Pinus radiata	Radiata Pine	14.32					76.19	
32	Pinus radiata	Radiata Pine	13.05					62.30	
33	Pinus radiata	Radiata Pine	14.32					76.19	
34	Pinus radiata	Radiata Pine	15.28					87.59	
35	Pinus radiata	Radiata Pine	17.35					115.26	
36	Pinus radiata	Radiata Pine	15.60					91.59	
37	Pinus radiata	Radiata Pine	14.01					72.58	
38	Pinus radiata	Radiata Pine	17.51					117.56	
39	Pinus radiata	Radiata Pine	14.32					76.19	
40	Pinus radiata	Radiata Pine	13.27					64.62	
	Total Dry Weight (kg)							2977.62	
	Total Biomass (tons/ha)							94.53	

Sample Plot No. 4		Plot Size: 21 m x 15 m			Collection Date: 02/02/99			Time: 4:25 p.m.	
Tree #	**Scientific Name**	**Common Name**	**Dbh (cm)**	**Tht (m)**	**Cover (m)**	**ABD (cm)**	**ABL (m)**	**Total Dry Weight (kg)**	**Remarks**
1	Pinus radiata	Radiata Pine	13.37	12.25	4.85	3.80	2.40	65.63	Branching Pattern: 6 -8
2	Pinus radiata	Radiata Pine	15.28					87.59	branches encircling the
3	Pinus radiata	Radiata Pine	13.37					65.63	stem about 6 in. from
4	Pinus radiata	Radiata Pine	9.55					31.72	the ground to the top
5	Pinus radiata	Radiata Pine	14.96					83.70	of the tree.
6	Pinus radiata	Radiata Pine	12.41					55.92	:branches/whorls
7	Pinus radiata	Radiata Pine	13.37					65.63	approximately
8	Pinus radiata	Radiata Pine	15.92					95.67	1-2 ft. apart;
9	Pinus radiata	Radiata Pine	14.32					76.19	:20 - 30 % sky visibility
10	Pinus radiata	Radiata Pine	17.51					117.56	:6 yrs. old
11	Pinus radiata	Radiata Pine	12.73					59.06	:Total ht., cover, ave.
12	Pinus radiata	Radiata Pine	14.32					76.19	branch diameter, and
13	Pinus radiata	Radiata Pine	14.96					83.70	average branch length
14	Pinus radiata	Radiata Pine	12.41					55.92	generally the same for
15	Pinus radiata	Radiata Pine	12.10					52.87	each tree.
16	Pinus radiata	Radiata Pine	14.32					76.19	
17	Pinus radiata	Radiata Pine	12.57					57.48	
18	Pinus radiata	Radiata Pine	11.94					51.37	
19	Pinus radiata	Radiata Pine	15.28					87.59	
20	Pinus radiata	Radiata Pine	15.60					91.59	
21	Pinus radiata	Radiata Pine	16.87					108.51	
22	Pinus radiata	Radiata Pine	12.10					52.87	
23	Pinus radiata	Radiata Pine	16.55					104.14	
24	Pinus radiata	Radiata Pine	19.74					152.31	
25	Pinus radiata	Radiata Pine	14.32					76.19	
26	Pinus radiata	Radiata Pine	12.73					59.06	
27	Pinus radiata	Radiata Pine	14.64					79.89	
28	Pinus radiata	Radiata Pine	10.82					41.57	
29	Pinus radiata	Radiata Pine	15.60					91.59	
30	Pinus radiata	Radiata Pine	13.37					65.63	
31	Pinus radiata	Radiata Pine	14.01					72.58	
32	Pinus radiata	Radiata Pine	11.14					44.26	
33	Pinus radiata	Radiata Pine	15.60					91.59	
34	Pinus radiata	Radiata Pine	15.28					87.59	
35	Pinus radiata	Radiata Pine	18.94					139.34	
36	Pinus radiata	Radiata Pine	15.92					95.67	
37	Pinus radiata	Radiata Pine	14.64					79.89	
38	Pinus radiata	Radiata Pine	12.41					55.92	
39	Pinus radiata	Radiata Pine	12.73					59.06	
40	Pinus radiata	Radiata Pine	14.15					74.19	
41	Pinus radiata	Radiata Pine	18.46					131.86	
42	Pinus radiata	Radiata Pine	15.92					95.67	
43	Pinus radiata	Radiata Pine	18.46					131.86	
	Total Dry Weight (kg)							3428.44	
	Total Biomass (tons/ha)							108.84	

Sample Plot No. 5		Plot Size: 21 m x 15 m	Date: 02/02/99		Collection Date: 02/02/99			Time: 5:10 p.m.	
Tree #'	**Scientific Name**	**Common Name**	**Dbh (cm)**	**Tht (m)**	**Cover (m)**	**ABD (cm)**	**ABL (m)**	**Total Dry Weight (kg)**	**Remarks**
1	Pinus radiata	Radiata Pine	14.96	11.36	5.20	5.20	3.78	83.70	Branching Pattern: 6 -8
2	Pinus radiata	Radiata Pine	12.41					55.92	branches encircling the
3	Pinus radiata	Radiata Pine	14.01					72.58	stem about 6 in. from
4	Pinus radiata	Radiata Pine	14.64					79.89	the ground to the top
5	Pinus radiata	Radiata Pine	16.87					108.51	of the tree.
6	Pinus radiata	Radiata Pine	14.96					83.70	:branches/whorls
7	Pinus radiata	Radiata Pine	17.98					124.60	approximately
8	Pinus radiata	Radiata Pine	14.32					76.19	1-2 ft. apart;
9	Pinus radiata	Radiata Pine	17.51					117.56	:10 - 20 % sky visibility
10	Pinus radiata	Radiata Pine	14.01					72.58	:6 yrs. old
11	Pinus radiata	Radiata Pine	15.92					95.67	
12	Pinus radiata	Radiata Pine	13.69					69.06	
13	Pinus radiata	Radiata Pine	17.51					117.56	
14	Pinus radiata	Radiata Pine	14.01					72.58	
15	Pinus radiata	Radiata Pine	14.64					79.89	
16	Pinus radiata	Radiata Pine	14.01					72.58	
17	Pinus radiata	Radiata Pine	14.96					83.70	
18	Pinus radiata	Radiata Pine	14.01					72.58	
19	Pinus radiata	Radiata Pine	14.32					76.19	
20	Pinus radiata	Radiata Pine	17.19					112.99	
21	Pinus radiata	Radiata Pine	16.23					99.86	
22	Pinus radiata	Radiata Pine	18.46					131.86	
23	Pinus radiata	Radiata Pine	15.28					87.59	
24	Pinus radiata	Radiata Pine	14.64					79.89	
25	Pinus radiata	Radiata Pine	19.42					147.05	
26	Pinus radiata	Radiata Pine	17.83					122.23	
27	Pinus radiata	Radiata Pine	17.51					117.56	
28	Pinus radiata	Radiata Pine	16.87					108.51	
29	Pinus radiata	Radiata Pine	14.96					83.70	
30	Pinus radiata	Radiata Pine	16.23					99.86	
31	Pinus radiata	Radiata Pine	14.32					76.19	
32	Pinus radiata	Radiata Pine	12.10					52.87	
33	Pinus radiata	Radiata Pine	20.05					157.67	
34	Pinus radiata	Radiata Pine	14.32					76.19	
35	Pinus radiata	Radiata Pine	15.28					87.59	
36	Pinus radiata	Radiata Pine	14.01					72.58	
37	Pinus radiata	Radiata Pine	15.44					89.58	
38	Pinus radiata	Radiata Pine	17.19					112.99	
	Total Dry Weight (kg)							3531.76	
	Total Biomass (tons/ha)							112.12	

Sample Plot No.6		Plot Size: 21 m x 15 m		Collection Date: 02/02/99				Time: 6:05 p.m.	
Tree #	**Scientific Name**	**Common Name**	**Dbh (cm)**	**Tht (m)**	**Cover (m)**	**ABD (cm)**	**ABL (m)**	**Total Dry Weight (kg)**	**Remarks**
1	Pinus radiata	Radiata Pine	17.51	11.27	3.90	3.30	2.36	117.56	Branching Pattern: 6 -8
2	Pinus radiata	Radiata Pine	15.92					95.67	branches encircling the
3	Pinus radiata	Radiata Pine	14.01					72.58	stem about 6 in. from
4	Pinus radiata	Radiata Pine	17.83					122.23	the ground to the top
5	Pinus radiata	Radiata Pine	16.55					104.14	of the tree.
6	Pinus radiata	Radiata Pine	16.87					108.51	:branches/whorls
7	Pinus radiata	Radiata Pine	12.89					60.67	approximately
8	Pinus radiata	Radiata Pine	15.92					95.67	1-2 ft. apart;
9	Pinus radiata	Radiata Pine	15.76					93.62	:90 -100 branches/tree
10	Pinus radiata	Radiata Pine	17.83					122.23	:30 - 50 % sky visibility
11	Pinus radiata	Radiata Pine	15.92					95.67	:6 yrs. old
12	Pinus radiata	Radiata Pine	18.14					127.00	
13	Pinus radiata	Radiata Pine	12.73					59.06	
14	Pinus radiata	Radiata Pine	13.37					65.63	
15	Pinus radiata	Radiata Pine	15.60					91.59	
16	Pinus radiata	Radiata Pine	14.64					79.89	
17	Pinus radiata	Radiata Pine	15.76					93.62	
18	Pinus radiata	Radiata Pine	12.57					57.48	
19	Pinus radiata	Radiata Pine	12.73					59.06	
20	Pinus radiata	Radiata Pine	14.48					78.03	
21	Pinus radiata	Radiata Pine	16.39					101.99	
22	Pinus radiata	Radiata Pine	16.55					104.14	
23	Pinus radiata	Radiata Pine	14.16					74.37	
24	Pinus radiata	Radiata Pine	20.85					171.50	
25	Pinus radiata	Radiata Pine	14.80					81.78	
26	Pinus radiata	Radiata Pine	14.32					76.19	
27	Pinus radiata	Radiata Pine	11.78					49.90	
28	Pinus radiata	Radiata Pine	11.30					45.63	
29	Pinus radiata	Radiata Pine	19.89					154.98	
30	Pinus radiata	Radiata Pine	13.05					62.30	
31	Pinus radiata	Radiata Pine	17.51					117.56	
32	Pinus radiata	Radiata Pine	16.39					101.99	
33	Pinus radiata	Radiata Pine	14.96					83.70	
34	Pinus radiata	Radiata Pine	12.25					54.38	
35	Pinus radiata	Radiata Pine	15.92					95.67	
36	Pinus radiata	Radiata Pine	16.55					104.14	
37	Pinus radiata	Radiata Pine	23.71					226.53	
38	Pinus radiata	Radiata Pine	8.44					24.26	
39	Pinus radiata	Radiata Pine	7.64					19.58	
	Total Dry Weight (kg)							3550.51	
	Total Biomass (tons/ha)							112.71	

Sample Plot No. 7		Plot Size: 21 m x 15 m		Collection Date: 06/02/99				Time: 4:10 p.m.	
Tree #	**Scientific Name**	**Common Name**	**Dbh (cm)**	**Tht (m)**	**Cover (m)**	**ABD (cm)**	**ABL (m)**	**Total Dry Weight (kg)**	**Remarks**
1	Pinus radiata	Radiata Pine	23.24	21.34	4.60	3.70	4.00	216.79	Branching Pattern: 6 -8
2	Pinus radiata	Radiata Pine	23.87					229.83	branches encircling the
3	Pinus radiata	Radiata Pine	20.37					163.13	stem about 6 in. from
4	Pinus radiata	Radiata Pine	18.78					136.82	the ground to the top
5	Pinus radiata	Radiata Pine	21.65					185.97	of the tree.
6	Pinus radiata	Radiata Pine	19.74					152.31	:branches/whorls
7	Pinus radiata	Radiata Pine	17.19					112.99	approximately
8	Pinus radiata	Radiata Pine	20.69					168.69	1-2 ft. apart;
9	Pinus radiata	Radiata Pine	25.46					264.24	:90 -100 branches/tree
10	Pinus radiata	Radiata Pine	20.05					157.67	:10 - 15 % sky visibility
11	Pinus radiata	Radiata Pine	15.60					91.59	:22 yrs. old
12	Pinus radiata	Radiata Pine	19.74					152.31	
13	Pinus radiata	Radiata Pine	20.69					168.69	
14	Pinus radiata	Radiata Pine	22.92					210.42	
15	Pinus radiata	Radiata Pine	20.69					168.69	
16	Pinus radiata	Radiata Pine	20.05					157.67	
17	Pinus radiata	Radiata Pine	18.78					136.82	
18	Pinus radiata	Radiata Pine	22.60					204.16	
19	Pinus radiata	Radiata Pine	22.28					197.99	
20	Pinus radiata	Radiata Pine	21.96					191.93	
21	Pinus radiata	Radiata Pine	20.37					163.13	
22	Pinus radiata	Radiata Pine	21.96					191.93	
23	Pinus radiata	Radiata Pine	18.78					136.82	
24	Pinus radiata	Radiata Pine	24.19					236.51	
25	Pinus radiata	Radiata Pine	23.24					216.79	
26	Pinus radiata	Radiata Pine	23.87					229.83	
27	Pinus radiata	Radiata Pine	22.28					197.99	
28	Pinus radiata	Radiata Pine	21.33					180.11	
29	Pinus radiata	Radiata Pine	24.19					236.51	
30	Pinus radiata	Radiata Pine	25.94					275.06	
31	Pinus radiata	Radiata Pine	21.33					180.11	
32	Pinus radiata	Radiata Pine	23.87					229.83	
33	Pinus radiata	Radiata Pine	22.28					197.99	
34	Pinus radiata	Radiata Pine	24.83					250.17	
35	Pinus radiata	Radiata Pine	21.65					185.97	
36	Pinus radiata	Radiata Pine	22.92					210.42	
	Total Dry Weight (kg)							6787.86	
	Total Biomass (tons/ha)							215.49	

Sample Plot No.8		Plot Size: 21 m x 15 m		Collection Date: 03/02/99				Time: 11:00 a.m.	
Tree #	**Scientific Name**	**Common Name**	**Dbh (cm)**	**Tht (m)**	**Cover (m)**	**ABD (cm)**	**ABL (m)**	**Total Dry Weight (kg)**	**Remarks**
1	Pinus radiata	Radiata Pine	18.78	12.87	5.20	5.00	2.30	136.82	Branching Pattern: 6 -8
2	Pinus radiata	Radiata Pine	18.78					136.82	branches encircling the
3	Pinus radiata	Radiata Pine	17.98					124.60	stem about 6 in. from
4	Pinus radiata	Radiata Pine	21.65					185.97	the ground to the top
5	Pinus radiata	Radiata Pine	12.73					59.06	of the tree.
6	Pinus radiata	Radiata Pine	20.85					171.50	:branches/whorls
7	Pinus radiata	Radiata Pine	21.96					191.93	approximately
8	Pinus radiata	Radiata Pine	18.78					136.82	1-2 ft. apart;
9	Pinus radiata	Radiata Pine	24.19					236.51	:90 -100 branches/tree
10	Pinus radiata	Radiata Pine	18.14					127.00	:10 - 15 % sky visibility
11	Pinus radiata	Radiata Pine	15.28					87.59	:9 yrs. old
12	Pinus radiata	Radiata Pine	17.83					122.23	
13	Pinus radiata	Radiata Pine	18.14					127.00	
14	Pinus radiata	Radiata Pine	20.37					163.13	
15	Pinus radiata	Radiata Pine	16.87					108.51	
16	Pinus radiata	Radiata Pine	19.10					141.89	
17	Pinus radiata	Radiata Pine	14.48					78.03	
18	Pinus radiata	Radiata Pine	16.87					108.51	
19	Pinus radiata	Radiata Pine	14.64					79.89	
20	Pinus radiata	Radiata Pine	15.92					95.67	
21	Pinus radiata	Radiata Pine	17.51					117.56	
22	Pinus radiata	Radiata Pine	13.37					65.63	
23	Pinus radiata	Radiata Pine	16.87					108.51	
24	Pinus radiata	Radiata Pine	21.96					191.93	
25	Pinus radiata	Radiata Pine	16.87					108.51	
26	Pinus radiata	Radiata Pine	14.64					79.89	
27	Pinus radiata	Radiata Pine	18.14					127.00	
28	Pinus radiata	Radiata Pine	18.14					127.00	
29	Pinus radiata	Radiata Pine	12.10					52.87	
30	Pinus radiata	Radiata Pine	18.78					136.82	
31	Pinus radiata	Radiata Pine	13.37					65.63	
32	Pinus radiata	Radiata Pine	13.69					69.06	
33	Pinus radiata	Radiata Pine	19.10					141.89	
34	Pinus radiata	Radiata Pine	13.37					65.63	
	Total Dry Weight (kg)							4077.44	
	Total Biomass (tons/ha)							129.44	

Sample Plot No .9		Plot Size: 21 m x 15 m		Collection Date: 03/02/99				Time:11:35 a.m.	
Tree #	**Scientific Name**	**Common Name**	**Dbh (cm)**	**Tht (m)**	**Cover (m)**	**ABD (cm)**	**ABL (m)**	**Total Dry Weight (kg)**	**Remarks**
1	Pinus radiata	Radiata Pine	16.55	13.81	6.25	4.00	4.00	104.14	Branching Pattern: 6 -8
2	Pinus radiata	Radiata Pine	17.51					117.56	branches encircling the
3	Pinus radiata	Radiata Pine	16.55					104.14	stem about 6 in. from
4	Pinus radiata	Radiata Pine	17.51					117.56	the ground to the top
5	Pinus radiata	Radiata Pine	18.46					131.86	of the tree.
6	Pinus radiata	Radiata Pine	18.78					136.82	:branches/whorls
7	Pinus radiata	Radiata Pine	16.87					108.51	approximately
8	Pinus radiata	Radiata Pine	15.28					87.59	1-2 ft. apart;
9	Pinus radiata	Radiata Pine	17.51					117.56	:90 -100 branches/tree
10	Pinus radiata	Radiata Pine	17.35					115.26	:25 - 30 % sky visibility
11	Pinus radiata	Radiata Pine	17.19					112.99	:9 yrs. old
12	Pinus radiata	Radiata Pine	18.14					127.00	
13	Pinus radiata	Radiata Pine	17.19					112.99	
14	Pinus radiata	Radiata Pine	16.55					104.14	
15	Pinus radiata	Radiata Pine	17.03					110.74	
16	Pinus radiata	Radiata Pine	17.51					117.56	
17	Pinus radiata	Radiata Pine	18.46					131.86	
18	Pinus radiata	Radiata Pine	17.51					117.56	
19	Pinus radiata	Radiata Pine	15.60					91.59	
20	Pinus radiata	Radiata Pine	18.14					127.00	
21	Pinus radiata	Radiata Pine	15.92					95.67	
22	Pinus radiata	Radiata Pine	16.55					104.14	
23	Pinus radiata	Radiata Pine	16.55					104.14	
24	Pinus radiata	Radiata Pine	17.35					115.26	
25	Pinus radiata	Radiata Pine	15.76					93.62	
26	Pinus radiata	Radiata Pine	16.87					108.51	
27	Pinus radiata	Radiata Pine	15.60					91.59	
28	Pinus radiata	Radiata Pine	16.55					104.14	
29	Pinus radiata	Radiata Pine	17.83					122.23	
30	Pinus radiata	Radiata Pine	14.32					76.19	
31	Pinus radiata	Radiata Pine	17.83					122.23	
32	Pinus radiata	Radiata Pine	17.83					122.23	
33	Pinus radiata	Radiata Pine	14.32					76.19	
34	Pinus radiata	Radiata Pine	14.96					83.70	
35	Pinus radiata	Radiata Pine	14.32					76.19	
36	Pinus radiata	Radiata Pine	17.51					117.56	
37	Pinus radiata	Radiata Pine	18.06					125.80	
38	Pinus radiata	Radiata Pine	17.51					117.56	
	Total Dry Weight (kg)							4151.36	
	Total Biomass (tons/ha)							131.79	

Sample Plot No. 10		Plot Size: 21 m x 15 m		Collection Date: 03/02/99				Time: 12:00 noon	
Tree #	**Scientific Name**	**Common Name**	**Dbh (cm)**	**Tht (m)**	**Cover (m)**	**ABD (cm)**	**ABL (m)**	**Total Dry Weight (kg)**	**Remarks**
1	Pinus radiata	Radiata Pine	14.64	16.30	6.00	5.60	4.30	79.89	Branching Pattern: 6 -8
2	Pinus radiata	Radiata Pine	17.83					122.23	branches encircling the
3	Pinus radiata	Radiata Pine	15.28					87.59	stem about 6 in. from
4	Pinus radiata	Radiata Pine	16.55					104.14	the ground to the top
5	Pinus radiata	Radiata Pine	19.10					141.89	of the tree.
6	Pinus radiata	Radiata Pine	17.03					110.74	:branches/whorls
7	Pinus radiata	Radiata Pine	16.87					108.51	approximately
8	Pinus radiata	Radiata Pine	18.78					136.82	1-2 ft. apart;
9	Pinus radiata	Radiata Pine	17.19					112.99	:30 - 40 % sky visibility
10	Pinus radiata	Radiata Pine	18.46					131.86	:10 yrs. old
11	Pinus radiata	Radiata Pine	17.51					117.56	
12	Pinus radiata	Radiata Pine	16.87					108.51	
13	Pinus radiata	Radiata Pine	18.62					134.33	
14	Pinus radiata	Radiata Pine	15.60					91.59	
15	Pinus radiata	Radiata Pine	17.83					122.23	
16	Pinus radiata	Radiata Pine	17.51					117.56	
17	Pinus radiata	Radiata Pine	15.28					87.59	
18	Pinus radiata	Radiata Pine	15.92					95.67	
19	Pinus radiata	Radiata Pine	16.87					108.51	
20	Pinus radiata	Radiata Pine	15.28					87.59	
21	Pinus radiata	Radiata Pine	16.87					108.51	
22	Pinus radiata	Radiata Pine	14.96					83.70	
23	Pinus radiata	Radiata Pine	17.83					122.23	
24	Pinus radiata	Radiata Pine	17.83					122.23	
25	Pinus radiata	Radiata Pine	16.55					104.14	
26	Pinus radiata	Radiata Pine	17.19					112.99	
27	Pinus radiata	Radiata Pine	16.87					108.51	
28	Pinus radiata	Radiata Pine	18.14					127.00	
29	Pinus radiata	Radiata Pine	17.51					117.56	
30	Pinus radiata	Radiata Pine	15.60					91.59	
31	Pinus radiata	Radiata Pine	14.64					79.89	
32	Pinus radiata	Radiata Pine	14.64					79.89	
33	Pinus radiata	Radiata Pine	16.87					108.51	
34	Pinus radiata	Radiata Pine	15.12					85.63	
35	Pinus radiata	Radiata Pine	14.96					83.70	
36	Pinus radiata	Radiata Pine	17.51					117.56	
37	Pinus radiata	Radiata Pine	17.19					112.99	
38	Pinus radiata	Radiata Pine	14.96					83.70	
39	Pinus radiata	Radiata Pine	12.10					52.87	
40	Pinus radiata	Radiata Pine	15.28					87.59	
41	Pinus radiata	Radiata Pine	15.28					87.59	
42	Pinus radiata	Radiata Pine	15.60					91.59	
43	Pinus radiata	Radiata Pine	15.36					88.58	
	Total Dry Weight (kg)							4466.38	
	Total Biomass (tons/ha)							141.79	

Sample Plot No. 11		Plot Size: 21 m x 15 m		Collection Date: 03/02/99				Time: 1:40 p.m.	
Tree #	**Scientific Name**	**Common Name**	**Dbh (cm)**	**Tht (m)**	**Cover (m)**	**ABD (cm)**	**ABL (m)**	**Total Dry Weight (kg)**	**Remarks**
1	Pinus radiata	Radiata Pine	20.69	14.44	4.65	3.90	3.70	168.69	Branching Pattern: 6 -8
2	Pinus radiata	Radiata Pine	13.69					69.06	branches encircling the
3	Pinus radiata	Radiata Pine	21.65					185.97	stem about 6 in. from
4	Pinus radiata	Radiata Pine	23.55					223.26	the ground to the top
5	Pinus radiata	Radiata Pine	20.21					160.38	of the tree.
6	Pinus radiata	Radiata Pine	18.78					136.82	:branches/whorls
7	Pinus radiata	Radiata Pine	19.10					141.89	approximately
8	Pinus radiata	Radiata Pine	16.87					108.51	1-2 ft. apart;
9	Pinus radiata	Radiata Pine	23.87					229.83	:10 - 15 % sky visibility
10	Pinus radiata	Radiata Pine	19.42					147.05	:10 yrs. old
11	Pinus radiata	Radiata Pine	18.14					127.00	
12	Pinus radiata	Radiata Pine	18.78					136.82	
13	Pinus radiata	Radiata Pine	19.74					152.31	
14	Pinus radiata	Radiata Pine	16.23					99.86	
15	Pinus radiata	Radiata Pine	14.32					76.19	
16	Pinus radiata	Radiata Pine	13.05					62.30	
17	Pinus radiata	Radiata Pine	18.46					131.86	
18	Pinus radiata	Radiata Pine	19.42					147.05	
19	Pinus radiata	Radiata Pine	15.60					91.59	
20	Pinus radiata	Radiata Pine	16.23					99.86	
21	Pinus radiata	Radiata Pine	16.55					104.14	
22	Pinus radiata	Radiata Pine	14.32					76.19	
23	Pinus radiata	Radiata Pine	16.87					108.51	
24	Pinus radiata	Radiata Pine	17.51					117.56	
25	Pinus radiata	Radiata Pine	14.96					83.70	
26	Pinus radiata	Radiata Pine	17.51					117.56	
27	Pinus radiata	Radiata Pine	14.32					76.19	
28	Pinus radiata	Radiata Pine	15.92					95.67	
29	Pinus radiata	Radiata Pine	16.55					104.14	
30	Pinus radiata	Radiata Pine	17.51					117.56	
31	Pinus radiata	Radiata Pine	17.19					112.99	
32	Pinus radiata	Radiata Pine	18.46					131.86	
33	Pinus radiata	Radiata Pine	17.83					122.23	
34	Pinus radiata	Radiata Pine	16.87					108.51	
35	Pinus radiata	Radiata Pine	14.64					79.89	
36	Pinus radiata	Radiata Pine	19.74					152.31	
37	Pinus radiata	Radiata Pine	14.64					79.89	
38	Pinus radiata	Radiata Pine	16.87					108.51	
39	Pinus radiata	Radiata Pine	17.60					118.95	
40	Pinus radiata	Radiata Pine	18.14					127.00	
	Total Dry Weight (kg)							4839.66	
	Total Biomass (tons/ha)							153.64	

Sample Plot No.12		Plot Size: 21 m x 15 m		Collection Date: 03/02/99				Time: 2:10 p.m.	
Tree #	**Scientific Name**	**Common Name**	**Dbh (cm)**	**Tht (m)**	**Cover (m)**	**ABD (cm)**	**ABL (m)**	**Total Dry Weight (kg)**	**Remarks**
1	Pinus radiata	Radiata Pine	15.92	13.55	4.00	3.80	4.20	95.67	Branching Pattern: 6 -8
2	Pinus radiata	Radiata Pine	16.39					101.99	branches encircling the
3	Pinus radiata	Radiata Pine	19.42					147.05	stem about 6 in. from
4	Pinus radiata	Radiata Pine	18.46					131.86	the ground to the top
5	Pinus radiata	Radiata Pine	20.37					163.13	of the tree.
6	Pinus radiata	Radiata Pine	18.30					129.42	:branches/whorls
7	Pinus radiata	Radiata Pine	19.89					154.98	approximately
8	Pinus radiata	Radiata Pine	12.10					52.87	1-3 ft. apart;
9	Pinus radiata	Radiata Pine	17.83					122.23	:30 - 50 % sky visibility
10	Pinus radiata	Radiata Pine	16.23					99.86	:10 yrs. old
11	Pinus radiata	Radiata Pine	20.69					168.69	
12	Pinus radiata	Radiata Pine	20.05					157.67	
13	Pinus radiata	Radiata Pine	16.07					97.75	
14	Pinus radiata	Radiata Pine	17.19					112.99	
15	Pinus radiata	Radiata Pine	15.92					95.67	
16	Pinus radiata	Radiata Pine	16.55					104.14	
17	Pinus radiata	Radiata Pine	15.92					95.67	
18	Pinus radiata	Radiata Pine	22.44					201.06	
19	Pinus radiata	Radiata Pine	17.51					117.56	
20	Pinus radiata	Radiata Pine	21.33					180.11	
21	Pinus radiata	Radiata Pine	20.05					157.67	
22	Pinus radiata	Radiata Pine	18.94					139.34	
23	Pinus radiata	Radiata Pine	19.10					141.89	
24	Pinus radiata	Radiata Pine	20.05					157.67	
25	Pinus radiata	Radiata Pine	16.87					108.51	
26	Pinus radiata	Radiata Pine	21.01					174.35	
27	Pinus radiata	Radiata Pine	16.87					108.51	
28	Pinus radiata	Radiata Pine	17.51					117.56	
29	Pinus radiata	Radiata Pine	19.74					152.31	
30	Pinus radiata	Radiata Pine	14.96					83.70	
31	Pinus radiata	Radiata Pine	15.92					95.67	
32	Pinus radiata	Radiata Pine	13.37					65.63	
33	Pinus radiata	Radiata Pine	18.78					136.82	
34	Pinus radiata	Radiata Pine	16.39					101.99	
35	Pinus radiata	Radiata Pine	17.83					122.23	
36	Pinus radiata	Radiata Pine	21.33					180.11	
37	Pinus radiata	Radiata Pine	13.37					65.63	
38	Pinus radiata	Radiata Pine	10.50					38.97	
39	Pinus radiata	Radiata Pine	10.03					35.24	
	Total Dry Weight (kg)							4714.15	
	Total Biomass (tons/ha)							149.66	

Sample Plot No. 13		Plot Size: 21 m x 15 m		Collection Date: 03/02/99				Time: 3:05 p.m.	
Tree #	**Scientific Name**	**Common Name**	**Dbh (cm)**	**Tht (m)**	**Cover (m)**	**ABD (cm)**	**ABL (m)**	**Total Dry Weight (kg)**	**Remarks**
1	Pinus radiata	Radiata Pine	21.49	18.050	4.800	3.600	3.500	183.02	Branching Pattern: 6 -8
2	Pinus radiata	Radiata Pine	24.19					236.51	branches encircling the
3	Pinus radiata	Radiata Pine	23.24					216.79	stem about 6 in. from
4	Pinus radiata	Radiata Pine	24.67					246.71	the ground to the top
5	Pinus radiata	Radiata Pine	24.51					243.29	of the tree.
6	Pinus radiata	Radiata Pine	22.28					197.99	:branches/whorls
7	Pinus radiata	Radiata Pine	20.05					157.67	approximately
8	Pinus radiata	Radiata Pine	27.69					316.77	1-2 ft. apart;
9	Pinus radiata	Radiata Pine	25.46					264.24	:10 - 15 % sky visibility
10	Pinus radiata	Radiata Pine	13.37					65.63	:19 yrs. old
11	Pinus radiata	Radiata Pine	13.69					69.06	
12	Pinus radiata	Radiata Pine	22.92					210.42	
13	Pinus radiata	Radiata Pine	31.19					409.73	
14	Pinus radiata	Radiata Pine	20.69					168.69	
15	Pinus radiata	Radiata Pine	19.10					141.89	
16	Pinus radiata	Radiata Pine	14.01					72.58	
17	Pinus radiata	Radiata Pine	23.55					223.26	
18	Pinus radiata	Radiata Pine	20.05					157.67	
19	Pinus radiata	Radiata Pine	20.05					157.67	
20	Pinus radiata	Radiata Pine	25.15					257.15	
21	Pinus radiata	Radiata Pine	13.53					67.33	
22	Pinus radiata	Radiata Pine	15.92					95.67	
23	Pinus radiata	Radiata Pine	25.46					264.24	
24	Pinus radiata	Radiata Pine	27.37					308.95	
25	Pinus radiata	Radiata Pine	23.87					229.83	
26	Pinus radiata	Radiata Pine	23.08					213.59	
27	Pinus radiata	Radiata Pine	23.55					223.26	
28	Pinus radiata	Radiata Pine	25.31					260.68	
29	Pinus radiata	Radiata Pine	24.19					236.51	
30	Pinus radiata	Radiata Pine	21.65					185.97	
	Total Dry Weight (kg)							6082.77	
	Total Biomass (tons/ha)							193.10	

Sample Plot No.14		Plot Size: 21 m x 15 m		Date: 03/02/99				Time: 4:00 p.m.	
Tree #	**Scientific Name**	**Common Name**	**Dbh (cm)**	**Tht (m)**	**Cover (m)**	**ABD (cm)**	**ABL (m)**	**Total Dry Weight (kg)**	**Remarks**
1	Pinus radiata	Radiata Pine	16.23	19.75	4.05	3.80	2.20	99.86	Branching Pattern: 6 -8
2	Pinus radiata	Radiata Pine	22.12					194.95	branches encircling the
3	Pinus radiata	Radiata Pine	28.97					349.09	stem about 6 in. from
4	Pinus radiata	Radiata Pine	21.96					191.93	the ground to the top
5	Pinus radiata	Radiata Pine	22.92					210.42	of the tree.
6	Pinus radiata	Radiata Pine	20.69					168.69	:branches/whorls
7	Pinus radiata	Radiata Pine	22.28					197.99	approximately
8	Pinus radiata	Radiata Pine	24.19					236.51	1-3 ft. apart;
9	Pinus radiata	Radiata Pine	19.42					147.05	:40 % sky visibility
10	Pinus radiata	Radiata Pine	21.33					180.11	:19 yrs. old
11	Pinus radiata	Radiata Pine	20.05					157.67	
12	Pinus radiata	Radiata Pine	20.37					163.13	
13	Pinus radiata	Radiata Pine	22.92					210.42	
14	Pinus radiata	Radiata Pine	23.87					229.83	
15	Pinus radiata	Radiata Pine	20.37					163.13	
16	Pinus radiata	Radiata Pine	28.33					332.72	
17	Pinus radiata	Radiata Pine	18.78					136.82	
18	Pinus radiata	Radiata Pine	22.92					210.42	
19	Pinus radiata	Radiata Pine	16.23					99.86	
20	Pinus radiata	Radiata Pine	24.19					236.51	
21	Pinus radiata	Radiata Pine	14.64					79.89	
22	Pinus radiata	Radiata Pine	21.96					191.93	
23	Pinus radiata	Radiata Pine	21.01					174.35	
24	Pinus radiata	Radiata Pine	22.92					210.42	
25	Pinus radiata	Radiata Pine	19.42					147.05	
26	Pinus radiata	Radiata Pine	20.69					168.69	
27	Pinus radiata	Radiata Pine	20.05					157.67	
28	Pinus radiata	Radiata Pine	21.65					185.97	
29	Pinus radiata	Radiata Pine	18.14					127.00	
30	Pinus radiata	Radiata Pine	20.69					168.69	
31	Pinus radiata	Radiata Pine	20.05					157.67	
32	Pinus radiata	Radiata Pine	21.01					174.35	
33	Pinus radiata	Radiata Pine	13.69					69.06	
34	Pinus radiata	Radiata Pine	18.61					134.08	
35	Pinus radiata	Radiata Pine	23.87					229.83	
	Total Dry Weight (kg)							6293.72	
	Total Biomass (tons/ha)							199.80	

Sample Plot No. 15		Plot Size: 21 m x 15 m		Collection Date: 03/02/99				Time: 4:20 p.m.	
Tree #	**Scientific Name**	**Common Name**	**Dbh (cm)**	**Tht (m)**	**Cover (m)**	**ABD (cm)**	**ABL (m)**	**Total Dry Weight (kg)**	**Remarks**
1	Pinus radiata	Radiata Pine	16.87	19.74	5.45	4.20	3.60	108.51	Branching Pattern: 6 -10
2	Pinus radiata	Radiata Pine	18.46					131.86	branches encircling the
3	Pinus radiata	Radiata Pine	18.14					127.00	stem about 6 in. from
4	Pinus radiata	Radiata Pine	22.92					210.42	the ground to the top
5	Pinus radiata	Radiata Pine	23.08					213.59	of the tree.
6	Pinus radiata	Radiata Pine	20.69					168.69	:branches/whorls
7	Pinus radiata	Radiata Pine	21.01					174.35	approximately
8	Pinus radiata	Radiata Pine	21.65					185.97	1-3 ft. apart;
9	Pinus radiata	Radiata Pine	17.19					112.99	:30 - 40 % sky visibility
10	Pinus radiata	Radiata Pine	18.78					136.82	:19 yrs. old
11	Pinus radiata	Radiata Pine	19.10					141.89	
12	Pinus radiata	Radiata Pine	18.46					131.86	
13	Pinus radiata	Radiata Pine	17.51					117.56	
14	Pinus radiata	Radiata Pine	17.83					122.23	
15	Pinus radiata	Radiata Pine	21.01					174.35	
16	Pinus radiata	Radiata Pine	16.71					106.31	
17	Pinus radiata	Radiata Pine	19.74					152.31	
18	Pinus radiata	Radiata Pine	18.62					134.33	
19	Pinus radiata	Radiata Pine	19.10					141.89	
20	Pinus radiata	Radiata Pine	20.53					165.89	
21	Pinus radiata	Radiata Pine	14.96					83.70	
22	Pinus radiata	Radiata Pine	20.69					168.69	
23	Pinus radiata	Radiata Pine	21.33					180.11	
24	Pinus radiata	Radiata Pine	22.92					210.42	
25	Pinus radiata	Radiata Pine	23.87					229.83	
26	Pinus radiata	Radiata Pine	15.28					87.59	
27	Pinus radiata	Radiata Pine	18.78					136.82	
28	Pinus radiata	Radiata Pine	19.42					147.05	
29	Pinus radiata	Radiata Pine	16.87					108.51	
30	Pinus radiata	Radiata Pine	20.05					157.67	
31	Pinus radiata	Radiata Pine	17.51					117.56	
32	Pinus radiata	Radiata Pine	19.42					147.05	
33	Pinus radiata	Radiata Pine	19.26					144.45	
34	Pinus radiata	Radiata Pine	20.37					163.13	
35	Pinus radiata	Radiata Pine	18.14					127.00	
36	Pinus radiata	Radiata Pine	15.76					93.62	
37	Pinus radiata	Radiata Pine	17.51					117.56	
38	Pinus radiata	Radiata Pine	18.94					139.34	
39	Pinus radiata	Radiata Pine	16.87					108.51	
40	Pinus radiata	Radiata Pine	18.14					127.00	
41	Pinus radiata	Radiata Pine	16.55					104.14	
42	Pinus radiata	Radiata Pine	17.67					119.88	
43	Pinus radiata	Radiata Pine	16.23					99.86	
44	Pinus radiata	Radiata Pine	17.83					122.23	
	Total Dry Weight (kg)							6200.54	
	Total Biomass (tons/ha)							196.84	

Sample Plot No. 16		Plot Size: 21 m x 15 m		Collection Date: 03/02/99				Time: 4:35 p.m.	
Tree #	**Scientific Name**	**Common Name**	**Dbh (cm)**	**Tht (m)**	**Cover (m)**	**ABD (cm)**	**ABL (m)**	**Total Dry Weight (kg)**	**Remarks**
1	Pinus radiata	Radiata Pine	24.19	21.34	3.85	3.50	2.40	236.51	Branching Pattern: 6 - 8
2	Pinus radiata	Radiata Pine	23.87					229.83	branches encircling the
3	Pinus radiata	Radiata Pine	30.24					383.10	stem about 6 in. from
4	Pinus radiata	Radiata Pine	23.24					216.79	the ground to the top
5	Pinus radiata	Radiata Pine	26.10					278.73	of the tree.
6	Pinus radiata	Radiata Pine	21.01					174.35	:branches/whorls
7	Pinus radiata	Radiata Pine	23.87					229.83	approximately
8	Pinus radiata	Radiata Pine	24.19					236.51	1-2 ft. apart;
9	Pinus radiata	Radiata Pine	22.28					197.99	:20 - 25 % sky visibility
10	Pinus radiata	Radiata Pine	20.69					168.69	:22 yrs. old
11	Pinus radiata	Radiata Pine	21.96					191.93	
12	Pinus radiata	Radiata Pine	24.83					250.17	
13	Pinus radiata	Radiata Pine	18.46					131.86	
14	Pinus radiata	Radiata Pine	24.83					250.17	
15	Pinus radiata	Radiata Pine	18.46					131.86	
16	Pinus radiata	Radiata Pine	22.60					204.16	
17	Pinus radiata	Radiata Pine	20.69					168.69	
18	Pinus radiata	Radiata Pine	21.65					185.97	
19	Pinus radiata	Radiata Pine	20.69					168.69	
20	Pinus radiata	Radiata Pine	19.10					141.89	
21	Pinus radiata	Radiata Pine	18.46					131.86	
22	Pinus radiata	Radiata Pine	20.69					168.69	
23	Pinus radiata	Radiata Pine	21.33					180.11	
24	Pinus radiata	Radiata Pine	19.74					152.31	
25	Pinus radiata	Radiata Pine	15.60					91.59	
26	Pinus radiata	Radiata Pine	20.69					168.69	
27	Pinus radiata	Radiata Pine	24.83					250.17	
28	Pinus radiata	Radiata Pine	21.01					174.35	
29	Pinus radiata	Radiata Pine	20.07					157.94	
30	Pinus radiata	Radiata Pine	19.74					152.31	
31	Pinus radiata	Radiata Pine	21.65					185.97	
32	Pinus radiata	Radiata Pine	19.42					147.05	
33	Pinus radiata	Radiata Pine	17.51					117.56	
34	Pinus radiata	Radiata Pine	20.69					168.69	
35	Pinus radiata	Radiata Pine	19.74					152.31	
36	Pinus radiata	Radiata Pine	18.46					131.86	
	Total Dry Weight (kg)							6709.11	
	Total Biomass (tons/ha)							212.99	

Sample Plot No.17		Plot Size: 21 m x 15 m		Collection Date: 03/02/99				Time: 5:10 a.m.	
Tree #	**Scientific Name**	**Common Name**	**Dbh (cm)**	**Tht (m)**	**Cover (m)**	**ABD (cm)**	**ABL (m)**	**Total Dry Weight (kg)**	**Remarks**
1	Pinus radiata	Radiata Pine	20.69	21.53	6.75	5.20	4.80	168.69	Branching Pattern: 6 - 8
2	Pinus radiata	Radiata Pine	21.65					185.97	branches encircling the
3	Pinus radiata	Radiata Pine	20.05					157.67	stem about 6 in. from
4	Pinus radiata	Radiata Pine	19.74					152.31	the ground to the top
5	Pinus radiata	Radiata Pine	18.78					136.82	of the tree.
6	Pinus radiata	Radiata Pine	21.17					177.21	:branches/whorls
7	Pinus radiata	Radiata Pine	18.78					136.82	approximately
8	Pinus radiata	Radiata Pine	18.78					136.82	1-2 ft. apart;
9	Pinus radiata	Radiata Pine	20.37					163.13	:10 - 15 % sky visibility
10	Pinus radiata	Radiata Pine	20.05					157.67	:22 yrs. old
11	Pinus radiata	Radiata Pine	17.51					117.56	
12	Pinus radiata	Radiata Pine	17.51					117.56	
13	Pinus radiata	Radiata Pine	22.92					210.42	
14	Pinus radiata	Radiata Pine	20.69					168.69	
15	Pinus radiata	Radiata Pine	21.01					174.35	
16	Pinus radiata	Radiata Pine	21.01					174.35	
17	Pinus radiata	Radiata Pine	18.78					136.82	
18	Pinus radiata	Radiata Pine	22.28					197.99	
19	Pinus radiata	Radiata Pine	20.53					165.89	
20	Pinus radiata	Radiata Pine	21.33					180.11	
21	Pinus radiata	Radiata Pine	18.78					136.82	
22	Pinus radiata	Radiata Pine	19.42					147.05	
23	Pinus radiata	Radiata Pine	17.51					117.56	
24	Pinus radiata	Radiata Pine	21.33					180.11	
25	Pinus radiata	Radiata Pine	19.42					147.05	
26	Pinus radiata	Radiata Pine	18.78					136.82	
27	Pinus radiata	Radiata Pine	21.65					185.97	
28	Pinus radiata	Radiata Pine	16.71					106.31	
29	Pinus radiata	Radiata Pine	17.51					117.56	
30	Pinus radiata	Radiata Pine	20.85					171.50	
31	Pinus radiata	Radiata Pine	19.89					154.98	
32	Pinus radiata	Radiata Pine	18.46					131.86	
33	Pinus radiata	Radiata Pine	19.74					152.31	
34	Pinus radiata	Radiata Pine	18.78					136.82	
35	Pinus radiata	Radiata Pine	19.74					152.31	
36	Pinus radiata	Radiata Pine	20.69					168.69	
37	Pinus radiata	Radiata Pine	20.21					160.38	
38	Pinus radiata	Radiata Pine	18.30					129.42	
39	Pinus radiata	Radiata Pine	14.32					76.19	
40	Pinus radiata	Radiata Pine	17.83					122.23	
41	Pinus radiata	Radiata Pine	17.51					117.56	
42	Pinus radiata	Radiata Pine	17.83					122.23	
43	Pinus radiata	Radiata Pine	17.19					112.99	
44	Pinus radiata	Radiata Pine	17.03					110.74	
45	Pinus radiata	Radiata Pine	17.19					112.99	
46	Pinus radiata	Radiata Pine	17.38					115.72	
	Total Dry Weight (kg)							6741.01	
	Total Biomass (tons/ha)							214.00	

Sample Plot No.18		Plot Size: 21 m x 15 m		Collection Date: 04/02/99				Time: 11:10 p.m.	
Tree #	**Scientific Name**	**Common Name**	**Dbh (cm)**	**Tht (m)**	**Cover (m)**	**ABD (cm)**	**ABL (m)**	**Total Dry Weight (kg)**	**Remarks**
1	Pinus radiata	Radiata Pine	23.87	21.72	4.90	3.50	4.05	229.83	Branching Pattern: 6 - 8
2	Pinus radiata	Radiata Pine	21.33					180.11	branches encircling the
3	Pinus radiata	Radiata Pine	19.42					147.05	stem about 6 in. from
4	Pinus radiata	Radiata Pine	20.05					157.67	the ground to the top
5	Pinus radiata	Radiata Pine	22.28					197.99	of the tree.
6	Pinus radiata	Radiata Pine	20.05					157.67	:branches/whorls
7	Pinus radiata	Radiata Pine	19.10					141.89	approximately
8	Pinus radiata	Radiata Pine	18.46					131.86	1-2 ft. apart;
9	Pinus radiata	Radiata Pine	23.87					229.83	:10 - 15 % sky visibility
10	Pinus radiata	Radiata Pine	20.05					157.67	:22 yrs. old
11	Pinus radiata	Radiata Pine	18.14					127.00	
12	Pinus radiata	Radiata Pine	18.46					131.86	
13	Pinus radiata	Radiata Pine	21.33					180.11	
14	Pinus radiata	Radiata Pine	19.74					152.31	
15	Pinus radiata	Radiata Pine	19.10					141.89	
16	Pinus radiata	Radiata Pine	20.69					168.69	
17	Pinus radiata	Radiata Pine	16.87					108.51	
18	Pinus radiata	Radiata Pine	21.65					185.97	
19	Pinus radiata	Radiata Pine	17.51					117.56	
20	Pinus radiata	Radiata Pine	19.74					152.31	
21	Pinus radiata	Radiata Pine	19.74					152.31	
22	Pinus radiata	Radiata Pine	21.33					180.11	
23	Pinus radiata	Radiata Pine	23.87					229.83	
24	Pinus radiata	Radiata Pine	20.05					157.67	
25	Pinus radiata	Radiata Pine	19.42					147.05	
26	Pinus radiata	Radiata Pine	25.46					264.24	
27	Pinus radiata	Radiata Pine	23.24					216.79	
28	Pinus radiata	Radiata Pine	21.65					185.97	
29	Pinus radiata	Radiata Pine	20.05					157.67	
30	Pinus radiata	Radiata Pine	25.31					260.68	
31	Pinus radiata	Radiata Pine	18.46					131.86	
32	Pinus radiata	Radiata Pine	21.33					180.11	
33	Pinus radiata	Radiata Pine	20.37					163.13	
34	Pinus radiata	Radiata Pine	20.69					168.69	
35	Pinus radiata	Radiata Pine	20.05					157.67	
36	Pinus radiata	Radiata Pine	21.96					191.93	
37	Pinus radiata	Radiata Pine	20.69					168.69	
38	Pinus radiata	Radiata Pine	20.05					157.67	
39	Pinus radiata	Radiata Pine	20.47					164.78	
40	Pinus radiata	Radiata Pine	21.65					185.97	
	Total Dry Weight (kg)							6820.54	
	Total Biomass (tons/ha)							216.53	

Sample Plot No. 19		Plot Size: 21 m x 15 m		Collection Date: 04/02/99				Time: 11:35 p.m.	
Tree #	**Scientific Name**	**Common Name**	**Dbh (cm)**	**Tht (m)**	**Cover (m)**	**ABD (cm)**	**ABL (m)**	**Total Dry Weight (kg)**	**Remarks**
1	Pinus radiata	Radiata Pine	25.15	22.60	4.90	3.50	4.05	257.15	Branching Pattern: 6 - 8
2	Pinus radiata	Radiata Pine	23.87					229.83	branches encircling the
3	Pinus radiata	Radiata Pine	20.69					168.69	stem about 6 in. from
4	Pinus radiata	Radiata Pine	23.24					216.79	the ground to the top
5	Pinus radiata	Radiata Pine	22.60					204.16	of the tree.
6	Pinus radiata	Radiata Pine	21.01					174.35	:branches/whorls
7	Pinus radiata	Radiata Pine	23.87					229.83	approximately
8	Pinus radiata	Radiata Pine	20.37					163.13	1-2 ft. apart;
9	Pinus radiata	Radiata Pine	17.83					122.23	:10 - 15 % sky visibility
10	Pinus radiata	Radiata Pine	20.05					157.67	:24 yrs. old
11	Pinus radiata	Radiata Pine	20.69					168.69	
12	Pinus radiata	Radiata Pine	23.55					223.26	
13	Pinus radiata	Radiata Pine	21.33					180.11	
14	Pinus radiata	Radiata Pine	18.14					127.00	
15	Pinus radiata	Radiata Pine	21.01					174.35	
16	Pinus radiata	Radiata Pine	26.74					293.63	
17	Pinus radiata	Radiata Pine	19.42					147.05	
18	Pinus radiata	Radiata Pine	21.65					185.97	
19	Pinus radiata	Radiata Pine	22.92					210.42	
20	Pinus radiata	Radiata Pine	20.69					168.69	
21	Pinus radiata	Radiata Pine	20.69					168.69	
22	Pinus radiata	Radiata Pine	24.19					236.51	
23	Pinus radiata	Radiata Pine	27.06					301.24	
24	Pinus radiata	Radiata Pine	27.69					316.77	
25	Pinus radiata	Radiata Pine	22.92					210.42	
26	Pinus radiata	Radiata Pine	21.96					191.93	
27	Pinus radiata	Radiata Pine	21.33					180.11	
28	Pinus radiata	Radiata Pine	18.14					127.00	
29	Pinus radiata	Radiata Pine	21.96					191.93	
30	Pinus radiata	Radiata Pine	23.87					229.83	
31	Pinus radiata	Radiata Pine	24.51					243.29	
32	Pinus radiata	Radiata Pine	25.46					264.24	
33	Pinus radiata	Radiata Pine	19.26					144.45	
34	Pinus radiata	Radiata Pine	24.19					236.51	
35	Pinus radiata	Radiata Pine	20.69					168.69	
36	Pinus radiata	Radiata Pine	22.60					204.16	
37	Pinus radiata	Radiata Pine	19.64					150.72	
38	Pinus radiata	Radiata Pine	23.87					229.83	
	Total Dry Weight (kg)							7599.26	
	Total Biomass (tons/ha)							241.25	

Sample Plot No. 20		Plot Size: 21 m x 15 m		Collection Date: 04/02/99				Time: 12:00 noon	
Tree #	**Scientific Name**	**Common Name**	**Dbh (cm)**	**Tht (m)**	**Cover (m)**	**ABD (cm)**	**ABL (m)**	**Total Dry Weight (kg)**	**Remarks**
1	Pinus radiata	Radiata Pine	24.35	23.18	5.25	4.90	4.20	239.88	Branching Pattern: 6 - 8
2	Pinus radiata	Radiata Pine	21.33					180.11	branches encircling the
3	Pinus radiata	Radiata Pine	25.46					264.24	stem about 6 in. from
4	Pinus radiata	Radiata Pine	24.19					236.51	the ground to the top
5	Pinus radiata	Radiata Pine	24.19					236.51	of the tree.
6	Pinus radiata	Radiata Pine	24.03					233.16	:branches/whorls
7	Pinus radiata	Radiata Pine	23.55					223.26	approximately
8	Pinus radiata	Radiata Pine	23.40					220.01	1-2 ft. apart;
9	Pinus radiata	Radiata Pine	25.94					275.06	:10 - 15 % sky visibility
10	Pinus radiata	Radiata Pine	17.51					117.56	:24 yrs. old
11	Pinus radiata	Radiata Pine	23.87					229.83	
12	Pinus radiata	Radiata Pine	22.60					204.16	
13	Pinus radiata	Radiata Pine	24.19					236.51	
14	Pinus radiata	Radiata Pine	26.10					278.73	
15	Pinus radiata	Radiata Pine	24.51					243.29	
16	Pinus radiata	Radiata Pine	23.87					229.83	
17	Pinus radiata	Radiata Pine	12.41					55.92	
18	Pinus radiata	Radiata Pine	15.76					93.62	
19	Pinus radiata	Radiata Pine	25.78					271.43	
20	Pinus radiata	Radiata Pine	18.14					127.00	
21	Pinus radiata	Radiata Pine	23.24					216.79	
22	Pinus radiata	Radiata Pine	28.33					332.72	
23	Pinus radiata	Radiata Pine	28.17					328.69	
24	Pinus radiata	Radiata Pine	23.71					226.53	
25	Pinus radiata	Radiata Pine	22.76					207.28	
26	Pinus radiata	Radiata Pine	24.83					250.17	
27	Pinus radiata	Radiata Pine	25.46					264.24	
28	Pinus radiata	Radiata Pine	23.55					223.26	
29	Pinus radiata	Radiata Pine	21.33					180.11	
30	Pinus radiata	Radiata Pine	25.78					271.43	
31	Pinus radiata	Radiata Pine	21.65					185.97	
32	Pinus radiata	Radiata Pine	24.51					243.29	
33	Pinus radiata	Radiata Pine	18.78					136.82	
34	Pinus radiata	Radiata Pine	22.92					210.42	
35	Pinus radiata	Radiata Pine	20.37					163.13	
	Total Dry Weight (kg)							7637.44	
	Total Biomass (tons/ha)							242.46	

Sample Plot No. 21		Plot Size: 21 m x 15 m		Collection Date: 04/02/99				Time: 12:25 p.m.	
Tree #	**Scientific Name**	**Common Name**	**Dbh (cm)**	**Tht (m)**	**Cover (m)**	**ABD (cm)**	**ABL (m)**	**Total Dry Weight (kg)**	**Remarks**
1	Pinus radiata	Radiata Pine	27.06	21.96	5.60	5.00	4.20	301.24	Branching Pattern: 6 - 10
2	Pinus radiata	Radiata Pine	13.37					65.63	branches encircling the
3	Pinus radiata	Radiata Pine	23.55					223.26	stem about 6 in. from
4	Pinus radiata	Radiata Pine	22.60					204.16	the ground to the top
5	Pinus radiata	Radiata Pine	23.24					216.79	of the tree.
6	Pinus radiata	Radiata Pine	23.24					216.79	:branches/whorls
7	Pinus radiata	Radiata Pine	22.28					197.99	approximately
8	Pinus radiata	Radiata Pine	25.15					257.15	1-2 ft. apart;
9	Pinus radiata	Radiata Pine	23.40					220.01	:10 - 15 % sky visibility
10	Pinus radiata	Radiata Pine	19.74					152.31	:24 yrs. old
11	Pinus radiata	Radiata Pine	28.65					340.85	
12	Pinus radiata	Radiata Pine	27.37					308.95	
13	Pinus radiata	Radiata Pine	23.55					223.26	
14	Pinus radiata	Radiata Pine	20.85					171.50	
15	Pinus radiata	Radiata Pine	22.60					204.16	
16	Pinus radiata	Radiata Pine	27.06					301.24	
17	Pinus radiata	Radiata Pine	21.65					185.97	
18	Pinus radiata	Radiata Pine	25.78					271.43	
19	Pinus radiata	Radiata Pine	26.10					278.73	
20	Pinus radiata	Radiata Pine	18.14					127.00	
21	Pinus radiata	Radiata Pine	22.60					204.16	
22	Pinus radiata	Radiata Pine	19.74					152.31	
23	Pinus radiata	Radiata Pine	18.46					131.86	
24	Pinus radiata	Radiata Pine	25.78					271.43	
25	Pinus radiata	Radiata Pine	24.19					236.51	
26	Pinus radiata	Radiata Pine	26.74					293.63	
27	Pinus radiata	Radiata Pine	27.37					308.95	
28	Pinus radiata	Radiata Pine	13.69					69.06	
29	Pinus radiata	Radiata Pine	24.35					239.88	
30	Pinus radiata	Radiata Pine	21.01					174.35	
31	Pinus radiata	Radiata Pine	21.65					185.97	
32	Pinus radiata	Radiata Pine	23.24					216.79	
33	Pinus radiata	Radiata Pine	23.87					229.83	
34	Pinus radiata	Radiata Pine	23.87					229.83	
35	Pinus radiata	Radiata Pine	25.78					271.43	
	Total Dry Weight (kg)							7684.38	
	Total Biomass (tons/ha)							243.95	

Sample Plot No. 22		Plot Size: 21 m x 15 m		Collection Date: 05/02/99				Time: 5:40 p.m.	
Tree #	**Scientific Name**	**Common Name**	**Dbh (cm)**	**Tht (m)**	**Cover (m)**	**ABD (cm)**	**ABL (m)**	**Total Dry Weight (kg)**	**Remarks**
1	Pinus radiata	Radiata Pine	29.28	25.31	4.20	4.00	3.75	357.43	Branching Pattern: 6 - 8
2	Pinus radiata	Radiata Pine	33.74					485.47	branches encircling the
3	Pinus radiata	Radiata Pine	26.42					286.12	stem about 6 in. from
4	Pinus radiata	Radiata Pine	23.55					223.26	the ground to the top
5	Pinus radiata	Radiata Pine	28.01					324.69	of the tree.
6	Pinus radiata	Radiata Pine	34.38					505.49	:branches/whorls
7	Pinus radiata	Radiata Pine	30.24					383.10	approximately
8	Pinus radiata	Radiata Pine	33.42					475.63	1-3 ft. apart;
9	Pinus radiata	Radiata Pine	28.33					332.72	:20 % sky visibility
10	Pinus radiata	Radiata Pine	33.42					475.63	:26 yrs. old; thinned
11	Pinus radiata	Radiata Pine	29.92					374.44	
12	Pinus radiata	Radiata Pine	20.05					157.67	
13	Pinus radiata	Radiata Pine	31.83					428.02	
14	Pinus radiata	Radiata Pine	31.19					409.73	
15	Pinus radiata	Radiata Pine	33.42					475.63	
16	Pinus radiata	Radiata Pine	24.83					250.17	
17	Pinus radiata	Radiata Pine	23.55					223.26	
18	Pinus radiata	Radiata Pine	27.69					316.77	
19	Pinus radiata	Radiata Pine	25.15					257.15	
20	Pinus radiata	Radiata Pine	33.42					475.63	
21	Pinus radiata	Radiata Pine	24.83					250.17	
22	Pinus radiata	Radiata Pine	35.33					536.33	
23	Pinus radiata	Radiata Pine	33.42					475.63	
24	Pinus radiata	Radiata Pine	30.24					383.10	
25	Pinus radiata	Radiata Pine	31.19					409.73	
26	Pinus radiata	Radiata Pine	31.19					409.73	
27	Pinus radiata	Radiata Pine	35.01					525.94	
28	Pinus radiata	Radiata Pine	30.24					383.10	
29	Pinus radiata	Radiata Pine	31.19					409.73	
30	Pinus radiata	Radiata Pine	22.60					204.16	
31	Pinus radiata	Radiata Pine	28.03					325.09	
32	Pinus radiata	Radiata Pine	29.28					357.43	
	Total Dry Weight (kg)							11888.18	
	Total Biomass (tons/ha)							377.40	

Sample Plot No. 23		Plot Size: 21 m x 15 m		Collection Date: 05/02/99				Time: 6:15 noon	
Tree #	**Scientific Name**	**Common Name**	**Dbh (cm)**	**Tht (m)**	**Cover (m)**	**ABD (cm)**	**ABL (m)**	**Total Dry Weight (kg)**	**Remarks**
1	Pinus radiata	Radiata Pine	36.61	24.20	4.50	3.50	3.50	578.98	Branching Pattern: 6 - 8
2	Pinus radiata	Radiata Pine	33.42					475.63	branches encircling the
3	Pinus radiata	Radiata Pine	30.24					383.10	stem about 6 in. from
4	Pinus radiata	Radiata Pine	39.79					693.33	the ground to the top
5	Pinus radiata	Radiata Pine	41.38					754.67	of the tree.
6	Pinus radiata	Radiata Pine	33.42					475.63	:branches/whorls
7	Pinus radiata	Radiata Pine	31.83					428.02	approximately
8	Pinus radiata	Radiata Pine	30.24					383.10	1-3 ft. apart;
9	Pinus radiata	Radiata Pine	28.01					324.69	:15 - 20 % sky visibility
10	Pinus radiata	Radiata Pine	26.74					293.63	:26 yrs. old; thinned
11	Pinus radiata	Radiata Pine	28.65					340.85	
12	Pinus radiata	Radiata Pine	35.01					525.94	
13	Pinus radiata	Radiata Pine	25.46					264.24	
14	Pinus radiata	Radiata Pine	23.87					229.83	
15	Pinus radiata	Radiata Pine	20.69					168.69	
16	Pinus radiata	Radiata Pine	31.19					409.73	
17	Pinus radiata	Radiata Pine	25.46					264.24	
18	Pinus radiata	Radiata Pine	22.28					197.99	
19	Pinus radiata	Radiata Pine	26.10					278.73	
20	Pinus radiata	Radiata Pine	23.55					223.26	
21	Pinus radiata	Radiata Pine	29.60					365.88	
22	Pinus radiata	Radiata Pine	25.46					264.24	
23	Pinus radiata	Radiata Pine	26.10					278.73	
24	Pinus radiata	Radiata Pine	23.24					216.79	
25	Pinus radiata	Radiata Pine	37.56					612.13	
26	Pinus radiata	Radiata Pine	26.74					293.63	
27	Pinus radiata	Radiata Pine	23.24					216.79	
28	Pinus radiata	Radiata Pine	22.28					197.99	
29	Pinus radiata	Radiata Pine	29.92					374.44	
30	Pinus radiata	Radiata Pine	31.19					409.73	
31	Pinus radiata	Radiata Pine	22.28					197.99	
	Total Dry Weight (kg)							11122.63	
	Total Biomass (tons/ha)							353.10	

Sample Plot No. 24		Plot Size: 21 m x 15 m		Collection Date: 05/02/99				Time: 6:40 p.m.	
Tree #	**Scientific Name**	**Common Name**	**Dbh (cm)**	**Tht (m)**	**Cover (m)**	**ABD (cm)**	**ABL (m)**	**Total Dry Weight (kg)**	**Remarks**
1	Pinus radiata	Radiata Pine	35.65	26.52	5.00	4.50	3.50	546.83	Branching Pattern: 6 - 8
2	Pinus radiata	Radiata Pine	32.15					437.33	branches encircling the
3	Pinus radiata	Radiata Pine	37.88					623.39	stem about 6 in. from
4	Pinus radiata	Radiata Pine	31.83					428.02	the ground to the top
5	Pinus radiata	Radiata Pine	36.61					578.98	of the tree.
6	Pinus radiata	Radiata Pine	37.56					612.13	:branches/whorls
7	Pinus radiata	Radiata Pine	30.88					400.75	approximately
8	Pinus radiata	Radiata Pine	28.01					324.69	1-3 ft. apart;
9	Pinus radiata	Radiata Pine	28.65					340.85	:15 - 20 % sky visibility
10	Pinus radiata	Radiata Pine	35.01					525.94	:27 yrs. old; thinned
11	Pinus radiata	Radiata Pine	38.20					634.77	
12	Pinus radiata	Radiata Pine	27.69					316.77	
13	Pinus radiata	Radiata Pine	29.28					357.43	
14	Pinus radiata	Radiata Pine	34.70					515.66	
15	Pinus radiata	Radiata Pine	29.92					374.44	
16	Pinus radiata	Radiata Pine	28.65					340.85	
17	Pinus radiata	Radiata Pine	33.42					475.63	
18	Pinus radiata	Radiata Pine	29.28					357.43	
19	Pinus radiata	Radiata Pine	31.19					409.73	
20	Pinus radiata	Radiata Pine	30.88					400.75	
21	Pinus radiata	Radiata Pine	30.24					383.10	
22	Pinus radiata	Radiata Pine	33.10					465.89	
23	Pinus radiata	Radiata Pine	28.97					349.09	
24	Pinus radiata	Radiata Pine	27.06					301.24	
25	Pinus radiata	Radiata Pine	29.92					374.44	
26	Pinus radiata	Radiata Pine	27.06					301.24	
27	Pinus radiata	Radiata Pine	29.28					357.43	
28	Pinus radiata	Radiata Pine	27.06					301.24	
29	Pinus radiata	Radiata Pine	28.81					344.96	
30	Pinus radiata	Radiata Pine	34.89					521.82	
31	Pinus radiata	Radiata Pine	27.69					316.77	
	Total Dry Weight (kg)							13019.59	
	Total Biomass (tons/ha)							413.32	

Sample Plot No. 25		Plot Size: 21 m x 15 m		Collection Date: 06/02/99			Time: 10:00 a.m.		
Tree #	**Scientific Name**	**Common Name**	**Dbh (cm)**	**Tht (m)**	**Cover (m)**	**ABD (cm)**	**ABL (m)**	**Total Dry Weight (kg)**	**Remarks**
1	Pinus radiata	Radiata Pine	38.20	27.16	4.35	4.20	3.20	634.77	Branching Pattern: 6 - 8
2	Pinus radiata	Radiata Pine	24.19					236.51	branches encircling the
3	Pinus radiata	Radiata Pine	27.69					316.77	stem about 6 in. from
4	Pinus radiata	Radiata Pine	30.88					400.75	the ground to the top
5	Pinus radiata	Radiata Pine	35.97					557.44	of the tree.
6	Pinus radiata	Radiata Pine	45.20					913.35	:branches/whorls
7	Pinus radiata	Radiata Pine	39.47					681.39	approximately
8	Pinus radiata	Radiata Pine	28.65					340.85	1-3 ft. apart;
9	Pinus radiata	Radiata Pine	29.60					365.88	:10 - 20 % sky visibility
10	Pinus radiata	Radiata Pine	33.74					485.47	:27 yrs. old; thinned
11	Pinus radiata	Radiata Pine	29.92					374.44	
12	Pinus radiata	Radiata Pine	17.19					112.99	
13	Pinus radiata	Radiata Pine	33.42					475.63	
14	Pinus radiata	Radiata Pine	27.53					312.84	
15	Pinus radiata	Radiata Pine	19.10					141.89	
16	Pinus radiata	Radiata Pine	32.47					446.74	
17	Pinus radiata	Radiata Pine	24.83					250.17	
18	Pinus radiata	Radiata Pine	20.05					157.67	
19	Pinus radiata	Radiata Pine	24.19					236.51	
20	Pinus radiata	Radiata Pine	41.38					754.67	
21	Pinus radiata	Radiata Pine	21.33					180.11	
22	Pinus radiata	Radiata Pine	34.06					495.43	
23	Pinus radiata	Radiata Pine	28.65					340.85	
24	Pinus radiata	Radiata Pine	31.51					418.83	
25	Pinus radiata	Radiata Pine	21.96					191.93	
26	Pinus radiata	Radiata Pine	44.56					885.77	
27	Pinus radiata	Radiata Pine	48.70					1073.19	
28	Pinus radiata	Radiata Pine	22.60					204.16	
29	Pinus radiata	Radiata Pine	27.37					308.95	
30	Pinus radiata	Radiata Pine	25.46					264.24	
31	Pinus radiata	Radiata Pine	25.46					264.24	
32	Pinus radiata	Radiata Pine	29.28					357.43	
33	Pinus radiata	Radiata Pine	25.15					257.15	
34	Pinus radiata	Radiata Pine	33.74					485.47	
	Total Dry Weight (kg)							13924.48	
	Total Biomass (tons/ha)							442.05	

Appendix 7.3

In this appendix are graphs showing the relationship between total aboveground biomass and all individual radar bands and most radar band combinations for the broad-leaved and needle-leaved stands.

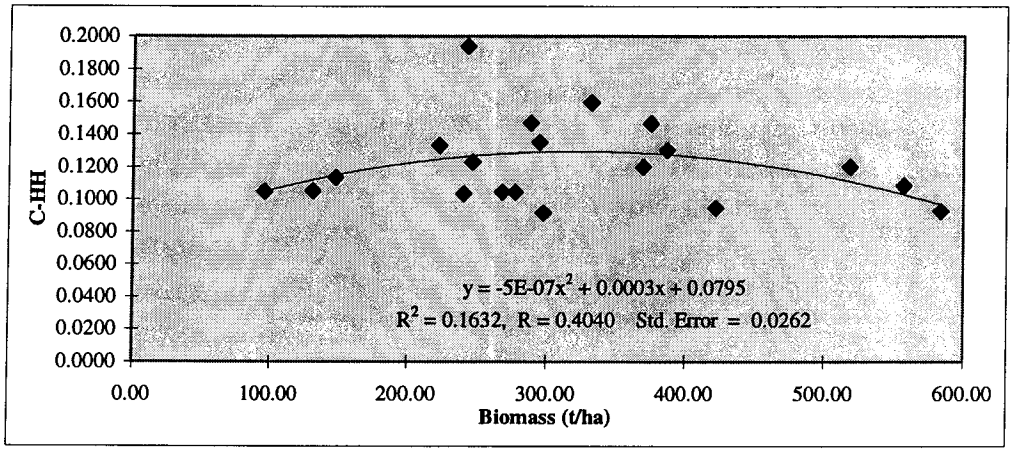

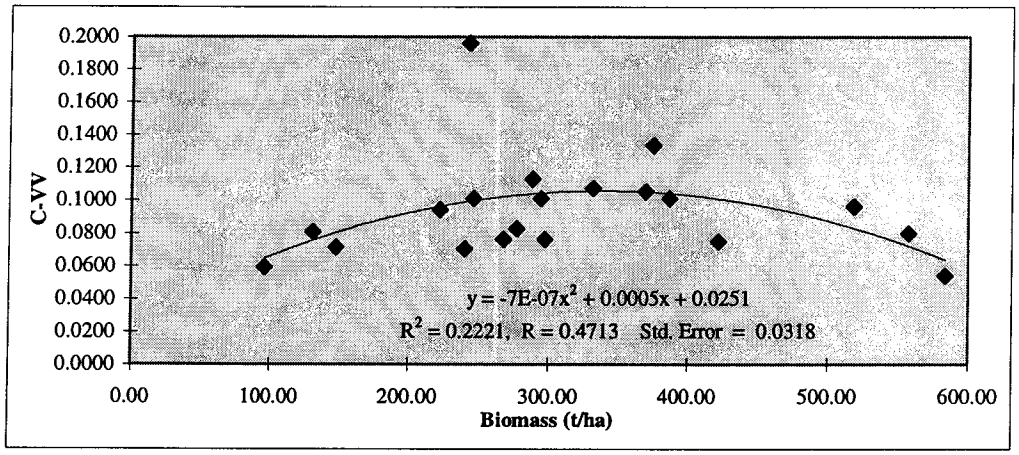

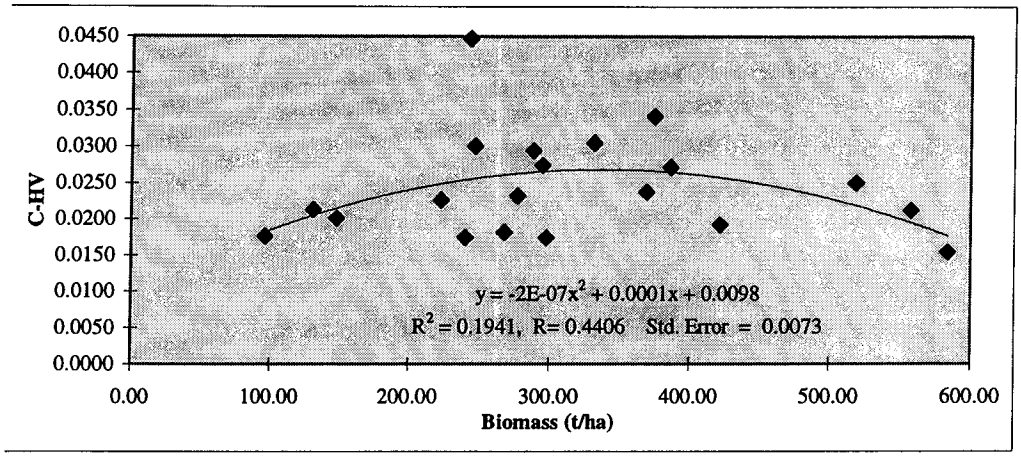

Figure 7.3.1 Total aboveground dry biomass (t/ha) versus C-HH, C-VV, and C-HV backscatter (intensity values) from broad-leaved stands

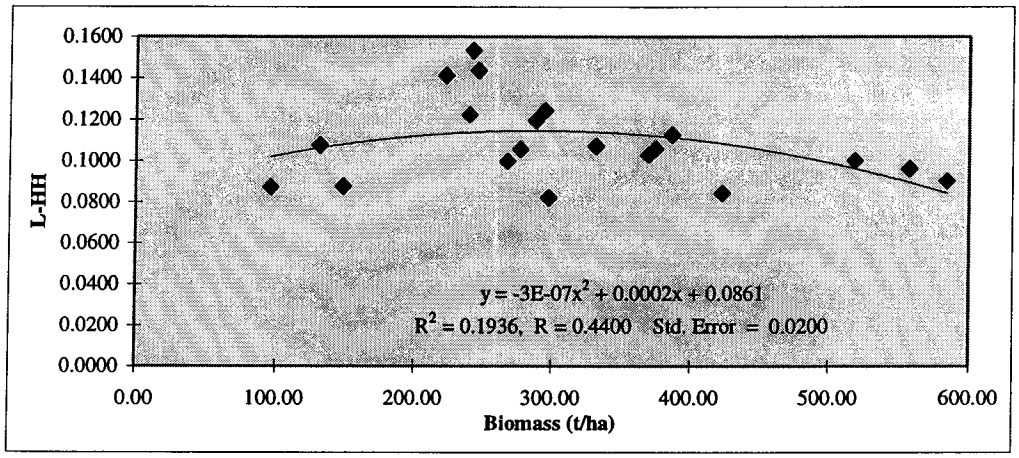

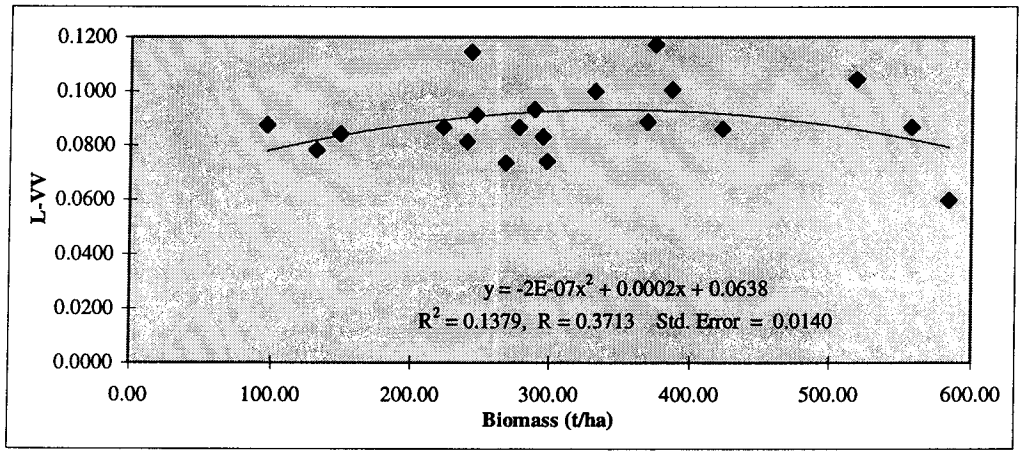

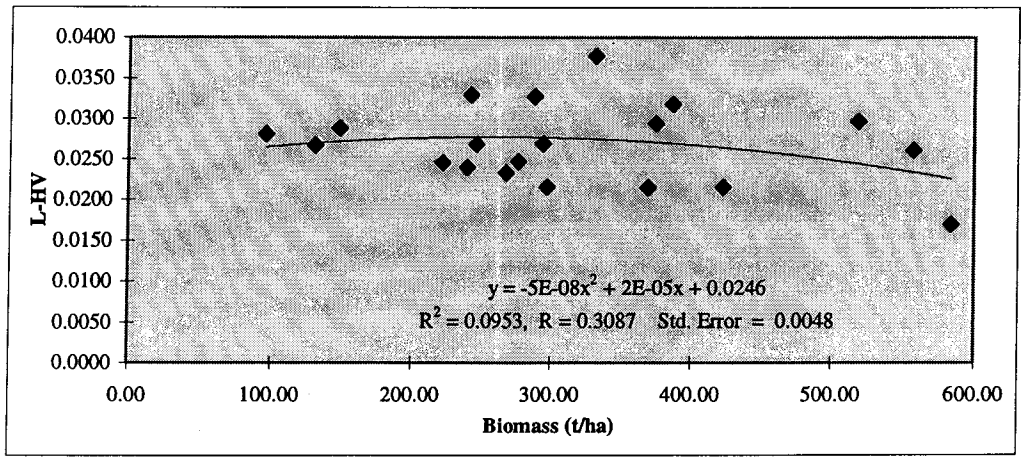

Figure 7.3.2 Total aboveground dry biomass (t/ha) versus L-HH, L-VV and L-HV backscatter (intensity values) from broad-leaved stands

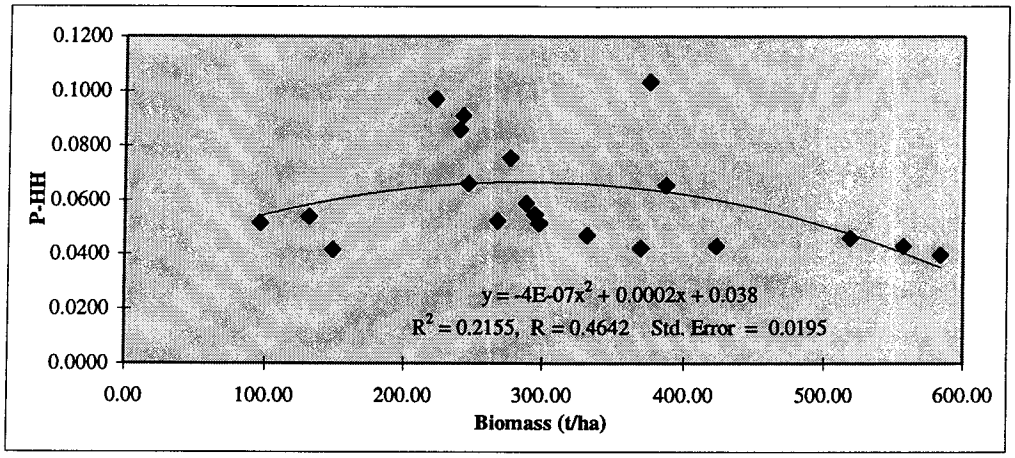

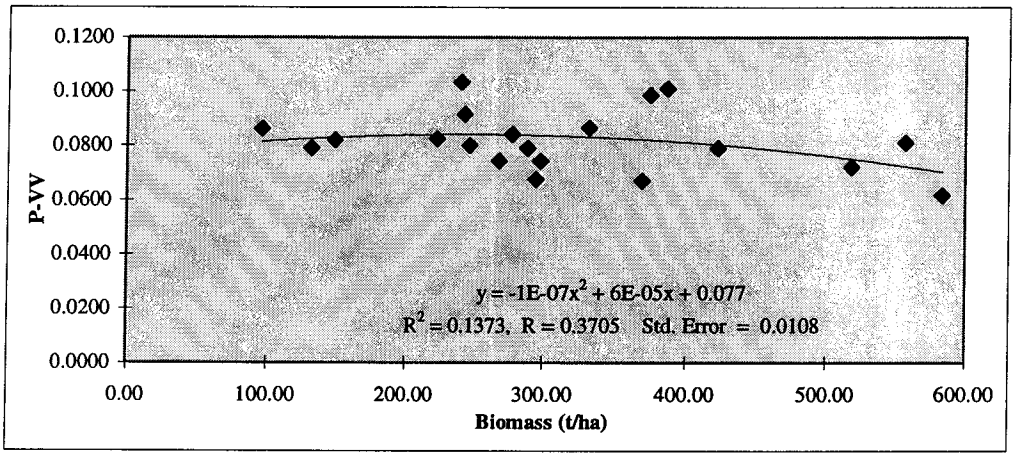

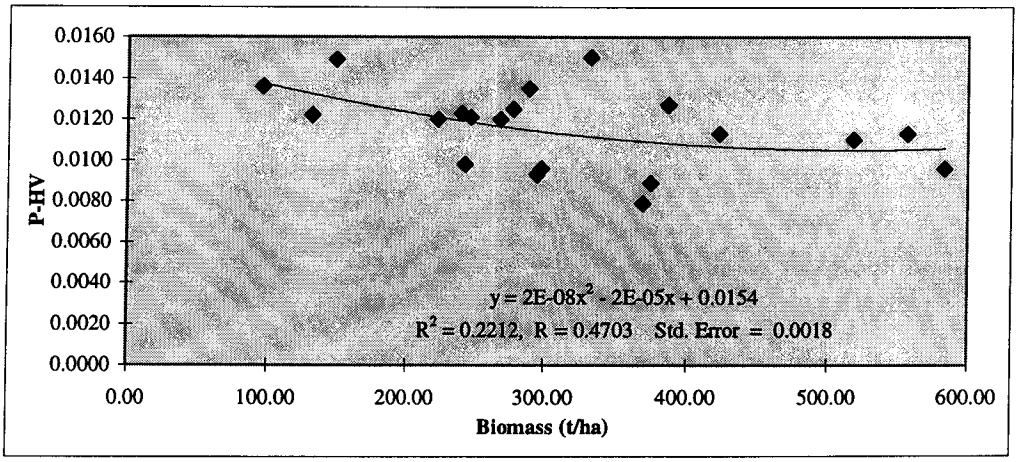

Figure 7.3.3 Total aboveground dry biomass (t/ha) versus P-HH, P-VV and P-HV backscatter (intensity values) from broad-leaved stands

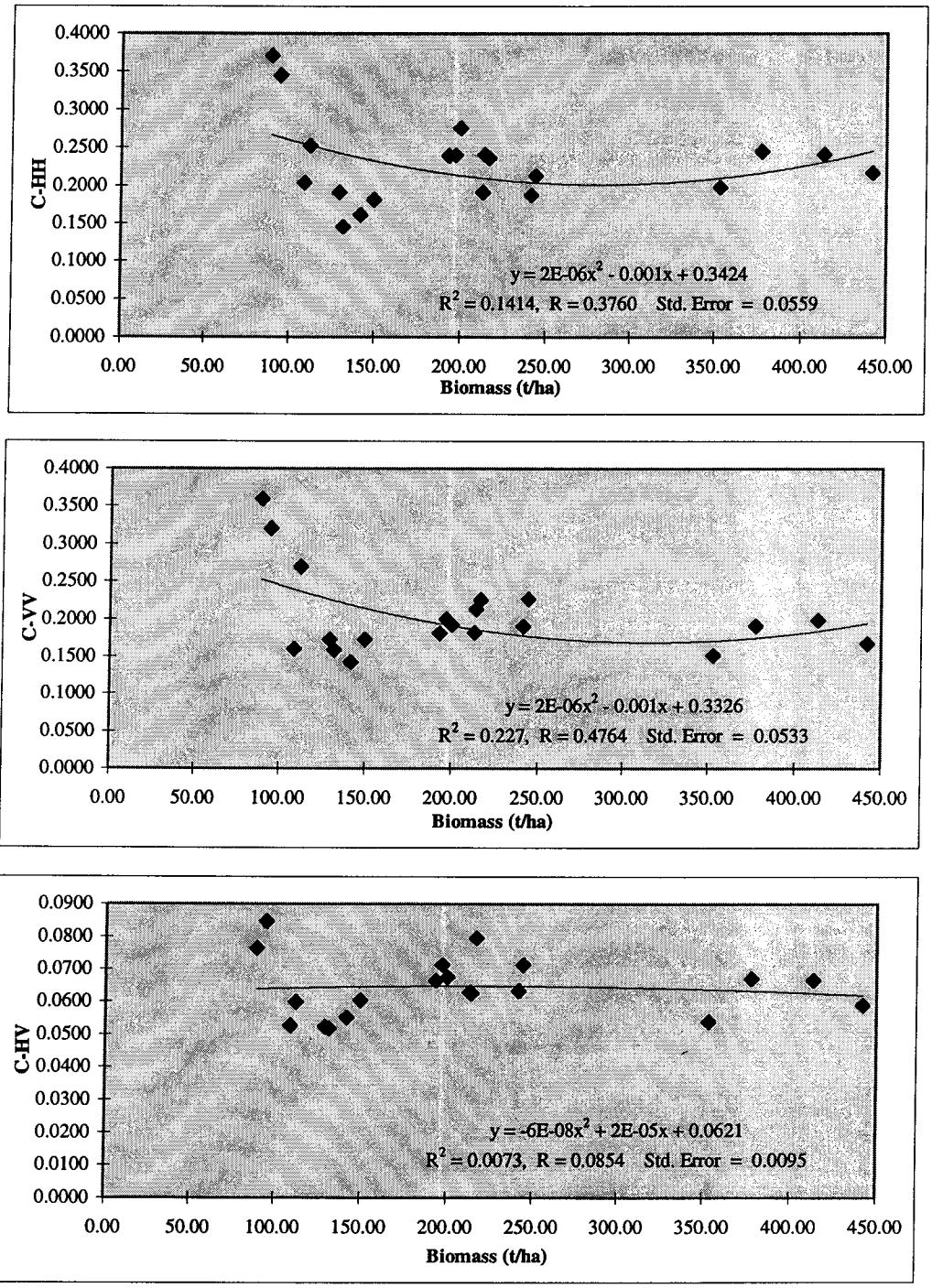

Figure 7.3.4 Total aboveground dry biomass (t/ha) versus C-HH, C-VV and C-HV backscatter (intensity values) from needle-leaved stands

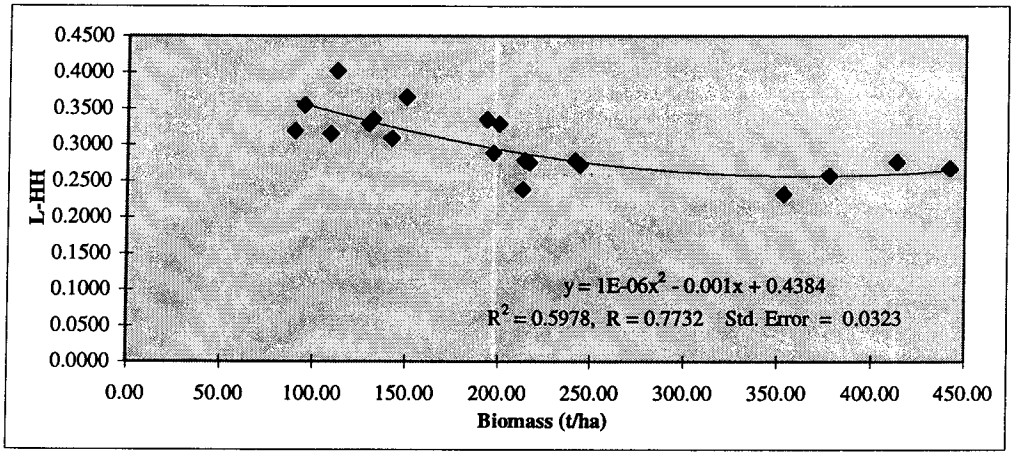

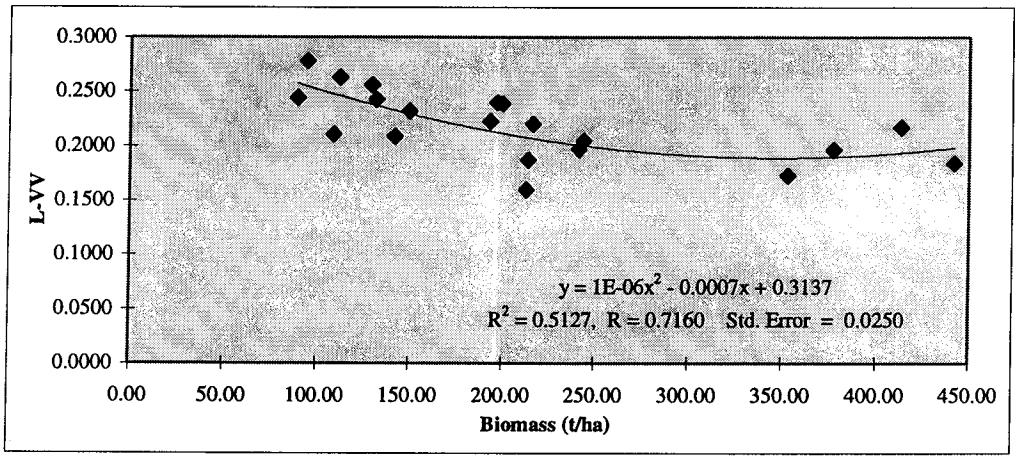

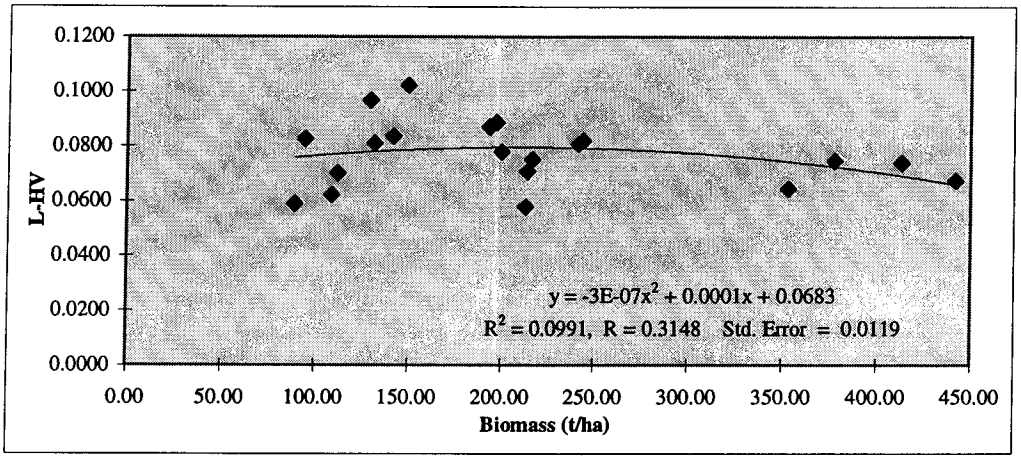

Figure 7.3.5 Total aboveground dry biomass (t/ha) versus L-HH, L-VV and L-HV backscatter (intensity values) from needle-leaved stands

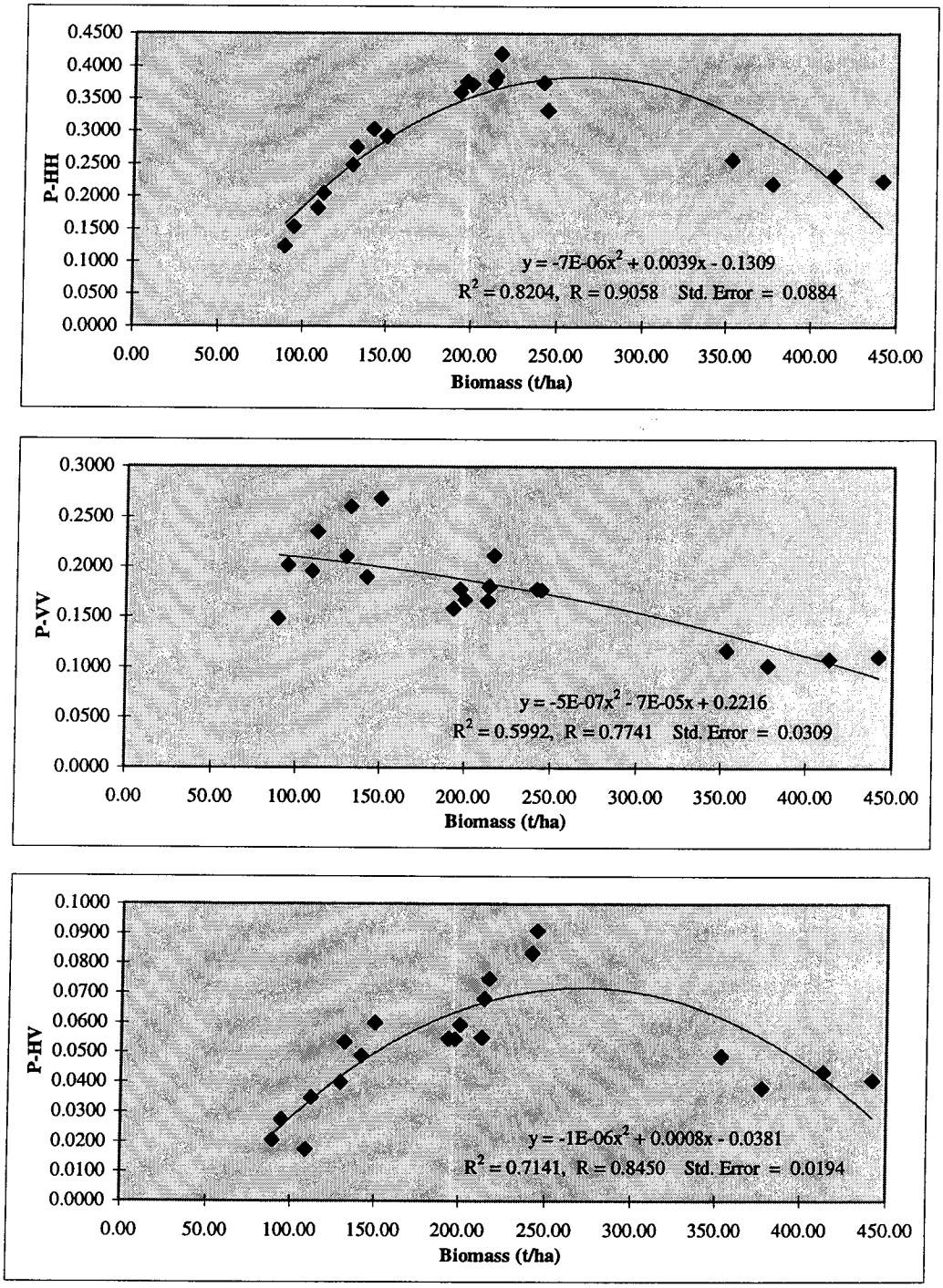

Figure 7.3.6 Total aboveground dry biomass (t/ha) versus P-HH, P-VV and P-HV backscatter (intensity values) from needle-leaved stands

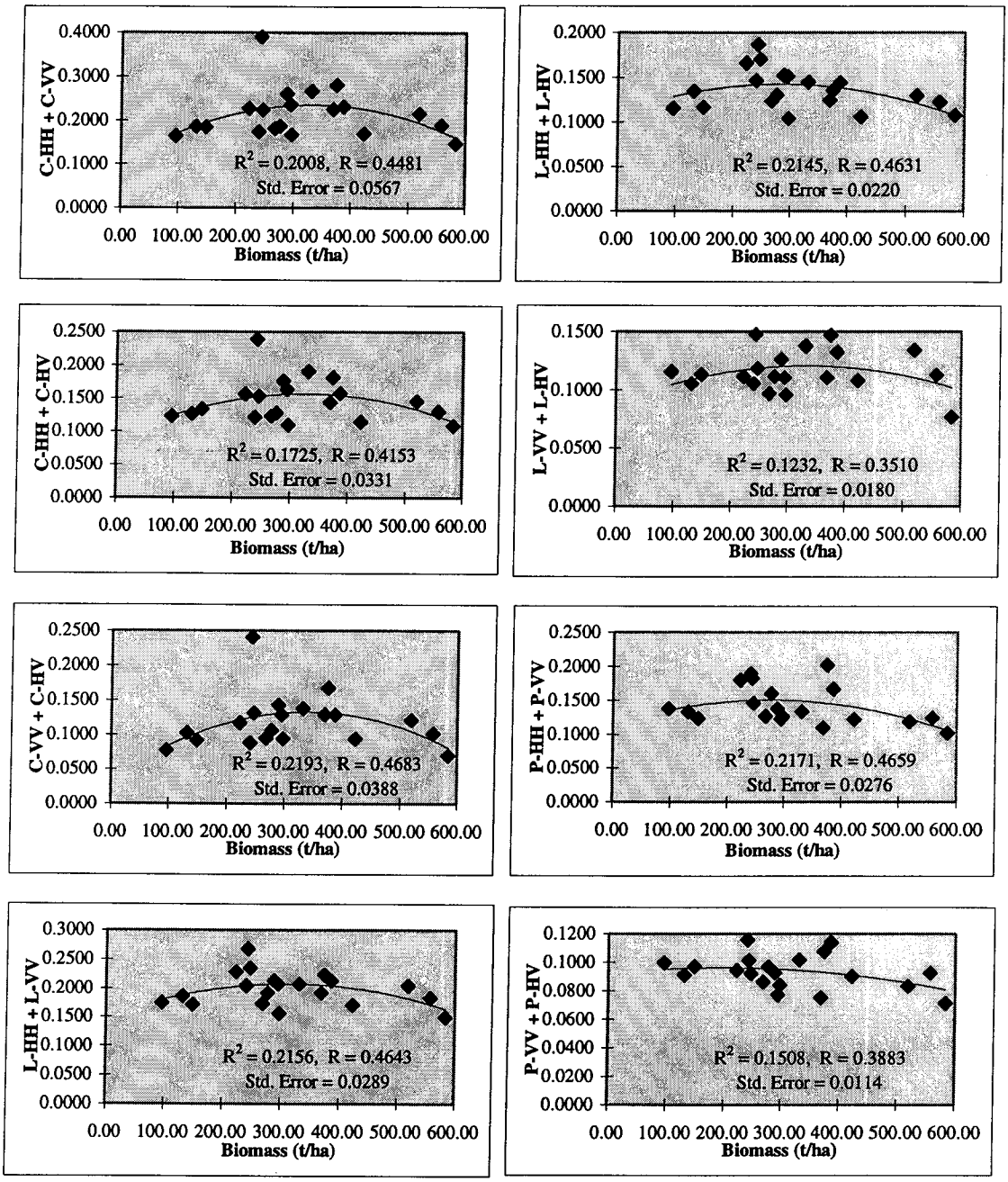

Figure 7.3.7 Total aboveground dry biomass (t/ha) versus C-HH + C-VV, C-HH + C-HV, C-VV + C-HV, L-HH + L-VV, L-HH + L-HV, L-VV + L-HV, P-HH + P-VV, and P-VV + P-HV backscatter (in intensity values) from broad-leaved stands

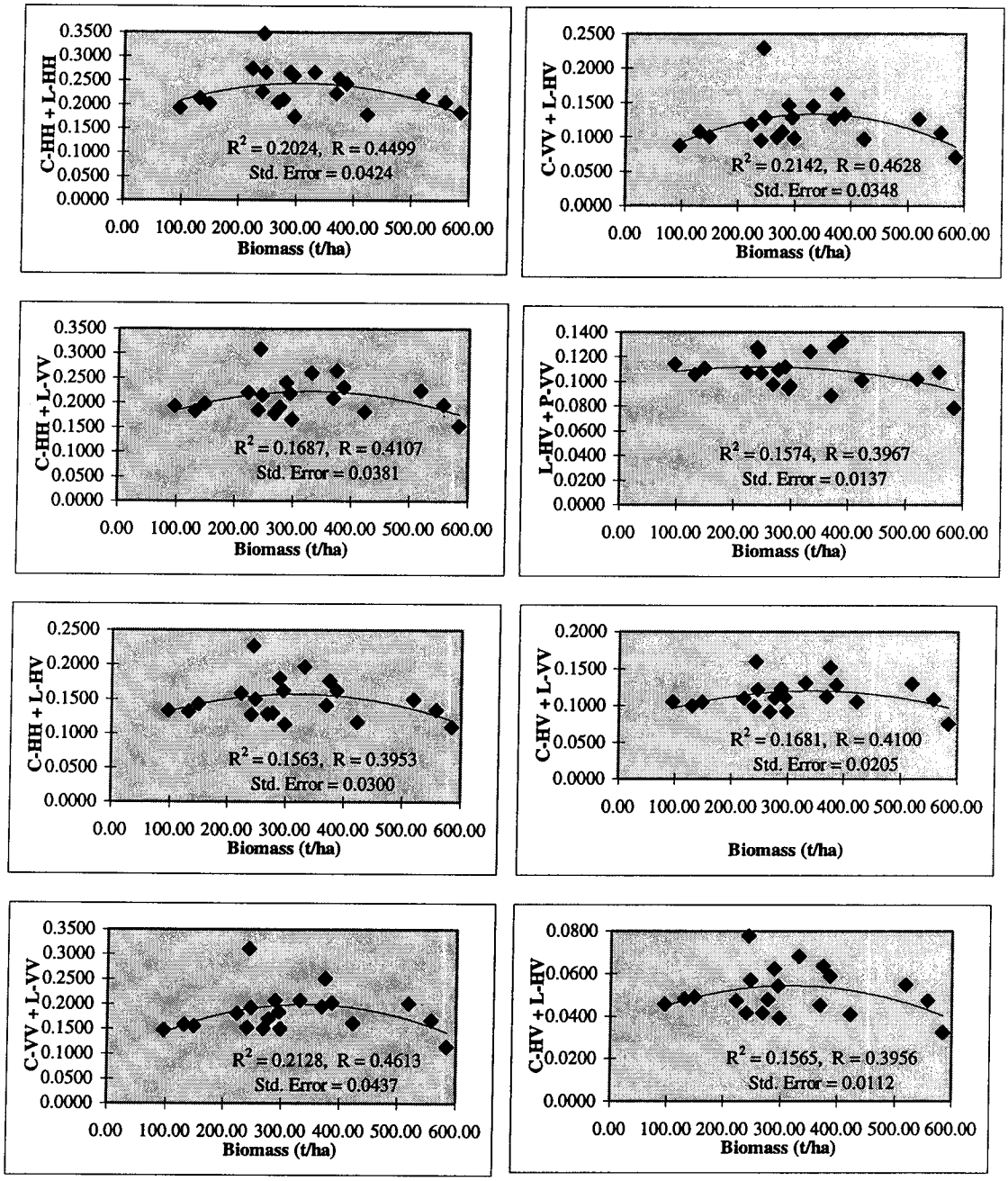

Figure 7.3.8 Total aboveground dry biomass (t/ha) versus C-HH + L-HH, C-HH + L-VV, C-HH + L-HV, C-VV + L-VV, C-VV + L-HV, L-HV + P-VV, C-HV + L-VV, and C-HV + L-HV backscatter (in intensity values) from broad-leaved stands

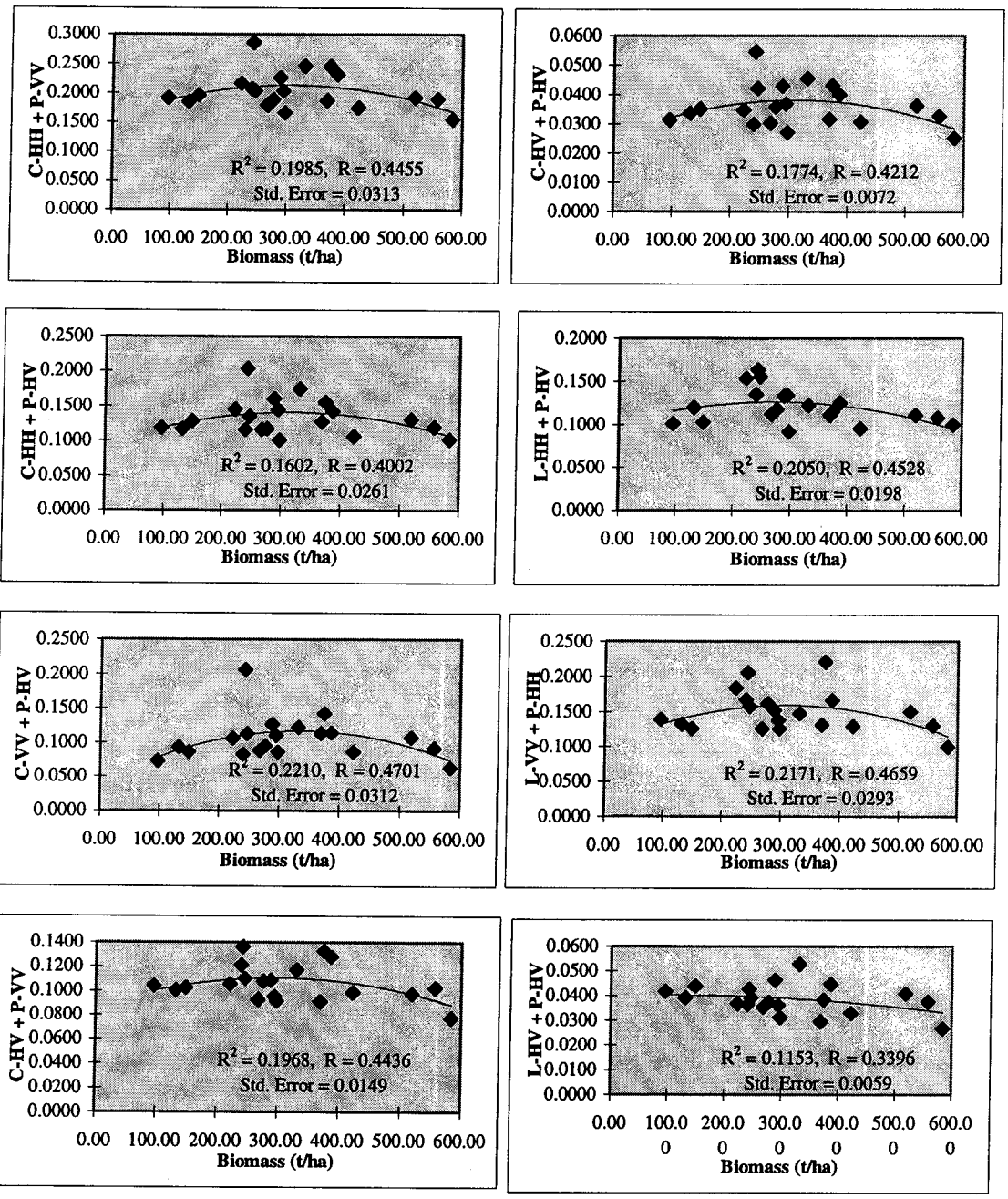

Figure 7.3.9 Total aboveground dry biomass (t/ha) versus C-HH + P-VV, C-HH + P-HV, C-VV + P-HV, C-HV + P-VV, C-HV + P-HV, L-HH + P-HV, L-VV + P-HH, and L-HV + P-HV backscatter (in intensity values) from broad-leaved stands

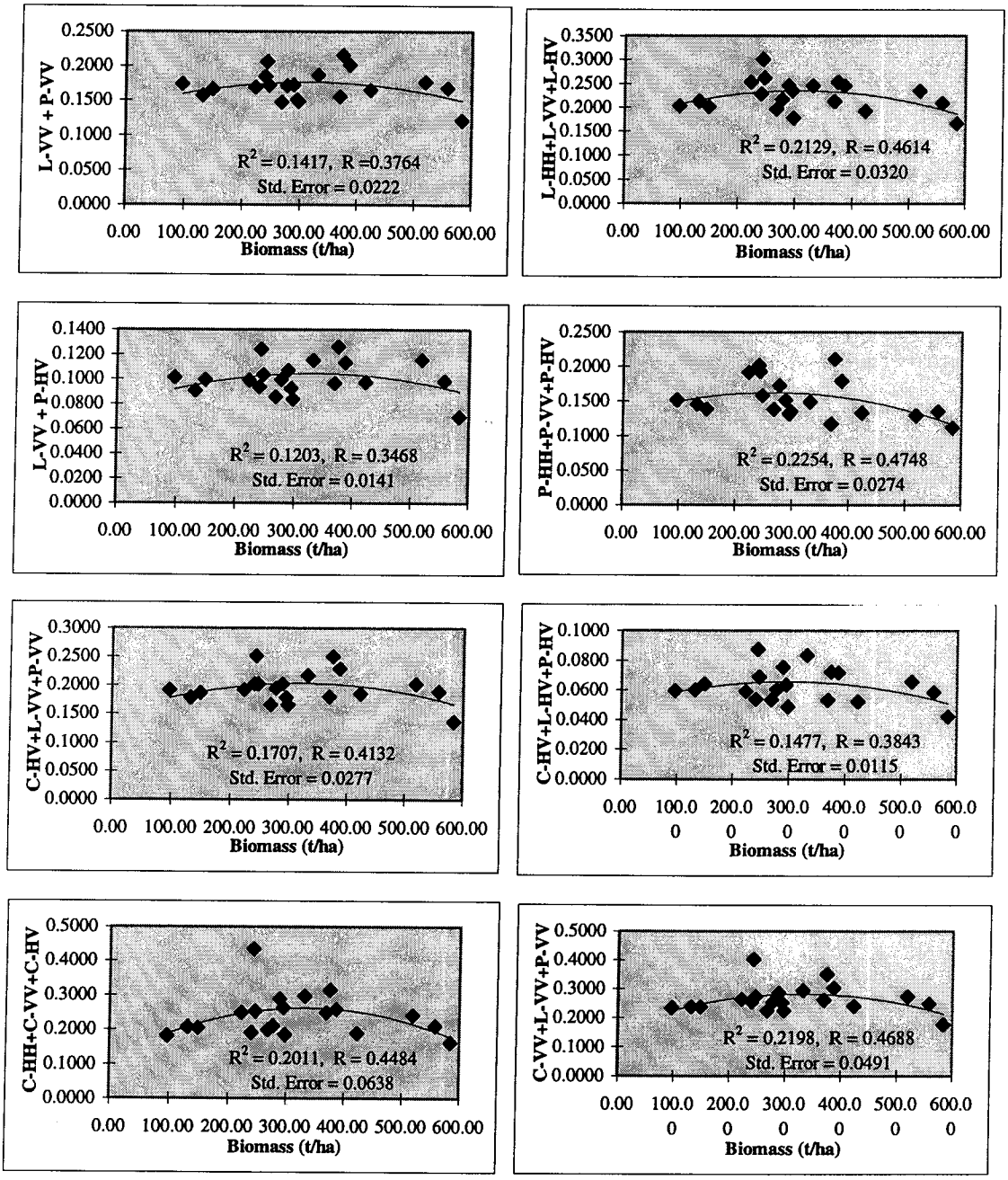

Figure 7.3.10 Total aboveground dry biomass (t/ha) versus L-VV + P-VV, L-VV + P-HV, C-HV + L-VV + P-VV, C-HH + C-VV + C-HV, L-HH + L-VV + L-HV, P-HH + P-VV + P-HV, C-HV + L-HV + P-HV, and C-VV + L-VV + P-VV backscatter (in intensity values) from broad-leaved stands

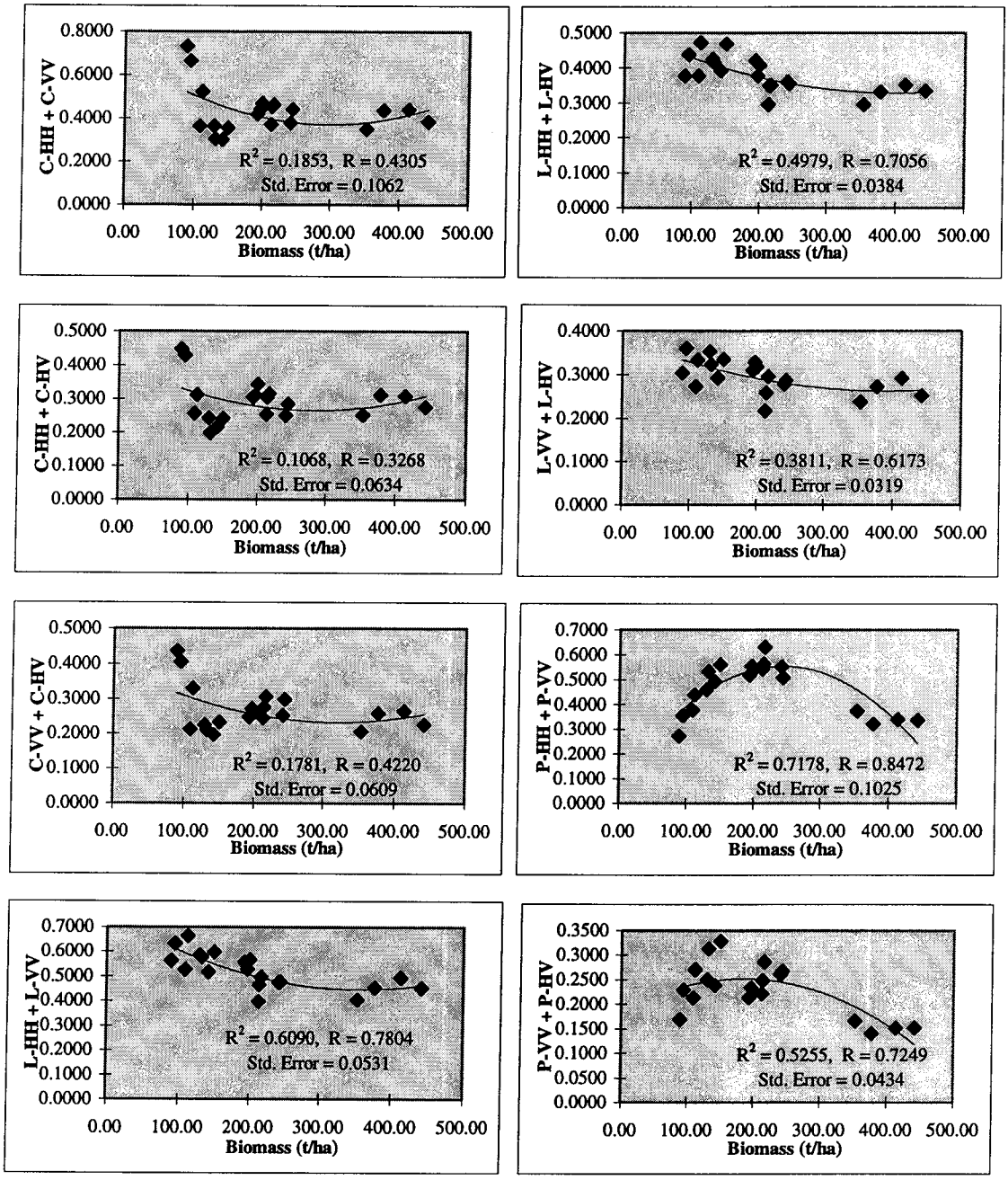

Figure 7.3.11 Total aboveground dry biomass (t/ha) versus C-HH + C-VV, C-HH + C-HV, C-VV + C-HV, L-HH + L-VV, L-HH + L-HV, L-VV + L-HV, P-HH + P-VV, and P-VV + P-HV backscatter (in intensity values) from needle-leaved stands

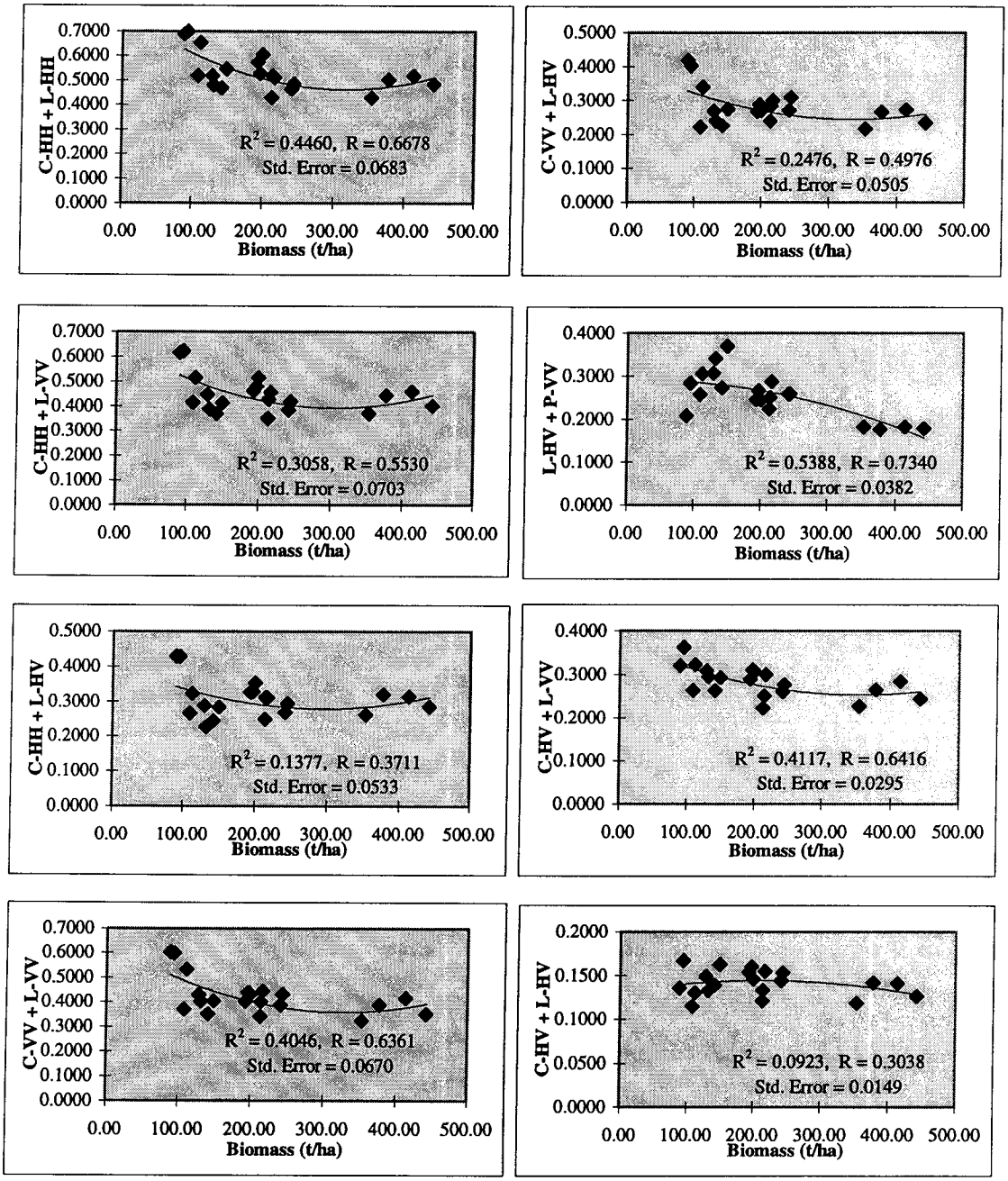

Figure 7.3.12 Total aboveground dry biomass (t/ha) versus C-HH + L-HH, C-HH + L-VV, C-HH + L-HV, C-VV + L-VV, C-VV + L-HV, L-HV + P-VV, C-HV + L-VV, and C-HV + L-HV backscatter (in intensity values) from needle-leaved stands

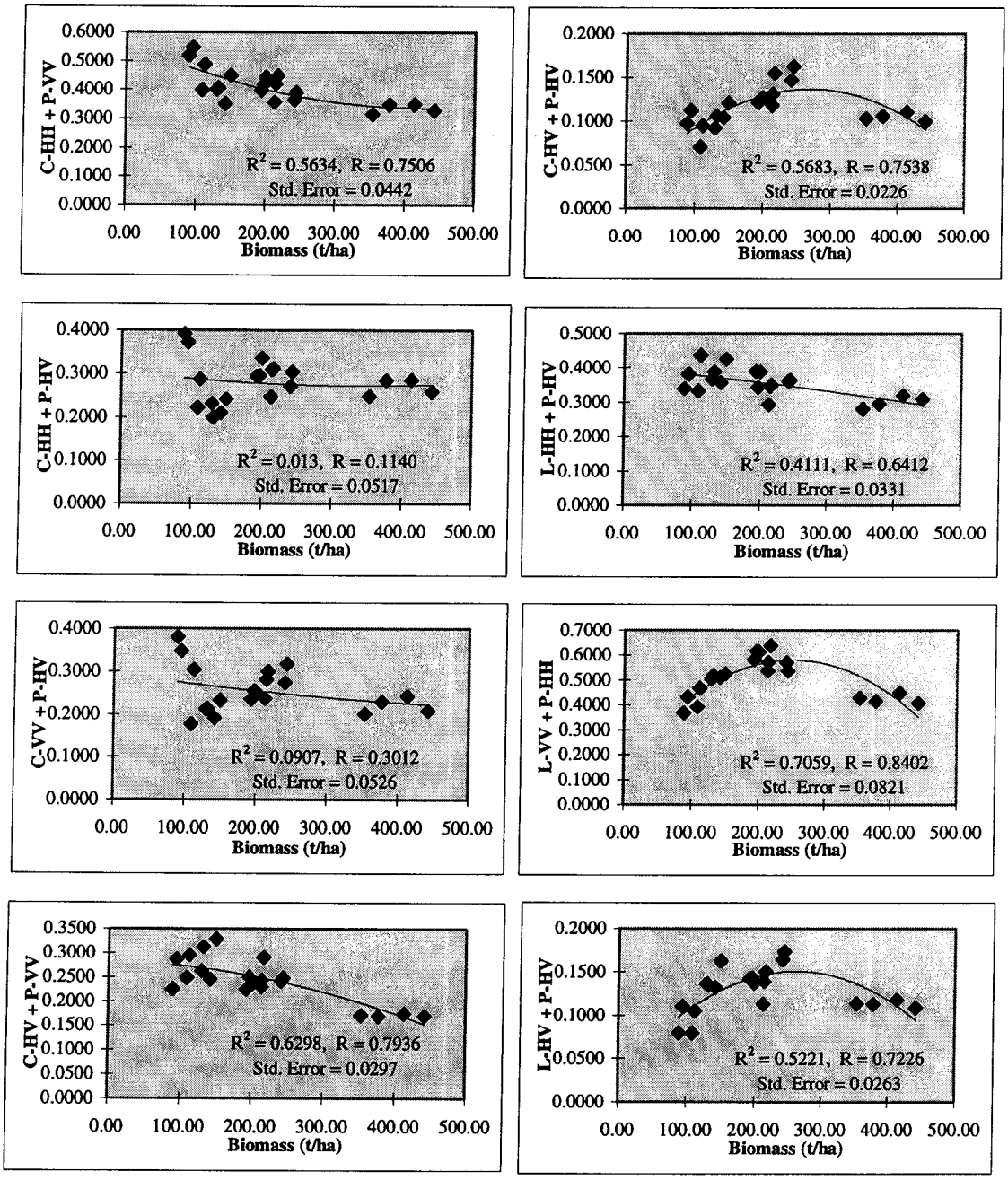

Figure 7.3.13 Total aboveground dry biomass (t/ha) versus C-HH + P-VV, C-HH + P-HV, C-VV + P-HV, C-HV + P-VV, C-HV + P-HV, L-HH + P-HV, L-VV + P-HH, and L-HV + P-HV backscatter (in intensity values) from needle-leaved stands

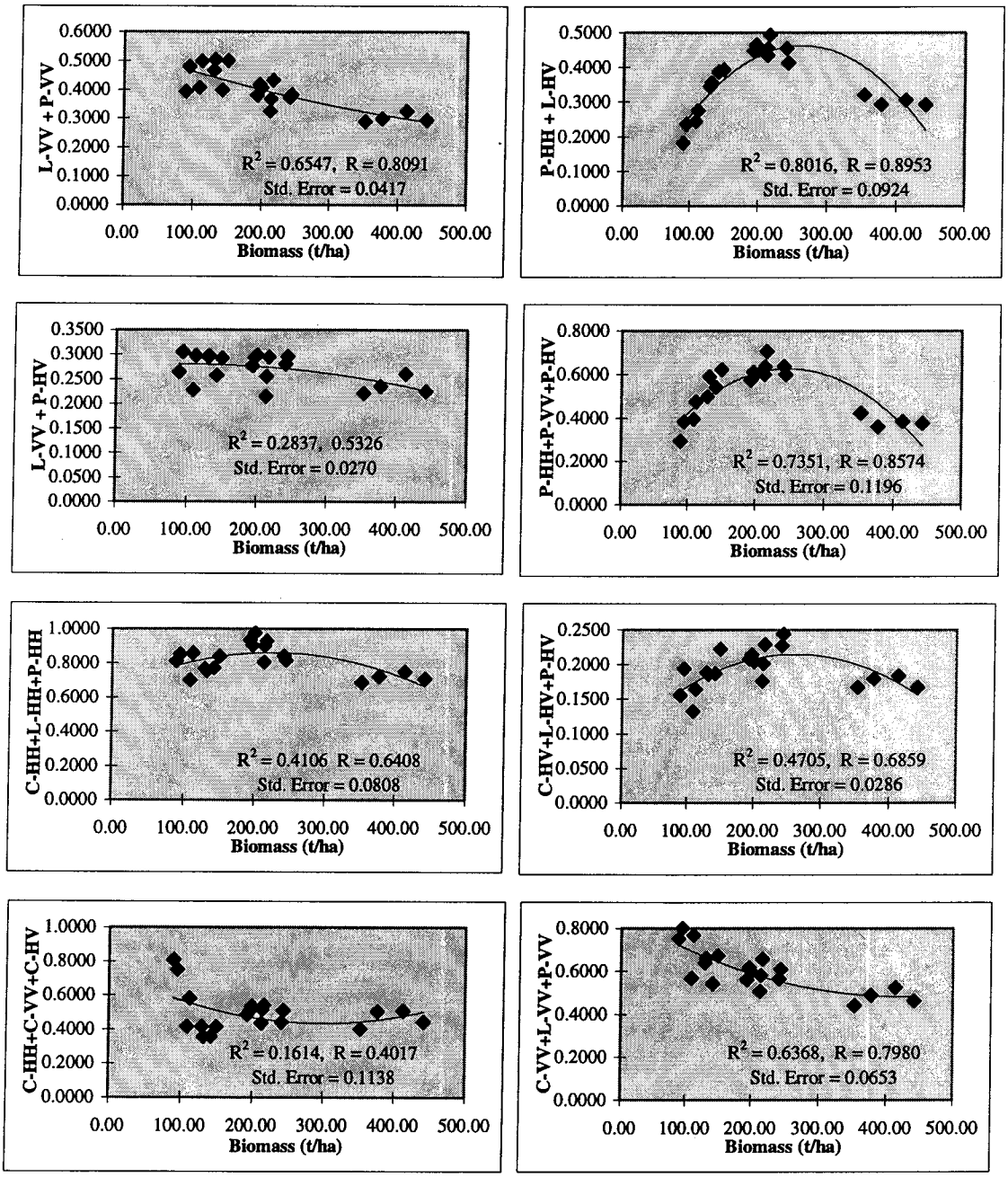

Figure 7.3.14 Total aboveground dry biomass (t/ha) versus L-VV + P-VV, L-VV + P-HV, C-HH + L-HH + P-HH, C-HH + C-VV + C-HV, P-HH + L-HV, P-HH + P-VV + P-HV, C-HV + L-HV + P-HV, and C-VV + L-VV + P-VV backscatter (in intensity values) from needle-leaved stands

Appendix 7.4

This appendix shows how stand age is related to total aboveground dry biomass and the new TCM and TCB indices.

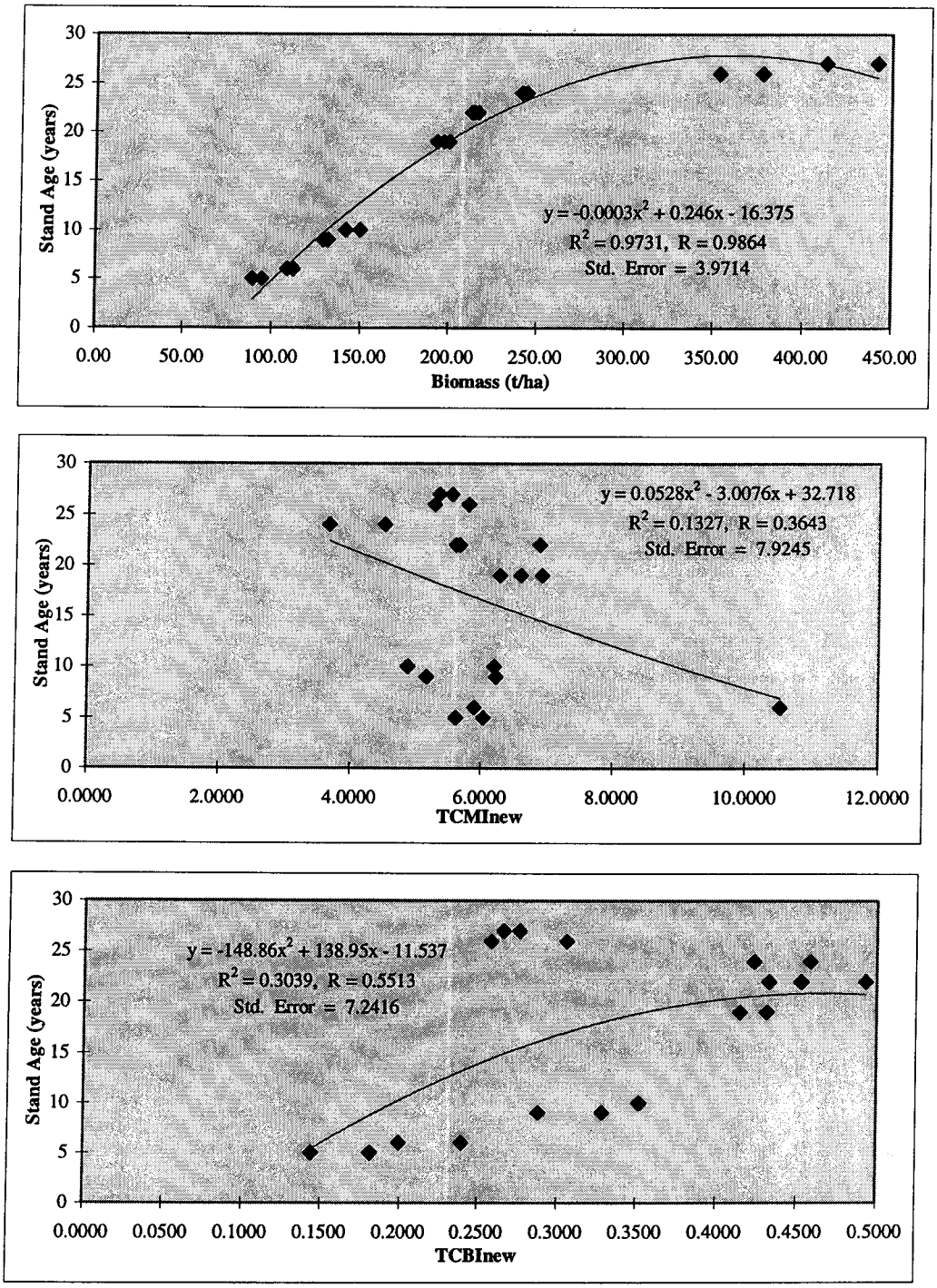

Figure 7.4.1 Stand age versus total aboveground dry biomass (t/ha), $TCMI_{new}$ and $TCBI_{new}$

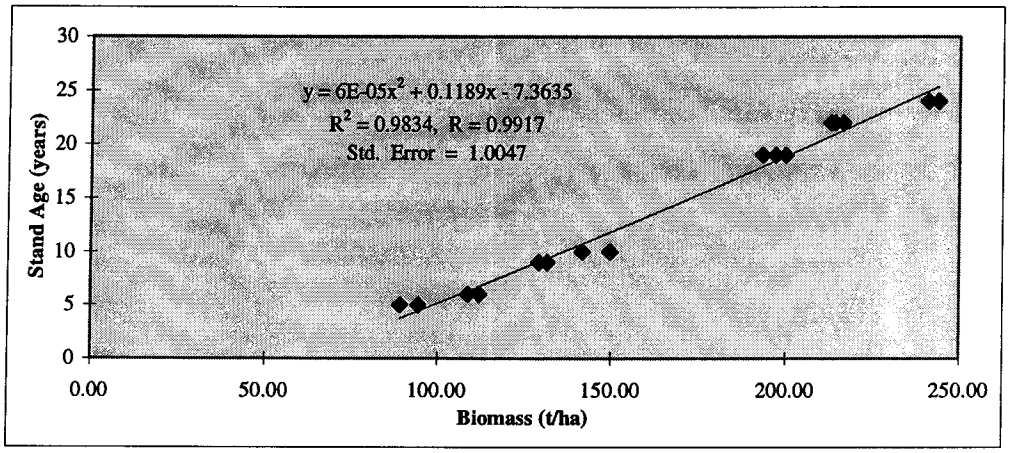

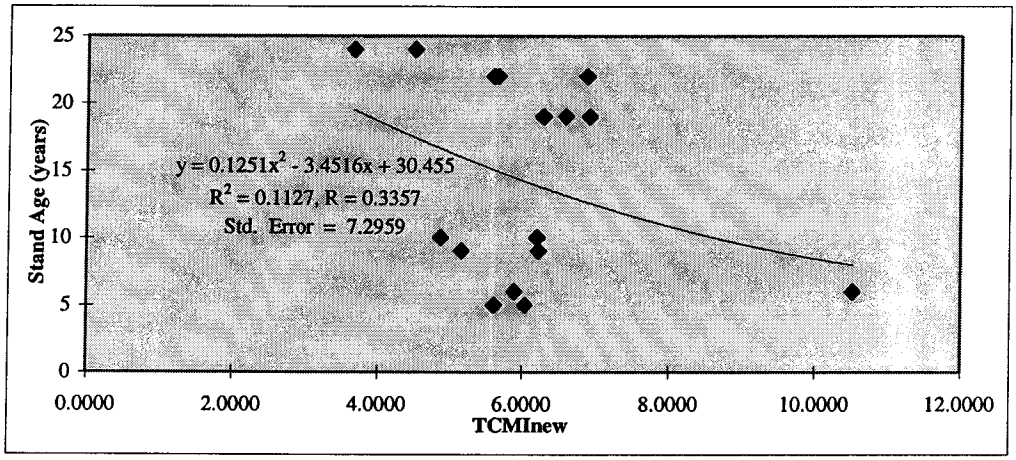

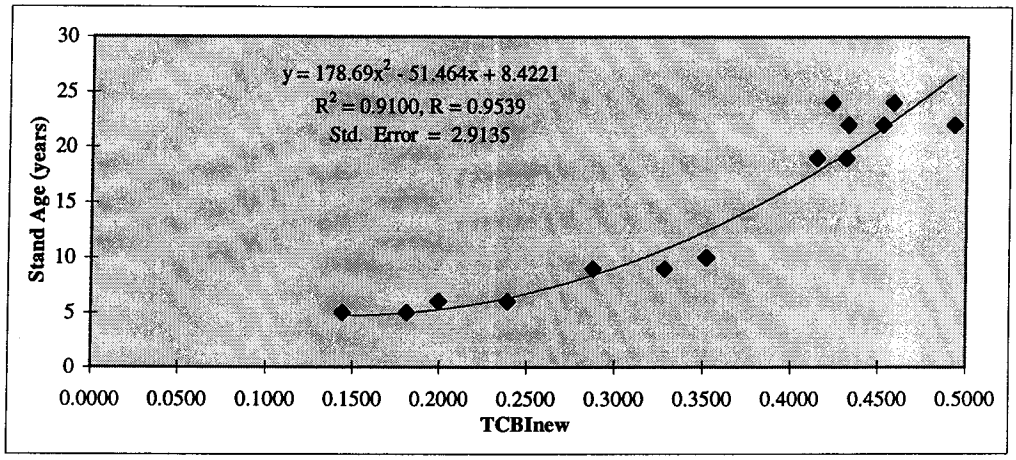

Figure 7.4.2 Stand age versus total aboveground dry biomass (t/ha), $TCMI_{new}$ and $TCBI_{new}$ within a 0 - 245 t/ha biomass range

Appendix 7.5

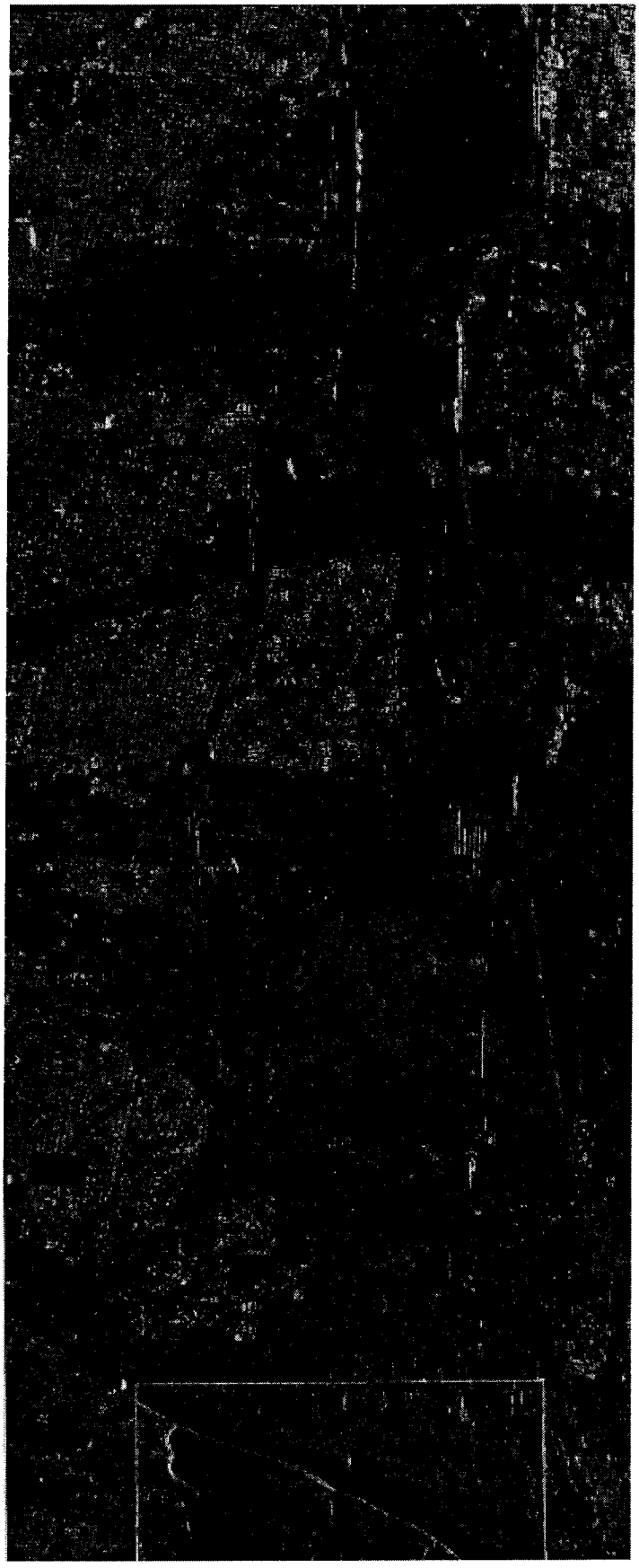

Figure 7.5.1 Single-band (L-HH) image of the whole radar scene which includes the Blue Mountains study site

7.5.2 Multi-band image (R=C-HV, G=L-HH, B=P-HH) of the whole radar scene which includes the Blue Mountains Study site

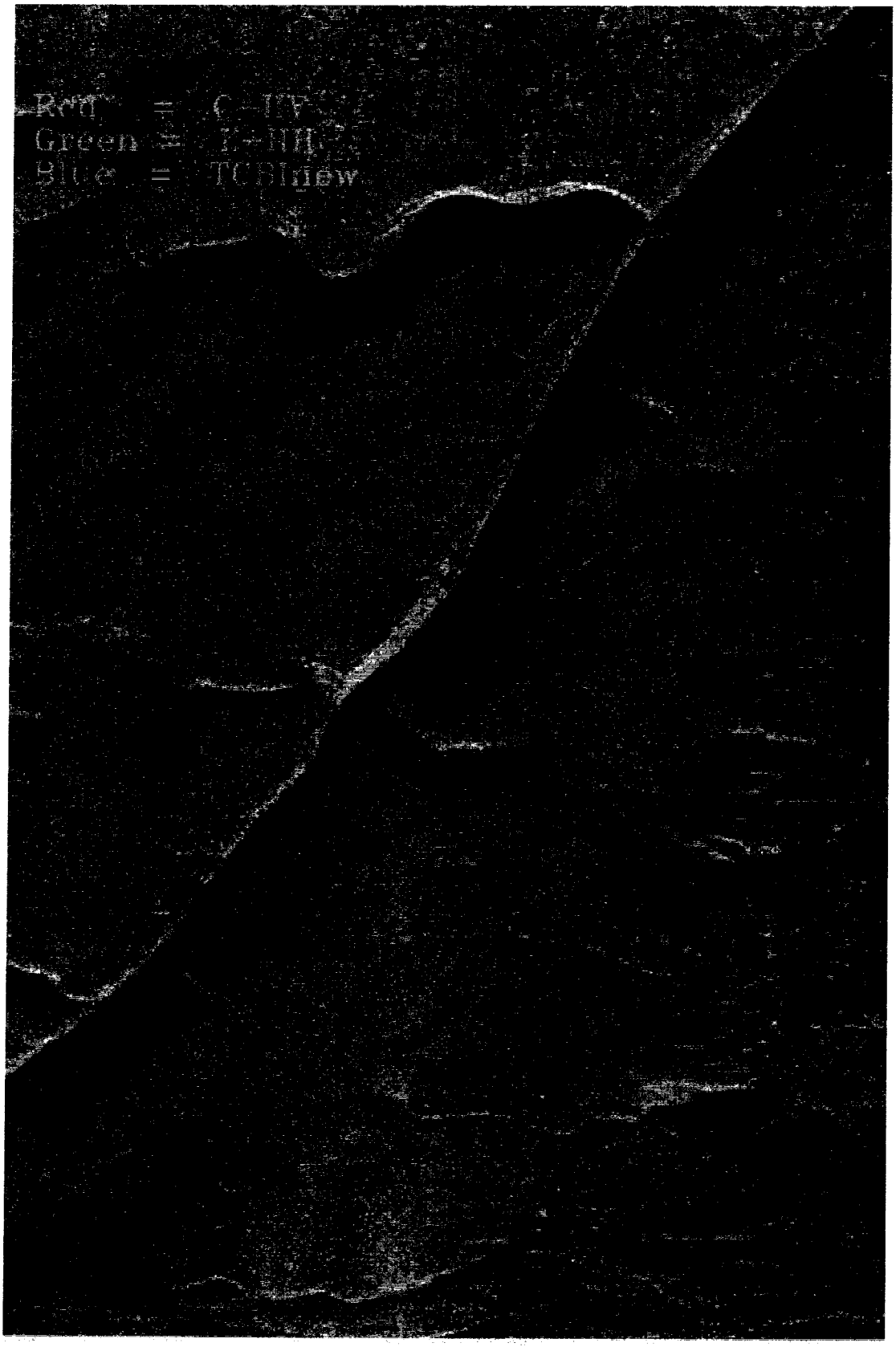

Figure 7.5.3 C-HV (Red), L-HH (Green) and $TCBI_{new}$ (Blue) image of study site 1 (Blue Mountains)

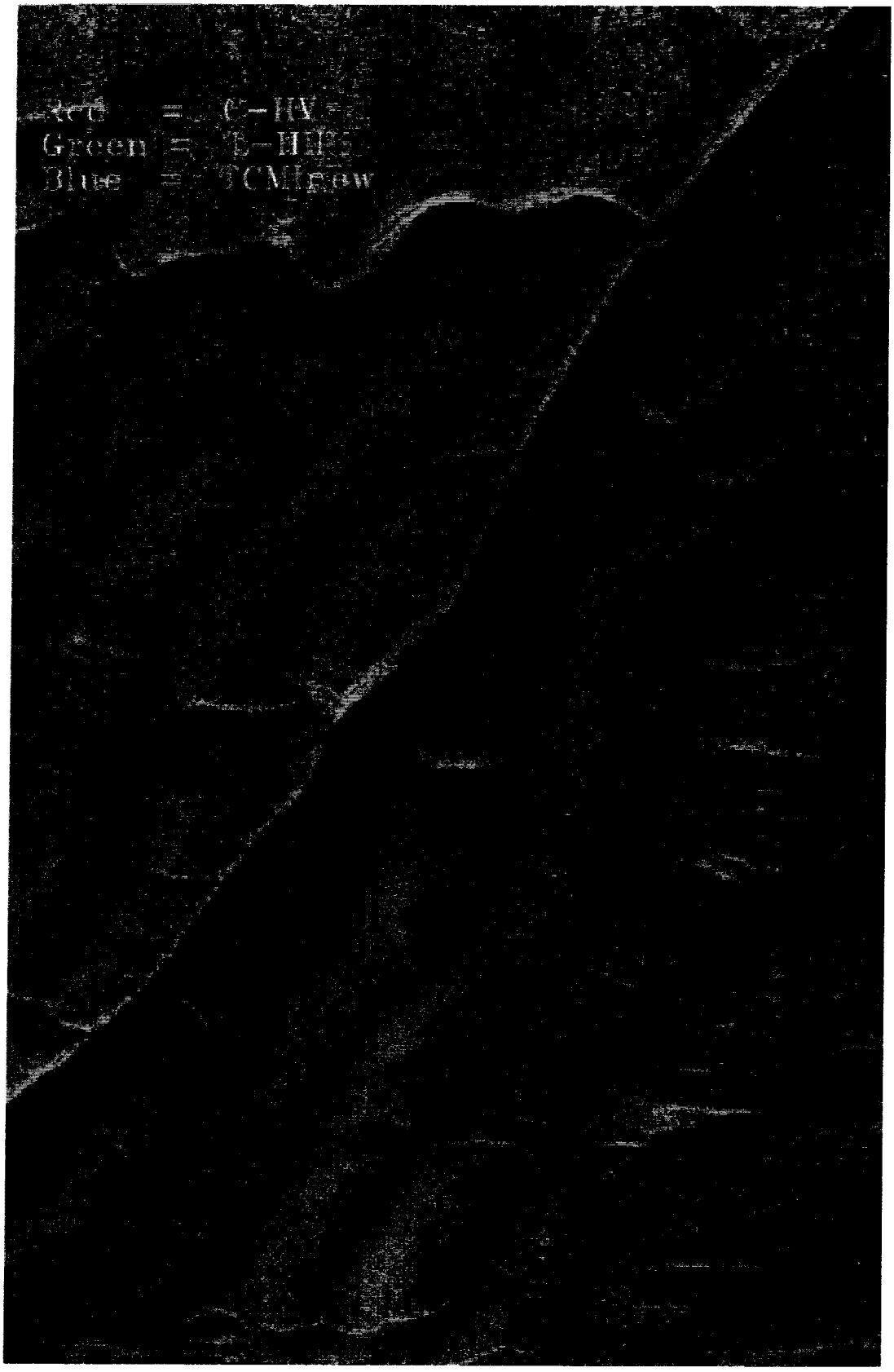

Figure 7.5.4 C-HV (Red), L-HH (Green) and $TCMI_{new}$ (Blue) image of study site 1 (Blue Mountains)

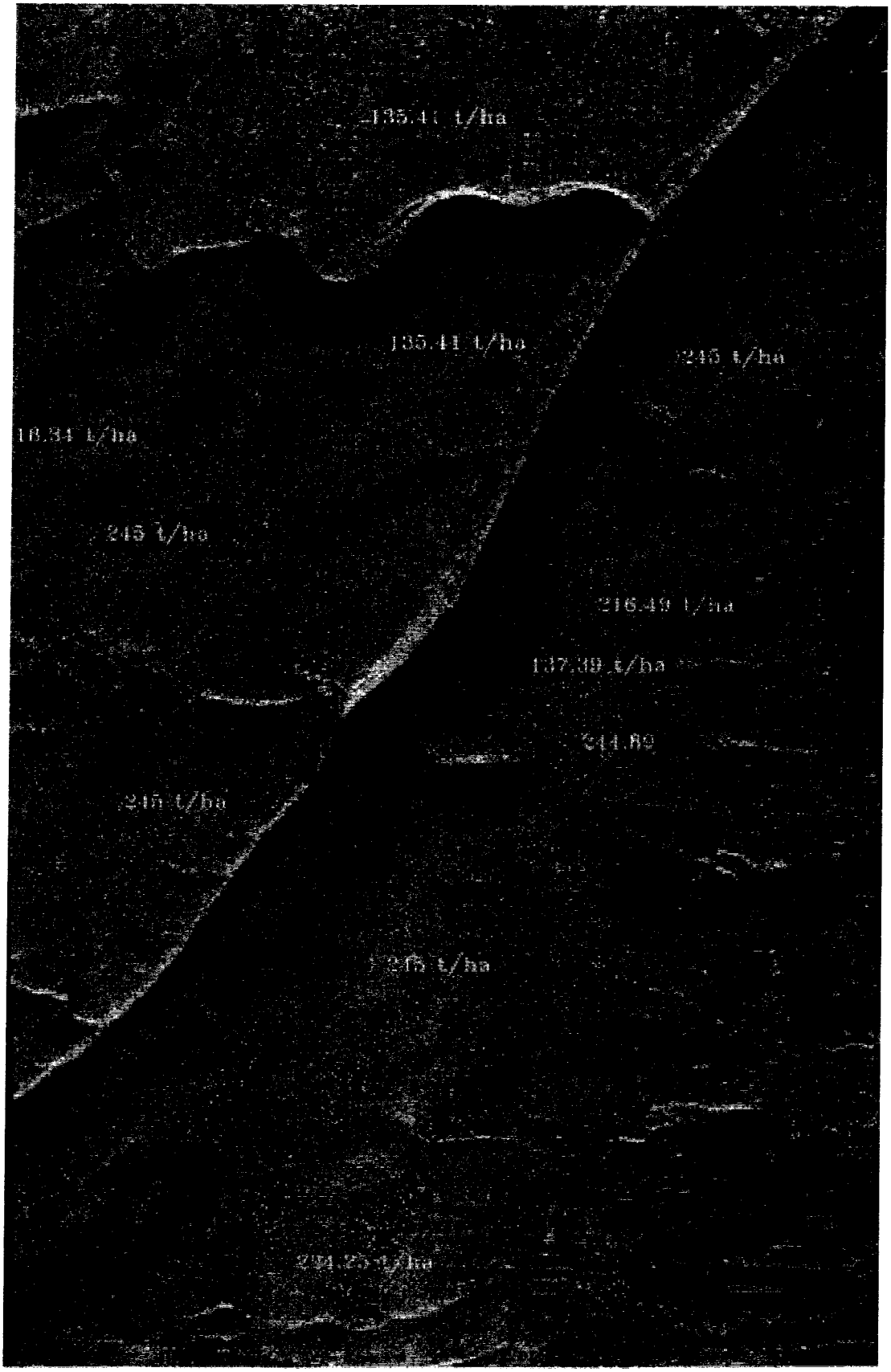

Figure 7.5.5 Image showing calculated biomass amounts in representative parcels in study site 1 (Blue Mountains)

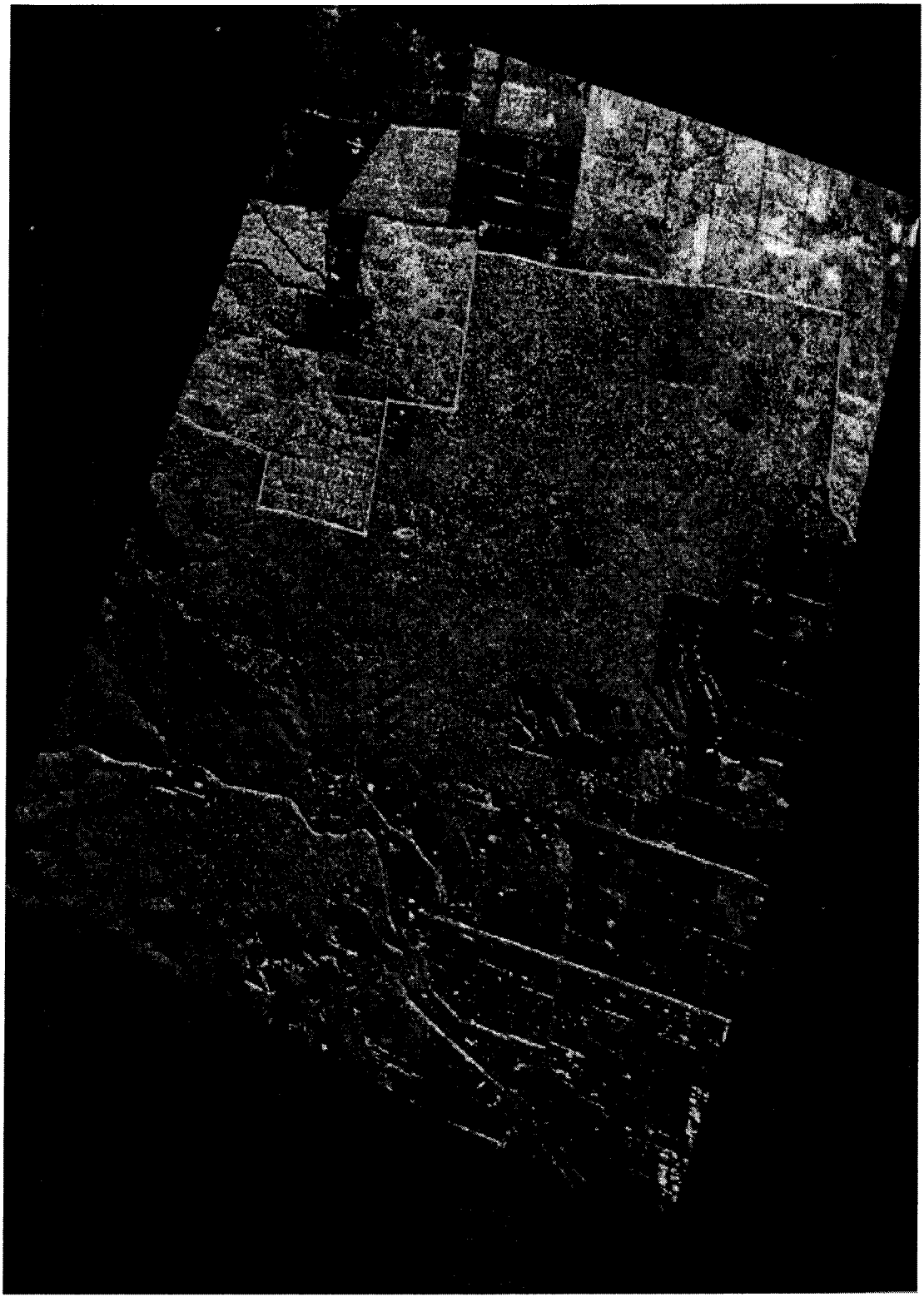

Figure 7.6.1 Single band image (L-HH) of the whole radar scene which includes the Gippsland study site (inset)

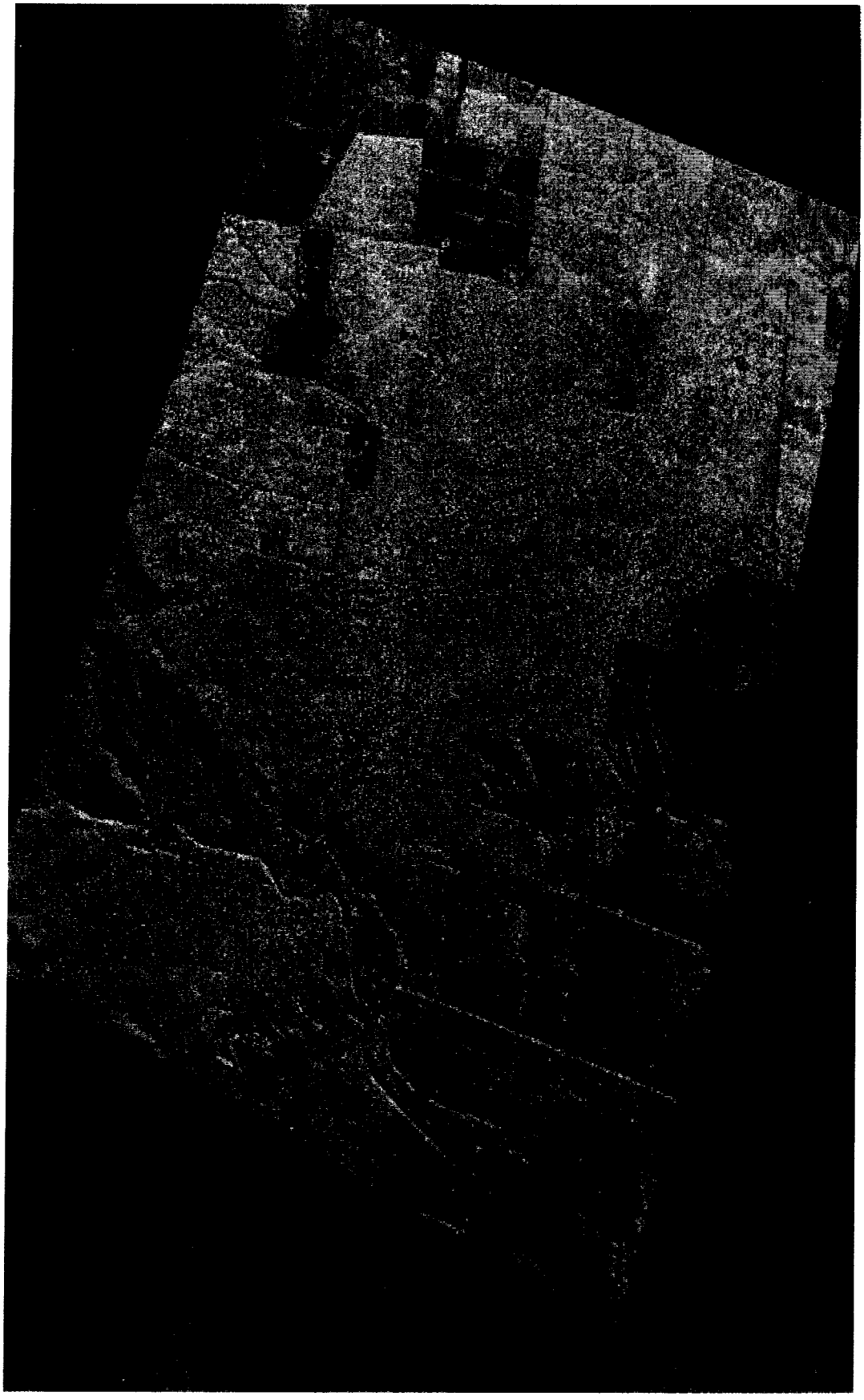

Figure 7.6.2 Multi-band image (R=C-HV, G=L-HH, B=P-HH) of the whole radar scene containing the Gippsland study site (top)

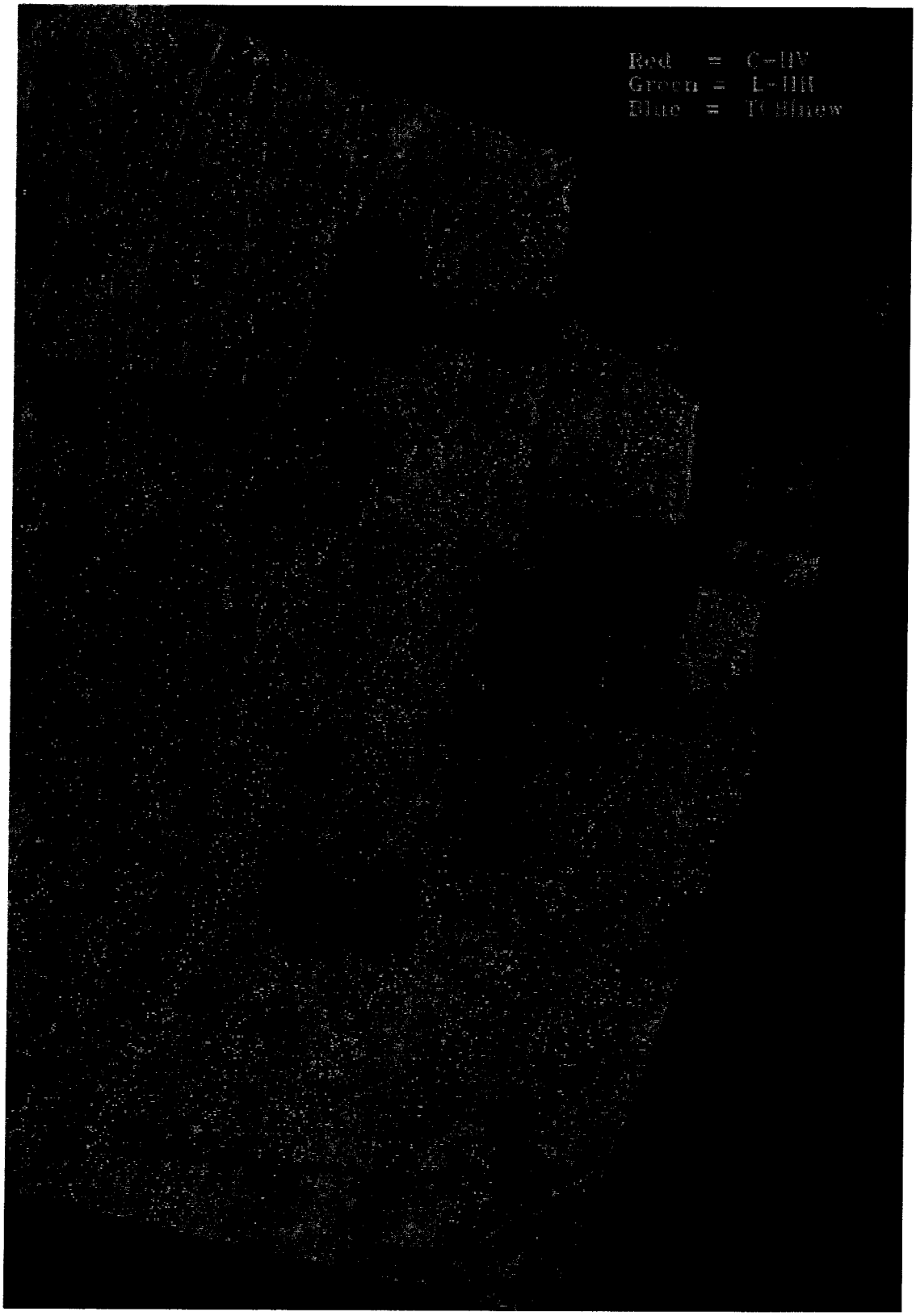

Figure 7.6.3 C-HV (Red), L-HH (Green) and $TCBI_{new}$ (Blue) image of study site 2 (Gippsland)

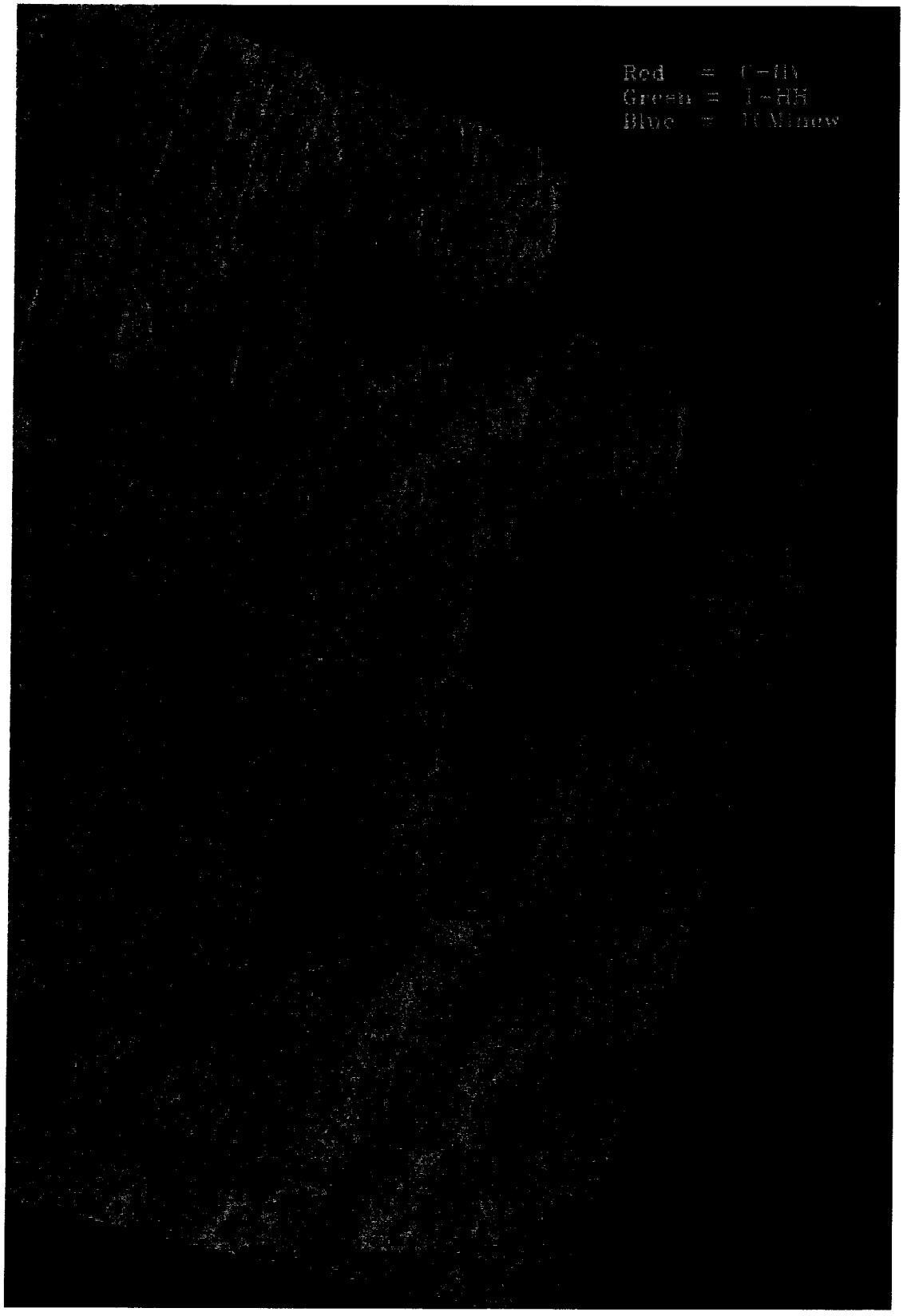

Figure 7.6.4 C-HV (Red), L-HH (Green) and $TCMI_{new}$ (Blue) image of study site 2 (Gippsland)

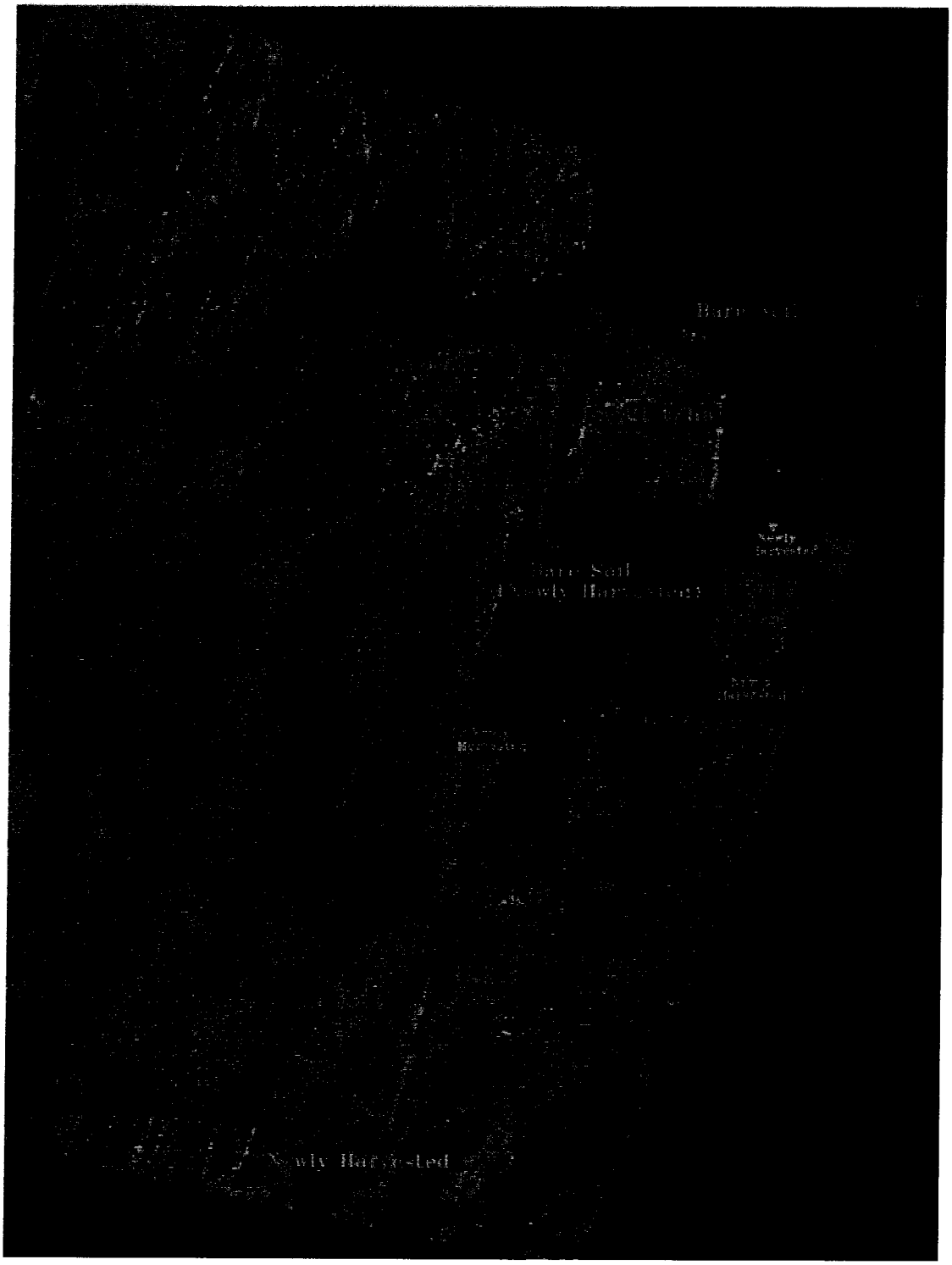

Figure 7.6.5 Image showing calculated biomass amounts in representative block compartments in study site 2

Publications from the

SCHOOL OF GEOMATIC ENGINEERING

THE UNIVERSITY OF NEW SOUTH WALES
ABN 57 195 873 179

To order, write to:
Publications Officer, School of Geomatic Engineering
The University of New South Wales, UNSW SYDNEY NSW 2052, AUSTRALIA

NOTE: ALL ORDERS MUST BE PREPAID. CREDIT CARDS ARE ACCEPTED.
ASK FOR OUR CREDIT CARD ORDER FORM.

UNISURV REPORTS - S SERIES

(Prices effective September 2000)

Australian Prices *:	S8 - S20		$11.00
	S29 onwards	Individuals	$27.50
		Institutions	$33.00
Overseas Prices **:	S8 - S20		$10.00
	S29 onwards	Individuals	$25.00
		Institutions	$30.00

* Australian prices include postage by surface mail and GST.
** Overseas prices include delivery by UNSW's air-lifted mail service (~2-4 weeks to Europe and North America). Rates for air mail rates through Australia Post on application.

S8. A. Stolz, "Three-D Cartesian Co-ordinates of Part of the Australian Geodetic Network by the Use of Local Astronomic Vector Systems", Unisurv Rep. S8, 182 pp, 1972.

S10. A. J. Robinson, "Study of Zero Error and Ground Swing of the Model MRA101 Tellurometer", Unisurv Rep. S10, 200 pp, 1973.

S12. G. J. F. Holden, "An Evaluation of Orthophotography in an Integrated Mapping System", Unisurv Rep. S12, 232 pp, 1974.

S14. E. G. Anderson, "The Effect of Topography on Solutions of Stokes` Problem", Unisurv Rep. S14, 252 pp, 1976.

S16. K. Bretreger, "Earth Tide Effects on Geodetic Observations", Unisurv S16, 173 pp, 1978.

S17. C. Rizos, "The Role of the Gravity Field in Sea Surface Topography Studies", Unisurv S17, 299 pp, 1980.

S18. B. C. Forster, "Some Measures of Urban Residential Quality from LANDSAT Multi-Spectral Data", Unisurv S18, 223 pp, 1981.

S19. R. Coleman, "A Geodetic Basis for Recovering Ocean Dynamic Information from Satellite Altimetry", Unisurv S19, 332 pp, 1981.

S20. D. R. Larden, "Monitoring the Earth's Rotation by Lunar Laser Ranging", Unisurv Report S20, 280 pp, 1982.

S29. G. S. Chisholm, "Integration of GPS into Hydrographic Survey Operations", Unisurv S29, 190 pp, 1987.

S30. G. A. Jeffress, "An Investigation of Doppler Satellite Positioning Multi-Station Software", Unisurv S30, 118 pp, 1987.

S31. J. Soetandi, "A Model for a Cadastral Land Information System for Indonesia", Unisurv S31, 168 pp, 1988.

S33. R. D. Holloway, "The Integration of GPS Heights into the Australian Height Datum", Unisurv S33, 151 pp, 1988.

S34. R. C. Mullin, "Data Update in a Land Information Network", Unisurv S34, 168 pp, 1988.

S35. B. Merminod, "The Use of Kalman Filters in GPS Navigation", Unisurv S35, 203 pp, 1989.

S36. A. R. Marshall, "Network Design and Optimisation in Close Range Photogrammetry", Unisurv S36, 249 pp, 1989.

S37. W. Jaroondhampinij, "A model of Computerised Parcel-Based Land Information System for the Department of Lands, Thailand," Unisurv S37, 281 pp, 1989.

S38. C. Rizos (Ed.), D. B. Grant, A. Stolz, B. Merminod, C. C. Mazur "Contributions to GPS Studies", Unisurv S38, 204 pp, 1990.

S39. C. Bosloper, "Multipath and GPS Short Periodic Components of the Time Variation of the Differential Dispersive Delay", Unisurv S39, 214 pp, 1990.

S40. J. M. Nolan, "Development of a Navigational System Utilizing the Global Positioning System in a Real Time, Differential Mode", Unisurv S40, 163 pp, 1990.

S41. R. T. Macleod, "The Resolution of Mean Sea Level Anomalies along the NSW Coastline Using the Global Positioning System", 278 pp, 1990.

S42. D. A. Kinlyside, "Densification Surveys in New South Wales - Coping with Distortions", 209 pp, 1992.

S43. A. H. W. Kearsley (Ed.), Z. Ahmad, B. R. Harvey and A. Kasenda, "Contributions to Geoid Evaluations and GPS Heighting", 209 pp, 1993.

S44. P. Tregoning, "GPS Measurements in the Australian and Indonesian Regions (1989-1993)", 134 + xiii pp, 1996.

S45. W.-X. Fu, "A Study of GPS and Other Navigation Systems for High Precision Navigation and Attitude Determinations", 332 pp, 1996.

S46. P. Morgan et al, "A Zero Order GPS Network for the Australia Region", 187 + xii pp, 1996.

S47. Y. Huang, "A Digital Photogrammetry System for Industrial Monitoring", 145 + xiv pp, 1997.

S48. K. Mobbs, "Tectonic Interpretation of the Papua New Guinea Region from Repeat Satellite Measurements", 256 + xc pp, 1997.

S49. S. Han, "Carrier Phase-Based Long-Range GPS Kinematic Positioning", 185 + xi pp, 1997.

S50. M. D. Subari, "Low-cost GPS Systems for Intermediate Surveying and Mapping Accuracy Applications", 179 + xiii pp, 1997.

S51. L.-S. Lin, "Real-Time Estimation of Ionospheric Delay Using GPS Measurements", 199 + xix pp, 1997.

S52. M. B. Pearse, "A Modern Geodetic Reference System for New Zealand", 324 + xviii pp, 1997.

S53. D. B. Lemon, "The Nature and Management of Positional Relationships within a Local Government Geographic Information System", 273 + xvi pp, 1997.

S54. C. Ticehurst, "Development of Models for Monitoring the Urban Environment Using Radar Remote Sensing", 282 + xix pp, 1998.

S55. S. S. Boey, "A Model for Establishing the Legal Traceability of GPS Measurements for Cadastral Surveying in Australia", 186 + xi pp, 1999.

S56. P. Morgan and M. Pearse, "A First-Order Network for New Zealand", 134 + x pp, 1999.

S57. P. N. Tiangco, "A Multi-Parameter Radar Approach to Stand Structure and Forest Biomass Estimation", 319 + xxii pp, 2000.

MONOGRAPHS

Australian prices include postage by surface mail.
Overseas prices include delivery by UNSW's air-lifted mail service (~2-4 weeks to Europe and North America).
Rates for air mail rates through Australia Post on application.
Australian prices include GST.

(Prices effective September 2000)

		Price Australia (incl. GST)	**Price** Overseas
M1.	R. S. Mather, "The Theory and Geodetic Use of some Common Projections", (2nd edition), 125 pp, 1978.	$ 16.50	$ 15.00
M2.	R. S. Mather, "The Analysis of the Earth's Gravity Field", 172 pp, 1971.	$ 8.80	$ 8.00
M3.	G. G. Bennett, "Tables for Prediction of Daylight Stars", 24 pp, 1974.	$ 5.50	$ 5.00
M4.	G. G. Bennett, J. G. Freislich & M. Maughan, "Star Prediction Tables for the Fixing of Position", 200 pp, 1974.	$ 8.80	$ 8.00
M8.	A. H. W. Kearsley, "Geodetic Surveying", 96 pp, 1988.	$ 13.20	$ 12.00
M11.	W. F. Caspary, "Concepts of Network and Deformation Analysis", 183 pp, 2000.	$ 27.50	$ 25.00
M12.	F. K. Brunner, "Atmospheric Effects on Geodetic Space Measurements", 110 pp, 1988.	$ 17.60	$ 16.00
M13.	B. R. Harvey, "Practical Least Squares and Statistics for Surveyors", (2nd edition, reprinted with corrections), 319 pp, 1998.	$ 33.00	$ 30.00
M14.	E. G. Masters and J. R. Pollard (Eds.), "Land Information Management", 269 pp, 1991. (Proceedings LIM Conference, July 1991).	$ 22.00	$ 20.00
M15/1	E. G. Masters and J. R. Pollard (Eds.), "Land Information Management - Geographic Information Systems - Advance Remote Sensing Vol. 1", 295 pp, 1993 (Proceedings of LIM & GIS Conference, July 1993).	$ 33.00	$ 30.00
M15/2	E. G. Masters and J. R. Pollard (Eds.), "Land Information Management - Geographic Information Systems - Advance Remote Sensing Vol. 2", 376 pp, 1993 (Proceedings of Advanced Remote Sensing Conference, July 1993).	$ 33.00	$ 30.00
M16.	A. Stolz, "An Introduction to Geodesy", 112 pp, 1994.	$ 22.00	$ 20.00
M17.	C. Rizos, "Principles and Practice of GPS Surveying", 565 pp, 1997.	$ 46.20	$ 42.00

Credit Card Orders / Payment

from / to

School of Geomatic Engineering

The University of New South Wales

Name and postal address of ordering person/organisation

_____

_____

_____

_____

_____

Date : _____

Day time phone number : _____

Credit Card debit for

_____ $ _____

_____ $ _____

_____ $ _____

_____ $ _____

Total $ _____

Please debit my credit card: ☐ Mastercard ☐ Visa ☐ Bankcard

Card Name: _____ Signature: _____

Card No: | | | | | | | | | | | | | | | | Expire Date : _____

Note: UNSW requires that you attach a photocopy of your credit card to this order